LEABHARLANN CHOLÁISTE NA TRÍONÓIDE, BAILE ÁTHA CLIATH | TRINITY COLLEGE LIBRARY DUBLIN
Ollscoil Átha Cliath | The University of Dublin

Terms and Conditions of Use of Digitised Theses from Trinity College Library Dublin

Copyright statement

All material supplied by Trinity College Library is protected by copyright (under the Copyright and Related Rights Act, 2000 as amended) and other relevant Intellectual Property Rights. By accessing and using a Digitised Thesis from Trinity College Library you acknowledge that all Intellectual Property Rights in any Works supplied are the sole and exclusive property of the copyright and/or other IPR holder. Specific copyright holders may not be explicitly identified. Use of materials from other sources within a thesis should not be construed as a claim over them.

A non-exclusive, non-transferable licence is hereby granted to those using or reproducing, in whole or in part, the material for valid purposes, providing the copyright owners are acknowledged using the normal conventions. Where specific permission to use material is required, this is identified and such permission must be sought from the copyright holder or agency cited.

Liability statement

By using a Digitised Thesis, I accept that Trinity College Dublin bears no legal responsibility for the accuracy, legality or comprehensiveness of materials contained within the thesis, and that Trinity College Dublin accepts no liability for indirect, consequential, or incidental, damages or losses arising from use of the thesis for whatever reason. Information located in a thesis may be subject to specific use constraints, details of which may not be explicitly described. It is the responsibility of potential and actual users to be aware of such constraints and to abide by them. By making use of material from a digitised thesis, you accept these copyright and disclaimer provisions. Where it is brought to the attention of Trinity College Library that there may be a breach of copyright or other restraint, it is the policy to withdraw or take down access to a thesis while the issue is being resolved.

Access Agreement

By using a Digitised Thesis from Trinity College Library you are bound by the following Terms & Conditions. Please read them carefully.

I have read and I understand the following statement: All material supplied via a Digitised Thesis from Trinity College Library is protected by copyright and other intellectual property rights, and duplication or sale of all or part of any of a thesis is not permitted, except that material may be duplicated by you for your research use or for educational purposes in electronic or print form providing the copyright owners are acknowledged using the normal conventions. You must obtain permission for any other use. Electronic or print copies may not be offered, whether for sale or otherwise to anyone. This copy has been supplied on the understanding that it is copyright material and that no quotation from the thesis may be published without proper acknowledgement.

DEVELOPMENT OF MICROEMULSIONS AND SELF-EMULSIFYING SYSTEMS FOR ORAL DRUG DELIVERY

by

Bożena E. Adamczyk, M.Sc. (Pharmacy)

being submitted a thesis submitted for the degree of

Doctor of Philosophy
in Pharmaceutics

at
University of Dublin
Trinity College

under the direction and supervision of

Anne Marie Healy, B.Sc. (Pharm.), Ph.D., M.P.S.I., F.T.C.D.
and
Professor O.I. Corrigan, B.Sc. (Pharm), M.A., Ph.D., F.T.C.D., F.P.S.I.

March 2012

TRINITY COLLEGE
2 4 MAY 2013
LIBRARY DUBLIN

Thesis 10095

DECLARATION

This thesis is submitted by the undersigned to the University of Dublin, Trinity College, for examination for the degree of Doctor of Philosophy. It has not been submitted as an exercise for a degree at any other university. I myself carried out all the practical work except where duly acknowledged.

I wrote this manuscript with the aid of editorial advice from Dr. Anne Marie Healy and Professor O.I. Corrigan.

I agree to deposit this thesis in the University's open access institutional repository or allow the library to do so on my behalf, subject to Irish Copyright Legislation and Trinity College Library conditions of use and acknowledgement.

Bozena E. Adamczyk

To my family and Giorgio, who have always been there for me in every way, and they are the reason I am here right now.

SUMMARY

The main aim of the current work was to explore microemulsions (ME) and self-emulsifying lipid formulations (SELFs) comprising derivatives of capric/caprylic acids (Captex 355, Captex 200P, Capmul PG-8, Capmul MCM) as drug delivery systems for oral administration of hydrophilic compounds (BCS class III) intended for encapsulation.

Physicochemical profiling of hydrophilic model compounds (two bisphosphonates: sodium alendronate trihydrate and disodium pamidronate pentahydrate and a decaptide, acyline monoacetate) was carried out. Sodium alendronate trihydrate and disodium pamidronate pentahydrate were found to be highly water soluble with the highest solubility achieved in the modified K-McIlvaine's buffers pH 7.8 (~52 mg/ml) and pH 4.4 (~70 mg/ml) respectively. Acyline monoacetate was found to be also highly water soluble, however rapid gelation (physical instability) was observed in aqueous solutions. Good solubility (up to 10 mg/g) and physical stability (lack of gelling) was observed in propylene glycol and the standard GIPET® II formulation. The isoelectric point of acyline was found to be ~11.4.

Oils (Captex 200P, Captex 355 and Capmul PG-8), cosurfactants (Capmul MCM, Capmul MCM C8 and Capmul MCM C10), one surfactant (Crillet 4 HP) and water were used to prepare several pseudoternary phase diagrams at 37 °C where the formation of SELFs and MEs was investigated by varying the type of oil, the type of cosurfactant and the combined HLB value. In the systems with low combined HLB values (6 – 9), preconcentrates (mixes of oil, the surfactant and the cosurfactant) formed microemulsions, which subsequently converted into emulsions upon further dilution with water. A number of preconcentrates formulated with Captex 355 (the most hydrophobic oil) and Capmul MCM C8 (as a cosurfactant) formed extensive microemulsion regions comprising up to 20 - 30% of water (at 37 °C). This cosurfactant was found to form larger microemulsion regions and reduced liquid crystalline phases compared to Capmul MCM C10. The systems with the high HLB values (9 –14), formed large liquid crystalline regions upon dilution but their emulsification behaviour could be improved by the addition of PEG 400 as a cosolvent or the use of artificial intestinal fluids (FaSSIF-V2, FeSSIF-V2) as titrants instead of water.

The microstructure in selected model colloidal samples (formed by gradual dilution of the preconcentrate comprising Captex 355/Capmul MCM C8/Crillet 4 HP, 40: 39: 21 %w/w) was investigated with conductivity and viscosity measurements, small-angle neutron scattering (SANS), pulsed-field-gradient spin-echo (PGSE-NMR), dynamic light scattering (DLS), differential scanning calorimetry (DSC), zeta potential, cryogenic transmission electron microscopy (cryo-TEM) and freeze-fracture transmission electron microscopy (FF-TEM). As a result of the characterisation performed, the colloidal samples containing from 10 to 20% were identified as inverse micelles with an average particle size below 10 nm. The samples comprising from 20 to 45% of water were identified as water-in-oil microemulsions with an average particle size between 11 and 17 nm. The sample containing 45% of water also showed some bicontinuous properties since it was 'located' close to the phase transition into an oil-in-water emulsion (at 50% of water).

Incorporation of the bisphosphonates into MEs suitable for encapsulation was not feasible. Both drugs were found to be poorly soluble in these formulations despite an effort to maximise the drug load by using the modified K-McIlvaine's buffers (as an aqueous phase) in which each drug showed the highest solubility. Acyline monoacetate was found to be soluble in non-aqueous microemulsions (SEDDSs) up to ~10 mg per g of SEDDS, however the physical stability of these formulations was very poor and significantly reduced dissolution rate of acyline *in vitro* was observed from gelled SEDDSs compared to the liquid. In a dog study (n= 5), the relative oral bioavailability of acyline was significantly improved from three liquid (non-gelled) SEDDSs by 8, 22 and 33 fold. Stability of acyline in liquid SEDDSs was poor due to the gelling and further work focussed on the development of solid self-emulsifying lipid formulations (S-SELFs) where a high drug load or chemical/ physical incompatibility with SELF should not be major obstacles to the development of a stable dosage form.

Characterisation of selected solid carriers (Sylysia 320, Aeroperl 300/30, Zeofree 5161, Hubersorb 600, Neusilin US2 and Fujicalin SG) was carried out using scanning electron microscopy (SEM), particle sizing by laser diffraction, measurements of specific surface area (BET) and porosity, bulk and tapped density, pH measurements, solid state Fourier transform infrared spectroscopy (FTIR), thermal analysis (DSC & TGA), powder X-Ray diffraction analysis (PXRD) and Adsorption Index (AI). Neusilin US2, Sylysia 320, Aeroperl 300/30 and Hubersorb 600 were found to be the most promising adsorbents based on the large specific surface area (SSA_{BET}) and high Adsorption Index. In addition, Zeofree 5161 was identified as a more hydrophilic grade of silicon dioxide than Sylysia 320 and Aeroperl 300/30. Hubersorb 600 was found to contain highly alkaline impurities.

Subsequently, the adsorption capacity of the solid carriers was investigated with rheometric measurements of flowability (Basic Flowability Energy, Specific Energy), density (Conditioned Bulk Density) and shear properties (Shear Stress). Changes in these physical properties were monitored as the percentage of added liquid SEDDS increased, in order to establish the transition point between a powder and a paste (the adsorption capacity). The highest adsorption capacity equal to ~70% was determined for Zeofree 5161, Hubersorb 600 and Neusilin US2, while Fujicalin showed the poorest adsorption capacity (~40%). The desorption characteristics from the solid systems were measured in a dispersion test where release of the adsorbed SEDDS was indirectly measured by particle sizing, transmittance and the percentage of dissolved water-insoluble Fat Red 7B dye. The best desorption characteristics were seen with Hubersorb 600 and Fujicalin SG.

The current thesis highlighted the role played by the type of oil, the type of a cosurfactant and the combination of the cosurfactant with a primary surfactant on the formation of self-emulsifying systems and microemulsions. The solubility and stability of model hydrophilic drugs in liquid MEs/SELFs were found to be major obstacles to develop liquid systems suitable for encapsulation, which subsequently led to the development of solid self-emulsifying systems with a potential to overcome these limitations.

TABLE OF CONTENTS

Acknowledgments i

Presentations and publications associated with this thesis ii

Abbreviations and symbols iii

Origin and Scope v

INTRODUCTION

1. Chapter: Lipid - based Drug Delivery Systems and Their Properties

1.1. Introduction 1

1.2. Solutions, self-emulsifying systems and microemulsions for oral delivery 2

1.2.1. Simple and micellar solutions 3

1.2.2. Self-emulsifying systems 5

1.2.3. Microemulsions 7

1.3. Composition of microemulsions and self-emulsifying lipid systems 8

1.3.1. Oil phase 8

1.3.2. Surfactants 9

1.3.3. Cosurfactants 9

1.3.4. Hydrophilic phase 10

1.3.5. Composition of the original microemulsions and self-emulsifying systems 11

1.4. Microstructure and phase behaviour 25

1.4.1. Mechanism of self-emulsification 25

1.4.2. Phase behaviour 26

1.4.3. Factors affecting formation of microemulsions 28

1.4.4. Techniques to characterise the microstructure 29

1.4.4.1. Cryogenic transmission electron microscopy (cryo-TEM) and Freeze-fracture transmission electron microscopy (FF-TEM) 29

1.4.4.2. Pulsed-field-gradient spin-echo nuclear magnetic resonance *(PGSE-NMR)* 30

1.4.4.3. Small angle neutron scattering (SANS) 31

1.5. Solid microemulsions and solid self-emulsifying systems 33

1.5.1. Techniques to characterise solid adsorbents 33

1.5.1.1. Laser diffraction to determine particle size 34
1.5.1.2. Specific surface area and porosity 34
1.5.2. Techniques to characterise solid microemulsion and solid self-emulsifying systems 36
1.5.2.1. Basic Flowability Energy (BFE) 37
1.5.2.2. Specific Energy (SE) 38
1.5.2.3. Conditioned Bulk density (CBD) 39
1.5.2.4. Shear Stress (SS) 39
1.6. Aims of experimental work 40

EXPERIMENTAL

2. Chapter: Materials And Methods

2.1. Materials 41
2.2. Methods: Characterisation of Model Compounds 44
2.2.1. Synthesis of monosodium pamidronate monohydrate 44
2.2.2. Solid state Fourier transform infrared spectroscopy (FTIR) 44
2.2.3. Thermal analysis (Differential scanning calorimetry & Thermal gravimetric analysis) 44
2.2.4. Powder X-Ray Diffraction analysis (PXRD) 44
2.2.5. Particle sizing by laser diffraction (PSD) 45
2.2.6. Isoelectric point (IEP) 45
2.2.7. Aqueous solubility 45
2.2.8. Solubility in the standard GIPET® II formulation and propylene glycol 47
2.2.9. Calculation of cLogP and cLogD 48
2.3. Methods: Characterisation of Microemulsion components 48
2.3.1. Thermal analysis (Differential scanning calorimetry & Thermal gravimetric analysis) 48
2.3.2. Calculation of cLogP 49
2.3.3. Calculation of solubility parameter 49
2.3.4. Calculation of HLB value 49
2.3.5. Calculation of a combined HLB value 50
2.4. Methods: Construction of pseudoternary phase diagrams 50
2.4.1. Titration procedure 50
2.4.2. Determination boundary points 53

2.5. Methods: Characterisation of Microemulsions 54
2.5.1. Cryogenic transmission electron microscopy (cryo-TEM) and Freeze-fracture transmission electron microscopy (FF-TEM) 54
2.5.2. Conductivity 54
2.5.3. Zeta potential 55
2.5.4. Rheology, absolute viscosity and density 55
2.5.5. Pulsed-field-gradient spin-echo nuclear magnetic resonance (PGSE-NMR) 56
2.5.6. Small- angle neutron scattering (SANS) 57
2.5.7. Differential scanning calorimetry (DSC) 58
2.5.8. Particle sizing by dynamic laser scattering (DLS) 58
2.6. Methods: Incorporation of Model Compounds into Liquid Microemulsions and SELFs 59
2.6.1. Incorporation of sodium alendronate trihydrate and disodium pamidronate pentahydrate 59
2.6.1.1. Drug loading procedure 59
2.6.1.2. Differential Scanning Calorimetry (DSC) 59
2.6.2. Incorporation of acyline monoacetate 60
2.6.2.1. Drug loading procedure 60
2.6.2.2. Assay & Dissolution testing 60
2.6.2.3. Stability studies 60
2.6.2.4. Dispersion test and particle size measurements by dynamic light scattering (DLS) of the dispersed preclinical SEDDSs 60
2.6.2.5. Preclinical study 62
2.7. Methods: Characterisation of Solid Carriers 64
2.7.1. Scanning electron microscopy (SEM) 64
2.7.2. Particle sizing by laser diffraction (PSD) 64
2.7.3. Specific Surface Area (BET) and Porosity (t-plot) 64
2.7.4. Bulk and tapped density 65
2.7.5. True density 65
2.7.6. pH measurements 65
2.7.7. Solid state Fourier transform infrared spectroscopy (FTIR) 66
2.7.8. Thermal analysis (DSC & TGA) 66
2.7.9. Powder X-Ray Diffraction analysis (PXRD) 66
2.7.10. Adsorption Index (AI) 66

2.8. Methods: Adsorption of liquid SEDDS onto Solid Carriers 68
2.8.1. Adsorption procedure 68
2.8.2. Staining using Fat Red 7B dye 68
2.8.3. Powder rheometry (BFE, SE, CBD, SS) 68
2.8.4. Dispersion and desorption tests 69
2.8.5. Particle size by dynamic light scattering (DLS) 69
2.8.6. Transmittance 70
2.8.7. Assay of Fat Red 7B 70
2.8.8. Scanning electron microscopy (SEM) 70

RESULTS AND DISCUSSION

3. Chapter: Physicochemical Profiling Of Model Compounds

3.1. Introduction 71
3.2. Characterisation of sodium alendronate trihydrate and disodium pamidronate pentahydrate 72
3.2.1. Solid state Fourier transform infrared spectroscopy (FTIR) 72
3.2.2. Thermal analysis (Differential scanning calorimetry & Thermal gravimetric analysis) 73
3.2.3. Powder X-Ray Diffraction analysis (PXRD) 75
3.2.4. Particle sizing by laser diffraction (PSD) 75
3.2.5. Aqueous, pH dependent solubility 76
3.2.6. Solubility in the standard GIPET ® II formulation and propylene glycol 81
3.2.7. Calculation of cLogP and cLogD 84
3.3. Characterisation of acyline monoacetate 86
3.3.1. Solid state Fourier transform infrared spectroscopy (FTIR) 86
3.3.2. Differential scanning calorimetry (DSC) 87
3.3.3. Powder X-Ray Diffraction analysis (PXRD) 87
3.3.4. Isoelectric point (IEP) 88
3.3.5. Gelling behaviour in aqueous solutions 89
3.3.6. Solubility in the standard GIPET ® II formulation and propylene glycol 90
3.3.7. Calculation of cLogP and cLogD 91
3.4. Overall Conclusions 92

4. Chapter: Pseudoternary Phase Diagrams

4.1. Introduction 93

4.2. Composition of pseudoternary phase diagram 93

4.2.1. Oils 94

4.2.2. Low and high HLB value surfactants 95

4.2.3. Aqueous phase 97

4.3. Pseudoternary phase diagrams with the low combined HLB value 97

4.3.1. Impact of different cosurfactants on the phase behaviour 101

4.3.2. Impact of different oils on the phase behaviour 103

4.4. Pseudoternary phase diagrams with the high combined HLB value 104

4.4.1. Impact of different cosurfactants on the phase behaviour 108

4.4.2. Impact of different oils on the phase behaviour 110

4.5. Impact of additional cosolvents on the phase behaviour 111

4.6. Impact of temperature on the phase behaviour 114

4.7. *In vivo* considerations, impact of intestinal fluids on the phase behaviour 114

4.7.1. Phase behaviour in fasted stated (FaSSIF-V2) 115

4.7.2. Phase behaviour in fed state (FeSSIF-V2) 115

4.8. Overall Conclusions 116

5. Chapter: Characterisation of Microemulsions

5.1. Introduction 117

5.2. Composition of the model colloidal samples 117

5.3. Cryogenic transmission electron microscopy (cryo-TEM) and Freeze-fracture transmission electron microscopy (FF-TEM) 118

5.4. Conductivity 122

5.5. Zeta potential 125

5.6. Rheology and absolute viscosity 126

5.7. Pulsed-field-gradient spin-echo nuclear magnetic resonance (PGSE-NMR) 128

5.8. Small- angle neutron scattering (SANS) 132

5.9. Differential scanning calorimetry (DSC) 134

5.10. Particle sizing by dynamic laser scattering (DLS) 140

5.11. Overall Conclusions 144

6. Chapter: Incorporation of Model Compounds Into Liquid Microemulsions

6.1. Introduction 147

6.2. Incorporation of sodium alendronate trihydrate and disodium pamidronate pentahydrate into liquid microemulsions 147

6.3. Incorporation of acyline monoacetate in liquid non-aqueous microemulsions (SEDDSs) 150

6.3.1. Preclinical study 157

6.4. Overall Conclusions 166

7. Chapter: Characterisation of Solid Carriers

7.1. Introduction 171

7.2. Scanning electron microscopy (SEM) 172

7.3. Particle sizing by laser diffraction (PSD) 175

7.4. Specific Surface Area (BET) and Porosity 176

7.5. Bulk and tapped density 180

7.6. pH measurements 181

7.7. Solid state Fourier transform infrared spectroscopy (FTIR) 182

7.8. Thermal analysis (Differential scanning calorimetry & Thermal gravimetric analysis) 184

7.9. Powder X-Ray Diffraction analysis (PXRD) 186

7.10. Adsorption Index (AI) 187

7.11. Overall Conclusions 191

8. Chapter: Adsorption onto Solid Carriers

8.1. Introduction 193

8.2. Adsorption of liquid SEDDS onto solid carriers 194

8.2.1. Basic Flowability Energy (BFE) 196

8.2.2. Specific Energy (SE) 199

8.2.3. Conditioned Bulk Density (CBD) 201

8.2.4. Shear Stress (SS) 203

8.3. Desorption from the S-SEDDSs 208

8.3.1. Desorption by particle sizing and transmittance 208

8.3.2. Desorption of Fat Red 7B dye 214

8.3.3. SEM analysis of the desorbed S-SEDDS 216

8.4. Overall Conclusions 219

9. Chapter: General Discussion

9.1. Introduction 223

9.2. Physical characterisation of non-ionic microemulsions and self-emulsifying systems composed of derivatives of caprylic and capric acids. 223

9.3. Liquid microemulsions and self-emulsifying systems for use with BSC Class III compounds 235

9.4. Solid forms of self-emulsifying lipid formulations (SELFs) for use with BCS Class III compounds 241

9.5. Main findings 246

9.6. Future work 248

References 249

Appendices

Appendix to Chapter 3 271

Appendix to Chapter 4 275

Appendix to Chapter 5 276

Appendix to Chapter 6 281

Appendix to Chapter 7 285

Appendix to Chapter 8 287

ACKNOWLEDGMENTS

First and foremost, I would like to sincerely thank my supervisors Dr. Anne Marie Healy and Professor Owen I. Corrigan for their patience, support and advice during the course of my research and in the preparation of this thesis.

I am grateful to Enterprise Ireland and Merrion Pharmaceuticals for providing me with financial support and the opportunity to use laboratory equipment in Merrion's facility. Thank you to all my work colleagues in Merrion Pharmaceuticals for their continuous encouragement. In particular, my warmest thanks goes to Edel O'Toole, who helped me to get through the worst moments and her never ending support and friendship brought me to the end of this journey. Also, a big thank you to all in the Analytical Department in Merrion Pharmaceuticals for performing part of analytical testing and for their advice in relation to other analytical analyses performed by me.

I would like to thank to Dr Anna Stenstam (Colloidal Resource AB, Sweden), Dr Sarah Rogers (ISIS, Rutherford Appleton Laboratory, UK) and Dr Tony Brain (King's College London, Centre for Ultrastructural Imaging, UK) for performing PGSE-NMR, SANS and cryo-TEM/FF-TEM experiments on my samples and for their help and advice in the interpretation of the results.

A big thank you to Dr. Lidia Tajber for her excellent technical and practical advice. I am especially grateful that she always found time when I needed help to sort out malfunctioning equipment.

I would also like to thank to all staff in Centre for Microscopy and Analysis: Neal Leddy, Leona Mulvey, Clodagh Dooley, Heath Bagshaw and Colin Reid, for technical support on SEM and mass spectroscopy.

Thank you to Patrick Quinlan, Ray Keaveny, Brian O'Reilly, Conan Murphy, Joseph Reilly and Dr Thomas McCabe for their advice and technical support during my research.

A special thanks goes to Joanne Crean, Evelyn O'Shea, Vincent Curtin and Kieran Madigan for their proof reading of the final thesis. Thanks to all my fellow postgrads and postdocs with whom I have had a pleasure to work over the past five years: Dr. Krzysztof Paluch, Joanne Crean, Anita Umerska, Christine Grossjohann, Evelyn O'Shea, Maria Ines Amaro, Dr. Orla Ni Ógáin, Dr. Frederic Tewes, Dr. Shadeed Gad, Stefano Bianco, Vincent Curtis and Dr. Vincent Caron.

Finally, I would like to thank all of my family and Giorgio for their continuous encouragement and support. Thank you for believing in me.

PRESENTATIONS AND PUBLICATIONS ASSOCIATED WITH THE THESIS

Poster presentations:

Adamczyk, B.E., Healy, A.M., Corrigan, O.I., Effect of oil phase polarity on the phase behaviour of oil/ polysorbate 80: glyceryl monocaprylate (35:65)/ water systems. *AAPS Annual Meeting and Exposition, Atlanta, USA, 2008.*

Adamczyk, B.E., Healy, A.M., Corrigan, O.I., Characterization of Microemulsion Structures in the Pseudoternary Phase Diagram of caprylate/caprate triglycerides /water/ polysorbate 80: glyceryl monocaprylate. *Joint Schools of Pharmacy Meeting, Trinity College Dublin, Dublin, Ireland, 2009.*

ABBREVIATIONS AND SYMBOLS

Symbol	Description	Unit
AI	Adsoprtion Index	%
API(s)	Active pharmaceutical ingredient(s)	N/A
AUC	Area under the curve	Ng/ml h
BA	Bioavailability (oral)	N/A
BET	Brunauer Emmett Teller (isotherm- analysis)	N/A
BFE	Basic Flowability Energy	mJ
BJH	Barrett-Joyner-Halenda (pore- analysis)	N/A
CBD	Conditioned Bulk Density	g/ml
C_{max}	Maximum concentration of a drug post administration	ng/ml
CoA	Certificate of Analysis	N/A
Cryo-TEM	Cryogenic transmission electron microscopy	N/A
D	Diffusion coefficient	m^2s^{-1}, μ^2s^{-1}
DSC	Dynamic scanning calorimetry	N/A
DLS	Dynamic Laser Scattering	N/A
Fabs %	Absolute bioavailability	%
FaSSIF-V2	Fasted-State Simulated Intestinal Fluid – version 2	N/A
FeSSIF-V2	Fed-State Simulated Intestinal Fluid – version 2	N/A
FF-TEM	Freeze-fracture transmission electron microscopy	N/A
Frel %	Relative bioavailability	%
FR7B	Fat Red 7B	N/A
FTIR	Fourier transform –infrared spectroscopy	N/A
GC-MS	Gas chromatography mass spectrometry	N/A
GIPET®	Gastrointestinal Permeation Enhancement Technology®	N/A
GnRH	Gonadotropin-releasing hormone	N/A
HLB	Hydrophilic-lipophilic balance	N/A
IEP	Isoelectric point	N/A
LBDD	Lipid Based Drug Delivery	N/A
LC	Liquid crystals	N/A
cLogD	Calculated Distribution coefficient	N/A
cLogP	Calculated Partition coefficient	N/A
ME	Microemulsion	N/A
MEP	Microemulsion preconcentrate	N/A
MSDS	Material Safety Data Sheet	N/A
M_w	Molecular weight	Da
o/w	Oil-in-water	N/A
PD	Pharmacodynamics	N/A
PG	Propylene glycol	N/A
PGSE-NMR	Pulsed-field-gradient spin-echo nuclear magnetic resonance	N/A
PEP	Powder End Point (adsorption capacity)	%
pH	Minus log of hydrogen ion concentration	N/A
PIT	Phase inversion temperature	°C (degree Celsius), K (degree Kelvin)
PK	Pharmacokinetics	N/A
PSD	Particle size distribution (by laser diffraction)	N/A
PVDF	polyvinyl difluoride (filter)	N/A

Symbol	Description	Unit
PXRD	Powder X-ray diffraction	N/A
RH	Relative humidity	%
RSD	Relative standard deviation	%
R^2	Correlation coefficient	N/A
SANS	Small angle neutron scattering	N/A
SD	Standard deviation	N/A
SDLF	Self-dispersing lipid formulation	N/A
SE	Specific Energy	mJ/g
SEDDS	Self-emulsifying drug delivery system	N/A
SELF	Self-emulsifying lipid formulation	N/A
SEM	Scanning electron microscopy	N/A
SEM_e	Standard error of the mean	N/A
SLN	Solid Lipid Nanoparticles	N/A
SMEDDS	Self-microemulsifying drug delivery system	N/A
SNEDDS	Self-nanoemulsifying drug delivery system	N/A
SEOF	Self-emulsifying oil formulation	N/A
S-SEDDS	Solid Self-emulsifying Drug Delivery Systems	N/A
S-SELF	Solid self-dispersing lipid formulation	N/A
S-ME	Solid microemulsion	N/A
SS	Shear Stress	kPa
SSA_{BET}	Specific surface area by BET	m^2/g
SSA_p	Specific surface area by particle size distribution	m^2/g
S-SMEDDS	Solid Self-microemulsifying Drug Delivery Systems	N/A
S-SNEDDS	Solid self-nanoemulsifying drug delivery system	N/A
t-plot ESA	t-plot External Surface Area	m^2/g
t	Time	S (second), min (minute) ,
T	Temperature	˚C (degree Celsius), K (degree Kelvin)
TGA	Thermogravimetric analysis	N/A
T_{max}	Time after administration of a drug when the maximum plasma concentration is reached	h
$T_{1/2}$	Elimination half-life	h
UV	Ultra violet	N/A
V	Volume	ml (millilitre)
W	Weight	g (gram), mg (milligram), µg (microgram)
w/o	Water-in-oil	N/A
w/w	Weight per weight	N/A
~	Approximately	N/A
δ_S	Solubility parameter	$(cal/cc)^{\wedge 0.5}$
®	Registered mark	N/A
η	Viscosity	mPa s
™	Trademark	N/A
Φ_c	Percolation threshold	N/A
Φ_e	Phase transition (microemulsion into emulsion)	N/A
γ	Interfacial tension	mN/m
Φ	Droplet volume fraction	N/A
%AL	Percentage of Added Liquid	%
λ	Wavelength	nm

ORIGIN AND SCOPE

Lipids can have significant and beneficial effects on the absorption of co-administered lipophilic and hydrophilic drugs (Constantinides, 1995; Constantinides et al., 1995; Constantinides et al., 1996; Porter et al., 2007; Pouton, 2006). Over the last twenty years, a substantial effort has been undertaken to develop microemulsions and/or self-emulsifying systems (containing lipids) that could improve oral absorption of lipophilic and/or hydrophilic compounds belonging to the BCS Class II – IV according to the classification system introduced by Amidon et al. (1995). A number of lipophilic drugs incorporated into lipid-based formulations have already reached the market. Invirase containing saquinavir mesylate (BCS class II) in a hard gelatine capsule was launched on the market in 1995. As its bioavailability was highly variable and as low as 4%, in 1997 Fortovase, a new formulation of the free base of the drug was introduced in a lipid formulation consisting of medium-chain monoglycerides and diglycerides which displayed three times higher bioavailability than Invirase in humans (Chakraborty et al., 2009). Neoral is a commercially available, improved version of an encapsulated microemulsifying system with cyclosporine A (BCS class II). The previous product, Sandimune, formulated as a self-emulsifying system showed erratic oral bioavailability of the drug in fasted and fed state (Strickley, 2004). The improved version is less subject to the effect of food and therefore offers flexibility with regards to dietary schedule of patients and their convenience (Chakraborty et al., 2009). A few studies focused on the development of lipid formulations suitable for BCS class IV e.g. amphotericin B formulated in a mono/diglyceride phospholipid (distearoylphosphatidyl-ethanolamine) -based oral formulation was reported to significantly improve intestinal absorption in rats (Wasan et al., 2009), however there are no commercially available examples of these formulations. Also, many BCS class III organic compounds as well as proteins and peptides, do not appear to be available on the market for oral administration in the form of microemulsions and/or self-emulsifying systems.

Merrion Pharmaceuticals is a product development company, engaged in the development of oral forms (tablets/capsules) of drugs that have poor oral absorption (permeability) and are generally given by injection. Gastrointestinal Permeation Enhancement Technology® (GIPET®) is a proprietary technology owned by Merrion Pharmaceuticals. GIPET® technology can be subdivided into two main platforms which are GIPET® I and GIPET® II. GIPET® I platform is based on medium-chain fatty acids and salts thereof (e.g., C_{10}), typically formulated as enteric-coated tablets and it was demonstrated to enhance oral bioavailability of BCS Class III compounds (such as alendronate, zoledronic acid and two types of low molecular weight heparin with molecular weight 4400 and 6010 Da respectively) in phase I clinical trials. GIPET® II technology is based on glycerides and propylene glycol esters of C_8 and C_{10} (mainly) formulated as liquid microemulsion or liquid self-emulsifying system and developed further as enteric-coated soft gels or hard capsules. Oral bioavailability of desmopressin and dalteparin sodium was significantly enhanced by GIPET® II absorption promotors in phase I clinical trials (Leonard et al., 2006).

Preclinical and clinical studies to date of GIPET® have focused on delivery of BCS class III compounds, since there are still many parenteral formulations where patients' compliance would be significantly improved if the oral equivalents could be offered.

GIPET® II technology is currently owned by Merrion Pharmaceuticals but it developed by another company. Main formulation concepts of this technology are presented in five patents. The main scope of the patents filed between 1995 and 1997 (US5444041A1, US5633226A1, US5646109A1, US5688761A1) refers to the development of water-in-oil (w/o) microemulsions that readily convert to an oil-in-water (o/w) emulsions by the addition of aqueous fluid whereby any water-soluble biologically active material in the aqueous phase is released for absorption by the body. The definition of a microemulsion (in terms of the composition) according to these patents is 'the microemulsions of this invention are self-emulsifying stable dispersions of oil and water, stabilized by interfacial films of surface-active molecules (Owen et al., 1995, Owen & Yiv, 1997, Owen & Yiv, 1997, Owen et al., 1997). The most recent patent (US5707648A1) describes 'stable transparent multi-component composition useful for the delivery of water-soluble active agents to animals are specially formulated to be compatible with capsules such as gelatine and starch capsules. The aqueous phase of the compositions contains a substantial amount of polyethylene glycol and can optionally contain a plasticizer' (Yiv, 1998).

The patents (US5444041A1, US5633226A1, US5646109A1, US5688761A1) contain a wide range of claims related to the combined HLB value such as 'from about 1 to 70 volume percent of a surfactant or mixture of surfactants, wherein the surfactant or surfactant mixture has a hydrophilic-lipophilic balance value from 7 to 14'. As the oil phase mainly C_{15}-C_{40} diesters of propylene glycol and C_9-C_{45} triglycerides are used although the range of potential surfactants/mixture of surfactants is very extensive including: ethoxylated castor oil; C_{5-29} mono-glycerides and ethoxylated derivatives thereof; C_{15-60} diglycerides and polyoxyethylene derivatives thereof having 1 to 90 POE groups; C_{10-40} esters of long chain fatty acids; C_{10-40} alcohols; C_{8-96} ethoxylated fatty esters; C_{14-130} sucrose fatty esters; and C_{20-130} sorbitol and sorbitan monoesters, diesters, and triesters, and polyoxyethylene (POE) derivatives thereof having 1 to 90 POE groups. The water in the aqueous phase can be partially or fully replaced by the incorporation of another polar, biologically compatible solvent such as polyhydric alcohols having at least 2 hydroxyl groups, glycerol, propylene glycol, and mixtures thereof (Owen et al., 1995; Owen et al., 1997). The claims in the recent patent (US5707648A1) describe 'a stable, transparent drug delivery composition suitable for storage and administration of biologically active materials, comprising a delivery composition consisting of a) from about 1 to about 80 weight percent of a pharmaceutically acceptable oil phase; b) from about 3 to about 98 weight percent surfactant (a mixture of low and high HLB value surfactants wherein the low HLB value surfactant comprises C_{9-13} monoglycerides); c) from about 2 to about 60 weight percent polyethylene glycol; d) from about 0.5 to about 15 weight percent water (Yiv, 1998).

Clearly, the patents provide an almost inexhaustive list of combinations of the surfactants and therefore potential GIPET® II formulations. In practice, little is known about which materials and what combinations should be ideally used to achieve physically and chemically stable formulations that would demonstrate improved oral bioavailability of BCS Class III drugs and be compatible with capsule shells at the same time. The systems described in the patents that contain water can be considered as microemulsions according to the definition given by Danielsson & Lindman (1981) (Chapter 1, section 1.2.3). The systems, where water has been fully replaced by polar solvents (cosolvents), could be termed as self-emulsifying lipid formulations (SELFs) and further divided into self-emulsifying drug delivery systems (SEDDSs) and self-microemulsifying drug delivery systems (SMEDDSs) depending on the behaviour upon dilution (Lawrence & Rees, 2000; Pouton & Porter, 2008). Using the Lipid Formulation Classification Systems (LFCS) developed by Pouton (2000, 2006) these systems could be classified mainly as type II and III LFCS (Chapter 1, section 1.2). The type II would be formed if a single water insoluble surfactant with HLB value below 12 (e.g. polyoxyethylene sorbitol hexaoleate, HLB = 11.4) was employed. Type III encompasses SEDDSs and SMEDDSs formulated with a mix of surfactants comprising water insoluble and water-soluble surfactants (HLB > 12) and possibly some cosolvents (Pouton, 2006).

The first aim of the present work was to explore properties of microemulsions and self-emulsifying systems (type III according to Pouton's system) that were composed of glycerides and propylene glycol esters of caprylic/capric acids and a water-soluble surfactant (HLB = 15). The systems were further examined to evaluate formulation challenges and limitations in relation to the incorporation of BCS class III drugs (the second main aim). These aims were translated into the following objectives of the work:

- To examine the impact of the combined HLB value, the type of the low HLB value surfactant and the type of oil phase on formation of microemulsion and self-emulsifying formulations and their dilution behaviour.
- To analyse physical properties of model microemulsions to gain an understanding of drug distribution in formulations for encapsulation and the possible fate of the drug upon dilution *in vivo*.
- To examine the incorporation of hydrophilic compounds (using model drug compounds) into selected liquid microemulsions and/or self-emulsifying systems and investigate further their chemical and physical stability in the final encapsulated dosage forms.
- To examine the effect of developed microemulsions and/or self-emulsifying systems on the oral bioavailability of the selected model compounds.

Chapter 1

Lipid – based Drug Delivery Systems and Their Properties

1.1. Introduction

Oral drug delivery is continuously being developed in new ways aiming to improve poor drug solubility and/or oral absorption, eliminate high fluctuations in the drug plasma level and reduce the effect of food on the drug plasma level, all of which are still significant drawbacks to achieve efficacious, safe delivery of many drugs. Since the last decade, oral drug delivery has taken a new dimension with the increasing application of lipid materials as carriers of various drugs. Lipids have been loosely defined as biological substances that are generally hydrophobic in nature and in many cases soluble in organic solvents which covers a broad range of molecules such as fatty acids, phospholipids, sterols, sphingolipids, terpenes (Fahy et al., 2005). As many lipid materials are classified as GRAS (Generally Regarded As Safe), they present a reduced toxicological risk when used in oral formulations (Pouton, 2000) such as simple solutions, microemulsions (ME), emulsions, self-emulsifying systems SEDDSs), self-microemulsifying system (SMEDDSs), liposomes and solid lipid nanoparticles (Bagwe et al., 2001). Self-emulsifying lipid formulations (SELFs) and microemulsions have been investigated in oral delivery of lipophilic and hydrophilic molecules including peptides and proteins. The primary mechanisms by which lipid-based drug formulations enhance drug solubilisation within the GI tract are by presenting the drug in a solubilised form (thereby avoiding solid-state limitations) and by inducing changes to the GI environment such that solute–solvent interactions and drug solubility are enhanced (Porter et al., 2007). Other factors which directly improve intestinal drug absorption include: an increase in membrane fluidity facilitating transcellular absorption, opening of the tight junction (TJ) to allow paracellular transport (mainly relevant for ionized drugs or hydrophilic macromolecules), inhibition of P-gp and/or CYP450 to increase intracellular concentration and residence time, and stimulation of lipoprotein/chylomicron production (O'Driscoll, 2002). Oral delivery of peptide and protein-like macromolecules is challenging due to a number of reasons such as unfavourable physicochemical properties, large molecular size, susceptibility to enzymatic degradation, short plasma half-life, ion permeability, immunogenicity, the tendency to undergo aggregation, adsorption, and denaturation. These factors are frequently magnified by several physiological variables (gastric emptying, transit time, the presence of food, variation in pH across the GI tract, hydrolysis of peptides at several sites: luminally, at the brush border and intracellularly) which consequentially causes the absolute oral bioavailability levels of most peptides and proteins to be less than 1% (Mahato et al., 2003; Sarciaux et al., 1995). Several water-in-oil microemulsions have been found to be useful for delivery of proteinaceous materials such as epidermal growth factor, RGD peptide, calcein, GMDP by decreasing degradation in the intestinal tract (Celebi et al., 2002, Constantinides et al., 1995, Lyons et al., 2000).

1.2. Solutions, self-emulsifying systems and microemulsions for oral delivery

Simple lipid-based solutions and self-emulsifying lipid formulations (SELFs) are frequently employed to deliver lipophilic molecules, and for this reason dilution behaviour together with digestion patterns are closely examined for these formulations to prevent any drug precipitation upon release *in vivo*. The digestion process is known to significantly alter the emulsifying properties of the original formulation. The enzymatic hydrolysis by pancreatic lipase and co-lipase reduces triglycerides into the more polar products 2-monoglycerides and fatty acids (Embleton & Pouton, 1997). Digestion of medium chain glycerides is known to alter their solubilising capacity which could lead to precipitation of highly lipophilic drugs, and therefore their reduced oral absorption. Long-chain glycerides maintain their solubilising capacity even when the digestion process is advanced and drug solubilisation is often possible even at low concentrations of long-chain triglycerides (Porter et al., 2007). The colloidal species produced, in the form of micelles, mixed micelles, vesicles and free fatty acids as a result of lipid digestion, are taken up by passive diffusion or facilitated diffusion or active transport through the enterocyte membrane. It is worth mentioning that medium-chain and long-chain lipids, have a different effect on intestinal lymphatic transport (Porter & Charman, 2001). Medium-chain lipids are poor stimulators of intestinal lymphatic transport, while long chain lipids (fatty acids with chain lengths greater than 14) are primarily transported into intestinal lymph and were reported to enhance 'lymphatic uptake' of halofantrine, cyclosporine, naftifine, probucol and vitamin D (Porter et al., 2007; Porter & Charman, 1997).

Due to the variety in lipid-based formulations, the Lipid Formulation Classification System (LFCS) was introduced as a working model in 2000 (Pouton) to aid the comparison of published data from various laboratories. An extra 'type' of formulation was added in 2006 (Pouton) due to the growing complexity of lipid formulations. Although, Pouton has never stated explicitly that the LFCS applies to formulations designed for poorly water soluble compounds, the formulations are categorised based on their ability to ensure that a drug remains dissolved throughout its transit within the gastro-intestinal tract (Pouton, 2000). Therefore, the main two characteristic (classifying) features of these formulations are their dispersion behaviour (prior to digestion) and solubilising behaviour (post digestion). The characteristics of each formulation type according to the 'newer version' of the LFCS (Pouton, 2006) are summarised in Table 1.1.

With regard to hydrophilic drugs, not every formulation type according to Pouton's classification systems could be utilised because lipophilicity of certain vehicles is likely to prevent incorporation of a required drug load. In this review, suitability of each LFCS type for hydrophilic compounds (including peptides and proteins) will be discussed.

Table 1.1. The Lipid Formulation Classification System displaying typical features and compositions of lipid formulation types of proposed by Pouton (2000, 2006).

Excipients in formulations	**Increasing hydrophilic content ⟶**				
	Type I	**Type II**	**Type IIIA**	**Type IIIB**	**Type IV**
	Content of formulation (%, w/w)				
Triglycerides or mixed mono and diglycerides	**100**	**40 - 80**	**40 - 80**	**< 20**	-
Water-insoluble surfactants (HLB < 12)	-	**20 - 60**	-	-	-
Water-soluble surfactants (HLB value > 12)	-	-	**20 - 40**	**20 - 50**	**30 – 80**
Oil-free, hydrophilic cosolvents (e.g. PEG, propylene glycol, transcutol)	-	-	**0 - 40**	**20 -50**	**0 - 50**
Properties	**Type I**	**Type II**	**Type IIIA**	**Type IIIB**	**Type IV**
Typical particle size of dispersion	**Crude emulsion**	**250 nm - 2μm**	**100 – 250 nm**	**50 – 100 nm**	**micellar solution**
Significance of aqueous dilution	Non dispersing (very crude emulsion)	SEDDS is unlikely to loose solvent capacity on dispersion (coarse emulsion)	SEDDSs & SMEDDSs forms clear or almost clear dispersions - possible loss of solvent capacity upon dispersion	SMEDDSs forms clear or almost clear dispersions - possible loss of solvent capacity upon dispersion	Potential loss of solvent capacity
Significance of digestibility	Crucial condition (drug released upon digestion)	Not crucial but likely to occur	Not crucial but may be inhibited (less easily digested)	Not required and not likely to occur	Not required and not likely to occur (may not be digestible)

1.2.1. Simple and micellar solutions

The simplest lipid products, LFCS type I, are those in which the drug is dissolved in a digestible oil, usually a vegetable oil such as medium chain triglycerides. The low solvent capacity of triglycerides often prevents successful formulation of many drugs in this simple oil, but it may be a realistic option for potent drugs or for compounds with LogP > 4. Oil has been the standard way of administering oil-soluble vitamins (A and D) for many years (Pouton, 2000). Despite poor dilution behaviour, bioavailability of drugs from oil solutions can be still good since triglycerides are rapidly digested. The bioavailability and plasma profile of lipophilic 5α-reductase inhibitor from an oil solution were equivalent to those achieved using a self-emulsifying system (Loper et al., 1996). Pouton (2000, 2006) classified triglycerides and/or mixed glycerides as LFCS 'type I' (Table 1.1). However, monoglycerides are non-digestible and polar enough to be classified as low HLB value surfactants. Therefore, the compositions comprising oils with a substantial amount of monoglycerides are more likely to belong to LFCS type II what has been recently pointed out by

Müllertz, et al. (2010). A number of poorly water soluble drugs (BCS class II) are available on the market as capsules where a drug is simply dissolved in a single oil (Table 1.2).

Table 1.2 Encapsulated forms of one-phase lipid-based solutions available on the market (Rxlist, Strickley, 2004; Augustijns & Brewster, 2007).

Generic name	Brand name (company)	Dosage form	Capsule filling composition
Type I as per the LFCS			
Progesterone	Prometrium (Abbot)	capsule	Peanut oil
Dronabinol	Marinol (Unimed Pharmaceuticals,	softgel	Sesame oil
Valproic acid	Depakene (Abott)	softgel	Corn oil
Calcitrol	Rocaltrol (Roche)	softgel	Fractionated triglyceride of coconut oil
Paricalcitol	Zemplar (Abbott)	softgel	Fractionated medium-chain triglycerides of coconut oil or palm kernel oil

The LFCS type I formulations are unlikely to become useful with hydrophilic compounds or proteinaceous materials, as the highly lipophilic composition will not dissolve a sufficient amount of drug. The LFCS type I formulations can be considered as the most hydrophobic formulations, the opposite side of the LFCS are the most hydrophilic formulations, type IV. These formulations are predominantly composed of water-soluble surfactants and cosolvents. A water-soluble surfactant offers improved solvent capacity upon dilution (to keep the drug dissolved) while addition of cosolvents facilitates dispersion and reduces variability and irritancy caused by high local concentration of the surfactant (Pouton, 2006). The LFCS type IV formulations can be good vehicles for hydrophobic; however, they may not be well tolerated when taken on a chronic basis (Pouton, 2006). Two examples of commercially available LFCS type IV formulations are presented in Table 1.3.

Table 1.3 Encapsulated forms of hydrophilic solutions available in the market (Rxlist, Strickley, 2004; Augustijns & Brewster, 2007).

Generic name	Brand name (company)	Dosage form	Capsule filling composition
Type IV as per the LFCS			
Amprenavir	Agenerase (GlaxoSmithKline)	softgel	d-alpha tocopheryl polyethylene glycol 1000 succinate, PEG 400, propylene glycol
Bexarotene	Targretin (Ligand)	softgel	Polysorbate 20, PEG 400

The LFCS type IV formulations could be formulated with hydrophilic organic compounds, as the highly hydrophilic composition should facilitate the incorporation of a high drug load. The use of these formulations with peptides and proteins, which are degraded in the intestinal environment, might be limited as the LFCS type IV systems form instantly a clear micellar solution upon

dispersion. According to Lyons et al. (2000) and Constantinides et al. (1994), a water-in-oil microemulsion protects 'entrapped protein molecules' in the microemulsion core until the phase conversion occurs and the peptides is released and can be absorbed. The LFCS type IV formulations rapidly form micelles upon dispersion and they lack the oil phase, therefore may offer limited protection against enzymatic degradation.

1.2.2. Self-emulsifying systems

Self-emulsifying systems are not microemulsions according to the definition by Danielsson & Lindman (1981), although they may be considered as closely related systems. A basic self-emulsifying system, also called a preconcentrate, typically comprises a mixture of surfactants, oil and a drug (Lawrence & Rees, 2000). According to Hauss (2007), SEDDSs and SMEDDSs are physically stable isotropic mixtures of oil, surfactant, cosurfactants and a solubilised drug. According to Pouton (1997), self-emulsifying drug delivery systems (SEDDS) are ideally isotropic mixtures of oils and surfactants (and cosolvents in some instances), which emulsify under conditions of gentle agitation, similar to those encountered in the gastro-intestinal tract. With respect to the difference between self-emulsifying drug delivery systems (SEDDSs) and self-microemulsifying drug delivery systems (SMEDDSs), it seems that the distinction was somewhat arbitrary in scientific terms until recently. Pouton & Porter (2008) described SMEDDSs as formulations, which disperse to form transparent colloidal systems (possibly a microemulsion, however usually it is unknown if the formed system is truly a thermodynamically stable microemulsion), with a smaller the particle size compared to dispersed SEDDSs. The LFCS type II formulations considered as SEDDSs by Pouton (2006) typically show a particle size below 250 nm, what implies that SMEDDSs would form droplets smaller than 250 nm upon dispersion. This interpretation is in good agreement with the more recent publications where the SEDDS formulations were expected to produce an opaque dispersion with a particle size above 200 nm (Müllertz, et al., 2010; Kumar et al., 2010). The SMEDDS was expected to disperse into smaller droplets with a particle size below 200 nm and therefore form an optically clear or slightly opalescent dispersion, more consistent with the presence of a microemulsion (Müllertz, et al., 2010; Kumar et al., 2010). Self-nanoemulsifying drug delivery system (SNEDD) is a recent term construing the globule size range less than 100 nm (Kohli et al., 2010). In the published scientific literature, sometimes the term 'SEDDSs' is used describe all self-emulsifying lipid systems irrespective of their dilution characteristics. In the current work, the term 'self-emulsifying lipid formulations (SELFs)' will be used to describe all self-emulsifying systems (SEDDSs, SMEDDS, SNEDDs, etc.) as a group while the terms SEDDSs and SMEDDS will be used to differentiate between systems that form different dispersions (SMEDDSs < 200nm, SEDDSs > 200nm) upon dilution as per the definitions given above (Müllertz, et al., 2010; Kumar et al., 2010).

SEDDSs and SMEDDSs are classified as LFCS type II and III formulations (Pouton, 2000; Pouton; 2006). In the LFCS type II, the inclusion of a water-insoluble surfactant (HLB < 12) may improve the solvent capacity of the formulation, but is mainly used to improve emulsification behaviour. The LFCS type III formulations, in particular type IIIB, contain a small amount of the oil phase, and hydrophilic components such as water-soluble surfactants and polar solvents make a substantial fraction in these systems. Commercial examples of SELFs are shown in Table 1.4.

Table 1.4. Encapsulated forms of lipid-based SEDDSs/SMEDDSs with polar solvents available on the market (Rxlist, Strickley, 2004; Augustijns & Brewster, 2007).

Generic name	Brand name (company)	Dosage form	Capsule filling composition
Type II and III as per the LFCS			
Tipranavir	Aptivus	softgel	Ethanol, propylene glycol, Cremophor EL, medium chain monoglycerides
Clofaximine	Lamprene	softgel	Rapeseed oil, hydrogenated soybean, partially hydrogenated plant oil, propylene glycol
Cyclosporin A	Neoral	softgels	Ethanol, propylene glycol, Cremophor RH 40, corn oil mono-di-triglycerides, α-tocopherol
Cyclosporin A	Gengraf (Abbott)	hard gelatine capsule	Ethanol, propylene glycol, polyethylene glycol, Cremophor EL, sorbitan monooleate, Tween 80
Lopinavir	Kaletra (Abbot)	softgel	Oleic acid/Cremophor EL/propylene glycol
Dutasteride	Avodart (GSK)	softgel	Mixture of mono-diglycerides of capric/caprilic acid
Ritonavir	Norvir (Abbot)	softgel	Oleic acid/Cremophor EL/propylene glycol
Saquinavir	Fortovase (Roche)	softgel	Mixture of medium chain mono-diglycerides

LFCS type III formulations have been widely applied to BCS class II compounds, mainly due to the solubility and dissolution enhancement observed *in vivo* which produces more reproducible bioavailability of these drugs *in vivo*. Both LFCS types II and III could be potentially used with hydrophilic compounds. Based on the composition, the LFCS type III appears to be more suitable for BCS class III drugs and proteinaceous materials due to a higher content of polar solvents, which should facilitate a higher drug load. Talking into consideration the dispersion behaviour, both formulation types: LFCS II and III should be equally suitable for hydrophilic organic compounds (the drug is water soluble and does not require a stable emulsion or a microemulsion to dissolve and remain solubilised). In this case, the 'bio-enhancing effect' of lipid formulations is limited to their effect on permeability. In case of peptides and proteins, which become inactivated by digestive enzymes in the physiological conditions, a self-emulsifying lipid systems LFCS type II and III could also improve the stability of these molecules during absorption process.

1.2.3. Microemulsions

Microemulsions are clear, thermodynamically stable, isotropic mixtures of oil, water and surfactant frequently in combination with a cosurfactant (Danielsson & Lindman, 1981; Kumar & Mittal, 1999; Lawrence & Rees, 2000). The term "microemulsion" was first used by Schulman et al. (1959) to describe a multiphase system consisting of water, oil, surfactant and alcohol, which formed a transparent solution. In the light of this definition, microemulsions are beyond the LFCS developed by Pouton (2000, 2006) since the formulations described in this system are water-free. Nevertheless, in terms of the composition, microemulsions and self-emulsifying systems LFCS type II and III are closely related systems, which would show similar dispersion behaviour upon dilution. The LFCS type I and IV formulations are not similar to microemulsions, as the former one does not include any surfactants and the latter one does not contain any oil phase. Microemulsions that would have a similar composition to the LFCS type II, are likely have a very low capacity to incorporate water before a phase transition occurs due to the lack of hydrophilic surfactant. Microemulsions similar to LFCS type III formulations appear to be the most suitable for incorporation of hydrophilic compounds as the amount of 'hydrophilic phase' essential to dissolve a required dose of a drug can be maximised by combining water with other polar cosolvents. Microemulsions where water is fully substituted with polar solvents are in fact self-emulsifying systems, also called non-aqueous microemulsions or microemulsion preconcentrates (Strickley, 2004; Hauss, 2007). According to Augustijns & Brewster (2007) and Strickley (2004), all currently available commercial products are non-aqueous microemulsions (Table 1.4).

Microemulsions are formed spontaneously and remain physically stable infinitely. They are characterised by ultra low interfacial tension and a dynamic microstructure where the interface is continuously and spontaneously fluctuating. Low viscosity and Newtonian behaviour is typically observed for these systems (Talegaonkar et al., 2008). The reported particle size of microemulsions differs depending on the literature source and values of 15 – 150 nm (Friberg, 1990), 20- 200 nm (Talegaonkar et al., 2008) and 10- 100 nm (Bagwe et al., 2001) were reported. Lack of consistency regarding the particle size characteristic for microemulsions, could be due to the fact that only certain microstructures of the microemulsions exist as perfect, isolated droplets. The two main types of microemulsions, oil-in water or water-in-oil, can be visualised as droplets of one phase in another continuous phase. However the bicontinuous structure (or so-called sponge phase) is a quite different structure, where both water and oil are continuous phases and the typical model of 'droplets suspended in the continuous phase' does not apply. Typical lipid excipients used to formulate microemulsions and the mechanism of microemulsion formation, are discussed in detail in sections 1.3 and 1.4. A novel type of microemulsions, which are solid or semi-solid, is further presented in section 1.5.

1.3. Composition of microemulsions and self-emulsifying lipid systems

Many studies on the phase behaviour have been carried out using oil and surfactants (such as hydrocarbon oils: heptane or dodecane, or cyclohexane) that are not approved for use in pharmaceuticals (Lawrence & Rees, 2000). For the purpose of the work carried out in the course of this thesis, this paragraph will briefly review only pharmaceutically acceptable materials.

1.3.1. Oil phase

Definition of the oil phase in the lipid-based formulations appears to be rather vague. In terms of chemical composition natural triglycerides are the most frequently used. A number of natural product oils, derived primarily from plants have been very frequently used in microemulsions and other self-emulsifying lipid systems. Strickley (2004) published the following oils as solubilising excipients used in commercially available oral and injectable formulations: beeswax, oleic acid, soy fatty acids, vitamin E, corn oil, medium chain triglycerides derived from coconut oil or palm see oil, castor oil, corn oil, cottonseed oil, olive oil, peanut oil, peppermint oil, safflower oil, sesame oil, soybean oil, hydrogenated soya bean oil. Synthetic materials such as diesters of propylene glycol and caprylic/capric acids (Captex 200) are also commonly used as an oil phase (Gursoy & Benita, 2004; Kommuru et al., 2001). Pouton (2000, 2006) referred to 'oils' as triglycerides or mixed mono and diglycerides what poses a question about hydrophobicity of the oil phase. Materials such as Capmul MCM, or Imwitor 308 are mono and diglycerides of caprylic/capric acids, however due to the amphipilic character are considered as low HLB value surfactants by many researchers (Gursoy & Benita, 2004; Constantinides et al., 1995; Constantinides et al., 1994). Propylene glycol monocaprylate (Capmul PG-8, Capryol 90), a relatively hydrophilic material (HLB ~ 6, Pouton, 2007), have been used as oil in the work of Li et al. (2005) and Kang et al. (2004). On the other hand, use of glyceryl monolinoleate (Maisine 35-1 with HLB ~ 4, Pouton, 2007) as a surfactant was reported by Gursoy and Benita (2004). Lack of precise definition with respect to 'the nature of oil' in many SELFs may be caused by practical reason, i.e. how oil is selected for a SELF. The main criterion for selecting the oil phase when formulating SELFs especially with lipophilic drugs, is that the drug should have high solubility in this material in order to minimise the volume of the lipid formulation required to deliver the therapeutic dose. This suggests that choice of 'more or less hydrophobic oil' is conveniently driven by the solubility of a drug. In the work undertaken, lipid materials with HLB value below 6 and liquid at room temperature were considered as oils. The choice of oil is not only important to maximise the drug load, but it has a critical impact on the dispersion behaviour. The oil component influences curvature of microemulsion interface by its ability to penetrate and hence swell the tail group region of the surfactant monolayer. Long-chain triglycerides (e.g. with 18 carbons) are difficult to solubilise given their high molecular weight, which limits their flexibility at the interface and restricts film penetration. A strong interaction, frequently produced by oil molecules

with a small molecular weight (volume), leads to a large penetration of oil molecules into the surfactant chain layer (salvation), thus increasing curvature of the interface (Kumar & Mittal, 1999, Leung & Shah, 1987).

1.3.2. Surfactants

Conventional surfactant molecules comprise a polar head group region and a non polar tail region. When surfactants are incorporated into immiscible mixtures of oil and water, the surfactant molecules will locate at the oil/water interface which is thermodynamically very favourable.

The use of cationic and anionic surfactants (such as sodium bis-2-ethylhexylsulphosuccinate /AOT, hexadecyltrimethylammonium bromide/CTAB, sodium lauryl sulphate/SLS) in oral formulations is limited mostly due to their toxicity. On the other hand, ionic, zwitteronic surfactants such as phospholipids (major components of soybean and egg lecithin) are very frequently used due to their excellent biocompatibility (Lawrence & Rees, 2000). Non-ionic surfactants are often preferred for pharmaceutical applications since they are less toxic and less affected by pH and ionic strength changes of other components of the formulation. In addition, since emulsification process is dependent on the critical micelle concentration (CMC), non-ionic surfactant are superior over ionic since they have typically very low CMC values in water and therefore are very effective emulsifiers and solubilisers upon dilution *in vivo* (Kumar & Mittal, 1999). Strickley (2004) published a list of non-ionic surfactants suitable for oral and parenteral administration which includes: Cremophor EL, Cremophor RH 40, Cremophor RH 60, Polysorbate 20, Polysorbate 80, d-α-tocopheryl polyethylene glycol 1000 succinate (TPGS), Span 20, Solutol HS-15, Span 20, lauroyl polyoxylglycerides (Gelucire 44/14), stearoyl polyoxylglycerides (Gelucire 50/13), PEG 300 caprylic/capric glycerides (Softigen 767), PEG 400 caprylic/capric glycerides (Labrasol), PEG 300 oleic glycerides (Labrafil M-1944CS), PEG 300 linoleic glycerides (Labrafil M-2125CS), polyoxyl 8 stearate, polyoxyl 40 stearate.

1.3.3. Cosurfactants

In most cases, single-chain surfactants alone are unable to reduce the oil-in-water-interfacial tension sufficiently to enable a microemulsion to form. The presence of cosurfactants allows the interfacial film sufficient flexibility to take up different curvatures required to form microemulsion over a wide range of composition. If a single surfactant film is desired, the lipophilic chains of the surfactant should be sufficiently short, or contain fluidising groups (e.g. unsaturated bonds). Short to medium chain length alcohols (C_3-C_8) are commonly added as cosolvents, which further reduce the interfacial tension and increase the fluidity of the interface (Kumar & Mittal, 1999; Leung & Shah, 1987). The terms 'cosurfactant' and 'cosolvents' seem to be interchangeably used in the work published by many researchers, however for consistency and clarity, the distinction will be made in the current work. A material with surface- active properties, typically characterised by a low HLB value between 4 and 11 and semi-solid/solid at room

temperature will be considered as a cosurfactant. Unlike surfactants, the cosurfactant may not be capable of forming self-associated structures like micelles on its own. The quantity of cosurfactant in a system is usually less than that of the surfactant (Narang et al., 2007.) As cosurfactants, the following materials are commonly used: medium chain length alcohols, Span 20, Span 80, glyceryl caprylate/caprate (Campul MCM), glyceryl trioleate, decaglycerol monooleate, mono- and diglycerides of medium fatty chain acids (Imwitor ® 972, Imwitor ® 988), glyceryl monooleate, glyceryl monostearate, (Pouton, 2007; Narang et al., 2007; Strickley, 2004).

In the current, the term of cosolvents will apply to those materials, which could increase the effectiveness of the main surfactant, but are not amphiphilic in their own right.

1.3.4. Hydrophilic phase

Based on the definitions dicussed earlier, the hydrophilic phase may comprise polar solvents when formulating SELFs and polar solvents, water and other aqueous media when microemulsions are considered. The cosolvents are included to increase the solvent capacity of the formulation for drugs (with intermediate log P ($2 < \log P < 4$) which dissolve in cosolvents, as well as to aid dispersion of systems which contain a high proportion of water-soluble surfactants (Pouton, 2000). PEGs are very frequently used as cosolvents. By partitioning between aqueous and oil phases, PEGs can modify the solvent properties of these phases, i.e., making an oil phase relatively more hydrophilic or an aqueous phase relatively more hydrophobic. PEGs can prevent formation of rigid structures such as gels, liquid crystals, precipitates, etc., and to lower the viscosity of the system (Ke et al., 2005). Other cosolvents like, diethylene glycol monoethyl ether (Transcutol), propylene glycol, polyoxyethylene, propylene carbonate, tetrahydrofurfuryl alcohol polyethylene glycol ether (Glycofurol), glycerine, N-methyl-2 pyrrolidone, Poloxamer 407, etc., are frequently employed in encapsulated formulations for the same reasons. (Pouton, 2007; Strickley, 2004; Narang et al., 2007). The amount of water or another aqueous phase in microemulsion formulations for encapsulation is limited, otherwise water, as a potent plasticiser, will compromise the stability of the capsule shell. In general, the water content up to 5– 6% (w/w) was found as the maximum level compatible with hard gelatine capsules, while any higher quantity used would lead to capsule softening (Cole, 1999). The water level for soft-gelatine capsules is also limited depending on the viscosity of final formulation. If a drug molecule for incorporation into a microemulsion is ionisable, then pH adjustment can be used to increase water solubility because the ionized molecular species has higher water solubility than its neutral species (Strickley et al, 2004). Constantinides and Scalart (1997) used isotonic (0.010M) Tris pH 7.4, saline, isotonic water for injections pH 5.0, 0.040M acetate buffer pH 5.0 and phosphate-buffered saline pH 7.2 as the aqueous phase to provide optimum solubility of the studied molecule of peptides.

1.3.5. Composition of the original microemulsions and self-emulsifying systems

As stated in the 'Origin and Scope', the work presented in this thesis originates from the microemulsion technology considered as GIPET® II technology. The development of these microemulsions and self-emulsifying systems was described in five patents (US5444041A1, US5633226A, US5646109A1, US5688761A1, US5707648A1), however other sources of the scientific data (reports, raw data, logbooks) are not available. This paragraph will briefly summarise the main content of these patents to provide an insight into the origins of the work and to highlight the rationale for the current work presented in this thesis.

Among the five patents, patent US5444041A1 'Convertible microemulsion formulations' (Owen et al., 1995) appears to be the first and the main patent, which captures the origins of the invention and presents a number of experiments (examples) carried out to demonstrate the invention. The patents US5633226A, US5646109A1, US5688761A1, which were subsequently filed, expanded patent claims but their terms (expiry dates) were not extended beyond the expiration date of US5444041A1. The latest patent US5707648A1 differs form the preceding ones, with respect to the nature and compositions the systems described and it will be discussed in the latter part of this review. The definition of a microemulsion according to the main patent US5444041A1 is 'the microemulsions of this invention are self-emulsifying stable dispersions of oil and water, stabilized by interfacial films of surface-active molecules. These microemulsions are also characterised by their small average particle sizes, generally less than about 0.1 micron, by their wide range of temperature stability, typically from about 5 °C to 50 °C., and they appear to be thermodynamically stable, i.e., stable indefinitely over this range. They are also relatively insensitive to the pH or ionic strength of the aqueous internal phase. These microemulsions are further characterized in that they form spontaneously without the need for high shear equipment' (Owen et al., 1995). The main invention claims improved 'biological' and chemical stability of proteinaceous materials incorporated into a water-in oil microemulsion. According to the invention, the oil phase protects the drug in the intestines until it is slowly released as the body fluids convert the water-in-oil microemulsion into an emulsion. This leads to an improved stability and improved oral absorption of proteins, peptides and any other molecules that are readily attacked by digestive enzymes.

Three formulations, used in the animal study (Table 1.7, study no. 7) were derived from the pseudoternary phase diagrams that are shown in Fig. 1.1. A number of formulations representing convertible microemulsions, suitable to demonstrate the invention, are summarised in Table 1.5. The pseudoternary phase diagrams (Fig. 1.1) were constructed using a mix of surfactants based on three components (two low HLB value surfactants + one high HLB value surfactant), however many examples of binary combinations (one low HLB value surfactant + one high HLB value surfactant) were also given in the examples 1 – 13 (Table 1.5).

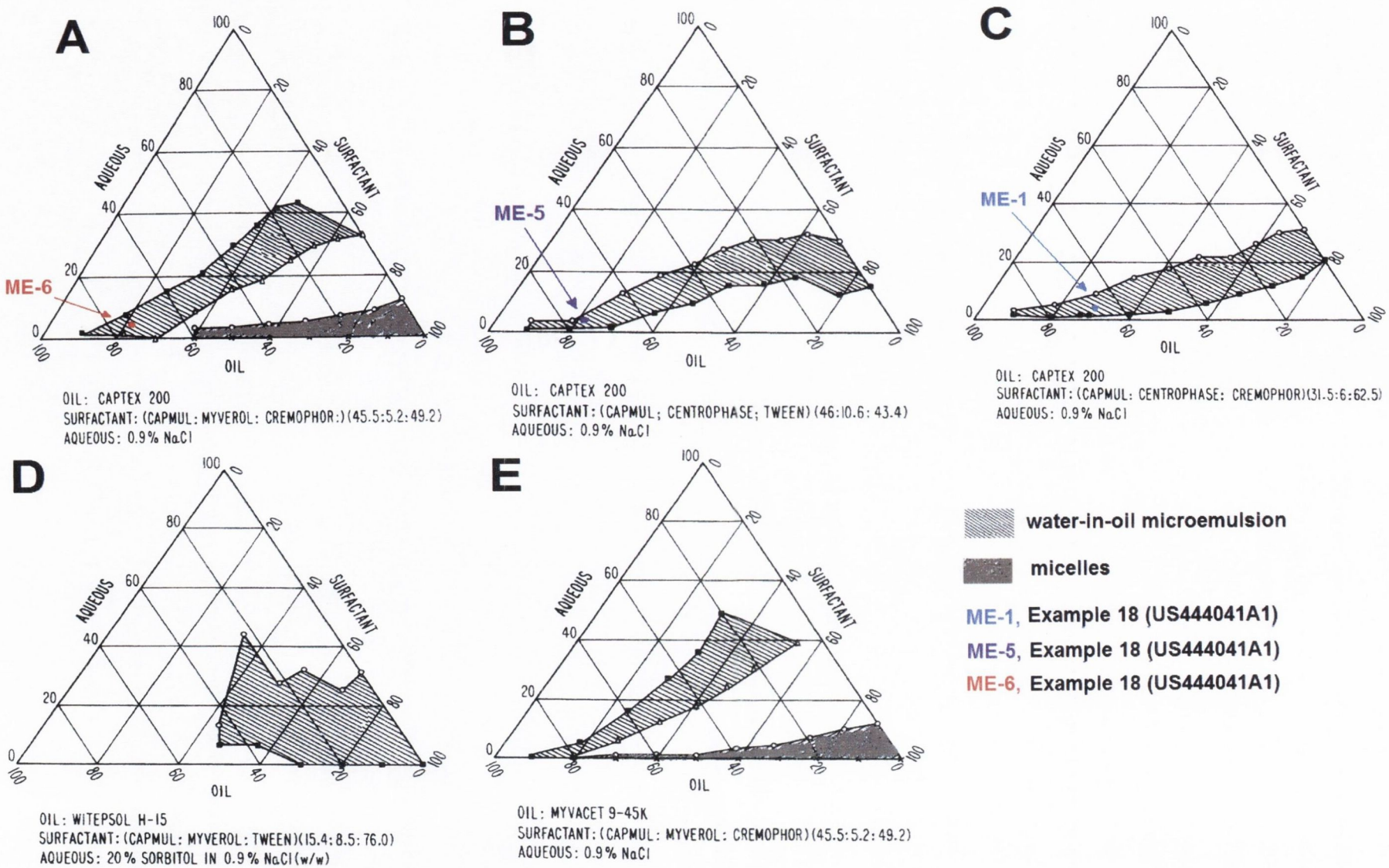

Fig. 1.1. Pseudoternary phase diagrams presented in the patent US5444041A1.

Table 1.5. Composition of convertible microemulsions (Examples) presented in US5444041A1.

Ingredients		Content % /v	Function in composition
Trade Name	*Chemical Name*		
EXAMPLE 1 / combined HLB value = 12.45			
Captex 200	propylene glycol dicaprylate	87.0	oil phase
POE 50 Sorbitol Hexaoleate	polyoxyethylene 50 sorbitol hexaoleate	5.0	low HLB surfactant
Cremophor EL	polyoxyethylene glycerol triricinoleate	5.0	high HLB surfactant
Saline (0.9% NaCl)	saline	3.0	aqueous phase
EXAMPLE 2/ combined HLB value = 12.50			
Captex 200	propylene glycol dicaprylate	87.0	oil phase
Centrophase 31	soybean based lecithin dissolved in soybean oil	1.05	low HLB surfactant
Cremophor EL	polyoxyethylene glycerol triricinoleate	8.95	high HLB surfactant
Saline (0.9% NaCl)	saline	3.0	aqueous phase
EXAMPLE 3/ combined HLB value = 10.0			
Captex 200	propylene glycol dicaprylate	87.0	oil phase
Centrophase 31	soybean based lecithin dissolved in soybean oil	4.55	low HLB surfactant
Tween 80	polyoxyethylene sorbitan monooleate	5.45	high HLB surfactant
Saline (0.9% NaCl)	saline	3.0	aqueous phase
EXAMPLE 4/ combined HLB value = 11.9			
Captex 200	propylene glycol dicaprylate	86.13	oil phase
Capmul MCM	glyceryl mono- & dicaprylate/caprate	0.87	low HLB surfactant
Centrophase 31	soybean based lecithin dissolved in soybean oil	1.05	low HLB surfactant
Cremophor EL	polyoxyethylene glycerol triricinoleate	8.95	high HLB surfactant
EXAMPLE 5/ combined HLB value = 12.50			
Captex 200	propylene glycol dicaprylate	35.0	oil phase
Centrophase 31	soybean based lecithin dissolved in soybean oil	5.26	low HLB surfactant
Cremophor EL	polyoxyethylene glycerol triricinoleate	44.74	high HLB surfactant
Saline (0.9% NaCl)	saline	15.0	aqueous phase
EXAMPLE 7 / combined HLB value = 12.14			
Captex 200	propylene glycol dicaprylate	86.13	oil phase
Monocapryloyl-rac-glycerol	Monocapryloyl-rac-glycerol	0.87	low HLB surfactant
Centrophase 31	soybean based lecithin dissolved in soybean oil	1.05	low HLB surfactant
Cremophor EL	polyoxyethylene glycerol triricinoleate	8.95	high HLB surfactant
Saline (0.9% NaCl)	saline	3.00	aqueous phase
EXAMPLE 8/ combined HLB value = 12.50			
Captex 200	propylene glycol dicaprylate	87.0	oil phase
Myverol 18-92	glycerol monolinoleate	1.05	low HLB surfactant
Cremophor EL	polyoxyethylene glycerol triricinoleate	8.95	high HLB surfactant
Saline (0.9% NaCl)	saline	3.00	aqueous phase
EXAMPLE 9/ combined HLB value = 11.9			
Myvacet 9- 45K	1-oleyl-2,3- diacetyl glycerol	86.13	oil phase
Capmul MCM	glyceryl mono- & dicaprylate/caprate	0.87	low HLB surfactant
Centrophase 31	soybean based lecithin dissolved in soybean oil	1.05	low HLB surfactant
Cremophor EL	polyoxyethylene glycerol triricinoleate	8.95	high HLB surfactant
Saline (0.9% NaCl)	saline	3.00	aqueous phase

Table 1.5. Composition of convertible microemulsions presented in US5444041A1 (cont'd).

EXAMPLE 13								
No	Surfactant			Oil phase		Aqueous phase		TOTAL (%)
	Content % /v							
	Myverol 18-92	Tween 20	Centrolene A (hydroxylated lecithin)	Captex 200	Triacetin	1% NaCl Sol	Water	
1	27	23	/	10	/	40	/	100
2	25	20	5	10	/	40	/	100
3	24	18	8	5	5	/	40	100
4	26	16	8	5	5	/	40	100
5	23.64	14.55	7.27	4.55	4.55	/	45.45	100
6	21.67	13.33	6.67	4.17	4.17	/	50.00	100
7	19.70	12.12	6.06	3.79	3.79	/	54.55	100

The invention was demonstrated in three biostudies with calcitonin (Table 1.7, studies no. 1 and 2) and SK&F 106760 (Table 1.7, study no. 7). Oral absorption of calcitonin in rats, measured as a pharmacodynamic response (reduction of calcium Ca^{2+}), appeared to be the best from the microemulsion formulation D (Table 1.7, study no. 2) composed of Captex 200 (oil), Capmul MCM (a low HLB value surfactant), Centrophase 31 (a low HLB value surfactant), Cremophor EL (a high HLB value surfactant) and a substantial amount (45%) of Hydrokote 108. Hydrokote 108 is a mixture of hydrogenated coconut and palm oils, with a melting point 108°C. This formulation was not derived from any of the pseudoternary phase diagrams presented in Fig. 1.1.

In the next animal study (Table 1.7, study no. 7), oral absorption of SK&F 106760 from various microemulsion formulations was compared against absorption of the drug from an unenhanced formulation (drug dissolved in saline), which was administered intraduodenally, in the same way as the microemulsions. When one-way ANOVA with multiple comparison post test Tukey–Kramer was used to compare the formulations, the microemulsion formulations based on Captex 200, 68%/ Capmul MCM/Centrophase 31/Cremphor EL/saline (ME-1, Table 1.7, study no. 7, Fig. 1.1.C) and Captex 200, 76%/Centrophase 31/Cremphor EL/saline (ME-2, Table 1.7, study no. 7) were found to significantly improve oral bioavailability of SK&F 106760 compared to the unenhanced formulation. The rest of the formulations, including ME-5 (Fig. 1.1.B) and ME-6 (Fig. 1.1.A) failed to show a statistically significant difference ($p < 0.05$) when compared the unenhanced formulation.

The patent claims presented in patent US5444041A1, based on the provided examples are very broad. They cover a very extensive list of surfactants (combinations of surfactants) and wide ranges for the content of each component in the convertible microemulsion formulations. The combined HLB value of a mixture of surfactants is preferably from 8 to 13 and the said mixture comprises a surfactant having an HLB value of less than 5, and a surfactant having an HLB value of greater

than 9' (Owen et al., 1995). The content of each component (phase) according to one of the independent claims is given as:

a) up to about 20 volume percent of an internal dispersed aqueous phase comprising an effective amount of a biologically-active material, said biologically-active material consisting of therapeutic water-soluble materials,

b) from about 30 to 99 volume percent of a continuous oil phase comprising diesters of propylene glycol having from about 15 to 40 carbon atoms,

c) from about 1 to 70 volume percent of a surfactant or a mixture of surfactants, wherein the surfactant or the surfactant mixture has a hydrophilic-lipophilic balance value from 7 to 14.

As the mixture of surfactants, the following materials can be used: ethoxylated castor oil; C_{5-29} mono-glycerides and ethoxylated derivatives thereof; C_{15-60} diglycerides and polyoxyethylene derivatives thereof having 1 to 90 POE groups; C_{10-40} esters of long chain fatty acids; C_{10-40} alcohols; C_{8-96} ethoxylated fatty esters; C_{14-130} sucrose fatty esters; and C_{20-130} sorbitol and sorbitan monoesters, diesters, and triesters, and polyoxyethylene (POE) derivatives thereof having 1 to 90 POE groups (Owen et al., 1995).

Additional claims were added in patent US5633226A (Owen &Yiv, 1997), to allow for the use of oil phase comprising C_9-C_{83} triglycerides and a surfactant or a mixture of surfactants that has an HLB value of at least 7 and comprises C_8 fatty acid salts, fatty acids or C_9-C_{13} monoglycerides (1-70%). New claims were added in patent US5646109A1 (Owen & Yiv, 1997), where an external oil phase ranging from 5 – 99% could comprise at least one pharmaceutically acceptable oil, which was not chemically defined.

Additional examples of convertible microemulsion formulations and a new claim were included in patent US5688761A1 (Owen et al., 1997). A new claim, with regard to a low HLB value surfactant appeared: 'a low HLB surfactant having a HLB value below about 8 and being at least 80% composed of C_9-C_{13} monoglycerides'. The invention was related to the use of high purity C_9-C_{13} monoglycerides (low HLB value surfactants) to enhance the uptake of the active material upon oral administration (Owen et al., 1997). The term 'C_9-C_{13} monoglycerides' referred to the overall number of carbon atoms in the material e.g. Imwitor 308 which is composed of approximately 80-90% of glycerol monocaprylate (derivative of C_8 acid) was considered as C_{11} monoglyceride (8 carbon from acid + 3 carbon atoms from glycerine). The new microemulsion formulations comprising Imwitor 308 were possibly derived from the pseudoternary phase diagrams mentioned in patent US5688761A1 (Table 1.6). However, the diagrams were not shown in the patent (the previous phase diagrams presented in Fig. 1.1 appeared to be mistakenly attached instead) and the exact compositions were not given (Owen et al., 1997).

Table 1.6. Composition of pseudoternary phase diagrams mentioned (but not shown) in patent US5688761A1.

Content % /v				
Surfactant	**Ratio of surfactants**	**Oil phase**	**Aqueous phase**	**Phase diagram**
Imwitor 308: Tween 80	Not disclosed	Captex 200	0.9% NaCl	Not shown in the patent
Imwitor 308: Tween 80	Not disclosed	Captex 8000 (tricaprylin)	0.9% NaCl	Not shown in the patent
Imwitor 308: Glucamate SSE-20 (PEG-20 methyl glucose sequistearate)	Not disclosed	Captex 200	0.9% NaCl	Not shown in the patent
Imwitor 308: Brij 30	Not disclosed	Captex 200	0.9% NaCl	Not shown in the patent
Imwitor 308: Tween 80	Not disclosed	Witepsol H-15: Captex 800	0.9% NaCl	Not shown in the patent

The invention was demonstrated on three biostudies with calcitonin (Table 1.7, study no. 3), calcein (Table 1.7, study no. 5) and an anticoagulant peptide (Table 1.7, study no. 8).

Oral absorption of calcitonin in rats (Table 1.7, study no. 3), measured as a pharmacodynamic response (reduction of calcium Ca^{2+}) was demonstrated with the microemulsion formulation composed of Captex 200/Imwitor 308/Tween 80 and lauroyl choline. Calcium levels were significantly lowered after 45 minutes (post administration of the microemulsion) compared to the pre-dosing state (15 minutes prior to dosing). In comparison to the previous studies with calcitonin (Table 1.7, study no. 1 and 2), the pharmacodynamic effect was achieved with a lower amount of microemulsion. However, different routes of administration were used in the studies no. 1 and 2 versus no 3. A significant reduction of calcium levels in study no. 3 was achieved after 45 minutes but this effect did not last beyond this time point while in studies no. 1 and 3, a significant reduction was still observed after 120 minutes despite the lower dose of the drug. Since the route of administration and the volume of the microemulsions dosed differed in studies 1, 2 and 3, a direct comparison of the 'bio-performance of these formulations cannot be made and it is not possible to say if the newer version of microemulsion (with Imwitor 308) was more 'bio-effective' than the previous formulations. Oral bioavailability of calcein (Table 1.7. study no. 5) was significantly improved from all three tested formulations composed mainly of Captex 200/ Imwitor 308/Tween 80 (Formula A), Captex 200/ Glyceryl monocaprate/Tween 80 (Formula B) and Captex 800 (propylene glycol dioctanoate)/ Imwitor 308/Tween 80 (Formula C). The amount of Imwitor 308 in the ME was not directly related to the adsorption extent, since Formula C contained approximately twice more of this material compared to the formulation A but all three formulations (A, B, C) demonstrated comparable bioavailability. Oral bioavailability of the anticoagulant peptide (Table 1.7, study no. 8) in rats was approximately four times better from the microemulsion formulation consisting mainly of Captex 200/Imwitor 308/Tween 80, compared to the absorption of the drug from saline solution (control).

The latest patent, US5707648A1 'Transparent liquid for encapsulated drug delivery' (Yiv, 1998) is not a close continuation of the four patents (presented above) but describes a stable transparent drug delivery composition suitable for storage and administration of biologically active materials, comprising:

a) an internal aqueous phase from about 0.5 to about 15 % water,

b) polyethylene glycol from about 2 to about 60%,

c) an external oil phase from about 1 to about 80% comprises at least one pharmaceutical oil,

d) a surfactant or a mixture of surfactants from 3 to about 98 %,

e) a therapeutic amount of a biologically active material having the octanol: water partition coefficient of less than 0.1, provided that the system does not contain a mixture of phospholipids and cholesterol and the ratio of polyethylene glycol to water is at least 2:1.

The invention presents delivery compositions, which are preferably transparent and thermodynamically stable solutions resembling swollen micelles and w/o microemulsions with the particle size preferably below about 5 nm. The compositions are specially formulated to be compatible with gelatine and starch capsules. The aqueous phase of the compositions contains a substantial amount of polyethylene glycol and can optionally also contain a plasticizer' (Yiv, 1998). Such drug delivery compositions are suitable for storage and administration of an active agent, preferably by an oral route (in an encapsulated form), which forms a microemulsion *in situ* in the intestines. These compositions do not require the presence of a phospholipid in conjunction with a cholesterol component. The surfactant component is a mixture of surfactants comprising a low HLB value surfactant (HLB value below 10) and a high HLB value surfactant (HLB value above 10) wherein the low HLB value surfactant comprises C_9-C_{13} monoglycerides (Yiv, 1998).

The bio-performance of new transparent liquid compositions was demonstrated in three biostudies with calcitonin (Table 1.7. study no. 4), calcein (Table 1.7. study no. 6) and desmopressin acetate (Table 1.7, study no. 9). None of these formulations was directly derived from the pseudoternary phase diagrams shown in Fig. 1.2.

A significant oral absorption of calcitonin in rats, measured as a pharmacodynamic response (reduction of calcium Ca^{2+}), was observed from the formulations A and B (Table 1.7, study no. 4) mainly composed of Captex 200, Imwitor 308 and Tween 80. The calcium levels were significantly reduced up to 3 hours post administration of calcitonin in these two formulations. The composition C (Tween 80 with polyoxyethylene-9 lauryl ether, PEG 1000) failed to show any significant reduction in calcium levels. The composition A and B in this study (study no. 4) were dosed in rats, in the same way as the formulation administered in study 3, however an approximately twice larger amount (volume) of lipid formulations was used in study no 4.

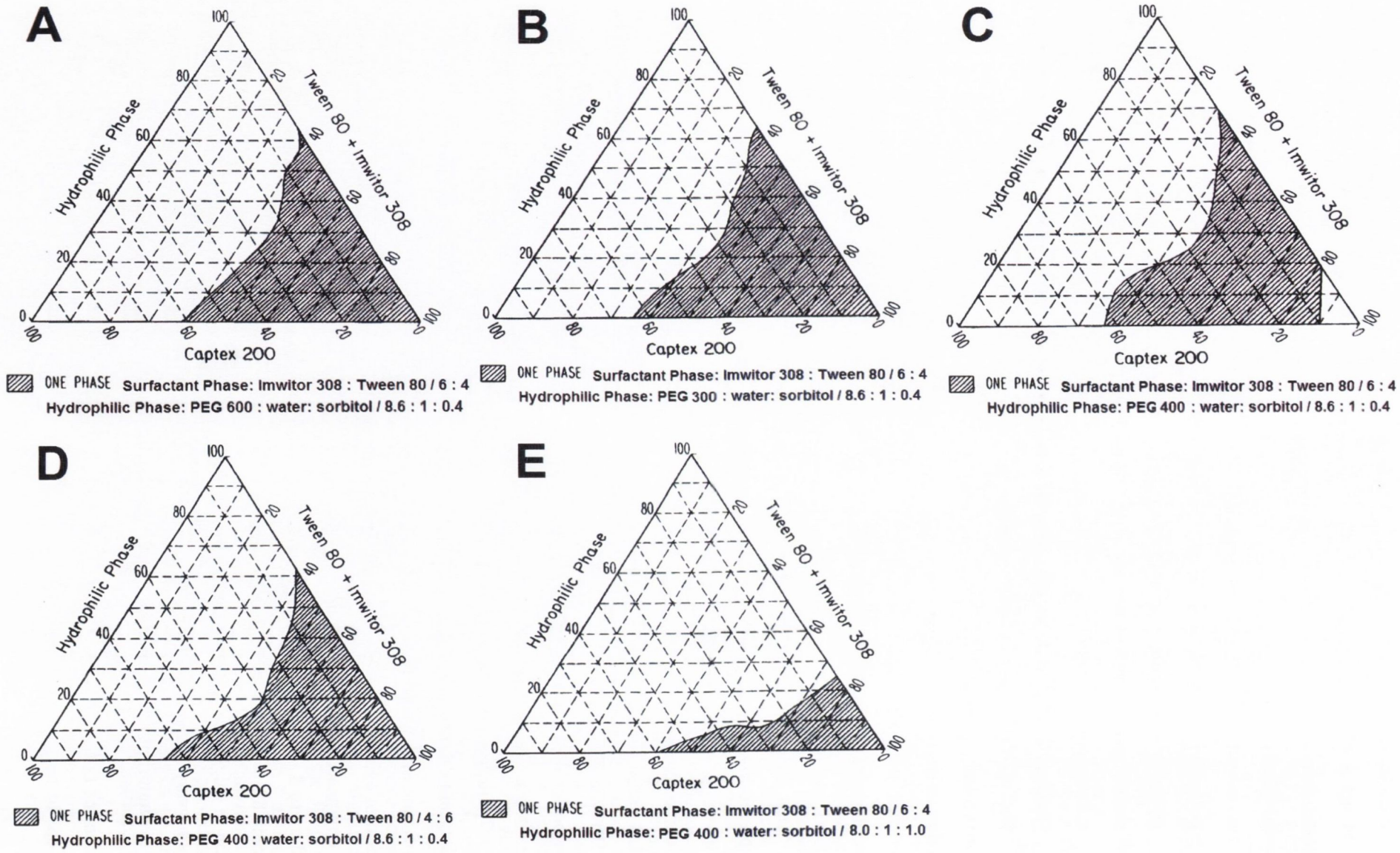

Fig. 1.2 Pseudoternary phase diagrams presented in patent US5707648A1.

Table 1.7. Summary of the pharmacokinetic & pharmacodynamic data presented in the patents US5444041A1, US5633226A, US5646109A1, US5688761A1, US5707648A1.

<table>
<tr><th>Compound/ Molecular weight (Reference)</th><th>Animal model (administration mode)</th><th colspan="4">Formulation</th><th>Bio-data</th></tr>
<tr><td rowspan="4">Study no. 1

Calcitonin
/
M_W= 3454.93

(US5444041A1, Example 14)</td><td rowspan="4">Fasted rats (n = 5), body weight 140 –170 gm, items orally gavaged with 250µl of the microemulsions</td><td><u>Group A</u>
10% of Capmul MCM in Captex 200 – 570 µl,
298 µl Cremophor EL,
35 µl Lecithin,
92 µl acetate buffer,
8 µl calcitonin,
10% Capmul in HB-108</td><td><u>Group B</u>
373 µl Myverol 18-92,
404 µl Tween 80,
124 µl Capmul MCM,
725 µl HB-95,
365 µl acetate buffer,
8 µl calcitonin</td><td colspan="2"><u>Group C</u>
373 µl Myverol 18-92,
404 µl Tween 80,
124 µl Capmul MCM,
725 µl HB-118,
365 µl acetate buffer,
8 µl calcitonin</td><td>PK parameters not measured,

PD response: changes in levels of Ca^{2+} and PO_4 after 2 hours compared to the controls (formulations A, B, C without the drug)</td></tr>
<tr><td colspan="3"><u>Ca^{2+}levels:</u>
Formula A vs. placebo/ $p < 0.05$
Formula B vs. placebo/ $p < 0.05$
Formula C vs. placebo/ $p > 0.05$</td><td colspan="2"><u>PO_4 levels:</u>
Formula A vs. placebo/ $p < 0.05$
Formula B vs. placebo/ $p < 0.05$
Formula C vs. placebo/ $p < 0.05$</td></tr>
<tr><td colspan="5">Total volume = 2.0 ml</td><td rowspan="2">Pharmacodynamic response (with ME)
Formula A) Ca^{2+} and PO_4 levels: reduced by ~ 4.4 & 3.5
Formula B) Ca^{2+} and PO_4 levels: reduced by ~ 2.9 & 13
Formula C) Ca^{2+} and PO_4 levels: reduced by ~ 0 & 2.6</td></tr>
<tr><td colspan="5">250 µl of ME containing 10 i.u. of API was dosed orally and the flush volume unknown</td></tr>
<tr><td rowspan="4">Study no. 2

Calcitonin
/
M_W= 3454.93

(US5444041A1, Example 15)</td><td rowspan="4">Fasted rats (n = 5), body weight approximately 100 g, items orally gavaged with 250µl of the microemulsions</td><td>Capmul MCM,
Captex 200
Centrophase -31 (lecithin)
Cremophor EL
Saline
Salmon calcitonin 10,000 U/ml
HB-108</td><td><u>Group B</u>
157 µl,
1.413 ml,
35 µl,
298 µl,
92 µl ,
8 µl
0 ml</td><td colspan="2"><u>Group D</u>
157 µl,
513 µl,
35 µl,
298 µl,
92 µl ,
8 µl calcitonin
0.9 ml</td><td>PK parameters not measured,

PD response: changes in levels of Ca^{2+} after 2 hours compared to the controls (formulations A & C without the drug)</td></tr>
<tr><td colspan="3"><u>Ca^{2+}levels:</u>
Formula B vs. placebo A/ $p > 0.05$
Formula D vs. placebo C/ $p < 0.05$</td></tr>
<tr><td colspan="5">Total volume = 2.0 ml</td><td rowspan="2">Pharmacodynamic response (with ME)
Formula D) Ca^{2+} levels: reduced by ~ 1.5</td></tr>
<tr><td colspan="5">250 µl of ME containing 10 i.u. of API was dosed orally and the flush volume unknown</td></tr>
<tr><td rowspan="6">Study no. 3

Calcitonin
/
M_W= 3454.93

(US5688761A1, Example 4)</td><td rowspan="6">Fasted rats (n = 5), body weight 90 -160g, items dosed via intraduodenal cannula (0.5 ml of ME per 1 kg)</td><td colspan="3">Trade Name</td><td>Content % /v</td><td>PK parameters not measured,
PD response: changes in levels of Ca^{2+} 15 minutes before dosing and after 15, 45, 135 and 165 min post dosing</td></tr>
<tr><td colspan="3">Captex 200</td><td>45.0</td><td rowspan="2"><u>Reduction in Ca^{2+}levels:</u>
45 min vs. –15 min/ $p < 0.01$</td></tr>
<tr><td colspan="3">Imwitor 308</td><td>25.0</td></tr>
<tr><td colspan="3">Tween 80</td><td>15.0</td></tr>
<tr><td colspan="3">Lauroyl choline</td><td>10.0</td></tr>
<tr><td colspan="3">Acetate buffer pH 4.5 containing Calcitonin</td><td>5.0</td><td rowspan="2">Pharmacodynamic response (with ME)
Ca^{2+} levels (45 min): reduced by ~ 1.4</td></tr>
<tr><td colspan="4">~ 75 µl of ME containing 17 i.u. of API was intraduodenally and the flush volume unknown</td></tr>
</table>

Table 1.7. Summary of the pharmacokinetic & pharmacodynamic data presented in the patents US5444041A1, US5633226A, US5646109A1, US5688761A1, US5707648A1 (cont'd).

Compound/ Molecular weight (Reference)	Animal model (administration mode)	Formulation				Bio-data
Study no. 4 **Calcitonin** / **M_W= 3454.93** **(US5707648A1, Example 10)**	Fasted rats (n = 3 -8), body weight 87 – 106 g, items dosed via intraduodenal cannula (1.0 ml of ME per 1 kg)	*Components*	**Comp A**	**Comp B**	**Comp C**	PK parameters not measured, PD response: changes in levels of Ca^{2+} after 0, 1 and 3 hours
		Captex 200	11.40	11.70	11.70	
		Imwitor 308	23.30	28.00	28.00	
		Polyoxyethylene 9 Lauryl Ether	/	/	18.70	
		Tween 80	21.70	18.70	/	None of the formulations showed a significant reduction in Calcium levels at the dose 15 i.u./kg and 50 i.u./kg of calcitonin. Formulation A (150 i.u./kg) showed a very significant reduction between T_{0h} and T_{1h} and T_{3h} ($p < 0.01$ and $p < 0.001$ respectively). Formulation B (150 i.u.//kg) showed a significant reduction between T_{0h} and T1 and T_{3h} ($p < 0.05$ and $p < 0.05$ respectively). Formulation C showed no statistically significant difference between T_{0h}, T_{1h} and T_{3h}.
		Molecusol (β-cyclodextrin)	/	3.00	/	
		Glycocholic acid	3.70	/	/	
		Chenodeoxycholic acid	3.70	/	/	
		Linoleic Acid	/	/	/	
		PEG 400	/	31.30	/	
		PEG 600	28.60	/	/	
		PEG 1000	/	/	31.00	
		Sorbitol	/	1.70	1.70	
		Glycerine	1.30	/	/	
		Acetic acid	0.53	/	/	
		1N HCl	/	0.33	/	
		Sterile water	4.40	1.43	5.1	**Pharmacodynamic response (with ME)** Ca^{2+} levels (Formulation A 150 i.u./kg, T_{3h}): reduced by ~ 1.4 Ca^{2+} levels (Formulation B 150 i.u./kg, T_{3h}): reduced by ~ 1.3
		1N Sodium Hydroxide	1.40	/	/	
		750 µg/ml Calcitonin solution	3.90	3.90	3.90	
		~ 100 µl of ME containing 1.5, 5, 15 i.u. of API was intraduodenally and the flushed with 100 µl saline				

Table 1.7. Summary of the pharmacokinetic & pharmacodynamic data presented in the patents US5444041A1, US5633226A, US5646109A1, US5688761A1, US5707648A1 (cont'd).

<table>
<tr><th>Compound/ Molecular weight (Reference)</th><th>Animal model (administration mode)</th><th colspan="8">Formulation</th><th colspan="3">Bio-data</th></tr>
<tr><td rowspan="11"><u>Study no. 5</u>

Calcein
/
M_W= 623

(US5688761A1, Example 1)</td><td rowspan="11">Fasted rats (n = unknown), body weight unknown, items dosed via intraduodenal cannula (1.0 ml of ME per 1 kg body weight)</td><td>Components</td><td colspan="2">Form A</td><td colspan="2">Form B</td><td colspan="2">Form C</td><td>Formulation</td><td colspan="2">Fabs% ± SD / one way ANOVA</td></tr>
<tr><td>Captex 200</td><td colspan="2">59.4</td><td colspan="2">59.8</td><td colspan="2">/</td><td>Saline (I.D)</td><td colspan="2">1.3 ± 0.5</td></tr>
<tr><td>Captex 800</td><td colspan="2">/</td><td colspan="2">/</td><td colspan="2">50</td><td>Formula A</td><td colspan="2">22</td></tr>
<tr><td>Imwitor 308</td><td colspan="2">15.3</td><td colspan="2">/</td><td colspan="2">36</td><td>Formula B</td><td colspan="2">22.2 ± 6.1</td></tr>
<tr><td>Glycerol mono-caprate</td><td colspan="2">/</td><td colspan="2">15.4</td><td colspan="2">/</td><td>Formula C</td><td colspan="2">22.9 ± 5.3</td></tr>
<tr><td>Tween 80</td><td colspan="2">15.3</td><td colspan="2">15.4</td><td colspan="2">8</td><td colspan="3" rowspan="3">All 3 ME appear significantly better compared to control (statistical analysis not performed – number of animals unknown)

Formulas A, B and C, oral bioavailability increased by 17 fold (on average)</td></tr>
<tr><td>Aqueous phase</td><td colspan="2">10</td><td colspan="2">9.4</td><td colspan="2">6</td></tr>
<tr><td colspan="8">Total volume = 100%</td></tr>
<tr><td colspan="8">~ 0.15ml of ME (1.0 ml/kg) containing 3µmol/kg of API was dosed intraduodenally and the flush volume unknown</td></tr>
<tr><td rowspan="16"><u>Study no. 6</u>

Calcein
/
M_W= 623

(US5707648A1, Example 9)</td><td rowspan="16">Fasted rats body weight unknown, items dosed via intraduodenal cannula</td><td>Components</td><td>Com pA</td><td>Com pB</td><td>Com pC</td><td>Com pD</td><td>Com pE</td><td>Com pF</td><td>Formulation</td><td>N</td><td>Fabs% ± SEM / one way ANOVA</td></tr>
<tr><td>Captex 200</td><td>12.0</td><td>13.0</td><td>12.0</td><td>11.5</td><td>7.00</td><td>10.0</td><td>Buffer (I.D)</td><td>5</td><td>1.3 ± 0.5</td></tr>
<tr><td>Cod liver</td><td>/</td><td>/</td><td>/</td><td>/</td><td>5.00</td><td>/</td><td>Comp A</td><td>10</td><td>27.6 ± 4.8</td></tr>
<tr><td>Imwitor 308</td><td>29.8</td><td>26.0</td><td>28.8</td><td>23.4</td><td>28.6</td><td>25.0</td><td>Comp B</td><td>5</td><td>25.8 ± 7.1</td></tr>
<tr><td>Tween 80</td><td>19.2</td><td>/</td><td>22.3</td><td>21.8</td><td>19.1</td><td>/</td><td>Comp C</td><td>12</td><td>39.7 ± 6.8/ Comp C vs. Cont p < 0.01</td></tr>
<tr><td>Cremophor RH40</td><td>/</td><td>26.0</td><td>/</td><td>/</td><td>/</td><td>/</td><td>Comp D</td><td>4</td><td>35.4 ± 1.5</td></tr>
<tr><td>Glycocholic acid</td><td>/</td><td>/</td><td>1.90</td><td>3.70</td><td>/</td><td>5.00</td><td>Comp E</td><td>4</td><td>33.4 ± 13.1</td></tr>
<tr><td>Sodium Taurocholate</td><td>/</td><td>/</td><td>1.90</td><td>3.70</td><td>/</td><td>5.00</td><td>Comp F</td><td>5</td><td>39.5 ± 5.6/ Comp F vs. Cont p < 0.05</td></tr>
<tr><td>Linoleic Acid</td><td>/</td><td>/</td><td>/</td><td>/</td><td>/</td><td>20.0</td><td colspan="3" rowspan="10">Composition C and F, oral bioavailability increased by 30 fold (on average)</td></tr>
<tr><td>PEG 400</td><td>32.4</td><td>28.0</td><td>/</td><td>/</td><td>34.0</td><td>/</td></tr>
<tr><td>PEG 600</td><td>/</td><td>/</td><td>31.0</td><td>28.7</td><td>/</td><td>29.0</td></tr>
<tr><td>Sorbitol</td><td>1.60</td><td>/</td><td>/</td><td>/</td><td>1.60</td><td>1.50</td></tr>
<tr><td>Glycerine</td><td>/</td><td>2.80</td><td>3.10</td><td>1.30</td><td>/</td><td>/</td></tr>
<tr><td>Sterile water</td><td>3.00</td><td>/</td><td>1.20</td><td>1.50</td><td>2.90</td><td>/</td></tr>
<tr><td>1N NaOH</td><td>/</td><td>/</td><td>0.70</td><td>1.40</td><td>0.20</td><td>/</td></tr>
<tr><td>Calcein solution in Tris, pH 7.4</td><td>3.0</td><td>4.2</td><td>2.9</td><td>3.0</td><td>1.5</td><td>4.5</td></tr>
<tr><td>Volume of ME dosed [µl] containing 2.5 µmol/kg of API</td><td>83.3</td><td>59.5</td><td>86.2</td><td>83.3</td><td>166.7</td><td>55.6</td></tr>
</table>

Table 1.7. Summary of the pharmacokinetic & pharmacodynamic data presented in the patents US5444041A1, US5633226A, US5646109A1, US5688761A1, US5707648A1 (cont'd).

<table>
<tr><th>Compound/ Molecular weight (Reference)</th><th>Animal model (administration mode)</th><th colspan="7">Formulation</th><th colspan="4">Bio-data</th></tr>
<tr><td rowspan="13"><u>Study no. 7</u>

SK&F 106760
/
M_W= 634

(US5444041A1, Example 18)</td><td rowspan="13">Fasted rats, body weight unknown, items dosed via intraduodenal cannula (3.3 ml of ME per 1 kg body weight)</td><td>Components</td><td>ME-1</td><td>ME-2</td><td>ME-3</td><td>ME-4</td><td>ME-5</td><td>ME-6</td><td>Formulation</td><td>Dose mg/kg</td><td>N</td><td>Fabs% ± SD / one way ANOVA</td></tr>
<tr><td>Captex 200</td><td>68.30</td><td>76.47</td><td>/</td><td>76.57</td><td>76.65</td><td>76.49</td><td>Saline (I.D)</td><td>10.0</td><td>3</td><td>0.5 ± 0.3</td></tr>
<tr><td>Myvacet 9- 45K</td><td>/</td><td>/</td><td>76.91</td><td>/</td><td>/</td><td>/</td><td>ME-1</td><td>6.5</td><td>3</td><td>29.1 ± 7.1/ ME-1 vs. Cont p < 0.001</td></tr>
<tr><td>Capmul MCM</td><td>8.31</td><td>/</td><td>9.09</td><td>/</td><td>9.28</td><td>9.26</td><td>ME-2</td><td>6.5</td><td>3</td><td>19.4 ± 11.8/ ME-2 vs. Cont p < 0.05</td></tr>
<tr><td>Dicaprin</td><td>/</td><td>/</td><td>/</td><td>9.26</td><td>/</td><td>/</td><td>ME-3</td><td>10.0</td><td>3</td><td>5.4 ± 2.2</td></tr>
<tr><td>Centrophase 31</td><td>1.60</td><td>1.61</td><td>/</td><td>0.96</td><td>2.13</td><td>/</td><td>ME-4</td><td>10.0</td><td>3</td><td>2.5 ± 1.9/ / ME-4 vs. ME-2 p< 0.05</td></tr>
<tr><td>Myverol 18-92</td><td>/</td><td>/</td><td>1.04</td><td>/</td><td>/</td><td>1.06</td><td>ME-5</td><td>10.0</td><td>1</td><td>7.4</td></tr>
<tr><td>Cremophor EL</td><td>16.52</td><td>16.63</td><td>9.82</td><td>10.01</td><td>/</td><td>10.0</td><td>ME-6</td><td>10.0</td><td>3</td><td>14.4 ± 4.4</td></tr>
<tr><td>Tween 80</td><td>/</td><td>/</td><td>/</td><td>/</td><td>8.74</td><td>/</td><td colspan="4" rowspan="3">Formula ME-1, oral bioavailability increased by 58 fold (on average)

Formula ME-2, oral bioavailability increased by 39 fold (on average)</td></tr>
<tr><td>Saline (peptide)</td><td>5.26</td><td>5.30</td><td>3.13</td><td>3.19</td><td>3.20</td><td>3.19</td></tr>
<tr><td colspan="7">Total volume = 100%</td></tr>
<tr><td colspan="7">~ 1ml of ME (3.3ml/kg) containing 6-10 mg/kg of API was dosed intraduodenally and the flush volume unknown</td></tr>
<tr><td rowspan="8"><u>Study no. 8</u>

N-methyl-D-phenylalanyl-n-proplyl-L-argininal sulphate (Anticoagulant)
/
M_W= 515

(US5688761A1, Example 7)</td><td rowspan="8">Fasted rats (n = 3), body weight unknown, items dosed via intraduodenal cannula (1.0 ml of ME per 1 kg)</td><td colspan="5">Trade Name</td><td>Content % /v</td><td colspan="4" rowspan="8">Fabs% (unenhanced, saline) = 10.5%

Fabs% (microemulsion) = 40%

Oral bioavailability increased by 4 fold (on average)</td></tr>
<tr><td colspan="5">Captex 200</td><td>60.0</td></tr>
<tr><td colspan="5">Imwitor 308</td><td>15.0</td></tr>
<tr><td colspan="5">Tween 80</td><td>15.0</td></tr>
<tr><td colspan="5">20 mM acetate buffer</td><td>9.0</td></tr>
<tr><td colspan="5">Peptide (5mg/ml in the final composition)</td><td>0.7</td></tr>
<tr><td colspan="5">1 N HCl</td><td>0.3</td></tr>
<tr><td colspan="6">Total volume = 100%</td></tr>
<tr><td colspan="6">~ 115 µl of ME containing5mg/kg of API was intraduodenally and the flush volume unknown</td></tr>
</table>

Table 1.7. Summary of the pharmacokinetic & pharmacodynamic data presented in the patents US5444041A1, US5633226A, US5646109A1, US5688761A1, US5707648A1 (cont'd).

<table>
<tr><th>Compound/ Molecular weight (Reference)</th><th>Animal model (administration mode)</th><th>Formulation</th><th>Bio-data</th></tr>
<tr><td rowspan="11"><u>Study no. 9</u>

Desmopressin acetate
/
M_W= 1183.34

(US5707648A1, Example 7)</td><td rowspan="11">Fasted beagle dogs (n = unknown), body weight 9 - 12 kg, items dosed orally as enteric capsules</td><td><table>
<tr><td>Components</td><td>6A</td><td>6B</td><td>6C</td><td>6D</td></tr>
<tr><td>Captex 200</td><td>12.0</td><td>12.0</td><td>12.0</td><td>12.0</td></tr>
<tr><td>Imwitor 308</td><td>28.8</td><td>28.8</td><td>28.8</td><td>28.8</td></tr>
<tr><td>Tween 80</td><td>19.2</td><td>19.2</td><td>19.2</td><td>19.2</td></tr>
<tr><td>PEG 400</td><td>32.4</td><td>32.4</td><td>32.4</td><td>32.4</td></tr>
<tr><td>1N HCL</td><td>0.74</td><td>0.74</td><td>0.74</td><td>0.74</td></tr>
<tr><td>Sorbitol</td><td>1.60</td><td>1.60</td><td>1.60</td><td>1.60</td></tr>
<tr><td>Water</td><td>1.45</td><td>4.67</td><td>5.08</td><td>5.26</td></tr>
<tr><td>dDAVP in acetate buffer pH 5.0</td><td>3.81</td><td>0.59</td><td>0.18</td><td>0.0</td></tr>
<tr><td>DDAVP (µg/g)</td><td>171</td><td>59</td><td>18</td><td>0</td></tr>
<tr><td colspan="5">Total volume = 100%</td></tr>
<tr><td colspan="5">1 enteric capsule given orally, flushed volume unknown</td></tr>
</table></td><td>PK parameters not measured,

PD response: changes in levels of Factor VIII after up to 6 hours post dosing</td></tr>
<tr><td>Pharmacodynamic response (with ME)

A subcutaneous injection at the dose of 0.4. µg/kg produced similar increase in Factor VIII levels as the oral dose 125 µg/capsule (6A)</td></tr>
<tr><td rowspan="11"><u>Study no. 10</u>

Desmopressin acetate
/
M_W= 1183.34

(Leonard et al., 2006)</td><td rowspan="11">Fasted human (n = 18), dosed orally as enteric capsule</td><td><table>
<tr><td>Trade Name</td><td>Content % /v</td></tr>
<tr><td>Captex 200</td><td>12.0</td></tr>
<tr><td>Imwitor 308</td><td>28.0</td></tr>
<tr><td>Tween 80</td><td>19.82</td></tr>
<tr><td>PEG 400</td><td>32.4</td></tr>
<tr><td>Sorbitol</td><td>1.6</td></tr>
<tr><td>Purified water</td><td>2.44</td></tr>
<tr><td>dDVAP in pH 5.5</td><td>3.0</td></tr>
<tr><td>1 M HCl</td><td>0.74</td></tr>
<tr><td colspan="2">Total = 100%</td></tr>
<tr><td colspan="2">1 enteric capsule containing approximately 0.7 ml of ME and 200 µg of dDVAP given orally</td></tr>
</table></td><td>Frel% (ME vs. reference 4 µg s.c.) = 2.4% ± 2.9

Frel% (Minirin tablet 200µg vs. reference 4 µg s.c) = 0.2% ± 0.2

Oral bioavailability increased by 12 fold (on average)</td></tr>
<tr><td rowspan="5"><u>Study no. 11</u>
Dalteparin sodium/
M_W= ~5000 Da (Merrion, unpublished data)</td><td rowspan="5">Fasted human (n = 12), dosed intraduodenally</td><td><table>
<tr><td>Trade Name</td><td>Content % /v</td></tr>
<tr><td>Captex 355</td><td>5</td></tr>
<tr><td>Capmul MCM</td><td>90</td></tr>
<tr><td>Tween 80</td><td>5</td></tr>
<tr><td colspan="2">Total = 100%</td></tr>
<tr><td colspan="2">Intraduodenally as 2.5 ml of ME chased by 15ml of aqueous solution containing 45000 IU</td></tr>
</table></td><td>Frel% (ME vs. reference 5000 IU s.c) = 4.52% ± 2.53</td></tr>
</table>

Oral bioavailability of calcein (Table 1.7, study no. 6) was significantly improved from the compositions C and F compared to the absorption of the drug from a buffer solution. On average, oral bioavailability was improved by 30 fold which is higher by approximately 15 fold compared to the previous results from study no. 5 (Table 1.7). This higher absorption appeared to be achieved with approximately half the volume of lipid formulations previously dosed. In terms of composition, formula C (study no. 6) contained a higher percentage of Imwitor 308 and Tween 80, while approximately 45% of Captex 200 was substituted mainly with PEG 600 compared to the formulation A (study no. 5). The second formulation which showed a significant improvement in calcein bioavailability in the study no. 6 was the formulation F, where Tween 80 was replaced with linoleic acid glycocholic acid, and sodium taurocholate.

An improved oral absorption of desmopressin acetate (Table 1.7, study no. 9) from a transparent liquid composition was observed in dogs as a change in levels of Factor VIII after up to 6 hours post dosing. A dose of desmopressin, 0.4 μg/kg administered subcutaneously produced a similar increase in Factor VIII levels as the oral dose of desmopressin, 125 μg incorporated into a liquid composition comprising mainly Captex 200, Imwitor 308, Tween 80 and PEG 400 and administered orally as an enteric capsule. The formulation used with desmopressin is similar to the phase systems presented in Fig. 1.2. C, however the components of the aqueous phase were combined in a slightly different ratio in the desmopressin formulation (PEG 400: water: sorbitol/ 8.3: 1.3: 0.4). The same liquid composition was administered in humans (Leonard et al., 2006, Table 1.7, study no. 10) and the absorption of desmopressin from enteric capsules containing 200μg of desmopressin incorporated into the lipid formulation was found to be approximately 12 times better than the reference product, 200μg Minirin immediate release tablet. Another clinical study mentioned in the 'Origin and Scope' where a lipid formulation was found to improve oral absorption of a large molecule, dalteparin sodium, is presented as study no. 11 (Table 1.7). The composition of this formulation differs from the ones previously presented but C_8/C_{10} monoglycerides (Capmul MCM) are still the main components in this system.

The patents present several 'original' microemulsion formulations (examples) prepared with various lipid excipients and surfactants. However, physical characterisation of these formulations e.g. viscosity, particles size, dilution behaviour at 37°C, etc. is not provided and therefore little is known about stability and/or final manufacturing of these formulations as encapsulated dosage forms. A few pseudoternary phase diagrams are shown in the patents but many formulations presented in the examples are derived from different systems. The patents do not disclose how the combination of surfactants (the combined HLB value) affects the phase behaviour, neither if there is a relationship between the composition of lipid formulations, dilution behaviour and the oral bioavailability observed. Although the same model compounds (calcein, calcitonin) were used in the several biostudies, the comparison of the 'bio-enhancing effect' of these formulations cannot be made due to a number of differentiating factors between the studies

(e.g. different way of administration, different volumes of ME administered and the way how absorption was estimated, etc). $C_{9\text{-}13}$ monoglycerides were proven to improve oral bioavailability of the model compounds, however there isn't enough evidence in the patents to say that these materials are significantly better 'absoprtion promoters' than any other lipid materials mentioned in the claims. Therefore, in order to develop GIPET® II microemulsion formulations so that they could become commercially viable products, there is a need to explore some formulation parameters such as the type of oil phase, the type of cosurfactant and the impact of the combined HLB value on the formation of these microemulsions, their dilution behaviour and the possibility of any bioavailability improvement.

1.4. Microstructure and phase behaviour

1.4.1. Mechanism of self-emulsification

Microemulsions are formed spontaneously when the interfacial tension between water and oil is decreased, close to zero. Three different theories have been proposed to explain the microemulsion formations which are: 1) interfacial or mixed film theory, 2) solubilisation theory and 3) thermodynamic theory. These theories are not mutually exclusive as elements of each can contribute to an understanding of microemulsion formation and stability.

In the interfacial or mixed film theory, the interface is assumed to be a duplex film having different properties on the water-side and the oil-side. Formation of different types of microemulsions (water-in-oil or oil-in-water) depends on the bending or curvature of the interface (Schulman et al., 1959, Prince, 1977). In the solubilisation theory, microemulsions are considered as swollen systems, where one phase is solubilised by surfactants i.e. oil is solubilised by normal micelles and water is solubilised by reverse micelles (Shinoda & Friberg, 1975; Ahmad et al., 1974). Finally, according to the thermodynamic theory, the spontaneous formation of microemulsions can only be expected if the interfacial tension is so low that the remaining free energy of the interface is overcompensated by the entropy of dispersion of the droplets in the medium (Ruckenstein & Chi, 1975; Ruckenstein & Krishnan, 1979). Every molecular assembly, including microemulsions, theoretically organises itself so that the Gibbs free energy of the system is minimised. The Gibbs energy depends on the interfacial energy ($\gamma\ \Delta A$) and the change in entropy of the system upon droplet formation ($T\Delta S$):

$$\Delta G = \gamma \Delta A - T\Delta S \qquad \text{Eqn.1.1}$$

where γ is the interfacial tension, ΔG is the Gibbs free energy, ΔA is the surface area of the droplets, T is the temperature and ΔS is the entropy of the system. In microemulsions the Gibbs energy is transiently negative or almost equal to zero, due to the interfacial tension being extremely small given the high proportions of surfactant(s)/cosurfactant(s). A single surfactant lowers the interfacial tension but in most cases the critical micelle concentration (CMC) is reached before the interfacial

tension is close to zero, and therefore the addition of a second surfactant of a completely different nature is required. With the second surfactant (cosurfactant) the interfacial tension is further reduced, what causes the microemulsions to form spontaneously (Tadros, 2005, Kumar & Mittal, 1999; Lawrence & Rees, 2000).

1.4.2. Phase behaviour

The relationship between the composition and the phase behaviour can be deduced with the aid of a phase diagram (a typical example is presented in Fig. 1.3). Compositional variables can also be studied as a function of temperature and pressure although the large majority of microemulsions are studied under conditions of ambient pressure (Lawrence & Rees, 2000).

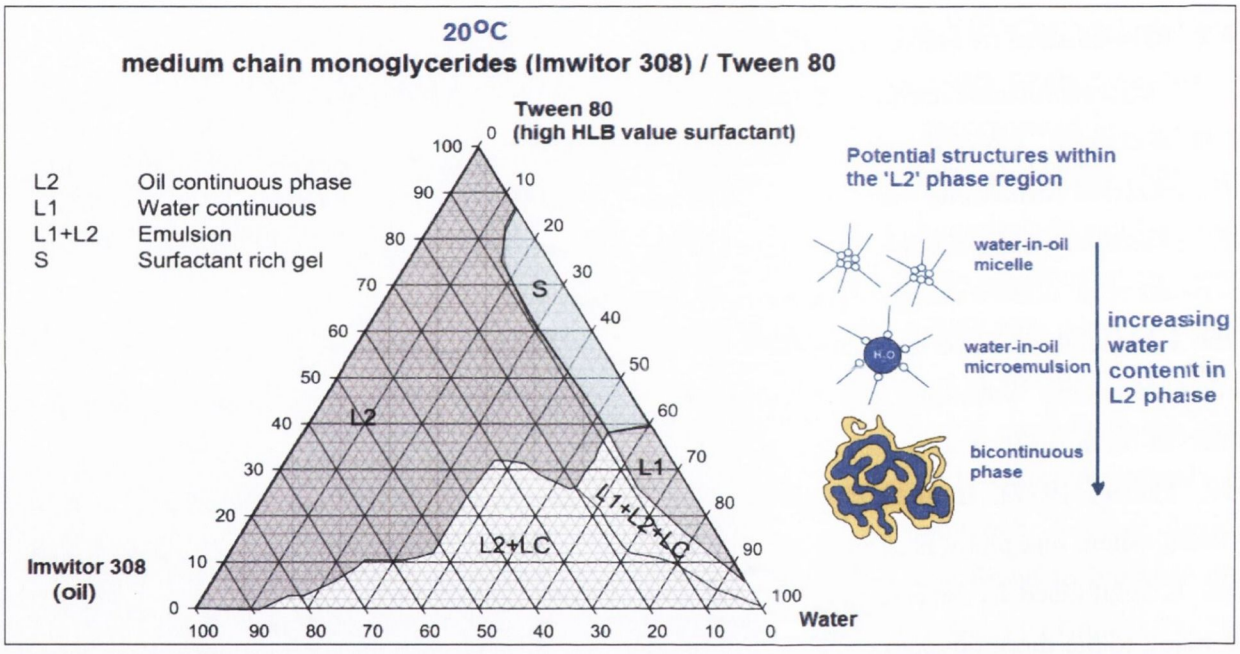

Fig. 1.3. A hypothetical ternary phase diagram representing three component system, in which Imwitor 308 was considered as the oil phase, Tween 80 as the surfactant and water as the hydrophilic phase (Pouton, 2007).

The phase behaviour of a basic microemulsion consisting of oil, water and surfactant is studied with a ternary phase diagram where each corner represents 100% of that particular component. In the case where four or more components are investigated, pseudoternary phase diagrams are used where one of the corners will typically represent a binary mixture of two components such as surfactant/cosurfactant, water/drug or oil/drug (Lawrence & Rees, 2000). A well-known classification system for microemulsions is that of Winsor (Winsor, 1948) who identified four general types of phase equilibria:

1) Winsor I, which indicates a surfactant-rich water phase that coexists with surfactant-poor oil phase (an oil-in-water microemulsion),

2) Winsor II , which indicates a surfactant-rich oil phase that coexists with surfactant-poor water phase (a water-in-oil microemulsion),

3) Winsor III, which represents the surfactant rich middle-phase that coexists with both water and oil surfactant-poor phases (a bicontinuous microemulsion) and

4) Winsor IV, which is a single- phase homogeneous mixture (Chevalier & Zemb, 1990; Kumar & Mittal, 1999).

The extent of formation of water-in-oil, oil-in-water and bicontinuous microemulsions, as well as formation of other structures upon dilution such as viscous gels, liquid crystalline phase and emulsions is studied within use of phase diagrams to enable scientists to design stable microemulsions and self-emulsifying systems with desirable dispersion behaviour. Outside the microemulsion region, multiple phases can exist simultaneously and the complexity of which increase with the number of components in a formulation. Emulsions, which are frequently formed once microemulsions or SELFs have been diluted with a high volume of water, are thermodynamically unstable which fundamentally differs them from microemulsions. Some of them could exhibit excellent kinetic stability, however they will eventually phase separate (Lawrence & Rees, 2000). Droplet size of emulsions would be typically in a range of 0.5 –5 microns (Bagwe et al., 2001). Formation of a liquid crystalline region upon dispersion from self-emulsifying lipid formulations can be considered as an undesirable effect if rapid emulsification of the system is required. According to Pouton (2000), at high surfactant concentrations, greater then approximately 65% depending on the materials, the progress of emulsification is compromised by viscous liquid crystalline gels (lyotropic liquid crystals), which form at the oil-water interface. These mixtures require energy to break up and in practise are not self-emulsifying systems (Pouton, 2000). In order to eliminate formation of liquid crystals upon dispersion, cosurfactants and cosolvents are added to promote emulsification of the system. Formation of liquid crystals (LC) is mainly related to the properties and concentration of the primary surfactant. Surfactants that have anisotropic shape (e.g. are elongated) and have a fairly good rigid backbone containing double bonds (what defines the long axis of the molecule) are likely to form liquid crystalline structures in aqueous solutions (Andrienko, 2006). Liquid crystals can be considered as an intermediate state of a matter in between the liquid and the crystal (solid form). LCs must possess some typical properties of liquids e.g. fluidity, formation and coalescence of droplets, as well as some properties of crystals e.g. anisotropy in their optical, electrical, and magnetic properties and the periodic arrangement of molecules in one spatial direction, etc. (Andrienko, 2006). Because of their ability to rotate polarised light, liquid crystals are visible when placed between crossed polarisers and this provides a useful means of detecting the liquid crystalline state. The formation of the two main types of liquid crystalline assemblies which are lyotropic and thermotropic is related the concentration of the surfactant (the concentration of the solvent) and heat respectively. Formation of lyotropic liquid crystals is mainly affected by the concentration of the solvents but can be also

affected by temperature at the same time (Stegemeyer, 1994). The typical crystalline phases distinguished for lyotropic crystals are hexagonal, cubic and lamellar. Because some types of micelles, change their structure from spherical to cylindrical to lamellar with an increase in the surfactant concentration, hexagonal phases are usually encountered at a lower surfactant concentration than lamellar phase (Rosen, 2004; Stegemeyer, 1994). Thermotropic liquid crystals are generally recognisable as one of three principal types: smectic, nematic or cholesteric (chiral nematic) (Andrienko, 2006; Van Hecke et al., 2005). Liquid crystals observed upon dispersion of SELFs are mainly lyotropic. However when non-ionic surfactants are used, which show temperature dependent solubility in water, both the concentration of the surfactant and the temperature will affect the formation of these assemblies. LCs have found use in stabilizing many pharmaceutical dosage forms including simple and multiple emulsions, creams, and gels (Alany et al., 2001) but they have not been utilised in encapsulated dosage forms intended for oral, rapid delivery.

1.4.3. Factors affecting formation of microemulsions

The formation and stability of a microemulsion can be affected by various factors, including nature and molecular weight of the primary surfactant and cosurfactant, salinity and temperature (Kumar & Mittal, 1999). One of the most critical factors affecting formation of the microemulsion is the choice of a primary surfactant. Attempts have been made to rationalise surfactant behaviour in terms of the hydrophile–lipophile balance (HLB), as well as the critical packing parameter (CPP). Both approaches are fairly empirical but can be a useful guide to surfactant selection (Lawrence & Rees, 2000). The CPP is a measure of the preferred geometry adopted by the surfactant, and as a consequence is predictive of the type of aggregate that is likely to form (Israelachvili et al., 1976). Theoretically, a CPP value less than 1/3 corresponds to spherical micelles, between 1/3 and 1/2 corresponds to rod-like micelles and between 1/2 and 1 to a planar structure (Israelachvili et al., 1976). Changes in a microemulsion composition (e.g. the presence of a cosurfactant and cosolvents) will modify the microenvironment of the surfactant, which leads to changes in the apparent CPP of the surfactant. The concept of HLB (Hydrophilic-Lipophilic Balance) was introduced by Griffin in 1949, but subsequently Davies et al. (1959) offered a general empirical equation to calculate it. The HLB takes into account the relative contribution of hydrophilic and hydrophobic fragments of the surfactant molecule. It is generally accepted that low HLB (3 – 6) surfactants are favoured for the formation of water-in-oil microemulsions whereas surfactants with high HLB (8 – 18) are preferred for the formation of oil-in-water microemulsion systems (Tadros, 2005). The chain length, the type and the nature of a cosurfactant or a cosolvent also affect the formation of microemulsions. Addition of shorter chain alcohols promotes formation of o/w type of microemulsion, while longer chain alcohols favours w/o type by alcohol swelling more in the chain region than the head region of a surfactant (Moulik

& Paul, 1998). Any material present in a formulation may influence the solubility properties of the aqueous and oily phases due to its partitioning between these phases. It has been suggested that some oils, for example the ethyl esters of fatty acids, also act as 'cosurfactants' by penetrating the hydrophobic chain region of the surfactant monolayer (Lawrence & Rees, 2000). Temperature plays an important role in determining the effective head group size of nonionic surfactants. Microemulsions stabilised by non-ionic surfactants, especially these based on polyoxyethylene are very susceptible to temperature because a decrease in surfactant solubility occurs with increasing temperature and as a result systems shows characteristic phase inversion temperature (PIT). The PIT of the microemulsion varies with the amount of oil present, the nature of the surfactant(s) (Lawrence & Rees, 2000). Microemulsions and self-emulsifying systems consisting of non-ionic components are in general not affected by the pH and/or ionic strength of the aqueous phase in the pH range between 3 and 10 (Constantinides, 1995).

1.4.4. Techniques to characterise the microstructure

The elucidation of the internal structure of a microemulsion, although important, can be very complex, and sophisticated physical techniques are required for this purpose. Of all the methods used, the Small-angle neutron scattering (SANS), Small-angle X-ray scattering (SAXS), DLS (Dynamic light scattering), Cryogenic transmission electron microscopy (cryo-TEM), Freeze-fracture transmission electron microscopy (FF-TEM) and Pulsed-field-gradient spin-echo nuclear magnetic resonance (PGSE-NMR) methods are most important and they can provide complementary data on microemulsion structure (Paul & Moulik, 1997). Other methods, i.e. conductance, viscosity, ultrasonic interferometry, ultrasonic absorption, dielectric permittivity, thermal conductivity, transient electrical birefringence, infrared spectroscopy, calorimetry, etc., are also frequently employed for the understanding of the internal physicochemical states of microemulsions (Paul & Moulik, 1997). This section will briefly present three techniques such as cryo-TEM/FF-TEM, PGSE-NMR and SANS which were later on employed to characterise model microemulsion.

1.4.4.1. Cryogenic transmission electron microscopy (cryo-TEM) and Freeze-fracture transmission electron microscopy (FF-TEM)

In the cryogenic transmission electron microscopy (cryo-TEM), direct imaging at high resolution of a vitrified sample is performed. The produced specimen needs to be thin enough (100-200 nm) to transmit a substantial portion of illuminating beam and any aqueous phase needs to be vitrified to prevent ice crystal damage which requires extremely fast cooling rates and sometimes addition of cryoprotectants (e.g. dextran, glycerol, etc.). Typical cryogens are liquid gases: helium, nitrogen, propane, hydrogen, freons. Slow cooling rates result from the use of cryogens with poor heat-transfer capabilities and immersion techniques that contact the sample too slowly with the

cryogen, e.g., hand-plunging. Slow cooling rates cause undesirable effects such as phase separation, crystallization which alters the physical structure of the original sample. In the cryo-TEM, the specimens are viewed in the cold microscope. The advantage of this method is that no replica of a frozen sample is needed (where sometimes it is difficult to avoid artifacts) and hence the system can be imaged directly. The weak points are the extreme sensitivity of the sample to beam damage, which requires the use of a 'low-dose beam' mode giving lower image resolution (Kumar & Mittal, 1997). Another disadvantage for samples lacking sufficient contrast (when the structure that should be imaged has a low contrast with respect to the bulk) is addition of stains that can alter the original self-assembled structure. A variation of the cryo- TEM technique is FF-TEM. In the freeze-fracture transmission electron microscopy (FF-TEM), a liquid specimen is rapidly frozen and fractured. The fractured surface is mirrored by coating with platinum and subsequently the platinum coat is reinforced with carbon. The created metal replica can be imaged by TEM at room temperature. This method is especially useful in the case of highly viscous samples (Kumar & Mittal, 1999).

1.4.4.2. Pulsed-field-gradient spin-echo nuclear magnetic resonance (PGSE-NMR)

Pulsed-field-gradient spin-echo NMR (PGSE-NMR) is a well-established method for studying diffusive molecular motions in isotropic liquids. This method measures molecular motion via the attenuation of a spin-echo signal. This paragraph will briefly present the main principle of PGSE-NMR without detailing all mathematical conversions and propagations carried out to calculate the final diffusion coefficient of studied molecules. Many nuclei (such as ^{1}H, ^{2}H and ^{13}C) have a magnetic moment and in effect behave like little magnets (ignoring some of the more subtle points in quantum mechanics). The strength of the nuclear magnetism decreases as the mass of the nucleus increases thus the most NMR sensitive nucleus is the proton (^{1}H). A sample in macroscopic view is composed of a number of nuclei on the order of Avogadro's number. Normally the magnetic moments of the nuclei are distributed randomly. If the sample is placed in a strong magnetic field the magnetic moments of the nuclei will have a preference to align along the field in the same manner that a compass needle has a preference to align north (the preference is slight as the molecules are all in thermal motion). The PGSE-NMR technique is based on spatial encoding of the Larmor frequency by applying a strong magnetic field gradient to a studied sample. Coherent transverse nuclear magnetization is transformed ('encoded') into a well-defined spatial structure, a helix. The process that formed the helix is then reversed, and the coherent transverse magnetization is recovered and measured. The greater the diffusion during the 'pulse time' is, the less successful the restoration and therefore, the smaller the resulting NMR signal. The spatial encoding and decoding of the magnetization in diffusion experiments is normally performed as part of a modified spin-echo pulse sequence (normally a Hahn-echo or stimulated-echo) (Paul & Moulik, 1997; Price, 2005; Yadav & Price, 2007). In the simplest version, PGSE-NMR experiment

consists of two equal and rectangular gradient pulses of magnitude g and length δ, sandwiched on either side of the 180° rf pulse in a Hahn echo experiment, the PGSE sequence is shown in Fig. 1.4.

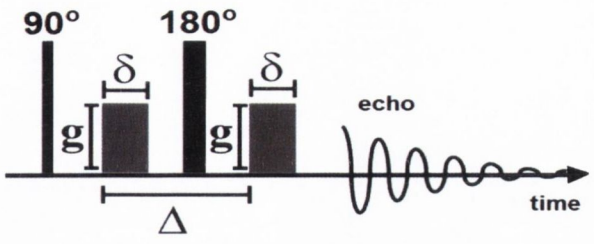

Fig. 1.4. The pulsed spin-echo pulse sequence: 90° and 180° are the two rf pulses. Two field gradient pulses of magnitude g, duration δ, and separation Δ are applied before and after the 180° refocusing pulse. The second half of the spin is Fourier transformed, and the relative intensities of the resolved absorption peaks are measured (Kumar & Mittal, 1999).

For molecules undergoing free diffusion characterised by a diffusion coefficient D, the echo attenuation due to diffusion is given by:

$$I(\Delta,\delta,g) = I_0 \exp[-\gamma_{mr}{}^2 g^2 \delta^2 (\Delta - \frac{\delta}{3})D] \qquad \text{Eqn. 1.2}$$

where Δ represents the distance between the leading edges of the two gradient pulses, γ_{mr} is the magnetogyric ratio of the monitored spin, I_0 denotes the echo intensity in the absence of any field gradient. By varying $g\delta$ or Δ (while at the same time keeping the distance between two rf pulses constant), D is obtained by fitting Eqn. 1.2 to the observed intensities (Price, 2007; Kumar & Mittal, 1999). The diffusion coefficient that can be measured with the PGSE method covers the range from the fast diffusion of small molecules in solutions with D typically around 10^{-9} m^2/s to very slow diffusion of polymers in the semidilute concentration regime, where D values down to 10^{-16} m^2/s can be measured (Kumar & Mittal, 1999).

1.4.4.3. Small angle neutron scattering (SANS)

SANS method can provide detailed structural information over the whole range of dimensions 1-1000 nm. The SANS analysis of microemulsions is capable of showing polydispersity of the droplet size, shape and their fluctuations (Paul & Moulik, 1997). The technique requires a neutron source, i.e. a nuclear reactor or an accelerator based spallation source and therefore the experiments are performed at large scale facilities. During a SANS experiment a beam of neutrons is directed at a sample and the neutrons are elastically scattered by changes of refractive index on a nanometer scale inside the sample (due to the interaction of the beam with the nuclei of the atoms present in the sample). The neutrons interact with the nuclei in the sample and the extent of the interaction depends on the isotope. The scattering vector (sometimes called momentum transfer) (Q) is the modulus of the resultant between the incident and scattered wavevectors (see Fig. 1.5) and is expressed as:

$$Q = / k_f - k_i / = \frac{4\pi n}{\lambda} \sin(\theta / 2) \qquad \text{Eqn. 1.3}$$

where k_i is the incident beam, k_f is the scattered beam, λ is the neutron waive length and θ is scattering angle.

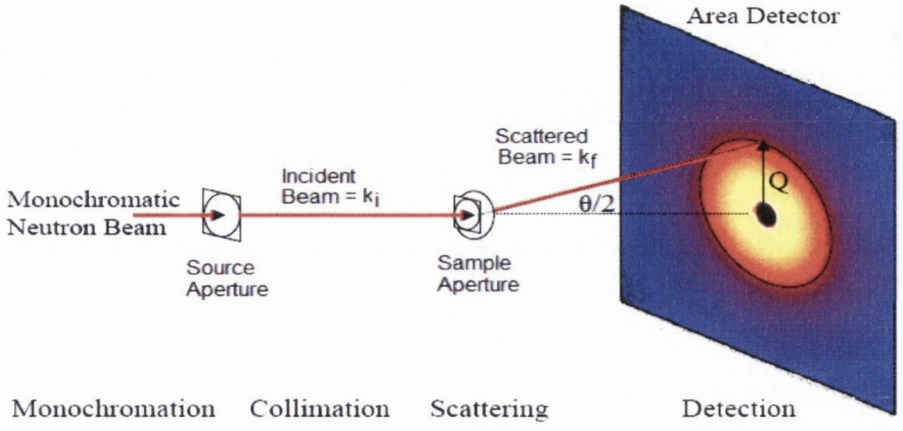

Fig. 1.5. Neutron scattering path in the SANS technique.

In a SANS experiment, the differential cross-section is measured, which contains all the information on the shape, size and interactions of the scattering bodies (assemblies of scattering centres) in the sample. The scattering cross section is a measure of how "big" the nucleus appears to the neutron and thus how strongly neutrons will be scattered from it.

The differential cross-section ($\frac{\partial \sigma}{\partial \Omega}(Q)$) is given by:

$$\frac{\partial \sigma}{\partial \Omega}(Q) = N_p V_p^2 (\Delta \delta_n)^2 P(Q) S(Q) + B_{inc} \qquad \text{Eqn. 1.4}$$

where N_p is the number concentration of scattering bodies (given the subscript "p" for "particles"), V_p is the volume of one scattering body, $(\Delta \delta_n)^2$ is the square of the difference in neutron scattering length density, $P(Q)$ is a function known as the form or shape factor, $S(Q)$ is the interparticle structure factor, Q is the scattering vector and B_{inc} is the (isotropic) incoherent background signal. The difference in scattering length density (δ) values between that part of the sample of interest, and the surrounding medium or matrix is called the contrast. A 'SANS pattern' from a multi-component sample is essentially a contrast-weighted summation of the SANS from each individual component. The technique of contrast matching can be used to dramatically simplify the scattering pattern. By changing the isotopic composition of the components (e.g. using deuterated oil and H_2O-D_2O) once can match the scattering lengths density of the various components (e.g. by matching δ of the water core with that of then oil, the scattering from the surfactant "shell" can be investigated). The equations used to calculate the form factor, P(Q) (according to Van de Hulst's

equation) and the interparticle structure factor, S(Q) are not presented in this review and can be found in the literature published by King (1999).

1.5. Solid microemulsions and solid self-emulsifying systems

Development of solid microemulsions (S-MEs), solid self-emulsifying drug delivery systems (S-SEDDSs) and solid self-microemulsifying drug delivery systems (S-SMEDDSs) have been extensively exploited in recent years, as they frequently represent more effective and stable alternatives to conventional liquid forms (Tang et al., 2008). The main techniques for transforming liquid and semi-solid lipid-based formulations into solid particles or granules are presented in Table 1.8 together with potential advantages and disadvantages of each technique with respect to the lipid content and the drug loading.

Table 1.8. Considerations in selection of solidification techniques with lipid-based excipients (Jannin et al., 2008).

Formulation techniques for solid and semi-solid formulations	Physical property of the lipid excipients applied		Formulation advantages and limits	
	Liquid	Semi-solid to Solid	Maximum lipid exposure‡ (% w/w)	Maximum drug loading‡ (% w/w)
Spray-cooling		X	99	30
Spray-drying	X	X	60	50
Adsorption on solid carrier	X		80	10
Melt granulation		X	50	80
Melt extrusion		X	50	60
Supercritical fluid based methods		X	99	20
Solid lipid nanoparticles	X	X	99	50

‡Percentage calculated after evaporation of solvent whenever applicable.

Adsorption onto solid carriers is one of the solidification techniques that can produce free flowing powders from liquid lipid formulations. The adsorption process is simple and involves addition of the liquid formulation onto the carrier of choice by mixing in a blender. The carriers used for this purpose, should be selected for their ability to adsorb a great quantity of liquid excipients and for the flowability of the mixture after adsorption if the created S-ME/S-SELF is intended for direct capsule filling or compression. A significant benefit of the adsorption technique is good content uniformity as well as the possibility for high lipid exposure (Jannin et al., 2008).

1.5.1. Techniques to characterise solid adsorbents

Adsorption onto solid carriers requires the selection of a suitable solid adsorbent. Properties such as particle size, specific surface area, pore size, and pore size distribution together

with the particle morphology, are mainly responsible for high adsorptive capacity of solid carriers. Additional complementary characterisation (e.g. TGA, DSC, pH measurements, PXRD, FTIR) can be performed to gain information on potential chemical compatibility and stability of the adsorbent with the liquid adsorbed formulation. The principles of particle sizing and determination of surface area will be briefly presented in this paragraph since these techniques provide the most critical characterisation of solid carriers.

1.5.1.1. Laser diffraction to determine particle size

Laser diffraction is an ensemble particle-sizing technique, which means it provides a result for the whole sample, rather than building up distributions from data for individual particles, in the way that, for example, image analysis or microscopy does. In laser diffraction particle size analysis, a representative cloud or 'ensemble' of particles passes through a broadened beam of laser light which scatters the incident light onto a Fourier lens. This lens focuses the scattered light onto a detector array and, using an inversion algorithm, a particle size distribution is inferred from the collected diffracted light data (Virden, 2010). As particle size decreases, the observed scattering angle increases logarithmically. Large particles therefore scatter light at narrow angles with high intensity whereas small particles scatter at wider angles but with low intensity (MRK1399 technical note). With the application of an appropriate model of light behaviour, the particle-size distribution of the sample can be determined from the scattering data, via a deconvolution step. The Mie and Fraunhofer theories are used routinely although the Mie theory is a preferred model for wide dynamic range measurements, since it gives improved accuracy for small particles compared to the Fraunhofer theory (MRK1399 technical note). Nevertheless, both models assume that the measured particles are spherical, so for nonspherical samples the size distribution returned is one that is based on equivalent of sphere. A number of useful parameters are obtained from particle size measurements including D(10), D(50), D(90), D[4,3] D[3,2] and Span. D[3,2], called Surface Area Moment Mean (Sauter Mean Diameter) defines the diameter of sphere of equivalent surface area. D[4,3], Volume or Mass Moment Mean (De Brouckere Mean Diameter) is the diameter of sphere of equivalent volume. Span is calculated as the difference between D(90) (90% of tested particles shows the diameter smaller than this value) and D(10) (10% of tested particles shows the diameter smaller than this value) divided by D(50) (50% of tested particles shows the diameter smaller than this value). A high value of Span indicates broad particle size distribution (Technical note MRK0345, Mastersizer's technical instruction).

1.5.1.2. Specific Surface Area and Porosity

The physical adsorption of gases is the most frequent measurement used for determining specific properties of solids. Adsorption, in general, occurs whenever a substance (the adsorbate, such as an adsorbable gas) accumulates at an interface or in an interfacial region. If the adsorption

process involves only the weaker intermolecular forces that result from van der Waals interactions and if there is no significant change in the electronic orbital states of the interacting species then the process is called physical adsorption. Physisorption (physical adsorption) should not be confused with chemical adsorption (chemisorption). Chemical adsorption is an adsorption process in which significant chemical bonds are formed at the interface or in the interfacial region. Depending on the physical characteristic of materials, various adsorption profiles can be observed in the range of relative pressure from 0.05 to 1. Sing et al. (1985) divided adsorption isotherms into six categories and derived information on the material properties based on shape of these curves defining the following types: I - predominantly microporous structure, II – non-porous solids, III - both non-porous and microporous adsorbents, IV - the presence of mesoporosity, V - indicative of microporous or mesoporous solids, VI - extremely homogeneous, non-porous surfaces where the monolayer capacity corresponds to the step height. Sing et al. (1985) also classified pores according to their size in the following order: micropores (widths) less than 2 nm, mesopores (width) between 2 nm and 50 nm and macropores (widths) above 50 nm, in order to create a consistent terminology for microporous, mesoporous and macroporous materials. Gas adsorption technique is applied to measure the surface area of solid particles. The "specific surface area" is defined as the area of solid surface per unit mass of material. In practice, what is actually determined is the accessible (or detectable) area of solid surface per unit mass of material. The specific surface area is evaluated using Stephen Brunauer, Paul Hugh Emmett and Edward Teller theory (Brunauer et al., 1938) where the main BET equation is:

$$\frac{p/p_0}{n_a(1-(p/p_0))} = \frac{1}{n_m C} + \frac{C-1}{n_m C} * \frac{p}{p_0} \qquad \text{Eqn. 1.5}$$

where n_a is the weight of adsorbed gas (nitrogen is the most commonly used) at a given p/p_0 which is the equilibrium in the saturation pressure of adsorbate at the temperature of adsorption, and n_m the weight of gas to give monolayer coverage and C- a constant that is related to the heat of adsorption. A linear relationship between $1/n_m[(p_0/p)-1]$ and p/p_0 is required to obtain the quantity of gas adsorbed. This linear portion of the curve is restricted to a limited portion of the isotherm, generally between 0.05-0.30.

De Boer et al. (1966) proposed a model to investigate porosity using the thickness of an adsorbate. Multi-layer formation is modelled mathematically to calculate a layer "*thickness, t*" as a function of increasing relative pressure (p/p_0). The resulting t-curve is compared with the experimental isotherm in the form of a t-plot. That is, the experimental volume adsorbed is plotted versus statistical thickness for each experimental p/p_0 value typically in the range 0.2 – 0.5. The linear range lies between monolayer and capillary condensation. The slope of the t-plot (V/t) is equal to the "external area", i.e. the area of those pores that are not micropores. Mesopores, macropores and

the outside surface are able to form a multilayer, whereas micropores, which have already been filled, cannot contribute further to the adsorption process (De Boer et al., 1966).

1.5.2. Techniques to characterise solid microemulsion and solid self-emulsifying systems

Physical properties of solid microemulsions (S-ME) and solid self-emulsifying lipid systems (S-SELFs) will vary depending on the preparation method used to create them. Characterisation techniques adequate for each 'type' of S-MEs/S-SELFs are not clearly given in the literature and need to be identified by scientists developing these systems. In case of solid systems formed by adsorption onto solid carriers, the difference in the behaviour of non-loaded and loaded particles will be determined by physical characteristics of the solid carrier and how the liquid is deposited into the particles during adsorption process. Therefore, it would be useful to monitor physical properties such as flow, density, shear rate, as a function of the amount of the liquid adsorbed. Observing these properties during a gradual adsorption process will help not only to determine the transition from powder into a paste state (end of adsorption and beginning of agglomeration) but also to characterise flowability and density of the final S-SELFs prior to further processing these into the final dosage form such as capsules and/or tablets.

Changes in flow behaviour, density and behaviour under shear stress as a function of 'progressing adsorption' process could be measured by powder rheometery. This paragraph will briefly summarise principles of powder- rheometric methods that can be employed to establish the end of adsorption with the use of FT4 powder rheometer (Chapter 2, section 2.8.3). Basic Flowability Energy (BFE), Flow Rate Index (FRI), Stability Index (SI), Specific Energy (SE) are the measurement methods which use a standard FT4 blade. Prior to each measurement (and each individual testing cycle), a studied sample is conditioned to eliminate the influence of random distribution of particle in the samples and remove any 'processing history' so that extremely reproducible baseline measurements can be generated for aerated, conditioned and consolidated samples. After conditioning, the 'split mass' is obtained which subsequently can be used to calculate Conditioned Bulk Density or can be used to correct measured parameters with the bulk density of the sample. During testing, the rotational and axial forces acting on a helical blade are measured as the blade passes through a sample and the measured energy required to 'pass through the sample' is defined as 'Energy Test' or 'Energy Cycle'. The Helix Angle and Blade Tip speed are specific for each measurement method and define the angle at which the blade approaches the powder and the rate at which it moves through it. Each measurement method is based on the fixed number of full cycles. Each full cycle consist of one testing cycle and one conditioning cycle. 'Energy Test' or 'Energy Cycle' is measured during a testing or conditioning cycle and reflects the energy required to perform a required motion (e.g. downward traverse movement of a blade), which is strongly influenced by the powder properties. The measurement of Shear Stress requires

the use of shear assembly (shear head and shear cell) and is carried out in a series of individual cycles (typically five) where the shear head moves in a conditioned and 'mass split' sample in two directions. Combining dynamic measurement with bulk properties and shear properties measurements allows the characterisation of powders in a range of complementary ways.

1.5.2.1. Basic Flowability Energy (BFE)

The Basic Flowability Energy (BFE) can be regarded as a measure of the powder rheology. It is measured as 'Energy Test' (Eqn. 1.6) and corresponds to the energy needed to displace a conditioned powder sample during downwards testing at specific consolidating conditions (Freeman, 2007). The flow pattern established during the BFE test is a downward anticlockwise motion (Fig. 1.6). This ensures the powder is pushed forwards and downwards in front of the blade, in a relatively high stress flow mode. The resulting resistance to flow is dependant on the many physical properties such as particle size, shape, density, etc. and the way in which they interact. The Basic Flow Energy can correspond to 'Energy Test 1' during a single full cycle for stable powders, or 'Energy Test 7' in a measurement that consists of multiple full cycles for unstable powders (typically seven or eleven full cycles are performed). 'Energy Test' is measured in the testing cycle as the blade moves downwards to the bottom of the vessel. Once the bottom has been reached, the blade retracts to the surface of the powder. In the multiple cycle measurement, subsequently a conditioning cycle is performed and the blade moves into the powder sample again to perform another testing cycle (another 'Energy Test' is measured again). Since one conditioning step may be insufficient to eliminate random packing of particles in the unstable powders, the BFE is measured after several repeated testing and conditioning cycles. BFE is calculated according to the equations:

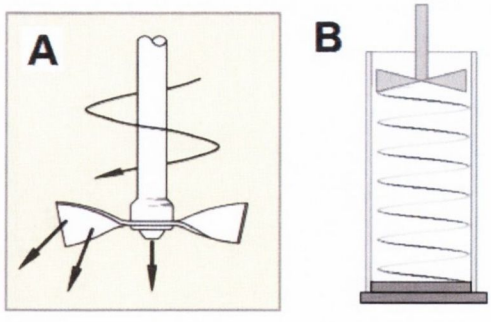

BFE for stable powders = Energy Test 1 or
BFE for unstable powders = Energy Test 7

Eqn. 1.6

Fig. 1.6. The blade (A) moving through the powder sample (B) from the top of the vessel to the bottom, i.e. during the downward traverse (BFE measurement).

It is often assumed that a low BFE represents a powder with "good" flow properties and a powder with a high BFE will flow poorly. In many cases this is true, particularly if the difference between powder samples is due to particle surface texture or amount of flow additive. However, the

opposite can also be true, where powders that flow freely under gravity result show a high BFE and powders that are cohesive show a low BFE (Freeman, 2007).

A Stability Index (SI) should be calculated to decide which 'Energy Test' should be used as the BFE (Eqn. 1.6). A Stability Index is a factor by which the measured flow energy changes during repeated testing or processing:

$$Stability\ Index\ (SI) = \frac{Energy\ Test\ 7}{Energy\ Test\ 1} \qquad \text{Eqn. 1.7}$$

Small changes ($0.9 < SI < 1.1$) are normal for most powders and are to be expected. SI values above 1 may indicate de-aeration, agglomeration, segregation, moisture uptake or electrostatic charge. SI values below 1 may be caused by attrition, de-agglomeration, over blending of an additive or coating of the vessel by additive (Freeman Technology, work instructions).

A Flow Rate Index (FRI) is the factor by which the flow energy is changed when the flow rate (tip speed) is reduced by a factor of 10 (Freeman, 2007) and is calculated using the following equation:

$$Flow\ Rate\ Index\ (FRI) = \frac{Energy\ Test\ 11}{Energy\ Test\ 8} \qquad \text{Eqn. 1.8}$$

The typical range of FRI for most of powders is from 1.5 to 3.0. Very cohesive powders would exhibit a FRI above 3. A FRI value round 1 could be obtained from measurements of large, granular materials that flow relatively well (Freeman Technology, work instructions).

1.5.2.2. Specific Energy (SE)

The Specific Energy (SE) can be defined as the energy per gram needed to displace a conditioned powder during upwards testing using a negative 5° helix (Fig. 1.7) (Freeman, 2007). The SE is calculated from the average energy of the upwards traverses of conditioning cycles 6 and 7, then divided by the split mass of the sample:

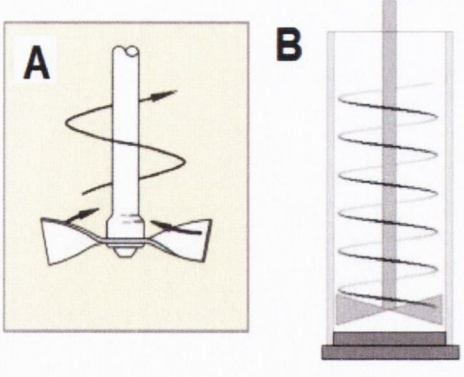

$$SE = \frac{(Up\ Energy\ Cycle\ 6 + Up\ Energy\ Cycle\ 7)/2}{Split\ Mass} \qquad \text{Eqn. 1.9}$$

Fig. 1.7. The blade (A) moving through the powder sample (B) from the bottom of the vessel to the top, i.e. during upward clockwise motion (SE measurement).

The Split Mass is defined as a weight of the conditioned sample, which takes a known volume in the testing cylinder. The SE measurement is a carried out in a sequence of testing and conditioning cycles (seven or eleven of full cycles). 'Up Energy Cycle 6 and 7' are measured in the conditioning cycles as the blade moves from the bottom of the vessel to the surface of the powder. Unlike the BFE measurement, where bulk compressibility can significantly contribute to the measured flow energy, the SE mostly relates to cohesion and other physical properties like particle size, shape and texture of particles in the studied sample. As a general rule, the higher the SE, the more cohesive the powder is. SE value below 5 would indicate low cohesion, SE between 5 and 10 denotes powders with moderate cohesion and SE above 10 indicated highly cohesive powders (Freeman Technology, work instructions).

1.5.2.3. Conditioned Bulk Density (CBD)

The Conditioned Bulk Density (CBD) can be defined as bulk density of conditioned powder. Conditioning is a gentle disturbance of the powder sample to prepare for testing using a slicing helix downwards and a lifting helix upwards (Freeman, 2007). Conditioned Bulk Density is measured prior to each test and calculated using the split mass:

$$\textit{Conditioned Bulk Density (CBD)} = \frac{\textit{Split Mass}}{\textit{Split Volume}} \qquad \text{Eqn. 1.10}$$

1.5.2.4. Shear Stress (SS)

Shear properties are important for understanding how easily a previously at rest, consolidated powder will begin to flow. Measurements of shear properties will provide important information as to whether the powder will flow through the process or whether bridging, blockages and stoppages are likely. During the Shear Stress test, the powder sample is first conditioned to achieve a homogeneous reproducible state, a 'split mass' is obtained and then the sample is slowly pre-compacted by applying the pre-shear normal load to allow the entrapped air to escape. The consolidated sample is pre-sheared to achieve a critical state, after which the normal stress is lowered, and the sample is sheared further to obtain a yield point. The rotational shear cell module consists of a vessel containing the powder sample and a shear head to induce both vertical and rotational stresses. The shear head moves downwards inserting the blades into the powder and induces a normal stress as the shear head face contacts the top of the powder. The shear head continues to move downwards until the required normal stress (σ) is established. Slow rotation of the shear head then begins, inducing a shear stress (τ) (Fig. 1.8.A).

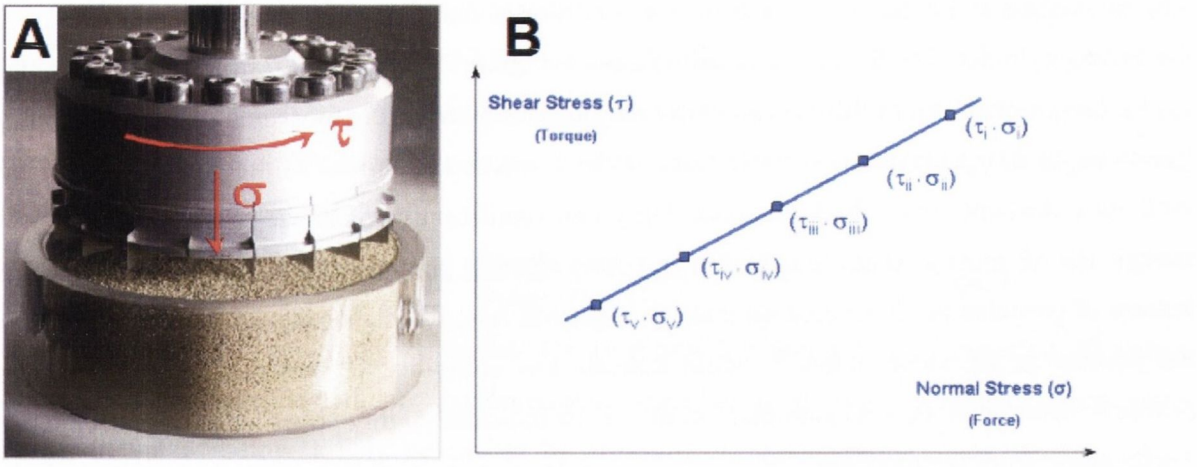

Fig. 1.8. Shear Stress (SS) measurement. A) shear head with marked direction to induce normal (σ) and shear (τ) stress. B) Typical Yield Loci obtained by plotting normal and shear stress.

As the powder bed resists the rotation of the shear head, the shear stress increases until the bed fails or shears, at which is time a maximum shear stress is observed. The normal stress is maintained constant throughout the shear step. This maximum shear stress is the point of Incipient Failure or the yield point. Plotting each of the incipient failure points against their corresponding normal stresses allows construction of the yield locus. The pre-shear/shear sequence is typically repeated five times to obtain a yield locus (Fig. 1.8.B). For each measurement of incipient failure, the shear head starts from zero shear stress, having previously rotated backwards to reduce the shear stress to zero from the previous shear step. For some materials, the repeated consolidation of the sample can change slightly during a series of shear measurements. Pro-rating is used to compensate for this situation by recalculating (correcting) the shear stress for each test point achieved using average of pre-shear shear stresses and measured pre-shear shear stress preceding shear step which makes the results of each cycle more precise and unaffected by the previous cycle (Freeman et al., 2009). Each yield locus could be analyzed using Mohr stress circle analysis to obtain the values of major principal stress, unconfined yield strength and cohesion if required (Vasilenko et al., 2011).

1.6. Aims of the experimental work

Chapter 1 briefly presented main terminology, formulation development and various characterisation techniques used with microemulsions and self-emulsifying systems. The experimental work undertaken in this research aimed to develop stable microemulsions and self-emulsifying systems with hydrophilic compounds, which would be suitable for encapsulation. The work was divided into experimental parts to thoroughly explore properties of hydrophilic compounds (model drugs), properties microemulsions/self-emulsifying systems composed of glycerides and propylene glycol esters of caprylic/capric acids and a water-soluble surfactant Polysorbate 80 and any formulation dependencies (interactions, relationships) between these two key items.

Chapter 2

Materials and methods

Fujicalin SG (dibasic calcium phosphate anhydrous)	Fuji Chemical Industry Co, Ltd (Japan), *[intake of 214mg/kg for 14 days in rats showed no abnormalities]*
Glycerine	Riedel de Haën (Germany)
Heavy water (99.9 atom % D)	Sigma Aldrich (Ireland)
Hubersorb 600 (calcium silicate)	Huber Engineered Materials (USA) *[LD_{50} (rats) > 5000 mg/kg]*
Hydrochloric acid	Sigma Aldrich (Ireland)
Lipoid EPC, (>98%, lecithin)	Lipoid GmbH
Lutrol 400 (PEG 400)	BASF (Germany)
Lutrol 300 (PEG 300)	BASF (Germany)
Maleic acid	Sigma Aldrich (Ireland)
Methanol (HPLC grade)	Sigma Aldrich (Ireland)
Methylene chloride	Fischer Scientific (Ireland)
Neusilin US2 (magnesium aluminometasilicate)	Fuji Chemical Industry Co, Ltd (Japan) *[LD_{50} (rats) > 16 g/kg, LD_{50} (rabbits, dogs) > 10 g/kg]*
Pamidronic acid ((3-amino-1-hydroxypropane-1,1-diyl)bis(phosphonic acid))	Nivon Specialties (India)
Potassium bromide (FT-IR grade)	Sigma Aldrich (Ireland)
Sodium alendronate trihydrate (4-amino-1-hydroxybutylidene) bisphosphonic acid monosodium salt trihydrate)	Polpharma S.A (Poland)
Sodium borate	Sigma Aldrich (Ireland)
Sodium citrate dihydrate	Sigma Aldrich (Ireland)
Sodium chloride	Sigma Aldrich (Ireland)
Sodium hydroxide	Riedel de Haën (Germany)
Sodium taurocholate (≥95%, TLC)	Sigma Aldrich (Ireland)
Sodium oleate	Sigma Aldrich (Ireland)
Softgels size 22 (empty)	Catalent Inc. (France)
Sylysia 320 (silicon dioxide)	Fuji Sylysia Chemical Ltd (Japan) *[LD_{50} (mice) > 5000 mg/kg]*
Peceol (glyceryl monooleate)	Gattefosse (France)
Phosphoric acid	Sigma Aldrich (Ireland)
Phosphorus pentoxide desiccant	Fluka (Ireland)

Polysorbate 80 (polyoxyethylene (20) sorbitan monooleate)	Sigma Aldrich (Ireland) *[LD_{50} (rats) > 63.840 g/kg]*
Potassium dihydrogen phosphate	Riedel de Haën (Germany)
1,2 -Propylene Glycol Pharma (propylene glycol)	BASF (Germany)
Purified water	Purite Prestige Analyst HP, Millipore Elix 3 (UK)
Trifluoroacetic acid	Sigma Aldrich (Ireland)
Zeofree 5161 (silicon dioxide)	Huber Engineered Materials (USA) *[LD_{50} (rats) > 5000 mg/kg]*

* *LD_{50} or other toxicity data provided for main components of SELFs and solid carriers.*

2.1. Materials

Trade Name (chemical name)	**Manufacturer/ Supplier (Origin)** *[LD_{50} *]*
Acetic acid	Riedel de Haën (Germany)
Acetonitrile	Fischer Scientific (Ireland)
Acyline monoacetate	NeoMPS SA (USA)
Aeroperl 300/30 (silicon dioxide)	Evonik Industries (Germany) *[LD_{50} (rats) > 10000 mg/kg]*
Anhydrous dibasic sodium phosphate	Sigma Aldrich (Ireland)
Bacteriostatic Water, USP	Fisher Scientific (USA)
Capmul MCM (glyceryl mono-dicaprylate/dicaprate)	Abitec Corporation (USA) *[LD_{50} (rats) = 5 g/kg]*
Capmul MCM C8 (glyceryl mono-dicaprylate/dicaprate)	Abitec Corporation (USA) *[LD_{50} (rats) = 5 g/kg]*
Capmul MCM C10 (glyceryl mono-dicaprate)	Abitec Corporation (USA) *[LD_{50} (rats) = 5 g/kg]*
Capmul PG-8 (propylene glycol monocaprylate)	Abitec Corporation (USA) *[Repeated doses: 1000 mg/kg and 2500 mg/kg in dogs over 28 days were found non-toxic]*
Captex 355 EP/NF & Captex 355 (glyceryl tricaprylate/tricaprate)	Abitec Corporation (USA) *[LD_{50} (rats) > 36 ml/kg, LD_{50} (mice) > 25 ml/kg]*
Captex 200P (propylene glycol dicaprylocaprate)	Abitec Corporation (USA) *[LD_{50} (mice) = 5 g/kg]*
Citric acid	Sigma Aldrich (Ireland)
Crillet 4 HP (polyoxyethylene (20) sorbitan monooleate)	Croda Inc (USA) *[LD_{50} (rats) > 63.840 g/kg]*
Disodium pamidronate pentahydrate ((3-amino-1-hydroxypropylidne) bisphosphonic acid disodium salt pentahydrate)	Nivon Specialties (India)
Disodium hydrogen phosphate	Riedel de Haën (Germany)
Fat Red 7B (> 95%, *N*-Ethyl-1-((4-phenyldiazenyl)phenyl)diazenyl)naphthalen-2-amine)	Sigma Aldrich (Ireland)
9-Fluorenylmethyl chloroformate	Fluka (Germany)

2.2. Methods: Characterisation of Model Compounds

2.2.1. Synthesis of monosodium pamidronate monohydrate

Monosodium pamidronate monohydrate was synthesized according to the preparation method shown in the patent WO03/053985A1. 1g of pamidronic acid (0.0425 mol) was suspended in 10 ml of water and mixed with 4.25 ml of 1M NaOH (0.0425 mol) to form a solution with the final pH of 4.3. The resulting clear solution was left to stand for an hour at room temperature, to crystallize a solid, which was subsequently filtered and dried in an oven at 45°C.

2.2.2. Solid state Fourier transform infrared spectroscopy (FTIR)

The three model compounds were analysed with the same FTIR method. Nicolet Magna IR 560 E.S.P. spectrophotometer equipped with MCT/A detector, operated by Omnic software version 4.1 was used to collect infrared spectra in range of 650-4000 cm^{-1}. Dehumidified potassium bromide (KBr) was used to prepare a disk with approximately 0.5% -1% of a sample. KBr disks were made by direct compression under 8 bar pressure for 1 minutes (Healy et al., 2008). Spectra were collected immediately after preparation of the disks.

2.2.3. Thermal analysis (Differential scanning calorimetry & Thermal gravimetric analysis)

The three model compounds were analysed with the same DSC procedure. DSC results were collected with Mettler Toledo DSC 821^e, operated by Mettler Toledo STAR^e software (version 6.10). Nitrogen was used as the purge gas. Approximately 3- 5mg of a sample was weighed into an aluminium pan. The aluminium pan was sealed with a lid and the lid was perforated to create three vent holes. DSC measurements were performed (in duplicate) in the temperature range from 25 – 300 (disodium pamidronate pentahydrate) and 25 - 350°C (sodium alendronate trihydrate) with the heating rate of 10°C/min.

TGA measurements of bisphosphonates were performed using a Mettler TG 50 unit, operated by Mettler Toledo STAR^e software (version 6.10) and connected to Mettler MT5 balance. Approximately 5-12mg of a sample was weighed into an aluminium pan or lid. Analysis was carried out (in duplicate) in the furnace under nitrogen purge and with the heating rate of 10°C/min, within the temperature range from 25 – 300 (disodium pamidronate pentahydrate) and 25 - 350°C (sodium alendronate trihydrate) (Tajber et al., 2005).

2.2.4. Powder X-Ray Diffraction analysis (PXRD)

Miniflex II Desktop X-ray diffractometer Rigaku was used to collect powder XRD scans for the bisphosphonates. The tube output voltage of 30 kV was used and tube output current was 15 mA. A Cu-tube with Ni-filter suppressing Kβ radiation was used. Measurements were taken from 5

to 40 on the 2 theta scale at a step size of 0.05° at room temperature (Tajber et al., 2009). Powder XRD analysis of acyline monoacetate was carried out by AAIPharma (USA) using automated powder Diffractometer Siemens D500. The measurements were taken from 2 to 40 on the 2 theta scale at a step size of 0.05° at room temperature.

2.2.5. Particle sizing by laser diffraction (PSD)

Measurements of particle size distribution for bisphosphonates were obtained using a laser diffraction particle sizer Mastersizer 2000 (Malvern Instruments, UK). A dry method, using a Scirocco dry feeder instrument and a micro-volume tray (2-10g) was used. Pressure/particle size titration experiments were carried out (Appendix, Fig. A.3.1 and A.3.2) to select an adequate dispersive pressure (Virden, 2010 and Jones, 2002) for each bisphosphonate. Dispersive pressures of 2 bar and 3 bar were selected for sodium alendronate trihydrate and disodium pamidronate pentahydrate respectively. The vibration feed rate from 40 - 50% was used. The General-purpose method with normal sensitivity was used to compute the mean particle size. Absorption Index of 0.1 and Refractive Index value of 1.52 (default) were used for both materials. Obscuration limit was set to 0.5 – 6%. Results for each sample were reported as an average of minimum three runs. A standard supplied by Malvern, made of calibrated glass beads, was measured prior to testing to verify the laser beam.

2.2.6. Isoelectric point (IEP)

Isoelectric point was determined in solutions of acyline with the concentration of 1mg/ml prepared in 0.1N HCl and 0.25N acetic acid. The solutions were prepared directly prior to measurements. Gradual titration of acyline solutions was performed using MPT-2 Autotitrator using 0.5N HCl, 0.1N NaOH and 0.5N NaOH as titrants. Continuous measurements of zeta potential in the titrated solutions were carried out with Zetasizer Nano ZS (ZEN 3600) from Malvern Instruments (UK) at 25 °C ± 0.5°C, A standard disposable zeta cell was used. The equipment was verified on zeta-standard of 50 mV ± 5mV prior to the measurements.

2.2.7. Aqueous solubility

Solutions of acyline monoacetate were prepared by 1) suspending the drug in a required medium, 2) gentle manual shaking of the suspension for approx 5 minutes, 3) leaving the sample at room temperature for next 24 hours. The content of acyline in non-gelled and gelled solutions was assayed by HPLC using a method developed by the Analytical Department, in Merrion Pharmaceuticals Ltd. The gelled and non-gelled samples were diluted with acetonitrile prior measurements. The details of the method are summarised below:

- HPLC System: Waters 2695 HPLC system equipped with a Waters 486 Tunable Absorbance detector

- Column: Grace Vydac 218TP54 C18 4.6 x 250 mm, 5 µm
- Column Temp: 25°C
- Inj. Vol: 10 µL
- Flow rate: 1.0 ml/min
- Detection: UV, 215 nm
- Mobile Phase A: 0.1 % trifluoroacetic acid (TFA) in Water
- Mobile Phase B: 0.1% TFA in Acetonitrile
- Acyline retention time: approx 11min
- Acyline working concentration = 0.1 mg/ml, Run Time = 35 min
- Gradient: 10 to 40 % B in 25 minutes

Time (min)	Flow Rate (ml/min)	% B
0	1	25
25	1	55
35	1	25

Solubility studies of bisphosphonates were carried in water and the modified K-McIlvaine's buffers. Sodium ion in the standard McIlvaine's buffers was replaced by potassium to avoid the common-ion effect. The modified K-McIlvaine's buffers were made by mixing solutions of 0.2 M dipotassium hydrogen phosphate and 0.1 M citric acid in the required ratio as shown in Table 2.1

Table 2.1. Composition of K-McIlvaine's buffers to prepare a final buffer volume of 20 ml.

pH measured	Volume (ml) of 0.2N K_2HPO_4 used	Volume (ml) of 0.1N citric acid used
pH 2.2	0.4	19.6
pH 4.4	8.82	11.18
pH 5.5	10.72	9.28
pH 6.8	14.55	5.45
pH 7.8	18.17	1.83

The glass vials with the suspended drug (approx 2.5 g suspended in 6 ml) were placed in a reciprocal shaking water bath Thermo Scientific model Precision. The temperature was set to 25 °C and the water bath was operated under 50 oscillations per minute for 24 - 48 hours. Following this the samples were filtered through 0.45 µm filters to obtain clear solutions and remove undissolved drug. Solubility of sodium alendronate trihydrate and disodium pamidronate pentahydrate was determined by a HPLC method based on the USP method for the determination of sodium alendronate in a raw material (sodium alendronate) and alendronic acid tablets. As per the method, derivatisation with 9-fluorenylmethyl chloroformate and extraction with methylene chloride were carried out. The details of the method are summarised below:

- HPLC system used was a Shimadzu HPLC Class VP series with a LC-10AT VP pump, autosampler SIL-10AD VP and SCL-10AVP system controller.
- Column: Hamilton PRP-1, 5 µm, 250 x 4.1 mm (USP L21 Packing)

- Column Temp: 35.0 °C
- Inj. Vol: 20 µL
- Flow rate: 1.0 ml/min
- Detection: UV, 266 nm
- Retention time: approx 3.5 min for alendronate and approx 3.2 min for pamidronate
- Run Time = 6 min
- Diluent: Sodium citrate dihydrate solution
- Mobile phase: Buffer /Acetonitrile/ Methanol (70:25:5) (filtered through 0.45 µm membrane filter before use)

Details of the calibration curves prepared are given in Appendix, Table A.3.1.

2.2.8. Solubility in the standard GIPET® II formulation and propylene glycol

Solubility of bisphosphonates and acyline monoacetate in the standard GIPET ® II formulation (composition given in Table 2.2) and propylene glycol was examined visually.

Table 2.2. Composition of the standard (non-aqueous) GIPET ® II formulations.

Ingredients	Chemical Names	% in formulation
Captex 355 EP/NF	caprylic/ capric triglyceride	5.5
Capmul MCM	glyceryl caprate/caprylate	55.0
Crillet 4HP/ Polysorbate 80	polyoxyethylene sorbitan monooleate	15.0
1,2 -Propylene Glycol Pharma	propylene glycol	5.0
Lutrol E 400	PEG 400	19.5

Acyline solutions were prepared by 1) suspending a known amount of the drug (milligrams) in a known amount of a medium (grams), 2) gentle, manual shaking (for approx 5 minutes), 3) leaving the sample at room temperature for next 24 hours. The solubility limit was examined visually. A clear solution indicated that the drug dissolved fully and therefore the solubility of the drug in this medium was at minimum equal to the concentration at which the sample was prepared. A solid material present in the sample after 24 hours indicated a lower solubility of the drug than the concentration at which the sample was prepared. The solubility limit of acyline monoacetate was determined in duplicates.

Solubility limit of bisphosphonates was evaluated by 1) suspending a known amount of the drug (milligrams) in a known amount of medium (grams) 2) placing the glass vials with the suspended drug in a reciprocal shaking water bath Thermo Scientific model Precision for 24 - 48 hours at 25°C (50 oscillations per minute), 4) examining visually the content of the glass vials. Presence of the solid powder in the glass vials indicated that the solubility of the drug was below the concentration at which the sample was prepared. A clear solution indicated the solubility at least equal to the concentration at which the sample was prepared. The solubility limit for

bisphosphonates was determined on duplicates. Solid material recovered after the study was dried at room temperature on a paper filter or in a desiccator filled with phosphorus pentoxide desiccant. The dry material was tested by DSC and TGA according the method described in section 2.2.3).

The content of propylene glycol in the solvate of alendronate was determined by gas chromatography – mass spectrometry (GC-MS) in the CMA (Centre for Microscopy and Analysis, TCD, Ireland). A known weight of each sample was placed in a glass vial to which 5 ml of deionised water was added. 1 µl of the solution was directly injected onto the GC-MS Varian Saturn 22700 column. Propylene glycol eluted at 17.5 minutes. The column used for the analysis was a WCOT fused Silica 60m x 0.32mm ID coating CP-SELECT 624 CB DF= 1.8.

2.2.9. Calculation of cLogP and cLogD

Calculation of cLogP for bisphosphonates was performed using ACD/ChemSketch (freeware) version 12.01, which estimates partition coefficient between water and octanol (at 25°C) based on the molecular structure. Algorithm used by ACD/cLogP function involves 1) structure fragmentation and assignment constants to estimate missing fragment by atomic increments similar to Ghose-Crippen (estimated constants), 2) assignment of implemented constants which are calculated for missing interfragmental interactions by polylinear expression similar to Hammett-Palm equation and 3) summation of the implemented and estimated constants (Mannhold et al., 2007). The application accurately predicts cLogP for simple organic molecules, but gives less reliable results for complex molecules such as peptide and proteins. Therefore cLogP for acyline was not calculated with this application.

The estimation of LogD (distribution coefficient between a buffer medium and octanol) and Charge/IEP (for acyline only) over the pH range of 0 - 14 were calculated using ChemAxon (Marvin) calculator. The estimation of these parameters is derived from their molecular structure. The calculator is available at http://www.chemaxon.com/marvin/sketch/index.php. The current algorithm is based on the method published by Viswanadhan et al. (1989), but was modified at several points based on the work of Klopman et al. (1994).

2.3. Methods: Characterisation of Microemulsion components

2.3.1. Thermal analysis (Differential scanning calorimetry & Thermal gravimetric analysis)

DSC measurements of oils and low HLB value surfactants were performed with a Metler Toledo DSC 821° operated by Metler Toledo STAR^e software (version 6.10) and equipped with a refrigerated cooling system. Nitrogen with a flow rate of 80 ml/min was used as purge gas. One drop (the weight between 10 to 20 mg) of liquid was weighted precisely into hermetic aluminum pans. An empty hermetically sealed pan was used as a reference (lids were not perforated).

Samples were cooled from 25°C to −20°C at a cooling rate of 10°C /min and then heated to 200°C at a heating rate of 10°C /min.

TGA measurements were performed using a Mettler TG 50 unit, operated by Mettler Toledo STAR^e software (version 6.10) and connected to Mettler MT5 balance. One drop (the weight between 10 to 20 mg) of liquid was used. Analysis was carried out in the furnace under nitrogen purge in the temperature range 25-200°C with the heating rate of 10°C/min.

2.3.2. Calculation of cLogP

Calculation of cLogP (partition coefficient between water: octanol) for individual components was calculated using ACD/ChemSketch (freeware) version 12.01.

2.3.3. Calculation of solubility parameter

Calculation of solubility parameter (δ) for individual components was calculated using online calculator available from Virtual Materials Simulation Center /Estimations Tools Collection (http://www.wag.caltech.edu/msc99/talks/p12/etukoE/SP/ourSP.htm). Smiles sequence, required as the input, was generated using ACD/ChemSketch (freeware) version 12.01 from the molecular structure.

2.3.4. Calculation of HLB value

Calculation of HLB for individual components was performed according to the equation below published by Pasquali et al. (2008):

$$HLB\ ester\ (a) = \frac{[Mr_{ester\ (a)} - a\ x\ Mr_{acid}]\ x\ 20}{Mr_{ester\ (a)}} \qquad \text{Eqn. 2.1.}$$

Mr ester (a) – Molecular weight of ester e.g. monoglyceride, diglyceride, triglyceride
Mr acid – Molecular weight of acid that the ester is made of
a – estrification number, e.g. 1 for monoglycerides, 3 for triglycerides

The average HLB value was calculated based on the percentage of each subcomponent in the material, wt% (according to the product specification) and its individual HLB value, according to the equation below:

$$Average\ HLB = \frac{(C_1\ x\ HLB_1) + (C_2\ x\ HLB_2) + (C_3\ x\ HLB_3) + (C_n\ x\ HLB_n)}{100\%} \qquad \text{Eqn. 2.2.}$$

HLB_1 – HLB_n – hydrophilic-lipophilic values calculated for individual components
C_1 – C_n – content of individual components in the material, expressed as the percentage of components in the material (100%).

2.3.5. Calculation of a combined HLB value

A combined HLB value was calculated based on the percentage of a surfactant in the blend (wt%) and its HLB value according to the following the equation which was also used by Owen et al. (1995):

$$Combined\ HLB = \frac{(C_L \times HLB_L) + (C_H \times HLB_H)}{100\%} \quad \text{Eqn. 2.3.}$$

HLB_L – hydrophilic-lipophilic value for the low HLB value surfactant

HLB_H – hydrophilic-lipophilic value for the high HLB value surfactants respectively

C_H – content of the high HLB value surfactant in the blend (100%), expressed as percentage

C_L – content of the high HLB value surfactant in the blend (100%), expressed as percentage

2.4. Methods: Construction of pseudoternary phase diagrams

The codes of phase ternary diagrams were introduced to easily identify difference between the studied systems. The main coding was based on combination of two digits and one letter, e.g. 1A2, 3B2, etc. The letter (in the middle) indicated the type of the system with 'A' standing for systems with the low combined HLB value while 'B' denoted the ones with the high HLB value. The first digit indicated the type of a cosurfactant used with 1) for Capmul MCM, 2) for Capmul MCM C8, and 3) for Capmul MCM C10. The last digit denoted the type of oil used with 1) for Captex 200P, 2) for Captex 355 and 3) for Capmul PG-8. For example, a system with the code 1A3 was formulated with Capmul MCM (as a cosurfactant), Capmul PG-8 (as the oil) and the system had a low HLB value. The system 3A3 would differ from the former one by a type of the cosurfactant. The codes with additional extensions such as T2, T3, T4 indicated systems that contained SEDDSs used in the preclinical study (termed as T2, T3, T4) or the systems that very closely resembled them. Only the Capmul MCM and Capmul MCM C10 were used as cosurfactants in the test items dosed in the preclinical study (Chapter 6, section 6.3.1) e.g. 1A3_T3 was the general system where one of preconcentrates was used to formulate the SEDDS T3.

2.4.1. Titration procedure

Pseudoternary phase diagrams were prepared using preconcentrates composed of the mix of the surfactants with oil in the following main ratios: 10: 90, 20: 80, 30: 70, 40: 60, 50: 50, 60: 40, 70: 30, 80: 20, 90: 10 w/w). The mix of surfactants was prepared with the cosurfactants that were melted at 55 - 60 °C and combined with Crillet 4 HP at the required ratio. The mix of surfactants was mixed thoroughly and allowed to equilibrate for 24 hours prior use. The required amount of the mix of surfactants and oil was weighed out in a jacketed beaker to form a preconcentrate. To each preconcentrate, gently stirred with a mixing bar using Heidolph magnetic stirrer, purified water was added drop wise and any visual change in the content of the beaker was

recorded. All dilutions were carried out at 37°C unless indicated otherwise. All components (oil, the mix of surfactants, water) were equilibrated at 37°C for 1 hour to ensure quick equilibration of temperature during dilution with water. Purified water was kept at 37°C during titration. Watson Marlow 101U/R was used to continuously circulate water (heated to 37°C on Precision water bath) through the jacketed vessel.

The phase diagrams were drawn based on the collected visual observation, by classifying samples according to various scales presented in detail in Table 2.3. As water was added, every change in visual appearance and behaviour (such as turbidity, opalescence, complete transparency, increase in viscosity, phase separation, etc.) was recorded and classified according to Transparency, Phase Behaviour and Visual Texture scales (Table 2.3). The amount of each component was known at phase transition points and recalculated as the % of the entire sample (water + oil + the mix of surfactants) to draw dilution curves. The visual assessment relays on the fact that once dispersed droplets are smaller than ¼ λ (ca.1400 Å, 140 nm) in diameter, white light can pass trough the dispersion and these systems appear transparent or slightly opalescent to the naked eye (Prince, 1977). All clear and very slightly opalescent, isotropic (based on microscopic observation) samples representing a 'green area' were classified as micelles/microemulsions because it is not possible to visually distinguish between true solutions, micelles and various types of microemulsions.

Opalescent but still clear and isotropic samples (light blue area) were considered as microemulsions as these were approaching the phase transition and therefore could not be micelles. A 'yellow area' represented clear but anisotropic (showing birefringence) samples which were considered to be liquid crystals. Hazy, turbid phases were represented as a 'grey area'. The detailed and full characterisation of the 'grey area' on the phase diagrams was not attempted. However, when anisotropy was detected within the 'grey field' and the region was substantial enough, it was distinguished as a separate turbid, liquid crystalline region ('brown area'). The dilution curves were visualized using Triplot 4.1.1 (freeware) to select boundary points demarking main phases.

Table 2.3. Phase behaviour scales developed for evaluation of titrated samples and boundary points.

Transparency Scale

C1 – Clear, transparent mix
C2 - Almost clear, transparent mix
C3 – Opalescent, translucent mix
C4 – Hazy, translucent mix
C5 – Murky, cloudy mix
C6 – Very cloudy mix
C7 – Opaque, milky mix

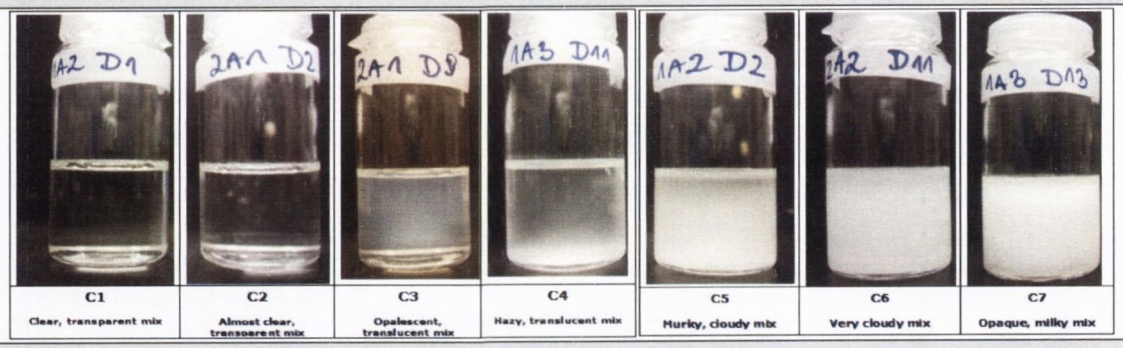

Phase Behaviour Scale

P1 – Single phase
P2 – Two phases
P3 - Three phases
P4 – Four phases
P5, P6, etc.
S – Sharp, distinct, clear line between adjoining phases
B – Blurred line between adjoining phases

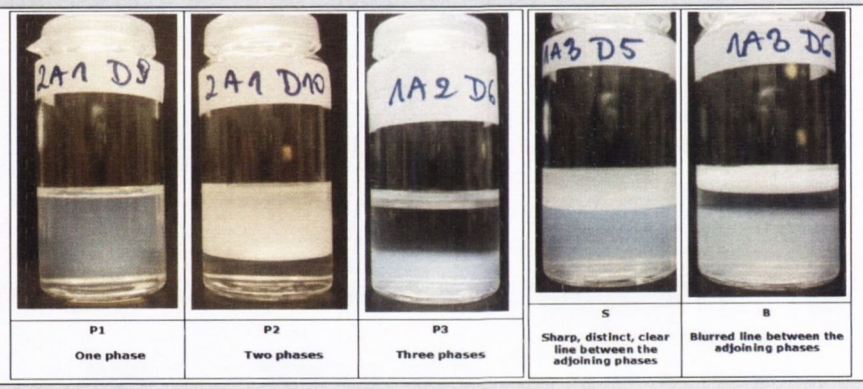

Visual Texture Scale

Without 'V' – low viscosity, the sample looks and flows like liquid
V1 – increased viscosity, semi viscous, viscoelastic, still flows in the bottle
V2 – very high viscosity, the sample flows very poorly or doesn't flow at all, the sample resembles a gel rather than a liquid, very often aerated with many air bubbles entrapped

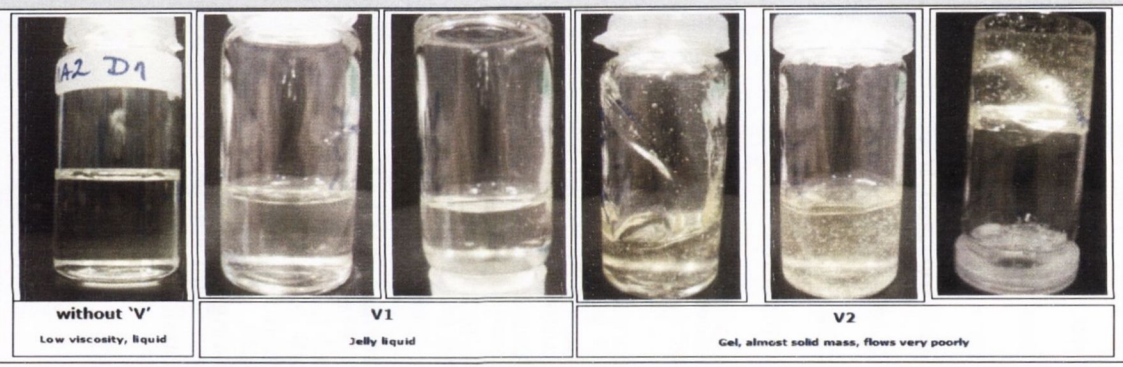

Titration of selected model systems was also carried out with artificial intestinal fluids FaSSIF-V2 and FeSSIF-V2, published by Jantratid et al. (2008) which compositions are given in Table 2.4

Table 2.4. Composition of full FaSSIF-V2 and full FeSSIF-V2 (Jantratid et al., 2008).

Ingredients	**Full FaSSIV-V2** (with surfactants)	**Full FeSSIV-V2** (with surfactants)
Sodium taurocholate	3 mM	10 mM
Lecithin	0.2 mM	2 mM
Glyceryl monooleate	/	5 mM
Sodium oleate	/	0.8 mM
Maleic acid	19.12 mM	55.02 mM
Sodium hydroxide	34.8 mM	81.65 mM
Sodium chloride	68.62 mM	125.5 mM
Purified water	ad 1000 ml	ad 1000 ml
pH	6.5	5.8
Osmolality (mOsm/kg)	180 ± 10	390 ± 10
Surface tension (mN/m)	54.3	40.5 ± 0.2

2.4.2. Determination of boundary points

Samples representing exact boundary points and points close to the expected phase border of various phases were prepared in duplicate and stored for 24 hours at 37°C before visual inspection was carried out (or at 25°C if the boundary points for dilution at 25°C were required). This procedure was designed to ensure that the boundary points, established with less than ± 3% error, represented true 'clear microemulsions'. Titration method is known to be fast but could overestimate a microemulsion region because little energy is required to convert fine emulsions (located close to the phase borders) into visually clear emulsions. Preparation of individual samples in a large number (150– 200) to evaluate phase diagrams is recommended (Bhargava et al., 1987), if the diluted mixtures do not reach equilibrium rapidly. After 24 hours of storage at 37°C, the prepared samples were visually classified according to Transparency, Phase Behaviour and Visual Texture scales (Table 2.3) and examined for birefringence using Vickers MIO microscope. A small portion of each sample was removed and spread relatively thickly onto a microscopic slide. A cover glass was not used to maintain a high thickness of the spread material and avoid thinning of the sample layer. Isotropic samples were detected where there was no change in appearance (polarization) as an analyzer in the microscope was rotated versus a polarizer, meaning the properties of a material were the same in all directions. Anisotropy was detected when distinctive colours, shapes (including Maltese crosses) were revealed depending on the position of the analyzer versus the polarizer (meaning there was a certain organized self-assembly of surfactant that caused polarizing light in one direction). The samples and slides were maintained at 37°C prior viewing and the examination was carried out rapidly (within a few seconds) to prevent a phase change (transition) caused by the room temperature. Images of selected liquid crystalline phases

were taken using Olympus SZX10 stereo- microscope with polarizer/analyzer, connected to a digital camera.

The final pseudoternary diagrams were drawn using ProSim Ternary diagram software (freeware).

2.5. Characterisation of Microemulsions

Isotropic character of the model colloidal samples was confirmed by examination the samples under microscope, the same way as described in section 2.4.2.

2.5.1. Cryogenic transmission electron microscopy (cryo-TEM) and freeze-fracture transmission electron microscopy (FF-TEM)

Cryo- TEM and freeze fracture replicas were performed by Center for Ultrastructural Imaging, King's College London, UK. The prepared samples were shipped to the to the testing site. Due to uncontrolled storage/shipment temperature the 'reconstitution' procedure was carried out prior testing. The samples were shaken manually for approx 5 minutes, equilibrated for 20 -30 minutes at temperature of 25 °C prior to experiments. In order to obtain direct cryo-TEM images, 5ul of sample was placed on a holey carbon film (300 mesh gold grid – Agar Scientific Ltd S147A3), blotted with filter paper, frozen by rapid immersion in 'slushed' nitrogen (- 210°C) and transferred to the specimen holder under liquid nitrogen. The samples were imaged in an FEI Tecnai T20 at -175°C using 200kV and low dose imaging with a Gatan Ultrascan 2K camera. The cryo-TEM was repeated 3 times for each sample. Freeze fracture preparations were carried out on the samples immediately after reconstitution and 24 hours afterwards. In order to obtain FF-TEM images, samples were frozen as a thin film between two copper double-sided replica specimen holders (Bal-tec AG, BU0 12 055-T) using 'slushed' nitrogen (-210 °C). Samples were fractured at -150°C, shadowed with platinum/carbon and coated with carbon in a Polaron E7500 freeze fracture unit mounted on a Polaron E6000 series high vacuum station (Quorum Technologies). The replicas were recovered by submerging the specimen holder and replica in 2:1 v/v chloroform: methanol (Analar grade) for 2 – 3 minutes and then floating the replica off in distilled water. Replicas were transferred with a platinum loop to copper 460 lines/inch hexagonal mesh grids (Agar Scientific Ltd. G2750C) and imaged at 75Kv in a Hitachi H7600 TEM with an AMT CCD camera.

2.5.2. Conductivity

Electrical conductivity was measured using CyberScan con 500 (Eutech Instruments, The Netherlands) with Eutech Instruments electrode. The conductivity measurements were performed in samples made with purified water, without addition of any electrolyte. All samples were equilibrated at 25°C for at least 30 min prior measurements and the temperature of each sample was measured together with conductivity (also by CyberScan con 500). The final reading for each

sample was based on three measurements obtained by dipping the electrode in the sample until equilibrium was reached (three times). Each sample was prepared and measured in duplicate at 23 - 25°C. The equipment was calibrated with a conductivity standard of 1,413 μS/cm and purified water prior to the measurements. 1st derivative [Conductivity] was calculated using the equation:

$$1^{st}\ derivative\ [Conductivity] = \frac{Log\ \rho_n - Log\ \rho_{n+1}}{\Phi\ w_n - \Phi\ w_{n+1}} \qquad \text{Eqn. 2.4.}$$

ρ_n – conductivity measured in sample n

ρ_{n+1}– conductivity measured in next sample n+1

$\Phi\ w_n$ – volume fraction of water in sample n

$\Phi\ w_{n+1}$– volume fraction of water in next sample n+1

2.5.3. Zeta potential

Measurements of zeta potential were carried out with Zetasizer Nano ZS (ZEN 3600) from Malvern Instruments (UK) using Zeta dip cell. The measurements were performed in samples made with purified water, without addition of any electrolyte. All samples were filtered before measurements through 0.45 μm filter directly to the glass optical cell. The zeta potential was taken as the mean value of at least 3 measurements carried out at 25 °C ± 1°C. The equipment was verified with a zeta-standard of 50 mV ± 5mV prior to the measurements. The measurements required manually set voltage since the automated mode with 40V was causing some charring of the samples.

2.5.4. Rheology, absolute viscosity and density

Rheological properties of samples were evaluated using a Brookfield LVDV-II rheometer (Brookfield Engineering Laboratories Inc, Middleboro, MA). The rheometer was used with S18 spindle and a small sample adapter that requires a sample size of 8 ml. All measured samples were equilibrated at 25°C for at least 30 min prior measurements and the temperature of each sample was measured at the beginning and the end of each measurement. All measurements were made in temperature of 26°C ± 1°C. The final reading for each sample was based on three results obtained from three runs of the samples (from the lowest to the highest shear rate, from the highest to the lowest shear rate and again from the lowest to the highest shear rate). Each sample was prepared and measured in duplicate.

In addition, three Newtonian fluids ($\eta_{Captex\ 355}$ = 23 mPas at 25°C, $\eta_{Propylene\ Glycol}$ = 48.6 mPas at 25°C and η_{PEG400} = 90.0 mPas at 25°C), having viscosities comparable to the samples were tested, to establish appropriate shear rates (speeds of the spindle) that could truly reflect the Newtonian or non-Newtonian behaviour of the tested samples. The shear rates/spindle speeds, which showed changeable viscosities for the Newtonian standards where considered as inadequate and excluded.

The viscosity values used to evaluate differences between the samples R1 - R13 were calculated as the average of viscosity values obtained under different shear rates.

Absolute viscosity of 'experimental external phases' (used in the DLS simulation) was measured with Sine-wave Vibro Viscometer SV-10 (A&D Company Limited, Tokyo, Japan) with a small cup for 10 ml. All samples were equilibrated at 25 °C for at least 30 min prior measurements and temperature of each sample was measured together with viscosity (also by SV-10). The final reading for each sample was based on three results. Each sample was prepared and measured in duplicate. All measurements were carried out at temperature of 25°C ± 1°C. The equipment was calibrated on purified water prior to measurements. The measured values on SV-10 needed to be corrected by dividing the measured viscosity by density of the sample in order to calculate the final absolute viscosity value (Sine-wave Vibro Viscometer SV-10 is automatically set on density of water at 25°C, ρ = 1g /cm^3). Density of external phases was measured using TD1 Lauda Tensiometer (LAUDA DR. R. WOBSER GMBH & CO. KG, Lauda- Königshofen, Germany). The final reading for each sample was based on three results/runs on the samples. The measurements were performed on single samples. The equipment was calibrated on purified water prior to the measurements.

2.5.5. Pulsed-field-gradient spin-echo nuclear magnetic resonance (PGSE-NMR)

PGSE-NMR measurements were performed by Colloidal Resource AB (Sweden), using a Bruker DMX 200 spectrometer equipped with a gradient probe (max gradient strength 9 T/m) following standard recommendations. All measurements were carried out at 25 ± 0.5 °C.
All samples had the following settings: Δ = 100ms, δ =1ms, number of gradients step = 32, number of scans (transients 8 or 16), waiting time (D1) = 2s, pulse sequence = stimulated echo (STE) delivered by Bruker. Evaluation and data analysis was carried out with the program delivered by Bruker. Data analysis was carried out based on Gaussian self-diffusion of a single species, the intensity, I, of the NMR signal decay can be written as:

$$I = \frac{I_0}{2} \exp(-2\tau_1/T_2 - \tau_2/T_1) \exp(-kD) \qquad \text{Eqn. 2.5.}$$

where k is defined as $k = \delta^2 g^2(\Delta - \Delta/3)$, I_0 is the intensity following a single 90° pulse, $T1$ and $T2$ are the longitudinal and transverse relaxation times, D is the self-diffusion coefficient, and τ_1 is the gyromagnetic ratio of the spin bearing nucleus. For two or more overlapping peaks, a biexponential fit was used (Söderman et al., 2004.). With the PGSE diffusion NMR method, the self-diffusion of different molecules was measured initially to retrieve the proton spectrum. From this, a distinct peak was chosen for use in the diffusion experiment. Water has one proton peak (Fig. 2.1, water peak at 4.7 ppm – red eclipse) and this can be easily distinguished from any other organic protons. The characteristic peak for polysorbate 80 was initially chosen around 3.6 ppm (violet eclipse), however the meaningful data were not obtained in tested samples and self-diffusion coefficient for

this surfactant was finally subtracted from the peak observed at 1.3 pm (blue eclipse). Capmul MCM C8 and Captex 355 are chemically very similar, therefore a characteristic, distinctive peak for each material could not be seen. The peak around 1.3 ppm (blue eclipse) corresponding to CH2 group, was selected as 'marker' of the oil and polysorbate 80.

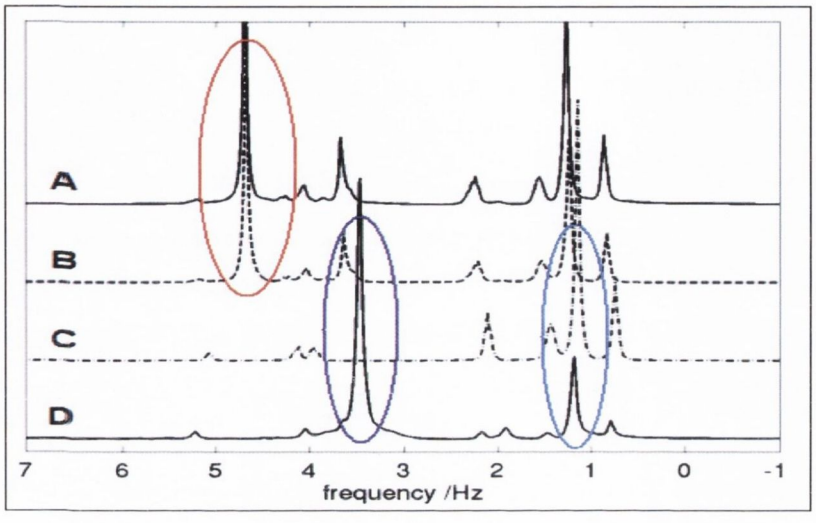

Fig. 2.1. Proton spectrum for A) sample R7, B) sample R3, C) Captex 355, D) Crillet 4 HP/Polysorbate 80. The red eclipse denotes water peak (4.7 ppm), the violet eclipse denotes polysorbate 80 (3.6 ppm), the blue eclipse corresponds to CH2 group (oil phase).

The prepared samples were shipped to the testing site. The samples were kept at 25 °C for 6 days prior to measurements. Due to uncontrolled storage/shipment temperature the 'reconstitution' procedure was carried out prior testing. The samples were shaken manually for approx 5 minutes, equilibrated for 20 - 30 minutes at temperature of 25 °C prior to experiments. All samples were transferred to 5 mm NMR tubes with a glass pipette. All samples but one were clear and homogeneous when transferred to the NMR tube. Sample R9 was turbid when transferred to the 5 mm NMR tube and was carefully shaken before transfer. After the transfer of sample R9 to the NMR tube the sample remained slightly bluish but was clear. All samples were clear and transparent when measured.

2.5.6. Small- angle neutron scattering (SANS)

Heavy water (D_2O) was used to prepare samples: R3, R4, R5, R6, R7 and R9 measured by SANS. SANS data were obtained on the LOQ small-angle diffractometer at the ISIS Pulsed Neutron Source (STFC Rutherford Appleton Laboratory, Didcot, U.K.). This is a fixed-geometry "white beam" time-of-flight instrument, which utilizes neutrons with wavelengths, λ, between 0.2 and 1 nm (2.2-10Å), and a 64 cm x 64 cm position-sensitive detector, at 4.1 m from the sample. Data are simultaneously recorded on two-dimensional, position-sensitive, neutron detectors, to provide a simultaneous Q range of 0.007– 0.287$Å^{-1}$. The R3 –R9 samples and suitable background

samples were shipped to the to the testing site. Due to uncontrolled storage/shipment temperature the 'reconstitution' procedure was carried out prior testing. The samples were manually shaken for approx 5 minutes, equilibrated for 20 - 30 minutes at temperature of 25 °C prior to experiments. Measurements were made at 25 °C and the samples were run in 1 mm quartz cells. Absolute intensities for I(Q) (cm^{-1}) were determined within 5% by measuring the scattering from a partially deuterated polymer standard. Each raw scattering data set was then corrected for the detector efficiencies, sample transmission and background scattering and converted to scattering cross-section data ($\partial\Sigma/\partial\Omega$ vs Q) using the instrument-specific software Collette. The FISH analysis program was used for data modelling. The model which was used to fit the data was the 'uniform ellipsoid * hard sphere S(Q)'. S(Q) is the structure factor and is present as there is some hard sphere interaction between the particles (due to the volume of the particles in the system). There are two types of ellipsoid: oblate where $X < 1$ (Fig. 2.2.A) and prolate where $X > 1$ (Fig. 2.2.B). X is the axial ratio i.e. the primary radius is R_1 and so the secondary radius $R_2 = R_1.X$. In order to calculate the average size of water droplets and a volume fraction, the 'uniform ellipsoid * hard sphere S(Q)' model was used to fit the data. The oblate model ($X < 1$) showed the best fit.

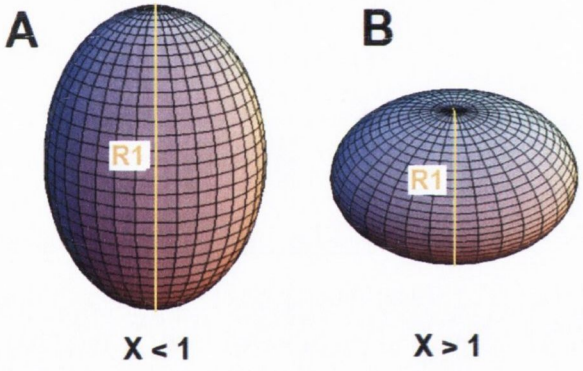

Fig. 2.2. Two structural dimensions in the ellipsoidal form factor A) oblate, B) prolate.

2.5.7. Differential scanning calorimetry (DSC)

DSC measurements of samples R1 – R13 were performed with a Metler Toledo DSC 821° operated by Metler Toledo STAR^e software (version 6.10) and equipped with a refrigerated cooling system. Nitrogen with a flow rate of 80 ml/min was used as purge gas. One drop (weight between 10 to 20 mg) of liquid was weighted precisely into hermetic aluminum pans. An empty hermetically sealed pan was used as a reference (lids were not perforated). Samples were cooled from 25°C to −60°C at a cooling rate of 5°C /min, held for 5 minutes at −60°C and then heated to 80°C at a heating rate of 10°C /min. All measurements were preformed at least in triplicate.

2.5.8. Particle sizing by dynamic laser scattering (DLS)

Particle size (Z-Aver) and polydispersity (PDI) of samples R1- R10 were measured by dynamic light scattering using Zetasizer Nano ZS (ZEN 3600) from Malvern Instruments (173°

backscatter). Viscosity of Captex 355 (η = 25.2100 mPas) and water (η = 0.8872 mPas) were used as the dispersant for R2 – R9 and R10 respectively, except for the simulation experiment. Refractive index values for Captex 355 (RI = 1.446) and water (RI = 1.330) were used. General purpose (normal resolution) mode was used to process data. All samples were filtered directly before measurements through 0.45-μm filter directly to the glass optical cell. The temperature of the scattering cell was controlled at 25°C ± 1.0°C. The equipment was verified on 60 nm latex in purified in 0.9% saline prior to the measurements. Each sample was measured at least three times. The diffusion coefficients (measured with Zetasizer) were corrected assuming the presence of hard-sphere interactions, using the following equation (Cheung et al., 1987; Aboofazeli et al., 2000):

$$D_{or} = D_{corr}*(1+1.56*\Phi) \qquad \text{Eqn. 2.6.}$$

D_{or} is the measured diffusion coefficient, D_{corr} is the corrected diffusion coefficient, Φ is the droplet volume fraction

The corrected particle size (hydrodynamic radius) was calculated according to the Einstein–Stokes equation (Nobbmann et al., 2007):

$$R = k*T/(3*\pi*\eta*D_{corr}) \qquad \text{Eqn. 2.7.}$$

where R is the hydrodynamic radius, k is Boltzmann's constant (k = 1.3806488(13)×10^{-23} J K^{-1}), T is the absolute temperature (T= 298 K (25°C)) , η is the viscosity of dispersant (water or Captex 355) and D_{corr} is the corrected diffusion coefficient according to equation 2.6.

2.6. Methods: Incorporation of Model Compounds into Liquid Microemulsions and SELFs

2.6.1. Incorporation of sodium alendronate trihydrate and disodium pamidronate pentahydrate

2.6.1.1. Drug loading procedure

Placebo microemulsion formulations were prepared by combining weighed amounts of excipients and hand shaking for 1-2 minutes. All semi-solid materials were melted at 40°C prior to weighing and mixing with the rest of liquid materials. The solubility limit for bisphosphonates in the microemulsion formulations was determined in the same ways as previously described in section 2.2.8.

2.6.1.2. Differential Scanning Calorimetry

The solid material that was recovered after determination of the solubility limit was dried on a paper filter at room temperature and tested by DSC using the method and equipment described in section 2.2.3.

2.6.2. Incorporation of acyline monoacetate

2.6.2.1. Drug loading procedure

Preformulation and formulation development work with acyline monoacetate was carried in an isolator designed for high potency APIs, located in Merrion Pharmaceuticals Ltd. All SEDDSs were prepared by combining weighed amounts of excipients and hand shaking for 1-2 minutes. All semi-solid materials were melted at 40°C prior to weighing and mixing with a rest of liquid materials. Acyline monoacetate was incorporated into SEDDSs 1) suspending the drug in a required medium, 2) gentle manual shaking of the suspension for approx 5 minutes, 3) leaving the sample at room temperature for next 24 hours until a clear formulation was formed or gelling occurred.

2.6.2.2. Assay and Dissolution testing

The analytical method used for assay and dissolution testing of acyline was developed by the Analytical Department, in Merrion Pharmaceuticals Ltd. The details of HPLC method were previously given in section 2.2.7. The developed assay method was not stability indicating. Samples used for determination of acyline content in SEDDSs were prepared by dissolving approximately 0.1 g of SEDDS formulation containing acyline monoacetate in 100 ml of acetonitrile: water 50:50 v/v to give the concentration of acyline of approximately 0.01 mg/ml. Diluted samples were prepared in duplicate, each sample injected twice.

Dissolution testing was performed by withdrawing of approximately 5 ml of dissolution media at the required time point. The sample was filtered through 0.45 µm PVDF filter, first 2-3 ml were discarded and the rest of the solution was assayed by the HLPC method (section 2.2.7).

2.6.2.3. Stability study

All liquid (non-encapsulated) formulations were stored in glass, parafilmed bottles placed in climatic chambers or a fridge (2 - 8°C). The climatic chambers set to 25 °C/60 % RH and 40 °C/75 % RH according to the ICH standards were used in Merrion Pharmaceuticals Ltd. The encapsulated formulations (into softgels) were stored in glass, tightly closed and parafilmed bottles.

2.6.2.4. Dispersion test and particle size measurements by dynamic light scattering (DLS) of the dispersed preclinical SEDDSs

The dispersion test was employed to evaluate dispersion (emulsification) behaviour of the preclinical SEDDSs. The method used in the present study was based on the methods published by Kommuru et al. (2001) and Kadu et al. (2011) where a liquid formulation was introduced into a glass beaker with a dispersing medium and gently stirred with a magnetic bar to produce a dispersed system. The dispersion test in this study was performed in a miniscale using 20 ml of blank FaSSIF-V2 to mimic an *in vivo* scenario where 1g of SEDDS (1 capsule containing 1g of

SEDDS) would be dispersed in 200 ml of FaSSIF-V2 (fasted state). To simulate fasted conditions in the small intestine, a volume of up to 200 ml is consistent with the values reported in the literature (Jantratid et al., 2008, Schiller et al., 2005).

0.1 g of each placebo SEDDS (Test Item 2, 3 and 4) was added to a glass bottle (Fig. 2.3.A) with 20 ml of pre-heated to 37°C blank FaSSIF-V2 (the composition of full FaSSIF-V2 is given in Table 2.5, the blank version is without sodium taurocholate and lecithin). A magnetic stirring bar (Fig. 2.3.B) was added; the bottle was closed and immersed (up to the neck of the bottle) into a vessel filled with pre-heated water to 37°C.

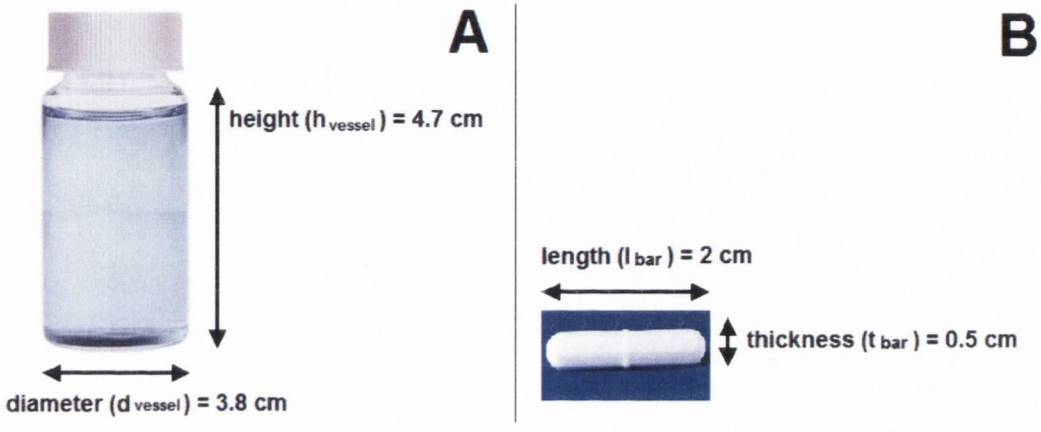

Fig. 2.3. A vessel (A) and mixing bar (B) used in the dispersion (and desorption) test.

The content was mixed for 15 minutes under 300 rpm and heating at 37 °C using magnetic stirrer Stuart SD162. An emulsion formed after 15 minutes, was sampled with a syringe, filtered through 0.45 μm filter directly into a disposable low-volume optical cell and measured immediately. Particle size (Z-Aver) and polydispersity (PDI) were measured by dynamic light scattering using a Zetasizer Nano ZS (ZEN 3600) from Malvern Instruments (173° backscatter). Viscosity and Refractive Index of water were used as dispersant. The temperature of the scattering cell was controlled at 37°C ± 1.0°C. Z-Aver and PDI were calculated as means of six runs on one sample. The dilution procedure for each formulation was carried out in duplicate. The equipment was verified on 60nm latex in purified in 0.9% saline prior to the measurements.

An overall HLB value was calculated based on the percentage of individual component in the three-component blend (wt%) and its HLB value according to the following the equation:

$$Overall\ HLB = \frac{(C_L \times HLB_L) + (C_H \times HLB_H) + (C_O \times HLB_O)}{100\%} \qquad \text{Eqn. 2.8.}$$

HLB_L – hydrophilic-lipophilic value for the low HLB value surfactant

HLB_H – hydrophilic-lipophilic value for the high HLB value surfactants respectively

HLB_O – hydrophilic-lipophilic value for the high HLB value surfactants respectively

C_H – content of oil in the three-component blend (100%), expressed as percentage

C_L – content of the high HLB value surfactant the three-component blend, expressed as percentage

C_O – content of the high HLB value surfactant the three-component blend, expressed as percentage

2.6.2.5. Preclinical study

The preclinical study (in-life portion) was conducted at Pre-Clinical Research Services Inc., 1512 Webster Court. Fort. Collins, Co, 80524. USA. The non-GLP exploratory study was carried out according to the study protocol MP-0702, which was reviewed and approved by the local animal ethics committee. Five adult non-naïve female beagle dogs approximately 14 -16 months of age, with a body weight ranging from 5.0 to 8.4 kg were used in the study. The sample size (n = 5) was selected using the equation Eqn. 2.9, where a sample size between 5 and 6 is acceptable under assumptions that 1) the coefficient of variation in the drug absorption is approximately 30% ($\sigma = 0.30$) and 2) the absorption of the drug from the SEDDSs is expected to be significantly higher by ~50% ($\Delta = 0.50$), compared to the unenhanced test item. For a statistical test at the 0.05 level and 0.80 chance of detecting the difference Δ (if it really exists), a sample size can be calculated according to the equation:

$$n \geq 15.68\,\sigma_b^2 / \Delta_b^2 \qquad \text{Eqn. 2.9.}$$

where n is the sample size, σ is the error standard deviation of the mean of drug absorbed , Δ is the minimum difference in amount of drug absorbed (from different formulations) that must be detected (Swarbrick, 1973).

For the purpose of dose administration, the dogs used in this study had been surgically implanted with duodenal access ports (DAP). Each DAP was connected to a cannula which was inserted into the duodenum. There was no randomisation of the animals in the study; each dog was given each test item at different stages of the study. Each dog was fasted for at least 12 hours prior dosing and fed between 2 and 5 hours following dosing. All SEDDSs formulations were kept frozen (2- 8°C) for less than 5 days till the date of dosing. Directly prior to dosing, the formulations were liquefied by heating at 30 °C for approximately 20 minutes. The SEDDSs were injected into the installed duodenal access port through a Huber-point non-coring hypodermic needle attached to a 10 ml syringe. Each injection of the tested formulation was followed by a flush of the duodenal port with 3 ml (Test Item 1) or 7 ml (Test Item 2, 3 and 4) of sterile water. A 7-day washout period followed each dose. Approximately 2ml of whole blood was collected (via jugular method) just prior to dosing and approximately 30 minutes and 1, 2, 4, 6, 8, 12, 24 and 48 hours post dosing. The blood samples were placed into plastic tubes for serum separation and allowed to clot at room temperature for approximately 20 minutes before being spun in a refrigerated centrifuge until serum was harvested. Serum samples were stored frozen (-110°C) until shipped on dry ice to BioClin Research Laboratories Ltd. for bioanalysis.

The bioanalytical was conducted at BioClin Research Laboratories Ltd. Monksland, Athlone, Co. Westmeath, Ireland. The method used was a liquid/liquid extraction. The LC/MS/MS system consisted of an Applied Biosystems API 4000 triple quadrupole mass spectrometer, (Applied Biosystems, UK) a Perkin Elmer series 200 autosampler (Foss, Ireland) and a Perkin Elmer series 200 pump (Foss, Ireland). Sildenafil was used as an internal standard. The limit of quantification of this method was 0.2 ng/ml. The calibration line of reference standards was in the range of 0.2- 40 ng/ml. Validation experiments including the assessment of accuracy and precision, extraction efficiency, repeatability, recovery, specificity, process stability and limit of quantitation within run and between run were carried out. Each analytical run consisted typically of a blank, eight standards and six QC samples interspersed between study samples. Acceptance criteria for standards is ± 15% deviation from the true value with the exception of the LOQ where it is ± 20% deviation from the true value. No more than two standards were omitted from the standard line.

Upon receipt of bioanalytical data, the individual animal serum concentration data was loaded into an Excel spreadsheet (Microsoft® office Excel 2003). Pharmacokinetic parameters such as AUC_{0-t}, AUC_{0-inf}, C_{max}, T_{max}, elimination half-life and elimination constant rate were calculated using macros written for MS Excel by Usansky J.I. *et al*, PK functions for Microsoft Excel available at www.boomer.org/pkin/xcel/pkf.pkf.doc.

Elimination half-life and elimination rate constant were calculated using last three time points.

Relative Bioavailability ($F_{rel\%}$) was calculated according the equation below:

$$Frel\ \%_{Dog\ X} = \frac{AUC_{(0\text{-}48h)}\ of\ Test\ Y\ in\ Dog\ X}{AUC_{(0\text{-}48h)}\ of\ Unenhanced\ Test\ in\ Dog\ X} \times 100\% \qquad \text{Eqn. 2.10}$$

Every mean value (AUC_{0-t}, AUC_{0-inf}, C_{max}, T_{max}, etc.) was calculated as a mean of parameters for individual animals.

Statistical analysis was performed using GraphPad InStat version 3.00 for Windows 95, GraphPad Software, San Diego California USA, www.graphpad.com (free-trial version) using the parametric two ways (repeated measures) ANOVA for matched (paired) groups to evaluate a statistical difference in $LogAUC_{0-48h}$ between the test items. A comparison of pairs was performed using Tukey-Kramer multiple comparisons post test. Non-parametric repeated measures ANOVA (Friedman test) was used to calculate any significant differences in T_{max} and elimination half-life ($T_{1/2}$) between the test items and a non-parametric multiple comparison (Dunn test) post test was performed between the pairs.

2.7. Methods: Characterisation of Solid Carriers

2.7.1. Scanning electron microscopy (SEM)

SEM analysis was carried out using a Zeiss Supra Variable Pressure Field Emission Scanning Electron Microscope with the resolution of 3 nm at 30 kV and the accelerating voltage 5 kV. The detector was secondary electron. Samples were spread onto aluminium stubs and sputter-coated with gold under vacuum prior to examination.

2.7.2. Particle sizing by laser diffraction (PSD)

Particle size distribution was measured by a dry method using a laser diffraction particle sizer Mastersizer 2000 (Malvern Instruments, UK). Samples were dispersed using a Scirocco dry feeder instrument fitted with a micro-volume tray (2- 10 g). Pressure/particle size titration experiments were performed for each carrier to select appropriate dispersive pressures and the final pressure parameters were: 2.0 bar for Sylysia 320 (Appendix Fig. A.7.1), 0.2 bar for Aeroperl 300/30 (Appendix Fig. A.7.2), 2.5 bar for Zeofree (Appendix Fig. A.7.3), 2.5 bar for Hubersorb 600 (Appendix Fig. A.7.4), 0.2 bar for Neusilin US2 (Appendix Fig. A.7.5) and 0.2 bar for Fujicalin SG (Appendix Fig. A.7.6). The acceptable obscuration limit was set to 0.5- 6.0%. The vibration feed rate from 40 - 90% was used depending on a tested sample. The General-purpose method with normal sensitivity was used to compute the mean particle size. Absorption Index of 0.1 was used for all materials. Refractive Index values of 1.610, 1.650, 1650, 1.460, 1.460, 1460 were used for Fujicalin SG, Neusilin US2 and Hubersorb 600, Aeroperl and Zeofree 5161 and Sylysia 320, respectively. During the set up of sizing method, the samples were also examined under Vickers MIO microscope and the particle size was compared to Malvern standard glass beads. Results were reported as an average of at least five measurements and RSD values complied with USP/ Ph. Eur. acceptance criteria (RSD < 10% on Dv50, RSD < 15% on Dv10 and Dv90, the limits doubled if particles are smaller than 10 μm).

2.7.3. Specific Surface Area (BET) and Porosity (t-plot)

Samples in duplicate were dried prior to analysis for 12 hours at 30°C, under nitrogen flow, using a Gemini SmartPrep drying station. Micromeritics Gemini VI surface area analyzer was used to carry out full isotherms in the relative pressure (P/P_0) range 0 – 1.0. Compressed nitrogen was used as an adsorptive gas. The measurements collected were used to compute BET and t-plot (Porosity). BET calculation was based on six measurements carried out in a range of relative pressure P/P_0 from 0.05 to 0.30 with an equilibration time of 10 s. T-plot calculation was based on six measurements carried out in a range of relative pressure P/P_0 from 0.20 to 0.55 with a equilibration time of 10 s. Free space was determined separately for each sample using helium gas. Saturation pressure P_0 was determined prior to measurement of each sample. All values of correlation coefficient (BET) were above 0.9975 and the Intercept was positive (met compendial

acceptance criteria Ph. Eur. and USP). All values of correlation coefficient (t-plot) were equal 1.0000.

2.7.4. Bulk and tapped density

The bulk and tapped density measurements were performed according to USP method I using Pharmatest Tapped Density Tester PT-TD1. Measurements were carried out on the reduced volumes (a 25 ml glass cylinder was used). Each sample was analysed in duplicate. Bulk and tapped density values were used to calculate Compressibility Index and Hausner ratio according to the following equations:

$$Compressibility\ Index = \frac{100\ (V_0 - V_f)}{V_0} \qquad \text{Eqn. 2.11.}$$

$$Hausner\ Ratio = \frac{V_0}{Vf} \qquad \text{Eqn. 2.12}$$

V_0 – bulk volume, V_f - final tapped volume

Table 2.5. Flow character based on Compressibility Index and Hausner ratio.

Compressibility Index	Flow Character	Hausner Ratio
1-10	Excellent	1.00-1.11
11-15	Good	1.12-1.18
16-20	Fair	1.19-1.25
21-25	Passable	1.26-1.34
26-31	Poor	1.35-1.45
32-37	Very poor	1.46-1.59
> 38	Very, very poor	> 1.60

2.7.5. True density

AccuPyc 1330 Pycnometer Micromeritics TM was used to measure the volume of samples, (having known weights) and compute the true density values. The volume of samples was measured by gas adsorption using helium (99.995% purity). A 1 cm^3 sample holder was used. The instrument was calibrated prior to each testing. True density value for each sample was an average of five measurements. Prior to analysis, all the samples were dried for at least 12 hours at 30 °C under nitrogen flow, using a Gemini SmartPrep drying station.

2.7.6. pH measurements

5% w/v slurries were prepared with each solid carrier (solid carriers are water insoluble). Measurements of pH were performed using Orion 420A+ portable pH/ISE meter, 3 hours after preparation of the slurries and once again after 24 hours. Calibration was performed prior to measurements of the samples. Each sample was measured twice at room temperature (20 - 25°C).

2.7.7. Solid state Fourier transform infrared spectroscopy (FTIR)

FTIR analysis of the solid carriers was performed using the same method and equipment as previously described in section 2.2.2 for the model compounds.

2.7.8. Thermal analysis (DSC & TGA)

DSC and TGA analysis of the solid carriers was performed using the same method and equipment as previously described in section 2.2.3 for bisphosphonates.

2.7.9. Powder X-Ray Diffraction analysis (PXRD)

PXRD analysis of the solid carriers was performed using the same method and equipment as previously described in section 2.2.4 for the bisphosphonates.

2.7.10. Adsorption Index (AI)

Adsorption Index was a parameter created based on the Oil Absorption parameter determined by "Oil Absorption by Spatula Rub-out" according to ASTM D 281 method (Koleske, 1995; Schoff, 2009). The Adsorption Index was determined in the following steps: 1) a powder sample of a solid carrier was weighed on a Petri dish 2) a liquid was added drop-wise (maximum 2-3 drops at one time) and mixed with the powder sample thoroughly using a spatula to ensure even distribution of the liquid 3) as the liquid was added any change in visual appearance of the sample was recorded together with the weight of added liquid and classified according to the Adsorption Stages shown in Table 2.6) the experiment was completed once the powder sample turned into wet, plastic mass, forming a consistent ball which could be lifted with a spatula as one piece (Adsorption Stage 6, Table 2.6). The amount of liquid required to form a 'one-piece' ball was used to calculate the Adsorption Index according to the following equation:

$$\textit{Adsorption Index (AI)} = \frac{\textit{weight of added liquid required to form 'one-piece' mass [g]}}{\textit{weight of dry sample of solid carrier [g]}} \times 100\% \qquad \text{Eqn. 2.13}$$

The procedure was carried out very slowly to minimize errors caused by uneven distribution of liquid onto a solid carrier. Screening through a 450 μm screen was employed to break up lumps as required, any loss of powder during screening was accounted for. Final values of Adsorption Index were calculated as a mean of two experiments.

Table 2.6 Classification of Adsorption Stages during determination of Adsorption Index.

Adsorption Stages		Visual appearance/ properties	Adsorption Stages		Visual appearance/ properties
1		dry, non-sticky powder, resembles the non-adsorbed solid carrier	4	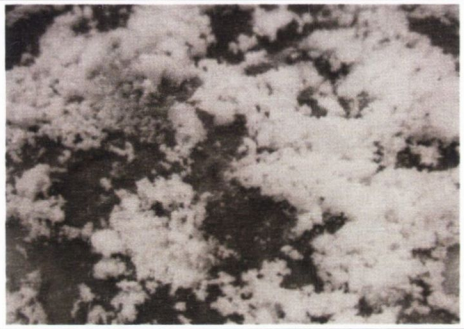	moderately plastic, forms small granules, evidently wet appearance
2		dry, slightly cohesive but non-sticky, tends to form weak agglomerates,	5		very wet appearance, large granules and lumps that still exist separately and don't form one mass
3	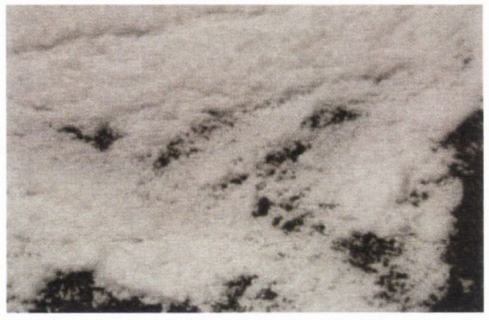	slightly sticky, cohesive, forms larger agglomerates, (could possibly cause stickiness/ adhesions to punches/dosators during tabletting and encapsulation)	6 (Adsorption Index)	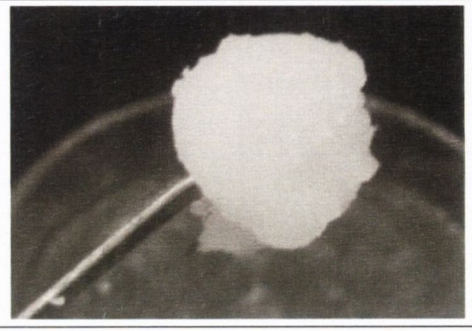	completely wet, pasty mass agglomerated into one piece (ball-like piece), doesn't break into separate lumps, the mass can be lifted with a spatula as one piece

The densities of the liquids used to determine the Adsorption Index were measured in duplicates at room temperature using a 25cm^3 glass pycnometer. The viscosities of these liquids were measured in triplicates at room temperature, using Sine-wave Vibro Viscometer SV-10 with a 10ml polycarbonate cup.

2.8. Methods: Adsorption of liquid SEDDS onto Solid Carriers

2.8.1. Adsorption Procedure

The S-SEDDSs were created by adsorption of preconcentrate 2A2 50: 50 onto the solid carriers using a blending procedure. The S-SEDDSs in a range from 40% to 70% of Added Liquid (calculated according to Eqn. 2.12) were prepared by adding the preconcentrate onto a solid carrier. Each S-SEDDSs was produced using following the steps: 1) a known amount of the solid carrier was weighed out into a 100 ml volume glass bottle (the volume of the powder sample was less than 40 ml to keep a void space of approximately 60%), 2) a required amount of preconcentrate was added drop-wise onto a solid powder sample to distribute the liquid as evenly as possible 3) any bigger lumps of wetted materials were sized down with a spatula 4) the bottle was closed and assembled into the cube shell of Erweka blender AR400 5) the sample was blended for 10 minutes at 25 rpm, 6) the sample was screened twice through a 425 μm screen (or 850 μm screen for the samples with the highest %AL), 7) the sample was blended for another 10 minutes at 25 rpm.
The efficiency of this adsorption procedure to produce uniform samples with a homogenously distributed preconcentrate was verified by preparation of single samples (%AL = ~ 40%) with the stained preconcentrate 2A2 50: 50 for each solid carrier. The adsorption procedure was found suitable for all the solid carriers, irrespective of their physical characteristics. The stained S-SEDDSs representing Powder End Point (PEP), were produced using the stained preconcentrate and the blending procedure described above. The % of Added Liquid (%AL) for each S-SEDDS was calculated according to the equation:

$$\%\ of\ Added\ Liquid\ (\%AL) = \frac{weight\ of\ added\ liquid\ [g]}{weight\ of\ added\ liquid + weight\ of\ solid\ carrier\ [g]} \times 100\% \qquad \text{Eqn. 2.14}$$

2.8.2. Staining Procedure using Fat Red 7B dye

The preconcentrate 2A2 50: 50 was stained with Fat Red 7B dye (FR7B). At the concentration of 0.2% FR7B was fully soluble in the preconcentrate 2A2 50: 50 which was verified (after dilution 1: 200 w/w with methanol) by the HPLC method described in section 2.8.7.

2.8.3. Powder rheometry (BFE, SE, CBD, SS)

Basic Flowability Energy (BFE), Conditioned Bulk Density (CBD), Specific Energy (SE) and Shear Stress (SS) were measured using a Powder Rheometer FT4.

BFE, CBD and SE were measured using a standard FT4 blade and 25ml volume glass cylinders. SS was measured using a FT4 shear head and 10ml volume cylinder. The final values of BFE, SE, SS experiments were the mean of two measurements, the final CBD was the mean of four measurements.

2.8.4. Dispersion and desorption tests

The dispersion test of liquid preconcentrate 2A2 50: 50 was performed by dispersing 0.1g of the preconcentrate in 20 ml of blank FaSSIF-V2, according to the method described in section 2.6.2.4. The lowest dilution (1: 200) obtained in this test was subsequently diluted with blank FaSSIF-V2 to produce higher dilutions up to 1: 4000 as required to prepare a calibration curve. The samples were prepared in duplicate.

The desorption test was carried according to a very similar procedure as the dispersion test. The amount of each S-SEDDSs used in the dispersion test contained 0.1g of the liquid preconcentrate adsorbed onto a solid carrier (the required weight of S-SEDDS varied depending on the % of Added Liquid in each S-SEDDS). The required amount of S-SEDDS was weighed and added to a bottle (d_{vessel} = 3.8 cm, h_{vessel} = 4.7 cm, section 2.6.2.4) that contained 20 ml of pre-heated blank FaSSIF-V2. A magnetic stirring bar (l_{bar} = 2 cm, t_{bar} = 0.5 cm) was inserted, the bottle was closed and immersed into a vessel with pre-heated water to 37°C. Magnetic stirrer Stuart SD162 with the mixing speed of 300 rpm and heating set to 37°C was used to produce mild stirring and maintain a constant temperature during the test. After 15 minutes, the dispersing medium was withdrawn with a syringe and immediately filtered through a membrane disposable PVDF filter, pore size 0.45 μm. The first 2-3 ml of filtrate were discarded, the rest of the liquid was used for particle sizing and transmittance testing. The desorption test for each S-SEDDS was carried out in triplicate. The desorption test was also performed in duplicate with pure (non-adsorbed) solid carriers. Approximately 0.5 g of each solid carrier was used to perform the desorption test according to the procedure described above. The filtrated solutions were tested by particle size and transmittance. Particle size was not measurable in all cases and transmittance was 100% what indicated that solid carriers did not affect particle size and transmittance measured in emulsions desorbed from the S-SEDDSs.

2.8.5. Particle size by dynamic light scattering (DLS)

All particle measurements were carried out within 30 minutes after completion of the dispersion or desorption test. Particle size (Z-Aver) and polydispersity (PDI) were measured at 25°C ± 1.0 °C, by dynamic light scattering using a Zetasizer Nano ZS (ZEN 3600) from Malvern Instruments (173° backscatter). Viscosity and Refractive Index of water were used as the dispersant. Z-Aver and PDI were calculated as the means of a minimum of three runs on the sample. The equipment was verified using 60nm latex in purified 0.9% saline prior to the measurements.

2.8.6. Transmittance

Transmittance was measured at room temperature using UV-VIS 1700 Shimadzu spectrophotometer with 10.00 mm quartz cuvettes and blank FaSSIF-V2 as the reference solution. Transmittance was measured at the wavelength of 500nm, as previously chosen by Afach et al. (2008) and Cameron et al. (1991) to investigate stability of emulsions. Each sample was measured three times after equilibration at 25 °C for approximately 30min.

2.8.7. Assay of Fat Red 7B

HPLC analysis of Fat Red 7B was based on the method described by Kowalski J., Restek Corporation (electronic resource). The details of the method are summarised below:

- HPLC system used was a Shimadzu HPLC Class VP series with a LC-10AT VP pump, autosampler SIL-10AD VP and SCL-10AVP system controller.
- Column: Symmetry C18 5μm 4.6x150cm, Waters (WAT045905)
- Column Temp: ambient
- Inj. Vol: 50 μL
- Flow rate: 1.0 ml/min
- Detection: VIS, 510 nm
- Retention time: approx 15 min for Fat red 7B
- Run Time = 20 min
- Mobile phase: Water: Methanol (3:97) (filtered through 0.45 μm e filter before use)

Details of the calibration curves prepared are given in Appendix Table A.8.9. The concentration of the preconcentrate in the tested emulsions was approx 500 times higher than the concentration of FR7B. The standard samples were spiked with the preconcentrate (the quantity at least doubled to the maximum amount that could be recovered from a S-SEDDS) and the concentration of FR7B was determined in the presence of the preconcentrate (Appendix Table A.8.10). The preconcentrate was found not to affect the separation of FR7B. Determination of FR7B from emulsions with a known concentration of Fat Red 7B and the preconcentrate was also carried out to evaluate reproducibility of sampling and repeatability between injections (Appendix Table A.8.11). The recovery of FR7B from emulsions was found to be reproducible on five samples (RSD < 3.2 %) and between the injections (RSD < 3.0 %). Each emulsion obtained from the S-SEDDS in the desorption test was tested in duplicate and each sample was injected twice.

2.8.8. Scanning electron microscopy (SEM)

The remaining powder after the desorption test with the S-SEDDSs was collected and dried out on a paper filter at room temperature. The 'desorbed' S-SEDDSs were imaged using the SEM method described in section 2.7.1.

Chapter 3

Physicochemical Profiling of Model Compounds

3.1. Introduction

Three hydrophilic compounds, sodium alendronate trihydrate, disodium pamidronate pentahydrate and acyline acetate, were selected as model drug compounds for development of microemulsions based on derivatives of caprylic and capric acids.

Sodium alendronate trihydrate and disodium pamidronate pentahydrate belong to the same group of analogues of inorganic pyrophosphate called bisphosphonates and therefore have similar chemical structures (Fig. 3.1. A & B). Acyline is a new chemical entity, a novel biopotent GnRH antagonist, formulated as the monoacetate salt (Fig. 3.1. C).

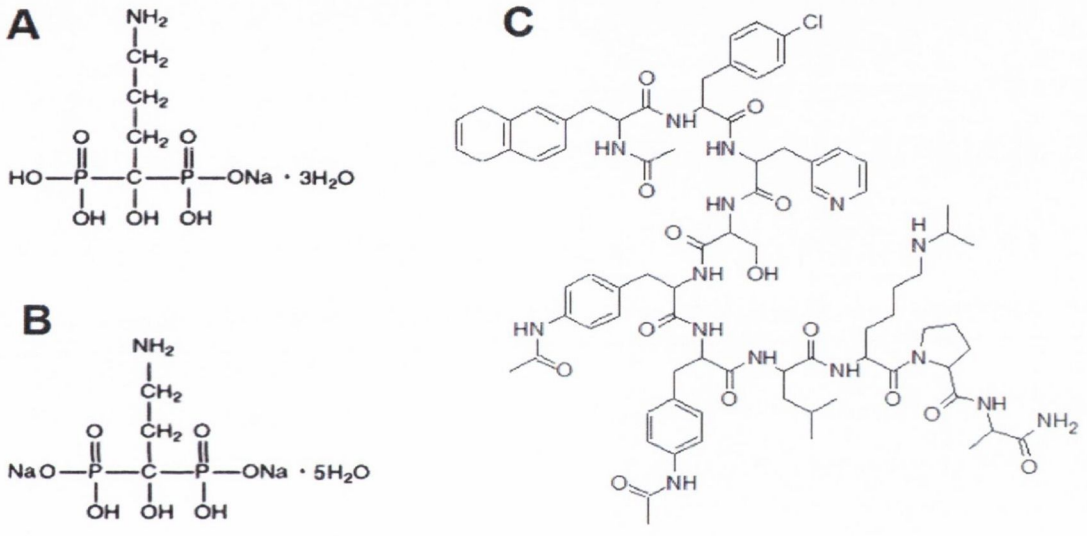

Fig. 3.1. Chemical structure of A) sodium alendronate trihydrate, B) disodium pamidronate pentahydrate, C) acyline (free-base, it has not been established so far which functional group is exactly involved in formation of the acetate salt).

Table 3.1. Structural properties of the model compounds.

Parameter	**Sodium alendronate trihydrate**	**Disodium pamidronate pentahydrate**	**Acyline (free base)**
Chemical Name	Sodium trihydrogen (4-amino-1-hydroxybutylidene) diphosphonate, trihydrate	Disodium dihydrogen (3-amino-1-hydroxypropylidene) diphosphonate, pentahydrate	[Ac-*D*-2Nal[1], *D*-4Cpa[2], *D*-3Pal[3], Aph(Ac)[5], *D*-Aph(Ac) [6], Ilys[8], *D*-Ala[10]] GnRH *
Chemical formula	$C_4H_{12}NNaO_7P_2 \cdot 3H_2O$	$C_3H_9NNa_2O_7P_2 \cdot 5H_2O$	$C_{80}H_{104Cl}N_{15}O_{14}$
Molecular weight	325.12 (271.12 anhydrous)	369.11 (279.11 anhydrous)	1535.23 (free base)
pKa values	five pKas values: 0.8, 2.2, 6.3, 10.9, 12.2 (Lin et al., 1994). 1.33, 2.22, 6.39, 10.96, 11.82 (Hägele et al., 2000).	five pKas values: 1.24, 1.93, 6.04, 10.18, 12.14 (Hägele et al., 2000).	N/A

*Abbreviations: Ac = acetyl; 2Nal = 3-(2-naphthyl)alanine; 4Cpa = 4-chlorophenylalanine; 3Pal = 3-(3-pyridyl)alanine, Aph = 4-aminophenylalanine; Ilys = N-isopropyllysine.

Alendronate and pamidronate, both exist in a zwitterionic form over a wide range of pH. The ionized forms of alendronate are shown in Fig. 3.2. Pamidronate is ionized in the similar way according to its pKa values (Table 3.1). Both compounds are highly negatively charged in the physiological pH of the small intestine (Lin et al., 1994; Lin, 1996).

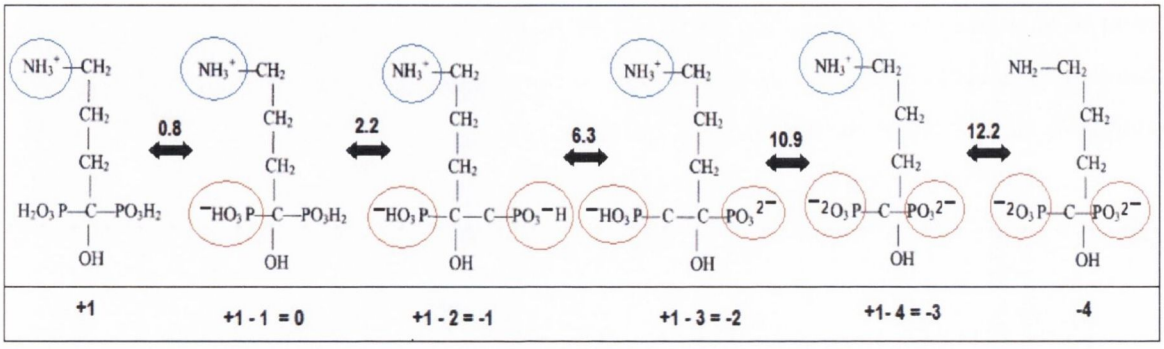

Fig. 3.2. Ionized forms of sodium alendronate depending on pKa values: 2.2, 6.3, 10.9 (Lin et al., 1994).

The aim of this work was to evaluate physical and chemical properties of the model drug compounds to understand their suitability for microemulsion formulations. It was expected that physicochemical characterisation would enable suitable versions of microemulsions or self-emulsifying systems to be designed and suitable testing methods of these formulations to be chosen.

3.2. Characterisation of sodium alendronate trihydrate and disodium pamidronate pentahydrate

3.2.1. Solid state Fourier transform infrared spectroscopy (FTIR)

Identification of bisphosphonates is typically carried out by FTIR, although these compounds have only a few characteristic functional groups. The FTIR spectra collected for sodium alendronate trihydrate and disodium pamidronate pentahydrate are presented in Fig. 3.3. The presence of crystalline water, typically observed as absorption bands in the range 3200 to 3500 cm^{-1}, overlapped with the band characteristic of the hydroxyl group (stretching) and amine (stretching) in both bisphosphonates (Fig. 3.3). The peaks and bands were identified based on the results of Negrea et al. (2010) and Liu et al. (2009) for sodium alendronate trihydrate and the typical interpretation of peaks and bands established for various groups detected by IR (Settle, 1997; Coates, 2000). Table 3.2 summarises the main characteristic peaks and bands observed in the studied bisphosphonates.

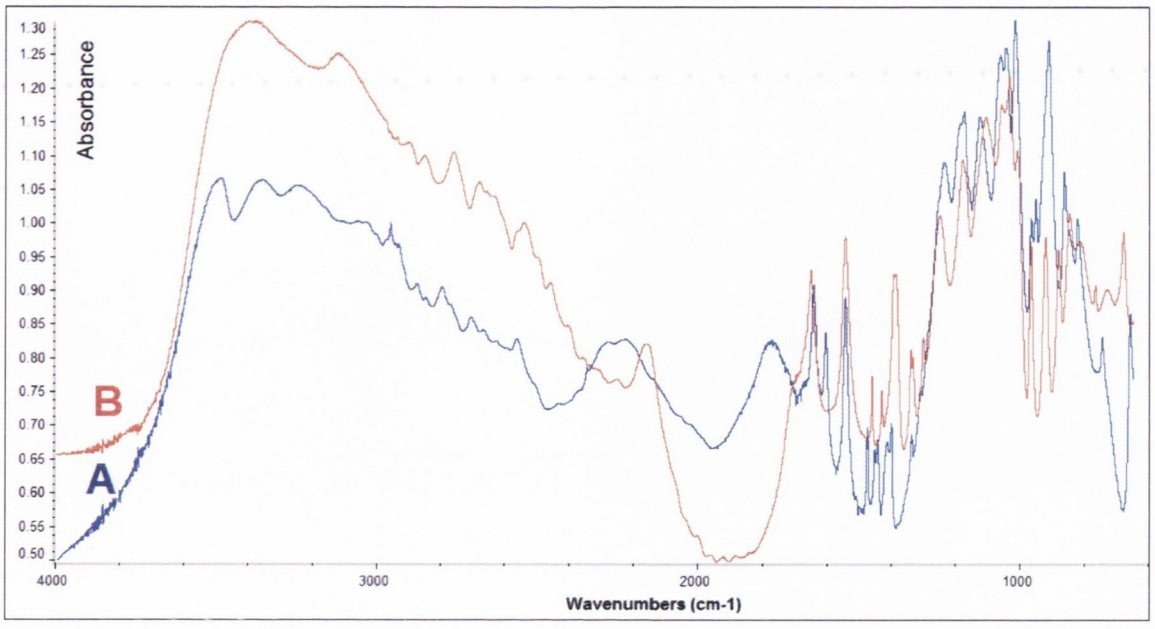

Fig. 3.3. FTIR spectrum of A) sodium alendronate trihydrate B) disodium pamidronate pentahydrate

Table 3.2. Identification of characteristic peaks for bisphosphonates in FT-IR spectrum in the range 700 – 4000 cm^{-1}.

Detected peaks		Identification	
Sodium alendronate trihydrate	**Disodium pamidronate pentahydrate**	Characteristic group	Comment
3487.47	~3450	***-OH***	O–H stretching, typically seen between 3500 and 3200 cm^{-1}
914.24	922.24		O–H bending vibration, around 910 - 950 cm^{-1}
3365.24	3355.35	***-NH_2***	N–H stretching (primary amines) seen between 3400-3250 cm^{-1}
1645.78	1651.82		N–H bend (primary amines only), from 1650-1580 cm^{-1}
1127.18, 1175.86	1107.21, 1178.58	***≡P=O***	P=O stretching vibration typically seen between 1100-1200 cm^{-1}

3.2.2. Thermal analysis (Differential scanning calorimetry & Thermal gravimetric analysis)

DSC characterisation of sodium alendronate trihydrate revealed three main thermal events. An endothermic peak observed at approximately 128°C (onset at 119.6 °C) was associated with a weight loss of approximately 16.2% that corresponded to liberation of 3 molecules of hydrated water (Fig. 3.4). The second thermal event, an endothermic peak around 265°C, reflected melting and was closely followed by decomposition of the compound (the third exothermic peak). The observed thermal behaviour of sodium alendronate trihydrate was in agreement with results presented by Asnani et al. (2009). Disodium pamidronate pentahydrate showed similar thermal behaviour to sodium alendronate trihydrate. An endothermic peak observed at approximately

116°C (onset 107.7°C) was related to a weight loss of approximately 24%, equivalent to the removal of 5 molecules of hydrated water (Fig. 3.5). The melting peak observed around 210 °C was followed by decomposition.

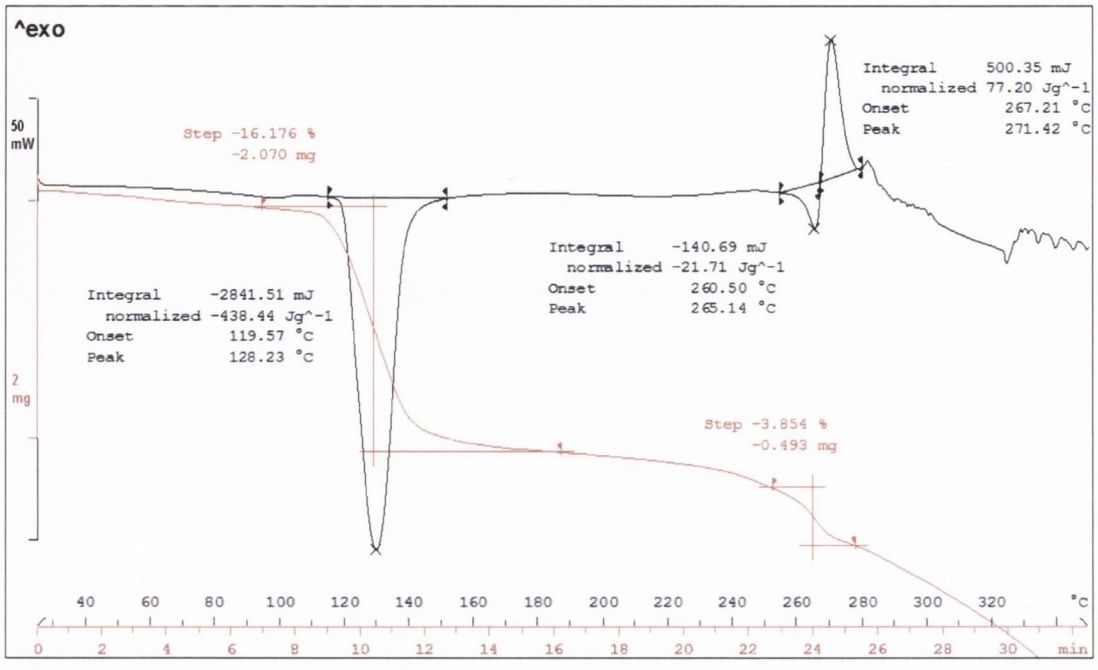

Fig. 3.4. DSC and TGA curves of sodium alendronate trihydrate

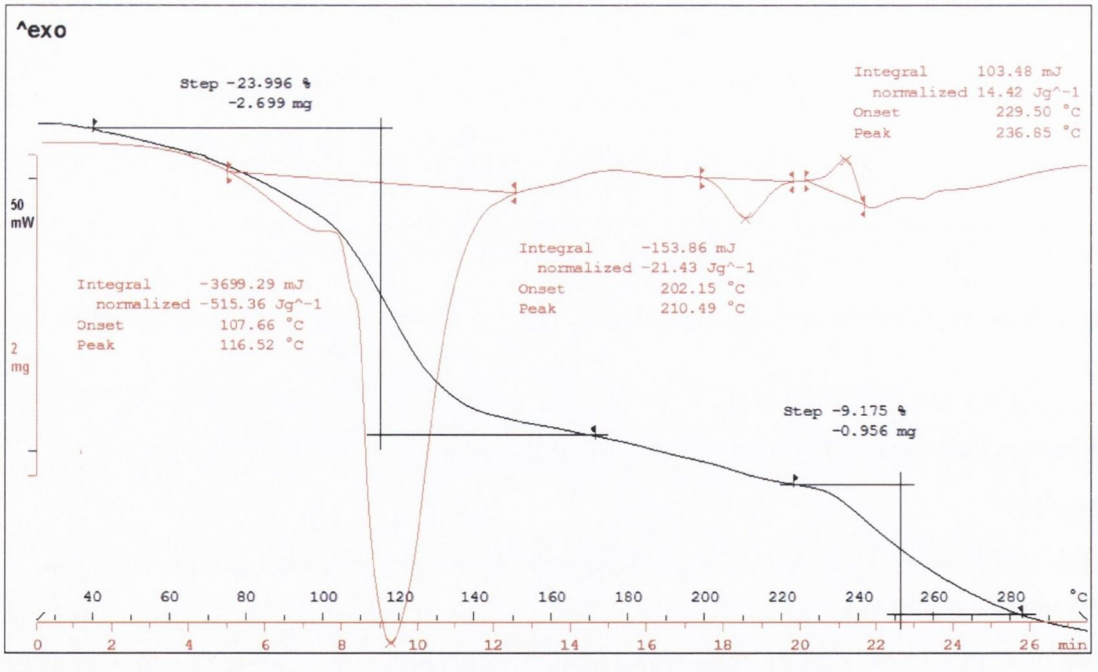

Fig. 3.5. DSC and TGA curves of disodium pamidronate pentahydrate

3.2.3. Powder X-Ray Diffraction analysis (PXRD)

Both compounds when analysed by powder X-ray diffraction were found to be crystalline (Fig. 3.6). A number of characteristic peaks for sodium alendronate trihydrate and disodium pamidronate pentahydrate were identified and are summarised in Table 3.3.

Table 3.3. Characteristic peaks for crystalline forms of sodium alendronate trihydrate and disodium pamidronate pentahydrate observed in XRD diffractogram in range 5 – 40 degrees.

Material	Characteristic peaks (2θ, degrees)
Sodium alendronate trihydrate	9.25, 12.40, 13.50, 17.50, 18.55, 19.70, 20.25, 21.00, 23.35, 24.25, 24.95, 26.20, 26.90, 28.40, 30.0, 31.95, 34.3, 35.50, 37.80, 38.55
Disodium pamidronate pentahydrate	9.50, 8.55, 8.90, 15.80, 25.35, 29.45, 33.00, 34.80

Sodium alendronate trihydrate appeared to have a more defined crystalline pattern compared to disodium pamidronate pentahydrate. Multiple, high intensity peaks were observed in the former compound, while the latter showed only several peaks with medium intensity.

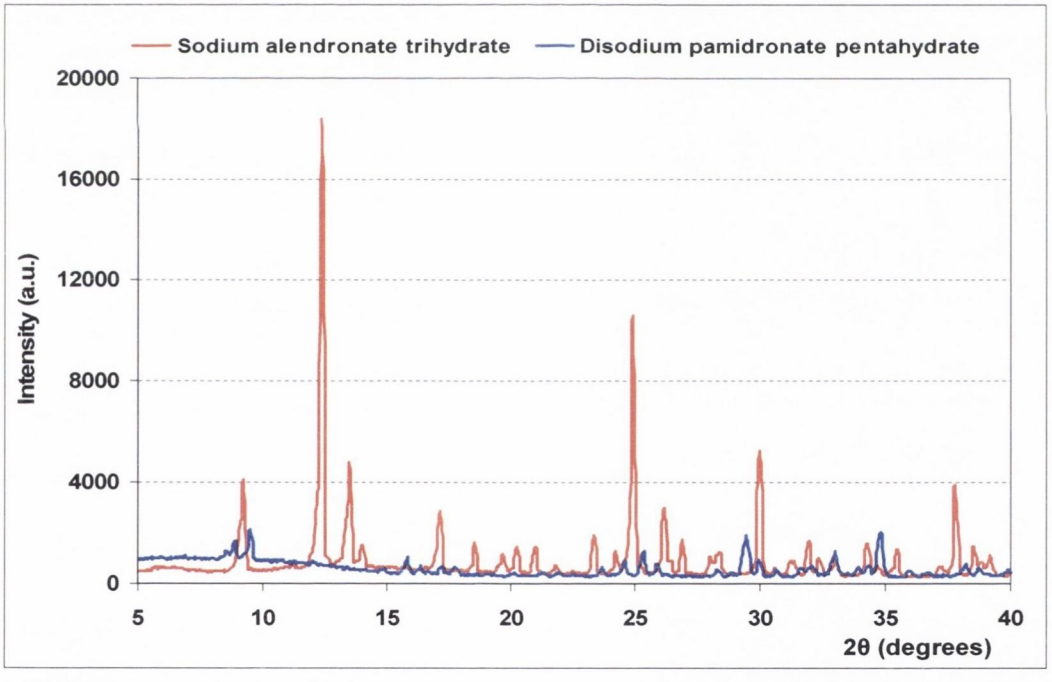

Fig. 3.6. PXRD diffractogram of bisphosphonates.

3.2.4. Particle sizing by laser diffraction (PSD)

Both bisphosphonates were measured as supplied, without any prior processing that could affect particle size distribution (PSD). Sodium alendronate trihydrate appeared to be a coarser material compared to disodium pamidronate pentahydrate (Fig. 3.7). The material consisted of approximately 90% of particles, which were smaller than 288 μm and contained approximately 10% of very fine particles below 7μm (Table 3.4). The particle size distribution for both materials

was bimodal (Fig. 3.7). Disodium pamidronate pentahydrate consisted of very small fine particles where the majority (Dv90) was below 40μm and approximately 50% of particles were below 16 μm (Table 3.4).

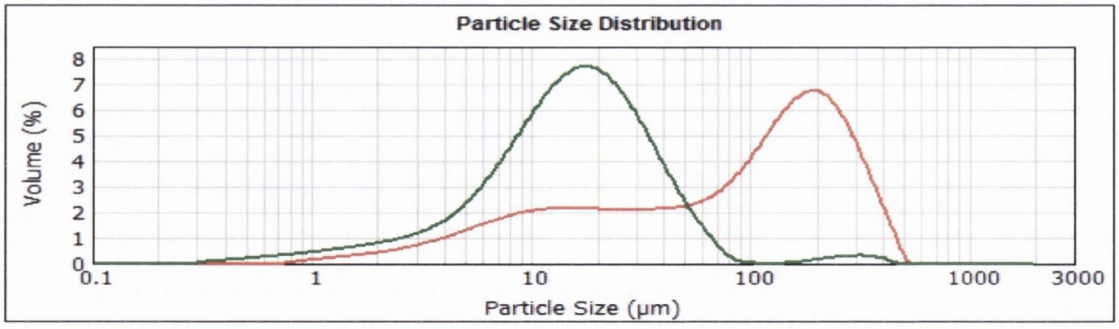

Fig. 3.7. Particle Size Distribution of sodium alendronate trihydrate dispersed at 2 bar (red line) and disodium pamidronate pentahydrate dispersed at 3 bar (green line).

Table 3.4. Comparison of the Particle Size Distribution obtained for bisphosphonates.

Sample Name		Dv10 [μm]	Dv50 [μm]	Dv90 [μm]	Specific surface area [m2/g]	Span	D [4, 3] - Volume weighted mean [μm]	D [3, 2] - Surface weighted mean [μm]
Sodium alendronate trihydrate (dispersing pressure: 2 bar, feeding rate: 50%)	**Average**	**7.3**	**102.7**	**288.5**	**0.305**	**2.736**	**125.6**	**19.7**
	SD	0.1	2	1.0	0.006	0.044	1.1	0.4
	RSD	1.4	1.9	0.3	2.0	1.6	0.9	2.0
Disodium pamidronate pentahydrate (dispersing pressure: 3 bar, feeding rate: 40%)	**Average**	**4.1**	**15.6**	**40.2**	**0.787**	**2.315**	**22.6**	**7.6**
	SD	0.1	0.4	2.4	0.018	0.091	3.8	0.2
	RSD	2.4	2.6	6.0	2.3	3.9	16.8	2.6

3.2.5. Aqueous, pH dependent solubility

Solubility of sodium alendronate trihydrate and disodium pamidronate pentahydrate was mesured in water and modified (potassium) K-McIlvaine's buffers. Sodium alendronate trihydrate was found to be the most soluble in pH 6.5 (final pH, after incorporation of the drug) and also showed high solubility in pH 2.7 (Table 3.5, Fig. 3.8). Solubility of sodium alendronate trihydrate in an aqueous medium (presumably water) was reported to be 40 mg/ml (Ezra & Golomb, 2000). There is no data in the literature on the solubility of sodium alendronate trihydrate in other buffered media.

Table 3.5. Solubility of sodium alendronate trihydrate in various aqueous media, measured at 25°C after 24 hours.

Initial pH (measured prior to incorporation of the drug)	**Final pH** (after incorporation of the drug)	**Solubility of sodium alendronate trihydrate [mg/ml]**		
		Average	SD	RSD%
Purified water (pH 5.6)	pH 4.5	**34.53**	0.85	2.46
pH 2.2	pH 2.7	**43.11**	0.73	1.69
pH 4.4	pH 4.4	**26.99**	0.72	2.67
pH 5.5	pH 5.2	**25.26**	0.34	1.36
pH 6.8	pH 6.1	**35.05**	0.85	2.41
pH 7.8	pH 6.5	**51.73**	1.43	2.77

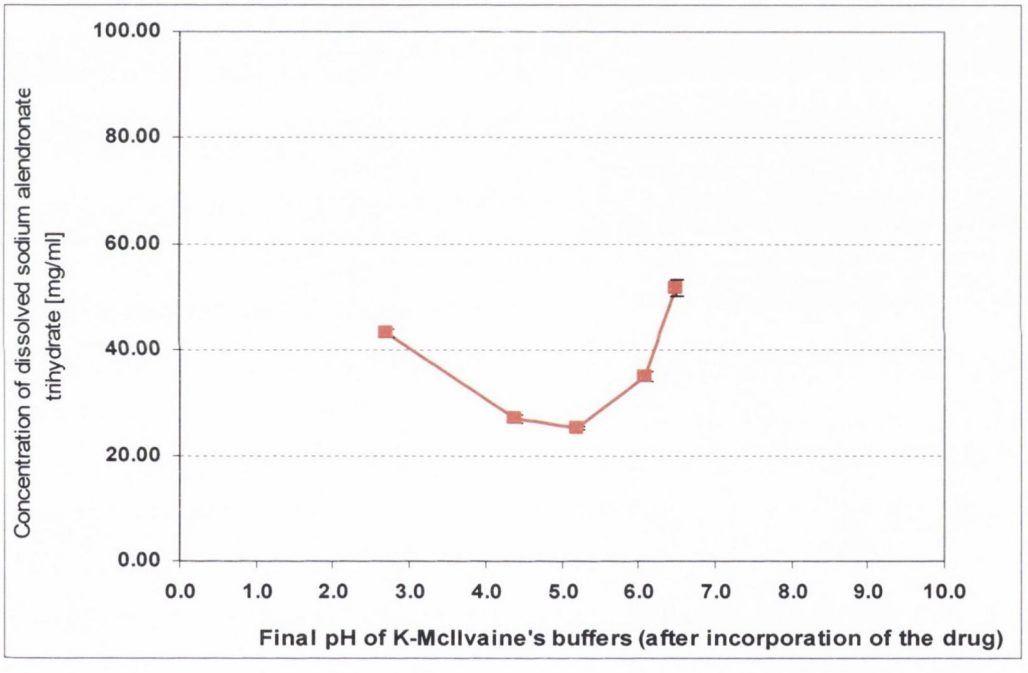

Fig. 3.8. Relationship between solubility of sodium alendronate trihydrate and pH of the media.

The relationship between solubility and pH of the final K-McIlvaine's buffers is shown in Fig. 3.8. Within the used range of pH, solubility of sodium alendronate trihydrate was high in highly acidic pH, decreased slightly in weakly acidic pH and increased again in weakly alkaline pHs. The solid material recovered after 24-hour solubility study using water and the modified K-McIlvaine's buffers, was recovered, dried and subsequently identified as sodium alendronate trihydrate by DSC in all pHs (Fig. 3.9).

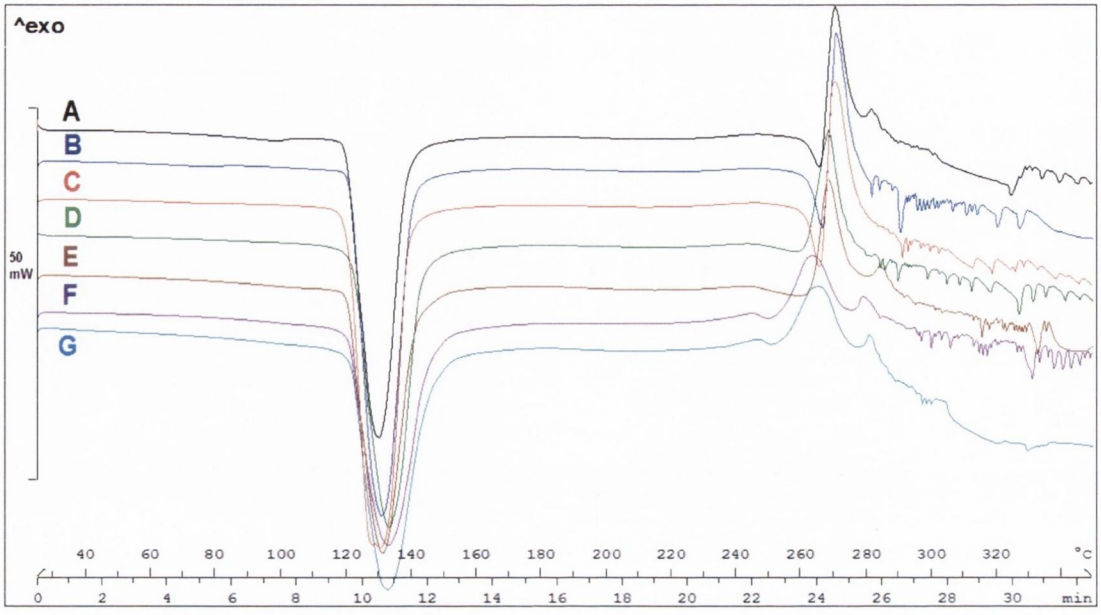

Fig. 3.9. DSC thermograms of the solid material recovered after 24 hour solubility study of sodium alendronate trihydrate at 25°C in media having initial pHs of B) 5.6 (purified water), C) pH 2.2, D) pH 4.4, E) pH 5.5, F) pH 6.8, G) pH 7.8 compared to the original material A).

The highest solubility of disodium pamidronate pentahydrate was found in the modified K-McIlvaine's buffers having initial pH 4.4 (prior to incorporation of the drug) and the final pH of 6.1 (Table 3.6, Fig. 3.10). The solubility of disodium pamidronate pentahydrate was also high in the K-modified McIlvaine's buffers with the final pH 6.5 and 7.2 but significantly lower compared to the one observed in pH 6.1. Good solubility of disodium pamidronate in pH 6.1 and above (when K-modified buffers pH 4.4 –7.8 were used) was likely to be associated with the formation of more negatively charged form of pamidronate, which existed above pH 6.04 up to 10.18 (pKa_3 = 6.04, pKa_4 = 10.18). Sodium pamidronate pentahydrate is described in the literature as soluble in water but exact solubility values are not given.

Table 3.6. Solubility of disodium pamidronate pentahydrate in various aqueous media, measured at 25°C after 24 hours.

Initial pH (measured prior to incorporation of the drug)	**Final pH** (after incorporation of the drug)	**Solubility of disodium pamidronate pentahydrate [mg/ml]**		
		Average	SD	RSD%
Purified water (pH 5.6)	pH 8.8	**43.39**	1.44	3.32
pH 2.2	pH 6.1	**30.49**	0.22	0.71
pH 4.4	pH 6.1	**70.47**	2.29	3.25
pH 5.5	pH 6.5	**62.04**	3.33	5.37
pH 6.8	pH 7.2	**59.84**	0.91	1.52
pH 7.8	pH 8.1	**64.17**	0.68	1.05

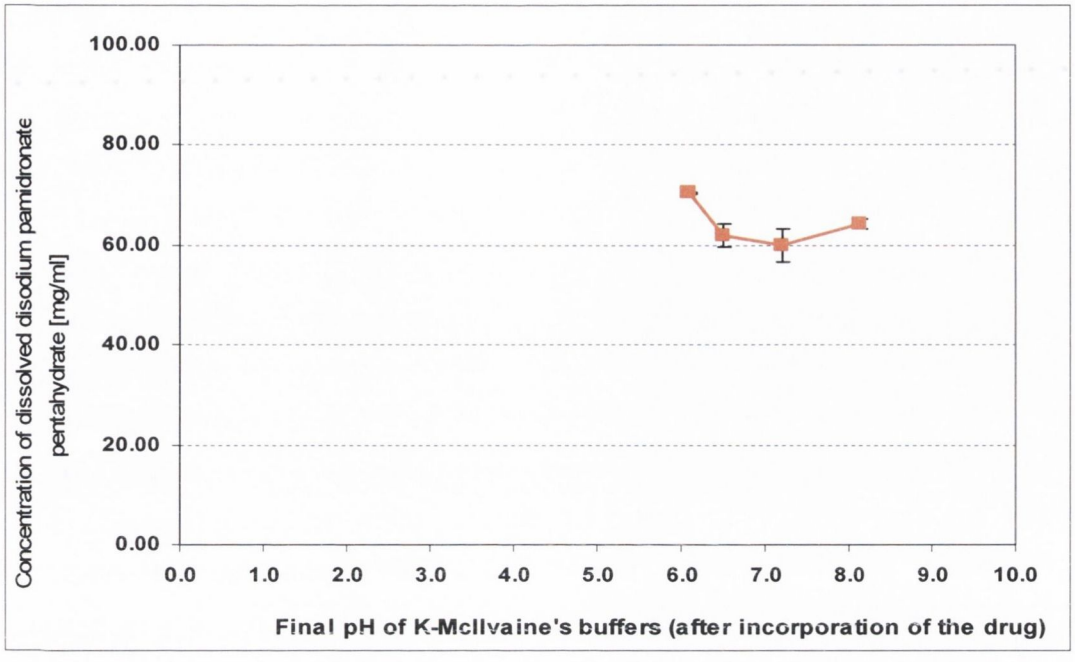

Fig. 3.10. Relationship between solubility of disodium pamidronate pentahydrate and pH of the used media.

The lowest solubility observed in pH 6.1, when the K-modified buffer pH 2.2 was used, appared to be caused by the formation of different form of pamidronate. The new salt of pamidronate was revealed when the solid material recovered post 24-hour solubility study with disodium pamidronate pentahydrate, was tested by DSC (Fig. 3.11).

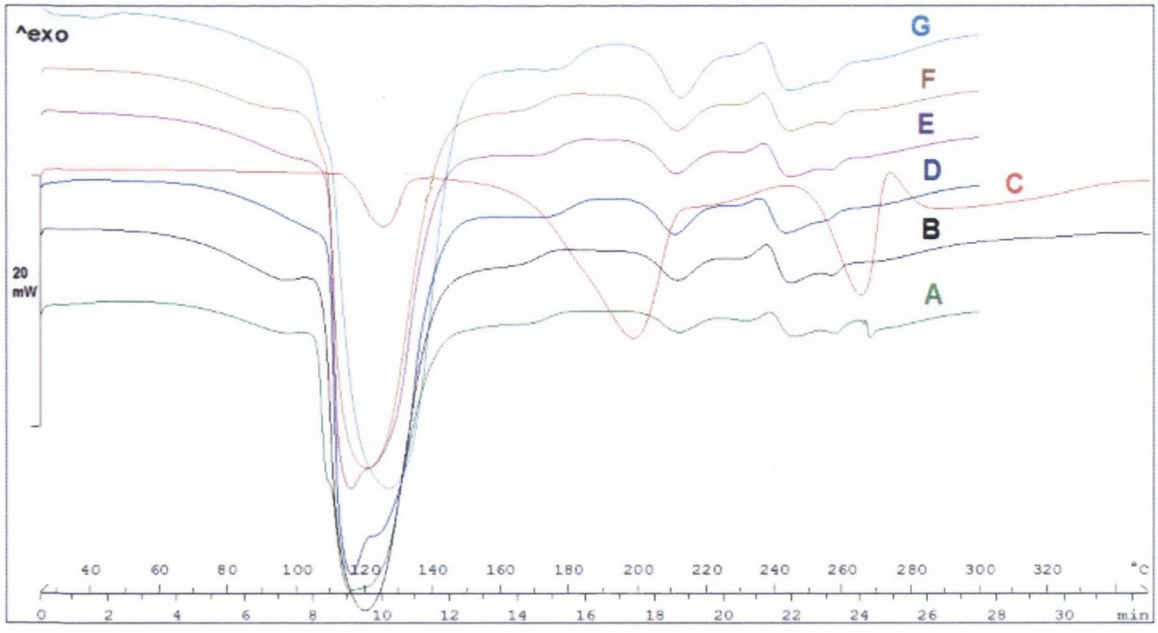

Fig. 3.11. DSC thermograms of the solid material recovered after 24 hour solubility study of disodium pamidronate pentahydrate at 25°C in media having initial pHs of B) 5.6 (purified water), C) pH 2.2, D) pH 4.4, E) pH 5.5, F) pH 6.8, G) pH 7.8 compared to the original material A).

The same characteristic peaks as for the original material were observed in the solid samples recovered from all used media, except for the modified K-McIlvaine's buffer having the initial pH of 2.2 (Fig. 3.11). In the solid material recovered from the modified K-McIlvaine's buffer with an initial pH of 2.2, a characteristic peak corresponding to dehydration of 3 molecules of water was substantially reduced and an additional, small endothermic peak around 190°C was detected. This peak was also associated with a weight loss that indicated a hydrated molecule. It was suspected that some type of monosodium salt could have been formed. The monosodium pamidronate monohydrate was synthesised according to the preparation method presented in the patent WO03/053985A1(Chapter 2, section 2.2.1). DSC and TGA testing of the synthesised material revealed an endothermic peak around 190°C which was associated with a weight loss of approximately 7%, corresponding to liberation of one molecule of hydrated water (Appendix, Fig. A.3.3). The second endothermic peak at approximately 262 °C and the exothermic peak round 272 °C, related to the weight loss of approximately 12.4%, were explained as melting followed by rapid decomposition of monosodium pamidronate. The PXRD diffractogram of the in-house synthesised monosodium pamidronate monohydrate and the material presented in the patent WO03/053985A1, were identical (Appendix Fig. A.3.4). Therefore it was confirmed that the in-house synthesis produced monosodium pamidronate monohydrate. Comparison between the solid material recovered after 24-hour solubility study in modified K-McIlvaine's buffer with an initial pH 2.2, and the synthesised monosodium pamidronate monohydrate (shown in Fig. 3.12) identified the undissolved material as a mixture of original material (disodium pamidronate pentahydrate) and monosodium pamidronate monohydrate. Precipitated monosodium pamidronate monohydrate and undissolved disodium pamidronate pentahydrate appeared to be inhomogeneously mixed in the solid sample recovered from pH 2.2 (a different ratio was seen between these materials on repeated DSC diagrams form the sample).

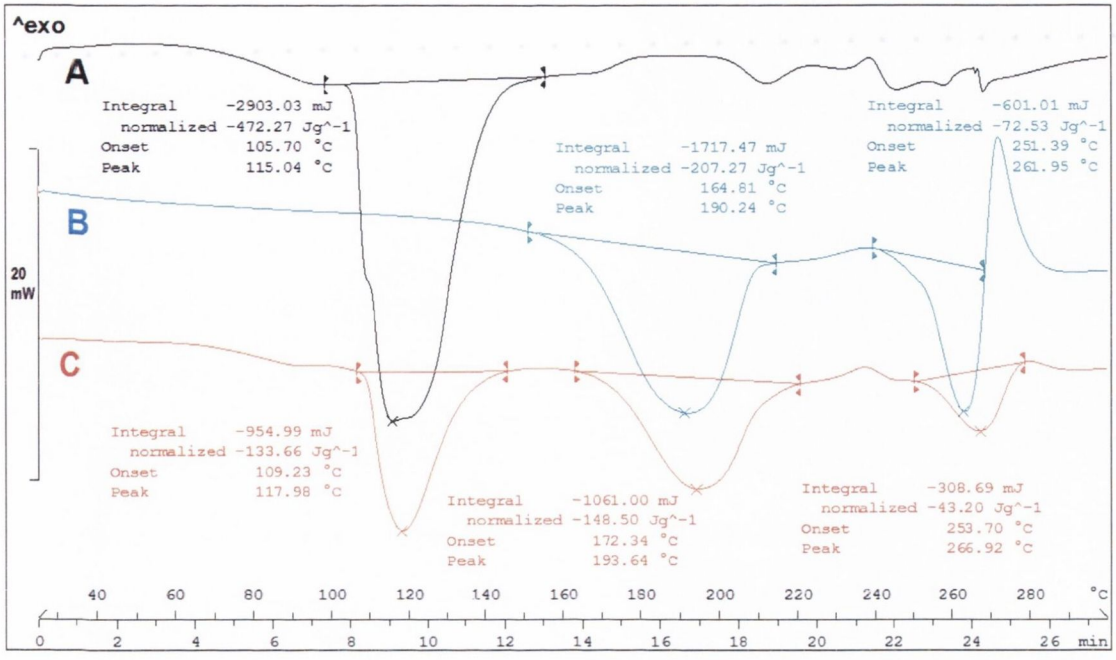

Fig. 3.12. DSC thermograms of the solid material recovered after 24 hour solubility study of disodium pamidronate pentahydrate at 25°C in K-McIlvaine's buffer with an initial pH 2.2 C) compared to the original material (disodium pamidronate pentahydrate) A) and synthesised monosodium pamidronate monohydrate (B).

3.2.6. Solubility in the standard GIPET® II formulation and propylene glycol

Solubility of the bisphosphonates was evaluated in propylene glycol and the standard GIPET® II formulation comprising glycerides of caprylic/capric acids, polysorbate 80 and typical quantities of propylene glycol and PEG 400 that are allowed in liquid formulations for encapsulation (the exact composition is given in the Chapter 2, section 2.2.8). Propylene glycol is a very good polar solvent in which to dissolve hydrophilic compounds. Unfortunately it can be used only in a small percentage (max 5-10% depending on type of capsule) in liquid fillings for encapsulation since the excess of propylene glycol causes softening of the capsule shell (Cole, 2007; Meissonier, 2007). Drug solubility in the standard GIPET® II formulations gives a preliminary estimation of drug solubility in derivatives of caprylic and capric acids. Although LogP is typically used to assess affinity to dissolve in water and in the lipophilic medium (octanol), it is also known that compounds having similar LogP values can have significantly different solubility in lipidic materials such as triglycerides (Stella, 2007).

Solubility of sodium alendronate trihydrate (at 25° C, after 24 and 48 hours) in the standard GIPET® II formulation and propylene glycol was found to be very poor, lower than 1 mg per 1 g of the solvent. Choi et al. (2008) found the solubility of alendronate in propylene glycol to be 2110.3 ng/ml ± 432.6 after 48 hours at 37°C. Solubility of alendronate, tested after 48 hours at 37°C, in other lipid vehicles such as propylene glycol monolaurate, propylene glycol

monocaprylate, oleyl alcohol was reported to be very poor, 15.1 ng/ml ± 2.6, 19.4 ng/ml ± 3.7, 3.8 ng/ml ± 0.7 respectively (Choi et al., 2008).

The solid material recovered after the solubility study in the standard GIPET® II formulation was identified as the original material (sodium alendronate trihydrate) by DSC testing (Fig. 3.13).

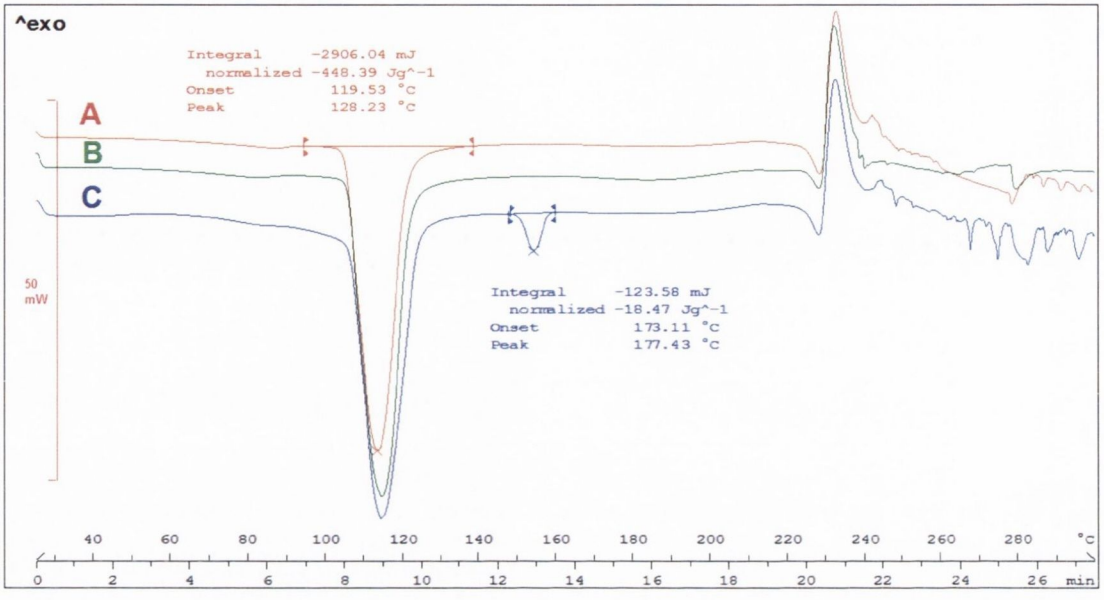

Fig. 3.13. DSC thermograms of sodium alendronate trihydrate -original material (A), the solid material recovered 48 hour solubility study in the standard GIPET2 formulation (B) and the solid material recovered 48 hour solubility study in propylene glycol (C).

The solid material obtained after the solubility study in propylene glycol was not identical to the original material (Fig. 3.13). An additional, endothermic peak was detected around 177°C, while the melting point of sodium alendronate (anhydrous) observed at 265°C remained unchanged.

A long-term study (approximately 13 months) of sodium alendronate trihydrate in propylene glycol (at a temperature of 25°C) was carried out to identify the unknown peak (compound). As 'more aged' samples recovered from propylene glycol were tested, it was observed that the size of the unknown peak increased while the size of the 'dehydration peak' of the trihydrate decreased. This suggested a conversion of sodium alendronate trihydrate into some type of solvate containing propylene glycol instead of water. It was also observed that the solvate was unstable and appeared to convert easily back to the trihydrate form when relative humidity was equal and higher than 50%. A conversion into trihydrate was observed when wet samples recovered from propylene glycol were left to dry at room temperature (23-24°C, RH% = 50%) for 24 hours prior to DSC/TGA testing. The 'most aged' samples (4E- 4G) were dried in anhydrous conditions (a desiccator filled with phosphorus pentoxide desiccant). An attempt to assay the content of propylene glycol by GC-MS chromatography was made, however the results did not correlate with

the size of the 'solvate' peak and the weight loss determined by DSC/ TGA testing (Table 3.7, Appendix Fig. A.3.5 - A.3.6.).

Table 3.7. DSC, TGA and GC-MS characterisation of two samples recovered from propylene glycol representing a mixture of the solvate and trihydrate (4E) and pure solvate (4G).

Testing		Sample 4E (322 days)	Sample 4G (382 days)
Peak corresponding to trihydrate	Normalized enthalpy	-138.72 Jg^{-1}	Peak was not observed
	Peak temperature	128.81 °C	
	Onset temperature	121.31 °C	
	Weight loss	**5.620 %**	
Peak corresponding to the solvate of propylene glycol	Normalized enthalpy	-177.48 Jg^{-1}	-275.48 Jg^{-1}
	Peak temperature	181.07 °C	181.08 °C
	Onset temperature	173.31 °C	172.03 °C
	Weight loss	**13.930 %**	**21.952 %**
Content of propylene glycol in the sample determined by GC-MS		**8.23 %**	**9.12 %**

The GC-MS chromatography detected the presence of propylene glycol; however the assayed content of propylene glycol was lower than expected based on the TGA results. Lack of correlation between the other methods and GC-MS chromatography could be attributed to instability of the solvate observed at room temperature. Sample 4G represented the 'pure solvate' (based on the DSC and TGA testing) since the characteristic 'trihydrate' peak for sodium alendronate trihydrate was not detected. DSC and TGA testing (after 24 hours drying at anhydrous conditions) indicated that the substance formed was a solvate of sodium alendronate with one molecule of propylene glycol (Appendix Fig. A.3.6). The endothermic peak around 181°C was associated with the weight loss of approximately 22%, which corresponded to liberation of 1 molecule of propylene glycol. Also the PXRD pattern of the formed solvate differed from the original material (Appendix Fig. A.3.7).

Solubility of disodium pamidronate pentahydrate (at 25° C, after 24 and 48 hours) in the standard GIPET® II formulation and propylene glycol was found to be very poor, lower than 1 mg per 1 g of the solvent. The solid material which remained after the solubility study in both solvents, was identified as the original material by DSC testing (Fig. 3.14).

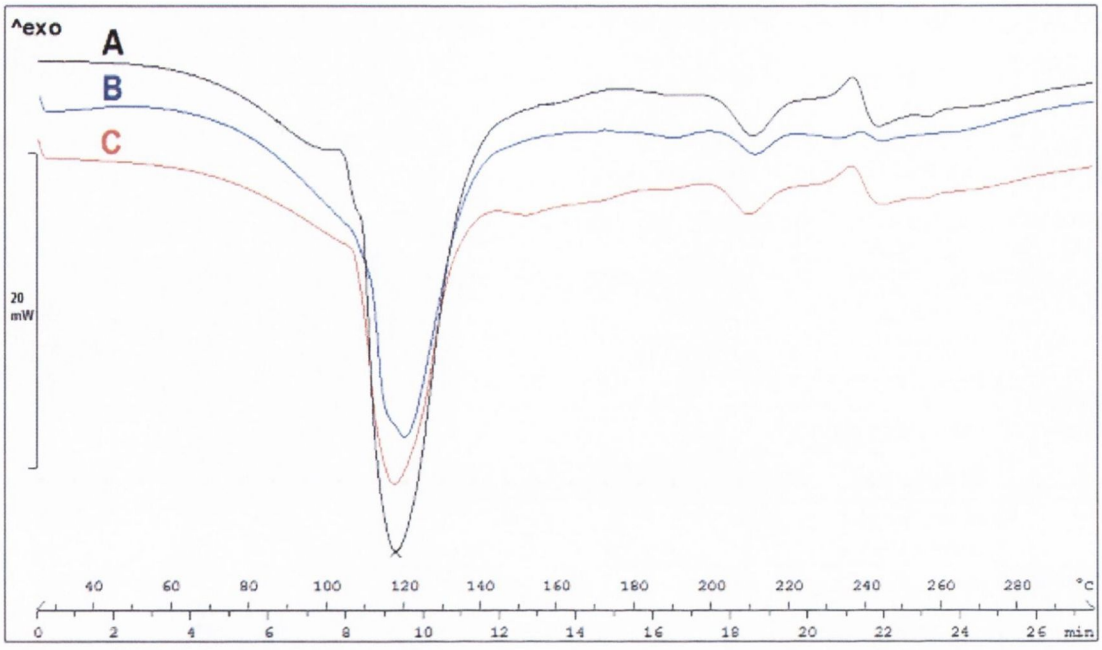

Fig. 3.14. DSC thermograms of disodium pamidronate pentahydrate -original material (A), the solid material recovered 48 hour solubility study in the standard GIPET2 formulation (B) and the solid material recovered 48 hour solubility study in propylene glycol (C).

3.2.7. Calculation of cLogP and cLogD

The calculated partition coefficient (cLogP) was computed (with the use of software) for un-ionized forms of alendronic and pamidronic acids (Table 3.8). In both cases the cLogP values were highly negative indicating a strongly hydrophilic character of the molecules and poor lipophilicity.

Table 3.8. Calculated cLogP and main cLogD values for the bisphosphonates.

Calculated parameter		Alendronic acid	Sodium alendronate	Pamidronic acid	Disodium pamidronate
cLogP		-3.52 ± 0.72	/	-3.40 ± 0.85	/
cLogD at pHs	1.50	-4.28	-3.76	-4.65	-3.15
	5.00	-6.21	-5.75	-6.56	-4.94
	6.50	-6.28	-5.86	-6.63	-5.07
	7.40	-6.56	-6.00	-6.92	-5.08

The distribution coefficient (cLogD), calculated for all forms (ionized and un-ionized) in the range of pH from 0 to 14 is presented in Fig. 3.15 for sodium alendronate/alendronic acid and in Fig. 3.16 for disodium pamidronate/pamidronic acid.

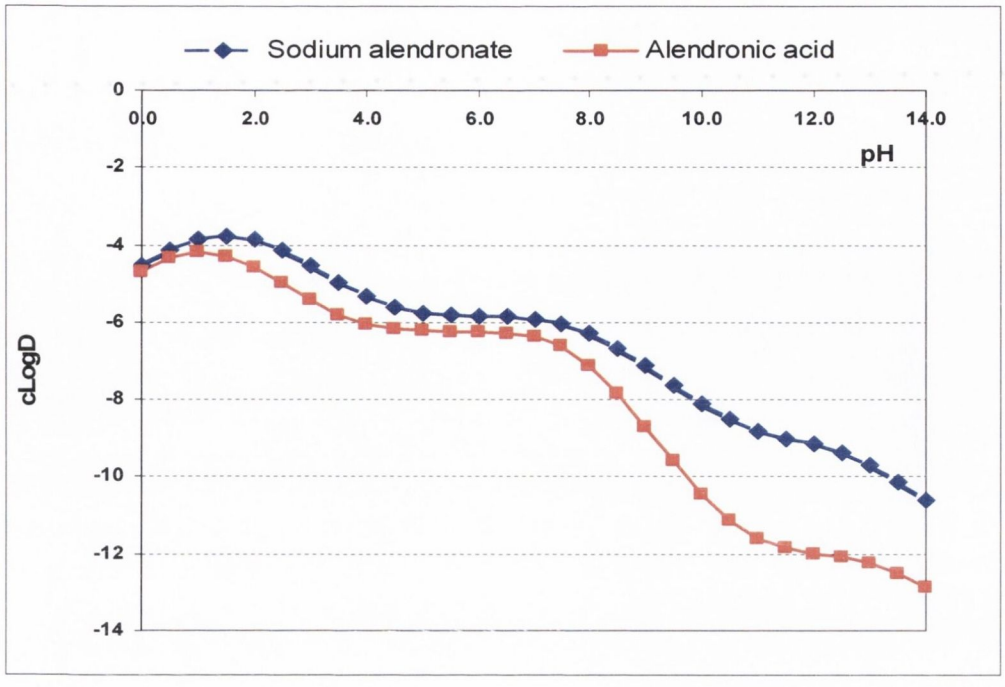

Fig. 3.15. Relationship between cLogD and pH calculated for sodium alendronate and alendronic acid.

In both cases, as the pH increased the hydrophilic character increased, due to stronger ionisation. In the physiological pH of the intestinal tract between pH 6.5 and 7.40, both bisphosphonates would be hydrophilic and highly ionized negatively, which is one of the main reasons for poor oral bioavailability of these compounds (Lin, 1996).

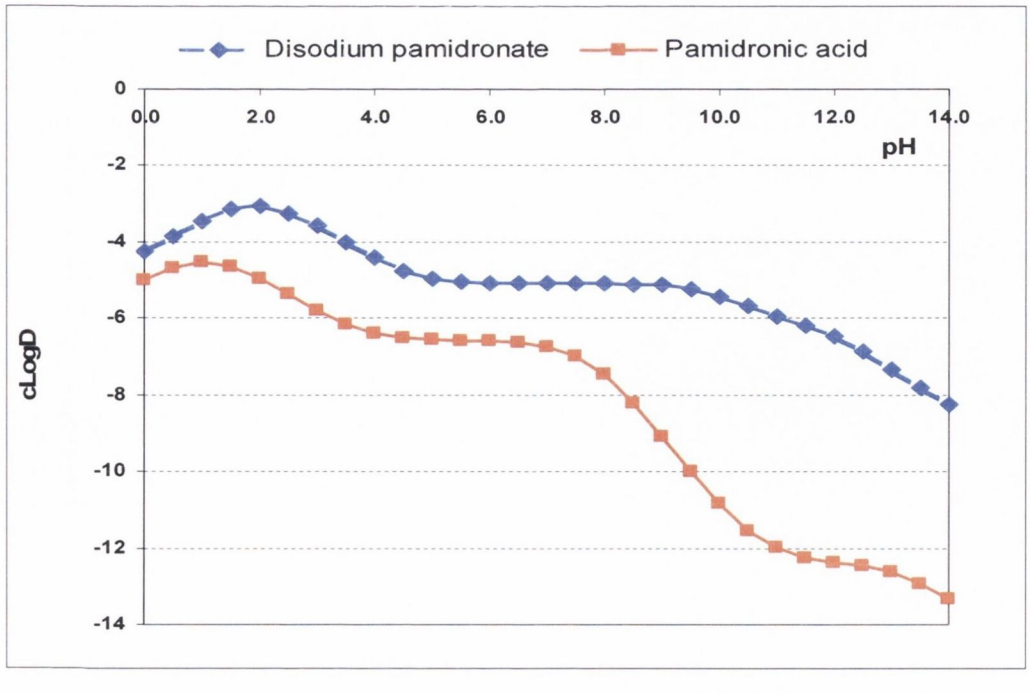

Fig. 3.16. Relationship between cLogD and pH calculated for disodium pamidronate and pamidronic acid.

3.3. Characterisation of acyline monoacetate

Acyline (monoacetate) is classified as a high potency material and therefore requires containment when handling. Due to safety concerns, limited physicochemical characterisation was carried out in order to limit exposure to the compound.

3.3.1. Solid state Fourier transform infrared spectroscopy (FTIR)

In relation to the FTIR spectrum of acyline acetate, shown in Fig. 3.17, main bands and peaks were identified based on typical assignment of functional groups (Settle, 1997; Coates, 2000) as summarised in Table 3.9.

Table 3.9. Identification of characteristic peaks observed in FT-IR spectrum of acyline monoacetate in the range 700 – 4000 cm^{-1}.

Detected main peaks	**Identification**	
Acyline monoacetate	Characteristic group	Comment
3297.43	**-OH --NH_2**	O–H stretching, typically seen between 3500 and 3200 cm^{-1} or N–H stretching (secondary amines) seen between 3350-3310 cm^{-1}
2957.99	**C-H**	C-H, aliphatic stretching typically seen from 3000–2850 cm^{-1}
3059.90	**C-H (aromatic)**	C-H, aromatic stretching, typically seen at 3100-3000 cm^{-1}
1655.90	**C=O**	C=O, stretching typically seen between 1710–1665 cm^{-1}
1540.06	**C-C (aromatic)**	C-C, aromatic stretching typically seen between 1600–1585 cm^{-1}
1268.86	**C-N (aromatic)**	C–N stretching (aromatic amines) from 1335-1250 cm^{-1}
816.76	**Cl-C**	C–Cl stretching 850-550 cm^{-1}

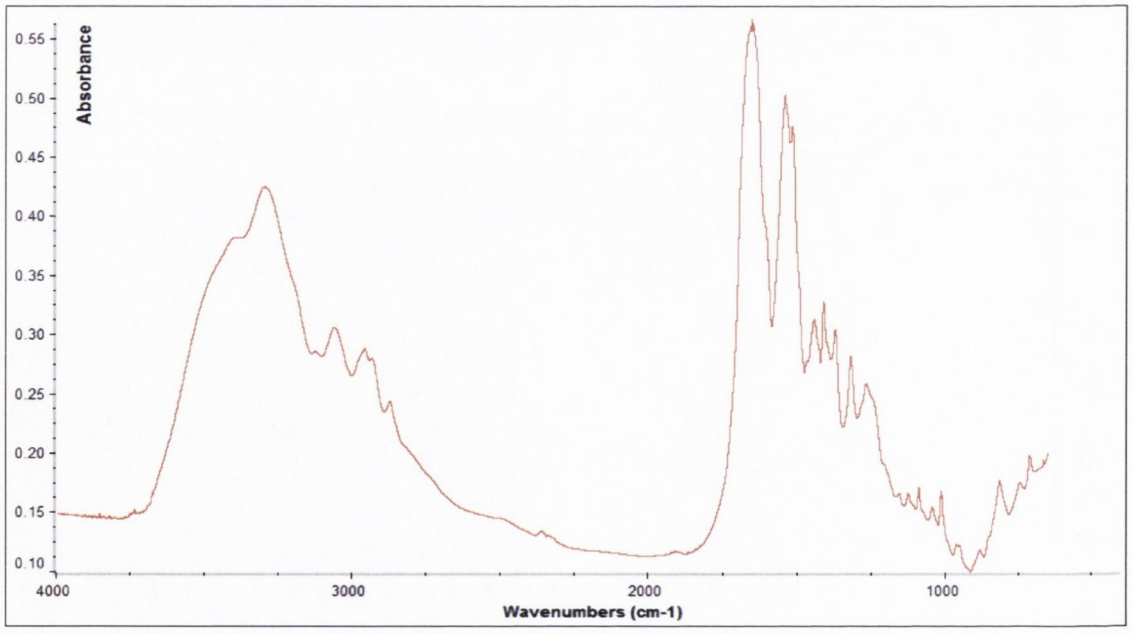

Fig. 3.17. FTIR spectrum of acyline monoacetate.

3.3.2. Differential scanning calorimetry (DSC)

DSC of acyline acetate revealed three main peaks (Fig. 3.18). The first endothermic peak around 57 °C could be explained by the loss of adsorbed water since the material contained approximately 2-7% of residual moisture according to the Certificate of Analysis (CoA). The second peak, detected around 178°C, was exothermic and could possibly have represented recrystallization. The 'recrystallisation peak' was very small and shallow. The last, endothermic peak around 231°C was likely to represent melting followed by decomposition (degradation) of acyline. The "melting peak" was small, which suggested that only a small portion of the sample was crystalline. The normalised enthalpy of this melting process was very low, ~ 2.7 Jg^{-1}. A relatively low normalised enthalpy, ~ 23 Jg^{-1}, was measured during melting of leuprolide acetate, a GnRH analogue (Slager & Domb, 2004), which is chemically similar to acyline. However, crystallinity of this material was not tested.

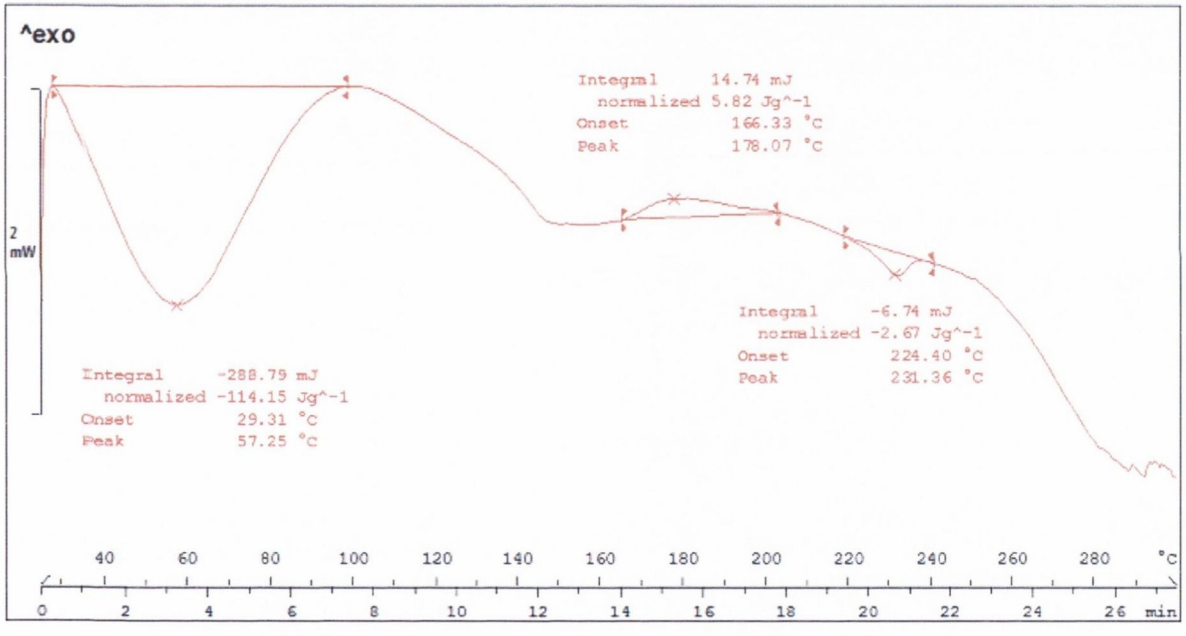

Fig. 3.18. DSC thermogram of acyline monoacetate.

3.3.3. Powder X-Ray Diffraction analysis (PXRD)

Based on powder XRD diffractogram of acyline acetate (Fig. 3.19), it appeared that the material was predominantly amorphous. This observation correlated with the thermal behaviour previously reported in section 3.3.2. Crystallinity of acyline has not been tested before. Leuprolide acetate, the most widely studied compound from the 'GnRH family' was found to be predominantly amorphous, showed almost no XRD peaks by Astaneh, et al. (2007).

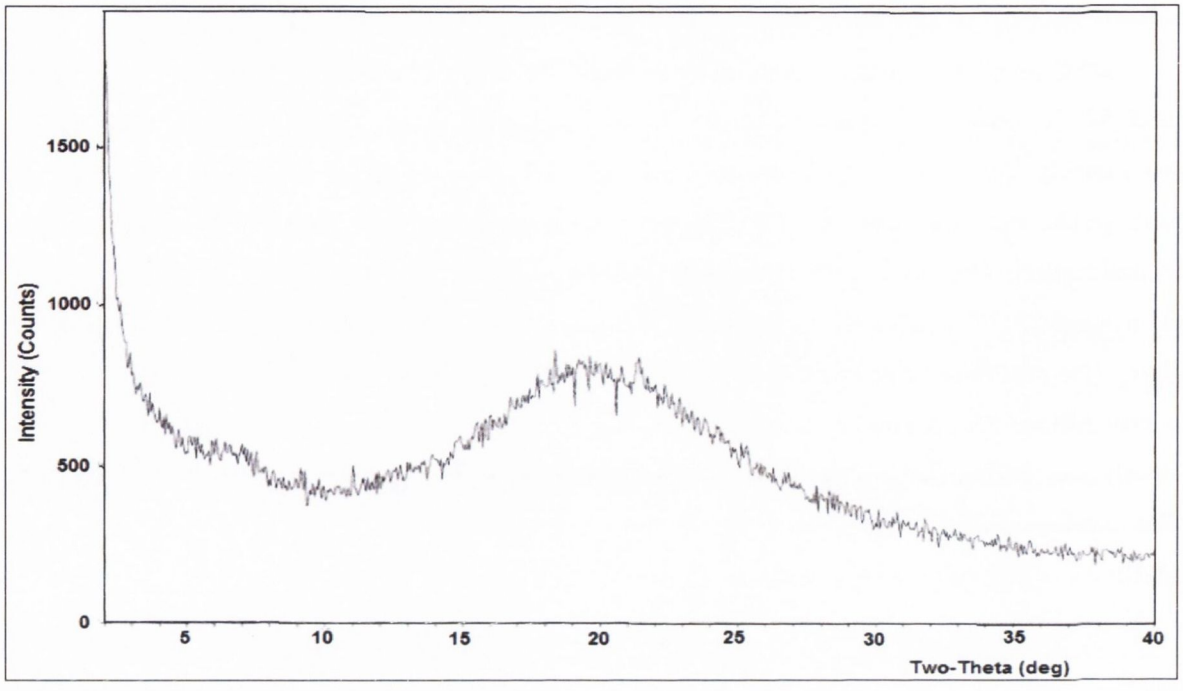

Fig. 3.19. PXRD diffractogram of acyline monoacetate.

3.3.4. Isoelectric point (IEP)

The isoelectric point (IEP) of acyline acetate was determined based on zeta potential measurements. Gradual titration of acyline acetate dissolved in two different acidic media led to determination of the IEP in the highly alkaline pH around 11.3-11.5 (Fig. 3.20).

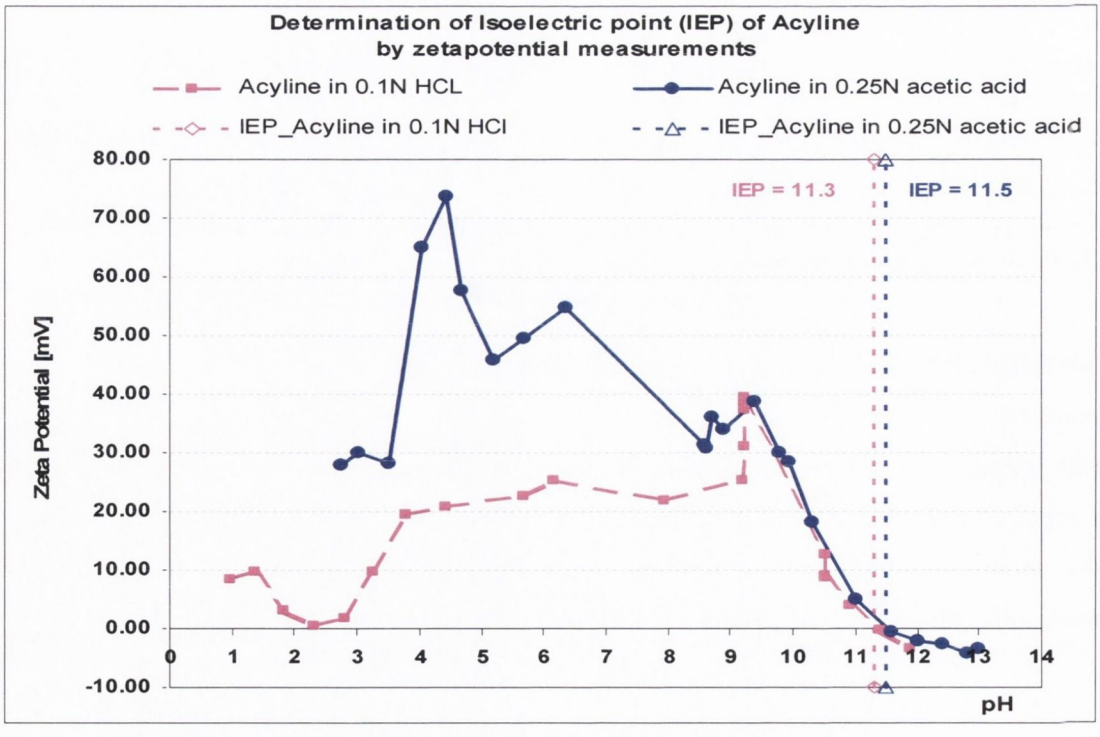

Fig. 3.20. Determination of isoelectric point of acyline monoacetate.

Based on the isoelectric point, it appeared that acyline was positively charged over a wide range of pH from 0 to 11 and its solubility in acidic and neutral media should have been better than in the highly alkaline solutions.

3.3.5. Gelling behaviour in aqueous solutions

GnRH (Gonadotropin-Releasing Hormone) antagonists are known to form gels, due to the formation of beta-sheet structures (Jiang et al., 1997, Rivier et al., 1995). Use of azaline B, which is a close analogue of acyline, was limited to concentrations lower than 10 mg/ml, due to relatively low solubility and propensity to form gels in buffer solutions (Jiang et al., 2001). Also, acyline readily forms gels in aqueous solutions at concentrations higher than 10 mg/ml (Rivier et al., 1996). A solution of acyline in bacteriostic water, having a concentration of 2 mg/ml showed no evidence of gelling within 1 hour prior to subcutaneous injection (Herbst et al., 2002). Aqueous solutions of GnRH antagonists, when administered subcutaneously, form a depot 'gel form' that prevents rapid absorption of these compounds into the blood stream. When 2.4 ml of acyline in bacteriostatic water (the concentration of 8.8 mg/ml) was administered subcutaneously, a nodule was formed at the site of injection (lingering for as long as 30 days post injection) suggesting that the drug might have formed a gel in the fat tissue in a volume large enough to be palpable, similar to other GnRH antagonists (Herbst, 2004, Herbst et al., 2002). Orntide, another GnRH antagonist was found to form a discernable gel-like white mass at the injection site (under the skin), which appeared to be chemically identical to the injected ornitide and therefore it was suggested that the compound precipitated or gelled in the 'chemically intact form'. The detailed mechanism of gel formation *in vivo* was not clear, but it was suspected that ornitide gelling in the tissue could have been caused by a change of pH or a localised increase of ornitide concentration as water and other excipients in the solution formulation diffused rapidly, leaving the ornitide more concentrated to aggregate, precipitate or form the gel. Another reason could have been that the body fluids containing some salts, induced association of ornitide molecules into a beta-sheet structure to fulfill the peptide hydrogen bonding requirements and allow a more ordered, solvated packing structure (Jiang, 2002). Another explanation of the 'gel-structure' formed by GnRH antagonists, could be a phenomenon observed with GnRH agonists by Powell et al. (1991, 1994). Hydrophobic GnRH agonists such as nafarelin and detirelix, having similar chemical structures to GnRH and GnRH antagonists, also undergo peptide aggregation and solution gelation resulting in compromised physical stability. It was discovered that detirelix and nafarelin in aqueous solutions at concentrations greater than 4 mg/ml and 8 mg/ml respectively formed gels which showed birefringence and therefore were considered to be peptide liquid crystals. Formation of stable peptide liquid crystals required extensive peptide counterion desolvation, making the onset of PLC formation slow but once aggregates were formed, they were not easily resolvated (Powell et al., 1991, Powell et al., 1994).

The solubility limit of acyline in various media was not clearly established as rapid gelling was observed in many aqueous solutions. Gelling appeared to be dependent mainly on the concentration, however the volume of medium was also important since gelling of 0.1 mg/ml solution was more rapid in 1 ml HPLC vial than in volumetric flasks. Gelling behaviour was visually evaluated in a number of aqueous media (Table 3.10). Rapid gelling was observed in water, the phosphate buffer pH 6.8 and saline, while gelling rate appeared to be slower in the bacteriostic water containing another less polar solvent (benzyl alcohol).

Table 3.10. Concentration of acyline determined in the combined media.

Medium	Solubility & gelling observations
Purified water	0.1 mg/ml soluble initially but seen to form a gel down to 0.005 mg/ml within 16-48 hours
Bacteriostatic Water (0.9 % benzyl alcohol)	Soluble up to 0.18 mg/ml – no apparent gelling after 24 hours
Saline	0.1 mg/ml, soluble initially but forms gel within 24 hours
Phosphate buffer (USP) pH 6.8	Reduced solubility to approx 0.074 mg/ml (only 74% recovered from 0.1 mg/ml acyline solution)

3.3.6. Solubility in the standard GIPET® II formulation and propylene glycol.

Acyline solubility up to 10 mg/ml in the standard GIPET ® II formulation and propylene glycol was evaluated visually (Table 3.11).

Table 3.11. Solubility/gelling of acyline monoacetate in the standard GIPET ® II formula and PG.

Appearance of samples	**Standard (non-aqueous) GIPET® II formula**	**Propylene glycol (PG)**	
	10 mg of acyline monoacetate /1g of solvent (~ 10mg/ml)	5 mg of acyline monoacetate /1g of solvent (~ 5mg/ml)	10 mg of acyline monoacetate /1g of solvent (~ 10mg/ml)
at T_{0h} (freshly made)	A suspension - some material undissolved in a liquid	A suspension - some material undissolved in a liquid	A suspension - some material undissolved in a liquid
at T_{2hours}	Clear, transparent, non viscous liquid	Clear, non viscous liquid	A suspension - some material undissolved in a liquid
at $T_{16\ hours}$ (next day)	Clear, transparent, non viscous liquid	Clear, non viscous liquid	Gelled material, cloudy, whitish gel mass (high viscosity)
at $T_{32\ hours}$ (2 days)	Clear, transparent, non viscous liquid	not performed	not performed

Acyline appared to go into solution up to the concentration of 10 mg/1 g in the standard GIPET ® II formulation and appeared to be less soluble, between 5 mg/g - 10mg/g in propylene glycol. The rapid gelling was not evident in those samples. In both cases, the established solubility limits were significantly higher than the ones observed in purified water and aqueous media (without other polar solvents). Propylene glycol appeared to be a very good solvent to dissolve acyline without signs of rapid gelling. Interestingly, the addition of propylene glycol (approximately 10- 15%) to aqueous solutions of detirelix and nafarelin suppressed solution gelation and formation of peptide liquid crystals (Powell et al., 1991).

3.3.7. Calculation of cLogP and cLogD

Acyline was ionized in the wide range of pH from 1 to 11 (Fig. 3.21). Coefficient distribution (cLogD) values, indicated a hydrophilic character from pH 1 - 8 and 12.5 – 14. Within the pH region, from 8 - 12.5, as acyline was reaching its isoelectric point, ionisation decreased leading to the potentially increased lipophilic character. At the isoelectric point, the distribution coefficient should be equal to cLogP. The cLogP value of approximately 2, was read from Fig. 3.21. The charge calculated for acyline in various pHs, indicated that the molecule was positively charged at physiological pH (pH 6 - 8).

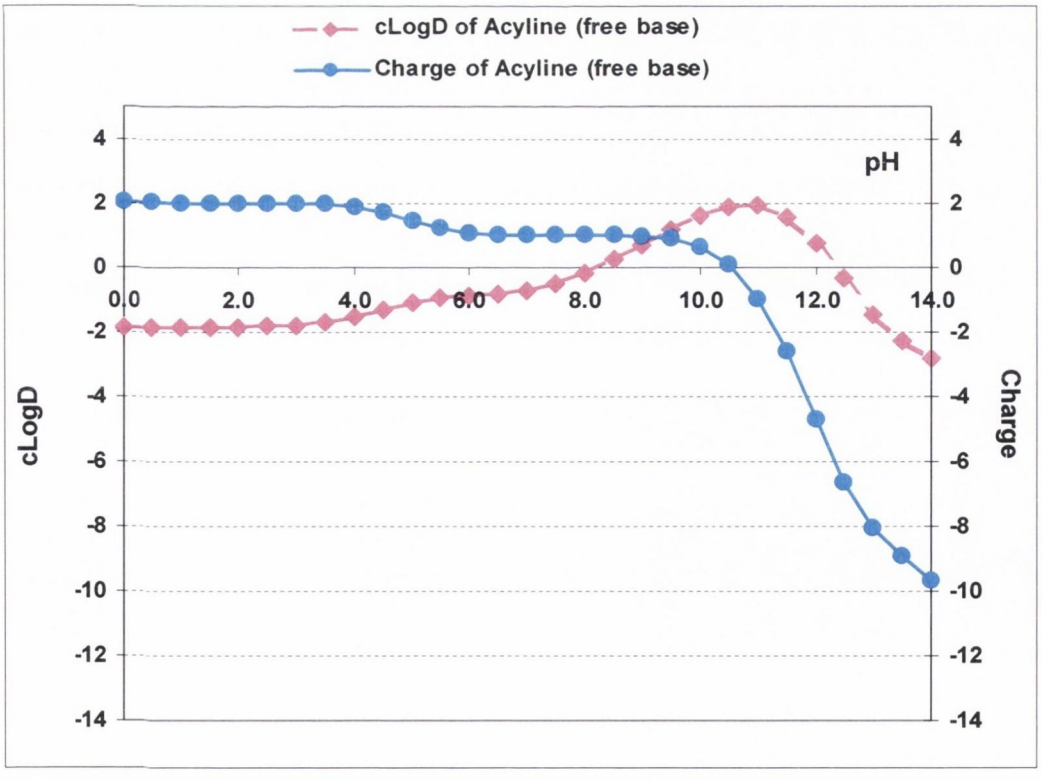

Fig. 3.21. Relationship between cLogD, charge and pH calculated for acyline.

3.4. Overall Conclusions

Three model drugs were characterised in terms of physicochemical properties to understand their suitability for incorporation into microemulsion formulations. Sodium alendronate trihydrate and disodium pamidronate pentahydrate appeared to be crystalline, highly water soluble organic molecules. Solubility in the aqueous buffers was superior compared to solubility in the other polar solvents (propylene glycol) and the standard GIPET ® II formulation. Disodium pamidronate pentahydrate was found to be unstable in the modified K-McIlvaine's buffer pH 2.2 and converted into monosodium pamidronate monohydrate. In addition, sodium alendronate appeared to be physically unstable as trihydrate in propylene glycol where formation of a solvate was observed over time. Therefore, it was evident that aqueous versions of microemulsion formulations should be developed with these model drugs in order to maximise their drug load.

Acyline monoacetate, as a decapeptide, differed significantly from the bisphosphonates. The material appeared to be amorphous, showing rapid gelation in the aqueous solutions. Solubility in propylene glycol and the standard GIPET ® II formulation appeared to be substantially better compared to the aqueous media. In addition, gelling did not develop rapidly in these solutions. Based on these observations, it appeared that development of non-aqueous microemulsions (SELFs) would be a more successful approach. All three compounds appeared to be highly ionized in the physiological pH of the intestinal tract. Many physiological studies demonstrated that absorptive cells in the lumen are negatively charged (Li & Hu, 2011, Gershanik & Benita, 2000; Tang et al., 2007) and therefore highly negatively charged drug molecules such as bisphosphonates show poor oral absorption. Hydrophilic molecules (mainly absorbed by the passive transport) that are negatively charged, are repelled as the junctional complex with a net negative charge, whereas positive charged molecules pass more readily (Li & Hu, 2011). Although, acyline appeared to be positively charged in physiological pH (6 - 7), which should facilitate its absorption, its oral bioavailability is likely to be poor due to its molecular size (it is approximately five times larger than bisphosphonates).

Chapter 4

Pseudoternary Phase Diagrams

4.1. Introduction

Phase diagrams are used to study the relationship between the phase behaviour of a mixture and its composition. The phase behaviour of simple microemulsion systems comprising of oil, water and a primary surfactant and cosurfactant can be studied with the aid of pseudoternary phase diagram, in which two corners of the diagram represents 100% of the two components (e.g. water and oil) while the third corner represents 100% of the 'pseudo component' which is a combination of the two remaining materials, e.g. a mix the primary surfactant and the cosurfactants as was chosen in the current work.

The aim of this work was to evaluate the effect of various low HLB value surfactants (cosurfactants) and the type of oil on formation of the microemulsion formulations. Understanding how to combine these materials to form clear, homogenous, physically stable preconcentrates and microemulsions suitable for encapsulation is critical to allow for successful application of the GIPET® II technology. Also, construction of phase diagrams provides an insight of the dilution behaviour of these formulations, which can be a critical factor affecting drug solubility and precipitation upon dilution *in vivo*. The focus was to capture a transition from clear monophasic formulations into turbid multi-phase regions.

4.2. Composition of pseudoternary phase diagram

Pseudo phase diagrams were constructed with three main components: oil, an aqueous phase and a mix of surfactants at a fixed ratio treated as a single 'pseudo-component'. The primary surfactant and the cosurfactant were mixed at four different ratios to obtain systems with a low combined HLB value, an intermediate combined HLB value and a high HLB value. The majority of the phase diagrams were prepared at 37°C to obtain 'universal' data. Firstly, preparation of the phase diagrams at 37°C examined the formation of microemulsions and the dilution behaviour of preconcentrates in the temperature representative of the human scenario. This is particularly important for systems comprising of non-ionic surfactant (showing phase inversion temperature) as droplet size and emulsification characteristic of such systems will vary depending on a temperature. The second reason why the ternary diagrams were prepared at 37°C was to gain preliminary information on physical stability of microemulsions and SELFs if these were used as encapsulated forms. As the solubility of the non-ionic surfactant decreases at a higher temperature, formulations which are physically stable (homogenous, monophasic, non-separating) at 37°C show good potential to remain physically stable encapsulated formulations when stored at intermediate (30°C/65 % RH) and normal long-term (25°C/60% RH) storage conditions, specified in the ICH guidelines (Q1A(R2), 2003). In addition, an encapsulation process typically takes place at a temperature higher than 25°C (Cole, 1999; Meissonnier, 2007). In order to reduce viscosity of the liquid formulation (facilitate dosing), it is essential to choose the temperature, which does not cause phase separation as this would result in uneven distribution of drug and excipients in capsules. By

performing phase diagrams at 37°C, microemulsions and SELFSs stable at higher temperature and therefore suitable for an efficient encapsulation process, could be identified.

4.2.1. Oils

Three excipients, Captex 200P (propylene glycol dicaprylocaprate), Captex 355 EP/NF (glyceryl tricaprylate/tricaprate), and Capmul PG-8 (propylene glycol monocaprylate) were chosen from pharmaceutically acceptable oils (based on the patent claims around the GIPET ® II technology, Chapter 1, section 1.3.5). Captex 355 EP/NF and Captex 200P have been previously used as oils in early GIPET ® II formulations developed by Merrion Pharmaceuticals. Capmul PG-8 was chosen due to a high content of monesters of caprylic acid and a good potential as an oral absorption promoter. Due to its relatively high hydrophilic character, Capmul PG-8 has been used as a cosurfactant (Prajapati et al., 2011) or an oil phase by other researchers (Spernath & Aserin, 2006). The key properties of the oils selected for the current work are summarised in Table 4.1.

Table 4.1. Comparison of composition and properties of the selected oils.

Excipient Name	Composition	Estimated			Appearance at room temperature
		Solubility parameter $(\mu Pa)^{1/2}$	cLog P	Average HLB	
Capmul PG – 8 (propylene glycol monocaprylate)	Monoesters: min 90% Diesters: max 10% of Caprylic acid: min 98.0% Capric acid: max 2.0%	**15.5- 20.9**	**2.9 - 6.7**	**~5.6**	Clear, colourless liquid
Captex 200P (propylene glycol mono-dicaprylate/ dicaprate)	Diesters: 100% of Caprylic acid: 50.0-80.0%. Capric acid: 20.0- 50.0%	**12.7 – 15.5**	**6.7- 8.8**	**~2.3**	Clear, colourless liquid,
Captex 355 (caprylate/ caprate triglycerides)	Triglycerides: 100% of Caprylic acid: 50-75%. Capric acid: 22- 45%	**7.4 – 9.8**	**9.3- 12.5**	**~ 1.5**	Colourless to light yellow odourless liquid

The HLB value for Capryol 90 (propylene glycol monocaprylate manufactured by Gattefossé), a material very chemically similar to Capmul PG-8, was reported to be 6 (Pouton, 2007). Labrafac™ PG (propylene glycol dicaprylocaprate) and Labrafac™ Lipophile WL1349 (caprylate/caprate triglycerides) produced by Gattefossé, are chemically similar to Captex 200P and Captex 355 respectively, and are given HLB values of 2 and 1 respectively (Gattefossé website). The HLB values reported are in a good agreement with the calculated numbers (Fig. 4.1). cLogP and the solubility parameter were calculated for individual subcomponents of the materials (according to the composition) and expressed as general ranges. DSC and TGA characterisation did not reveal

any thermal difference between the oils. Endothermic or exothermic peaks were not observed in the temperature range from -20°C to 200°C, neither was any mass loss was detected. Based on the calculated solubility parameters, cLogP values and HLB values (Table 4.1), Capmul PG-8 was found to be the most polar oil while Captex 355 was the least polar, the most hydrophobic one.

4.2.2. Low and high HLB value surfactants

In the investigated systems, Crillet 4 HP, a high HLB value surfactant was used as a primary surfactant while low HLB value surfactants Capmul MCM, Capmul MCM C8 and Capmul MCM C10 were considered to be cosurfactants. The key properties of the cosurfactants and the primary surfactant are summarised in Table 4.2.

Table 4.2. Comparison of composition and properties of the selected surfactants.

Excipient Name	Composition	Estimated			Appearance at room temperature
		Solubility parameter $(\mu Pa)^{1/2}$	cLog P	Average HLB	
Capmul MCM (glyceryl mono-dicaprylate/dicaprate)	Monoglycerides: 49.5 – 60.5% Diglycerides: 39.5 – 50.5% of Caprylic acid: 82-88%. Capric acid: 12-18%	**15.8- 23.7**	**1.9-8.0**	**~ 5.1**	Liquid/ semi-solid, yellowish mass or liquid
Capmul MCM C8 (glyceryl mono-dicaprylate/dicaprate)	Monoglycerides: 45.0 - 75.0% Diglycerides: 20.0 – 50.0% Triglycerides: max 10.0% of Caprylic acid: min 90.0%. Capric acid: max 10.0%	**9.8- 23.7**	**1.9-12.5**	**~ 5.2**	Liquid/ semi-solid, yellowish mass or liquid
Capmul MCM C10 (glyceryl mono-dicaprate)	Monoglycerides: min 45% Diglycerides: max 55% of Caprylic acid: max 55%. Capric acid: min 45%	**15.8– 23.7**	**1.9-8.0**	**~ 4.1**	Solid creamy to yellowish mass
Crillet 4 HP (polysorbate 80)	Polyoxyethylene (20) sorbitan monooleate 100%	**~ 9.8**	**~ -0.7**	**15**	Yellowish, viscous, liquid

The HLB value of Capmul MCM was reported to be 5.5- 6.0 (Constantinides, 1995) and between 5-6 for Capmul MCM C8, Capmul MCM 10 by Abitec, the manufacturer of the materials (Abitec Corporation website). The HLB value for Crillet 4 HP was not calculated because it is given by many scientific sources (Constantinides, 1995; Ke et al., 2005). cLogP and solubility parameters calculated for individual subcomponents of the cosurfactants and expressed as general ranges, did not indicate differences between these materials. In contrast to the oils which were made of different subcomponents, the cosurfactants were made of the same chemically compounds but combined in a different ratio for each Capmul type, therefore neither cLogP (the range) nor

solubility parameter (the range) could differentiate these materials The averaged HLB value demonstrated the difference between Capmul MCM, Capmul MCM C8 and Capmul MCM C10, because it was calculated as a mean value based on the weight ratio of the subcomponents (Table 4.2). Capmul MCM and MCM C8 appeared to have very similar properties; Capmul MCM C10 appeared to be slightly more hydrophobic. Capmul MCM is semi-solid or liquid at room temperature. On the DSC curve (Appendix Fig. A.4.1), two endothermic events were observed when the sample was heated in the temperature range from –20 °C to 200°C. Broad melting peaks were detected at 6°C and 32°C (onsets at -3°C and 22°C). Any significant weight loss was not observed in this temperature range, however a gradual weight decrease started around 180°C indicating a gradual decomposition of the material (Appendix Fig. A.4.2.). Capmul MCM C8 is chemically very similar to Capmul MCM. DSC testing revealed two main endothermic events between –20°C and 200°C (Appendix, Fig. A.4.1). The first broad melting peak was observed around 6 °C with onset at –11 °C. The second melting peak occurred around 26 °C with onset at 19°C. Any significant weight loss was not observed and the material started to gradually decompose around 180°C (Appendix, Fig. A.4.2). Only one endothermic event was detected in the temperature range from –20°C to 200°C (Appendix, Fig. A.4.1) for Capmul MCM C10. Melting occurred around 45 °C (onset 30°C). Any significant weight loss was not observed in this temperature range, however a gradual weight decrease started around 180°C indicating a gradual decomposition of the material (Appendix, Fig. A.4.2). DSC results demonstrated that Capmul MCM and Capmul MCM C8 were similar in terms of thermal behaviour, nevertheless both were quite inhomogeneous in terms of composition. Thermal behaviour of Capmul MCM C10 suggested that its composition differed significantly from the other two materials.

Polyoxyethylene-sorbitan-20-monooleate (also known as polysorbate 80, Tween 80 or Crillet 4 HP) is a mixture of partial esters of fatty acids, mainly oleic acid, with sorbitol and its anhydrides ethoxylated with approximately 20 moles of ethylene oxide for each mole of sorbitol and sorbitol anhydrides. The cloud point (the temperature above which surfactants begin to precipitate) is commonly seen with many nonionic polyoxyethylate surfactants in solution. At elevated temperatures, the surfactant separates as a precipitate and multi-component systems will separate into many phases creating the appearance of turbidity. The cloud point temperature has been reported as 65°C for a 3% (w/v) solution of polysorbate 80 in 1 M NaCl (Kerwin, 2008). The cloud point of surfactants is affected by the presence of other materials in a formulation. The cloud point of Tween 80 (0.1 mM) established as 95.1 °C, decreased in the presence of glycols and glycol ethers (Mahajan et al., 2004). In the experimental work of Na et al. (1999), the presence of PEG 400 and 2-hydroxypropyl-β-cyclodextrin decreased the cloud point of polysorbate 80 from 92 °C to 90 °C and 60 °C, respectively. On the other hand, the addition of sodium dioctyl sulfosuccinate and dimyristoylphosphatidyl glycerol to polysorbate 80, increased the cloud point considerably to 127°C and 132°C, respectively.

As the 'pseudo component', mixes of the low and high HLB value surfactants were used in fixed ratios to obtain systems with the low combined HLB value between 6 and 9 and systems with the high combined HLB value between 9 and 14. These ranges were chosen to represent systems on the opposite ends of the range for the combined HLB value specified in the patents (currently owned by Merrion Pharmaceuticals) which is 'the surfactant or mixture has a hydrophilic – lipophilic balance value 7 to 14, preferably 8 - 13' (Chapter 1, section 1.3.5).

4.2.3. Aqueous phase

Titration was carried out mainly with purified water. Full FaSSIF-V2 and full FeSSIF-V2 were used in some experiments to mimic dilution behaviour *in vivo* and evaluate the impact of additional surfactants on formation of microemulsion regions. The composition of full FaSSIF-V2 and full FeSSIF-V2 were published by Jantratid et al., (2008) and is given in Chapter 2, section 2.4.1.

4.3. Pseudoternary phase diagrams with the low combined HLB value

The mix of the surfactants and oil prior to the addition of an aqueous phase was called a preconcentrate in the current work. In general, preconcentrates are considered as SEDDSs, SMEDDSs or SNEDDSs that could also contain some cosolvents and other additives, however here the term 'preconcentrate' will only apply to mixes of the surfactants and the oil, expressed as the ratio of the mix of surfactants to oil (e.g. 40: 60 = a preconcentrate comprising 40% of surfactants and 60% of oil). Details of the systems having the low combined HLB value between 6 and 9 are summarised in Table 4.3. The prepared phase diagrams for these systems are shown in Fig. 4.1. The coding (the names) used for the systems presented in this work is explained in Chapter 2, section 2.4 to facilitate identification of key differences between systems and facilitate a comparison when visually assessing phase diagrams.

The first three phase diagrams shown in the first row in Fig. 4.1, represent the systems made with the same cosurfactant, Capmul MCM C8 while varying the oil phase: Captex 200P (Fig. 4.1.A), Captex 355 (Fig. 4.1.B), Capmul PG-8 (Fig. 4.1.C). The next three phase diagrams shown in the second row in Fig. 4.1, represent the systems made with Capmul MCM C10 as a cosurfactant, where Captex 200P (Fig. 4.1.D), Captex 355 (Fig. 4.1.E), Capmul PG-8 (Fig. 4.1.F) were used as the oil. The third row in Fig. 4.1 shows phase diagrams for the systems, which included preconcentrates used in the preclinical study (Fig.4.1.G and Fig. 4.1.I). The phase diagram coded as 1A2_T3 (Fig. 4.1.G) included the preconcentrate, which was used to prepare a self-emulsifying system and Test Item 3 with acyline monoacetate. The phase diagram coded as 3A2_T2 (Fig. 4.1.I) included the preconcentrate used to prepare a self-emulsifying system Test Item 2 with acyline monoacetate. Both SEDDSs were dosed in the preclinical study presented in Chapter 6, section 6.3.1).

Table 4.3. Composition of the phase diagrams for the systems with the low combined HLB value between 6 and 9.

Name of Phase Diagram	Oil	Low HLB value surfactant	High HLB value surfactant	Ratio, Low HLB vs High HLB surfactant	Combined HLB value	Figure No
2A1	Captex 200P	Capmul MCM C8	Crillet 4 HP	65:35	**8.6**	Fig. 4.1.A
2A2	Captex 355	Capmul MCM C8	Crillet 4 HP	65:35	**8.6**	Fig. 4.1.B
2A3	Capmul PG-8	Capmul MCM C8	Crillet 4 HP	65:35	**8.6**	Fig. 4.1.C
3A1	Captex 200P	Capmul MCM C10	Crillet 4 HP	65:35	**7.9**	Fig. 4.1.D
3A2	Captex 355	Capmul MCM C10	Crillet 4 HP	65:35	**7.9**	Fig. 4.1.E
3A3	Capmul PG-8	Capmul MCM C10	Crillet 4 HP	65:35	**7.9**	Fig. 4.1.F
1A2_T3	Captex 355	Capmul MCM	Crillet 4 HP	78.6 : 21.4	**7.2**	Fig. 4.1.G
2A2_T3	Captex 355	Capmul MCM C8	Crillet 4 HP	78.6 : 21.4	**7.3**	Fig. 4.1.H
3A2_T2	Captex 355	Capmul MCM C10	Crillet 4 HP	78.6 : 21.4	**6.4**	Fig. 4.1.I

The phase diagram coded as 2A2_T3 (Fig. 4.1.H) was prepared with Capmul MCM C8 as the cosurfactant and Captex 355 as the oil. This system was equivalent to 1A2_T3 system with regard to the composition, with the exception of the cosurfactant used. Capmul MCM was used as the cosurfactant in 1A2_T3 system (Fig. 4.1.G). As presented earlier in section 4.2.2, the composition and main properties of these two cosurfactants were very similar and they could be considered as almost the same (chemically) materials. No difference in the phase behaviour was observed when 1A2_T3 (Fig. 4.1.G) and 2A3_T3 (Fig. 4.1.H) diagrams were compared. Clear, homogenous preconcentrates were formed when the ratio of the mix of surfactants to oil varied between 5: 95 to 90: 10/and above (Fig. 4.1.G and Fig. 4.1H). The preconcentrates in the range 5: 95 to 60: 40 could incorporate approximately 5% of water before a phase transition occurred. The preconcentrates from 60: 40 to 90: 10/and above, could incorporate from approximately 10 – 15% of water before an emulsion was created. The clear region was isotropic and therefore identified as a microemulsion. Birefringence was also not observed upon transition into a hazy, turbid phase.

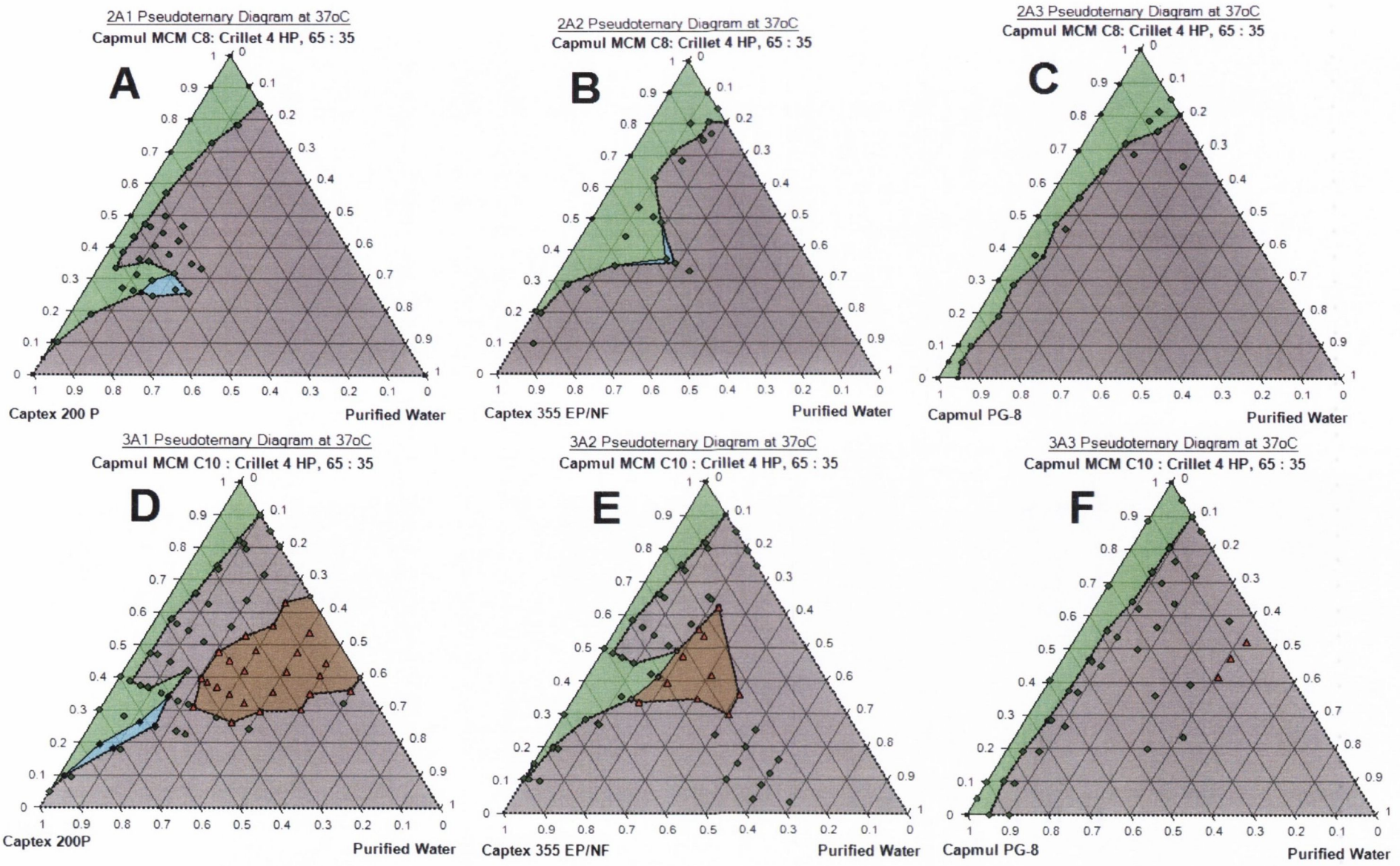

Fig. 4.1. Pseudoternary phase diagrams for the system with the low combined HLB value (the detailed explanation is given on the next page)

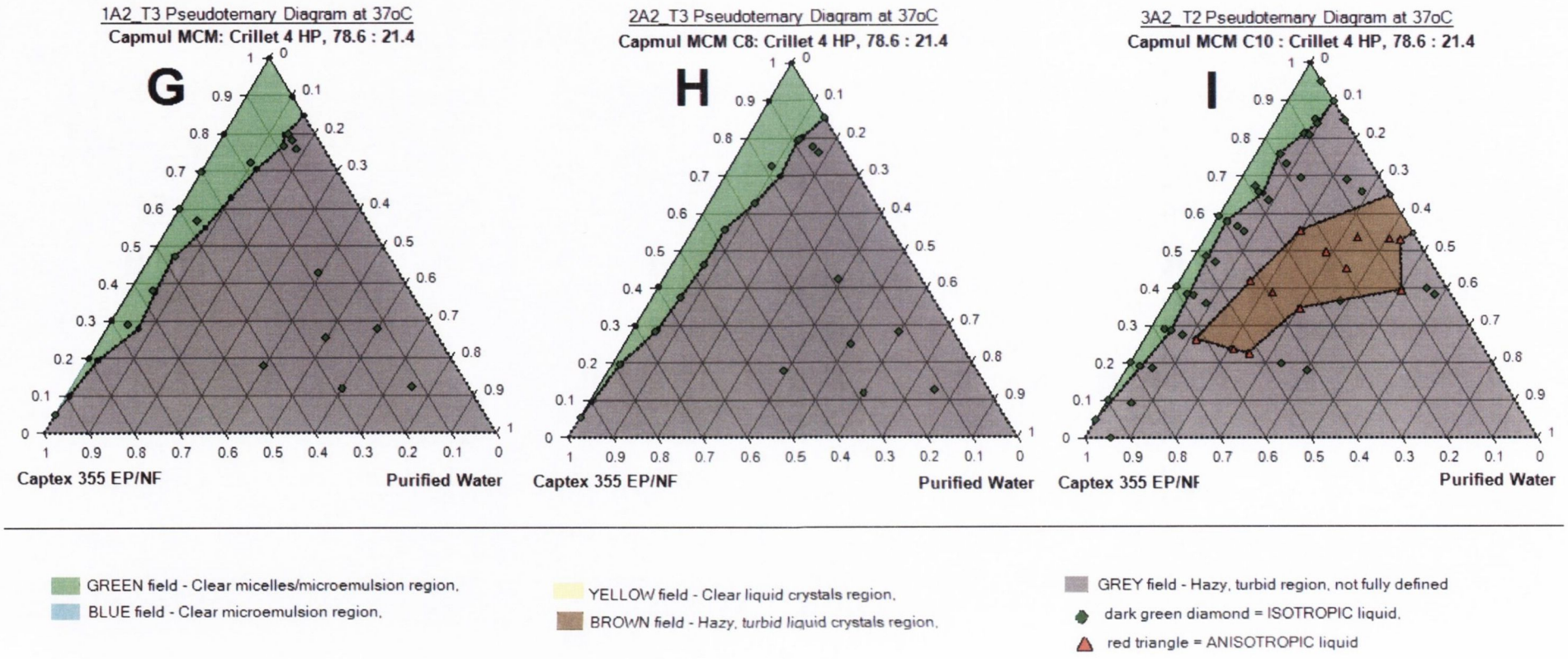

Fig. 4.1. Pseudoternary phase diagrams for the system with the low combined HLB value (cont'd):

A-C) systems where Capmul MCM C8 was used as a cosurfactant and a different oil phase was used Captex 355 (A), Captex 200P (B), Capmul PG-8 (C).

D-F) systems where Capmul MCM C10 was used as a cosurfactant and a different oil phase was used Captex 355 (D), Captex 200P (E), Capmul PG-8 (F).

G-I) systems where the same oil phase was used Captex 355, but a cosurfactant varied Capmul MCM (G), Capmul MCM C8 (H), Capmul MCM C10 (I).

These systems have a different ratio between the low HLB value surfactant and the high HLB value surfactant compared to the systems A-F.

4.3.1. Impact of different cosurfactants on the phase behaviour

The impact of different cosurfactants on the formation of clear preconcentrates and microemulsions was made by direct comparison of the phase diagrams prepared with Capmul MCM C8 and Capmul MCM C10 as the cosurfactant. Composition-wise, the phase diagrams coded as 2A1 – 2A3 (Fig. 4.1. A-C), prepared with Capmul MCM C8), were analogues to the phase diagrams 3A1- 3A3 (Fig. 4.1.D-F, prepared with Capmul MCM C10) with the cosurfactant used being the only difference. When Captex 200P was used as the oil, the pseudoternary phase diagram with Capmul MCM C8 showed a clear microemulsion region originating from the preconcentrates 5: 95 to 90: 10/and above (ratio between the mix of the surfactants and the oil) (Fig. 4.1.A). On average approximately 5- 10% of water could be incorporated by the preconcentrates 20: 80 and 50:50 to 70:30, and between 10- 15% by the preconcentrates 80: 20 to 90: 10/and above (Fig. 4.1.A). The best dilution behaviour was shown by the preconcentrate 35: 65, which could incorporate approximately 25 – 30% of water before a phase transition occurred. When comparing 2A1 system (Fig. 4.1.A) to its analogue system 3A1 formulated with Capmul MCM C10 (Fig. 4.1.D), it can be seen that a microemulsion region originated from the same preconcentrates and the best dilution behaviour was observed in the similar region. The best dilution behaviour (up to 15% of water) observed was the preconcentrates 30: 70 and 40: 60 made with Capmul MCM C10, before a phase transition occurred. Other preconcentrates also showed reduced capacity to incorporate water in comparison to those formulated with Capmul MCM C8. Within the grey zone in the system 3A1, a hazy, turbid, anisotropic region was detected (Fig. 4.1.D), which was considered to be a multiphase containing a liquid crystalline phase (Fig. 4.2).

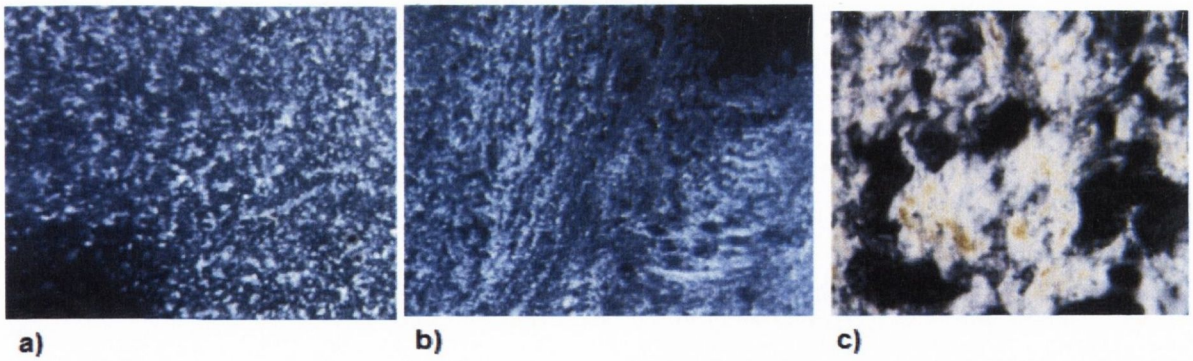

a) b) c)

Fig. 4.2. Images indicating presence of liquid crystals:

Figure 4.2/ images	Pseudoternary diagram	Mix of Surfactants	Oil	Water	Macroscopic appearance
a) (~ 40 x magnification)	**3A2_T2**	26.3	62.1	11.6	Hazy, turbid, low viscosity
b) (~ 40 x magnification)	**3A1**	55.8	13.9	30.3	Hazy, turbid, slightly viscous
c) (~ 60 x magnification)	**3A1**	55.8	13.9	30.3	Hazy, turbid, slightly viscous

Liquid crystals observed in this turbid region, appeared to be fine, uniformly dispersed, having rather loose, possibly lamellar arrangement (discussed in Chapter 1, section 1.4.2) because an increase of viscosity in this region was not observed. The presence of a turbid liquid crystalline region in 3A1 system (Fig. 4.1.D) and the lack of a similar liquid crystalline region in the same region in system 2A1 (Fig. 4.1.A) is an indication of poorer performance of Capmul MCM C10 as the cosurfactant. When Capmul MCM C8 was no longer able to facilitate formation of microemulsion, the preconcentrates 40: 60 and 50: 50 formed an emulsion (2A1 system (Fig. 4.1.A). The same preconcentrates in 3A1 system (Fig. 4.1.D) formed liquid crystals once the microemulsion phase could not be sustained in excess water.

A comparison of pseudoternary diagrams when Captex 355 was used as the oil revealed another significant difference between the co-emulsifying potential of the cosurfactants. The preconcentrate 50: 50 showed the best dilution behaviour in system 2A2 (Fig. 4.1.B). The preconcentrate could incorporate up to 30% of water before a phase transition occurred from a clear, isotropic microemulsion into a hazy but also an isotropic emulsion. Other preconcentrates in the range from 40: 60 to 90: 10/and above formed microemulsions up to approximately 10-15% of water. The phase diagram 3A2 (Fig. 4.1.E) revealed the best dilution behaviour for the same preconcentrate as observed in system 2A2. The preconcentrate 50: 50 (formulated with Capmul MCM C10) could incorporate up to 20% of water before a phase transition occurred, which indicated slightly inferior co-emulsifying properties compared to Capmul MCM C8 (up to 30% of water incorporated). In addition, the clear isotropic microemulsion converted directly into a hazy anisotropic phase when the water content exceeded 20%. The anisotropic phase closely resembled finely dispersed liquid crystals similar to the 3A1 system (Fig. 4.2). With less than 10% of water, the preconcentrates from 60: 40 to 80: 20 formed a turbid isotropic phase that gradually become anisotropic. Formation of an anisotropic, hazy multiphase area containing liquid crystals, once again suggested that Capmul MCM C10 was less effective as a cosurfactant compared to Capmul MCM C8.

When Capmul PG-8 was used as the oil, the pseudoternary phase diagrams with Capmul MCM C8 (2A3, Fig. 4.1.C) and Capmul MCM C10 (3A3, Fig. 4.1.F) did not differ substantially but the preconcentrates formulated with Capmul MCM C8 (from 80: 20 to 90: 10/and above) could incorporate a slightly higher amount of water (15-20%) before a phase transition occurred.

The combined HLB values of the systems 1A2_T3 (Fig. 4.1.G) and 2A2_T3 (Fig. 4.1.H) was low (~7) as these systems were prepared using a mix of the surfactants where the ratio between the low HLB value surfactant and the high HLB value was almost 80: 20. Compared to the phase diagram 2A2 where the ratio of the low HLB value surfactant to the high HLB value surfactant was 65: 35, these systems represented formulations with a very low, reduced content of the high HLB value surfactant (Crillet 4HP). The mix of surfactants with the reduced content of Crillet 4HP (80: 20) was more miscible with Captex 355 (Fig. 4.1.G and Fig. 4.1.H) compared to the former one (Fig. 4.1.B), and formed clear preconcentrates from 5: 95 to 90:10/and above. Nevertheless, the

reduction in the content of Crillet 4HP also resulted in a decreased microemulsion region as the water content increased. None of the preconcentrates showed a water-richer microemulsion region, which was previously observed for the preconcentrate 50: 50 in the phase diagram 2A2 (Fig. 4.1.B). This clearly indicated that Capmul MCM C8 and Capmul MCM did not have similar 'microemulsifying' properties to Crillet 4 HP, and reduction in the content of the primary surfactant worsened the capacity of the system to incorporate water and to form extensive microemulsion phases upon dilution. A similar observation was made when the phase diagram of 3A2_T2 system (Fig. 4.1.I) was compared with the diagram 3A2 (Fig. 4.1.E). The reduction in the content of Crillet 4 HP decreased formation of the microemulsion region, therefore Capmul MCM C10 was also less effective as a 'microemulsifying' surfactant compared to Crillet 4 HP. Comparison between the phase diagrams 2A2_T3 (Fig. 4.1.H) and 3A2_T2 (Fig. 4.1.I), which only differed in the type of cosurfactant used, demonstrated once again that Capmul MCM C8 was a better cosurfactant than Capmul MCM C10, as use of the former resulted in a larger microemulsion area.

4.3.2. Impact of different oils on the phase behaviour

The effect of different oils on the phase behaviour was made by comparison of phase diagrams where the same cosurfactant was used, either Capmul MCM C8 (Fig. 4.1.A-C) or Capmul MCM C10 (Fig. 4.1.D-F). The phase diagrams with Capmul MCM C8 were prepared with Captex 200P (2A1, Fig. 4.1A), Captex 355 (2A2, Fig. 4.1.B) and Capmul PG-8 (2A3, Fig. 4.1.C). Capmul PG-8 was miscible with the mix of surfactants in all ratios (Fig. 4.1.C) while Captex 200P (Fig. 4.1.A) and Captex 355 (Fig. 4.1.B) did not form clear homogenous preconcentrates when the ratio between the surfactants and the oil was lower than 5: 95 and 20: 80 respectively. This suggested that Capmul PG-8 was the most hydrophilic oil, while Captex 355 was the most hydrophobic one. The microemulsion region formed with Capmul PG-8 (Fig. 4.1.C) was narrow (up to 10% of water on average) and relatively similar for all the preconcentrates. The microemulsions with Captex 200P (Fig. 4.1.A) and Captex 355 (Fig. 4.1.B) showed superior dilution behaviour in particular for the preconcentrates 35: 65 (able to incorporate 25-30% of water) and 50: 50 (able to incorporate up to 25-30% of water) respectively. Captex 355 appeared to form a more extensive microemulsion area from the preconcentrates 30: 70 to 70: 30 compared to the one formed with Captex 200P. The preconcentrates 80: 20 and 90: 10/and above, formed a similar microemulsion region comprising up to 15-20% of water, irrespective of the oil type used. Since the oil phase was very limited in this region (less than 20%), oil had no observable impact on formation of the microemulsion.

Further evaluation of the impact that the oil phase had on formation of microemulsions was also carried out by comparing phase diagrams prepared with Capmul MCM C10 as a cosurfactant and Captex 200P (3A1, Fig. 4.1.D), Captex 355 (3A2, Fig. 4.1.E) or Capmul PG-8 (3A3, Fig. 4.1.F) as the oil phase. Capmul PG-8 was miscible with the mix of surfactants in all ratios (Fig. 4.1.F), but

the microemulsion region formed was narrow and contained a maximum of 10% water. Larger microemulsion regions were formed with Captex 200P (Fig. 4.1.D) and Captex 355 (Fig. 4.1.E), however these oils were not miscible with the mix of surfactants in all ratios. Captex 355 was the least miscible, as the most hydrophobic oil. The water-richer microemulsion areas (up to 20% of water) were observed with both oils, Captex 355 and Captex 200P. The microemulsion area appeared to be comparable for both oils, although the water –rich areas were observed in different regions of phase diagrams. The water rich microemulsion area with Captex 200P (Fig. 4.1.D) was derived for the preconcentrates, 30: 70 and 40: 60. The similar area in terms of shape and size, was derived from the preconcentrates 40: 60 and 50: 50 prepared with Captex 355 (Fig. 4.1.E). The 'shift' of the microemulsion area, could be potentially explained by the hydrophobic character of the oil. It appears that Captex 355 as the most hydrophobic oil, required a higher quantity of surfactants (higher than 40%) to become 'micro-emulsified' compared to Captex 200P which formed an extensive microemulsion region with 30% of surfactants (ratio 30:70 of the mix of surfactants to oil). The fact that, a very extensive microemulsion region was not seen with the higher content of the surfactants above 60% (for the preconcentrates 60: 40 and above) suggests that a unique balance between the amount of surfactants and oil phase drives formation of microemulsion.

4.4. Pseudoternary phase diagrams with the high combined HLB value

Details of systems having a high combined HLB value between 9 and 14 are summarised in Table 4.4 and the phase diagrams prepared are shown in Fig. 4.3.

The first three phase diagrams shown in the first row in Fig. 4.3, represent the systems made with the same cosurfactant, Capmul MCM C8 while varying the oil phase: Captex 200P (Fig. 4.3.A), Captex 355 (Fig. 4.3.B), Capmul PG-8 (Fig. 4.3.C). The next three phase diagrams shown in the second row in Fig. 4.3, represent the systems made with Capmul MCM C10 as a cosurfactant, where Captex 200P (Fig. 4.3.D), Captex 355 (Fig. 4.3.E), Capmul PG-8 (Fig. 4.3.F) were used as the oil phase. The third row in Fig. 4.3 shows a phase diagram 1B3_T4, which includes the preconcentrate used to prepare a self-emulsifying system (Test Items 4) with acyline monoacetate used in the preclinical study presented in Chapter 6, section 6.3.1.

Table 4.4. Composition of the phase diagrams for the systems with the high combined HLB value between 9 and 13.

Name of Phase Diagram	Oil	Low HLB value surfactant	High HLB value surfactant	Ratio, Low HLB vs High HLB surfactant	Combined HLB value	Figure No
2B1	Captex 200P	Capmul MCM C8	Crillet 4 HP	15 : 85	**13.5**	Fig. 4.3.A
2B2	Captex 355	Capmul MCM C8	Crillet 4 HP	15 : 85	**13.5**	Fig. 4.3.B
2B3	Capmul PG-8	Capmul MCM C8	Crillet 4 HP	15 : 85	**13.5**	Fig. 4.3.C
3B1	Captex 200P	Capmul MCM C10	Crillet 4 HP	15 : 85	**13.4**	Fig. 4.3.D
3B2	Captex 355	Capmul MCM C10	Crillet 4 HP	15 : 85	**13.4**	Fig. 4.3.E
3B3	Capmul PG-8	Capmul MCM C10	Crillet 4 HP	15 : 85	**13.4**	Fig. 4.3.F
1B3_T4	Capmul PG-8	Capmul MCM	Crillet 4 HP	33.3 : 66.7	**11.4**	Fig. 4.3.G
2B3_T4	Capmul PG-8	Capmul MCM C8	Crillet 4 HP	33.3 : 66.7	**11.7**	Fig. 4.3.H

The phase diagram coded as 2B3_T4 (Fig. 4.3.H) was prepared with Capmul MCM C8 as the cosurfactant and Capmul PG-8 as the oil. This system is equivalent to 1B3_T4 system (Fig. 4.3.G) with regard to the composition with the exception of the cosurfactant used. Capmul MCM was used as a cosurfactant in 1B3_T4 system (Fig. 4.1.G). No difference in the phase behaviour was observed between 1B3_T4 (Fig. 4.3.G) and 2B3_T4 (Fig. 4.3.H). Capmul PG-8 was miscible with the mix of surfactants in all ratios, forming clear preconcentrates. On average the preconcentrates 10: 90 to 70: 30 could incorporate approximately 5- 10% of water. The preconcentrate 90: 10 formed a microemulsion, which had capacity to hold up to 35% of water in both systems (Fig. 4.3.G and 4.3.H). Beyond this point, in the system 1B3_T4 (Fig. 4.3.G), a hazy region showing birefringence was formed. This region gradually became a clear anisotropic region that existed up to 80% of water. The similar transition from a microemulsion into a region of liquid crystals was observed in the system 2B3_T4 (Fig. 4.3.H) for the preconcentrate 90: 10. The observed liquid crystals appeared visually quite viscous, having a defined 'birefringence pattern' under polarised microscope (Fig. 4.4) which suggested a highly organised arrangements of surfactants, possibly a hexagonal phase (Chapter 1, section 1.4.2). The difference observed in the dilution behaviour of the preconcentrates 90:10 made with Capmul MCM (1B3_T4) and Capmul MCM C8 (2B3_T4) was not significant and the microemulsion region formed from the rest of the preconcentrates was similar. Therefore, it was again demonstrated that Capmul MCM C8 and Capmul MCM behaved similarly.

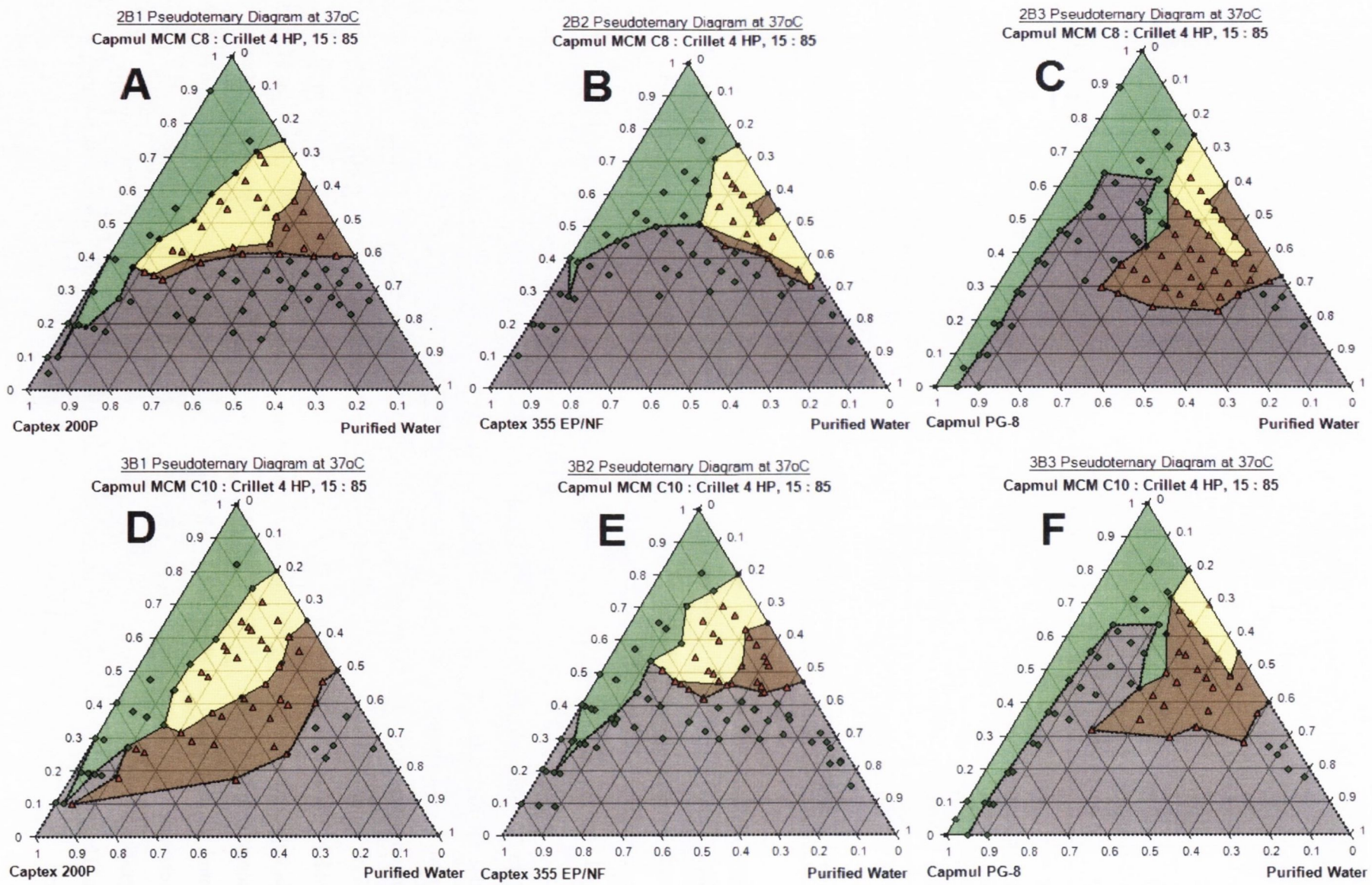

Fig. 4.3. Pseudoternary phase diagrams for the system with the low combined HLB value (the detail explanation given on the next page)

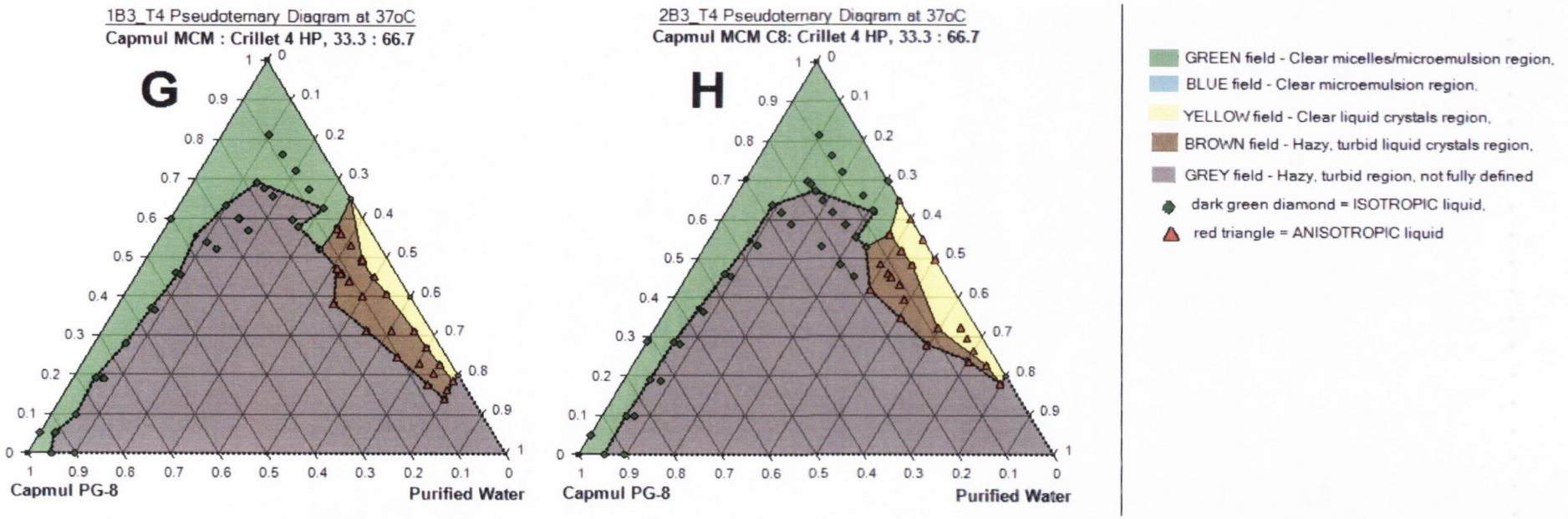

Fig. 4.3. Pseudoternary phase diagrams for the system with the high combined HLB value (cont'd):

A-C) systems where Capmul MCM C8 was used as cosurfactant and different oil phase was used Captex 355 (A), Captex 200P (B), Capmul PG-8 (C)

D-F) systems where Capmul MCM C10 was used as cosurfactant and different oil phase was used Captex 355 (D), Captex 200P (E), Capmul PG-8 (F)

G-H) systems where the same oil phase was used Capmul PG-8, but the cosurfactant varied Capmul MCM (G), Capmul MCM C8 (H). These systems have different ratio between the low HLB value surfactant and the high HLB value surfactant compare to the systems A-F.

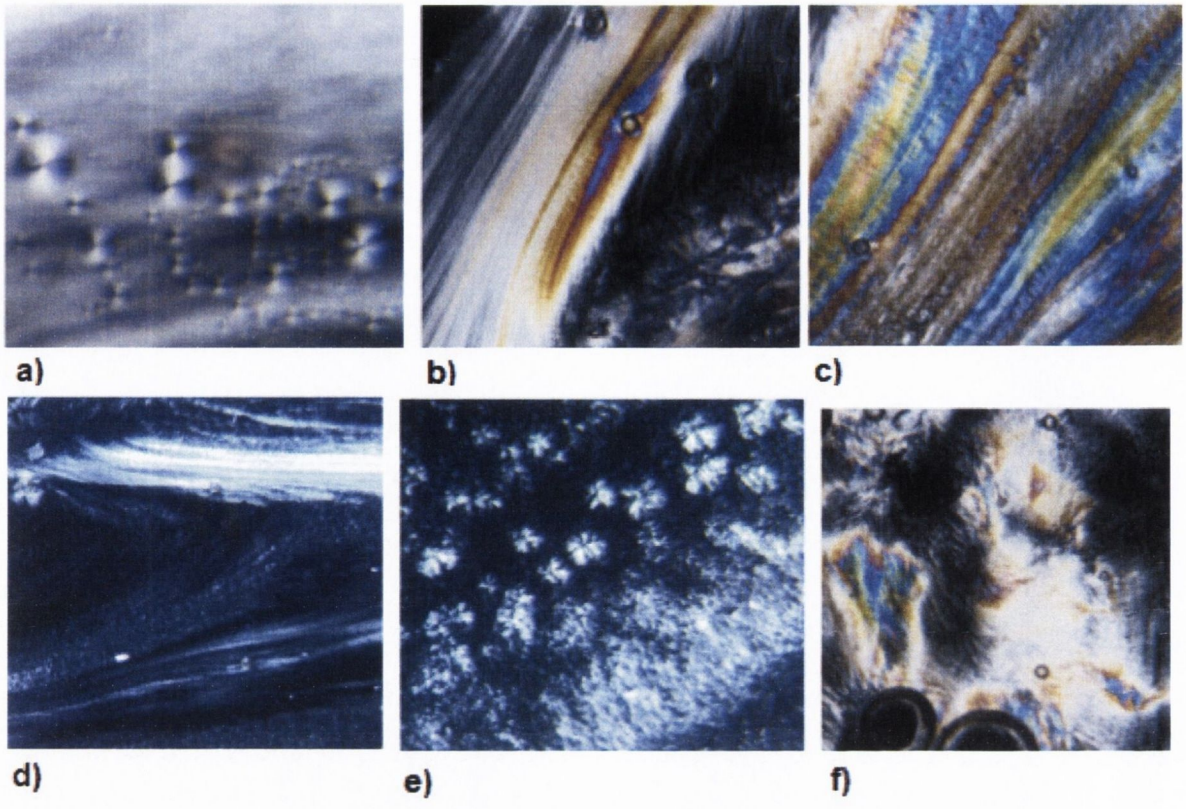

Fig. 4.4. Images indicating presence of liquid crystals (~ 40 x magnification):

Figure 4.4/ images	Pseudoternary diagram	Mix of Surfactants	Oil	Water	Macroscopic appearance
a	**1B3_T4**	53.1	5.9	41.0	Hazy, turbid, slightly viscous
b	**1B3_T4**	49.9	5.2	44.9	Clear, transparent, viscous
c	**1B3_T4**	49.1	5.5	45.5	Opalescent, transparent, viscous
d	**2B1**	39.9	39.8	20.3	Clear, transparent, slightly viscous
e	**2B3**	41.2	17.8	41.0	Hazy, turbid, viscous
f	**2B3**	51.7	13.0	35.3	Hazy, turbid, slightly viscous

4.4.1. Impact of different cosurfactants on the phase behaviour

The impact of different cosurfactants on the systems with the high combined HLB value, was made by direct comparison of phase diagrams prepared with Capmul MCM C8 (systems 2B1 – 2B3, Fig. 4.3.A-C) and Capmul MCM C10 (systems (3B1 – 3B3, Fig. 4.3.D-F) where the same three oils were used. In the system 2B1, Captex 200P was not miscible with the mix of surfactants in all ratios (Fig. 4.3.A) and clear preconcentrates were formed in the ratios 40: 60 to 90: 10 and above. The preconcentrates 20: 80 to 30: 70 were not clear, however when 2-5% of water was incorporated, a clear microemulsion was formed which only existed for up to 10% of water. The microemulsions formed from the preconcentrates 40: 60 to 90: 10 and above, showed a capacity to incorporate, on average, of between 10 to 20% of water before a clear, viscous liquid crystalline phase was formed upon further addition of water. In the system 3B1 (Fig. 4.3.D), where Capmul MCM C10 was used as a cosurfactant, the mix of surfactants was miscible with Captex 200P in the ratio 30: 70 and above. The preconcentrates from 40: 60 to 90:10 and above, could incorporate

between 10 – 20% of water before the microemulsion rearranged into clear liquid crystals, similar to the ones seen for the preconcentrates prepared with Capmul MCM C8. The microemulsion region and the clear anisotropic region of liquid crystals were comparable for the systems 2B1 and 3B1. In the system 2B1 (Fig. 4.3.A) further dilution of the clear liquid crystals, formed from the preconcentrates 40: 60 to 70: 30, led to formation of a very narrow hazy anisotropic phase, which converted into an isotropic emulsion when the water content increased by another 3-5% (20 - 40 % of water content). The same preconcentrates in the system 3B1 (Fig. 4.3.D), beyond the clear region of liquid crystals, formed a large region of hazy liquid crystals existing of up to 45 – 50% of water content. This indicated again that Capmul MCM C8 had a better co-emulsifying properties compared to Capmul MCM C10. When comparing the systems 2B2 (Fig. 4.3.B) and 3B2 (Fig. 4.3.E) where Captex 355 was used as the oil phase, a significantly larger microemulsion area was formed with Capmul MCM C8 as a cosurfactant. The mix of the surfactants was miscible with the oil from 40: 60 to 90: 10 and above, in both systems. In the system 2B2 (Fig. 4.3.B), the preconcentrate 70: 30 appeared to form the most extensive region of clear microemulsion containing up to 25-30% of water. The same preconcentrate in 3B2 system (Fig. 4.3.E) formed a clear isotropic microemulsion up to approximately 15% of water. Also, the region of clear liquid crystalline phase appeared to be larger for the system with Capmul MCM C8 as a cosurfactant.

Capmul PG-8 was miscible with the mix of surfactants in all ratios, irrespective of whether Capmul MCM C8 (Fig. 4.3.C) or Capmul MCM C10 (Fig. 4.3.F) was used as a cosurfactant. In both system 2B3 (Fig. 4.3.C) and 3B3 (Fig. 4.3.F), the preconcentrates from 10: 90 to 70: 30 formed a microemulsion region containing approximately 5-10%. In both systems, the preconcentrate 70: 30 formed a microemulsion region, which was separated by an isotropic turbid phase when the water content was between 10-25%. The preconcentrates 80: 10 and 90: 10, prepared with Capmul MCM C8 (Fig. 4.3.C) formed a clear microemulsion up to approximately 25% of water and a clear liquid crystalline region when the water content was between 25 and 55%. The same preconcentrates prepared with Capmul MCM C10 (Fig. 4.3.F) formed a microemulsion with the lower water content (~ 20%) before a clear liquid crystalline phase occurred (from 20 to 45%). As the microemulsion region and liquid crystalline region were larger in 2B3 system, Capmul MCM C8 was found to have stronger co-emulsifying properties than Capmul MCM C10.

The combined HLB values of the systems 1B3_T4 (Fig. 4.3.G) and 2B3_T4 (Fig. 4.3.H) were lower (~11.5) compared to the systems with high HLB value (~13) presented in Fig. 4.3 A-F. In systems 1B3_T4 and 2B3_T4, the ratio between the mix of the low HLB value surfactant to high HLB value was 33: 67, while it was 15: 85 in the other systems. The system 2B3_T4 represented formulations with a higher level of cosurfactant (lower level of the primary surfactant) compared to the system 2B2 (Fig. 4.3.F), which was made with the same type of oil, Capmul PG-8. Capmul PG-8 was found to form clear preconcentrates when combined with both mixes of surfactants (15: 85 and 33: 67) in every ratio. In both systems, the preconcentrates from 10: 90 to 70: 30 formed a

microemulsion phase with the same amount of water, between 5 and 10%. The preconcentrate 90: 10, with the higher content of the cosurfactant (the system 2B4_T4, Fig. 4.3.H) formed a more extensive microemulsion phase up to 35%. As the concentration of water increased beyond 35%, a clear liquid crystalline phase was formed for up to 80% of water. The same preconcentrate prepared with the lower content of cosurfactant (system 2B3, Fig. 4.3.C) formed a microemulsion region up to 25% of water and a clear liquid crystalline phase up to 55%. Therefore, it was demonstrated that the low concentration of the cosurfactant (despite the increased content of the primary surfactant), had a negative effect on formation of microemulsion and clear liquid crystalline region. Formation of microemulsion and clear liquid crystalline area decreased as the content of the cosurfactant decreased.

4.4.2. Impact of different oils on the phase behaviour

The effect of different oils on the phase behaviour was made by comparison of phase diagrams where the same low HLB value surfactant was used. The phase diagrams with Capmul MCM C8, were prepared with Captex 200P (2B1, Fig. 4.3.A), Captex 355 (2B2, Fig. 4.3.B) and Capmul PG-8 (2B3, Fig. 4.3.C). Capmul PG-8 was miscible with the mix of surfactants in all ratios (Fig. 4.3.C), however the microemulsion region was narrow with a maximum of 25% water for the preconcentrates 80: 20 and 90: 10 and above. Captex 355 (Fig. 4.3.B) and Captex 200P (Fig. 4.3.A) did not form clear preconcentrates when combined with the mix of surfactants in every ratio. Captex 355 was the least miscible as the most hydrophobic oil. The microemulsion region formed with Captex 355 (Fig. 4.3.B) slightly expanded compared to the system with Captex 200P. Clear preconcentrates with the ratio 70: 30 and above formed microemulsions with approximately 20 –30 % (Fig. 4.3.B). Captex 200P was more miscible with the mix of surfactants and therefore its microemulsion region (Fig. 4.3.A) was wider along the axis between 100% of oil and 100% of the mix of surfactants, compared to the system with Captex 355 (Fig. 4.3.B). On the other hand, a smaller region of microemulsion (as the concentration of water increased) was seen with Captex 200P compared to the one observed with Captex 355.

The phase diagrams with Capmul MCM C10 as a cosurfactant, were prepared with Captex 200P (3B1, Fig. 4.3.D), Captex 355 (3B2, Fig. 4.3.E) and Capmul PG-8 (3B3, Fig. 4.3.F). As before Capmul PG-8 appeared to be miscible with the mix of surfactants in every ratio (Fig. 4.3.F) but the microemulsion area was limited with the highest percentage of water incorporated by the preconcentrates of 80: 20 and above (up to 20% of water). Although, the preconcentrate 70:30 formed a clear microemulsion around 30% of water, its dilution behaviour was not superior as a turbid, hazy isotropic phase, possibly emulsion was observed between 10% and 20% of water. Captex 200P (Fig. 4.3.D) and Captex 355 (Fig. 4.3.E) showed larger areas of microemulsion derived from the preconcentrates of 40: 60 to 70: 30. The microemulsion region prepared with Captex 200P was wider compared to the microemulsion formed with Captex 355 (Fig. 4.3.E), due

to higher miscibility of Captex 200P with the mix of surfactants, but a similar amount of water could have been incorporated in both systems. None of the preconcentrates prepared with Captex 355 showed a superior dilution behaviour compared to the preconcentrates with Captex 200P.

4.5. Impact of additional cosolvents on the phase behaviour

The effect of additional cosolvent on the phase behaviour was evaluated with PEG 400 on two selected phase diagrams, the system 2A2 representing systems with a low combined HLB value and the system 2B2 representing systems with a high combined HLB value. Both these systems were made with the same type of oil and cosurfactant, so they differ only by the ratio of low and high HLB value surfactants (the combined HLB value). A comparison was made between the phase diagrams prepared without PEG 400 that were presented earlier on, and the phase diagrams prepared with approximately 20% of PEG 400 (preconcentrates made up 80% of the sample). To each preconcentrate in the range 10: 90 to 90:10, PEG 400 was added as 20% per final sample weight. Therefore, these SEDDS represented a potential capsule filling formulations with approximately 20% of PEG 400. In order to compare the phase diagram with PEG 400 (Fig. 4.5.B) to the one without PEG (Fig. 4.5.A), it was necessary to normalise the content of oil, water and the mix of surfactants to 100% so these components could be plotted on the three component diagram. Although PEG 400 is very frequently added to preconcentrates and microemulsions to improve their dilution behaviour, the addition of PEG 400 to the system 2A2 had a negative effect on formation of clear preconcentrates and dilution behaviour in some areas of the microemulsion region (Fig. 4.5.B). The presence of PEG 400 affected miscibility of the surfactants with Captex 355 and the clear SEDDS formulations were only formed with preconcentrates from 60: 40 to 90: 10 and above. The extensive microemulsion region formed from the preconcentrates 40: 60, 50: 50 and 60: 40 (without PEG 400) previously seen in 2A2 system (Fig. 4.5.A), disappeared. A very limited microemulsion area containing approx 2-3% of water was derived from the hazy preconcentrates 10: 60 to 50: 50, which existed of 7 and 10% water content. The preconcentrates 60: 40 with PEG 400, could incorporate between 15 and 20% of water before the microemulsion turned into a hazy emulsion. The same preconcentrates, without PEG 400 could incorporate approximately 10-15% of water, so it appeared that PEG 400 marginally improved dilution behaviour of the preconcentrates with the high content of surfactants (high ratio between the mix of the surfactants and the oil).

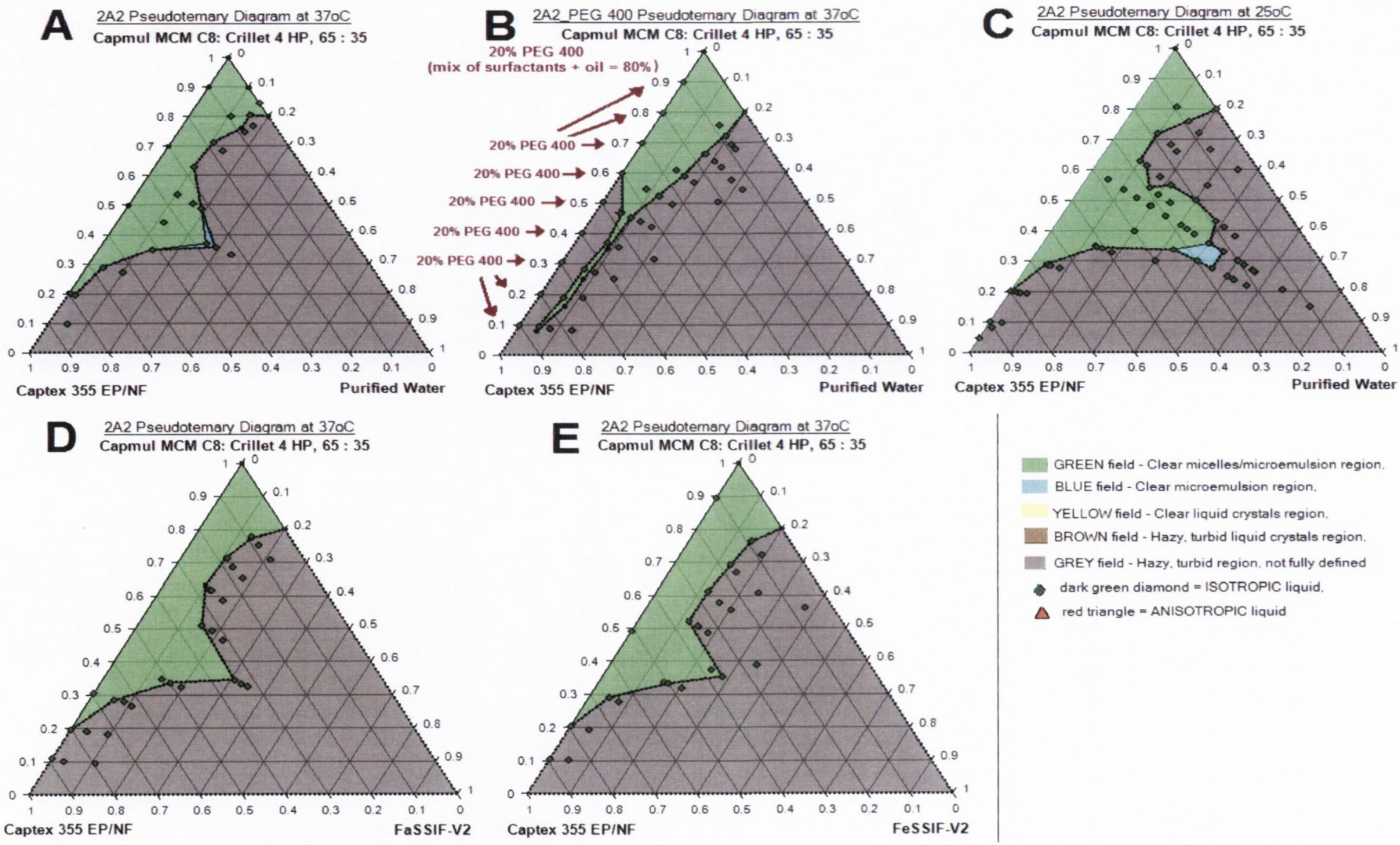

Fig. 4.5. Effect of various modifications on the phase behaviour in 2A2 systems: A) original system, B) addition of PEG 400, C) reduced temperature (25°C), D) FaSSIF-V2 as an aqueous phase, F) FeSSIF-V2 as an aqueous phase.

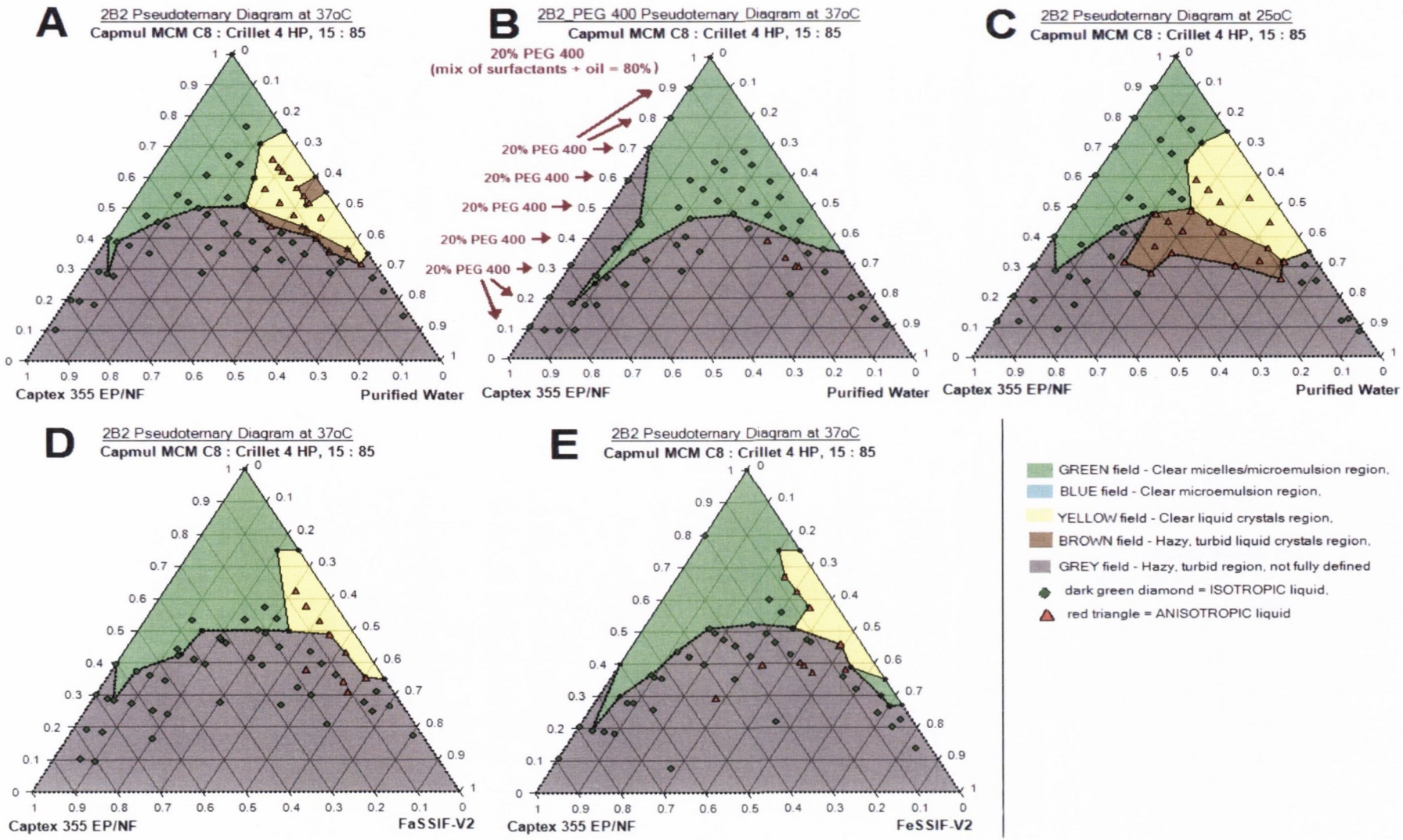

Fig. 4.6. Effect of various modifications on the phase behaviour in 2B2 systems: A) original system, B) addition of PEG 400, C) reduced temperature (25°C), D) FaSSIF-V2 as an aqueous phase, F) FeSSIF-V2 as an aqueous phase.

The addition of PEG 400 to the system 2B2 improved significantly the formation of the microemulsion region for the preconcentrates with the high content of surfactants such as 80: 20 and 90:10 (Fig. 4.6.B), where previously a liquid crystalline phase was observed (Fig. 4.6.A). The miscibility of the surfactants with Captex 355 decreased in the presence of PEG 400 (as previously seen in the system 2A2/PEG 400) and only the preconcentrates with the high amount of the surfactants (70: 30 to 90: 10/and above) were clear. The hazy, formulations based on the preconcentrates from 40: 60 to 70: 30 formed a reduced microemulsion region compared to the microemulsion region formed from the same preconcentrates in the absence of PEG 400 (Fig. 4.6.A).

4.6. Impact of temperature on the phase behaviour

The effect of temperature on phase behaviour was evaluated on the system 2A2 with the low combined HLB value and the system 2B2 with the high combined HLB value. The comparison was made between the phase diagrams prepared at 25°C and 37°C. Crillet 4 HP as a non-ionic surfactant containing polyoxyethylene chains, exhibits reverse solubility versus temperature behaviour in water, therefore it shows different 'microemulsifying' properties at various temperatures. In the system 2A2, the lower temperature increased the solubility of Crillet 4 HP, which resulted in an expanded microemulsion region derived from the preconcentrates 40: 60 to 70: 30 (Fig. 4.5.C). The preconcentrates 50: 50 and 60: 40 showed superior dilution behaviour as approximately 45% of water could be incorporate into a microemulsion before it turned a hazy, isotropic emulsion. In comparison to the preconcentrate 50: 50, which could incorporate up to 30% of water at 37°C (Fig. 4.5.A), the reduction of temperature by 12 degrees expanded the microemulsion region by an additional 15% of water. The microemulsion region derived from the preconcentrates 70: 30, 80: 20 and 90: 10 and above, was similar irrespective of the temperature. The temperature appeared to have no significant impact on phase behaviour of the system 2B2 (Fig. 4.6.C). The microemulsion and clear liquid crystalline regions were similar at 25° (Fig. 4.6.C) and 37°C (Fig. 4.6.A) The only difference caused by the temperature was the formation of a more extensive hazy liquid crystalline phase upon dilution of the preconcentrates from 40: 60 to 60: 40 at 25°C, while at 37° an isotropic emulsion was observed in this part of the phase diagram.

4.7. *In vivo* considerations, the impact of intestinal fluids on the phase behaviour

When microemulsions and SEDDSs are released from an enteric-coated capsule *in vivo*, the pH of the intestinal fluids and presence of natural surfactants could affect the dilution behaviour of these systems. The artificial intestinal fluid FaSSIF-V2 and FeSSIF-V2 were used to titrate two model systems: the system 2A2 with low combined HLB value and the system 2B2 with high

combined HLB value to examine the effect of natural surfactants (and physiological pH) on emulsification of the studied systems. The composition of the artificial, intestinal fluids is given in Chapter 2, section 2.4.1. Only dilution with intestinal fluids was investigated, as the GIPET® II capsules containing SEEDS, preconcentrates or microemulsions are enteric coated, intended to release the liquid content in the duodenum.

4.7.1. Phase behaviour in fasted stated (FaSSIF-V2)

The dilution with FaSSIF-V2 had no significant effect on the formation of microemulsion regions in the 2A2 system and a very similar pseudoternary diagram was obtained (Fig. 4.5.D) to the one produced with water (Fig. 4.5.A). The microemulsion region in the system 2B2 diluted with FaSSIF-V2 was slightly enlarged (Fig. 4.6.D) in comparison to the microemulsion formed with water (Fig. 4.6.A), in particular for the preconcentrate 80: 20. This indicated that the surfactants present in FaSSIF-V2 (sodium taurocholate, lecithin) facilitated formation of a larger microemulsion area. The preconcentrate 80: 20 when titrated with water formed a microemulsion containing approximately 25% of water (Fig. 4.6.A), while the same preconcentrate diluted with FaSSIF-V2 could incorporate up to approximately 35% of the aqueous phase (Fig. 4.6.D). The presence of sodium taurocholate in the diluting medium, also decreased formation of liquid crystals and in place of these structures, a microemulsion was formed. The dilution behaviour of the preconcentrate 90: 10 remained unchanged and similar phases of microemulsion and liquid crystals were observed with both diluting media. It appeared that the amount of sodium taurocholate/lecithin present in FaSSIF-V2 was insufficient to induce formation of microemulsion from this preconcentrate.

4.7.2. Phase behaviour in fed state (FeSSIF-V2)

The dilution with FeSSIF-V2 had no significant effect on the formation of microemulsion regions in the 2A2 system since no difference was observed between the original systems diluted with water (Fig. 4.5.A) and the one diluted with FeSSIF-V2 (Fig. 4.5.E). The microemulsion region in the system 2B2 diluted with FeSSIF-V2 was enlarged (Fig. 4.6.E) in comparison to the microemulsion formed with water (Fig. 4.6.A) as the additional surfactants (sodium taurocholate, lecithin sodium oleate, glycerol monooleate) facilitated formation of a larger microemulsion area. The microemulsion derived from the preconcentrate 80: 20 increased by approximately 10% when FeSSIF-V2 was used for titration. The additional region of isotropic microemulsion was observed for the preconcentrate 90: 10 when the content of the aqueous phase reached approximately 65% and existed for up to 75% of FeSSIF-V2.

4.8. Overall Conclusions

The main findings of this chapter relate to the effects that the type of the cosurfactant, the type of the oil phase and the combined HLB value has on the formation of clear preconcentrates and microemulsions. Based on the work carried out, Capmul MCM C8 was found to be a more effective cosurfactant compared to Capmul MCM C10 in all the systems examined, as this material facilated formation of larger microemulsion areas.

Capmul PG-8 as the most hydrophilic oil was found to be miscible with the surfactants (mixes of the low and the high HLB value surfactants) in every ratio, however these preconcentrates showed the limited microemulsion area upon dilution. Since the preconcentrates and microemulsions comprising of Capmul PG-8 can be considered as quite hydrophilic formulations, they could be used to incorporate highly hydrophilic drugs where prolonged existence of a water-in-oil microemulsion upon dilution *in vivo* is not required and the drug should be released rapidly. On the other hand, Captex 355, the most hydrophobic oil, did not form clear preconcentrates when combined with the mix of surfactants in every ratio, but a number of the preconcentrates (40: 60 to 60: 40) formed extensive microemulsion regions upon dilution. As these preconcentrates contain a relatively high percentage of the oil phase, they could be potentially used with more hydrophobic compounds (where the hydrophobic oil could help to dissolve the drug) and formation of the microemulsion on dilution would help maintain the drug in the solubilised form. In addition, these microemulsions could be potentially used to deliver hydrophilic, unstable drugs such as peptides, where the prolonged existence of water-in-oil microemulsion could protect the drug against enzymatic degradation (Lyons et al. (2000).

In terms of quantitative composition, formation of a microemulsion region was affected by the content of the primary surfactant, the content of cosurfactant and the ratio between them, which makes the combined HLB value. Within the systems examined in this work, the ratio of 65: 35 between the cosurfactant (the low HLB value surfactant) and the primary surfactant (the high HLB value surfactant) facilitated formation of extensive microemulsion regions in particular with Captex 355, and reduced formation of viscous liquid crystalline phase upon dilution. In addition, the impact of additional cosolvents, temperature and additional surfactants was evaluated on the model systems to understand how these factors affect the phase behaviour of the systems based on glycerides and esters of caprylic/capric acids.

The work presented in this chapter examined the interaction between the oil phase, the surfactants and the aqueous phase in order to learn how the choice of materials affects formation of preconcentrates, microemulsions (MEs) and SEDDSs and their dilution behaviour. Many potential SELFs and MEs for encapsulation were identified through preparation of phase diagrams. Prior to incorporation of the model compounds, it is important to gain an insight into the microstructure of the studied systems, which may affect drug distribution and stability in the formulation.

Chapter 5

Characterisation of Microemulsions

5.1. Introduction

Microemulsions are becoming increasingly complex systems in terms of their composition, e.g. containing polymers, biomolecules, complexing surfactants and/or mixtures of surfactants, etc. To have a detailed understanding of these more complex systems an increasingly more refined and comprehensive characterisation is required. Due to substantial improvements in experimental characterisation techniques over the last 10 years, a good understanding of the structure of microemulsions has been obtained using dynamic light scattering (DLS), small-angle X-ray scattering (SAXS) and, in particular, small-angle neutron scattering (SANS) and nuclear magnetic resonance (NMR) (Gradzielski, 2008). In addition, several other experimental techniques have been used to characterise the microstructure of microemulsions including electrical conductivity, viscosity, differential scanning calorimetry (DSC), freeze-fracture transmission electron microscopy (FF-TEM) and cryo-field emission scanning electron microscopy (Cryo-FESEM). Due to the complexity of the microemulsion structures, typically various experimental techniques have to be combined.

The aim of this work was to employ typical characterisation techniques to investigate the type and structure of model colloidal samples. It was important to understand which technique, if any, provided the best insight into the microstructure of the investigated microemulsions which comprised derivatives of caprylic/capric acids. Several experimental studies including conductivity, viscosity, self-diffusion NMR, DSC and cryo-TEM were carried out on the model colloidal samples in order to explain the type of microstructure. Understanding the relationship between the microstructure, the composition and the dilution behaviour of microemulsions helps to predict drug distribution in the formulations and its fate upon dilution.

5.2. Composition of the model colloidal samples

Clear, isotropic samples formed by dilution of the preconcentrate 2A2 60: 40 at 25°C (the phase diagram shown in Chapter 4, Fig. 4.5.C) were chosen as model colloidal samples representative of the systems studied in Chapter 4. These samples represented derivates of the preconcentrate that showed the best dilution behaviour. The preconcentrate 60: 40 could incorporate up to 45% water as a microemulsion (at 25°C) and therefore potentially various microphases existed as the water content varied. Investigation of the microstructures in these samples aimed to challenge the applicability of characterisation methods to examine various phases of microemulsions composed of derivates of caprylic/capric acids and polysorbate 90. The composition and appearance of each sample is presented in Table 5.1. R1 – R9 samples (up to 45% water) were clear, monophasic systems while R10- R13 corresponded to hazy turbid isotropic emulsions. The sample R10 was classified as in a turbid state after 24 hours equilibration at 25 °C, but this point seemed to be located very close to the border between the monophasic and the heterogeneous regions.

Table 5.1. Detailed composition of the samples derived from the preconcentrate 2A2 60:40 (R0).

Sample Name	Mix of surfactants, Capmul MCM C8: Crillet 4HP (65:35)	Captex 355 EP/NF	Purified Water	Visual Appearance at 25°C
R0	60	40	**0**	clear, monophasic solution
R1	57	38	**5**	clear, monophasic solution
R2	53	36	**11**	clear, monophasic solution
R3	51	34	**15**	clear, monophasic solution
R4	48	32	**20**	clear, monophasic solution
R5	45	30	**25**	clear, monophasic solution
R6	42	28	**30**	clear, monophasic solution
R7	39	26	**35**	clear, monophasic solution
R8	36	24	**40**	clear, monophasic solution
R9	33	22	**45**	almost clear, opalescent monophasic solution
R10	30	20	**50**	turbid, heterogeneous emulsion, becomes clear once temperature decreases by 2-3°C
R11	27	18	**56**	cloudy, turbid, heterogeneous emulsion
R12	21	14	**65**	cloudy, turbid, heterogeneous emulsion, separates very easily/quickly
R13	15	10	**75**	cloudy, turbid, heterogeneous emulsion, separates very easily/quickly

5.3. Cryogenic transmission electron microscopy (cryo-TEM) and Freeze-fracture transmission electron microscopy (FF-TEM)

Two samples likely to represent different microstructures were chosen for cryo-transmission electron microscopy (cryo-TEM) imaging and freeze-fracture transmission electron microscopy (FF-TEM). The characterisation was performed on sample R3, which could represent a water-in-oil system (15% water) and sample R9 (45% water), which was likely to differ significantly from the other sample considering the percentage of water incorporated (45%).

The cryo-TEM images indicated a lack of definite structure in both samples (Fig. 5.1). The dense black spots visible on Fig. 5.1.c were artifacts present on the carbon support film. The lack of visible structure could have been caused by several factors, including difficulties in sample preparation (the samples were too viscous to form thin enough films to visualise small structures) or an insufficient contrast between the different phases of the samples.

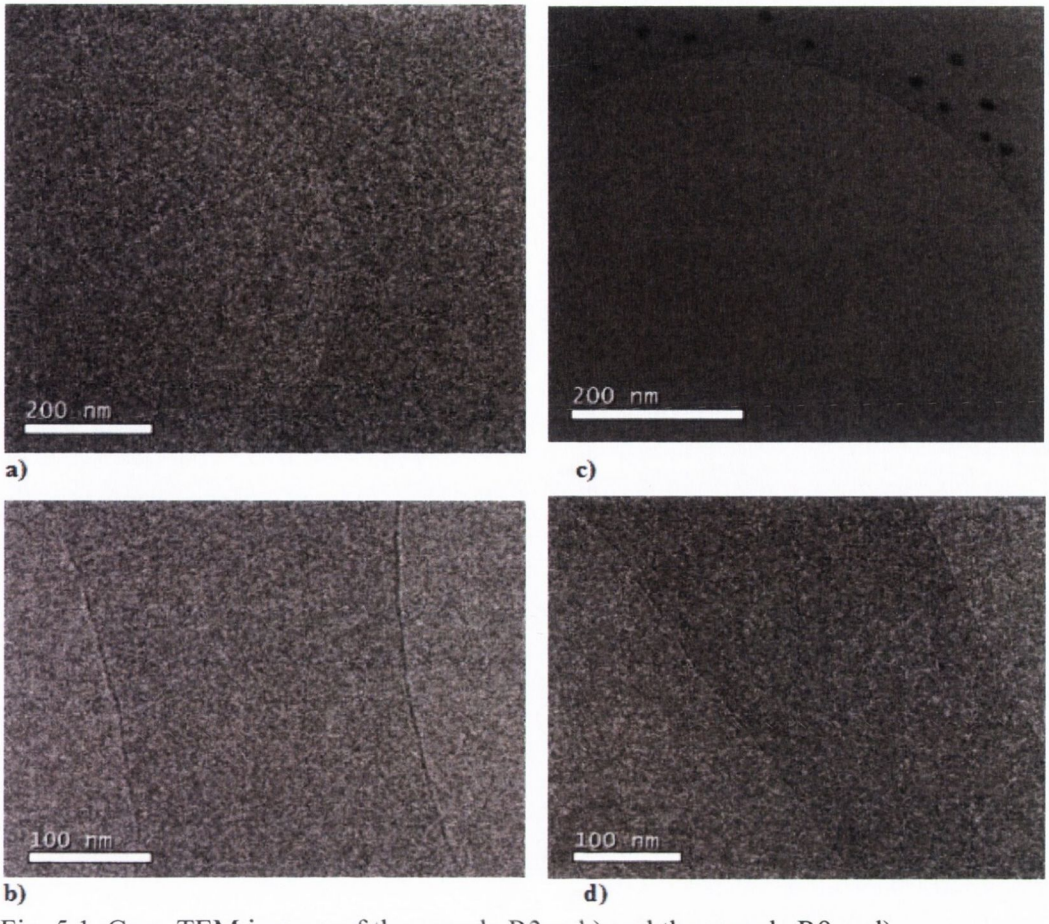

Fig. 5.1. Cryo-TEM images of the sample R3 a, b) and the sample R9 c, d)

Further characterisation was performed with freeze fracture replicas (FF-TEM) of the samples which were freshly mixed or stored for 24 hours at 25°C. The freeze fracture replicas from sample R3 showed no obvious, larger structures in either the freshly mixed (Fig. 5.2.a) or 24 hour samples (Fig. 5.2.b). The fractured surface looked 'rougher' than would be expected from, for example, a pure ice fracture face. FF-TEM images of R3 resembled very small discrete, overlaid droplets (possibly 10 nm or less) that were associated into extensive aggregates. Similar images, although slightly less rough were seen for 1-butyl-3-methylimidazolium tetrafluoroborate microemulsion in toluene with a weight ratio of 1.35:0.65 and with a molar ratio toluene: Triton X-100 equal to 0.66) (shown in Fig. 5.3.a) where the droplet size was on average was equal to 40nm (Voigt et al., 2008). Also, a rough surface (Fig. 5.3.b), similar to some extent to that in the images of the sample R3, was observed on the freeze fracture images for a quaternary microemulsion system of a cationic surfactant (cetyltrimethylammonium bromide, CTAB), octane, water, and 1-butanol) with a particle size ranging from 50 to 100 nm (Jian et al., 2001). Nevertheless, a definite conclusion that the sample R3 was made of very small droplets could not be made since the resolution of FF-TEM is poor for structures smaller than 10 nm (the resolution is limited by the grain size of the platinum coating used to make FF-TEM replicas; Brain, 2008).

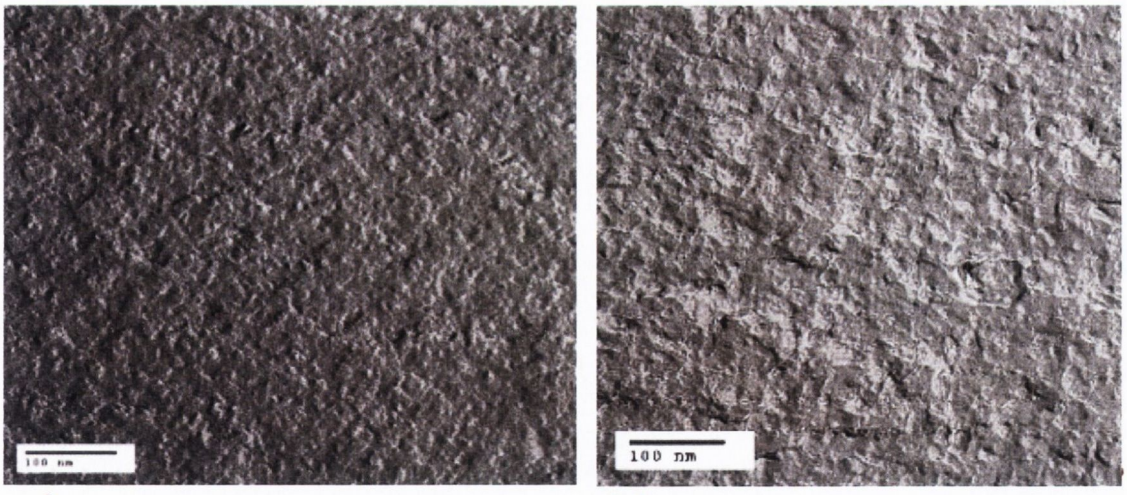

Fig. 5.2. Images of freeze-fracture replicates of R3 sample a) freshly mixed b) after 24 hours.

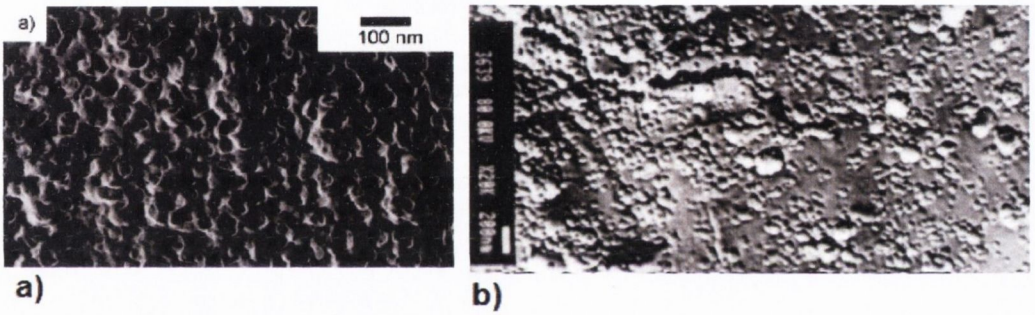

Fig. 5.3. Images of freeze-fracture replicates of a) a 1-butyl-3-methylimidazolium tetrafluoroborate-in-toluene microemulsion (Voigt et al., 2008), b) a microemulsion comprising cetyltrimethylammonium bromide, CTAB), octane, water (20%), and 1-butanol (Jian et al., 2001).

The freeze fracture replicas of the sample R9 showed some lamellar structures which were mostly more plate-like than vesicular and were more frequently observed in the freshly mixed sample (Fig. 5.4.a). In such a concentrated sample with a high amount of surfactants, a higher order of self-assembly would be common (Kumar & Mittal, 1999). The concept of single isolated vesicles suspended in a matrix differs substantially to the commonly observed lamellar, hexagonal, rod-like structures. The freshly shaken sample R9 resembles a lamellar, bi-layer microemulsion. After 24 hours, some feature of the lamellar state could still be seen, although the sample more resembled a vesicular structure bicontinuous phase (Fig. 5.4.b).

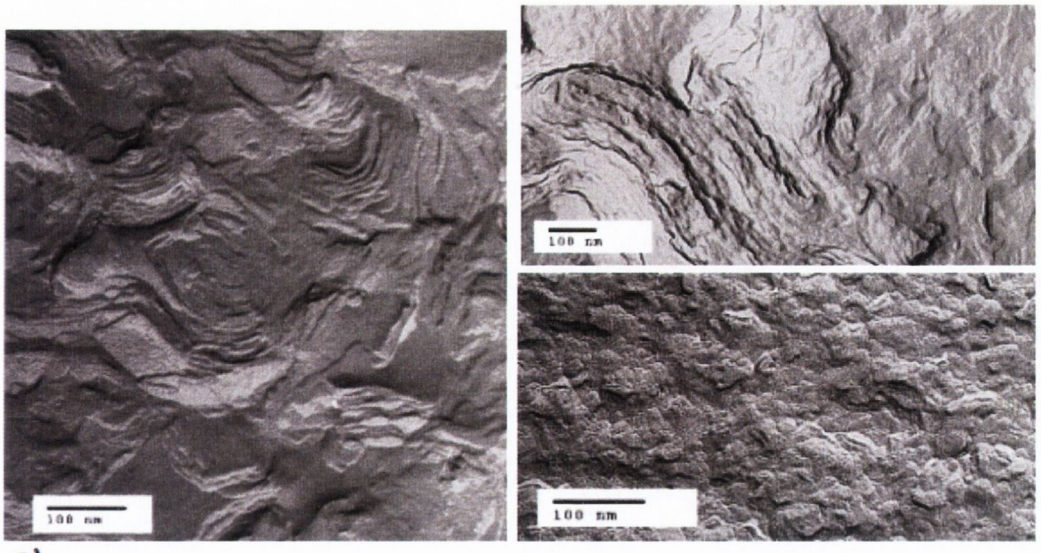

Fig. 5.4. Images of freeze-fracture replicates of R9 sample a) freshly mixed b) after 24 hours.

A bicontinuous microemulsion which resembled the structures observed here (in particular in Fig. 5.4.b) to some extent was observed by Boltzinger et al. (1998) for systems composed of sucrose monolaurate-sucrose dilaurate-medium chain alcohol-octyl octanoate-water (Fig. 5.5.a). Another bicontinuous structure, similar to the structure observed in R9 sample, was made of $C_{10}G_1$-water-n-octane-butan-1-ol (Fig. 5.5.b) and was reported by Hantzschel et al. (1999).

Based on the comparison with the results published by other researchers, the sample R9 appeared to be a bicontinuous microemulsion, although the oil and the aqueous phases were differentiated poorly on the pictures and additional characterisation would be required to verify this hypothesis.

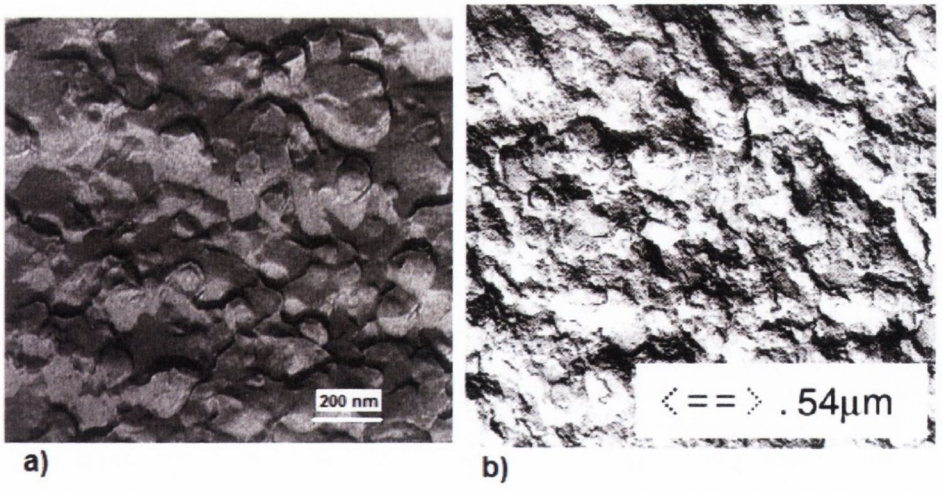

Fig. 5.5. Images of freeze-fracture replicas of a) a microemulsion composed of sucrose monolaurate-sucrose dilaurate-medium chain alcohol-octyl octanoate-water (Boltzinger et al., 1998), b) a microemulsion comprising of $C_{10}G_1$-water-n-octane-butan-1-ol (Hantzschel et al., 1999).

5.4. Conductivity

Measurements of electrical conductivity were used to detect structural changes in the samples. The conductivity measurements were performed without addition of any electrolyte. The incorporation of electrolytes in nonionic systems seems to be a common approach, which facilitates measurements through increased charge transport (Lutz et al., 2007). However, the change in ionic strength of the aqueous phase can lead to phase separation and therefore it was decided to perform direct measurements on the samples R1 - R13 made with purified water. Initially, the conductivity measurements of individual components used to prepare the samples R1 - R13 were carried out. The conductivity of individual materials was very low. The values obtained were 0.80 µS/cm, 1.86 µS/cm and 3.08 µS/cm for Captex 355 EP, purified water and mix of the surfactants (Crillet 4 HP: Capmul MCM C8, 35:65) respectively. The conductivity for all the samples R1 -R13 was found to be higher than for the individual materials as shown in Fig. 5.6 (details given in Appendix Table A.5.1). The samples R1- R4, containing 5-20% water, showed substantially lower conductivity than the samples R5- R13, 25-75% water, but still appeared to be twice to nine times more conductive than the mix of surfactants (the component with the highest conductivity).

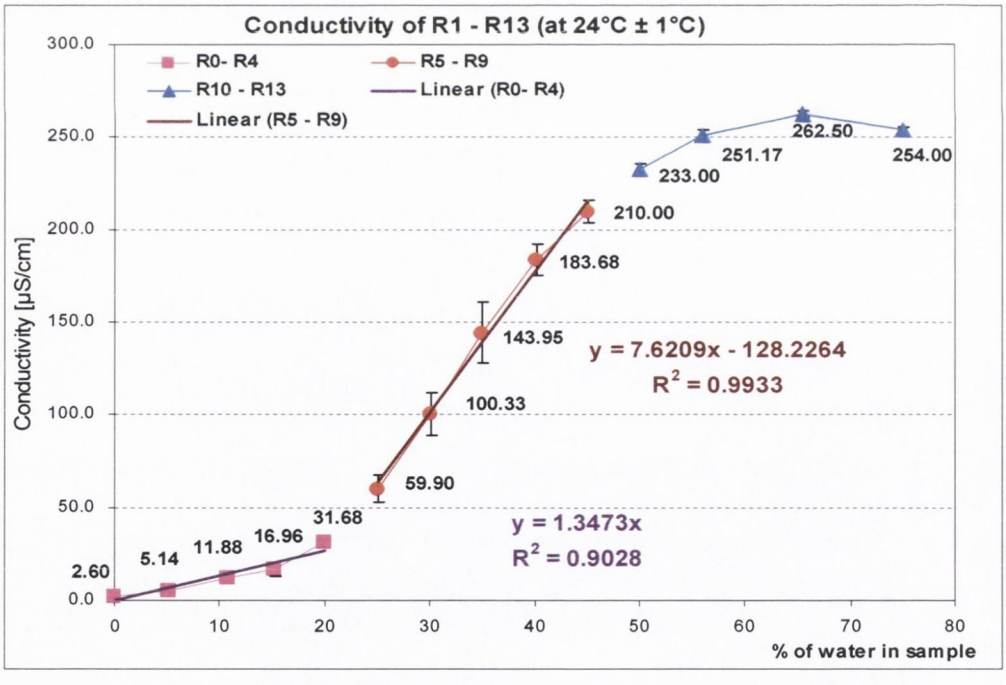

Fig. 5.6. Conductivity measurements for R0 -R13 samples with trendlines.

For the samples R0 - R4, a linear relationship between an increase of conductivity and a water increase up to 20% was observed with a correlation coefficient (Fig. 5.6, $R^2 = 0.9028$). The slope of the trendline was small, indicating that conductivity did not rise rapidly with the water increase, nevertheless conductivity for sample R4 was still significantly higher compared to samples R1 and R0. The relationship between conductivity and % water in the sample changed dramatically from sample R5, containing 25% water, onwards. In these samples a sharp increase in conductivity was

observed. Such a sudden increase in conductivity reflects the percolation threshold (Φ c). At low water content, individual droplets maintain low conductivity. As the percentage of water increases, the conductivity also increases facilitated by the assembly of droplets into clusters allowing ion diffusion or exchange of droplet content and thus the formation of an infinite percolating droplet network. It has been postulated that the threshold of electrical percolation corresponds to the formation of the first open structure of an infinite cluster (Mehta & Kaur, 2011). The conductivity above the percolation threshold has been attributed to either hopping of surfactant ions from droplet to droplet within droplet clusters or transfer of counter ions from one droplet to another through water channels opening between droplets during sticky collisions through transient merging of droplets. Percolation phenomena have been observed in ionic (Kumar & Mittal, 1999) but also in non-ionic (Mehta & Bala, 2000) microemulsions although it is not clear what exactly causes the phenomena (high conductivity) in these systems. Some researchers (Fanun, 2010) attributed the high conductivity measured in electrolyte-free microemulsion systems containing mixed nonionic surfactants (sucrose laurate and ethoxylated mono-di-glyceride) to the presence of 'conductive' impurities. The microemulsion droplets above the percolation threshold, aggregated in clusters, are considered to be phase different to that of non-percolating droplets, with distinct physical properties such as conductivity (Mehta & Kaur, 2011). Providing that there is a distinct inflection in the conductivity curve, an estimate of the percolation threshold can be obtained by plotting the first derivative, i.e. [d (log conductivity)/d volume fraction of water (φ w) or logarithmic values of conductivity against the percentage of water in the system (Alany et al., 2001), as shown in Fig. 5.7 (details in Appendix, Table A.5.2).

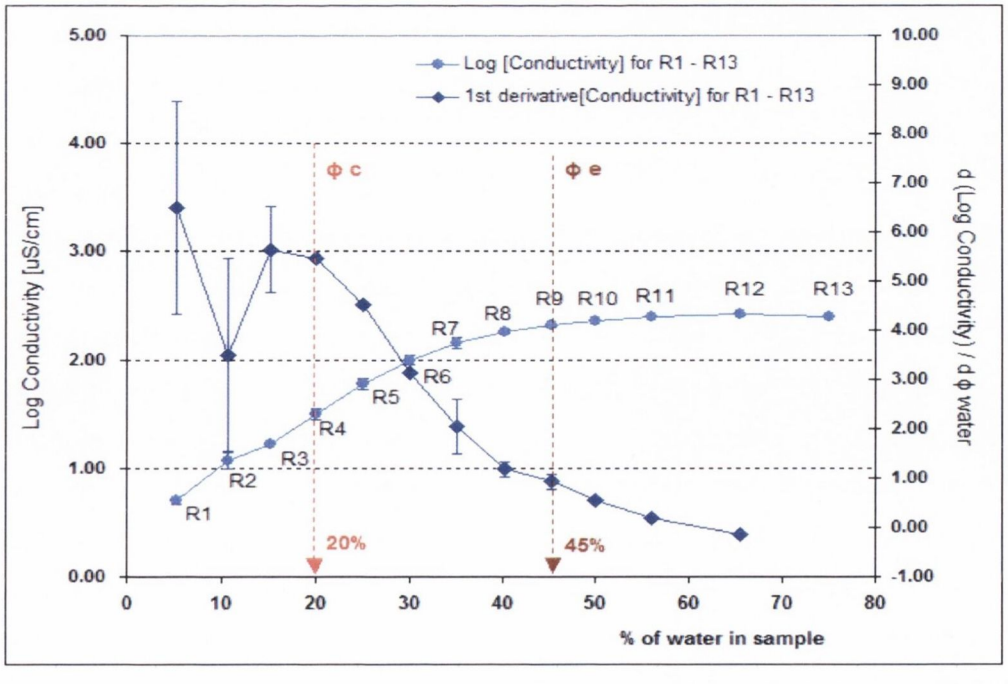

Fig. 5.7. Change of log (conductivity) for the samples R1-R13 and 1st derivative d (log conductivity) / d φ water.

The maximum peak of the 1st derivate plot is considered as the percolation threshold. In the studied samples, sample R4 (containing 20% water) was considered as the percolation threshold since high variability in the samples R1- R3 indicated non-reproducible (non-percolating) behaviour (Fig. 5.7). The conductivity of the samples R5 –R9 was significantly higher than for the R1-R4 points, which suggested the existence of some different, more conductive phase. All R5-R9 samples fitted well into a linear trendline (Fig. 5.6, $R^2 = 0.9933$). Based on the conductivity measurements only, it was not clear enough what sort of the system was formed when the water content ranged from 25-45%. High conductivity would be expected from oil-in-water microemulsions as well as from a bicontinuous phase. On the other hand, high conductivity (above the percolation threshold) was also reported for water-in-oil microemulsions where formation of conductive water cylinders or channels in an oil phase was observed. Xie et al. (2007) observed the percolation threshold at 20% wt% of water and this system consisted of biosurfactant-rhamnolipid/n-butanol/water/n-heptane remained a water-in-oil microemulsion up to 50% wt.% of water where a transformation into a bicontinuous microstructure occurred. In the gradually diluted microemulsion made of R(+)-limonene, water, propylene glycol, ethanol and Tween 60 or Brij 96v, studied by Yaghmur et al. (2003), the conductivity of the systems was negligible at low aqueous phase weight fraction, suggesting that the reverse discrete droplets existed up to 20 wt % (isolated droplets in a nonconducting oleic medium). The further, significant increase in conductivity beyond 20% of aqueous phase was attributed to the presence of a bicontinuous phase up to 60 wt % of the aqueous phase, where a structural transition to oil-in-water droplets occurred (Yaghmur et al., 2003). Boonme et al. (2006) reported the conductivity of microemulsions made of isopropyl palmitate/water/Brij 97:1-butanol/ water to be very low as long as the water fraction remained below 10% wt/wt. Above 10% wt/wt water, a drastic increase in conductivity (the percolation threshold) was observed leading to formation of a water-in oil microemulsion which converted into an oil-in-water microemulsion once 30% wt/wt water was incorporated. A bicontinuous phase was not detected in these microemulsions (Boonme et al., 2006). In the non-ionic microemulsions composed of cethyl polyethylene oxide, heptane, n-butanol and water studied by Wang et al. (2008), a water-in-oil microemulsion (showing high conductivity) existed up to 45% of water and beyond this point a bicontinuous phase was formed which was observed as a conductivity plateau (water channels were fully formed across the system between the electrodes, the charges were fully discharged through the channels). Based on the findings of these researchers, the most probable explanation was that the samples R1- R4 (5- 20% water) were inverse micelles, which transformed into a water-in-oil microemulsion at the percolation threshold (Φ c = 20% water). The second change in the conductivity (Φ e) occurred between the samples R9 and R10, which was also evident visually as the samples differed macroscopically (Table 5.1). Starting from sample R10 (corresponding to 50% water, w/w), the conductivity ceased increasing proportionally to the water increase and a plateau for the logarithmic curve was reached between the R10 - R13 points (Fig.

5.7). Based on this observation, the most probable explanation was that the transition between samples R9 and R10 was a conversion from a water-in-oil microemulsion into an oil-in-water emulsion. Since relatively high conductivity was still observed for samples R10-R13, these emulsions might have some bicontinuous properties, which would explain the high results. In the case of simple oil-in-water emulsions, once oil droplets grow large really quickly there are not enough small droplets to support charge transport and conductivity should be low, close to water.
The most probable explanation of the microstructure based on the conductivity results was suggested here. However, in the light of results published by other scientists, an increase of conductivity (versus a water content) may suggest transitions into various phases and therefore, conductivity results alone appear insufficient to formulate a conclusion about the microstructure with high confidence.

5.5. Zeta potential

As the samples R1 - R13 showed high conductivity, zeta potential was measured to evaluate if any charge on the surface of the droplets could be detected. It was not possible to establish any zeta potential values for the samples R1-R4. No definite values were obtained for the samples R5-R6 and R10 due to a very high standard deviation between the single runs but the average oscillated around zero. Zeta potential values recorded for the samples R8 and R9 were close to zero (Table 5.2)

Table 5.2. Zeta potential results for the samples R1 – R13.

Sample Name	Average Zeta potential [mV]	SD	RSD	No of Runs	No of sub-runs
R1	Not measurable	N/A	N/A	3	200
R2	Not measurable	N/A	N/A	3	200
R3	Not measurable	N/A	N/A	3	200
R4	Not measurable	N/A	N/A	3	200
R5	Not measurable *	N/A	N/A	3	200
R6	Not measurable *	N/A	N/A	5	200
R7	Not measurable *	N/A	N/A	3	200
R8	0.622	0.155	24.86	9	12-105
R9	-0.137	0.018	-13.29	4	16-168
R10	Not measurable *	N/A	N/A	6	32-200

* didn't meet the quality criteria but all measured values were close to 0 which suggested neutral zeta potential

The lack of positive or negative zeta potential for the tested samples was due to the non-ionic character of all components used to prepared R1-R13 samples. Despite high conductivity observed in the samples studied, zeta potential was neutral, close to zero. Extensive collision of small droplets leading to exchange of surface charges resulted in high conductivity, however the charge on the individual droplets appeared neutral. A non-ionic microemulsion containing Labrafac

CM10, Tween 80, polyethylene glycol 400 and distilled water that was developed by Surjyanarayan et al. (2009) also showed high conductivity (approximately 247 μS) and a zeta potential close to zero (-2.66 mV).

Conductivity results, which were measured in the studied samples (results not shown here) automatically by the instrument in order to calculate zeta potential, were in a very good agreement with the conductivity results presented in section 5.4.

5.6. Rheology and absolute viscosity

The viscosity (η) for all the samples R1- R13 remained relatively unaffected by the applied shear rate (Fig. 5.8, Appendix Table A.5.4.). The samples subjected to shear stress, exhibited comparable behaviour to the standards: PEG 400, propylene glycol and Captex 355 (known Newtonian fluids) and therefore were considered as Newtonian fluids. Newtonian flow behaviour is expected from the majority of microemulsions (Kumar & Mittal, 1999; Alany et al., 2001). However in concentrated systems, especially when the microemulsion contains elongated structures that strongly interact, non-Newtonian behaviour can be observed. Non-Newtonian behaviour has also been reported for a bicontinuous phase and a water-in-oil microemulsion (Anklam et al., 1995; Szymula, 2005).

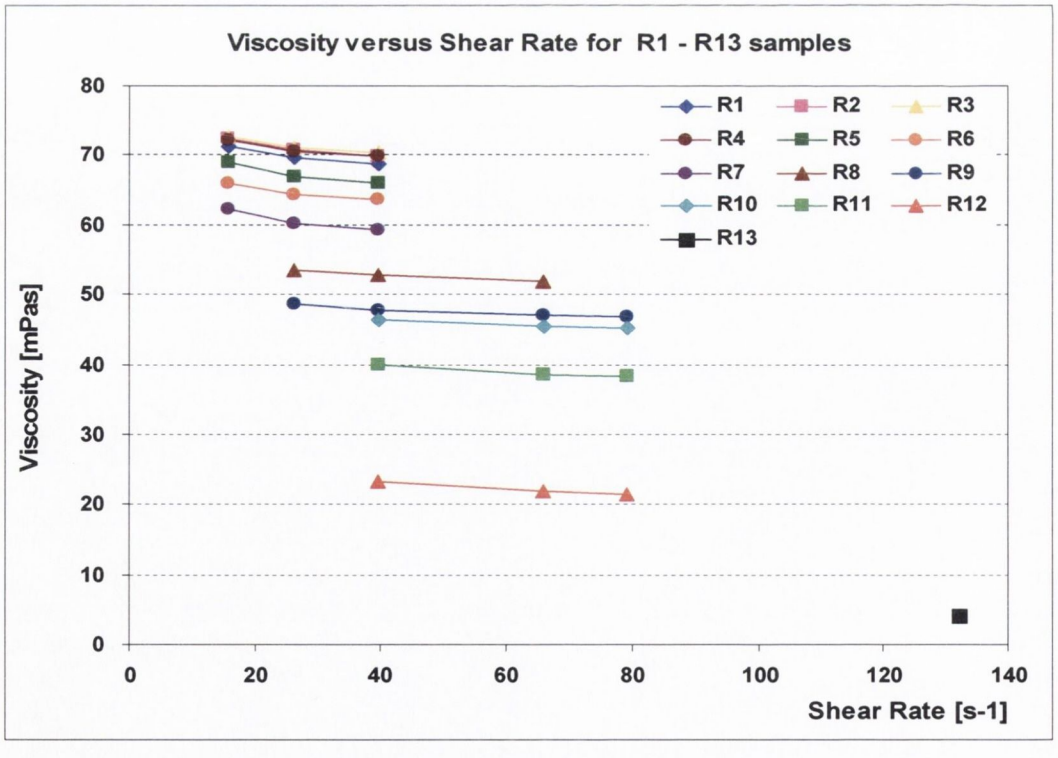

Fig. 5.8. Viscosity for the samples R1 – R13 versus shear rate.

Investigation of viscosity changes can provide information with respect to the occurrence of phase transition. When one of components of the system increases, e.g. the system is gradually diluted with water, the microstructure needs to rearrange to the most stable, energetically favourable state. This alteration of the microstructure should be reflected by noticeable changes in the viscosity (Sripriya et al., 2007; Mitra & Paul, 2005). However, depending on the composition of the studied systems these changes can be more or less substantial and it is quite difficult to confirm a phase transition based on viscosity testing only. The comparison of viscosity between the samples R1-R13 is shown in Figure 5.9 (the average viscosity values used on the graph were calculated as a mean of viscosity values obtained under various shear rates). It was noted that viscosity of the samples R1- R4 (corresponding to 5 – 20 % water) was noticeably higher than for the other R5 - R13 samples. The viscosity results for R1 –R4 samples were comparable and the samples did not differ statistically ($p < 0.05$) among each other which suggested the same type of microstructure. In the study carried out by Yaghmur et al. (2003), the maximum of viscosity occurred at 40 – 45% of water content and a further addition of aqueous phase caused a decrease in the viscosity, which was attributed to a structural transition from a water-in-oil into an oil-in-water microemulsion system. Mitra & Paul (2005) reported conversion from a water-in-oil system into an oil-in-water system through a bicontinuous state, when the viscosity of AOT/Brij-35 mixed surfactant system passed through the viscosity maximum. The sample R5 showed substantially lower viscosity compared to the R1-R4 samples. The viscosity of R6 –R13 samples further reduced as the water level in the samples increased. The decrease of viscosity for R5 - R9 samples versus the percentage of water could be described by a linear relationship (Fig. 5.9, $R^2 = 0.9718$).

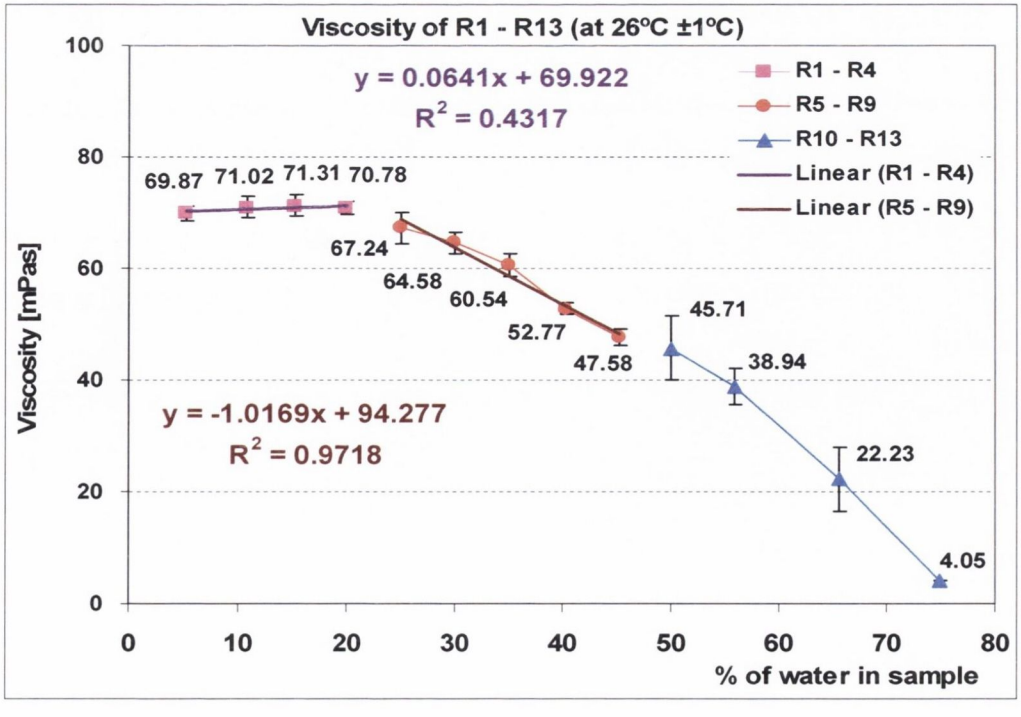

Fig. 5.9. Viscosity results for the samples R1 – R13 as a function of the water content.

The samples R10 – R13 (corresponding to 50- 75% water) were cloudy, turbid emulsions, which were less physically stable, which was seen as higher variability (higher standard deviation) in viscosity compared to any of the homogenous, clear samples. The decrease of viscosity was still proportional to the increase in the water content for the R10 -R13 samples. The relationship between viscosity and the water content was similar for R5-R9 and R10- R13 samples and the trendline based on all this points showed a good correlation coefficient ($y = -1.2348x + 102.7$, $R^2 = 0.9678$). The lowest viscosity, close to water viscosity, was noted for R13 where water constituted 75% (w/w) of the system. The viscosity measurements carried out on the samples R1-R13 demonstrated the evident difference between the R1-R4 and R5-R9 samples but were insufficient (without other techniques) to conclude what microstructure the samples represented. Due to high viscosity, the R1-R4 samples were suspected to be inverted micelles or water-in-oil microemulsions while the R5 - R10 could have represented oil-in-water microemulsions or a bicontinuous phase.

5.7. Pulsed-field-gradient spin-echo nuclear magnetic resonance (PGSE-NMR)

Pulsed-field-gradient spin-echo NMR (PGSE-NMR) is a well-established method for studying diffusive molecular motions in various liquids. Measurements of self-diffusion of water, oil and surfactant (Crillet 4 HP, polysorbate 80) were critical to derive structural information on the tested samples R3, R4, R5, R6, R7 and R9. The self-diffusion coefficients of water (D_{water}) could be measured and calculated without any problems in neat water and the studied samples since the characteristic peak for water (~4.7 ppm) was unique for this component only and did not occur in the other components. Self-diffusion coefficient values for water were calculated using a single exponential fit while for oil and Crillet 4 HP a biexpotential fit was used (Chapter 2, section 2.5.5). The values of self-diffusion coefficient of water obtained for the studied samples (Table 5.3) were clearly lower in the samples R3 - R9 compared to neat water.

Table 5.3. Self-diffusion coefficients of water (based on water peak at 4.7 ppm) measured for pure water and the samples.

Sample	Diffusion coefficient m^2s^{-1}	Comments about fitting
Pure water	$23.000*10^{-10}$ ($D_{0\ water}$)	Single expotential – very good
R3	$0.8758*10^{-10}$	Single expotential – very good
R4	$1.234*10^{-10}$	Single expotential – very good
R5	$1.795*10^{-10}$	Single expotential – very good
R6	$2.587*10^{-10}$	Single expotential – very good
R7	$3.570*10^{-10}$	Single expotential – very good
R9	$5.542*10^{-10}$	Single expotential – very good

The self-diffusion coefficient of water was approximately 26 times and approximately 4 times smaller in the samples R3 and R9 respectively in comparison to neat water, indicating a slower rate of diffusion of water in these systems compared to pure water. Also, the values of self-diffusion coefficient of water increased proportionally (linearly) as the water content in the samples increased (Fig. 5.10.A, R2 = 0.9732). When the self-diffusion coefficient of neat water was included it did not change the relationship significantly (R2 = 0.9769). The self-diffusion coefficient values for oil (presented in Table 5.4) in the samples R3- R7 were slightly lower (approx 1.5 times) compared to the neat oil but also appeared not to be related to the water content (Fig. 5.10.B). The self-diffusion coefficient values for Crillet 4 HP (polysorbate 80) in the samples R3-R7 were slightly higher compared to the neat Crillet 4 HP, which indicated that the material existed in a different form in the neat material compared to the diluted state. The self-diffusion coefficient values for Crillet 4 HP in the samples R3 – R7 also appeared to increase as the water content increased (Fig. 5.10.C). The self-diffusion coefficient values for the samples R3 and R7 were approximately 2.5 and 4 times higher compared to the neat surfactant.

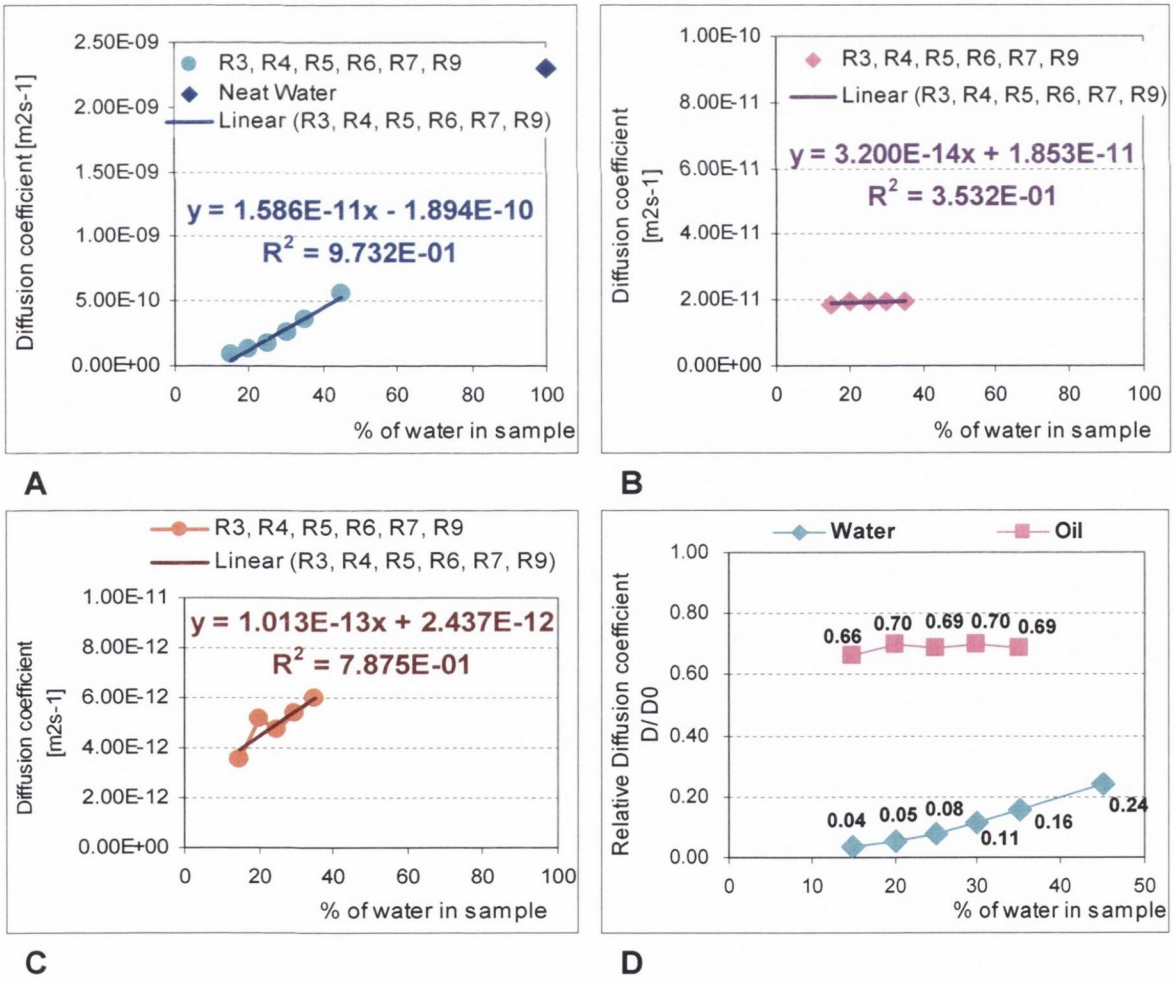

Fig. 5.10. Self-diffusion coefficient of A) water in the neat water and the samples R3 – R9, B) oil in the samples R3 – R7, C) Crillet 4 HP (polysorbate 80) in the samples R3 – R7. D) denotes relative self-diffusion coefficient of oil and water in the samples R3 - R9.

Table 5.4. Self-diffusion coefficients for the oil (based on CH_2 peak at 1.3ppm) and Crillet 4 HP (P80) measured for pure components and in the samples.

Sample	Diffusion coefficient m2s-1		Comments about fitting
Pure Polysorbate 80	$1.462*10^{-12}$ ($D_{0\ P80}$)		small deviation from single fit
Pure oil	$2.819*10^{-11}$ ($D_{0\ oil}$)		very good (single)
R3	**$1.860*10^{-11}$ (oil)**	$3.586*10^{-12}$ (P80)	perfect (biexponential)
R4	**$1.962*10^{-11}$ (oil)**	$5.157*10^{-12}$ (P80)	good (biexponential)
R5	**$1.942*10^{-11}$ (oil)**	$4.708*10^{-12}$ (P80)	perfect (biexponential)
R6	**$1.964*10^{-11}$ (oil)**	$5.402*10^{-12}$ (P80)	perfect (biexponential)
R7	**$1.939*10^{-11}$ (oil)**	$5.997*10^{-12}$ (P80)	perfect (biexponential)
R9	**$1.779*10^{-11}$ (oil)**	$2.985*10^{-12}$ (P80)	bad (biexponential)

The self-diffusion coefficient for Crillet 4 HP obtained for the sample R4 (corresponding to 20% water) was higher compared to the values obtained for the samples R3 and R5. Sample R4 was previously established to correspond to the percolation threshold, therefore this difference could have indicated that the mobility of surfactant increased as water droplets started clustering and became interconnected.

When interpreting the self-diffusion coefficients of water, oil and a surfactant together as the main components of microemulsions, it is necessary to understand how the type of microstructure affects the diffusion process of each component. If the microemulsion is of droplet-type, the self-diffusion coefficient (D) of the internal phase is determined by the diffusion of the droplet and will therefore be slower than that of the pure component. In addition, the diffusion of the surfactant or surfactant mixture is slow because of the formation of a monolayer around the droplet. In a bicontinuous microemulsion, where both oil and water are forming larger domains, the diffusion of these two components is high and often of the same magnitude as that observed for the pure components, while the surfactant is the slowest diffusing component (Boonme et al., 2006). Therefore the self-diffusion characteristics can have the following distinctions:

1. water-in-oil system: $D_{water} < D_{oil}$ and $D_{surfactant} \approx D_{water} \approx D_{droplet}$
2. oil-in-water system: $D_{oil} < D_{water}$ and $D_{surfactant} \approx D_{oil} \approx D_{droplet}$
3. bicontinuous state: D_{oil} and D_{water} are both higher but $D_{surfactant}$ is low because it exists in large aggregates (Moulik & Paul, 1998, Ceglie & Lindman, 1987).

In addition, it is known that the diffusion coefficient of a dispersed phase is typically 2–3 orders of magnitude lower than that of a neat solvent molecule, whereas the diffusion of a continuous (external) phase is normally only slightly retarded in comparison with its neat solvent molecule. For a bicontinuous structure, with both solvents forming domains that extend over macroscopic distances, both solvents have diffusion coefficients of the same order of magnitude as that of the neat solvent (Fanun et al., 2001; Yaghmur et al., 2003; Jian et al., 2001).

The self-diffusion coefficient values obtained for the samples R3– R9 showed that diffusion of water was restricted while the diffusion of oil remained similar to the neat material. This suggested a water-in-oil droplet type of system. However the values of self-diffusion of Crillet 4 HP (surfactant) were lower compared to water and oil, which suggested that this component diffused slowest, the situation typical for a bicontinuous phase. Further evaluation of the results was performed by calculating and comparing relative diffusion coefficients (D/D_0) which are shown in Fig. 5.10.D. It is well documented that if the D/D_0 values of water and oil differ by more than 1 order of magnitude, this is indicative of the presence of discrete droplets of the slowly diffusing solvent, whereas if the D/D_0 values of water and oil are of the same order of magnitude, a bicontinuous structure is suggested (Fanun, 2008). Yaghmur et al. (2003) analysed microemulsions composed of R(+)-limonene, water, propylene glycol (PG), ethanol (EtOH), and polyoxyethylene sorbitan monostearate (Tween 60) where three phases: a water-in-oil microemulsion (up to 20 wt % aqueous phase), a bicontinuous phase (20- 60% water) and an oil-in-water microemulsion (above 60% water) were identified based on the difference between the self-diffusion coefficients of water and oil (Fig. 5.11.A).

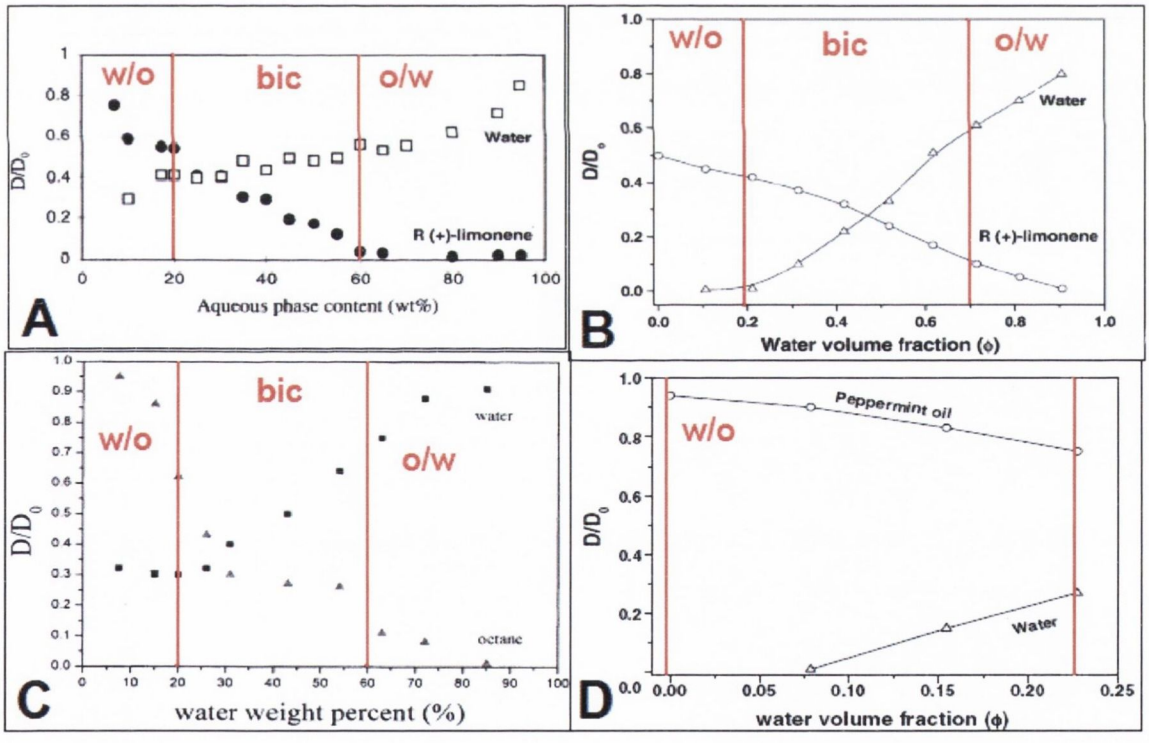

Fig. 5.11. Comparison of relative self-diffusion coefficient D/D_0 plotted against a water content in the samples: A) Yaghmur et al. (2003) empty square – D/D_0 for water, and filled/black dot - D/D_0 for (R(+) limonene; B) Fanun (2008) empty triangle – D/D_0 for water, and empty dot - D/D_0 for (R(+)) limonene; C) Jian et al. (2001), filled/black square – D/D_0 for water, and filled/grey triangle- D/D_0 for octane, D) Fanun (2009), empty triangle – D/D_0 for water, and empty dot - D/D_0 for peppermint oil. Red vertical separates various phases: w/o = water-in-oil system, bic = bicontinuous phase, w/o = water-in-oil system.

The microemulsions containing water/sucrose laurate/ethoxylated mono-di-glyceride/R (+)-limonene studied by Fanun (2008), were identified as oil-in water microemulsions (up 20 wt% water), a bicontinuous phase (with 20-70 wt%) and oil-in-water microemulsions (above 70% water) by comparing D/D_0 values of water and oil (Fig. 5.11.B). Jian et al. (2001) also identified a number of microphases in the system composed of CTAB/1-butanol/octane/water systems, by evaluating differences in the relative self-diffusion coefficients of water and oil plotted together against the water content (Fig. 5.11.C). The microemulsion composed of water/propylene glycol/sugar surfactant (L595)/ethanol/peppermint oil studied by Fanun (2009), was identified as a water-in-oil microemulsion based on the fact that D/D_0 values of water and oil differed by more than one order of magnitude (Fig. 5.11.D). In the samples R3 – R9 the values of the self-diffusion coefficient for water increased with increasing content of water, while the self-diffusion coefficient for the oil remained similar irrespective of the water content. The calculated relative diffusion coefficients values ($D/D_{0)}$ for water in the samples R3 – R9 differed by more than 1 order of magnitude from the oil value, which indicated an oil-continuous microstructure with discrete water domains (Fig. 5.10.D). The difference between self-diffusion coefficient of water and Crillet 4 HP could be explained by the contribution of water dissolved in the continuous oil phase, as explained previously by Jian et al. (2001). This free-water shows different, faster diffusion compared to water bound to surfactant molecules. The self-diffusion coefficient of water is a single number, which is the outcome of overlaid diffusion coefficient values for free and bound water, and therefore water appeared to diffuse faster the surfactant (Jian et al., 2001). All the samples R3 – R7 appeared to be different versions of the same microstructure, a water-in-oil system which showed 'droplet swelling' behaviour as the water content increased in the samples. A significant difference in the water diffusion behaviour was not observed between the samples R4 and R5, where previously some sort of transition was suggested based on the conductivity and viscosity results. The sample R9 was on the border of the phase transition (the subsequent sample, R10 was an emulsion). The measured self-diffusion coefficient of water in this sample indicated high mobility, proportional to the water content however self-diffusion coefficients of the oil and the surfactant could not be measured correctly. This suggested that sample R9 differed from the preceding samples and could not be strictly defined as a water-in-oil system.

5.8. Small- angle neutron scattering (SANS)

Small–angle neutron scattering (SANS) is a powerful technique for studying microemulsion structure because different regions can be contrasted by selective deuteration of components. The scattered neutron intensity as a function of the scattering angle (vector) was measured for the samples R3 – R7 and R9 (Fig. 5.12). The peak observed for each sample was present due to high particle interaction and it shifted slightly to lower scattering vector (Q) as the percentage of water increased.

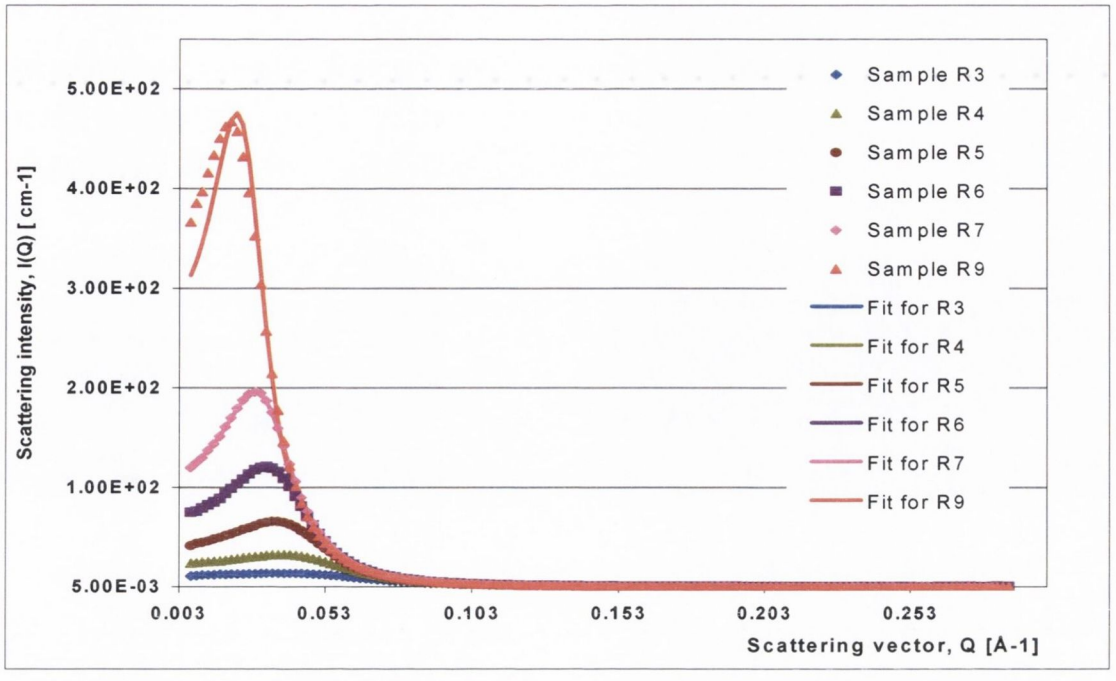

Fig. 5.12. Scattering intensity measured in the samples R3 – R9 and with the chosen fits for spherical water-in-oil microemulsions.

When the results were plotted on a logarithmic scale (Fig. 5.13), it was clearly visible that scattering intensity at low values of scattering vector increased proportionally to the water content, which could be explained as 'droplet growing' behaviour of the systems.

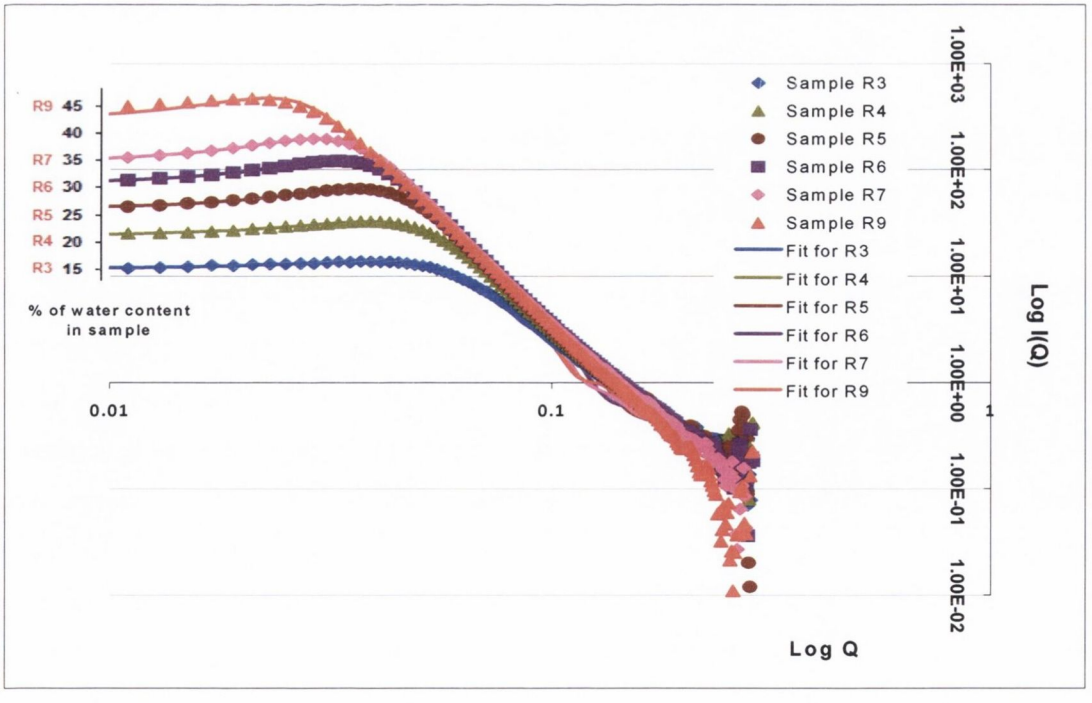

Fig. 5.13. Scattering intensity measured in the samples R3 – R9 and with the chosen fits for spherical water-in-oil microemulsions presented on a logarithmic scale.

The obtained scattering pattern was computed using various 'shape 'fits and the samples R3 – R7 were identified as droplets of water in the continuous oil phase systems. The sample R9 appeared to differ slightly (poorer fit obtained). This sample was close to a phase boundary and did not behave strictly as a water-in-oil microemulsion. The parameters derived from SANS measurements fitting are summarised in Table 5.5

Table 5.5. Parameters derived from the SANS measurements of the sample R3 - R9.

Sample ID	Calculated volume fraction of water (composition)	Radius, R_1 / Å	X	Particle diameter (nm)	Calculated volume fraction of water (fitting)
R3	0.15	40	0.38	**8.0**	0.08
R4	0.20	48	0.40	**9.6**	0.12
R5	0.25	56	0.41	**11.2**	0.15
R6	0.30	63	0.42	**12.6**	0.20
R7	0.35	71	0.42	**14.2**	0.25
R9	0.45	86	0.40	**17.2**	0.37

The droplet size was very small, between 8 -17 nm and increased as the water content increased. The volume fractions of water calculated from the fits were slightly lower than those calculated from the composition. This was due to the fact that some of the water was mixing into the surfactant layer, which was seen as an increased scattering length density of the surfactant shell layer compared to the expected value (additional parameters derived from SANS analysis and fitting are presented in Appendix Table A.5.5).

5.9. Differential scanning calorimetry (DSC)

Differential scanning calorimetry (DSC) was employed to determine the state of water in the samples R1- R13 and make a distinction between 'bulk' and 'bound' water. When water is incorporated into a microemulsion system, it can either exist, as 'bound' or 'free/bulk' water and the difference in the melting and freezing behaviour should be detectable with DSC measurements. Determination of 'bound' and 'bulk' water helps to understand interactions within self-assembled amphiphiles and water in microemulsions (Boonme et al., 2006; Podlogar et al., 2004, Senatra et al., 1988; Senatra, 2000). Senatra et al. (1988) differentiated between three types of water: free, bound and interphasal water. Based on the obtained endotherms, 'free water' was considered as a fraction that melted at 0°C, 'interphasal' type of water (confined in the region of not negligible volume and finite thickness separating the free water core of the droplets and the continuous medium) was a fraction that melted around -10°C and 'bound' water was a fraction which showed the melting point around –36 °C. The latter term was used to indicate the amount of water, very strongly bonded to the hydrophilic groups of surfactants, and counterions, that was found to melt at

temperatures lower than -10°C (Senatra et al., 1988). Garti et al. (2000) found that it was almost impossible to distinguish between 'bound' and 'interphasal (interfacial)' water in the samples they studied and therefore 'weakly' and 'strongly' bound water names were used. Bulk (free) water was assumed to have physicochemical properties not much different from those of pure water, showing a heat of fusion similar to that of ordinary water and freezing at approximately 0°C (Garti et al., 2000).

Initially, four pure components of the microemulsions were analysed with DSC to evaluate cooling and heating changes in the materials (Fig. 5.14).

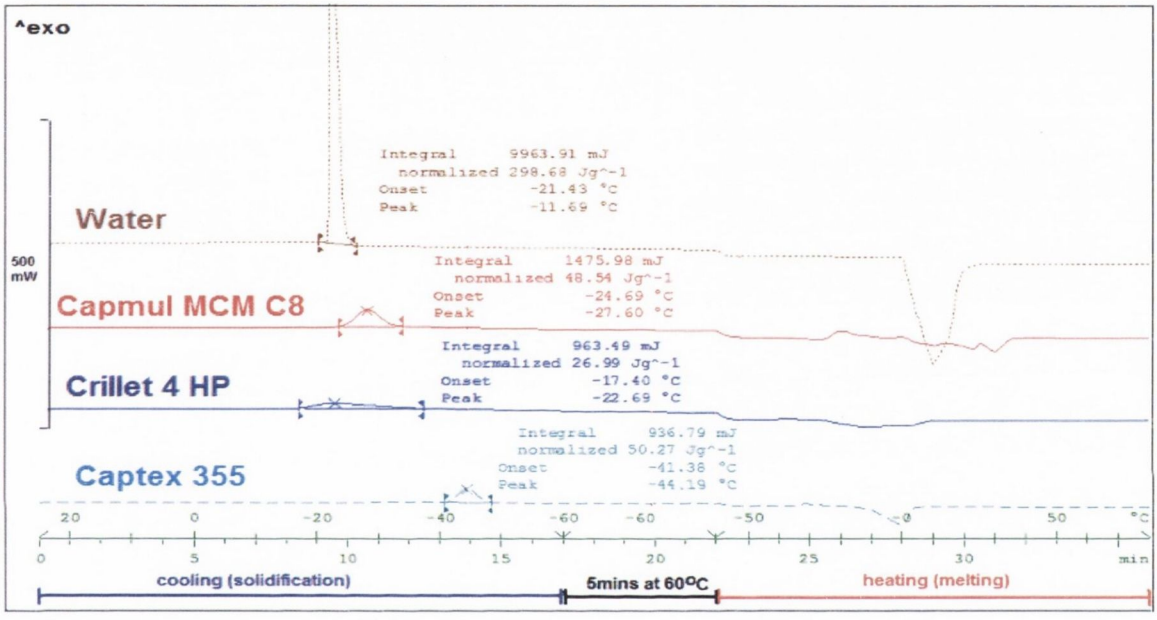

Fig. 5.14. DSC curves of individual components.

The water sample (pure) showed the freezing (solidification) point between –12 and -14°C (Fig. 5.14 & 5.18), which was clearly different to the solidification of the oil (Captex 355) observed at -45°C (Fig. 5.14 & 5.18). The low HLB value surfactant, Capmul MCM C8 and high HLB value surfactant Crillet 4 HP (polysorbate 80) showed solidification peaks around -28°C and -23°C respectively (Fig. 5.14). All components, except for Capmul MCM C8 melted below 5°C. As thermal behaviour of all components was clearly visible on the cooling curve, this part of the DSC curve was chosen for further evaluation. Also, the large difference in solidification points between water and Captex 355 was advantageous making the identification of each peak quite straightforward. In the samples R1- R4 (5-20% water content), only one solidification peak was observed around -45°C (Fig. 5.15), which clearly represented solidification of Captex 355. The solidification peak of water was not detected which suggested that water contained in the samples existed as 'bound' water. It appeared that this fraction of water (up to 20%) was so strongly bound to the surfactants that its thermal properties were completely altered. Since the investigated samples

R1 – R4 contained a very high percentage of the surfactant mixture (up to 48 wt. %), all water was bound and free (bulk) water did not exist in these samples.

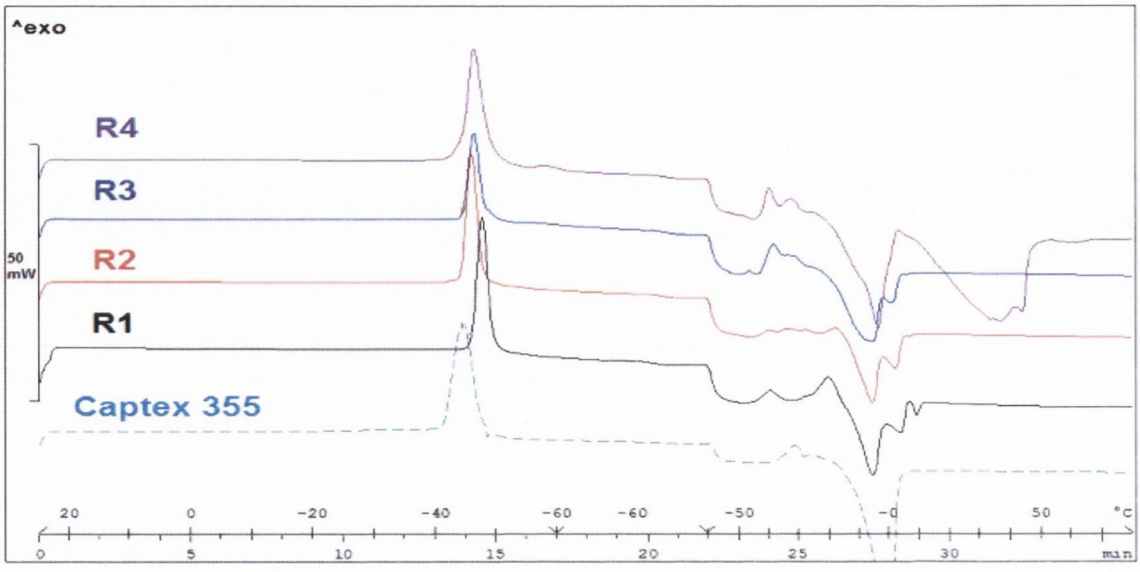

Fig. 5.15. DSC curves of the R1 – R4 samples compared with Captex 355.

In case of the samples R5- R13 (25-45% water content), two solidification peaks were observed (Fig. 5.16 – 5.17). A small peak detected around – 45 °C was identified as solidification of Captex 355 and the position of this peak remained unchanged irrespective of the water content. Starting from the sample R5 (corresponding to 25% water), a new peak appeared at approximately –35 °C (Fig. 5.16). With the increasing amount of water, the peak moved towards higher temperatures (Fig. 5.17) until it reached a temperature of approximately –12 °C in samples R12 and R13, which was equivalent to the freezing point of pure water.

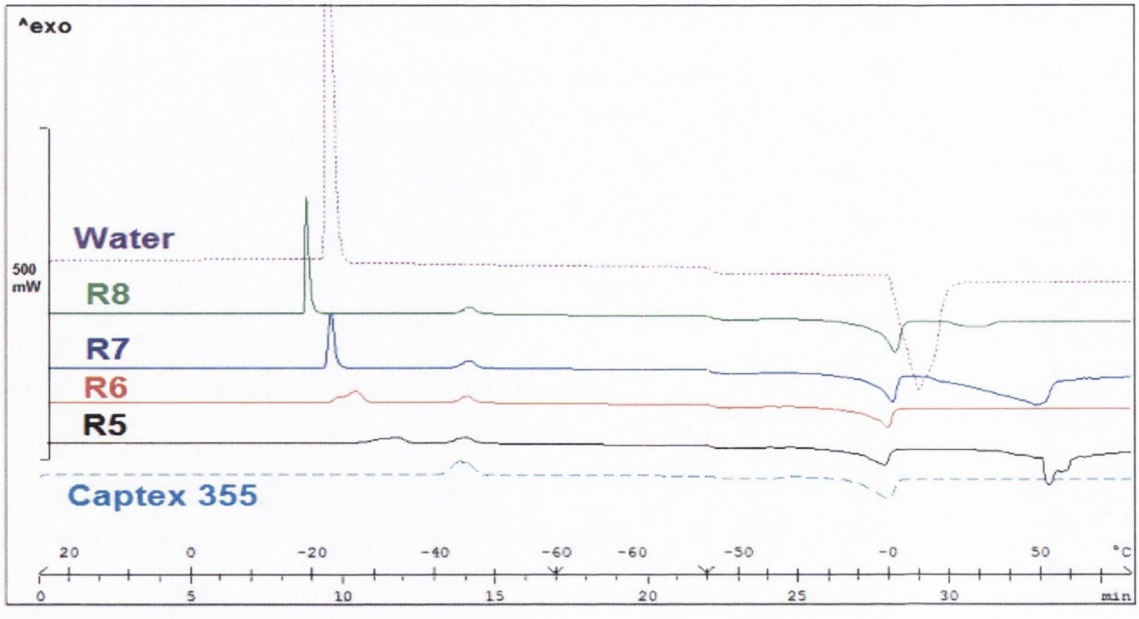

Fig. 5.16. DSC curves of the R5 – R8 samples compared with purified water and Captex 355

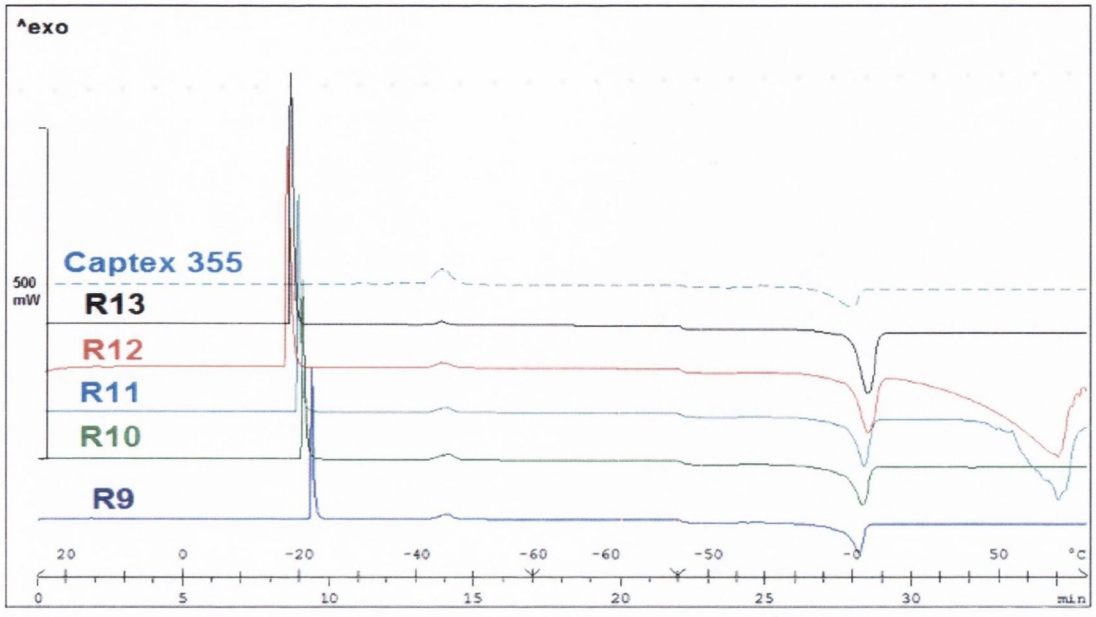

Fig. 5.17. DSC curves of R9– R13 samples compared with Captex 355.

This indicated that the second peak represented water, which could have been termed as an interfacial fraction in the samples R5-R9 (more weakly bound in comparison to bound water), and free water in the R10 - R13 samples. The solidification point of water in the samples R5 – R9 was clearly still altered by an association with the surfactants while water detected in samples R10 – R13 froze at the same temperature as the pure solvents (Fig. 5.18).

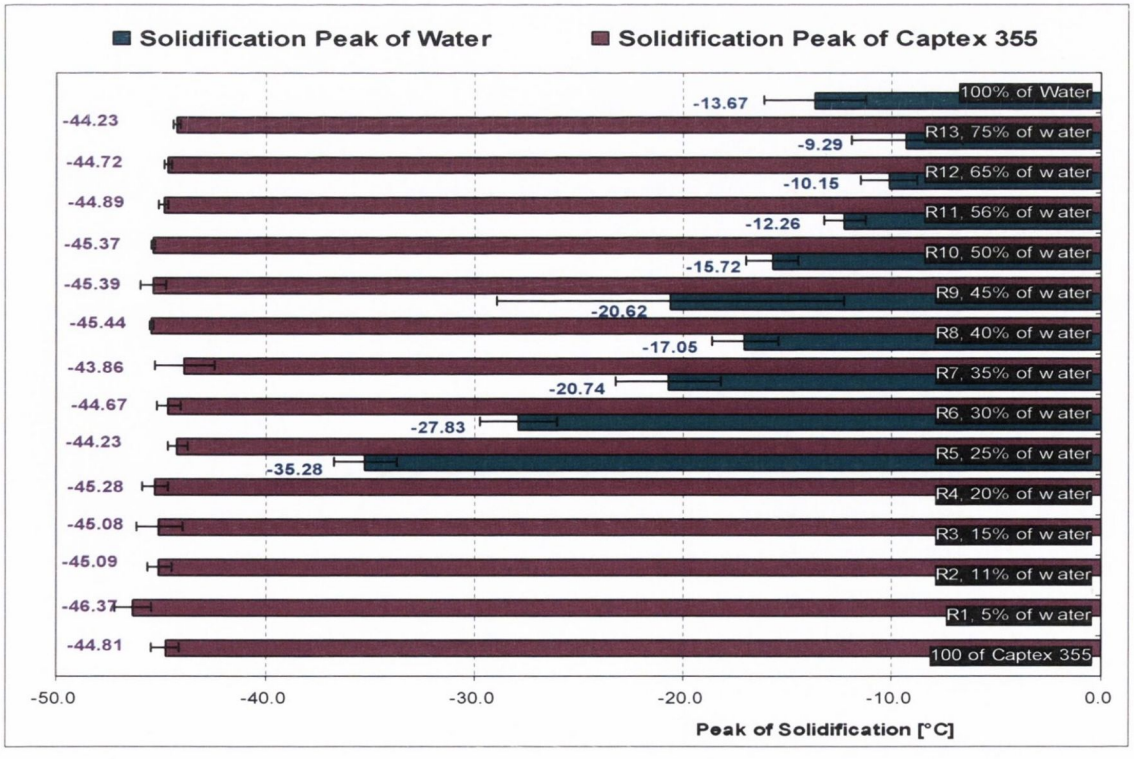

Fig. 5.18. Comparison of solidification peak temperature for water and Captex 355 in the R1– R13 samples.

Interestingly, the solidification point of Captex 355 remained unchanged irrespective of the water content (Fig. 5.18). It appeared that the intensity of the interaction between the oil and the surfactants did not depend on the concentration of the surfactants (57% to 15% for the samples R1-R13) and was not strong enough to alter the thermal behaviour of Captex 355. The size of the water and oil peaks changed with the water content in the microemulsion samples (Fig. 5.19; Appendix, Table A.5.3). As the water content increased (beyond R5 sample), the normalized enthalpy of solidification process increased proportionally (Fig. 5.19, $R^2 = 0.9974$). The normalized enthalpy measured for sample R4 was evidently higher (Fig. 5.19) than expected based on the linear plot. It appeared that the sample represented a transition from the bound water into the interfacial water and the measured normalized enthalpy (52.20 Jg $^{-1}$) was a sum of two peaks overlaid. Values of normalized enthalpy calculated according to the linear relationship between the water content and normalized enthalpy (the equations shown in Fig. 5.19) for each material were 18.27 Jg $^{-1}$ and 35.84 Jg -1 for water and Captex 355 respectively, for the R4 system. The sum of these values was 54.11 Jg $^{-1}$ which corresponded very well with the measured value of the peak. In addition, the linear relationship between the water content in a sample and normalized enthalpy (per 1g of sample) showed the intercept with 'Y' axis (% of water in sample) around 15% water. Based on the conductivity and viscosity results, sample R4 was previously considered to consist of inverse micelles.

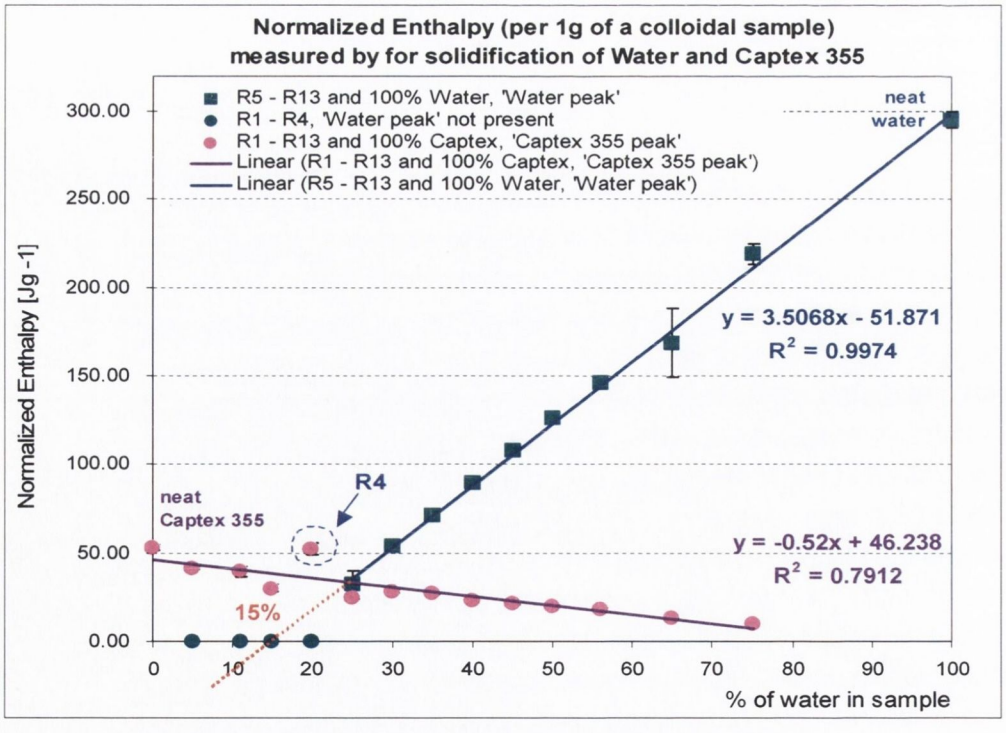

Fig. 5.19. Normalized enthalpy (per 1g of microemulsion) required to solidify water and Captex 355 in the R1– R13 samples plotted against the percentage of water in the samples.

In Fig. 5.19, samples R1-R3 (5-15% water) appear as 'water-free'. Correlating the water content with the normalized energy (per 1g of a colloidal sample) in diluted samples and finding the intercept with 'water content' axis may be a way to establish the quantity of the 'bound water' characteristic for each system based on its composition. When the normalized energy (per 1g of sample) was additionally corrected for water content in the samples (expressed as the normalized enthalpy per Jg $(water)^{-1}$) and plotted against the water content, it was demonstrated that thermal behaviour of water in samples R5- R9 still differed from that seen for pure solvents (Fig. 5.20). The energy required to solidify water in these samples was lower than expected, demonstrating that interfacial water differed from the pure solvent not only by a shift in the solidification temperature but also by the amount of energy required for the solidification process. Water behaviour in emulsion samples R11 – R13 resembled pure water in terms of temperature (Fig. 5.18) and energy (Fig. 5.20) and therefore this water could be termed free/bulk water. The thermal behaviour of Captex 355 was not affected by the presence of the surfactants or the water content in samples R5-R13 (Fig. 5.20). The energy required to solidify fractions of Captex 355 in the samples R1- R3 varied (likely due to presence of water) but it remained constant in R5-R13 irrespective of water content (Fig. 5.20).

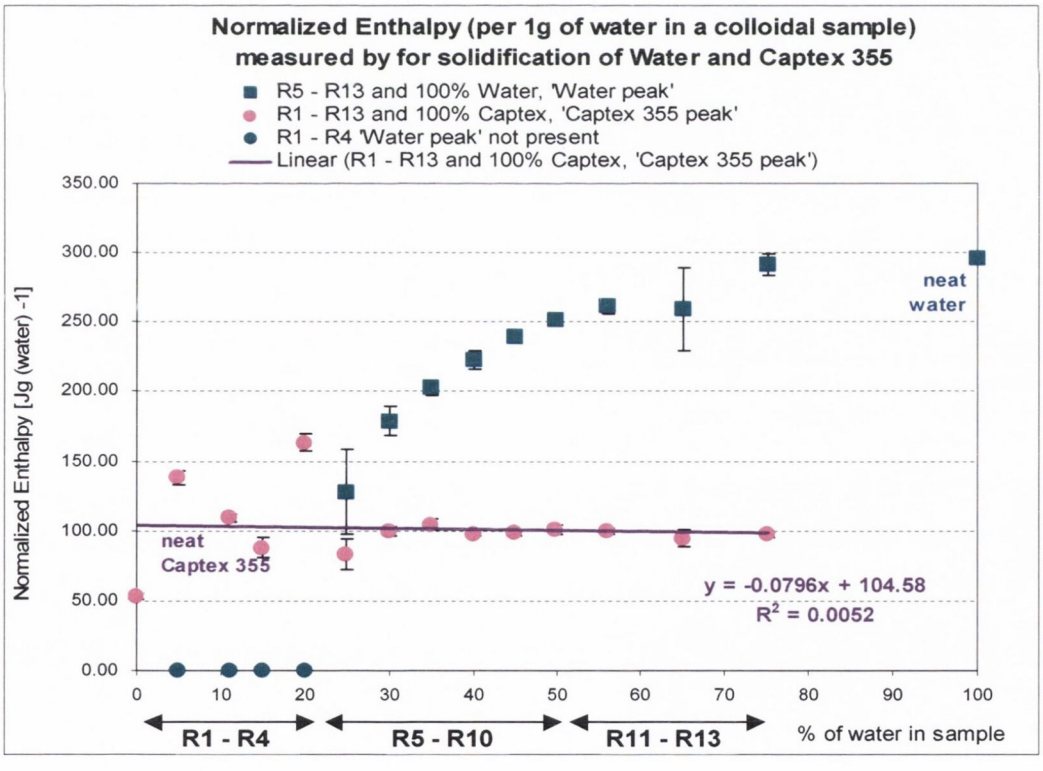

Fig. 5.20. Normalized enthalpy (per 1g of water in a colloidal sample) required to solidify water and Captex 355 in the R1– R13 samples plotted against the percentage of water in the samples.

Some researchers used the DSC results to interpret a transition between different phases of the microemulsions. Boonme et al. (2006) studied microemulsions made of isopropyl palmitate (IPP),

water, Brij 97:1 and butanol, where at water concentrations below 30% wt/wt, the freezing exotherm of water was not observed but became apparent as the water content increased beyond this point. Solidification and melting peaks for isopropyl palmitate (oil) were observed in the systems with 0 - 25% wt/wt water, but they disappeared at ~ 30-35% wt/wt. Based on these changes, it was suggested that IPP changed from an external to internal phase indicating the transition from a water-in-oil to an oil-in-water microemulsion (Boonme et al., 2006). Samples with a water content below 35% did not show the water peak in systems consisting of Tween 40, Imwitor 308 and isopropyl myristate studied by Podlogar et al. (2004). The water peak appeared above 35 wt% of water. Some interactions with the surfactant still existed; hence the shift of the freezing temperature towards lower temperatures (compared to pure water) was observed, as with the studied samples. Based on this observation, a conclusion was made that water in systems containing more than 35 wt.% was present as the outer phase, thus an oil-in-water or bicontinuous type of microemulsion was assumed (Podlogar et al., 2004). Liu et al. (2009) studied microemulsions containing water, Aerosol-OT, Tween 85 and isopropylmyristate. The appearance of a new endothermic peak around 0°C was attributed to melting of bulk water when the amount of water increased to 30 wt%, which became more pronounced at 40wt%. The water in systems containing more than 40.0 wt% was assumed to exist as the external (outer) phase and thus an oil-in-water type of microemulsion was assumed (Liu et al., 2009).

Although, the DSC results are useful to gain additional insight on the interaction between oil, water and the surfactants in microemulsion systems, one should be careful when interpreting the results. In the studied samples, the absence of water peak in the samples R1- R4 could have been explained by the strong interaction with the surfactants (existence of 'bound' water) and therefore water was considered as the internal phase. When the water reached more than 25% (samples R5 - R13), the solidification peak of water became detectable. This change was evidence of weakened interaction with the surfactants and the presence of water in a 'non-bound' state. Based on the work of other researchers, it would appear that the samples R5- R9 could have been bicontinuous or represented oil-in-water microemulsions. Nevertheless, the conclusions of other researchers were supported by the data from other characterisation techniques, which coincided with their interpretation of DSC results. In the current work, the DSC results did not correlate with the results obtained from other characterisation techniques if the common interpretation was to follow that occurrence of water peak (solidification of melting) implied water as the external phase.

5.10. Particle sizing by dynamic laser scattering (DLS)

The particle size and polydispersity were automatically computed by the DLS software based on the measured intensity of scattering, viscosity and refractive index values of the dispersant. It is well known that theory of DLS assumes the presence of spherical particles (droplets) in the dispersing medium and therefore it cannot give representative results for a

bicontinuous phase. Therefore, it is important to bear in mind that the DLS technique on its own may be insufficient in determining the microstructure (Kumar & Mittal, 1999; Stubenrauch, 2009; Goddeeris et al., 2006). In addition, a difficulty exists regarding the definition of the dispersant in which droplets are suspended. Some researchers (Constantinides & Yiv, 1995) have used the refractive index and viscosity of the whole microemulsion for their DLS analysis rather than those of the continuous phase, which clearly introduced errors into the analysis and underestimated droplet size (Aboofazeli et al., 2000). Also, without knowing whether samples represent water-in-oil or oil-in-water systems, it is not clear which external phase needs to be used as the dispersant. Initially, the size results for the samples R2 – R9 were calculated using both water and Captex 355 as the dispersant. The average particle size using water as the external phase was between 180 nm and 250 nm for completely clear, transparent samples, therefore these results were considered as incorrect as a particle size up to approximately 150 nm would be expected for completely clear systems (Prince, 1977). In addition, the particle size appeared to decrease as the water content increased, which was further proof that 'water' was incorrect as an external phase and Captex 355 was used as the dispersant in further evaluations. A system that contains more than a few volume percent of dispersed phase can be considered as concentrated and it is necessary to account for interparticulate interactions using the hard-sphere model proposed by Cheung (Cheung et al., 1987; Saint Ruth et al., 1995; Aboofazeli et al., 2000). The measured and corrected parameters for the samples R2 – R10 are summarised in Table 5.6. The sample R10 was a turbid emulsion. The average particle size indicated when Captex 355 was used as the dispersant, was between 20 and 30 nm which did not correlate with the appearance and therefore this sample was considered as an oil-in-water emulsion since an existence of bicontinuous phase cannot be detected with DLS. The corrected particle size measured by DLS for the samples R2- R9 was significantly higher than the values obtained by the SANS technique (Table 5.5). This clearly demonstrated that the overestimated particle size given by DLS was caused by the use of the simplified external phase (Captex 355 alone) and a wrong estimation of fraction of the internal phase (Φ) required for correction according to the hard sphere model. In the case of concentrated samples, the situation is complex. Because of the high concentration of surfactants, these components are likely to partition throughout the system and will not remain solely distributed as a surfactant layer (shell) around droplets (Aboofazeli et al., 2000). Considering the high solubility of Capmul MCM C8 in the oil phase, the low HLB surfactant could have been partially dissolved in Captex 355, especially when the water content in the samples was low. The same applies to Crillet 4 HP. Once the water was effectively bound by this surfactant, the excess of surfactant could remain non-bound, dissolved in the oil phase.

Table 5.6. Parameters derived from the DLS measurements of the samples R1 – R10.

Sample Name		Uncorrected Particle size (Z-Average diameter) [nm]	Polysidper-sity (PdI)	Diffusion Coefficient D_{or} [μ^2/s]	Mean particle size of 1st peak (Int) [nm]	Mean particle size of 2nd peak (Int) [nm]	Mean Area of 1st peak (Int) [%]	Mean Area of 2nd peak (Int) [%]	fraction of internal phase (core + surfactant shell), Φ	Corrected Diffusion Coefficient, D_{corr} [μ^2/s]	Corrected Particle size (diameter) [nm]
R1 *	not measurable										
R2 *	**Average**	**10.0**	**0.275**	**1.73**	**13.3**	**1.06**	**94.8**	**5.2**	**0.64**	**0.86486**	**40.1**
	SD	0.2	0.004	0.04	0.34	0.03	0.2	0.2	0	0.02037	0.9
R3 *	**Average**	**10.6**	**0.203**	**1.63**	**12.95**	**0**	**100**	**0**	**0.66**	**0.80147**	**43.2**
	SD	0.1	0.018	0.01	0.26	0	0	0	0	0.00402	0.2
R4 *	**Average**	**10.1**	**0.196**	**1.71**	**12.28**	**0**	**100**	**0**	**0.68**	**0.82897**	**41.8**
	SD	0.1	0.009	0.01	0.14	0	0	0	0	0.00714	0.4
R5 *	**Average**	**9.0**	**0.17**	**1.93**	**10.55**	**0**	**100**	**0**	**0.70**	**0.92097**	**37.6**
	SD	0.1	0.01	0.02	0.14	0	0	0	0	0.01118	0.5
R6 *	**Average**	**7.9**	**0.195**	**2.19**	**9.61**	**0**	**100**	**0**	**0.72**	**1.03068**	**33.6**
	SD	0.1	0.009	0.02	0.18	0	0	0	0	0.00811	0.3
R7 *	**Average**	**7.4**	**0.243**	**2.35**	**9.69**	**0**	**100**	**0**	**0.74**	**1.09234**	**31.7**
	SD	0.3	0.007	0.1	0.39	0	0	0	0	0.04497	1.2
R8 *	**Average**	**6.8**	**0.234**	**2.56**	**8.85**	**0**	**100**	**0**	**0.76**	**1.16978**	**29.6**
	SD	0	0.006	0.01	0.16	0	0	0	0	0.00625	0.2
R9 *	**Average**	**7.6**	**0.214**	**2.28**	**9.68**	**0**	**100**	**0**	**0.78**	**1.02926**	**33.7**
	SD	0.1	0.011	0.02	0.22	0	0	0	0	0.01045	0.3
R10 **	**Average**	**238.6**	**0.361**	**2.05**	**242.7**	**924.3**	**99.8**	**0.2**	**0.50**	**1.15169**	**854.9**
	SD	5.7	0.035	0.05	8.0	2264.1	0.4	0.4	0	0.02752	20.6

* Captex 355 used as the external phase (dispersant), η = 25.21 mPas at 25°C

** Water used as the external phase (dispersant), η = 0.8872 mPas at 25°C

A theoretical simulation of the scenario where some of the surfactants remained dissolved in the external phase was carried out. It was assumed that Crillet 4HP (polysorbate 80) as a high HLB value surfactant had a higher affinity for water than a 'water insoluble surfactant' Capmul MCM C8 (low HLB value surfactant). Therefore Capmul MCM C8 was more likely to remain dissolved in Captex 355 when the water concentration was low rather than form a surfactant layer in the 'abundance' of polysorbate 80. Based on the DSC results for the samples R1- R4, water up to 20% was fully bound and it was assumed that Crillet 4 HP was preferentially and exclusively engaged in this association. In the sample R4, saturation of Crillet 4 HP with water reached its limit as the water peak started to show on the DSC curves (R5-R9 samples). Based on the molar ratio between Crillet 4 HP and water in the sample R4, the saturation limit was estimated as 1: 87, meaning 1 molecule of the surfactant could form a close bond with 87 molecules of water (Appendix Table A.5.7). This ratio was applied to calculate quantities of bound and non-bound Crillet 4HP in the samples R1 – R3. Non-bound Crillet 4 HP and all Capmul MCM C8 were assumed to remain dissolved in Captex 355 (in samples R1-3). Starting from sample R5, the water peak was observed in the DSC, however the samples remained as transparent microemulsions, meaning the second surfactant started to partition into the surfactant layer supporting the microstructure of the microemulsion. The sample R9 was the last sample that remained clear which suggested that water content above 45% exceeded the saturation limit of Capmul MCM C8. Beyond this point, the insufficient amount of surfactants could not support the microemulsion structure any longer. Based on the molar ratio between Capmul MCM C8 and water in the sample R9, the saturation limit was estimated as 1: 25, meaning 1 molecule of the surfactant could form a close bond with 25 molecules of water. This ratio was applied to calculate quantities of bound and non-bound Capmul MCM C8 in the samples R5 – R9. In sample R5-R9, non-bound Capmul MCM C8 was assumed to remain dissolved in Captex 355, while all Crillet 4 HP was already bound in the surfactant layer. Following the assumptions made, above the external phases containing Captex 355, non-bound Crillet 4 HP and non-bound Capmul MCM C8 were prepared (details of the compositions in Appendix, Table A.5.8. and A.5.9). The viscosity of the external phases was measured and used together with the experimental fraction of internal phase (Φ_{exp}) to calculate the 'experimentally corrected' particle size of the samples R3- R5 & R7 (Appendix Table A.5.6.). A comparison between the average particle size measured by SANS and DLS (the simulation and Captex 355 used as the external phase) is given in Figure 5.21.

Using the experimental phases in the samples R3-R5 & R7 decreased the particle size, which clearly demonstrated the impact of viscosity of the external phase and Φ_{exp} . The experimental external phases enabled a significant reduction in the average particle size, however the average particle size was still approximately twice as large as that determined by SANS.

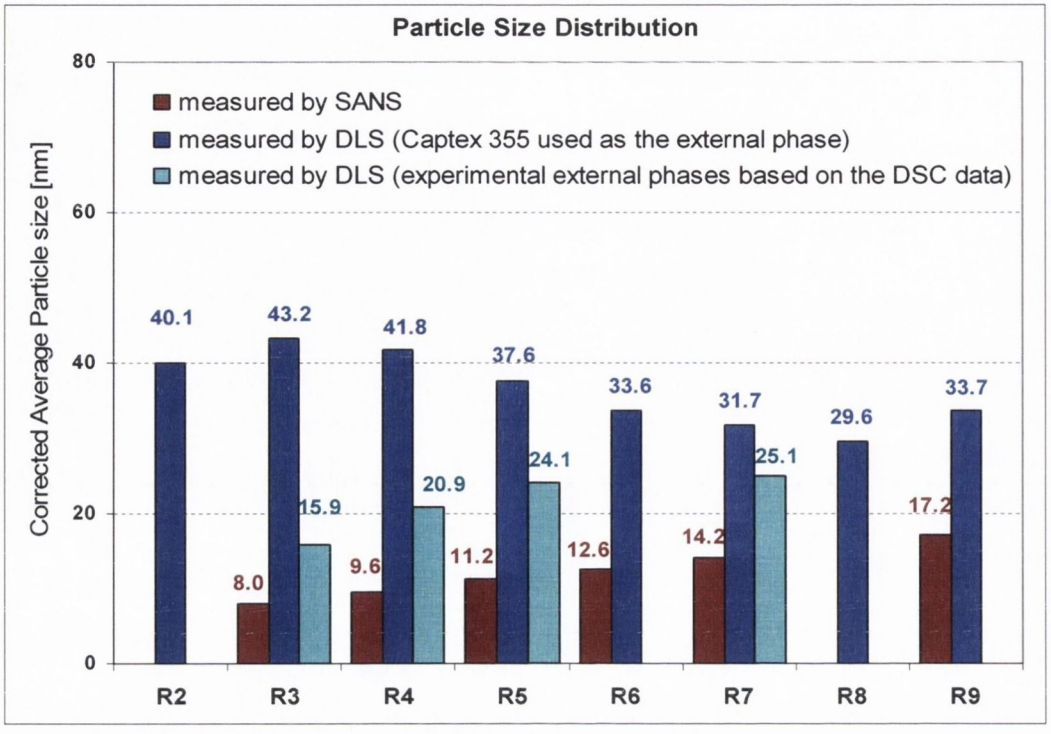

Fig. 5.21. Comparison of particle size derived from two different light scattering techniques.

The work carried out clearly demonstrated that dynamic light scattering is a challenging technique when applied to the concentrated microemulsions. Considering the number of assumptions required to perform the correction, obtained values of droplet size in concentrated systems should be taken as indicative only and possibly used for assessment of particle size stability rather than an estimation of the true droplet size. However, a useful observation was made with regard to the microstructure in samples R1 – R4 based on the observed light scattering in samples R2 - R4 and lack of scattering in sample R1. Sample R1, containing 5% of water could not be measured, which suggested lack of 'internal structures' such as droplets or micelles in this system. The lack of 'scattering' is typically seen in samples where the surfactant exists in unassociated monomers, while formation of micelles (above CMC) is detected as an increased intensity of reproducibly scattered light (Malvern's technical note MRK 801-01).

Based on PGSE-NMR, SANS, conductivity viscosity and DSC, the existence of inverse micelle up to 20% of water was established. Based on the DLS measurements, it appeared that surfactant molecules existed in unassociated monomers up 5% of water (an isotropic solution was formed), while the presence of micelles was detected at 10% of water content.

5.11. Overall Conclusions

The SANS and PGSE-NMR measurements appeared to be the most useful in determination of the microstructure in the samples R1 – R9. Nevertheless each of the used methods provided additional insights into the studied samples and was able to show certain changes as the water

percentage in the samples increased. The difficulty in relation to the observed changes was to understand their meaning and relate them to the phase behaviour. The conductivity and viscosity and DSC measurements clearly captured a change in the system that occurred at around 20% water content. This change was explained as the transition from inverse micelles (R2 -R4) into water-in-oil microemulsion (R5-R9) in the light of the SANS, PGSE-NMR and DLS measurements which also demonstrated particle growing ('swelling') behaviour of the system when the water content ranged from 15 to 45%. As the water content in these samples increased, many parameters such as viscosity, conductivity, normalized enthalpy for water and self-diffusion coefficient (water) changed simultaneous and proportionally and were well correlated to each other (Fig. 5.22). The increased diffusion of water in samples R4 –R9 showed an inverse correlation with kinematic (Fig. 5.22.A) and dynamic viscosity (Fig. 5.22.B) of the samples which suggested that as the microstructure became 'looser, less packed', water droplets were able to move more freely which also resulted in the increased conductivity (Fig. 5.22. C) and lower association with the surfactant (Fig. 5.22.D).

The presence of a water peak in the samples R5 - R9 was evidence that the occurrence of this peak is not always associated with the transition from a water-in-oil into an oil-in-water or bicontinuous system. The sample R9 was defined as 'not strictly' a water-in-oil microemulsion based on the SANS and PGSE-NMR results and appeared to have some bicontinuous properties based on the conductivity results and FF-TEM images.

Characterisation carried out on the model samples identified the microstructure in the samples, allowed the most suitable techniques to characterise systems based on derivatives of caprylic/capric acid to be established and provided a useful insight that the properties of water varies depending on its content in a sample.

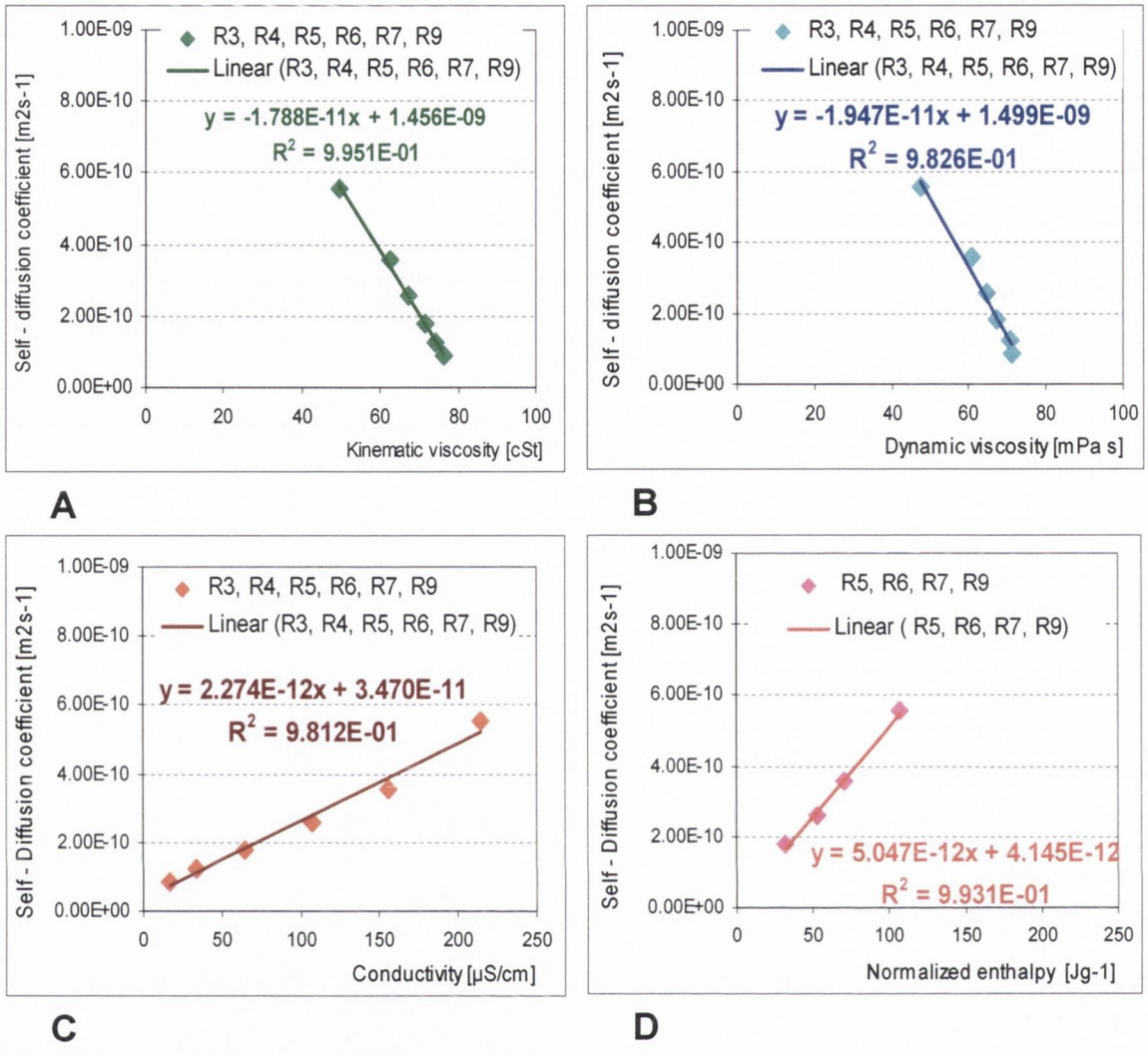

Fig. 5.22. Correlation between self-diffusion coefficient for water (PGSE-NMR) and other parameters: kinematic viscosity (A), dynamic viscosity (B), conductivity (C), normalized enthalpy per 1g of sample measured for water peak (D).

Chapter 6

Incorporation of Model Compounds into Liquid Microemulsions

6.1. Introduction

Any formulation approach to create a microemulsion and/or self-emulsifying lipid formulation (SELF) for encapsulation must consider the potential interaction between the composition of this formulation, the drug material and the capsule shell chosen. Many surfactants or lipid materials such as Capmul MCM, Capmul MCM C8, Imwitor 308 (if glycerine is above 5%), Cremophor EL or Span 80 are incompatible with hard gelatine capsules if used at the 100% level (Cole, 2007). Any high percentage of these materials in a complex formulation may compromise the stability of hard gelatine capsules. In addition, solubilisation of a sufficient load of hydrophilic drugs often requires an addition of polar solvents such as water, aqueous buffers, propylene glycol and/or ethanol. Stability of hard gelatine capsules may be compromised if high levels of ethanol, glycerine, propylene glycol, Transcutol P or PEGs (with molecular weight less than 4000) are used (Cole, 2007). These solvents would be less incompatible with thicker gelatine soft capsules but quantities of these materials also need to be limited (Meissonnier, 2007). A drug itself, depending on physiochemical properties, can affect the stability of a capsule filling and a capsule shell. Overcoming these issues is a challenge of formulation development as the drug load and the drug itself cannot be changed.

The aim of this chapter was to develop clear liquid microemulsion formulations with the model drug compounds, which could become commercially viable encapsulated products. One of the main objectives was to establish the maximum drug load (solubility limit) that could be solubilised in the typical microemulsion composed of derivates of caprylic/capric acids. Determination of the drug solubility limits in these caprylic/capric acid microemulsions would clarify if these formulations could contain a sufficient drug load to substitute existing treatments. The ultimate aim was to achieve liquid formulations that would be compatible with softgels and ideally also with hard gelatine capsules. Therefore, the formulations examined were prepared as microemulsions suitable for encapsulation where the aqueous phase or polar solvents were limited to 5- 8%, based on the information in the literature (Cole, 2007; Meissonnier, 2007). The capsule filling volume was targeted as approximately 1 ml, which corresponded to approximately 1 g of formulation.

6.2. Incorporation of sodium alendronate trihydrate and disodium pamidronate into liquid microemulsions

Solubility of sodium alendronate trihydrate was high in aqueous buffers (Chapter 3, section 3.2.5). The highest solubility, approximately 52 mg/ml, was observed in the modified K-McIlvaine's buffer with pH 7.8 (initial pH prior to incorporation of the drug), while the solubility in propylene glycol and the standard GIPET ® II formulation was very poor, less than 1 mg/1 g (Chapter 3, section 3.2.6). Therefore, aqueous versions of microemulsions were developed to

increase the solubilising capability of the system and maximise the drug load. The aqueous microemulsions were developed on the basis of two preconcentrates derived from systems 1A2_T3 and 1B3_T4 (Chapter 4, Fig. 4.1.G and Fig. 4.3.G respectively). The preconcentrate 1A2_T3 with the ratio of mix of surfactants to oil of 97.3: 7.3, was selected to maximise the load of C_9-C_{13} monoglycerides (Capmul MCM) which were found to be improve bioavailability of model drug molecules as presented in patent US5688761A1 (Owen et al., 1997) and the latest patent US5707648A1 (Yiv, 1998) (Chapter 1, section 1.3.5). In addition, monoglycerides are more hydrophilic than diglycerides and triglycerides therefore a microemulsion composed of these components should dissolve higher quantities of highly hydrophilic compounds. The second microemulsion based on the preconcentrate 1B3_T4 with the ratio between the mix of surfactants and oil of 40: 60 was also selected to maximise the drug load. Monoesters of propylene glycol (Capmul PG-8) were found to be very hydrophilic compared to the other oils (Chapter 4, Table 4.1). Clear aqueous (drug -free) versions of microemulsion formulations 1A2_T3 and 1B3_T4 containing approximately 8% of the modified K-McIlvaine's buffer pH 7.8 could not be prepared due to rapid precipitation observed upon mixing of the buffer with the preconcentrate. A high solubility of sodium alendronate trihydrate was also observed in pH 2.2, approximately 43 mg/ml, therefore this buffer was subsequently used to prepare clear (placebo) aqueous 1A2_T3 and 1B3_T4 microemulsions (hydrophilic phase type I). The composition of these microemulsions is given in Table 6.1 while the composition of the K-McIlvaine's buffers used was given previously in Chapter 2, section 2.2.7. Solubility of sodium alendronate trihydrate in both microemulsions 1A2_T3 (type I) and 1B3_T4 (type I) at 25°C was found to be less than 1 mg/g after 24 and 48 hours. The solid material recovered after the incorporation study was characterised by DSC and identified as the original material (Appendix Fig. A.6.1.)

Solubility of disodium pamidronate pentahydrate was previously found to be well below 1 mg/g in propylene glycol and the standard GIPET® II formulation (Chapter 3, section 3.2.6), while the solubility was found to be high in aqueous buffers (Chapter 3, section 3.2.5). The highest solubility, approximately 70 mg/ml, was observed in the modified K-McIlvaine's buffer pH 4.4 (prior to incorporation of the drug) and this buffer was used as the aqueous phase to prepare 1A2_T3 and 1B3_T4 (hydrophilic phase type II) microemulsions (composition presented in Table 6.1). Solubility of disodium pamidronate pentahydrate in both microemulsions at 25°C was found to be less than 1 mg/g after 24 and 48 hours. The solid material recovered after the incorporation study was characterised by DSC and identified as the original material (Appendix Fig. A.6.2). Pamidronic acid is known to be less soluble in water than its salt, disodium pamidronate pentahydrate. In theory it should be more soluble in non-polar or less polar materials such as lipid components of the studied microemulsions. Incorporation of pamidronic acid in propylene glycol and the standard non-aqueous GIPET® II formulation did not demonstrate an improved drug load

of pamidronate. Solubility of pamidronic acid was found to be below 1 mg/g and the solid material recovered after the incorporation study was identified by DSC as pamidronic acid (Appendix Fig. A.6.3).

Table 6.1 Drug-free microemulsion/SEDDS systems used to incorporate sodium alendronate trihydrate, disodium pamidronate pentahydrate and acyline monoacetate.

Ingredients		Chemical Names	Formula 1A2_T3		Formula 1B3_T4		Function in formulation
			mg/per capsule	% in formula-tion	mg/per capsule	% in formula-tion	
Preconcentrate							
Captex 355 EP/NF		caprylic/ capric triglyceride	55.0	5.5	/	/	oil phase
Capmul PG-8		propylene glycol monocaprylate	/	/	455.0	45.5	oil phase
Capmul MCM		glyceryl caprate/ caprylate	550.0	55.0	100.0	10.0	low HLB surfactant
Crillet 4 HP		polyoxyethylene sorbitan monooleate	150.0	15.0	200.0	20.0	high HLB surfactant
Polar phase *							
Aqueous phase (type I)	Modified K-McIlvaine's buffer pH 2.2	/	80.0	8.0	80.0	8.0	**aqueous phase**
	Lutrol E 400	PEG 400	165.0	16.5	165.0	16.5	hydrophilic solvent
Aqueous phase (type II)	Modified K-McIlvaine's buffer pH 4.4	/	80.0	8.0	80.0	8.0	**aqueous phase**
	Lutrol E 400	PEG 400	165.0	16.5	165.0	16.5	hydrophilic solvent
Non-aqueous phase (type III)	1,2 - Propylene glycol Pharma	propylene glycol	50.0	5.0	50.0	5.0	hydrophilic solvent
	Lutrol E 400	PEG 400	195.0	19.5	195.0	19.5	hydrophilic solvent
Non-aqueous phase (type IV)	Glycerine	glycerine	50.0	5.0	50.0	5.0	hydrophilic solvent
	Lutrol E 300	PEG 300	195.0	19.5	195.0	19.5	hydrophilic solvent
TOTAL = 75.5% preconcentrate + 24.5% of polar phase (only one type)			1000.0	100	1000.0	100	N/A

Polar phase used to form ME/SEDDS:

- **type I** indicates 24.5% of the hydrophilic phase used for sodium alendronate trihydrate and denotes K-McIlvaine's buffer pH 2.2/PEG 400 in the ratio 1:~2.
- **type II** indicated 24.5% of the hydrophilic phase used for disodium pamidronate pentahydrate and denotes K-McIlvaine's buffer pH 4.4/PEG 400 in the ratio 1:~2.
- **type III** indicates 24.5% of the hydrophilic phase used and denotes PG/PEG 400 in the ratio 1:~4.
- **type IV** indicates 24.5% of the hydrophilic phase used and denotes glycerine/PEG 300 ratio in the 1:~4.

Solubility of alendronic acid in microemulsions and SEDDSs was not tested as the calculated cLogP values (Chapter 3, Table 3.8) of alendronic and pamidronic acids were very similar and therefore solubility of alendronic acid in these formulations was not expected to differ significantly to that shown by pamidronic acid.

6.3. Incorporation of acyline monoacetate in liquid non-aqueous microemulsions (SEDDSs

Acyline monoacetate was found to gel rapidly in aqueous solutions (Chapter 3, section 3.3.5) and this was considered as physical instability (gelling). On the other hand, the drug appeared to be relatively well soluble and physically stable in propylene glycol and the standard (non-aqueous) GIPET ® II formulation (Chapter 3, section 3.3.6). Therefore, non- aqueous versions of microemulsions, containing propylene glycol (or glycerine) and PEG 300 or PEG 400 as a hydrophilic phase, were used to incorporate this model drug. Additional experiments were carried out to compare solubility and physical stability of the drug in propylene glycol and glycerine. Both propylene glycol and glycerine are highly polar solvents with high dielectric constants of 32 and 42 (Troy, 2006). Similar solubility and physical stability of the drug was observed in both these solvents upon preparation. As glycerine appears to be more polar (based on its dielectric constant), it could be a better vehicle to achieve a long-term stability of acyline. Replacement of PEG 400 with PEG 300 did not affect solubility or physical stability of the drug. The non-aqueous microemulsions (SEDDSs) were developed using the same two preconcentrates as previously used with the bisphosphonates. The composition of the non-aqueous microemulsions, type III and IV is presented in Table 6.1 (where type III and IV corresponds to different polar phases). Doses of acyline monoacetate equal to approximately 5-10 mg were soluble and appeared to be initially physically stable in the non-aqueous microemulsion 1A2_T3 (type III). The impact of 'water ingress' on physical stability of acyline monoacetate in the microemulsion was also evaluated. It is known that a manufacturing process of soft gels is carried out using hydrated plastic gelatine ribbons (sheets) that are cut and sealed to form capsules. The excess of water acting as a plasticizer/softener during the capsule formation and sealing is removed upon drying. During this encapsulation process, water enters the capsule filling. A certain percentage of water remains in the capsule filling even once the drying process has been completed. Therefore, liquid fillings of softgels always contain a small percentage of water even if the initial formulation for encapsulation was completely water free (Meissonnier, 2007). The water ingress in 1A2_T3 (type III) formulation was estimated as approximately 3% based on the composition (Meissonnier, 2007). In order to evaluate the impact of the 'water ingress' on the physical stability of acyline monoacetate, approximately 3% of water calculated assuming the formulation as 100% was added. The formulation remained clear, with no signs of precipitation or change in the viscosity over 2 days

when stored at room temperature. This demonstrated a lack of rapidly developed incompatibility that would have been manifested as quickly formed gel. The formulation 1A2_T3 (type IV, with glycerine and PEG 300) showed similar stability in the 'water ingress' experiments, which again suggested that glycerine had a similar effect to propylene glycol on the solubility and stability of acyline monoacetate. The non-aqueous microemulsion 1A2_T3 (type III) containing approximately 10 mg of dissolved acyline and approximately 3% of water added (to mimic 'water ingress' during encapsulation) was placed in glass vials on stability at 5 °C, 25 °C and 40 °C, and stored for 21 days. The content of acyline was tested after 7, 16 and 21 days and the results are summarised in Table 6.2.

Table 6.2. Content of acyline monoacetate in 1A2_T3 (type III) formulation.

Theoretical content of acyline monoacetate: 11.267 mg/g (approximately 10mg of acyline per 1g)							
Time Points (Days)	**0 days (Filtered)**	**7 days**		**16 days**		**21 days**	
		Filtered *	**Unfiltered**	**Filtered ***	**Unfiltered**	**Filtered ***	**Unfiltered**
Storage conditions: 5°C (Fridge)							
% of theoretical content	96.79	/	/	/	/	/	93.35
Visual appearance	Clear, non-viscous solution	Clear, non-viscous solution		Clear, non-viscous solution		Clear, non-viscous solution	
Storage conditions: 25°C							
% of theoretical content	96.79	91.73	97.87	41.77	105.90	34.62	94.94
Visual appearance	Clear, non-viscous solution	Clear, non-viscous solution		/		Gel, cloudy solid mass	
Storage conditions: 40°C							
% of theoretical content	96.79	20.00	90.16	16.19	95.58	5.74	70.27
Visual appearance	Clear, non-viscous solution	Gel, cloudy solid mass		Gel, cloudy solid mass		Gel, cloudy solid mass	

* filtered through 0.45 μm Millipore filter

In the gelled formulations, a substantial decrease of acyline content was observed in the filtered samples at 25 and 40 °C. The content in the equivalent unfiltered samples was significantly higher which indicated that the drug was relatively stable chemically but agglomerated extensively (the agglomerates were broken down by polar solvents used to prepare samples for assay testing). A substantial drug loss (approx 30%) was observed in the unfiltered sample stored at 40°C for 21 days. However, this result should not be attributed solely to the chemical instability since 'representative' sampling of the gelled mass was clearly an issue and variability in the content of the drug was also observed between 7 and 16 days (at 40°C). The impact of physical instability (gelling) on release of acyline was evaluated by dissolution testing. The gelled formulation stored at 25 °C for 21 days and the liquid formulation stored in a fridge for the same length of time were filled into empty softgels size 22 with a syringe and sealed with a flame. The dissolution profiles of

acyline from these capsules are shown in Fig. 6.1. The liquid formulation (stored refrigerated) reached 100% release within 15 minutes. The initial slow release, a lag time between 5- 10 minutes, was related to dissolution of the capsule shell (Fig. 6.1, Table 6.3).

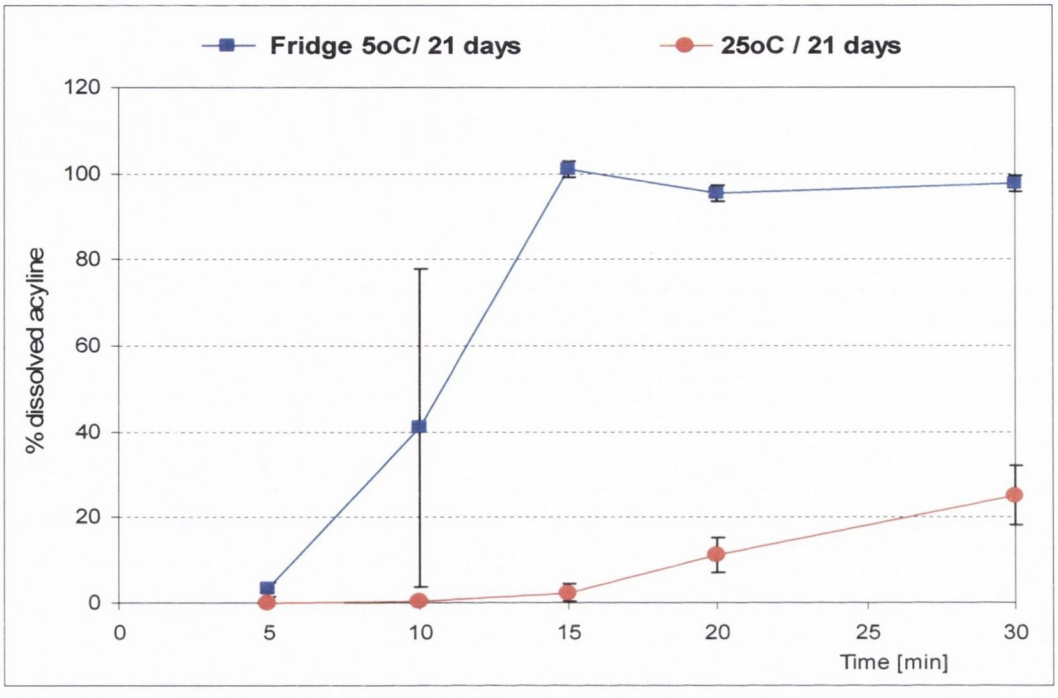

Fig. 6.1. Dissolution profile of acyline from 1A2_T3 (hydrophilic phase type III) encapsulated into soft gels carried out in 900 ml of phosphate buffer pH 6.8 (USP) with 1% of polysorbate 80, apparatus II (USP).

Table 6.3. Dissolution profile of acyline from gelled/ non-gelled 1A2_T3 (type III) formulations.

% of acyline dissolved in 900ml of phosphate buffer (USP) containing 1% of polysorbate 80, paddle 50rpm						
Storage Conditions : Fridge: 5°C, 21 days						
Time Points [min]	**5**	**10**	**15**	**20**	**30**	**INF**
V1 [a)]	4.5	67.1	99.8	96.7	98.9	98.2
V2 [b)]	1.9	14.7	102.2	94.0	96.3	96.7
AVERAGE (n= 2)	**3.2**	**40.9**	**101.0**	**95.4**	**97.6**	**97.5**
SD	1.8	37.1	1.7	1.9	1.8	1.1
% RSD	56.3	90.7	1.7	2.0	1.8	1.1
Storage Conditions : 25oC, 21 days						
Time Points [min]	**5**	**10**	**15**	**20**	**30**	**INF**
V1 [c)]	0.0	0.0	3.8	13.9	29.9	91.4
V2 [c)]	0.0	0.6	0.9	8.1	20.3	93.2
AVERAGE (n= 2)	**0.0**	**0.3**	**2.4**	**11.0**	**25.1**	**92.3**
SD	0.0	0.4	2.1	4.1	6.8	1.3
% RSD	/	133.3	87.5	37.3	27.1	1.4

[a)] Gelatine capsule burst just before 10 min, [b)] Gelatine capsule burst between 10 and 15 min,

[c)] Gelatine capsule burst after 15 min

The gelled formulation showed slow and incomplete release of acyline. Despite the presence of surfactant (1% of polysorbate 80) in the dissolution medium less than 30% of acyline was released within 30 minutes. The dissolution rate of acyline was improved once the infinity spin (defined as 15 minutes under 250 rpm, paddle) was performed and the amount of dissolved acyline increased to 90%. It appeared that vigorous mixing increased the release of acyline from the gelled samples. In the liquid sample, once the full release of acyline was reached within 15 minutes, acyline remained dissolved (> 95% dissolved) also after the infinity spin test.

Slow release of acyline from the gelled SEDDS compared to the liquid formulation was also observed for 1B3_T4 (type IV) non-aqueous microemulsion (composition in Table 6.1). The liquid SEDDS containing approximately 15mg of acyline (partially dissolved, partially suspended) was manually filled into size 22 empty soft gels. In the previous study (with 1A3_T3 type III formulation) the gelled mass was shaken and disintegrated prior to the dissolution testing to facilitate injection into capsules. This study was performed using capsules that were prepared with the clear (freshly made) 1B3_T4 (type IV) formulation and gel was formed inside the capsules over time, as they were stored at 40 °C. The capsules with the liquid content, stored in a fridge for 8 days, released more than 80% of acyline within 10 minutes (Fig. 6.2, Table 6.4).

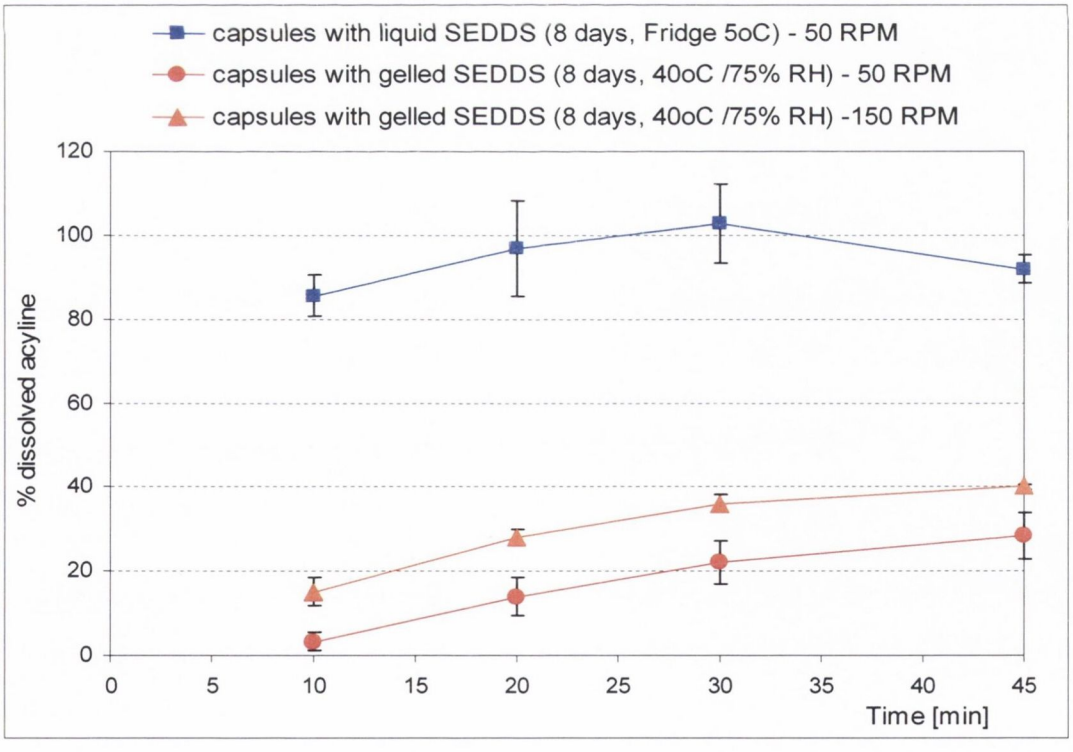

Fig. 6.2. Dissolution profile of acyline from 1B3_T4 (hydrophilic phase type IV) encapsulated in soft gels, carried out in phosphate buffer 900 ml, pH 6.8 (USP).

When the capsules stored at 40 °C for 8 days were examined visually the content was cloudy and appeared solid and gelled. Less than 30% of the drug was released from the 'gelled' capsules within 45 minutes using a mild agitation (paddle, 50 rpm). Also, only 40% of acyline was released when more vigorous mixing was used (150 rpm). Again, it was apparent that vigorous mixing better dispersed the gelled mass and improved release of acyline from the gelled mass. Nevertheless, a substantial amount of acyline remained insoluble irrespective of the agitation used and gelled mass was observed at the bottom of the dissolution vessel after the test was completed.

Table 6.4. Dissolution profile of acyline from gelled and non-gelled 1B3_T4 (type IV) formulation.

% of acyline dissolved in 900 ml of phosphate buffer (USP, paddle 50rpm)				
Capsules with the liquid formulation (8 days, Fridge 5°C) - 50 RPM				
Time Points [min]	**10**	**20**	**30**	**45**
AVERAGE (n= 3)	**85.5**	**96.7**	**102.6**	**91.8**
SD	4.9	11.5	9.4	3.4
% RSD	5.7	11.9	9.2	3.7
Capsules with the gelled formulation (8 days, 40°C) - 50 RPM				
Time Points [min]	**10**	**20**	**30**	**45**
AVERAGE (n= 3)	**3.2**	**13.9**	**22.1**	**28.4**
SD	2.2	4.6	5.2	5.5
% RSD	68.8	33.1	23.5	19.4
Capsules with the gelled formulation (8 days, 40°C) - 150 RPM				
Time Points [min]	**10**	**20**	**30**	**45**
AVERAGE (n= 3)	**15.0**	**28.0**	**36.0**	**40.1**
SD	3.3	2.0	2.0	0.6
% RSD	22.0	7.1	5.6	1.5

The complete release of acyline from the liquid formulation was observed after 30 minutes in phosphate buffer 6.8 (without any surfactants), however it appeared that solubility of acyline decreased over time in this medium. At the end of the dissolution test very small particles were seen floating on the surface of the medium. In the presence of polysorbate 80 (Fig. 6.1, Table 6.3) the content of dissolved acyline in the dissolution medium did not decrease over time. This suggested that polysorbate 80 might have stabilised acyline in the other medium and prevented precipitation (possibly gelling) over time.

Physical instability (gelling) of acyline monoacetate was demonstrated to have a significant, negative impact on the drug dissolution from the gelled SEDDSs compared to the freshly prepared liquid formulations. The temperature clearly had a significant effect on gelling rate but the drug load also appeared to affect it. A stability study was carried out to compare the combined effect of the drug load and the temperature on formation of gelling. Visual observations of gelling formation in 1A2_T3 (type IV) and 1B3_T4 (type IV) formulations are presented in Table 6.5 and Table 6.6 respectively. In the self-emulsifying system, 1A2_T3 (type IV), formation of the gel was dependent

on both the storage conditions and the concentration of the drug (Table 6.6). At the higher temperature (25 °C), gel formed faster and the samples with the concentration of acyline above 10 mg/g were physically stable for less than 9 days. The samples stored refrigerated were slightly more stable, however the difference was not substantial. Only samples with a very low concentration of the drug, from 1- 3 mg/g, appeared to be physically stable in 5 °C and 25 °C for a longer period of time i.e. approximately 2 months. Also it was noted that the extended preparation time (storage at room temperature for 7 days until the drug dissolved) had a negative impact on the high concentration samples (15-20 mg/g), which were already partially gelled before the stability study started. In those samples the drug did not dissolve completely but gelling occurred rapidly which suggested that undissolved particles of the drug might have acted as nucleating centres facilitating formation of aggregates. The reason why the drug was dissolved at room temperature was that 1A2_T3 formulation partially solidified at the low temperature (when stored in a fridge) which did not allow the drug to become dissolved.

Table 6.5. Physical stability of acyline in 1A2_T3 (type IV) formulation inspected visually.

Scale (visual inspection)	x = some particles of API still undissolved		Clear solution, no gelling		some precipitation, some gelling		partially gelled, cloudy suspension		Solid gel or almost solid gel, cloudy, whitish
1A2_T3 (type IV)	Preparation at room temp (7days)								
Acyline concentration [mg] in SEDDS [g]	**0 days**	**9 days**	**13 days**	**23 days**	**37 days**	**48 days**	**55 days**	**63 days**	**70 days**
Storage conditions: Fridge / 5°C									
1 mg/g									
3 mg/g									
5 mg/g									
10 mg/g	x								
15 mg/g	x								
20 mg/g	x								
Storage conditions: 25°C									
1 mg/g									
3 mg/g									
5 mg/g									
10 mg/g	x								
15 mg/g	x								
20 mg/g	x								

In 1B3_T4 system, formation of the gel also appeared to be dependent on the storage conditions and the concentration of acyline in the formulation (Table 6.6). Acyline gelled extremely rapidly at 40 °C and only the sample with acyline concentration of 1 mg/g was physically stable for approximately 1 month. The samples stored at 25 °C also demonstrated extensive gelling. Only the

samples with acyline concentration between 1-3 mg remained physically stable over 1 month, similarly to the stability of the drug in the 1A2_T3 (type IV) formulation. At the concentration of 5 mg/g (25 °C), the drug appeared to be more physically stable in the 1A2_T3 (type IV) formulation compared to the 1B3_T4 (type IV) formulation because gelling of these samples was observed after 37 and 18 days respectively. Due to the reduced preparation time (only 1 day because the formulation was still liquid when stored refrigerated), all the samples of 1B3_T4 (type IV) formulation were liquid at the start of the study (T0). However, the high concentration samples (15-30 mg/g) showed signs of gelling in less than 4 days when stored at 25 °C and 40 °C. No gelling was observed in the samples containing 1-30 mg/g of acyline in 1B3_T4 (type IV) formulation stored refrigerated for over 1 month.

Table 6.6. Physical stability of acyline in 1B3_T4 (type IV) formulation inspected visually.

Scale (visual inspection)	x = some particles of API still undissolved	Clear solution, no gelling	some precipitation, some gelling	partially gelled, cloudy suspension	Solid gel or almost solid gel, cloudy, whitish		
1B3_T4 (type IV)	Preparation at room temp (1day)						
Acyline concentration [mg] in SEDDS [g]	**0 days**	**4 days**	**6 days**	**10 days**	**18 days**	**26 days**	**33 days**
Storage conditions: Fridge/ 5°C							
1 mg/g							
3 mg/g							
5 mg/g							
10 mg/g	x						
15 mg/g	x	x	x	x			
20 mg/g	x	x	x	x	x	x	
30 mg/g	x	x	x	x	x	x	x
Storage conditions: 25°C							
1 mg/g							
3 mg/g							
5 mg/g							
10 mg/g	x						
15 mg/g	x						
20 mg/g	x						
30 mg/g	x						
Storage conditions: 40°C							
1 mg/g							
3 mg/g							
5 mg/g							
10 mg/g	x						
15 mg/g	x						
20 mg/g	x						
30 mg/g	x						

Physical stability of acyline (monoacetate) in 1A2_T3 (type IV) formulation when stored refrigerated appeared to be worse than in 1B3_T4 (type IV) system when the results in Table 6.5 and Table 6.6 where directly compared. However, it was concluded that the extended manufacturing time of 1A2_T3 (type IV) formulation at room temperature contributed significantly to 'initiation of gelling' in the samples with acyline concentration from 10 to 20mg/g, and therefore the direct comparison of acyline in these two formulations should not be made. In conclusion, acyline monoacetate appeared to have very limited physical stability in the developed SEDDSs stored at 25°C and 40°C if the drug concentration was 10 mg or higher.

6.3.1. Preclinical Study

In parallel with the stability evaluations shown above, it was decided to evaluate oral bioavailability of the drug from the developed SEDDSs. The objective was to understand if the oral absorption of acyline could be significantly improved by the lipid formulations based on derivatives of caprylic/capric acids. In a dog study, three self-emulsifying formulations containing approximately 5 mg of acyline (in a monoacetate form) were compared to the Test Item 1, which was a control formulation comprising 5 mg of acyline in 5 ml of purified water. The intravenous dose was abandoned during preliminary dosing due to significant adverse reactions in animals. The composition of the dosed SEDDSs is given in Table 6.7.

Table 6.7. A composition of the SEDDSs (non-aqueous microemulsions) dosed in the animal study.

5.981 mg of acyline monoacetate* per 1g of SEDDS (~ 5mg of acyline per 1g of SEDDS)				
Preclinical Test Item Name		**Test Item T2**	**Test Item T3**	**Test Item T4**
Original system		3A2_T2	1A3_T3	1B3_T4
Preconcentrate (mix of surfactants: oil)		92.7 : 7.3	92.7: 7.3	40 : 60
Combined HLB value		6.4	7.2	11.4
Overall HLB value		6.1	6.8	8.0
Formulation (including the hydrophilic phase)		**3A2_T2** (type IV)	**1A2_T3** (type IV)	**1B3_T4** (type IV)
Ingredients	Chemical Names	% in formulation		
Acyline monoacetate *	Acyline monoacetate	**0.595**	**0.595**	**0.595**
Capmul PG-8	propylene glycol monocaprylate	/	/	**45.229**
Captex 355 P/NF	caprylic/ capric triglyceride	**5.467**	**5.467**	/
Capmul MCM	glyceryl caprate/ caprylate	/	**54.673**	**9.941**
Capmul MCM 10	glyceryl caprate/ caprate	**54.673**	/	/
Polysorbate 80	polyoxyethylene sorbitan monooleate	**14.911**	**14.911**	**19.881**
Glycerine	glycerine	**4.970**	**4.970**	**4.970**
Lutrol E 300	PEG 300	**19.384**	**19.384**	**19.384**
TOTAL		100.0	100.0	100.0

* Load of acyline monoacetate was calculated based on the CoA (Assay and LOD)

Test Item 3 and Test Item 4, were the formulations 1A2_T3 (hydrophilic phase type IV) and 1B3_T4 (hydrophilic phase type IV), which were also used to evaluate physical stability of acyline and release from the gelled formulations. The third formulation, Test Item 2, was derived from the system 3A2_T2 (Chapter 4, Fig. 4.1.I) where Capmul MCM C10 was used as a cosurfactant (instead of Capmul MCM). This formulation was a close analogue of the formulation 1A2_T3 (type IV). The preclinical SEDDS differed by their combined HLB values (the calculation shown in section 2.3.5) and their overall HLB values (the calculation shown in section 2.6.2.4). The dilution behaviour of the preconcentrates of 3A2_T2, 1A2_T3, 1B_T4, (without cosolvents) was shown on the phase diagrams in Chapter 4 (Fig. 4.1.I, Fig. 4.1.G, Fig. 4.3.G respectively) and the formation of coarse emulsions was observed upon the incorporation of similar amounts of water despite various hydrophilic character of these compositions. It was also demonstrated in Chapter 4 (section 4.5) that an addition of cosolvent(s) had an impact on the dilution behaviour. Therefore, the dilution behaviour of the final preclinical formulation (type IV indicates glycerine and PEG 300 as cosolvents) was examined with water and fasted intestinal fluid FaSSIF-V2 (Fig. 6.3, Table 6.8). Test Item 3 appeared to have marginally better dilution behaviour compared to the other two Test Items. A microemulsion containing up to approximately 14% of the aqueous phase (calculated per as % of the formulation) could be formed, before a turbid, low viscosity emulsion was formed. Test Item 4 and Test Item 2 formed emulsions once 7% up to 10% of water (or FaSSIF-V2) was incorporated. The percentage of the aqueous phase was also calculated for a three component system (excluding PEG 300 and glycerine) to compare the dilution of the Test Items to the dilution of the preconcentrates they derived from. In all three cases, the presence of additional cosolvents had negligible effect on the dilution behaviour. The emulsification of Test Items in a larger volume of FaSSIF-V2 was tested. The dilution ratio 1: 200, typically employed to evaluate dispersion (emulsification) behaviour of SMEDDSs and SEDDSs (Porter et al., 2004) was used. All three formulations formed highly polydisperse, coarse emulsions (droplet size above 1μm). As the dilution of the Test Items did not differ significantly in vitro, it was not expected that a major difference in oral absorption of acyline could be caused by dilution of any of these formulations.

Table 6.8. Dilution behaviour of the preclinical items used with acyline acetate

Preconcentrate		% Glycerine/ PEG 300	% Diluent*	% Diluent **	Appearance
% Mix of Surfactants	% Oil				
Test Item 2					
69.97	5.51	24.50	0.00	**0.00**	Clear, transparent
Purified water as Diluent					
65.05	5.12	22.78	7.03	**9.11**	Transition point into hazy, turbid emulsion
FaSSIF-V2 as Diluent					
63.31	4.99	22.17	9.52	**12.24**	Transition point into hazy, turbid emulsion
Test Item 3					
69.96	5.51	24.50	0.00	**0.00**	Clear, transparent
Purified water as Diluent					
60.26	4.75	21.10	13.86	**17.58**	Transition point into hazy, turbid emulsions
FaSSIF-V2 as Diluent					
59.98	4.73	21.00	14.30	**18.10**	Transition point into hazy, turbid emulsion
Test Item 4					
30.06	45.46	24.50	0.00	**0.00**	Clear, transparent
Purified water as Diluent					
27.73	41.93	22.60	7.76	**10.02**	Transition point into hazy, turbid emulsion
FaSSIF-V2 as Diluent					
26.30	39.81	21.46	12.42	**15.82**	Transition point into hazy, turbid emulsion

* % of diluent calculated as the percentage of samples consisting of water+preconcentrate+glycerine+PE 300

** % of diluent calculated as the percentage of samples consisting of water+preconcentrate

In addition, the dilution characteristics of the original formulations were expected to change once the digestion process occurred. The dispersion behaviour of digestible lipid materials, such as the excipients used to formulate the SEDDSs, is altered once digested products are formed *in vivo* conditions (Pouton, 2000, Pouton, 2006). The digestion proceeds via interfacial binding of lipases to lipidic substrates (Embleton & Pouton, 1997). In theory, a very fine dispersion of an original formulation increases the contact area for digestive enzymes to bind and therefore can be digested more rapidly.

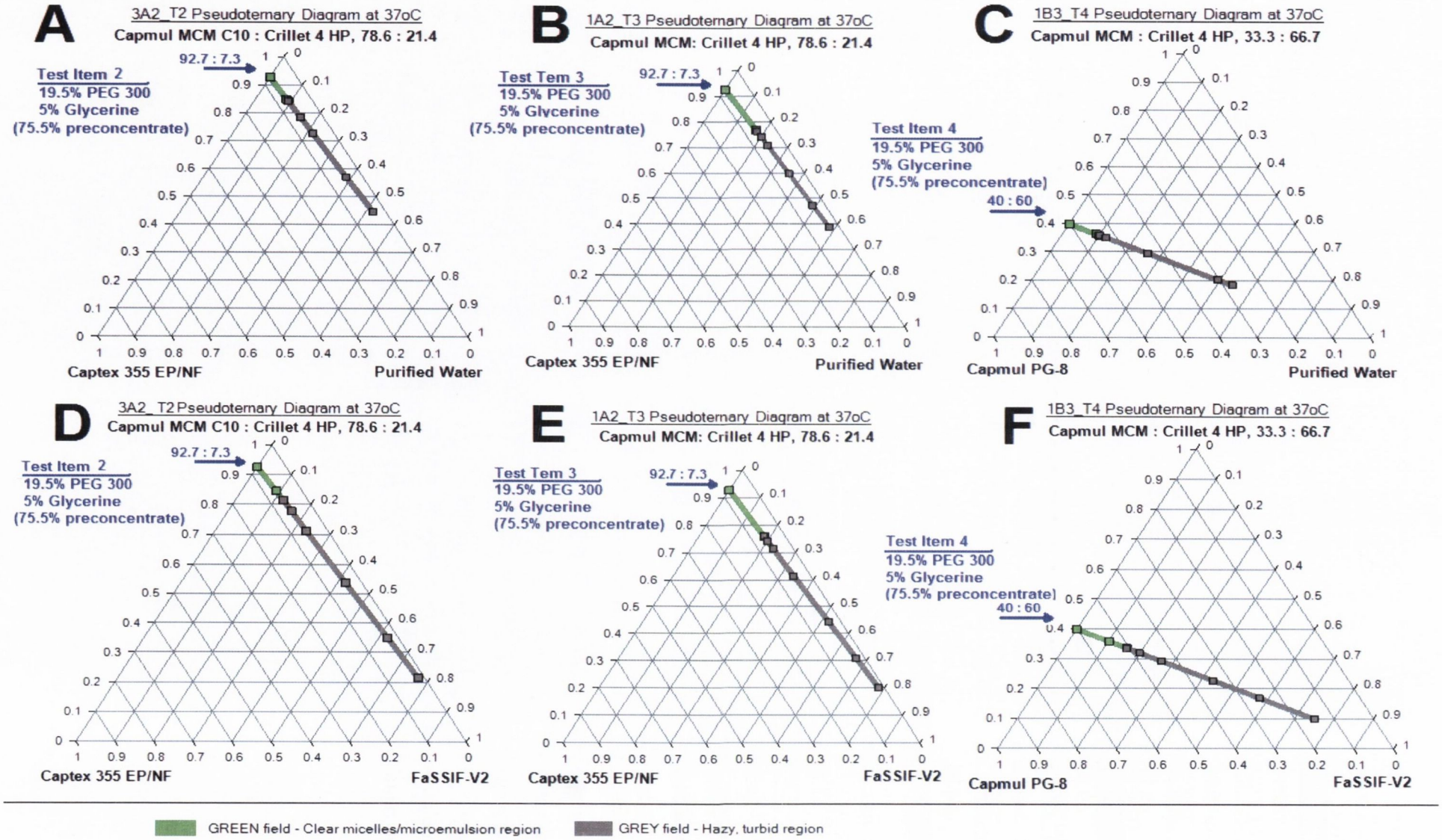

Fig. 6.3. Dilution behaviour in water (A-C) and FaSSIF-V2 (D-F) for Test Item 2 (A,D) , Test Item 3 (B, E) and Test Item 4 (C, F).

Lipid formulations composed of glycerides are digested to fatty acids and 2-monoglycerides, therefore relatively similar digested products would be formed from all three SEDDS in general. However, Test Item 3 and Test Item 2 differed by the type of cosurfactant where a different medium chain fatty acid was used. The digested products of Test Item 3 should contain mainly caprylic acid (C8) and its monoglycerides, compared to the digested products of Test Item 2 (mainly capric acid (C10) and its monoglycerides).

The preclinical study was carried out in cannulated beagle dogs (n = 5). The details of the study design, the bioanalytical method and the pharmacokinetic evaluation are presented in Chapter 2, section 2.6.2.5. At the time of dosing all three SEDDSs (Test Item 2, 3, and 4) were liquid, clear, low viscosity formulations without any signs of gelling. 1g of each SEDDS formulation (containing 5mg of acyline) was dosed through an intraduodenal port. As the reference (control), the unenhanced item, Test Item 1, containing 5mg of acyline was prepared in water directly prior to dosing (to avoid gelling) and dosed through the port, the same way as the self-emulsifying formulations.

Oral absorption of acyline was poorer from the unenhanced preparation compared to the SEDDSs (Fig. 6.4 – 6.7; Appendix Tables A.6.1- A.6.2), however high variability in the extent of absorption was observed for T3 and T4 formulations (Fig. 6.5) compared to the unenhanced test item T1 and T2.

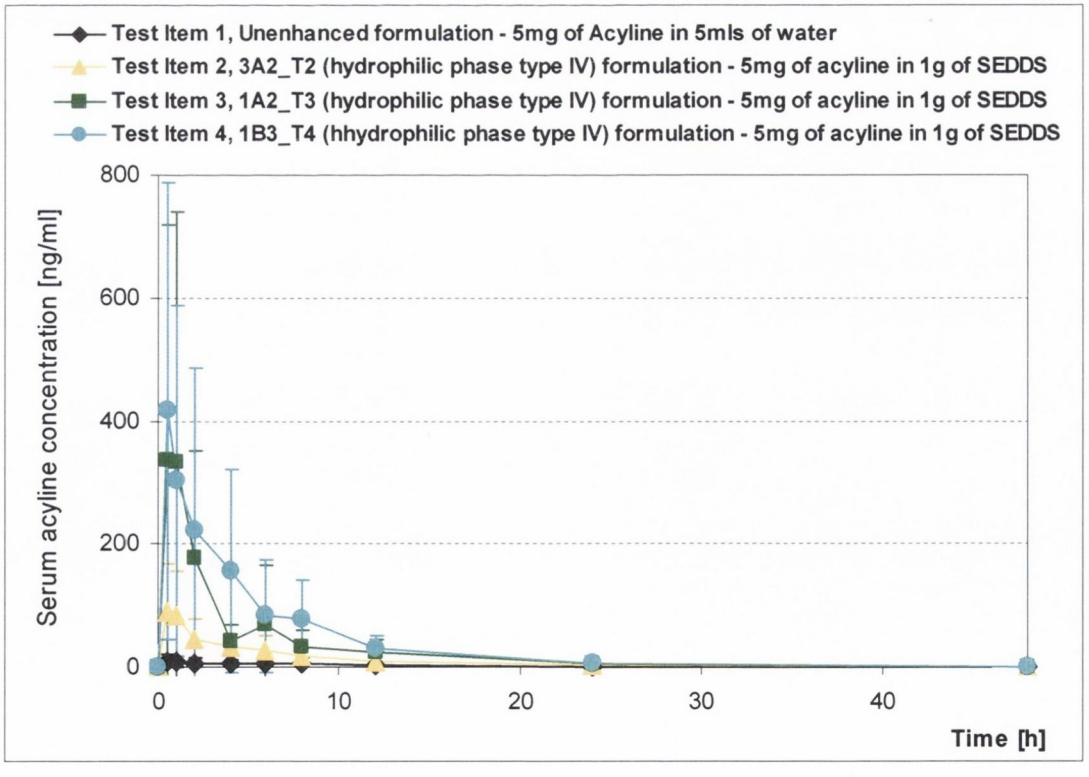

Fig. 6.4. Serum mean acyline concentration profile versus time (standard error bars indicate standard deviation).

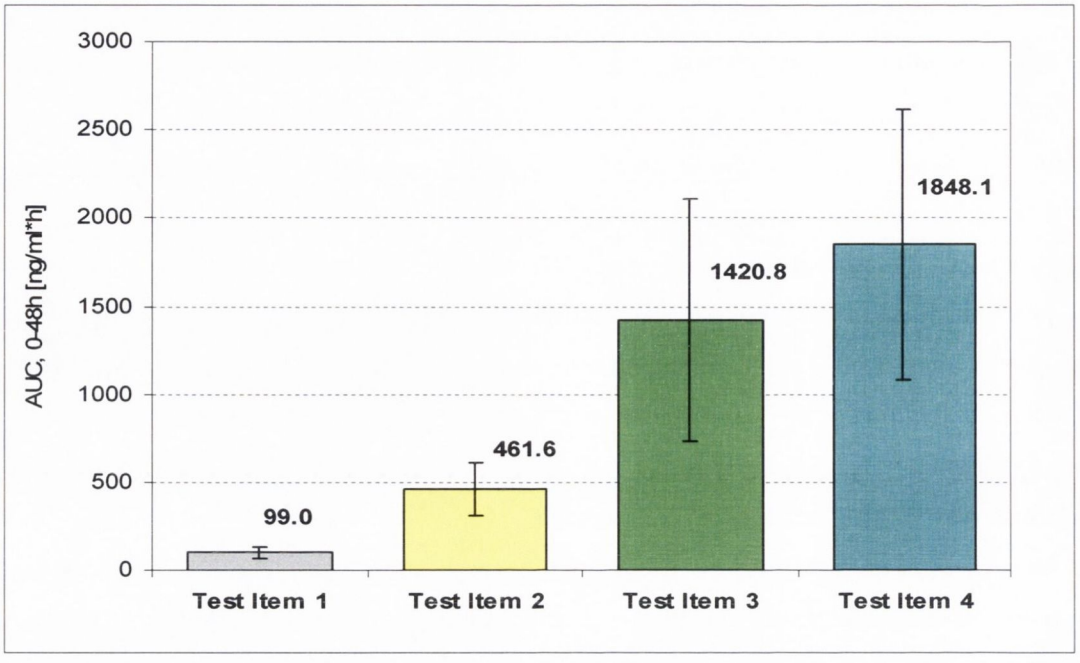

Fig. 6.5. Comparison of AUC $_{(0\text{-}48h)}$ calculated after administration of the preclinical formulations (error bars indicated SEM (standard error of the mean)).

A statistical analysis of AUC was performed using a parametric test, after log-transformation (Table 6.9). The extent of absorption (AUC) is a positive, right-skewed parameter (Qiu et al., 2008, CHMP/EWP/40326/2006, 2006) and therefore has been regarded as log normally-distributed. The comparison of log-transformed AUC$_{(0\text{-}48h)}$ results was performed using parametric repeated measures (paired) ANOVA test with multiple comparison post test.

Table 6.9. Summary of the statistical analysis performed with AUC$_{(0\text{-}48h)}$.

Tested parameter	**Parametric test** (assumes normal distribution of the overall population)
	Log-transformed extent of absorption/ Log [AUC$_{(0\text{-}48h)}$]
Difference between all 4 treatment	$p = 0.0001$, treatments are very significantly different ($p < 0.05$)
T1 (control) vs T3	very significantly different ($p < 0.001$)
T1 (control) vs T4	very significantly different ($p < 0.001$)
T1 (control) vs T2	significantly different ($p < 0.05$)
T3 vs T4	not significantly different ($p > 0.05$)
T3 vs T2	not significantly different ($p > 0.05$)
T4 vs T2	not significantly different ($p > 0.05$)

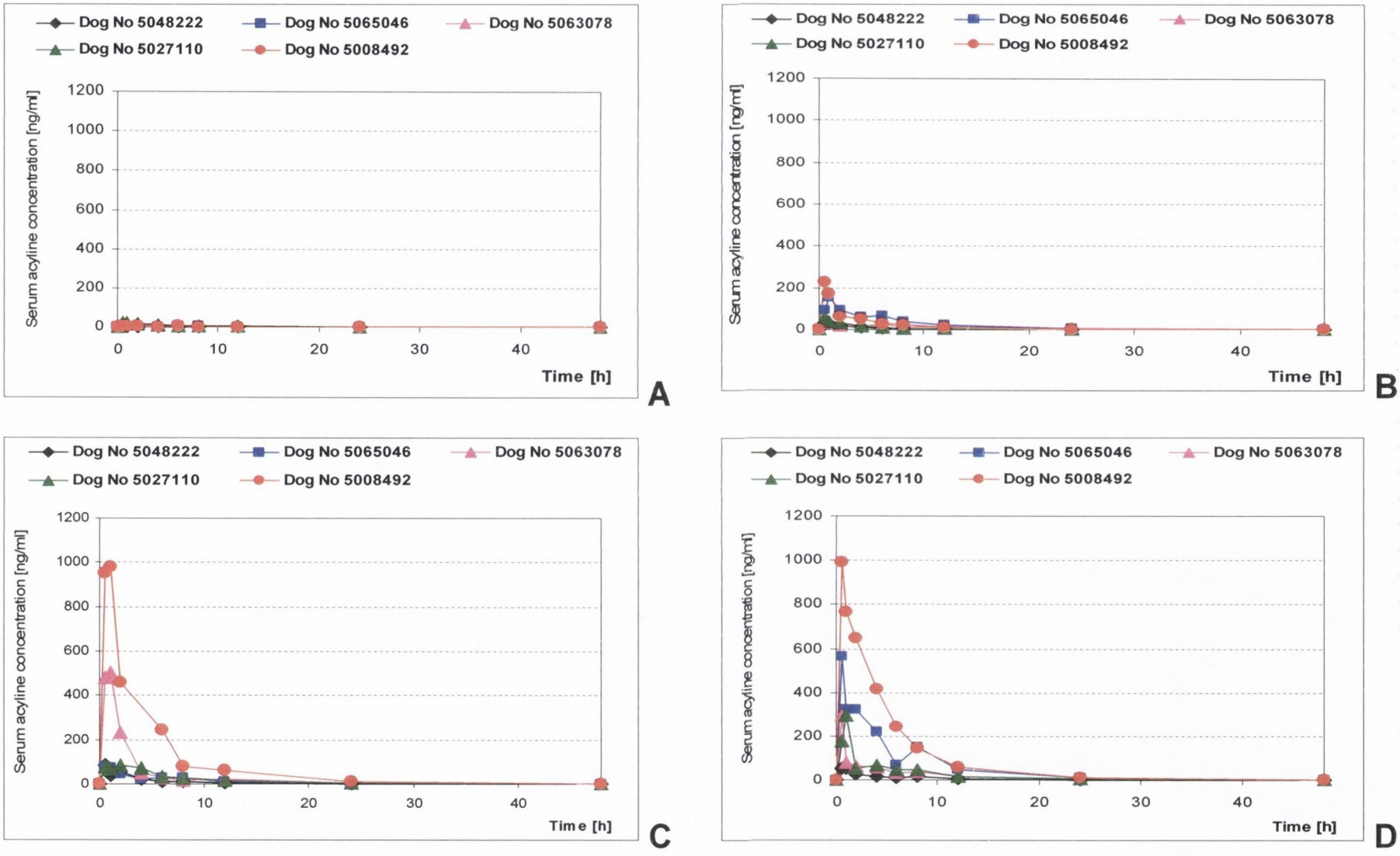

Fig. 6.6. Serum acyline concentration profile for individual dogs versus time: A) Test Item 1, B) Test Item 2, C) Test Item 3, D) Test Item 4.

Distribution in the samples was found to be normal although the limited sample size precludes a reliable determination of the distribution in the overall population (UCM070244, 2001; Motulsky, 1995). A small sample size is a problem in general, when using both parametric and non-parametric statistical tests, as the non-parametric tests lack statistical power while the parametric tests may not be robust enough for small samples (Motulsky, 1995).

The extent of acyline absorption from Test Item 4 was significantly better ($p < 0.001$) compared to the unenhanced formulation Test Item 1, irrespective of whether the parametric or non-parametric analysis was used. Absorption of acyline ($AUC_{(0\text{-}48h)}$) from the Test Item 3 was also demonstrated to be statistically better ($p < 0.05$) than the control (both approaches). The average relative bioavailability indicated approximately 26 and 33 fold increase (Fig. 6.7) in absorption of the drug from Test Item 3 (1A2_T3 SEDDS type IV) and Test Item 4 (1B3_T4 SEDDS type IV), however there was not statistical difference between these two test items. Acyline was significantly better absorbed form the Test Item 2 compared to the control formulation but only when comparing Log $AUC_{(0\text{-}48h)}$ using the parametric test. Based on the average value, Test Item 2 appeared to increase oral absorption of the drug by approximately 8 fold.

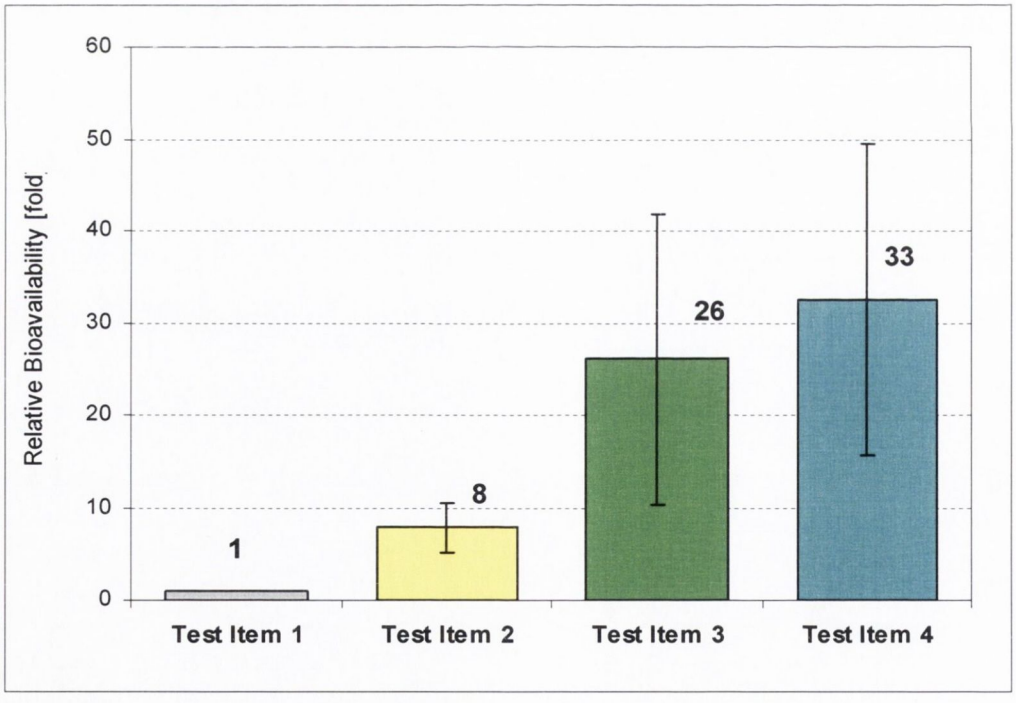

Fig. 6.7. Comparison between relative bioavailability (Frel) of acyline obtained after administration of the preclinical formulations (error bars indicated SEM).

The high variability in the extent of absorption prevented detection of any statistically significant differences between the SEDDS formulations. The recent pharmaceutical trends defined by the regulatory agencies for bioequivalence and clinical studies require a statistical analysis with parametric tests (CPMP/EWP/QWP/1401/98, 2010; UCM070244, 2001). In the current study, two

SEDDS were significantly better than the control even if a more conservative approach was used (the statistical significance was shown with both tests). Absorption of acyline from all three SEDDS formulations appeared rapid and T_{max} was achieved between 30 – 60 minutes for these formulations. Absorption rate of acyline appeared variable from the unenhanced item, and therefore no statistically significant difference ($p < 0.05$) between T_{max} of all four formulations was observed. Acyline monoacetate was previously shown to rapidly gel in aqueous media (Chapter 3, section 3.3.5). Therefore, one of the reasons for more variable absorption rate of acyline from the unenhanced formulation could be due to physical instability (gelling) of the drug *in vivo*. If this was the case, it appears that the SEDDS formulation (or their digestion products) produced an anti-gelling effect upon dilution and therefore the absorption from these formulations was not impeded by slower dissolution of gelled acyline. Based on the average relative bioavailability (Fig. 6.7) of acyline, the SEDDSs could be ranked from the least to the most 'effective' in the following order: Test Item 2, Test Item 3 and Test Item 4 which coincides with the order of the combined and overall HLB values (from the lowest to the highest values). The direct correlation between $AUC_{(0\text{-}48h)}$ and both HLB parameters was poor. On average, the drug absorption from Test Item 3 and Test Item 4 was very high and similar (Fig. 6.7) while their combined and overall HLB values differed significantly (Table 6.7). Also, the absorption from Test Item 2 appeared to be almost three times worse (on average) compared to the Test 3 while their combined and overall HLB values were very similar (Table 6.7). Since significant differences in absorption extent of acyline from the SEDDS could not have been demonstrated due to the high variability, it is also not possible to show a relationship between the HLB parameters and $AUC_{(0\text{-}48h)}$ based on the generated data. The observed trend may be random but it may also suggest differences in the dispersion behaviour of SEDDSs *in vivo* that were not seen in the *in vitro* testing. Although the dispersion behaviour of the SEDDSs observed *in vitro* did not demonstrate major differences between the formulations, perhaps physical stability of acyline (upon release) was different from these SEDDSs, especially if the digestion process was rapid. It is also possible that individual components of the system (rather than the whole dispersed system) somehow affected acyline 'stability in solution'. All three SEDDS comprised polysorbate 80 which is known as an excipient that can affect absorption in various ways including solubilisation, inhibition of P-gp (and potentially of other transporters) and stimulation of chylomicron production (O'Driscoll & Griffin, 2008). With regard to acyline, previously it was observed (during *in vitro* dissolution testing) that polysorbate 80 prevented precipitation of acyline from a solution. Therefore, it probable that polysorbate 80 had the same effect *in vivo*. Once the SEDDSs formed emulsions upon dispersion, acyline was released for absorption but it may have remained 'solubilised (in solution)' due to the presence of polysorbate 80. Again, the high variability observed in the study, does not allow to demonstrate a correlation between the extent of absorption and the content of polysorbate 80, but the highest $AUC_{(0\text{-}48h)}$ was observed for Test Item 4 that also contained the highest amount of polysorbate 80. Although the

effect of HLB parameters, the content of polysorbate 80 or simply the content of non-digestible (directly absorbable) components of SEDDSs on the adsorption of acyline cannot be established based on the generated data, it appears that all the SEDDSs could have enhanced physical stability of acyline *in vivo* compared to the Test Item 1.

Another possible explanation of the improved oral bioavailability of acyline from the SEDDSs could be related to the direct effect of SEDDSs, their components (or their digestion products) on permeability of the intestinal membrane. The oral absorption route of acyline has not been investigated and explained so far. As a hydrophilic and positively charged (in the intestinal tract) molecule it could be absorbed via the paracellular route, on the other hand its molecular weight (1535.23 Da as free base) may restrict this absorption route. The major products of lipid digestion, which are fatty acids and 2-monoglycerides, enter the enterocyte by simple diffusion across the plasma membrane. Some components of the SEDDSs (e.g. monoglycerides, monoesters of propylene glycol) did not require further digestion but could be absorbed directly. A considerable fraction of the fatty acids also enters the enterocyte via a specific fatty acid transporter protein in the membrane (Embleton, 1997). Although mixed 'intestinal' micelles appear to be the ideal vehicles for delivery of poorly water-soluble drugs, absorption of hydrophilic compounds can be also significantly enhanced in presence of these structures. It is possible that acyline was entrapped into micelles of bile acids and digested lipids and absorb together with these species. Polysorbate 80 as an inhibitor of P-gp and potentially of other transporters may have also affected permeability of acyline. The digestion of 'digestible components' of the SEDDSs was likely to occur rapidly as medium chain glycerides are very easily broken down in the intestinal tract (Kaukonen et al., 2004; Pouton & Porter, 2008). Polysorbate 80 was also shown to be susceptible to digestion by pancreatic enzymes (Christiansen et al., 2010).

Despite any effect that the SEDDSs may have exerted on the intestinal membrane, significant adverse results were not observed after administration of the preclinical items. Abnormal clinical signs were mild and limited to some vomiting within the first 15 minutes post-administration. None of the observed reactions were deemed severe enough to lead to any loss of the drug or the preclinical formulation dosed. Similar abnormal effects were observed in other preclinical studies and none raised concerns of the vet responsible for the health and safety of the animals.

6.4. Overall Conclusions

It was demonstrated on the model hydrophilic compounds that development of microemulsions and SEDDSs (non-aqueous microemulsions) suitable for encapsulation presents a number of formulation challenges. One of the main problems is to dissolve the required therapeutic dose of a drug in lipid formulations. While quantities of polar solvents need to remain low to ensure a long-term stability of capsule shells (Cole, 1999; Meissonnier, 2007), they also provide a limited vehicle to solubilise hydrophilic compounds. Both, sodium alendronate trihydrate and

disodium pamidronate pentahydrate showed very limited solubility in the developed microemulsions with the aqueous phase, which was supposed to maximise the drug load. Preparation of encapsulated clear microemulsions with the bisphosphonates that could become equivalents of the commercially available products does not appear feasible. Sodium alendronate trihydrate is available as Fosamax tablets for oral administration that contain 6.53, 13.05, 45.68, 52.21 or 91.37 mg of alendronate monosodium salt trihydrate (the molar equivalent of 5, 10, 35, 40 and 70 mg of alendronic acid). The oral bioavailability of alendronate in humans is very low, approximately 0.64% (Karamustafa et al., 2008; Ezra & Golomb, 2000). Preparation of clear, homogenous microemulsion (ME) warrants sodium alendronate trihydrate to have a sufficient solubility in the combined mix of excipients forming the microemulsion. Although a microemulsion could improve bioavailability significantly, taking into consideration the current low oral bioavailability of alendronate, an increase leading to oral bioavailability of approximately 25% would be a significant achievement. Assuming this bioavailability, the solubility of sodium alendronate trihydrate needs to be at minimum 2.34 mg per ~1 ml/1 g (one capsule) of microemulsion formulation (Table 6.10). The experiments performed clearly demonstrated that the solubility of alendronate in the lipid based microemulsions is very poor (well below 1 mg/g) and therefore preparation of clear, homogenous liquid microemulsions that could be equivalent to Fosamax doses is not feasible unless the oral bioavailability of alendronate from these formulations was significantly higher than 25%.

Table 6.10. Estimated load of sodium alendronate trihydrate to be dissolved into a liquid microemulsion assuming 25% oral bioavailability.

Fosamax doses: sodium alendronate trihydrate	Current oral bioavailability from Fosamax	Amount of the drug delivered to the systemic circulation	Oral bioavailability from a microemulsion (a significant increase assumed)	Required drug dose to be dissolved into a microemulsion (~1ml/1g)
The lowest dose: **6.53 mg**	0.64 %	~0.0418 mg	25%	**~ 0.167 mg**
The highest dose: **91.37 mg**	0.64 %	~0.5848 mg	25%	**~ 2.34 mg**

In the case of sodium pamidronate pentahydrate, a possibility to prepare microemulsions equivalent to the commercial forms of Aredia looks even less realistic. Aredia is available in 30 mg or 90 mg vials for intravenous administration. Oral bioavailability of pamidronate in humans was reported to be between 0.3-0.48% (Ezra & Golomb, 2000). Oral doses of disodium pamidronate of 150 – 300 mg were effective in preventing bone loss at both the lumbar spine and femoral neck in patients with established vertebral osteoporosis in the study performed by Ryan et al. (2000). Roldan et al. (2002) carried out a comparative clinical study between two enteric-coated formulations delivering a single dose of pamidronate 300 mg. Cheung et al. (1994) carried out a clinical trial with 300 mg

of pamidronate disodium in patients with postmenopausal osteoporosis. Brumsen et al. (2002) demonstrated a significant increase in bone mineral density of the lumbar spine and of the femoral neck when 150 mg/day of pamidronate were given for 3 years. Based on the studies presented above, the oral dose of pamidronate between 150- 300 mg appears to be suitable for treatment of osteoporosis, hypercalcemia and possibly osteolytic bone metastases of breast cancer. Assuming a significant improvement of oral bioavailability such as 25% with a microemulsion formulation, the solubility of disodium pamidronate pentahydrate would need to be at a minimum per ~1 ml/1 g (Table 6.11). Solubility of disodium pamidronate pentahydrate in the aqueous microemulsions was very low, well below 1 mg/g. Therefore the preparation of clear, homogenous liquid microemulsions with a sufficient drug load to match the doses used in the clinical studies (150-300 mg) appears to be unfeasible unless the oral bioavailability of pamidronate from these systems was almost 100%.

Table 6.11. Estimated load of disodium pamidronate pentahydrate to be dissolved into a liquid microemulsion assuming 25% oral bioavailability.

Oral doses in the clinical studies (disodium pamidronate pentahydrate	Current oral bioavailability	Amount of the drug delivered to the systemic circulation	Oral bioavailability from a microemulsion (a significant increase assumed)	Required drug dose to be dissolved into a microemulsion (~1ml/1g)
150 mg	~0.4 %	~0.6 mg	25%	**~ 2.4 mg**
300 mg	~0.4 %	~1.2 mg	25%	**~ 4.8 mg**

Incorporation of pamidronic acid into a microemulsion (undertaken to explore an option if another chemical form of the model compound could be more soluble in the studied microemulsions) was not successful as the same low solubility (less than 1 mg/g) was seen. In addition, this approach may not be possible when dealing with other compounds that don't have chemical alternatives. In addition, substitution of highly water soluble drugs with its more hydrophobic alternative could potentially increase the drug load in lipid based formulations, but at the same time it may compromise solubility of the drug upon dilution, when the drug is released from a capsule. In the case of bisphosphonates (sodium salts) that belong to BCS class III, permeability appears to be the only limiting factor in oral absorption and using more hydrophobic alternatives may decrease aqueous solubility and therefore worsen the oral bioavailability.

In the case of hydrophilic compounds such as bisphosphonates, preparation of a suspension could be a potential solution to overcome the solubility limit if the drug load is not very high. Nevertheless, there are a number of formulation challenges associated with preparation of stable suspension. Sedimentation of the drug followed by crystallisation onto the bottom of the shell that severely affects capsules stability could be one of major concerns. Use of micronized drug and

addition of thickening agents are typical formulation approaches to overcome this issue (Aulton, 2002). Addition of thickening agents and the presence of large doses of the drug suspended, effectively reduce the amount (the volume) of the lipid formulation that can be encapsulated. The encapsulation process of suspensions is significantly more complex compared to filling of solutions and microemulsions as a lack of flowability and segregation of suspended particles are common (Meissonnier, 2007). Preparation of suspensions with proteins and peptides is also not recommended as stability of these materials could be severely compromised by micronisation and high shear mixing typically required to prepare a homogenous suspension.

Acyline as a potent GnRH antagonist, has been investigated for the treatment of sex steroid hormone-dependent diseases (Herbst et al., 2002; Hild et al., 2004). The drug was found to inhibit gonadotropins and testosterone levels in men for 48 h after a single dose up to 75µg/kg was given subcutaneously (Herbst et al., 2002; Herbst et al., 2004). Acyline had not been previously administrated intravenously and orally in human and animals. Assuming that subcutaneous injection delivers approximately 50% of the dose, the total dose given by injection is approximately 2.625 mg (per adult, ~ 70kg). A substitution of one acyline injection (75µg/kg) with a single oral dosage form would require a minimum drug dose of 10 mg if the oral absorption is good i.e. 25%. The liquid SEDDSs developed for acyline showed physical instability (gelling) that was dose and temperature dependent and the formulations containing 10 mg of acyline developed gelling quite rapidly. Gelling had a highly negative effect on acyline solubility and release from the gelled formulations. It was suspected that gelled formulations would not show a satisfactory oral bioavailability and would underperform *in vivo* compared to the original, liquid formulations. Oral bioavailability from the gelled formulations *in vivo* was not investigated, however, when the acyline release from the gelled formulation was tested in phosphate buffer pH 6.8, with 1% of polysorbate 80 (Fig. 6.1), only approximately 30% of the drug was released after 30 minutes. For tamoxifen (BCS class II), a concentration as low as 0.175% of polysorbate 80 added to a dissolution medium was found to have similar 'solubilising effect' as the natural surfactants (Taupitz & Klein, 2010). Since release of acyline was very poor in the aqueous medium containing a much higher level of polysorbate 80 (1%), a significant improvement of acyline dissolution from the gelled formulations *in vivo* was not expected to occur in the presence of natural surfactants. Although the preclinical data demonstrated significantly improved absorption of acyline from the SEDDS formulations, long-term stability of the commercial product was questionable. In addition, the bench mark experiments did not reflect well enough the true encapsulation process where the 'water ingress' and elevated temperature during sealing and drying of capsules was likely to compromise physical stability of the drug even prior storage. A liquid SEDDS with acyline appeared unfeasible due to the limited physical stability as well as the limited drug load that could be dissolved in the lipid formulations.

As the drug load and stability appeared to be the main limitations in the successful development of microemulsions and non-aqueous microemulsions (SEDDSs) that could be applicable to a wide range of hydrophilic compounds, another formulation approach was undertaken. The next experiments in the following chapters investigated the development of a solid self-emulsifying drug delivery system, S-SEDDS (prepared via adsorption of liquid SEDDS onto a suitable solid carrier) as a potential solution to overcome the limitations of the liquid formulations.

Chapter 7

Characterisation of Solid Carriers

7.1. Introduction

Within last twenty years, porous adsorbents have been given a lot of attention due to their possible applications in drug delivery. Free flowing powders can be obtained from liquid formulations by adsorption onto solid carriers. The complexity and variety of porous materials has led to development and refinement of various methods for the determination of physical properties such as surface area and pore size distribution (Rouquerolt et al., 1994). The physicochemical properties of solid carriers are not only important in terms of enabling a high loading of liquid but also in achieving a long-term stability of dosage forms prepared via adsorption. Among the common carriers known to have a very large surface area attributed to their porosity, are calcium silicate, magnesium aluminometasilicate, silicon dioxide and carbon nanotubes. The chemical nature of these materials needs to be carefully considered when selecting a solid carrier. In adsorption, the contact between components of liquid formulation or a drug and a carrier surface, can lead to an interaction on the molecular level causing reduced chemical stability, e.g. the hydrolytic degradation of acetyl salicylic acid and the oxidative degradation of butylhydroxyanisole in dry silica adsorbates was caused by alkaline impurities of the adsorbent, while the oxidation of linoleic acid methylester in oleogels of colloidal silica was proved to be influenced both by carrier and its impurities (Daniels et al., 1986). On the other hand, a desirable interaction between a drug and an adsorbent could be developed if the properties of these components are well understood. Calcium silicates and silica gels are well known for their high moisture retention ability. When moisture is adsorbed, calcium silicate exhibits an alkaline pH in its local environment while silica gel exhibits a neutral pH. For acidic compounds such as ibuprofen and acetaminophen, loss of crystallinity and the enhanced dissolution behaviour was explained by dissolution of the drugs in the microenvironment and formation of hydrogen bonding between functional groups of the drug and the adsorbent (Madieh et al., 2007).

The aim of this work focussed on an investigation of the physical properties of various adsorbents (solid carriers) in order to identify the most suitable materials for development of solid self-emulsifying lipid formulations (SELFs). Six solid carriers: Sylysia 320 (silcon dioxide), Aeroperl 300/30 (silicon dioxide), Zeofree 5161 (silicon dioxide), Hubersorb 600 (calcium silicate), Fujicalin SG (dibasic calcium phosphate anhydrous), Neusilin US2 (magnesium aluminometasilicate) were chosen for the evaluation. Some of them have been previously used as adsorbents e.g. Neusilin US2 (Agarwal et al., 2009; Ito et al., 2005), Sylysia 320 (Ito et al., 2005), Aeroperl 300/30 (Goncalves & Rigassi, 2006). The others (Zeofree 5161, Hubersorb 600 and Fujicalin SG) are suitable for adsorption according to the suppliers. Once received, all materials except for Sylysia 320, were non-agglomerated, uniform in terms of physical appearance and therefore used as received. The received sample of Sylysia 320 was partially agglomerated into large (approx 0.5-3 cm) but brittle lumps. To ensure physical uniformity of this material during characterisation and processing, the material was manually sieved through a 180 μm screen, which

eliminated the lumps but was unlikely to reduce the primary particle size of the material (the average particle size between 2.9 - 3.5 μm according to the supplier's specification).

7.2. Scanning electron microscopy (SEM)

Scanning electron microscopy (SEM) analysis revealed significant variations between the selected solid carriers. Sylysia 320 consisted of multiple agglomerates formed with very small particles (Fig. 7.1. a, c, & d). The particle size of Sylysia 320 ranged from 1 to 6μm, with the majority of particles being around 3μm.

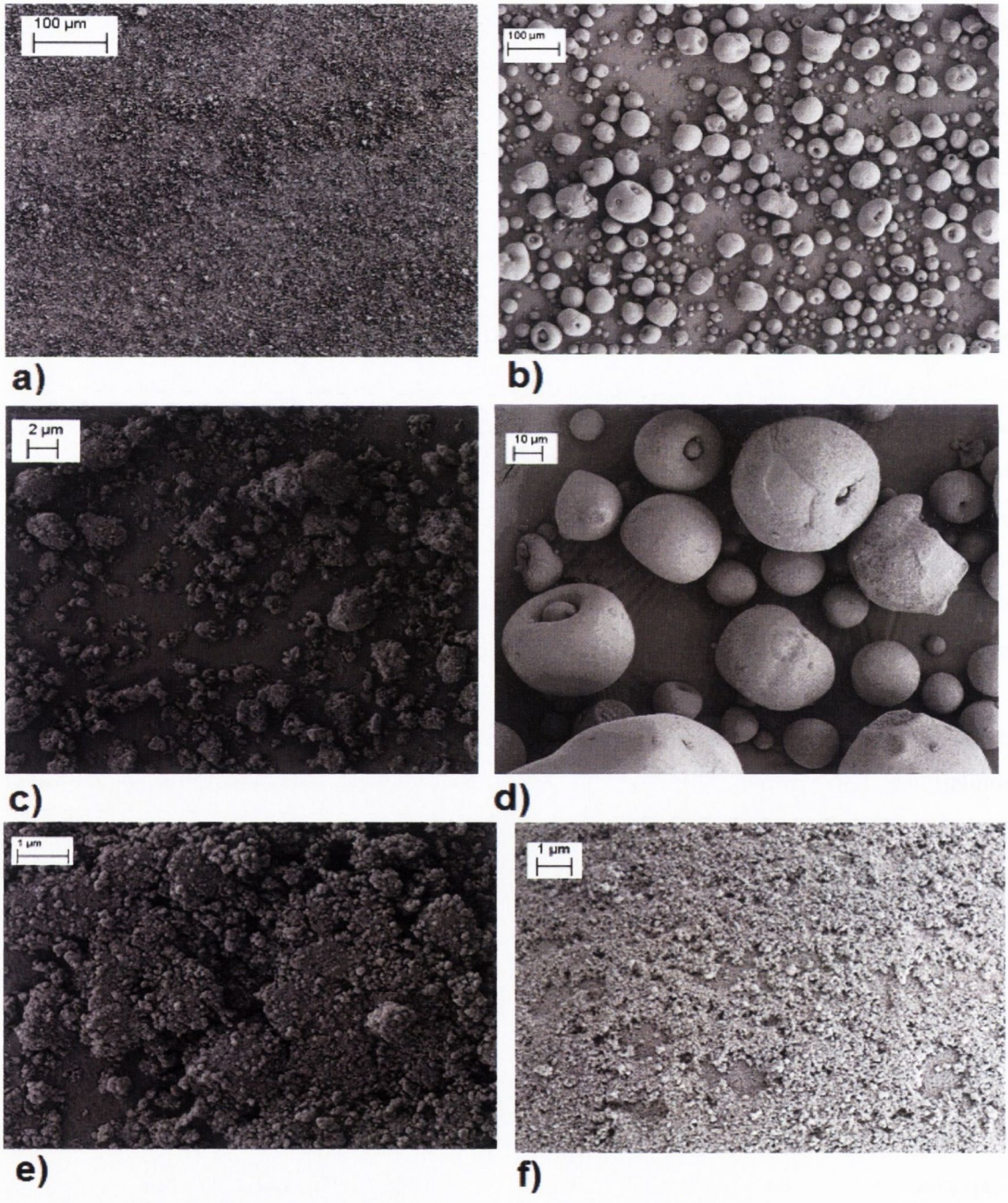

Fig. 7.1. SEM images of Sylysia 320 (a, c & e) and Aeroperl 300/30 (b, d & f)

Aeroperl 300/30 consisted of very round, spherical particles ranging from 10 to 100 μm, with the majority of particles between 30 and 50μm (Fig. 7.1.b, d & f). Close examination of the particle surface revealed a rough surface, as if the large particles were coated with very small, very fine grains (Fig. 7.1.c). Zeofree 5161 consisted of rounded particles ranging from 10 to 60 μm, with the majority of particles between 20 and 30μm (Fig. 7.2.a, b, c). The particles of Zeofree 5161 were less spherical compared to the particles seen with Aeroperl 300/30. The surface of particles appeared to be more porous when compared to Aeroperl 300/30.

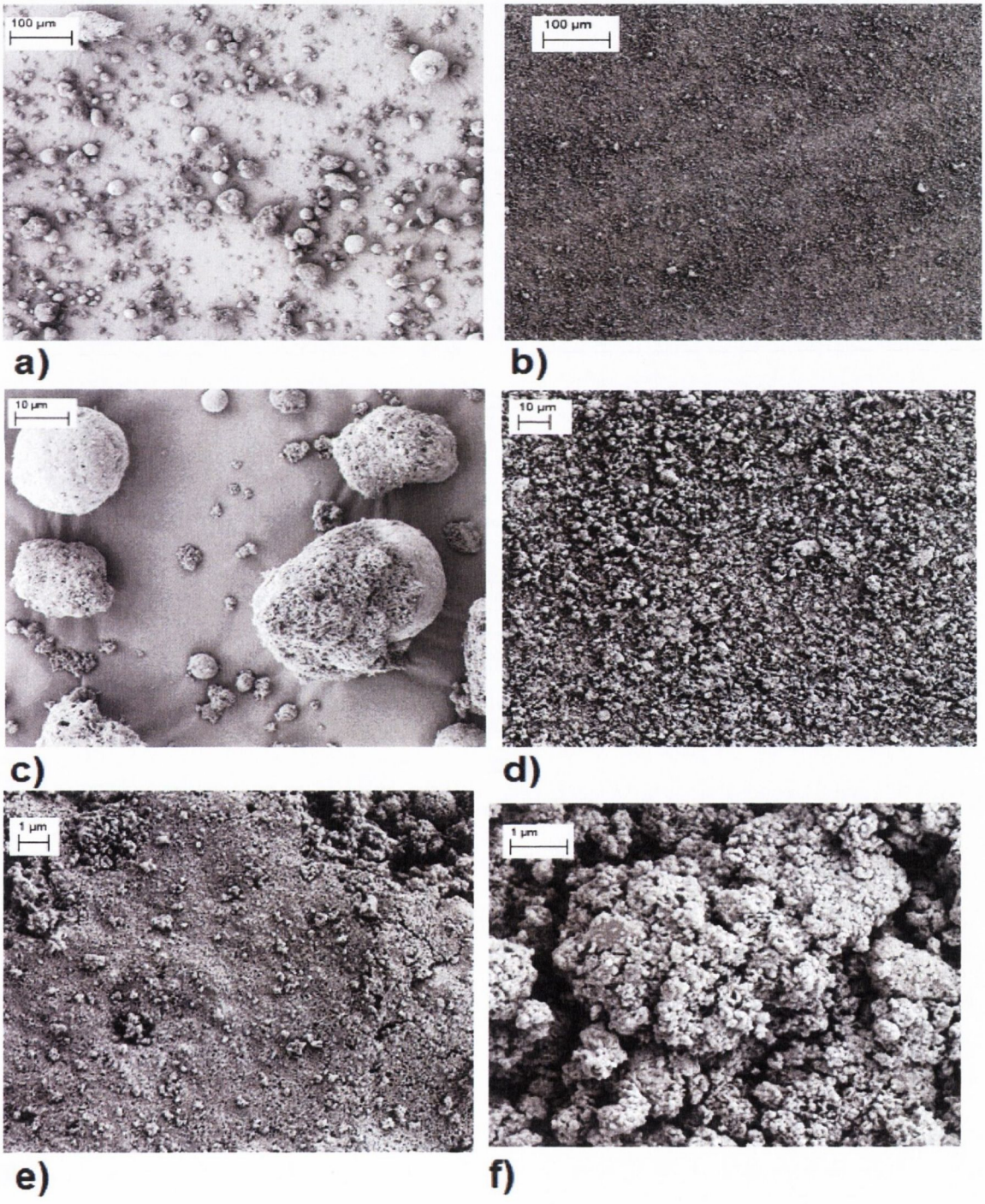

Fig. 7.2. SEM images of Zeofree 5161 (a, c & e) and Hubersorb 600 (b, d & f)

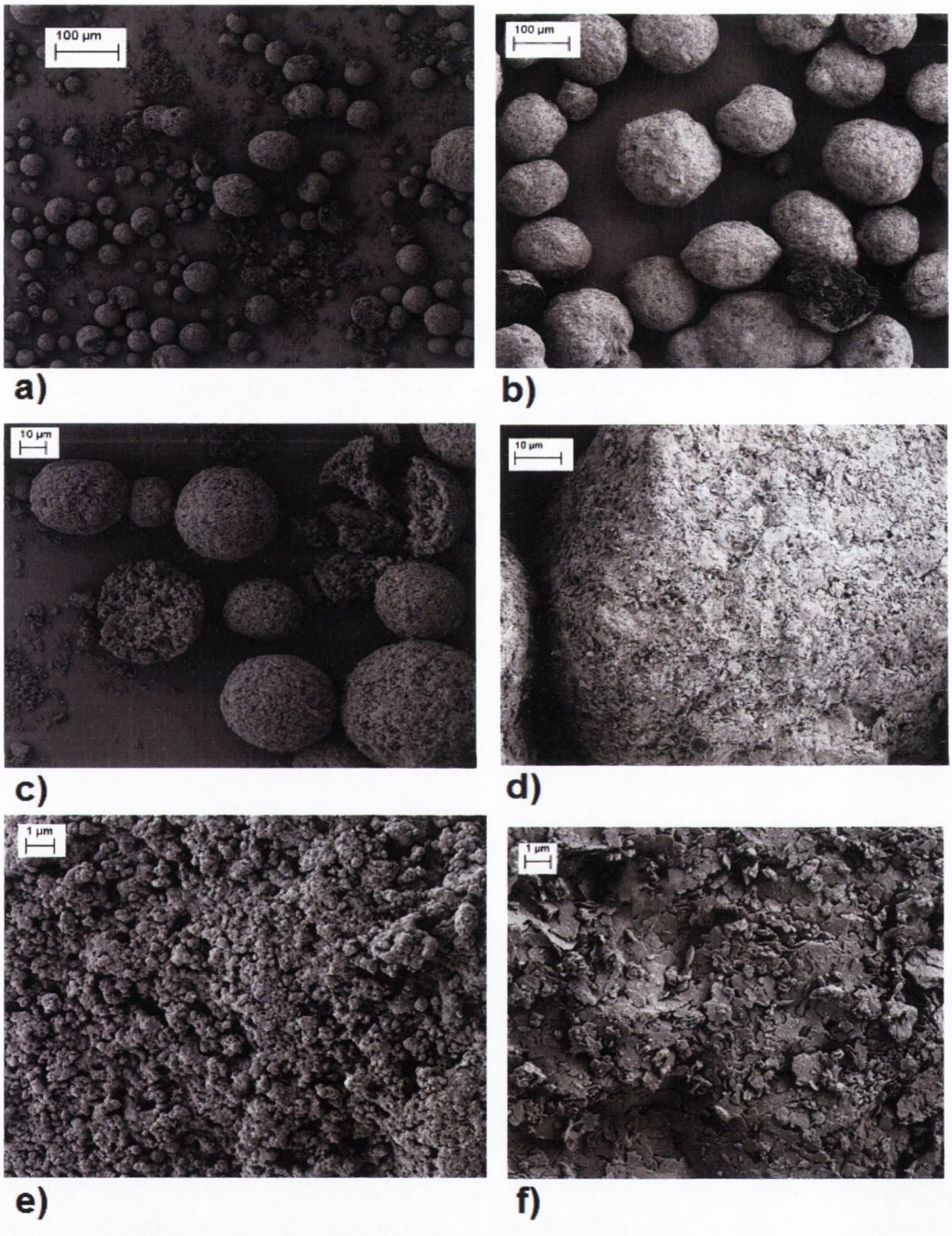

Fig. 7.3. SEM images of Neusilin US2 (a, c & e) and Fujicalin SG (b, d & f).

Hubersorb 600 consisted of very small, irregular in shape particles that ranged in size from 1 to 5µm (Fig. 7.2.b, d, f). Neusilin US2 was made of perfectly round, spherical, large particles ranging from 10 to 100 µm, with the majority of particles between 70 and 80µm. The surface as well as the interior of particles appeared to be highly porous (Fig. 7.3 a, c & e). Some damaged, split agglomerates could be observed on the SEM images (Fig. 7.3. a & c). Fujicalin SG consisted of

round, coarse granules ranging from 50 to 150 μm, with the majority of particles between 80 and 100 μm (Figure 7.3. d, e & f). The particles appeared quite solid and compacted, neither the surface of particles nor the inside of particles looked porous (Fig. 7.3.b). Only a few broken particles were observed. Among the examined solid carriers, Fujicalin SG and Neusilin US2 appeared to be coarser materials compared to the rest of the adsorbents and they also appeared to differ one from another with regard to porosity. Sylysia 320 and Hubersorb 600 were very fine materials, highly agglomerated materials.

7.3. Particle sizing by laser diffraction (PSD)

Particle size distribution (PSD) measured for Sylysia 320 was monomodal, uniform (Fig. 7.4) and narrow with the lowest Span value among all the carriers (Table 7.1). Zeofree 5161 also showed a single peak in the particle size distribution, but the distribution was the broadest among the all carriers (Fig. 7.4, Table 7.1). Aeroperl 300/30, Neusilin US2 and Fujicalin SG showed bimodal size distributions showing a small peak of fine particles and the main peak representing larger particles (Fig. 7.4). PSD of Hubersorb 600 was also bimodal but a smaller peak was observed at a larger particle size range, suggesting the presence of larger particles, possible stronger agglomerates that were not broken apart by the dispersive pressure (Fig. 7.4, Table 7.1).

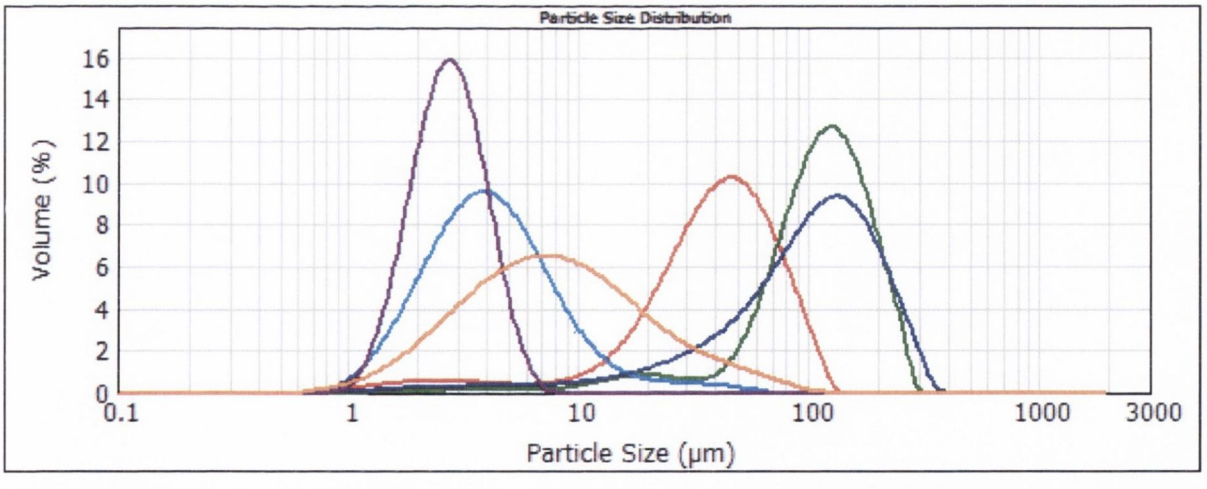

Fig. 7.4. Particle size distribution of Aeroperl 300/30 – red line, Zeofree 5161 – orange line, screened Sylysia 320 – purple line, Hubersorb 600 – sky blue line, Neusilin US2 – navy blue, Fujicalin SG – green line.

Table 7.1. Parameters computed form the PSD measured for the solid carriers.

Sample Name (Dispersive pressure/ feed rate)		Dv10 [µm]	Dv50 [µm]	Dv90 [µm]	Specific surface area (SSA_p) [m2/g] *	Span	D [4, 3] - Volume weighted mean [µm]	D [3, 2] - Surface weighted mean [µm]
Sylysia 320	**Average**	**1.7**	**2.7**	**4.4**	**1.096**	**0.985**	**2.9**	**2.6**
	SD	0.0	0.0	0.1	0.009	0.032	0.0	0.0
(2.0 bar/90%)	RSD	0.0	0.0	2.3	0.8	3.2	0.0	0.0
Aeroperl 300/30	**Average**	**14.3**	**41.0**	**80.3**	**0.146**	**1.611**	**44.5**	**18.8**
	SD	1.0	1.3	1.7	0.005	0.035	1.3	0.7
(0.2 bar/90%)	RSD	7.0	3.2	2.1	3.4	2.2	2.9	3.7
Zeofree 5161	**Average**	**2.5**	**7.7**	**27.6**	**0.550**	**3.243**	**12.3**	**5.4**
	SD	0.0	0.1	0.7	0.005	0.066	0.3	0.0
(2.5 bar/90%)	RSD	0.0	1.3	2.5	0.9	2.0	2.4	0.0
Hubersorb 600	**Average**	**1.9**	**4.1**	**9.8**	**0.923**	**1.965**	**5.6**	**3.4**
	SD	0.0	0.1	0.4	0.018	0.068	0.3	0.1
(2.5 bar/40%)	RSD	0.0	2.4	4.1	2.0	3.5	5.4	2.9
Neusilin US2	**Average**	**26.9**	**106.2**	**217.6**	**0.072**	**1.798**	**115.6**	**39.4**
	SD	1.7	4.5	6.2	0.006	0.041	4.1	3.3
(0.2 bar/90%)	RSD	6.3	4.2	2.8	8.3	2.3	3.5	8.4
Fujicalin SG	**Average**	**52.5**	**115.9**	**200.7**	**0.032**	**1.280**	**121.2**	**67.7**
	SD	5.0	3.6	4.1	0.004	0.050	3.8	7.4
(0.2 bar/50%)	RSD	9.5	3.1	2.0	12.5	3.9	3.1	10.9

* True density values were used to compute the estimated SSA_p values from the PSD.

Particle size distribution (Table 7.1) differed among the materials and was consistent with the SEM analysis. Based on Dv50 values, the materials could be ranked from the smallest to the largest particle size in the following order: Sylysia 320, Hubersorb 600, Zeofree 5161, Aeroperl 300/30, Neusilin US2 and Fujicalin SG. With regard to the estimated Specific Surface Area (SSA_p) from the particle size data, the materials could be ranked from the smallest to the largest SSA_p in the opposite order, as the specific surface of particles was inversely proportional to the particle size.

7.4. Specific Surface Area (BET) and Porosity

The full isotherms with adsorption and desorption plots were obtained for the solid carriers (Fig. 7.5). The isotherms of Zeofree 5161 (Fig. 7.5.C), Hubersorb 600 (Fig. 7.5.D) and Fujicalin SG (Fig. 7.5.F) were classified as type II as per IUPAC classification system for sorption isotherms (Sing et al., 1985) discussed briefly in Chapter 1, section 1.5.1.2. Type II isotherm is most commonly associated with macroporous and non-porous adsorbents (Sangwichien et al., 2002; Sing et el., 1985).

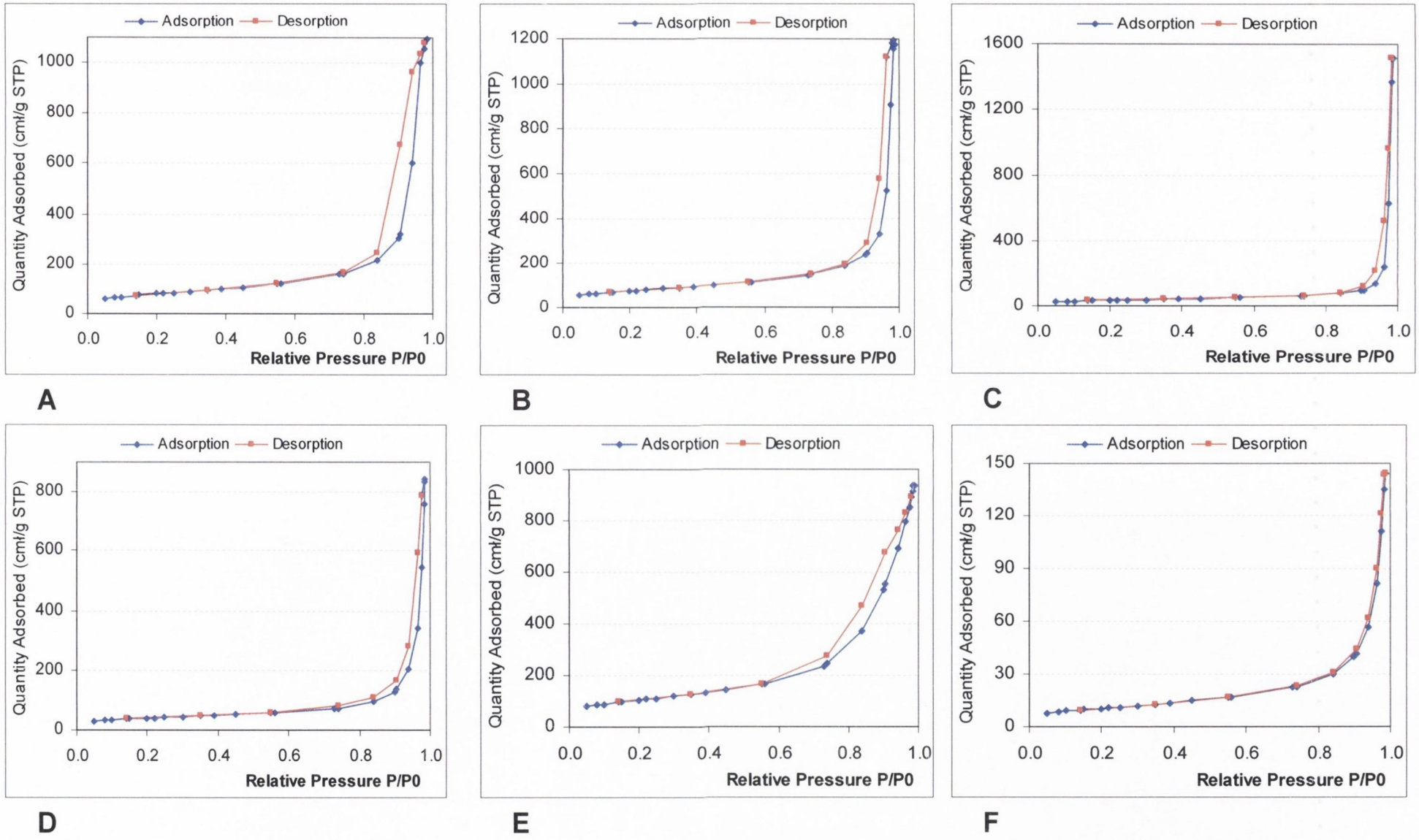

Fig. 7.5. Isotherm linear plot: Sylysia 320 (A), Aeroperl 300/30 (B), Zeofree 5161 (C), Hubersorb 600 (D), Neusilin US2 (E), Fujicalin SG (F).

Table 7.2. BET and t-plot results for the solid carriers.

Sample Name	BET Specific Surface Area (SSA_{BET}) [m^2/g]			t-plot External Surface Area (t-plot ESA)[m^2/g]			t-plot Micropore Area [m^2/g]			t-plot Micropore Area /SSA_{BET} x 100%	t-plot Micropore Volume [cm^3/g]		
	Average	SD	RSD	Average	SD	RSD	Average	SD	RSD		Average	SD	RSD
Sylysia 320	**282.3447**	0.4753	0.2	**246.023**	0.8428	0.3	**36.3218**	0.3675	1.0	13	**0.017080**	0.000199	1.2
Aeroperl 300/30	**263.1594**	5.5789	2.1	**229.0428**	4.1441	1.8	**34.1166**	1.4349	4.2	13	**0.015846**	0.000702	4.4
Zeofree 5161	**116.3604**	0.3349	0.3	**94.3739**	0.0141	0.0	**21.9866**	0.3208	1.5	19	**0.010865**	0.000204	1.9
Hubersorb 600	**138.8347**	3.4510	2.5	**113.8308**	3.1630	2.8	**25.0039**	0.2881	1.2	18	**0.012123**	0.000202	1.7
Neusilin US2	**359.0143**	11.1472	3.1	**342.6131**	11.1116	3.2	**16.4012**	0.0356	0.2	5	**0.006677**	0.000030	0.4
Fujicalin SG	**36.597**	1.0106	2.8	**37.3333**	0.3700	1.0	**0.12**	0.1697	141.4	0	**0.000000**	0.000000	/

Table 7.3. BJH pore size distribution analysis (based on the desorption isotherm)

Sample Name	BJH Desorption cumulative surface area of pores [m2/g]			BJH Desorption cumulative volume of pores between 17-3000 Å width [cm3/g]			BJH Desorption average pore width [Å]		
	Average	SD	RSD	Average	SD	RSD	Average	SD	RSD
Sylysia 320	**426.995**	0.000	0.0	**1.623050**	0.026982	1.7	**152.044**	2.527	1.7
Aeroperl 300/30	**332.377**	13.774	4.1	**1.771934**	0.047800	2.7	**213.308**	3.087	1.4
Zeofree 5161	**126.262**	11.100	8.8	**0.612705**	0.265108	43.3	**191.154**	67.183	35.1
Hubersorb 600	**170.664**	18.446	10.8	**0.767478**	0.216225	28.2	**178.183**	31.420	17.6
Neusilin US2	**653.722**	23.712	3.6	**1.261802**	0.043199	3.4	**77.210**	0.157	0.2
Fujicalin SG	**48.807**	1.331	2.7	**0.134603**	0.007234	5.4	**110.275**	2.922	2.6

The isotherms obtained for Sylysia 320 (Fig. 7.5.A), Aeroperl 300/30 (Fig. 7.5.B) and Neusilin US2 (Fig. 7.5.E), showed a shallow hysteresis loop at the high values of relative pressure P/P_0 which suggested type IV materials, commonly mesoporous solids (Sing et al., 1985; Sangwichien et al., 2002). Describing a material as microporous, mesoporous or macroporous, one refers to the size of pores in the material (Chapter 1, section 1.5.1.2). Specific Surface Area (SSA_{BET}) computed according to BET method is shown in Table 7.2. DeBoer T-Plot method was used to determine the external surface area and micropore area (Table 7.2), while the mesopore volume and mesopore diameter were calculated using Barrett, Joyner, and Halenda method (desorption isotherms) that assumes cylindrical pore geometry (Rocha et al., 2010). Based on the shape of the isotherms, none of the carriers was highly microporous and this was confirmed by very limited micropore area (less than 20% of the overall surface (SSA_{BET})). Values of cumulative surface area of pores and cumulative volume of pores were significantly higher for Sylysia 320, Aeroperl 300/30 and Neusilin US2 compared to the other materials (Table 7.3) which confirmed their mesoporous characters as previously suggested by the shape of the isotherms. Based on the cumulative volume of pores, the materials could be ranked from the most to the least mesoporous in the following order: Aeroperl 300/30, Sylysia 320, Neusilin US2, Hubersorb 600, Zeofree 5161, Fujicalin SG. In terms of the average pore width, the smallest pore opening between 8 and 11 nm, was calculated for Neusilin US2 and Fujicalin SG while the rest of the adsorbents showed slightly wider pore diameter in a range from 15 to 21 nm (Table 7.3). Neusilin US2, Sylysia 320 and Aeroperl 300/30 showed the largest t-plot External Surface Area values, which were 342.6131, 246.023 and 229.0428 m^2/g respectively. Although these values appeared to be very similar for Sylysia 320 and Aeroperl 300/30, the particle size distribution for these materials was very different. When the ratio between the t-plot External Surface Area (t-plot ESA) and Specific Surface Area (SSA_p) was calculated, Neusilin US appeared to be the most mesoporous material (Fig. 7.6.). Although, Fujicalin SG showed the lowest value of t-plot External Surface Area (t plot ESA = 33.3 m^2/g) among the tested solid carriers, it could be considered as more mesoporous than Hubersorb 600, Sylysia 320 screened and Zeofree 5161 when the particle size of this carrier was taken into consideration. As a coarse material, with the large particles it showed relatively small t-plot ESA and SSA_p but the calculated ratio indicated that these large particles were relatively more porous than particles of other three carriers. Hubersorb 600, Sylysia 320 and Zeofree 5161 appeared to show a large surface area (t-plot ESA) mainly due to their small particle size. The estimation of porosity related to PSD by the ratio t-plot-ESA/SSA_p may not be very accurate (especially if materials are not spherical), however it allows for more relative comparison between materials that differ significantly in particle size. Understanding whether a large surface area is related mainly to the porosity (void spaces in the material particles) or the surface area of small, but relatively non-porous particles, should help to understand how liquid would be distributed in the adsorption process onto those particles.

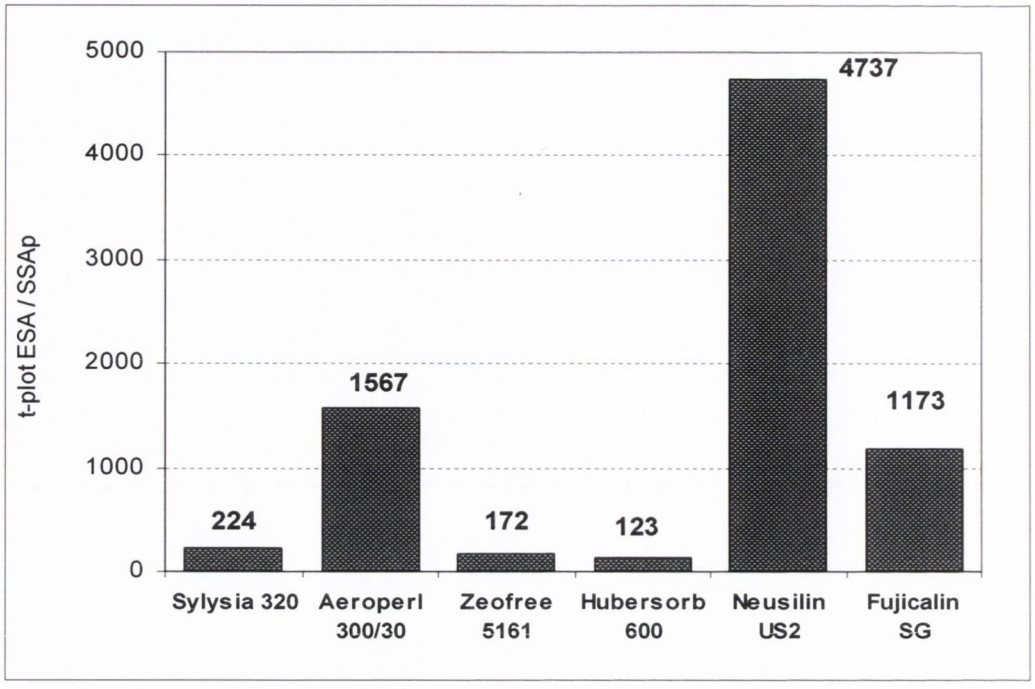

Fig. 7.6. Ratio between t-plot External Surface Area (t-plot ESA) calculated from gas adsorption data and Specific Surface Area (SSA_p) computed from particle sizing.

7.5. Bulk and tapped density

The solid carriers were characterised for bulk and tapped density and flow character, expressed as Compressibility Index and/or Hausner Ratio. Compressibility Index and/or Hausner Ratio represent one of several approaches to assess flowability of powders and granules. As with other methods, this evaluation is somewhat limited and doesn't comprehensively characterise the flow characteristics of various samples but can provide an insight on interparticulate interactions.

The solid carriers varied significantly in their density and flow properties. Sylysia 320 and Hubersorb 600 were the lightest materials (Table 7.4). Their highly cohesive behaviour was reflected by very poor flow characteristics. Fujicalin SG and Neusilin US2 were the materials with best flow. Despite having a very low bulk and tapped density values, Neusilin US was as flowable as Fujicalin SG, which was at least twice as dense as Neusilin US2. Both materials had similar particle size distribution and particle shape, so the density difference could be explained by the higher porosity of Neusilin US2.

Table 7.4. Comparison of bulk/ tapped density and flow characteristic of the solid carriers.

Sample Name		Bulk density [g/ml]	Tapped density [g/ml]	Compressibility Index	Hausner Ratio
Sylysia 320	**Average**	**0.06**	**0.08**	**22**	**1.28**
	SD	0.00	0.00	1.4	0.03
	RSD	0.0	0.0	6.4	2.3
	Flow character			Passable	Passable
Aeroperl 300/30	**Average**	**0.22**	**0.28**	**22**	**1.27**
	SD	0.00	0.00	0.7	0.01
	RSD	0.0	0.0	3.2	0.8
	Flow character			Passable	Passable
Zeofree 5161	**Average**	**0.14**	**0.20**	**31**	**1.45**
	SD	0.01	0.00	0.0	0.00
	RSD	7.1	0.0	0.0	0.0
	Flow character			Poor	Poor
Hubersorb 600	**Average**	**0.09**	**0.15**	**40**	**1.65**
	SD	0.00	0.01	2.1	0.06
	RSD	0.0	6.7	5.3	3.6
	Flow character			Very poor	Very poor
Neusilin US2	**Average**	**0.16**	**0.19**	**15**	**1.17**
	SD	0.00	0.01	2.1	0.04
	RSD	0.0	5.3	14.0	3.4
	Flow character			Good	Good
Fujicalin SG	**Average**	**0.45**	**0.52**	**13**	**1.15**
	SD	0.01	0.01	2.8	0.04
	RSD	2.2	1.9	21.5	3.5
	Flow character			Good	Good

7.6. pH measurements

All the solid carriers were water insoluble, therefore measurements of slurries provided information about residues on the surface of these materials and how they affected pH of water. Strong acidic or alkaline character of materials present on the surface of an adsorbent is something to consider with regard to the long term-stability of solid microemulsions or other solid self-emulsifying systems prepared by adsorption where an undesirable interaction between the adsorbate and the adsorbent could occur. Two grades of silicon dioxide, Sylysia 320 and Zeofree 5161 appeared to be almost neutral, while the third grade of silicon dioxide, Aeroperl 300/30 was found to be slightly acidic. This suggested that Aeroperl 300/30 might have been manufactured using a different method, which left a different type of impurity in the final product. Neusilin US2 and Fujicalin SG showed neutral and moderately acidic pH respectively. The slurry of Hubersorb 600 (Table 7.5) was very highly alkaline, which was due to residues of lime (calcium oxide or/and calcium hydroxide) that remained in the material after reacting lime with a precipitated silicon dioxide to form calcium silicate (Phillips, 2009).

Table 7.5. Comparison of pH measured in slurries of the solid carriers.

Sample Name	pH (3 hours post preparation)			pH (24 hours post preparation)		
	Average	SD	RSD	Average	SD	RSD
Sylysia 320	**6.85**	0.04	0.6	**7.43**	0.16	2.2
Aeroperl 300/30	**4.76**	0.11	2.3	**4.86**	0.02	0.4
Zeofree 5161	**6.78**	0.03	0.4	**7.19**	0.01	0.1
Hubersorb 600	**10.06**	0.06	0.6	**10.44**	0.08	0.8
Neusilin US2	**7.38**	0.14	1.9	**7.64**	0.07	0.9
Fujicalin SG	**5.79**	0.04	0.7	**5.77**	0.04	0.7

7.7. Solid state Fourier transform infrared spectroscopy (FTIR)

Solid state Fourier transform infrared spectroscopy (FTIR) analysis was carried out to investigate any further differences between the three grades of silicon dioxide. Silica is a substance of acidic and hydrophilic character reflecting its surface structure comprising silanol (Si–OH) and siloxane (Si–O–Si) groups. Siloxane groups ('bridges') appear as a result of condensation of free silanol groups at the elevated temperature (Siwinska-Stefanska et al., 2008). The IR spectrum of silica typically shows the most intense infrared band for the asymmetric stretching vibration of the siloxane group (Si–O–Si) around 1098 cm^{-1} (Jackson, 1998; Kim et al., 2009). Ying et al. (1992) reported SiO_2 overtone at 1640 cm^{-1}. Kim et al. (2009) identified the typical absorption peak for silica at 800 cm^{-1} for the symmetric stretching vibration of the siloxane group (Si–O–Si) using attenuated total reflection spectroscopy. Also, various researchers investigated the concentration and distribution of hydroxyl groups (silanol) on the silica surface. The hydroxyl groups on silica surfaces are important for various surface phenomena: adsorption of gases, dispersion in liquids, adhesion, surface reactions and wetting (Takei et al., 1999). The concentration and distribution of hydroxyl groups is directly related to the manufacturing process of silica. Hydrolysis followed by condensation is one of the most common manufacturing methods (Kim et al., 2009). Another common technique is the production of fumed silica by combustion of chlorosilanes in a hydrogen-oxygen flame (Zumbrum, 1994). In both cases, the final silica particles retain a number of hydroxyl groups on the surface. Several types of hydroxyl groups including isolated (single) silanols, germinal, and vicinal (hydrogen bonded) silanols appear to exist on the surface of silica particles (Fig. 7.7). However, it is ambiguous whether these three types (isolated, geminal and triple) of the hydroxyl groups on silica surfaces can be distinguished by their vibrational frequencies (Van Der Voort et al., 1991). The characteristic infrared peak for isolated (single) silanol groups is observed between 3745- and 3750 cm^{-1}.

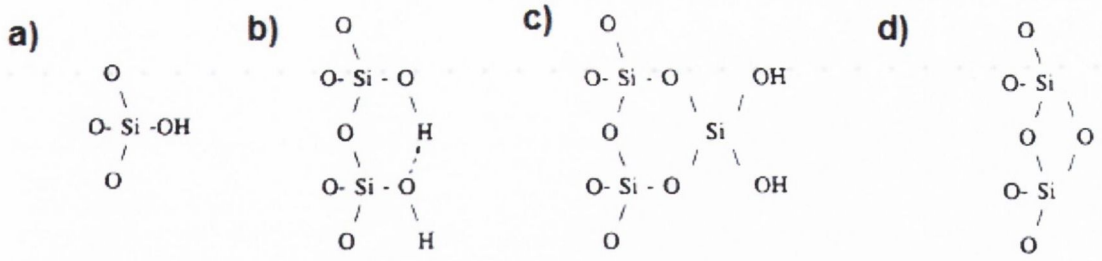

Fig. 7.7. The various types of hydroxyl group on the surface of silica gel: (a) free (isolated) OH, (b) vicinal (bridged) OH, (c) geminal OH, (d) siloxane bridge (Van Der Voort et al., 1991).

The geminal hydroxyl group can be detected around 3742 cm^{-1} and therefore some researchers concluded that isolated and geminal hydroxyl groups cannot be observed separately by means of infrared spectroscopy owing to a too small difference between the two peak positions (Chen et al., 1982; Van Der Voort et al., 1991). In addition, since the free hydroxyl band is known to shift as a function of temperature, it makes the differentiation between isolated and geminal groups less possible and any band detected between 3745 and 3750 cm^{-1} is likely to arise from a superposition of these two hydroxyl bands. The infrared band of physisorbed water is typically observed in the range 3400 - 3600 cm^{-1} (Van Der Voort et al., 1991; Zumbrum, 1994; Chen et al., 1982). In addition, the Si–OH stretching vibration band was reported at 953 cm^{-1} (Kim et al., 2009) and Si–OH peak at 973 cm^{-1} (White et al., 2000).

The FTIR data collected for Aeroperl 300/30, Zeofree 5161 and Sylysia 320 are shown in Fig. 7.8 and the interpretation of peaks and bands is reported Table 7.6.

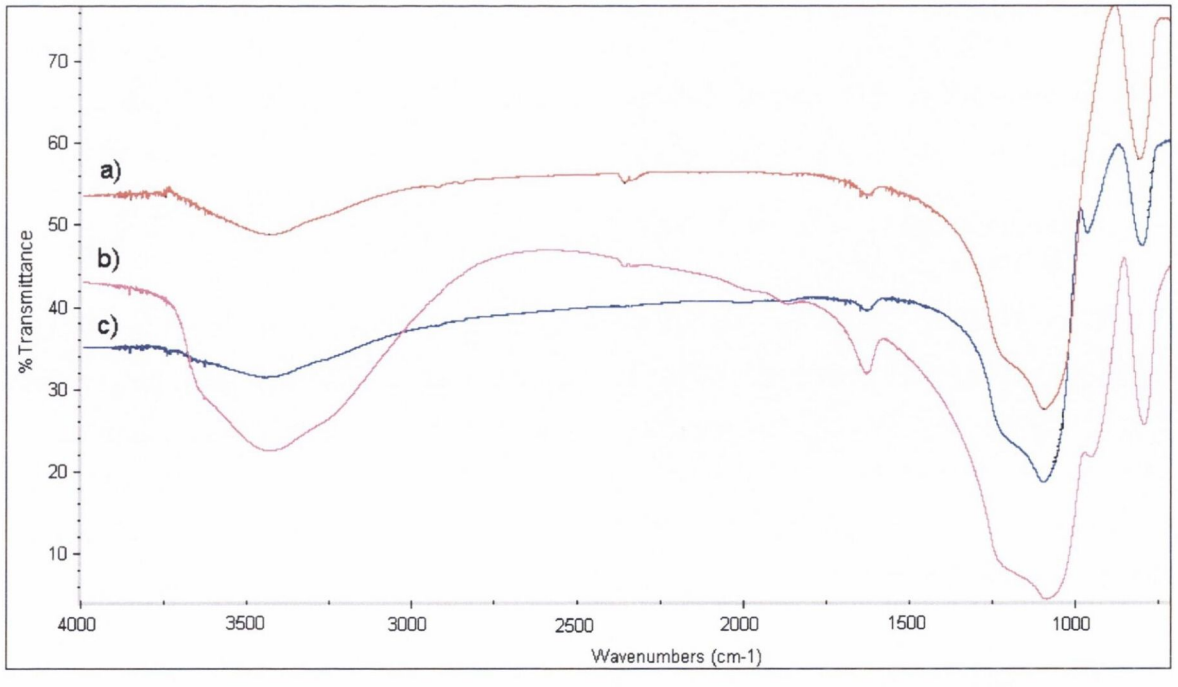

Fig. 7.8. Overlaid FTIR spectra of a) Aeroperl 300/30, b) Zeofree 5161 and c) Sylysia 320.

Table 7.6. Identification of main peaks in FTIR spectrum of the grades of silicon dioxides

Detected peaks						Explanation
Aeroperl 300/30		Sylysia 320		Zeofree 5161		
3743.61	Only detected with increased sensitivity	**3744.96**	Only detected with increased sensitivity	**3744.83**	Only detected with increased sensitivity	*Extremely small peaks likely caused the bound water, although superimposed isolated and geminal hydroxyl groups would be typically observed at 3745 -3750 cm^{-1}*
3430.76	broad, shallow	**3445.09**	broad, shallow	**3430.65**	broad, large	*Physisorbed water typically at 3400-3600cm^{-1}*
1096.53	broad, large	**1105.48**	broad, large	**1091.65**	broad, large	*Asymmetric stretching vibration (Si–O–Si) typically at 1098 cm^{-1}*
not present		**970.97**	sharp, small	**958.36**	sharp, small	*Si–OH stretching vibration typically at 953- 973 cm^{-1}*
813.84	sharp, large	**806.77**	sharp, large	**799.72**	sharp, large	*Symmetric stretching vibration (Si–O–Si) typically at 800 cm^{-1}*

An overtone band of the silicon-oxygen stretching vibrations was observed at 1640 cm-1 in all three samples. Each material contained some residual water. Based on the intensity of the peaks around 3430 $cm^{1,}$ (Fig. 7.8), it appeared that Zeofree 5161 contained the highest percentage of physisorbed water while Sylysia 320 and Aeroperl 300/30 appeared drier but comparable one to another. With the enhanced sensitivity, additional very small peaks were seen around 3430 cm^{-1}. Peaks within this region, could correspond to the superimposed isolated and geminal hydroxyl groups, however since the intensity of the detected peaks was extremely low, they were most likely caused by the physisorbed water. Additional peaks around 950 - 970 cm^{-1} associated with hydroxyl groups, were detected in Zeofree 5161 and Sylysia 320 but not in Aeroperl 300/30. Therefore, it appeared that the surface of Zeofree 5161 and Sylysia 320 was more hydrophilic (more hydroxyl groups present) in comparison to Aeroperl 300/30.

7.8. Thermal analysis (Differential scanning calorimetry & Thermal gravimetric analysis)

DSC and TGA analysis of Fujicalin SG didn't reveal any distinct thermal events. A gradual weight loss in this material of approximately 2.4% was observed in the temperature range from 25 – 350 °C (Table 7.7), which suggested that the material was quite dry, without residual moisture. The endothermic peak around 115 °C in the DSC spectrum of Hubersorb 600 was the most likely to be associated with the loss of residual moisture which was approximately 11% based on the TGA analysis (Table 7.7). Neusilin US2 as magnesium aluminometasilicate contains a certain percentage of hydrated water according to the supplier specification. Two thermal events were detected in this material (Table 7.7). The endothermic peak around 75 °C associated with the weight loss of approximately 8% was the most likely due to a removal of physisorbed water. The

second sharp peak detected at approximately 220 °C and associated with the weight loss of additional 8 % may have been associated with liberation of hydrated water.

Table 7.7. Summary of DSC and TGA results for the solid carriers.

Sample Name	DSC				TGA	
	Onset [°C]	Peak [°C]	Endset [°C]	Normalized energy [Jg-1]	Weight loss [%] associated with the peak	Overall weight loss in the range 25 to 350°C [%]
Sylysia 320	27.54	51.15	~100	-38.04	2.193	5.901
Aeroperl 300/30	27.11	55.96	~ 110	-48.54	0.414	1.662
Zeofree 5161	28.37	71.76	~140	-128.92	3.253	5.430
Hubersorb 600	26.69	116.74	~240	-374.59	10.763	12.900
Neusilin US2 (peak 1)	36.74	75.16	~160	-128.95	8.163	17.903
Neusilin US2 (peak 2)	197.16	221.42	~270	-94.98	8.170	
Fujicalin SG	N/A	N/A	N/A	N/A	N/A	2.422

Physisorbed water was previously detected in all three grades of silicon dioxide by FTIR and was also measured by DSC and TGA (Table 7.7). Based on the values of weight loss associated with the peaks, it appeared that Zeofree 5161 contained the highest percentage of residual water. This result was consistent with the observation made previously based on the FTIR data. Aeroperl 300/30 appeared to be the driest material as only approximately 0.4% of sample weight loss was measured up to 110 °C (Table 7.7). The residual moisture in the three grades of silicon dioxide was fully removed once the temperature of 140 °C was reached. No other thermal events at higher temperatures were detected (Fig. 7.9), although the TGA curves showed a continuous, steady-slow weight loss up to 350 °C of 3.7%, 1.2% and 2.2% for Sylysia 320, Aeroperl 300/30 and Zeofree 5161, respectively.

Several researchers reported two steps of weight loss for silicon dioxide. Kim et al. (2009) reported that the first rapid weight drop, occurred at 100 – 130°C due to dehydration meaning the removal of physisorbed water from the surface of the silica particles. The second step initiated above 190 ± 10 °C corresponded to dehydroxylation of the geminal and vicinal OH groups and formation of siloxane groups. This resulted in a significant weight drop for the silica particles across a broad temperature range from 200 up to about 600 °C. According to Van Der Voort et al. (1991) heating to temperatures below 127 °C removes physisorbed water and above this temperature silanols start to condensate and release additional water. According Sneh et al. (1995) neighbouring surface hydroxyls that are hydrogen-bonded together (vicinal) have been shown to desorb easily as water in the temperature range of 150 to 450 – 600 °C. Based on the findings of other researchers, the continuous weight loss recorded during TGA analysis for the grades of silicon dioxide in the

temperature range from approximately 100 °C (after the removal of the residual moisture) to 350 °C could be explained as gradual dehydroxylation.

When the dehydroxylation weight loss (considered as the further weight loss (%) recordered after the removal of residual moisture) was divided by the Specific Surface Area calculated by BET method (SSA_{BET}), Zeofree 5161 was found to have the 'highest packing' of hydrophilic groups on the surface. The ratio between dehydroxylated weight loss and the SSA_{BET} (Fig. 7.9) related the concentration of hydroxyl groups on the surface.

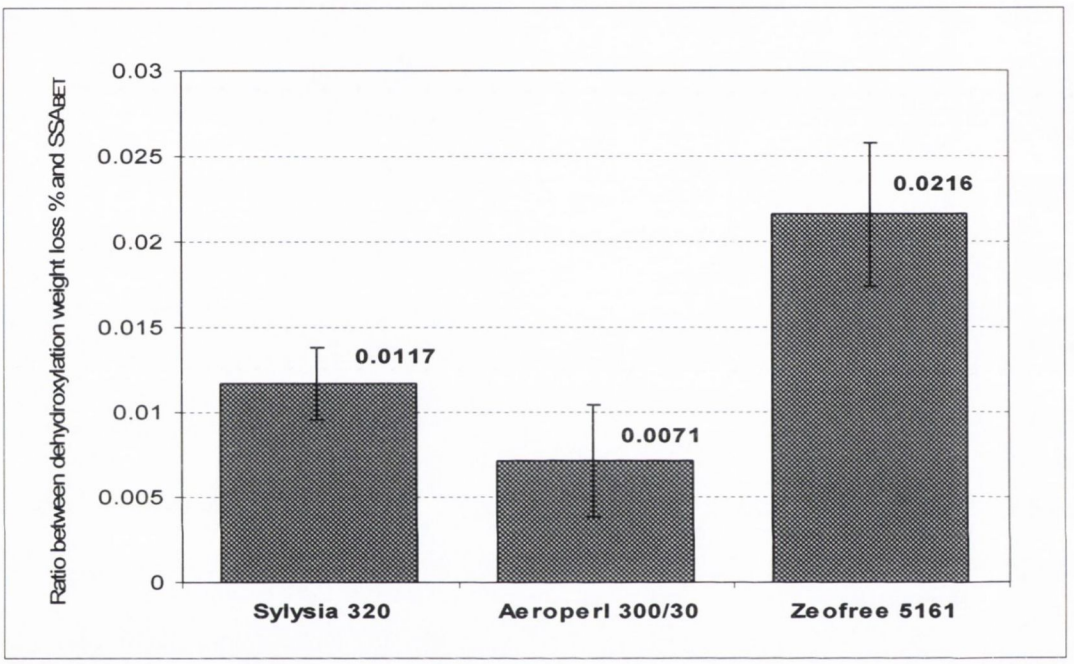

Fig. 7.9. Ratio between the dehydroxylation weight loss and the Specific Surface Area (SSA_{BET}) calculated from the gas adsorption data.

Although, the dehydroxylated weight loss (%) for Zeofree 5161 was lower than for Sylysia 320, the surface area of the former carrier was half that of the latter one. This suggested that a higher 'concentration' of hydroxyl groups per unit surface area was present in Zeofree 5161 compared to Sylysia 320. Aeroperl 300/30 appeared to release the lowest quantity of 'hydroxylated' water per unit surface area, meaning that its surface was likely to be already quite hydrophobic (many condensated siloxane groups already present).

7.9. Powder X-Ray Diffraction analysis (PXRD)

Sylysia 320, Aeroperl 300/30, Zeofree 5161 and Neusilin US2 were found to be amorphous based on their diffractograms (Fig. 7.10) which was consistent with the information supplied by the manufacturers. Hubersorb 600 appeared to be crystalline but few distinctive peaks were seen. Fujicalin SG was a crystalline material.

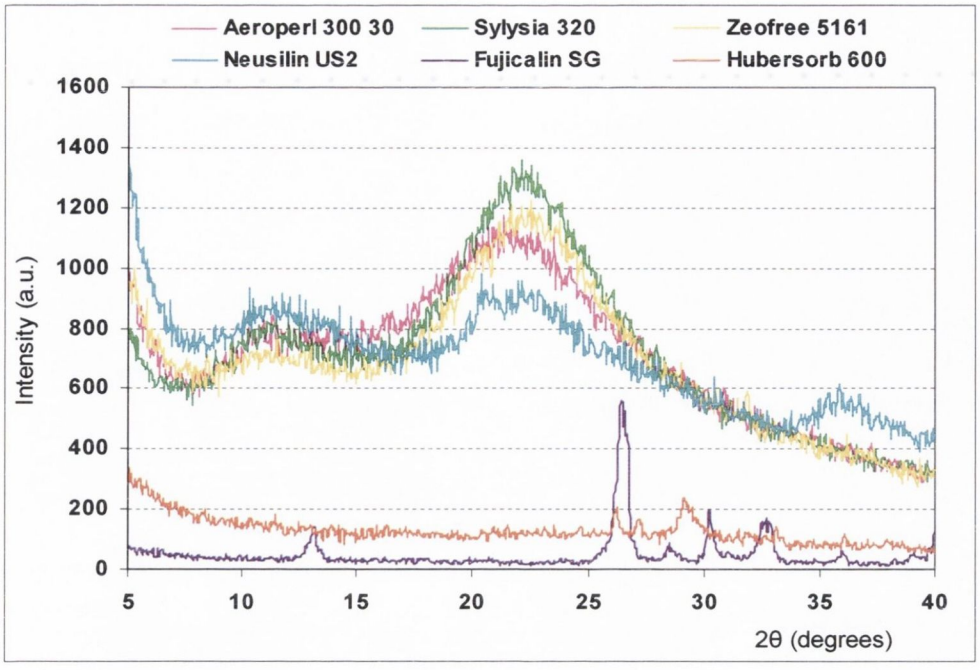

Fig. 7.10. XRD diffractograms of the solid carriers.

7.10. Adsorption Index

Adsorption Index was defined as the weight of added liquid required to form a paste-like mass divided by the weight of this paste-like mass multiplied by 100% (details presented in Chapter 2, section 2.7.10). The Adsorption Index was determined for the solid carriers using three different liquids. The two oils, Captex 355 and Capmul PG-8 that differed by hydrophilic/hydrophobic character (Chapter 4, section 4.2.1) were selected together with the preconcentrate 1B3_T4 40: 60 (the composition given in Chapter 6, Table 6.1). The selected liquids showed different viscosities at room temperature (Table 7.8) but were easily pourable and did not solidify during experiments.

Table 7.8. Properties of liquids used for Adsorption Index measured at room temperature.

Sample Name	Density [g/cm^3] at 20 °C			Absolute Viscosity [mPas] at 20 °C		
	Average	SD	RSD	**Average**	SD	RSD
Preconcentrate 1B3_T4 40: 60	**0.9893**	0.0000	0.0	**50.6**	0.6	0.0
Captex 355 EP/NF	**0.9490**	0.0002	0.0	**29.8**	0.1	0.0
Capmul PG-8	**0.9484**	0.0001	0.0	**15.2**	0.1	0.0

Viscosity and hydrophilicity of the liquids did not appear to significantly affect the adsorption/agglomeration and comparable values of Adsorption Index were obtained for each solid carrier when adsorbed with preconcentrate 1B3_T4 40: 60, Capmul PG-8 or Captex 355 (Table 7.9, Fig. 7.11). Fujicalin SG showed the lowest Adsorption Index among the carriers studied. A powder

sample of this material could adsorb a quantity of liquid equal to its own weight (AL = 100%) before a paste-like plastic mass was formed. Neusilin US2 was the most adsorptive material with the highest Adsorption Index of approximately 350%. The rest of the materials, Zeofree 5161, Aeroperl 300/30, Sylysia 320 and Hubersorb 600 showed lower Adsorption Indices (approximately 250 - 300%) compared to Neusilin US2, but they were still substantially better than Fujicalin SG.

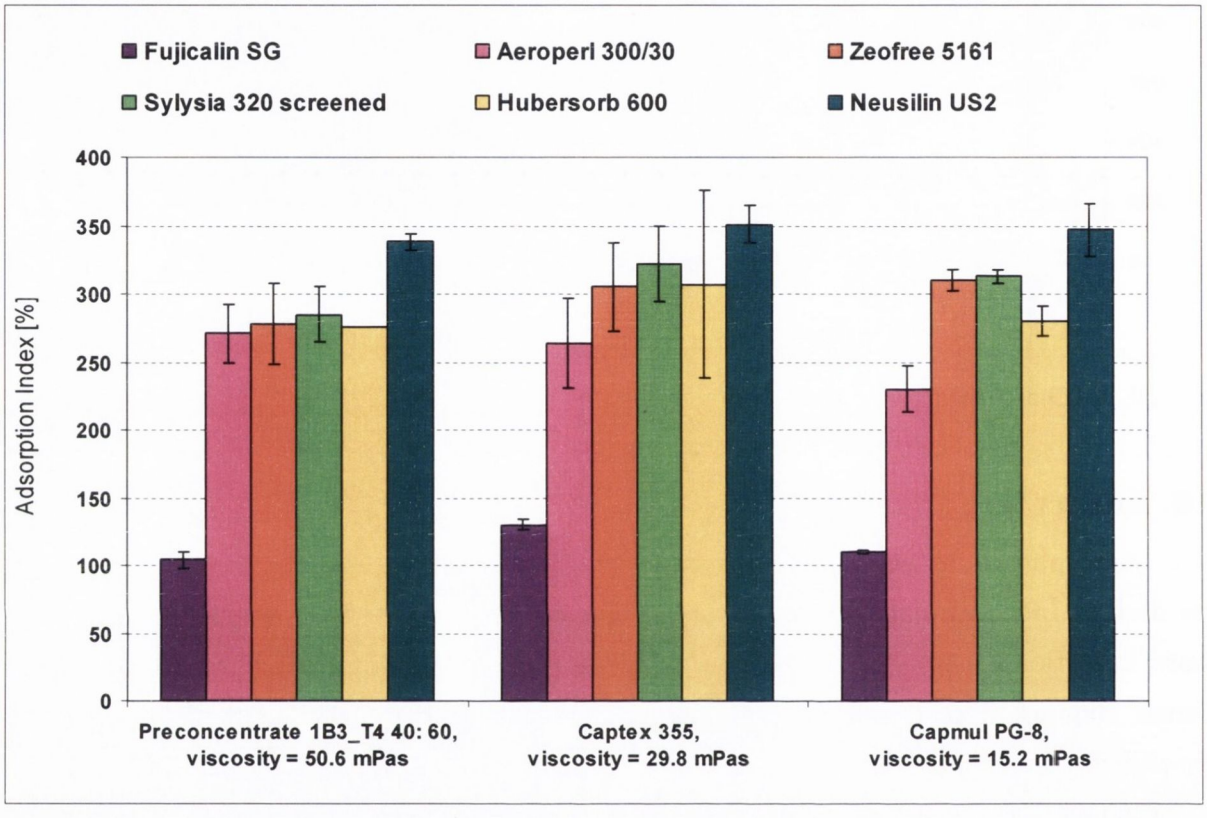

Fig. 7.11. Adsorption Index obtained with Capmul PG-8, Captex 355 and the preconcentrate 1B3_T4 40: 60.

Table 7.9. Determined values of adsorbed liquid (%) at various Adsorption stages and the final Adsorption Index (AI, stage = 6).

Sample Name	Preconcentrate 1B3_T4 40:60				Captex 355				Capmul PG-8			
	Adsorption stage	**Average % adsorbed**	**SD**	**RSD**	*Adsorption stage*	**Average % adsorbed**	SD	RSD	*Adsorption stage*	**Average % adsorbed**	SD	RSD
Sylysia 320	*2*	**196**	13	7	*2*	**165**	47	28	*1*	**124**	24	19
	3	**229**	6	3	*3*	**219**	4	2	*3*	**203**	23	11
	4	**272**	/	/	*4*	**241**	/	/	*4*	**286**	8	3
	5	**290**	/	/	*5*	**294**	17	6	*5*	**296**	6	2
	6	**285**	20	7	*6*	**322**	27	8	*6*	**313**	5	2
Aeroperl 300/30	*2*	**153**	0	0	*2*	**112**	22	20	*2*	**153**	0	0
	3	**178**	4	2	*3*	**151**	8	5	*3*	**179**	9	5
	4	**214**	3	1	*4*	**180**	4	2	*4*	**208**	1	0
	5	**248**	5	2	*5*	**227**	18	8	*5*	**222**	14	6
	6	**271**	21	8	*6*	**264**	33	13	*6*	**230**	17	7
Zeofree 5161	*2*	**168**	12	7	*2*	**142**	5	4	*2*	**195**	23	12
	3	**194**	1	1	*3*	**214**	9	4	*3*	**217**	8	4
	4	**238**	4	2	*4*	**255**	16	6	*4*	**270**	8	3
	5	**291**	/	/	*5*	**290**	35	12	*5*	**303**	8	3
	6	**278**	30	11	*6*	**305**	32	10	*6*	**310**	8	3
Hubersorb 600	*2*	**191**	/	/	*2*	**146**	/	/	*2*	**176**	/	/
	3	**206**	/	/	*3*	**198**	/	/	*3*	**222**	13	6
	4	**222**	4	2	*4*	**266**	/	/	*4*	**271**	42	15
	5	**260**	3	1	*4*	**255**	31	12	*5*	**271**	11	4
	6	**276**	0	0	*6*	**307**	69	22	*6*	**280**	11	4
Neusilin US2	*2*	**184**	15	8	*2*	**161**	29	18	*2*	**223**	23	10
	3	**223**	3	1	*3*	**226**	26	12	*3*	**240**	30	13
	4	**285**	8	3	*4*	**261**	23	9	*4*	**291**	2	1
	5	**320**	7	2	*5*	**306**	28	9	*5*	**326**	8	2
	6	**338**	6	2	*6*	**351**	14	4	*6*	**347**	19	5
Fujicalin SG	*2*	**49**	1	2	*2*	**56**	4	7	*2*	**68**	5	7
	3	**71**	4	6	*3*	**73**	1	1	*3*	**72**	4	6
	4	**81**	13	16	*4*	**88**	6	7	*4*	**79**	1	1
	5	**94**	4	4	*5*	**110**	11	10	*5*	**99**	6	6
	6	**104**	6	6	*6*	**130**	4	3	*6*	**110**	1	1

The Adsorption Index was determined once a powder sample turned into an agglomerated, plastic pasty wet mass, therefore this point was easy to detect visually. Detection of the middle point when a powder sample becomes sticky, overwetted and loses powder properties, cannot be captured visually in a precise way. Nevertheless, it may be possible to roughly determine the end of adsorption (the end of powder state) by extrapolating this value from the Adsorption Index. During the determination of Adsorption Index with the solid carriers, different stages of adsorption/agglomeration were recorded as the liquid was gradually added to a powder sample (Table 7.9). Visually, the end of powder state appeared to be typically somewhere between the Adsorption Stage 2 (corresponds to 'dry, slightly agglomerated but not sticky') and 3 (corresponds to 'slightly sticky, agglomerated powder') (Chapter 2, section 2.7.10). The percentage of adsorbed liquid recorded at the Adsorption stage 2 and 3 was compared to the values extrapolated as 60% and 70% of the Adsorption Index (Table 7.10).

Table 7.10. Powder end point extrapolated from the Adsorption Index (AI).

Sample Name	**Extrapolated Powder End point**											
	Preconcentrate 1B3_T4 40: 60				**Captex 355**				**Capmul PG-8**			
	Stage 2	60% of AI	70% of AI	**Stage 3**	**Stage 2**	60% of AI	70% of AI	**Stage 3**	**Stage 2**	60% of AI	70% of AI	**Stage 3**
Sylysia 320	**196**	171	200	**229**	**165**	193	225	**219**	**124**	188	219	**203**
Aeroperl 300/30	**153**	163	190	**178**	**112**	158	185	**151**	**153**	138	161	**179**
Zeofree 5161	**168**	167	195	**194**	**142**	183	214	**214**	**195**	186	217	**217**
Hubersorb 600	**191**	166	193	**206**	**146**	184	215	**198**	**176**	168	196	**222**
Neusilin US2	**184**	203	237	**223**	**161**	211	246	**226**	**223**	208	243	**240**
Fujicalin SG	**49**	62	73	**71**	**56**	78	91	**73**	**68**	66	77	**72**

The extrapolated values of 60% or 70% of Adsorption Index were in between the Adsorption stages 2 and 3. It appeared that powder end point could be roughly estimated if the Adsorption Index is known. Nevertheless, there is a need to determine the powder end point in a more precise way as any excess of liquid present on the surface of particles could negatively affect properties of the final composition (i.e. stability, flowability, adherence to tabletting punches, etc.).

7.11. Overall Conclusions

Physical characterisation of the solid carriers revealed different properties of these materials. Neusilin US2 and Fujicalin SG consisted of quite large coarse particles in the range between 70 and 150 μm, while Zeofree 5161, Hubersorb 600 and Sylysia 320 were very fine materials made of particles smaller than 10μm. Aeroperl 300/30 was somewhere in the middle with the majority of particles around 50 to 70 μm. All the solid carriers were found to be macroporous and/or mesoporous, with an insignificant micropore area, being less than 20% of the overall surface area estimated by BET. Based on the t-plot External Surface Area, BJH cumulative surface area of pores and BJH cumulative volume of pores, Neusilin US2, Sylysia 320, Aeroperl 300/30 and Hubersorb 600 appeared to be promising adsorbents while Fujicalin SG was likely to show a limited adsorptive capacity. Sylysia 320, Aeroperl 300/30 and Zeofree 5161, three grades of silicon dioxide, appeared to vary in terms of 'packing' of hydroxyl groups present on the surface, with Zeofree 5161 being the most hydrophilic grade.

The characterisation performed enabled identification the adsorbents with the highest adsorption capacity as well as understanding of their other properties (i.e. impurities on the surface, flowability, potential reactivity with an adsorbate) that could become critical to achieve a stable solid microemulsion or other solid self-emulsifying system. Detection of the precise powder end point during the adsorption process requires a more sensitive method than visual examination as distribution of liquid and any 'excess of free liquid' present on the surface of particles is likely to affect physical properties (flowability, cohesiveness, etc.) of the final S-SELF.

Chapter 8

Adsorption onto Solid Carriers

8.1. Introduction

Solid self-emulsifying lipid formulations (S-SELFs) can be produced using various methods as presented in Chapter 1, section 1.5. One of these methods involves adsorption of liquid self-emulsifying lipid formulations (SELFs) onto a suitable solid carrier. Good content uniformity and the possibility to incorporate a high load of lipid materials have been reported as significant benefits of this technique. Ito et al. (2005) formulated a SMEDDS that contained up to 70% w/w of the liquid formulation. The physicochemical properties of solid carriers are essential to enable a high loading of liquid and achieve long-term stability of dosage forms created by the adsorption process. The size and morphology of particles influence the powder behaviour observed during adsorption and determine the adsorption capacity of each solid carrier. Non-porous materials, with a relatively small surface area, are likely to have a limited capacity to adsorb liquid before they start agglomerating and become wet. Mesoporous and macroporous materials (Chapter 1, section 1.5.1.2) can potentially adsorb higher quantities of liquid before major changes in the powder behaviour are seen. Mesopores and macropores can fill up with liquid and therefore formation of multilayers of liquid onto the main surface of particles and formation of liquid bridges between the particles are delayed. Determination of the exact point where the adsorption ends (pores are fully loaded, the material remains as powder) and the agglomeration begins (liquid forms bridges between particles) is important to develop a robust S-SELF where the liquid is not only homogenously distributed inside pores but also remains relatively inert so the inter-particle behaviour is not affected. Ultimately, S-SELFs are intended to release their liquid content upon dilution *in vivo*, therefore the adsorption needs to remain reversible and the liquid is expected to be physisorbed onto a solid carrier. In the physisorption (physical adsorption), weak bonds, mainly Van der Waals interactions are formed between an adsorbate and an adsorbent. These bonds can be easily broken down to release the intact components in contrast to chemisorption (chemical adsorption) which is irreversible and involves a chemical reaction between the adsorbate and adsorbent (Harald, 2006).

The aim of this work was to determine the adsorption capacity for each of six solid carriers. The adsorption capacity was defined as the highest amount of liquid that can be adsorbed onto a solid carrier before any major changes in its physical properties are observed that indicate initiation of agglomeration (granulation) caused by excess of liquid on the surface of particles. Determination of the adsorption load would enable development of S-SELFs that could carry the maximum load of liquid but the liquid would remain relatively inert (incorporated into particles) and therefore unlikely to interact with a drug or a capsule shell. The additional aim of this work was to investigate desorption characteristics of solid self-emulsifying systems prepared with a selected preconcentrate.

8.2. Adsorption of liquid SEDDS onto solid carriers

Solid self-emulsifying drug delivery systems (placebo) were created by adsorption of the preconcentrate 2A2 50: 50 onto the solid carriers. The preconcentrate 2A2 50: 50 demonstrated very good emulsification behaviour at 25 °C (Chapter 4, Fig. 4.5.C) and 37 °C (Chapter 4, Fig. 4.1.B) in the previous experiments. The use of this preconcentrate in the adsorption experiments facilitated an investigation of desorption behaviour from the prepared S-SEDDS. The preconcentrate 2A2 50: 50 was composed of Captex 355 (50% w/w), Capmul MCM C8 (32.5% w/w) and Crillet 4 HP (17.5 % w/w). The load of the preconcentrate onto a solid carrier was expressed as % of Added Liquid (%AL) (details of the calculation are presented in Chapter 2, section 2.8.1). The Powder End Point (PEP), also called the adsorption capacity, was defined based on the specific change of material properties detected in the tests. The % of Added Liquid for the sample preceding the sample that showed a different behaviour (e.g. increase in density, decrease in Basic Flowability Energy, variability in measurement, etc.) was considered to be the Powder End Point.

The blending procedure described in Chapter 2 (section 2.8.1) was used to prepare S-SEDDSs with various % of Added Liquid using stained and non-stained preconcentrate 2A2 50: 50. The stained preconcentrate 2A 50: 50 was prepared as described in Chapter 2 (section 2.8.2) and these S-SEEDS were subsequently used to investigate release of Fat Red 7B. The appearance of each produced S-SEEDS was examined and the observations are summarised in Table 8.1.

Table 8.1. Visual characteristics of solid carriers and the carriers with liquid adsorbed.

Sample Name / w/w%	% of Added Liquid [%AL]	Appearance
Sylysia 320		
Sylysia 320 : preconcentrate/ 100:0	**0**	Very cohesive, agglomerated, poor flow
Sylysia 320 : preconcentrate/ 60:40	**40**	Similar to the pure material
Sylysia 320 : preconcentrate/ 50:50	**50**	Less cohesive, agglomerated and flows better than the pure material
Sylysia 320 : preconcentrate/ 40:60	**60**	Less cohesive, agglomerated and flows better than the pure material
Sylysia 320 : preconcentrate/ 35:65	**65**	Less cohesive, agglomerated and flows better than the pure material
Sylysia 320: STAINED preconcentrate/ 35:65	**65**	Less cohesive, agglomerated and flows better than the pure material
Sylysia 320 : preconcentrate/ 30:70	**70**	Sticky and wet, agglomerated, resembles a paste
Sylysia 320 : preconcentrate/ 25:75	**75**	Very wet, agglomerated paste
Aeroperl 300/30		
Aeroperl 300/30: preconcentrate/ 100:0	**0**	Slightly cohesive but not agglomerated, appears to flow well
Aeroperl 300/30: preconcentrate/ 60:40	**40**	Similar to the pure material
Aeroperl 300/30: preconcentrate/ 50:50	**50**	Similar to the pure material

Table 8.1. Visual characteristics of solid carriers and the carriers with liquid adsorbed (cont'd).

Sample Name / w/w%	% of Added Liquid [%AL]	Appearance
Aeroperl 300/30		
Aeroperl 300/30: preconcentrate/ 40:60	**60**	Similar to the pure material
Aeroperl 300/30: STAINED preconcentrate/ 40:60	**60**	Similar to the pure material
Aeroperl 300/30: preconcentrate/ 35:65	**65**	Sticky and wet, agglomerated, resembles a paste
Aeroperl 300/30: preconcentrate/ 30:70	**70**	Very wet, agglomerated paste
Zeofree 5161		
Zeofree 5161: preconcentrate/ 100:0	**0**	Non-cohesive, not agglomerated, moderately good flow
Zeofree 5161 : preconcentrate/ 60:40	**40**	Similar to the pure material
Zeofree 5161 : preconcentrate/ 49:51	**51**	Similar to the pure material
Zeofree 5161 : preconcentrate/ 40:60	**60**	Similar to the pure material
Zeofree 5161 : preconcentrate/ 35:65	**65**	Similar to the pure material
Zeofree 5161 : STAINED preconcentrate/ 35:65	**65**	Similar to the pure material
Zeofree 5161 : preconcentrate/ 30:70	**70**	Looks slightly sticky and agglomerated
Zeofree 5161 : STAINED preconcentrate/ 30:70	**70**	Looks slightly sticky and agglomerated
Zeofree 5161 : preconcentrate/ 24:76	**76**	Very wet, agglomerated paste
Hubersorb 600		
Hubersorb 600: preconcentrate/ 100:0	**0**	Very cohesive, agglomerated, poor flow
Hubersorb 600 : preconcentrate/ 29:61	**61**	Similar to the pure material
Hubersorb 600 : STAINED preconcentrate/ 30:60	**60**	Similar to the pure material
Hubersorb 600 : preconcentrate/ 29:71	**71**	Looks slightly sticky and agglomerated
Hubersorb 600 : STAINED preconcentrate/ 30:70	**70**	Looks slightly sticky and agglomerated
Hubersorb 600 : preconcentrate/ 25:75	**75**	Very wet, agglomerated paste
Neusilin US2		
Neusilin US2: preconcentrate/ 100:0	**0**	Non-cohesive, not agglomerated, very good flow
Neusilin US2 : preconcentrate/ 30:60	**60**	Similar to the pure material
Neusilin US2 : STAINED preconcentrate/ 30:60	**60**	Similar to the pure material
Neusilin US2 : preconcentrate/ 30:70	**70**	Similar to the pure material
Neusilin US2 : STAINED preconcentrate/ 30:70	**70**	Similar to the pure material
Neusilin US2 : preconcentrate/ 25:75	**75**	Very wet, agglomerated paste

Table 8.1. Visual characteristics of solid carriers and the carriers with liquid adsorbed (cont'd).

Sample Name / w/w%	% of Added Liquid [AL%]	Appearance
Fujicalin SG		
Fujicalin SG: preconcentrate/ 100:0	**0**	Non-cohesive, not agglomerated, very good flow
Fujicalin SG: preconcentrate/ 70:30	**30**	Similar to the pure material
Fujicalin SG: STAINED preconcentrate/ 69:31	**31**	Similar to the pure material
Fujicalin SG: preconcentrate/ 60:40	**40**	Similar to the pure material
Fujicalin SG: STAINED preconcentrate/ 60:40	**40**	Similar to the pure material
Fujicalin SG: preconcentrate/ 55:45	**45**	Sticky and wet, agglomerated, resembles a paste
Fujicalin SG: preconcentrate/ 50:50	**50**	Very wet, agglomerated paste

Physical properties of the stained and non-stained S-SEDDSs were subsequently evaluated in four tests that examined the impact of the increasing liquid load onto flowability, density and shear properties (resistance to flow) once the samples were slightly compacted (the employed tests were previously presented Chapter 1, section 1.5.3).

8.2.1. Basic Flowability Energy (BFE)

Basic Flowability Energy (BFE) of the S-SEDDSs formulated with Sylysia 320 (S-SEDDSs/Sylysia 320) showed an increase as the % of Added Liquid increased up to 70% (Fig. 8.1, Appendix Table A.8.1). The %AL up to 50% appeared to have little effect on the flowability and the adsorbed samples did not differ significantly from the pure, non-adsorbed Sylysia 320 ($p < 0.05$). The Basic Flowability Energy started increasing beyond 60% of Added Liquid and the samples with the %AL = 50% and %AL = 60% differed significantly ($p < 0.05$) but subsequently there was no statistical difference between the samples %AL = 60% and %AL = 65%. Visually, the samples containing up to 65% of Added Liquid resembled powder (Table 8.1). The change in the Basic Flowability between the samples with %AL = 65% and 70% was statistically significant ($p < 0.01$). The Powder End Point (PEP) for Sylysia 320 was determined as 65% as the previous change was less statistically significant. Also there was no difference between the samples with higher %AL (60% and 65%) which would be expected if the properties of these systems were reflecting initiation of agglomeration and granulation. The Basic Flowability Energy of the S-SEDDSs formulated with Aeroperl 300/30 exponentially increased with the percentage of the liquid up to 60% (Fig. 8.1, $R^2 = 0.9960$) until a sudden sharp increase occurred at the percentage of Added Liquid equal to 70%. The samples with the %AL = 60% and 65% differed significantly from the sample with the %AL = 70 ($p < 0.01$). The sample with the % AL = 65% looked sticky, agglomerated, resembled a paste (Table 8.1) and the mean BFE for this sample was calculated based on two variable measurements (RSD = 58.5%). Low repeatability of BFE measurements for

this sample (%AL= 65%) was considered as a change in the flow properties. Based on these measurements, the Powder End Point (PEP) for Aeroperl 300/30 was established as 60%.

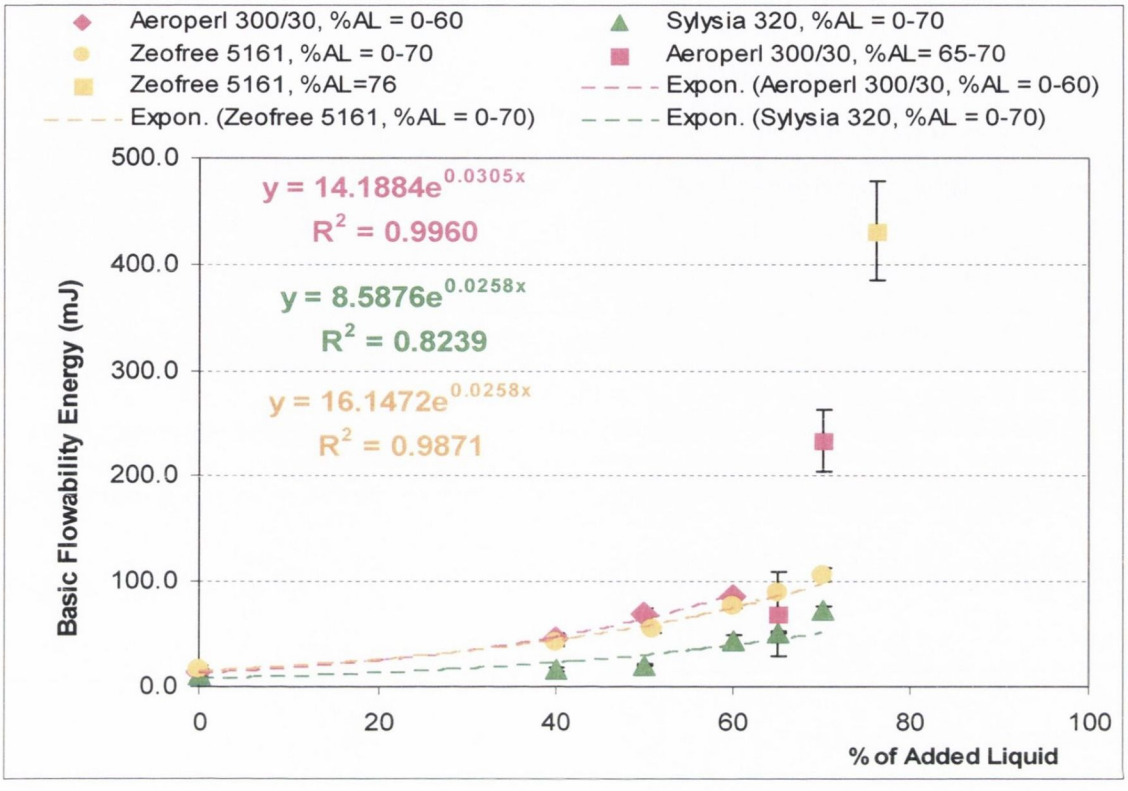

Fig. 8.1. Effect of the increased adsorption load (%AL) on the BFE for the three grades of silicon dioxide (error bars indicate SD).

The Basic Flowability Energy in the S-SEDDSs/ Zeofree 5161 increased exponentially (Fig. 8.1, $R^2 = 0.9871$) with the % of Added Liquid up to 70%. There was no statistical difference in the BFE values measured for the samples with the %AL from 0% up to 60%. A significant change in the BFE was observed between the samples with the %AL = 70% and 76%. Based on the measurements, the Powder End Point was established as 70% for Zeofree 5161. In the S-SEDDSs formulated with Hubersorb 600, the BFE increased up to 71% of Added Liquid. The exponential fit appeared to describe best the relationship between BFE and %AL (Fig. 8.2, $R^2 = 0.8808$) based on the limited data (3 points only). The sample with the %AL = 75% was a sticky wet paste and the average value of BFE was calculated based on two highly variable measurements (RSD = 140.8%) (Appendix, Table A.8.1). Although no statistical difference was seen between the samples from the %AL = 0% to %AL = 75%, the lack of repeatability in BFE measurements for the sample with the %AL = 75% was considered as a change in flowability and the Powder End Point for Hubersorb 600 was set as 71%. Flowability of the S-SEDDSs/ Neusilin US2, measured in terms of the BFE, was also correlated to the percentage % of Added Liquid (Fig. 8.2, $R^2= 0.9993$). The sample with the %AL = 75%, despite being a wet, sticky, paste-like mass (Table 8.1) did not differ statistically

from the preceding powder sample (%AL = 70%) when the BFE values were compared. The statistical difference was not shown between these samples because the relative standard deviation for the sample with the %AL= 75% was high, equal to 27.6 % (Appendix, Table A.8.1). Also, Stability Index showed variability between two individual measurements for this sample (RSD < 36.8%) (Appendix, Table 8.1) which suggested non-reproducible flow behaviour. The lack of reproducibility in the flow behaviour for the sample with %AL = 75% was considered as overloading with the preconcentrate and the Powder End Point for Neusilin US2 was set as 70%.

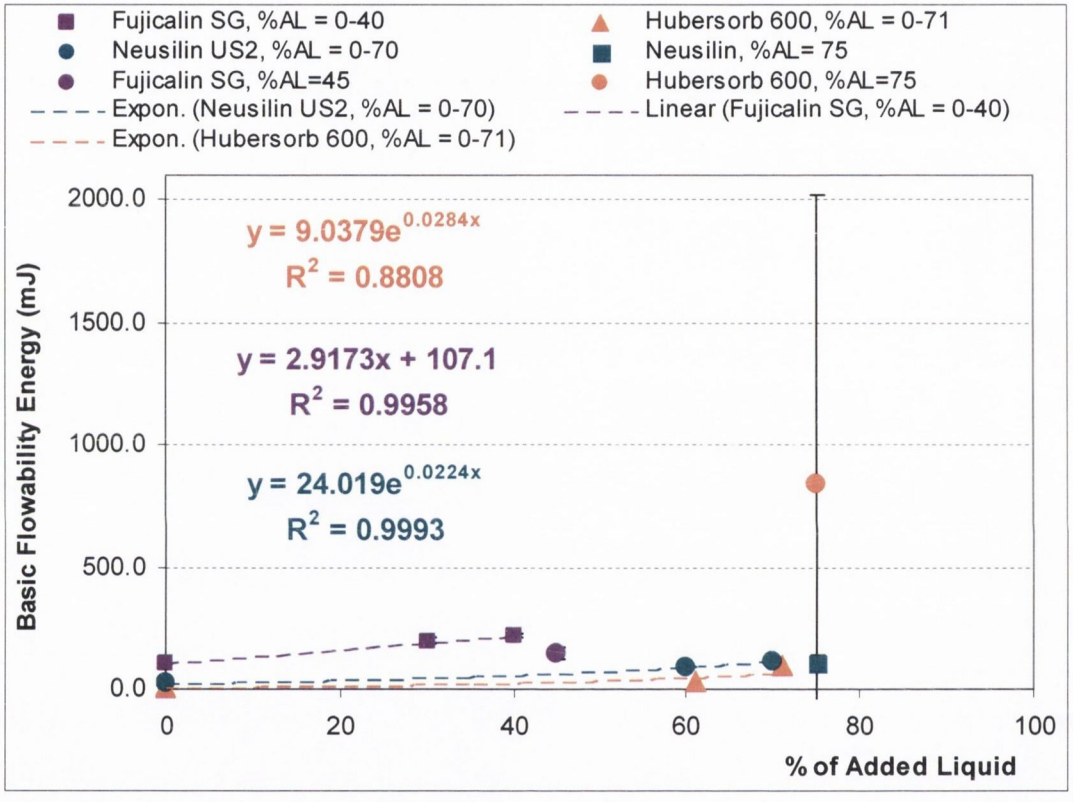

Fig. 8.2. Effect of the increased adsorption load (%AL) on the BFE for Hubersorb 600, Neusilin US2 and Fujicalin SG (error bars indicate SD).

Fujicalin SG showed the lowest adsorption capacity among the examined solid carriers (Fig. 8.2). The paste resembling sample (Fig. 8.2) with the %AL = 45% showed the BFE value significantly different ($p < 0.05$) from the preceding sample with %AL = 40%. The Powder End Point for Fujicalin SG was determined to be 40% based on the BFE measurements.

The pure, non-adsorbed solid carriers could be arranged from the poor flow (low BFE values) to the good flow (high BFE value) in the following order: Hubersorb 600 (9.6 mJ), Sylysia 320 (11.0mJ), Aeroperl 300/30 (14.2 mJ), Zeofree 5161 (17.1 mJ), Neusilin US2 (24.1 mJ) and finally Fujicalin SG (106.0 mJ).

8.2.2. Specific Energy (SE)

Specific Energy (SE) of the S-SEDDS/ Sylysia 320 showed little change as a measure of flowability as % of Added Liquid increased up to 50% (Fig. 8.3, Appendix Fig. A.8.2). The SE values of the S-SEDDS within this range did not differ significantly. The SE values significantly increased ($p < 0.01$) between for the samples with the %AL = 50% and 60%, however the consecutive samples with the %AL = 65% and 70% did not differ statistically ($p < 0.05$) from the samples with the %AL from 0% to 50%. It appeared that flowability decreased when the percentage of Added Liquid reached 60% but then it improved again. Visually, all the samples in the range from 50 to 65% resembled agglomerated powder but did not seem wet or sticky (Table 8.1). The sample with the highest %AL of 70% differed significantly ($p < 0.05$) from the preceding sample and was evidently wet, sticky and resembled paste (Table 8.1). The first significant change in the SE values between the samples with %AL = 50% and 60% was considered as the change in the flow behaviour and the Powder End Point for Sylysia 320 was set as 50%.

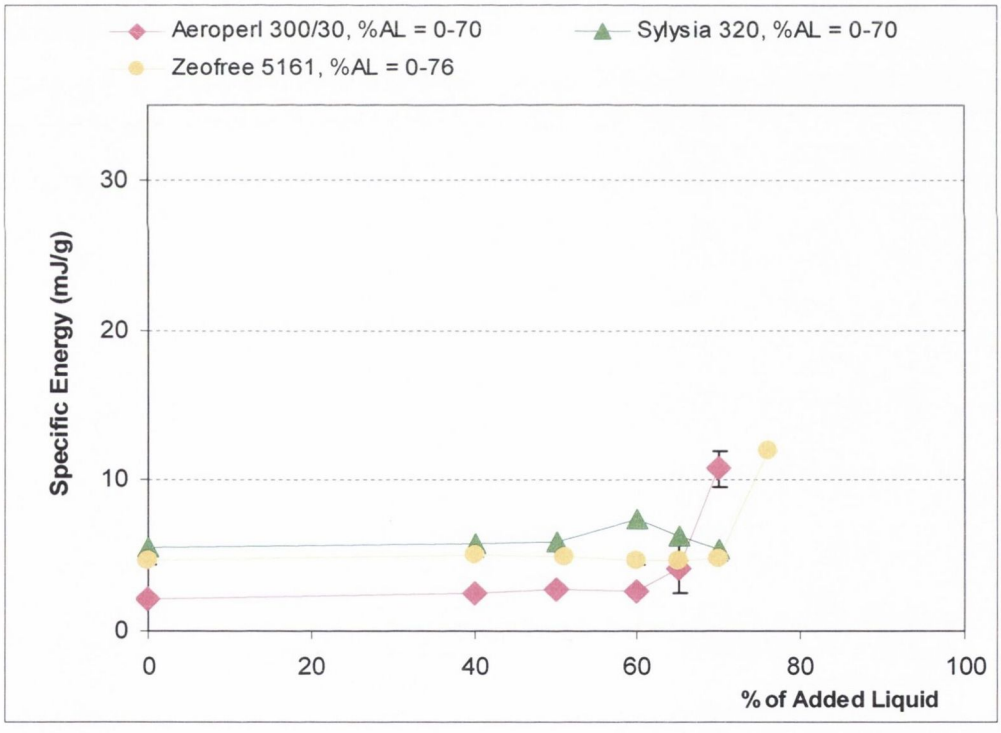

Fig. 8.3. Effect of the increased adsorption load (%AL) on the Specific Energy for the three grades of silicon dioxide (error bars indicate SD).

Specific Energy measured for Aeroperl 300/30 (pure material) was not significantly different from the values obtained for the S-SEDDSs/Aeroperl 300/30 with the %AL up to 65%. A significant increase ($p < 0.01$) in the SE values was detected between the samples with %AL of 65% and 70% (Fig. 8.3). There was no statistically significant difference between the sample with %AL of 60% and 65%, since the reproducibility of the SE measurement was poor (RSD = 39.4%) for the sample with %AL = 65% (Appendix, Table A.8.2). The S-SEDDSs with the %AL of 65% and 70%

showed RSD values of 39.4% and 11.1% respectively, while the measurements of the preceding powder samples (including Aeroperl 300/30 pure material) were more consistent (RSD < 6.9%). Based on the SE measurements, the Powder End Point for Aeroperl 300/30 was set to 60%. Specific Energy of the S-SEDDS formulated with Zeofree 5161 did not differ significantly from the pure material up to the %AL of 70% (Fig. 8.3). A sudden increase of the SE values was detected when the % of Added Liquid reached 76%. This sample also differed visually from the rest of the samples (Table 8.1). Based on this change, the Powder End Point for Zeofree 5161 was set to 70%. Measurements of Specific Energy (SE) in the S-SEDDSs/Hubersorb 600 indicated a transition from a powder state into a paste when %AL reached 71% (Fig. 8.3). There was no statistical difference between the mean SE values ($p < 0.05$) of all the samples. Nevertheless, variability in the SE observed between the individual measurements for the sample with %AL of 75% was very high (RSD = 105.5%) which indicated lack of reproducible flow behaviour. This change was considered as the end of adsorption and the Powder End Point for Hubersorb 600 was established as 71%. The sample of Neusilin US2 with the highest % of Added Liquid (%AL = 75%) showed higher variability in SE measurements (RSD =33.7%) in comparison to the previous samples (Appendix, Table A.8.2). Although the mean Specific Energy measured for this sample did not vary significantly from the preceding samples (Fig. 8.4), the unstable flow behaviour was considered as evidence of altered physical properties of the 'overloaded' material, and therefore the Powder End Point for Neusilin US was established as 70%.

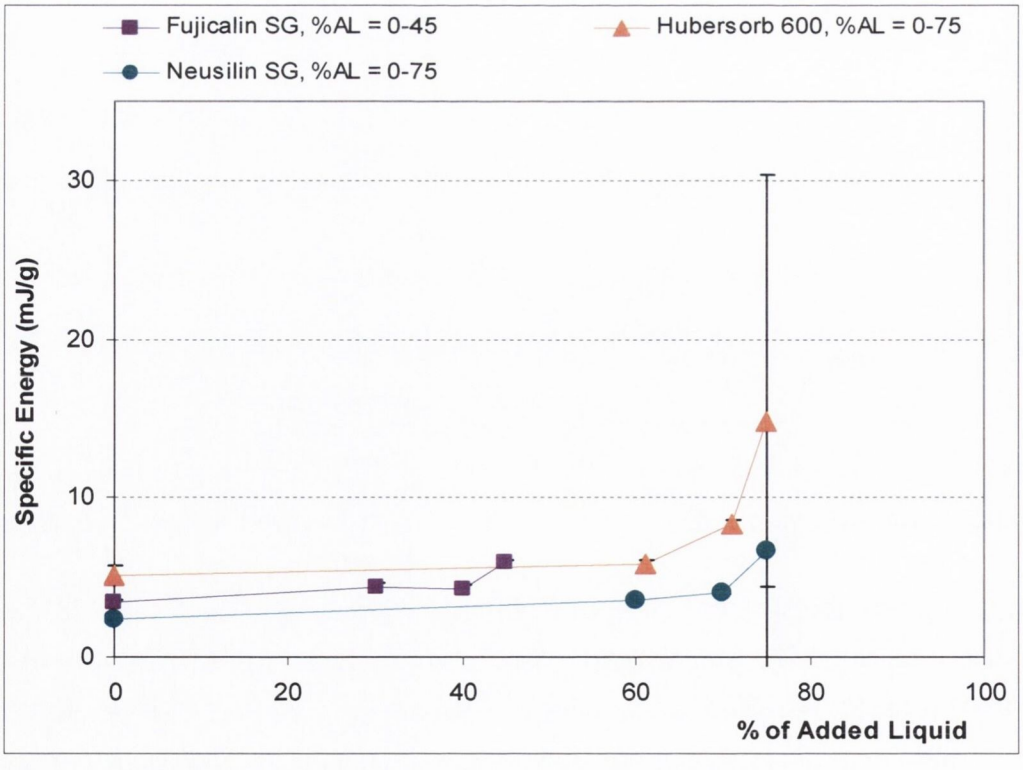

Fig. 8.4. Effect of the increased adsorption load (%AL) on the Specific Energy for Hubersorb 600, Neusilin US2 and Fujicalin SG (error bars indicate SD).

The Powder End Point for Fujicalin SG was determined as 40%. The Specific Energy for the sample with the highest % of Added Liquid equal to 45%, differed significantly ($p < 0.01$) from the preceding sample (Fig. 8.4).

The pure, non-adsorbed solid carriers could be arranged from the lowest to the highest values of the Specific Energy in the following order: Aeroperl 300/30 (2.14 mJ/g), Neusilin US2 (2.39 mJ/g), Fujicalin SG (3.52 mJ/g), Zeofree 5161 (4.69 mJ/g), Hubersorb 600 (5.11 mJ/g) and finally Sylysia 320 (5.58mJ/g). SE values above 5 typical indicate a moderate cohesion (Freeman's work instruction and equipment manual), therefore based on these results Sylysia 320 and Hubersorb 600 appeared to be moderately cohesive and more cohesive than the other four solid carriers.

8.2.3. Conditioned Bulk Density (CBD)

The Conditioned Bulk Density (CBD) of the adsorbed samples was compared to evaluate if any change in density could detect the beginning of agglomeration, the point where 'packing' of individual particles becomes altered as they started to form agglomerates. The Conditioned Bulk Density of Sylysia 320 showed a gradual increase up to the % of Added Liquid of 70 (Fig. 8.5).

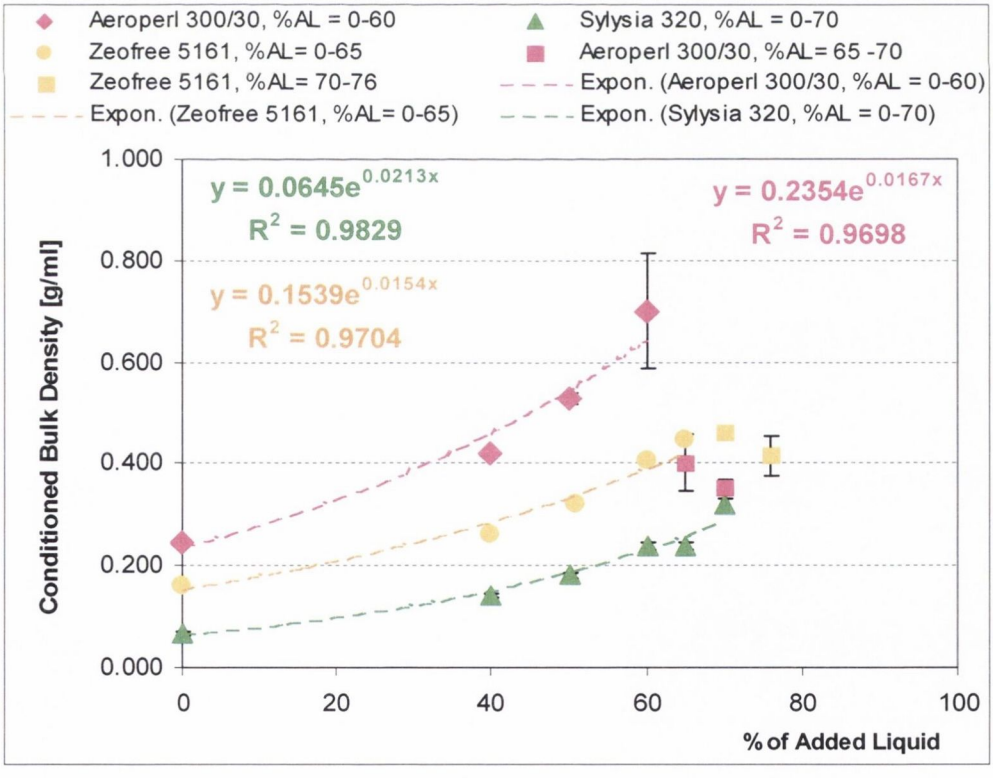

Fig. 8.5. Effect of % of Added Liquid on CBD for the three grades of silicon dioxide (error bars indicate SD).

A clearly visible change in density was not observed in the S-SEDDSs/Sylysia 320 but the sample with %AL = 65% appeared to have the same density as the preceding sample. The stained

equivalent of the sample with %AL of 65 showed variable RSD (11.8%), which was the highest among the adsorbed samples of Sylysia 320. All the adsorbed samples of Sylysia 320, except for the stained samples with %AL = 65%, showed RSD below 4% (Appendix Table A.8.3). The variability in density was considered as less reproducible 'packing' of the poured samples and therefore the Powder End Point for Sylysia 320 was set as 60% based on the CBD measurements.

The Conditioned Bulk Density of Aeroperl 300/30 showed a gradual exponential increase (Fig. 8.5, R^2 = 0.9829) up to the % of Adsorbed Liquid of 60%. Beyond this point, the density decreased substantially indicating a different 'packing' of particles. The Powder End Point for Aeroperl 300/30 was set to 60% based on these measurements. The Conditioned Bulk Density (Fig. 8.5) in the S-SEDDSs/ Zeofree 5161 appeared to increase exponentially with the %AL up to 70%. The adsorbed sample with %AL = 76% showed a decrease in the mean CBD value and also higher variability (RSD = 9.6%, Appendix Table A.8.3) compared to the preceding samples (RSD < 3.7%). The Powder End Point for Zeofree 5161 was established as 70% based on this change.

The Conditioned Bulk Density measured in the S-SEDDSs formulated with Hubersorb 600 was correlated with the % of Added Liquid up to 71% (Fig. 8.6, R= 0.9861).

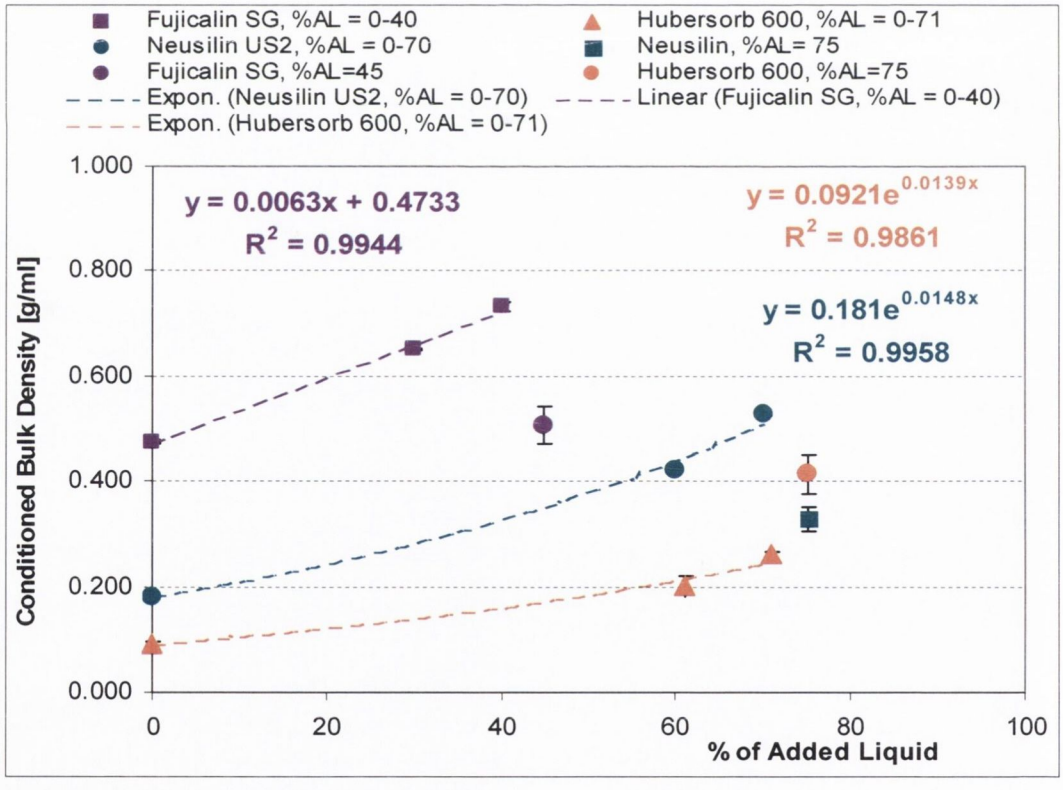

Fig. 8.6. Effect of % of Added Liquid on CBD for Hubersorb 600, Neusilin US2 and Fujicalin SG (error bars indicate SD).

A sudden increase in the BCD was observed for the sample with %AL of 70 (Fig. 8.6). This suggested a different 'packing of particles' in sample with %AL of 75% and therefore the Powder

Point End for Hubersorb 600 was established as 71%. The Powder End Point for Neusilin US2 and Fujicalin SG was established as 70% and 40% respectively, based on the decrease in density observed for the 'overloaded with liquid' samples that showed different packing of particles (Fig. 8.6).

The comparison of the Conditioned Bulk Density between the S-SEDDSs provided useful information with regard to changes of 'packing' and distribution of particles in the sample as the amount of adsorbed liquid increased. The lightest and the most cohesive powders, i.e. Hubersorb 600 and Sylysia 320 showed a moderate increase in density until the transition from a powder into a more condense paste-like state occurred. The 'overloaded with liquid' samples appeared denser because excess liquid acted as a binder, and loose and random packing of particles that was initially seen in the original materials was overcome. The transition from a powder state into agglomeration/granulation was seen as a decrease in density for the heavier and more flowable solid carriers (Aeroperl 300/30, Zeofree 5161, Neusilin US2 and Fujicalin SG). In this case, an excess of adsorbed liquid caused the particles to adhere one to another randomly and the 'packing' of particles worsen compared to the one seen with the pure, very flowable materials.

8.2.4. Shear Stress (SS)

The Shear Stress measurements evaluate how easily a previously at rest, consolidated powder will begin to flow. When a sample is subjected to some level of consolidation stress, this force increases the contact area between particles and may induce additional interparticulate bonding. In order to make a consolidated sample to flow again, resistance of consolidated particles needs to be overcome. This would typically require a higher force (energy) if the additional interparticulate bonding (for example due to excess of liquid on the surface of particles) was formed during the consolidation stage, compared to the force that is required to move non-consolidated particles. A comparison of resistance to flow for S-SEDDSs (after consolidation) enables understanding if any 'excess' of liquid is present on the surface of particles that may act as a binder and cause particles to agglomerate easily. In samples that contain the liquid fully incorporated inside pores of particles, the consolidation step should not trigger any additional inter-particulate interactions. The primary mode of flow of powders is shear, in which particles slide relative to each other and therefore the presence of 'excess of liquid' affects shear rate of the particles in the sample. Measurements of the Shear Stress are based on determination of yield loci (i.e. incipient failure points) that are obtained by plotting the measured values of actual (or actual pro-rated) shear stress on the Y-axis and actual normal stress (on X-axis) (as shown in Chapter 1, section 1.5.2.4). The measured shear stress and normal stress could be defined as the maximum stress recorded before the incipient failure occurs (powder begin to slide, the samples starts to flow) and are typically measured in the range of normal stress between 3 to 9 kPa. The effect of consolidation on flowability of the S-SEDDSs was evaluated by comparing the position of yield

loci determined in samples. The values of actual normal stress tended not to differ substantially in the pure material and the adsorbed samples, while the measured values of actual pro-rated shear stress were shifted towards higher values, meaning these yield loci were not overlapping with the other plots. For some materials, the repeated consolidation of the sample can change slightly during a series of shear measurements. Pro-rating is used to compensate for this situation by recalculating (correcting) the shear stress for each test point achieved using average of pre-shear shear stresses and measured pre-shear shear stress preceding shear step which makes the results of each run more precise and unaffected by the previous run. The plots of yield loci determined in Sylysia 320 and the S-SEDDS/ Sylysia 320 are shown in Fig. 8.7. The resistance to flow shown by the consolidated S-SEDDSs was similar to pure Sylysia 320 up to the percentage of Added Liquid equal to 70%. The plots of yield loci for these samples overlapped closely. The sample with the %AL of 75%, which looked like a wet paste (Table 8.1), showed a significant increase in the values of pro-rated shear stress in all five levels of the normal stress. Based on the Shear Stress measurements, the Powder End Point for Sylysia 320 was established as 70%.

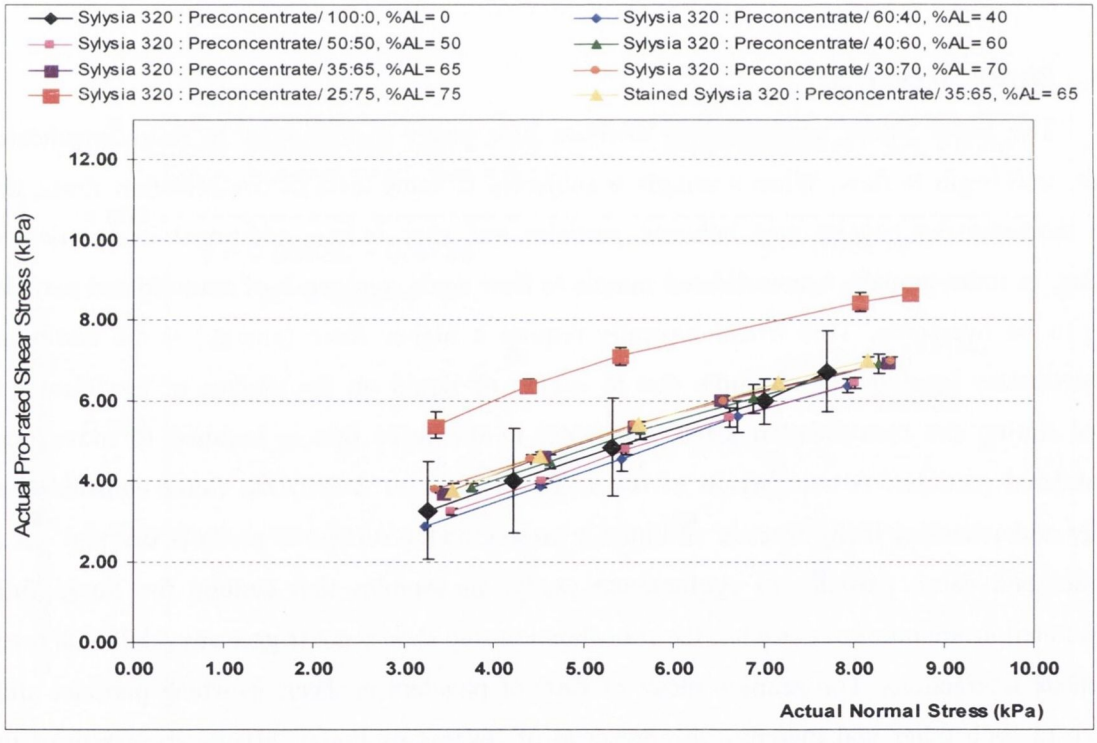

Fig. 8.7. Shear stress versus normal stress for Sylysia 320 (pure material) and its S-SEDDSs.

Similar values of pro-rated shear stress were measured in the consolidated Aeroperl 300/30 and its adsorbed samples with the %AL up to 60% (Fig. 8.8). The higher resistance to flow was shown by the samples with the %AL of 65% and 70% compared to the preceding samples. The plots of yield loci for these samples were positioned above the other plots which closely overlapped for the pure material and the S-SEDDSs up to %AL = 60%. The Powder End Point for Aeroperl 300/30 was set to 60% based on the observations from the Shear test.

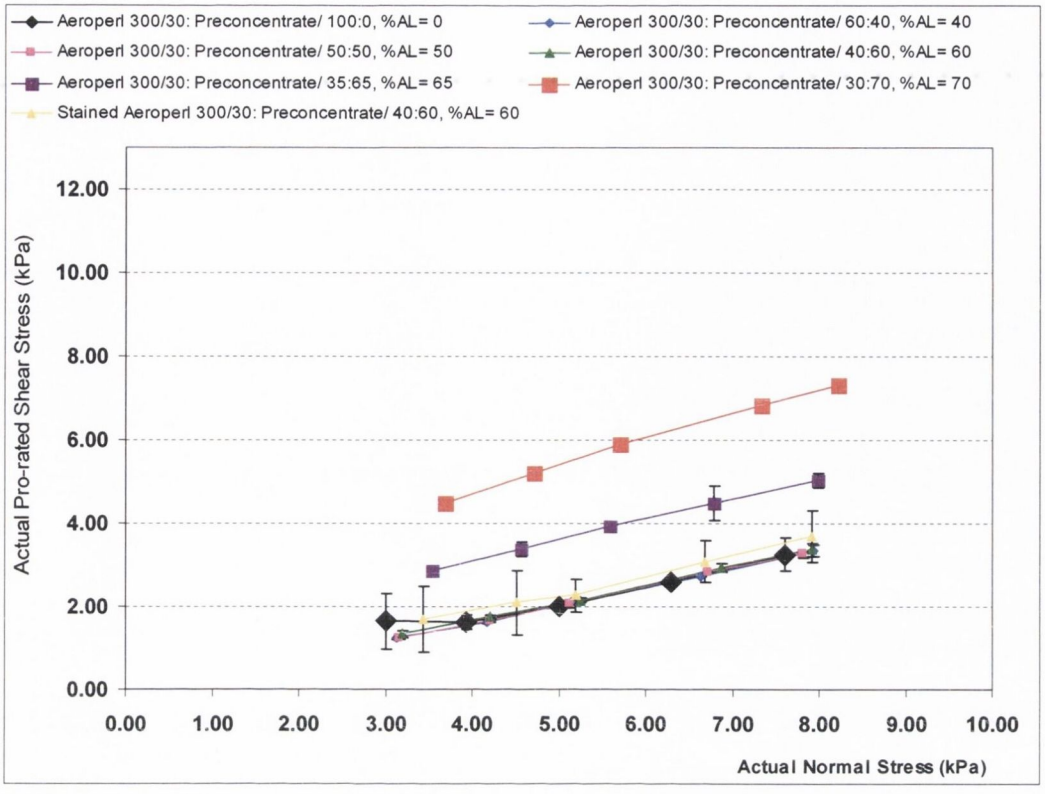

Fig. 8.8. Shear stress versus normal stress for Aeroperl 300/30 (pure material) and its S-SEDDSs.

A significantly higher pro-rated shear stress was determined in the consolidated S-SEDDS/Zeofree 5161 with the % of Added Liquid equal to 70%, compared to the preceding samples (Fig. 8.9). Visually, this sample looked wet and sticky (Table 8.1). The sample with the %AL equal to 70% looked slightly sticky and agglomerated, however its shear behaviour did not differ from the pure material and the adsorbed samples with %AL up to 65%. Based on the measured values of Shear Stress, the Powder End Point for Zeofree 5161 was set as 70%. When the flow behaviour of the consolidated, adsorbed samples formulated with Hubersorb 600 was compared (Fig. 8.10), an almost gradual increase of shear stress at all levels of normal stress was observed as % of Added Liquid increased. None of the adsorbed samples showed the similar flow behaviour to pure, non-adsorbed Hubersorb 600. Despite higher mean values of pro-rated shear stress measured in the S-SEDDSs/ Hubersorb 600 up to %AL of 71% (in comparison to the pure material), all the samples appeared to have relatively reproducible flow indicated by low variability between individual measurements (RSD < 10%, Appendix Table A.8.4). The sample with the % of Added Liquid equal to 75% differed substantially from the preceding samples with regard to variable RSD. It also showed a non-linear relationship between the pro-rated shear stress and the actual normal stress. This indicated that the consolidation steps affected 'packing' of particles significantly and the inter-particulate bonding increased significantly over time (during testing). The Powder End Point for Hubersorb 600 was set as 71% based on the outcome of the Shear Stress measurements.

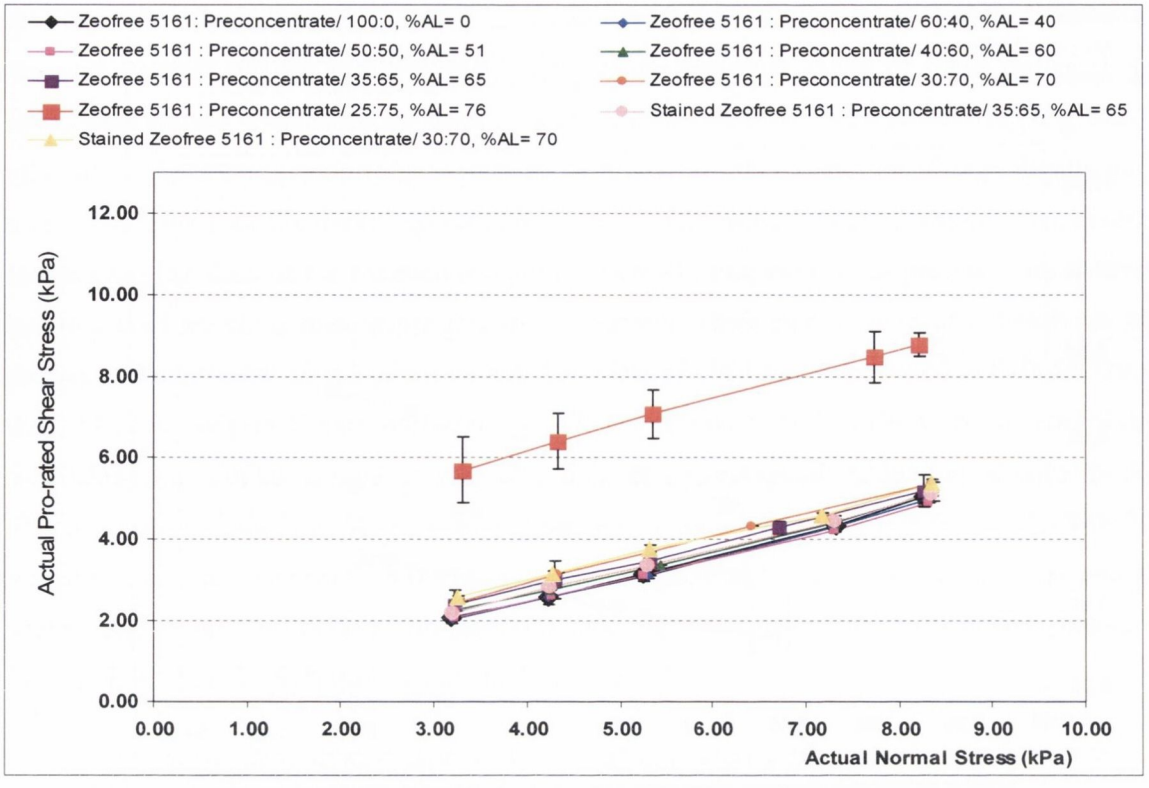

Fig. 8.9. Shear stress versus normal stress for Zeofree 5161 (pure material) and its S-SEDDSs.

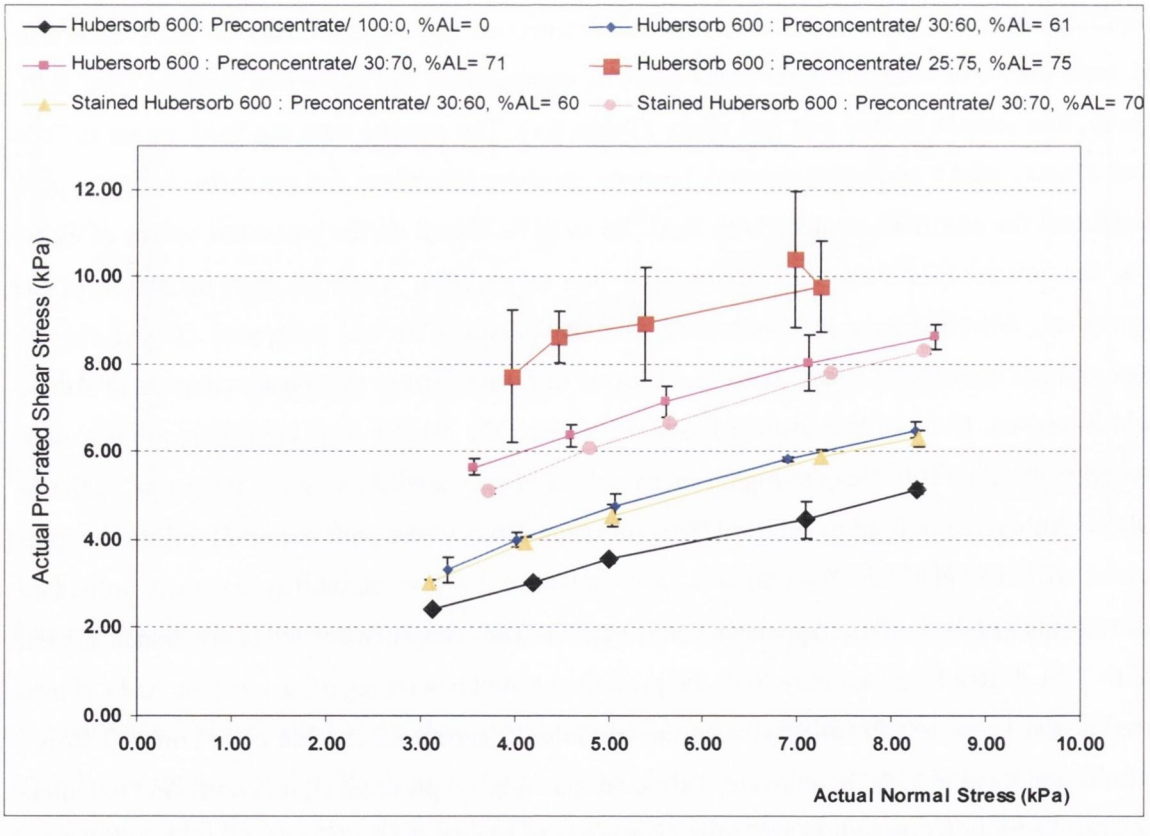

Fig. 8.10. Shear stress versus normal stress for Hubersorb 600 (pure material) and its S-SEDDSs.

The S-SEDDSs/ Neusilin US2 containing up to 70% of Added Liquid showed similar shear properties as the pure material (Fig. 8.11). The sample with the %AL of 75% showed a significantly higher resistance to flow compared to the preceding samples and the pure material. The detected change in the measured pro-rated shear stress corresponded to the visual appearance of this sample (Table 8.1). Based on the Shear Stress measurement, the Powder End Point for Neusilin US2 was determined to be 70%.

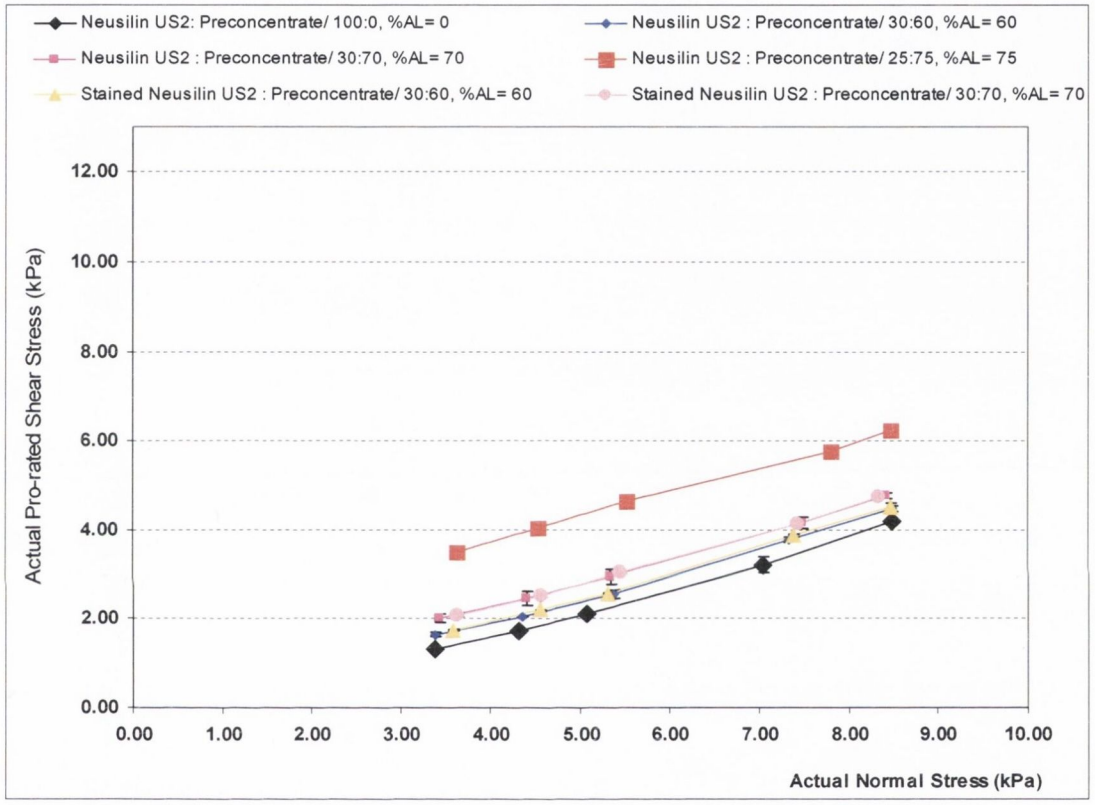

Fig. 8.11. Shear stress versus normal stress for Neusilin US2 (pure material) and its S-SEDDSs.

Similar shear properties were observed for pure non-adsorbed Fujicalin SG and the S-SEDDSs/Fujicalin SG with the percentage of Added Liquid up to 40% (Fig. 8.12). The consecutive sample (%AL = 45%) differed significantly to the preceding samples and the pure material, therefore the Powder End Point for Fujicalin SG was set to 40%.

The measurements of pro-rated shear stress which translated onto resistance of flow that was shown by particles after a consolidation step, was found to be a very good technique to detect the end of adsorption. This technique is likely to be more sensitive compared to the previously used methods (BFE, SE, CBD) in particular for difficult powders such as Sylysia 320. Determination of the Powder End Point in the adsorbed samples formulated with this carrier was not straight forward when with the other methods, while the Shear Stress measurement easily captured the transition from powder into paste. Due to the consolidation step which forces additional interactions between particles, this technique is likely to detect even 'small excess of liquid' present on the surface of

particles before it affects other physical properties such as flowability and density of loosely packed, non-consolidated particles.

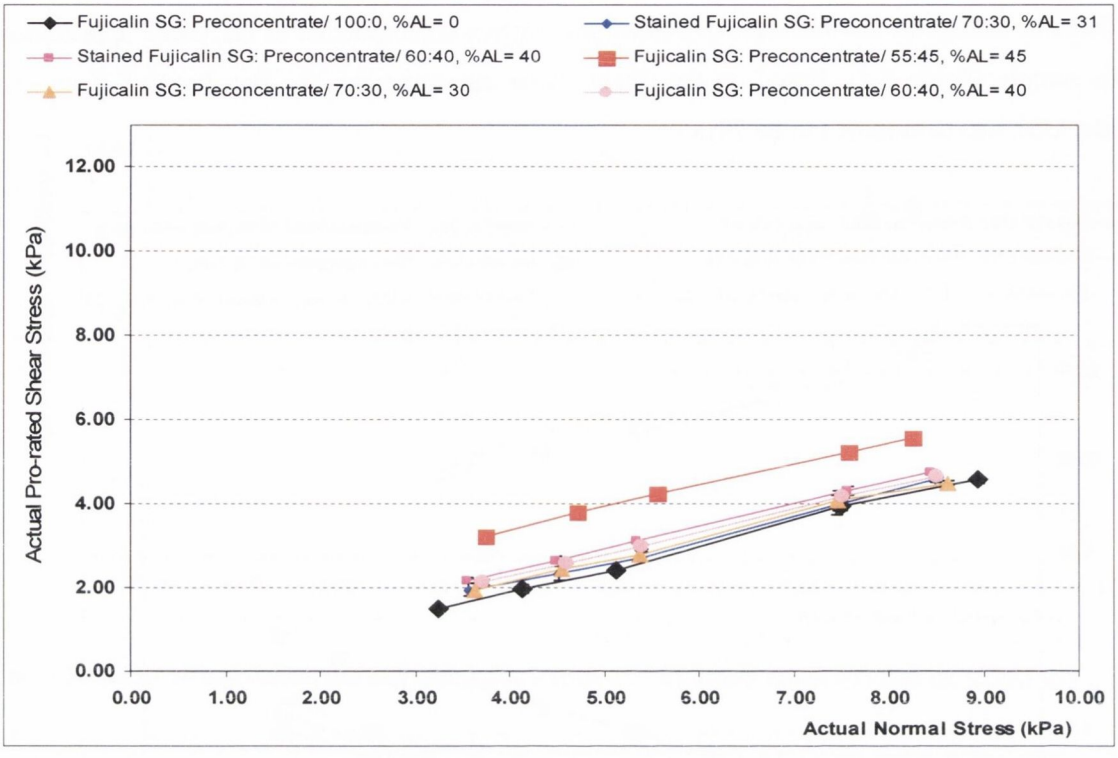

Fig. 8.12. Shear stress vs. normal stress for Fujicalin SG (pure material) and its S-SEDDSs.

The adsorption capacity determined for all the carriers, except for Fujicalin SG, was at minimum 60%. In particular, Zeofree 5161, Hubersorb 600 and Neusilin US2 appeared to be very promising carriers as their adsorption capacity was as high as 70%. Sylysia 320 and Aeroperl 300/30 were also significantly better (PEP = 65% and 60% respectively) compared to Fujicalin SG (PEP = 40%).

8.3. Desorption from S-SEDDSs

8.3.1. Desorption by particle sizing and transmittance

The desorption test (described in Chapter 2, section 2.8.4) was employed to investigate how rapidly the adsorbed preconcentrate 2A2 50: 50 could be released from the S-SEDDS. The S-SEDDSs that were equivalent to the Powder End Point were used in these experiments. The desorption of the preconcentrate adsorbed onto the solid carriers, was expected to occur upon contact with a dispersing medium. If the preconcentrate (as the whole system) or a portion of the preconcentrate was released from the S-SEDDS, the emulsion similar to the one formed by the liquid preconcentrate should have been observed. A combination of particle sizing and transmittance measurements was used to evaluate emulsification from the (non-stained) S-SEDDSs.

The DLS technique provides information on the particle size distribution (the average particle size (Z-Aver) and the polydispersity index (PDI)), but does not measure the concentration of droplets ('particle count') (Celis et al., 2008). Transmittance on the other hand, is a technique that measures the amount of light that passes through a sample compared to the reference beam. Microemulsions having the droplets smaller than $1/4^{th}$ the wavelength of visible light are characterised by very high transmittance at the wavelengths of 500- 600 nm (100% or slightly less for translucent systems). Any other dispersed systems with larger droplets such as emulsions (size above ~140 nm) would not be optically transparent (Patel et al., 2010). Transmittance measured in emulsions could be used to make a less subjective comparison between finer (clearer) and coarser (more opalescent) systems than the comparison by visual examination.

Initially, the particle size and transmittance of diluted samples with varied concentration of the liquid preconcentrate 2A2 50: 50 were measured to establish how the liquid SEDDS behaved upon dilution. This was important to understand so the comparison between the desorbed emulsions could be made with the systems formed by the original liquid preconcentrate. The diluted samples in the range of 0.2 mg/ml to approximately 3.8 mg/ml of the preconcentrate in blank FaSSIF-V2 were made. These concentrations corresponded to the dilution from 1: 200 to 1: 4000 and represented two scenarios: 1) if 1 g of the preconcentrate (100%) was emulsified in 200 ml of medium or 2) if only 0.05 g of the preconcentrate (5%) was emulsified in the same volume. The emulsification behaviour of SEDDSs and SMEDDSs is frequently measured in the volume of 200 – 250 ml to which 1 g of the formulation or 1 capsule (containing 1g of SELF) is added (Cuine et al., 2007). The lowest dilution corresponded to the one produced in the typical emulsification test, while the higher dilutions were prepared to mimic incomplete release of 1g of the preconcentrate adsorbed onto a solid carrier. The preconcentrate 2A2 50: 50 upon dilution in blank FaSSIF-V2 formed slightly opalescent and transparent systems. The average particle size (Z-Aver) and polydispersity index (PDI) did not differ substantially in the range of prepared dilutions (Fig. 8.13, Appendix Table A.8.5). The emulsions formed from the preconcentrate showed the average particle size in the range from 100 to 130 nm and the polydispersity index of approximately 0.200-0.240. All the systems were polydisperse and mostly bimodal. Nevertheless the scattering intensity (Int) of the main peak (maximum at ~100 nm) was higher than 85% in all the samples, which meant that the average particle size (Z-Aver) was principally derived from the main peak.

While the average particle size and polydispersity index did not differ significantly in these various emulsions, the appearance of the samples was visually very different. The lowest dilution (~3.8 mg/ml of the preconcentrate) was an opalescent, slightly whitish, translucent system, while the highest dilution (~0.2 mg/ml of preconcentrate) was clear, fully transparent and visually resembled a solution.

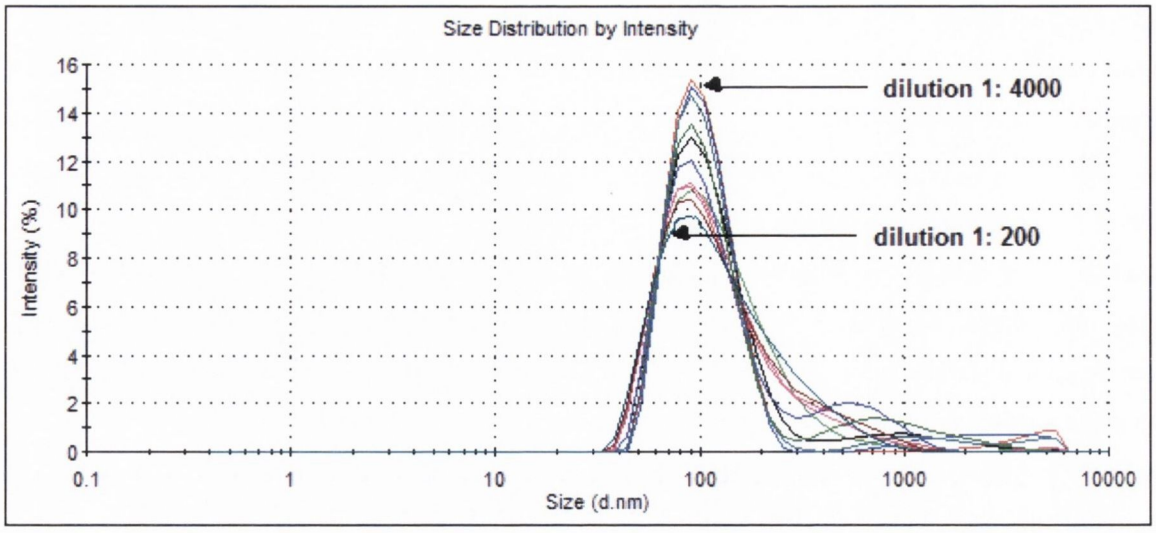

Fig. 8.13 Particle size distribution in the diluted samples of preconcentrate 2A2 50: 50 in blank FaSSIF-V2 (the highest peak corresponds to dilution 1: 4000. the smallest one represents 1: 200).

Transmittance of these samples appeared to be exponentially dependent on the concentration of the preconcentrate (Appendix Table A.8.6). The lowest dilution (~3.8 mg/ml of the preconcentrate) showed transmittance below 10% that gradually increased and became equal to 100% for the preconcentrate-free sample, blank FaSSIF-V2.

Desorption of the preconcentrate 2A2 50: 50 was evaluated with the S-SEDDSs with the highest adsorption capacity (the highest PEP). The emulsions formed after desorption from the S-SEDDS manufactured with Sylysia 320 (%AL = 65%), Aeroperl 300/30 (%AL = 60%), Zeofree 5161 (%AL = 70%), Hubersorb 600 (%AL = 71%) and Neusilin US2 (%AL = 70%) did not closely resemble the emulsions that were formed from the original preconcentrate (Fig. 8.14 and Fig. 8.15).

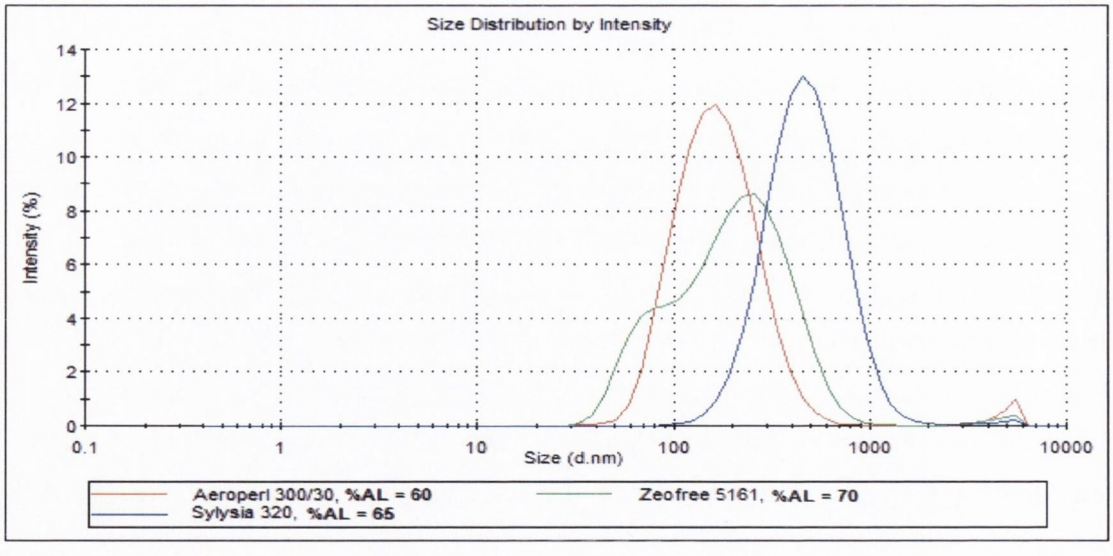

Fig. 8.14. Particle size distribution of the emulsions formed from the S-SEDDSs of Sylysia 320, Aeroperl 300/30 and Zeofree 5161.

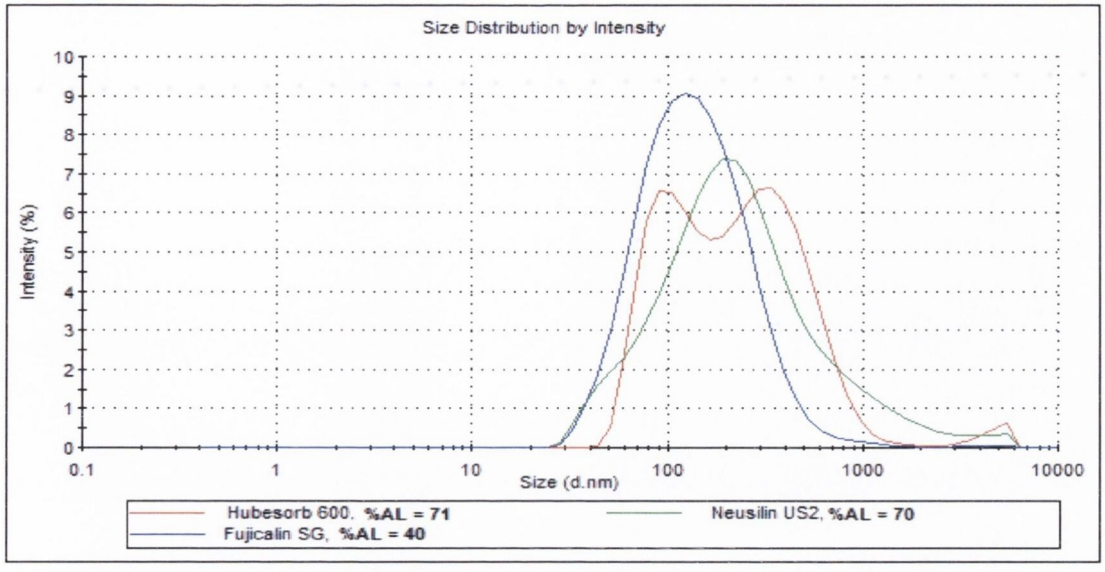

Fig. 8.15. Particle size distribution of the emulsions formed from the S-SEDDSs of Hubersorb 600, Neusilin US2 and Fujicalin SG.

The three emulsions formed from the S-SEDDSs formulated with Sylysia 320, Aeroperl 300/30 and Zeofree 5161 appeared coarser, having a larger average particle size, above 160nm (Fig. 8.16) compared to the particle size of the diluted preconcentrate (the original emulsion). Although the PDI values of the emulsions obtained from the solid systems with Sylysia 320 and Aeroperl 300/30 were similar to the one shown by the diluted preconcentrate (Fig. 8.17), it was not important since the average particle size differed. The emulsions desorbed from the S-SEDDSs of Hubersorb 600 and Neusilin US2 were also coarser and more polydispersed compared to the original emulsion (Fig. 8.16 and 8.17). The emulsion formed in the desorption test of the solid self-emulsifying system prepared with Fujicalin SG was very similar to the original emulsion (Fig. 8.16 and 8.17) as the similar average particle size and the polydispersity index were measured for both systems. This suggested that desorption of the preconcentrate from this S-SEDDS was more rapid than in the previous cases. Formation of the emulsion, having the same physical properties as the one formed by the liquid preconcentrate was very likely due to the presence of the desorbed preconcentrate as the whole system. None of the components appeared to be preferentially retained in the solid carriers and upon dilution these components self-emulsified into the system physically similar to the original emulsion. Alteration of the ratio between the components was likely to lead to formation of an emulsion with a different particle size distribution. The formation of the emulsions that physically differed from the original emulsion was seen with the other five carriers. This suggested that desorption of the components was not equally rapid (not simultaneous) and some components might have been released faster than the others. For examples, the emulsion formed from the desorbed S-SEDDS/ Sylysia 320 appeared to have low polydispersity but the average particle size was almost 450 nm. Theoretically, a 'reduced' amount of the primary surfactant would produce a coarser emulsion.

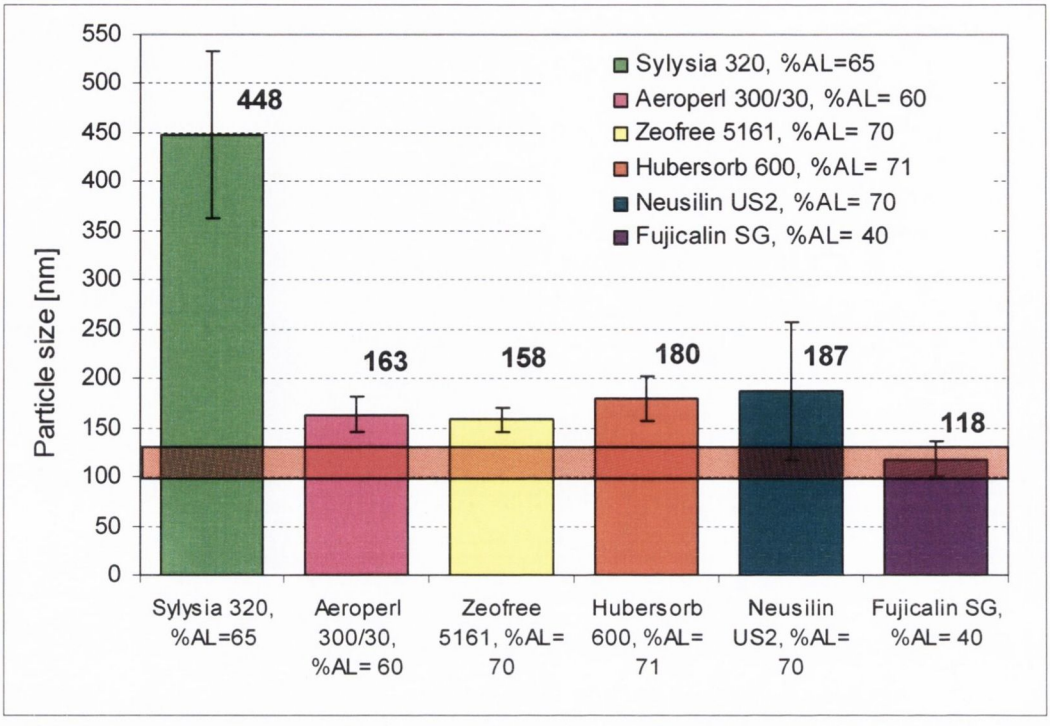

Fig. 8.16. Average particle size of the emulsions formed in the desorption study of S-SEDDSs. The red, semitransparent thick line denotes the expected Z-Average between 100 to 130 nm that would have been formed by the diluted liquid preconcentrate 2A2 50: 50.

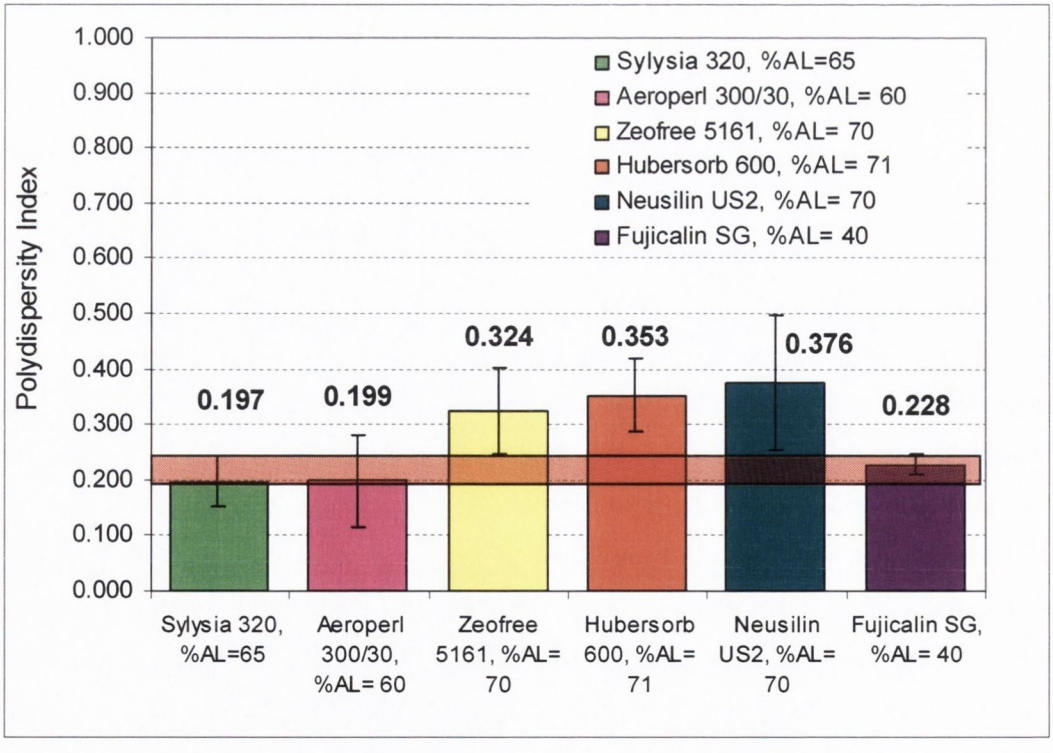

Fig. 8.17. Polydispersity Index of the emulsions formed in the desorption study of S-SEDDSs. The red, semitransparent thick line denotes the expected PDI from 0.200 to 0.240 that would have been formed by the diluted liquid preconcentrate 2A2 50: 50.

The emulsions obtained after desorption from the S-SEDDSs differed also visually in terms of opalescence and transparency. The emulsion created from the S-SEDDS/Zeofree 5161 was evidently clearer and more transparent compared to the emulsions formed from the solid systems formulated with Hubersorb 600 and Neusilin US2, although the particle size distribution of these three emulsions appeared very similar. The transmittance measurements were carried out on all the emulsions to make a relative comparison of transparency among the systems, compare them to a preconcentrate-free dispersing medium (blank FaSSIF-V2) and compare them to the original emulsion formed upon dilution 1: 200 (this mimics 100% release of preconcentrate) (Fig. 8.18).

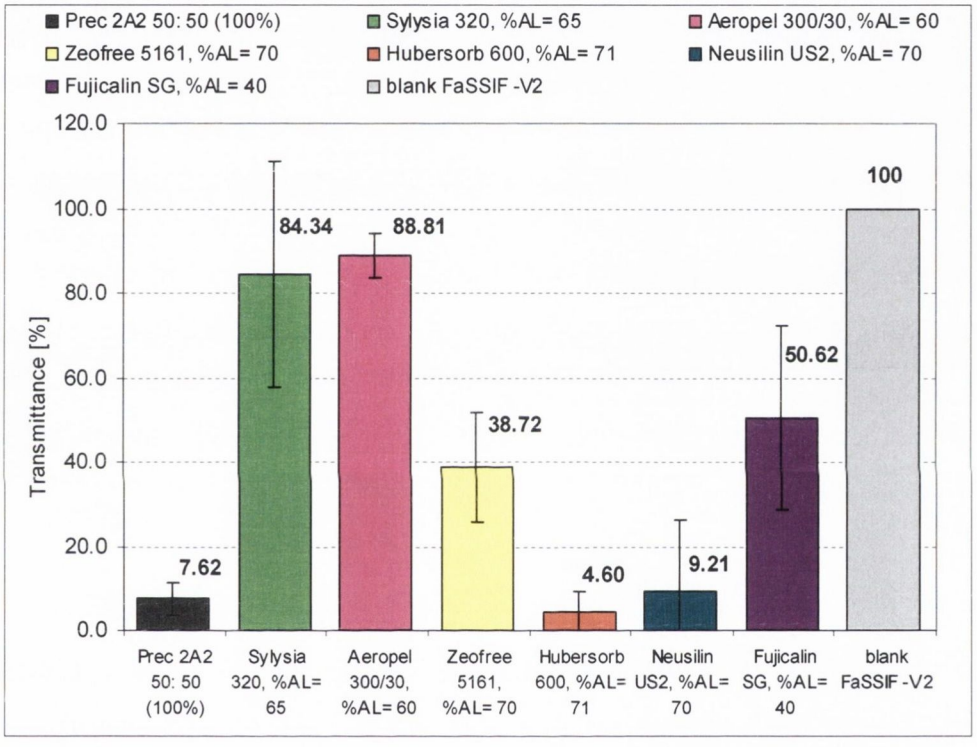

Fig. 8.18. Transmittance of the emulsions formed in the desorption study of S-SEDDSs.

The emulsions derived from the solid formulations of Sylysia 320 and Aeroperl 300/30 showed very high transmittance almost close to 90% (Fig. 8.18, Appendix Table A.8.8). Visually, these samples were clear and resembled blank FaSSIF-V2. On the other hand, the emulsions formed from the S-SEDDSs with Hubersorb 600 and Neusilin US2 were visually opalescent and showed the transmittance close to the original emulsion. The transmittance of the systems could be correlated to the concentration of the desorbed preconcentrate only if the original preconcentrate 2A2 50: 50 was desorbed. As the Z-Aver and PDI were different, based on the transmittance data it was not possible to estimate how much of the original preconcentrate was desorbed from the S-SEDDSs formulated with Zeofree 5161, Hubersorb 600 and Neusilin US2. Nevertheless, the high transmittance values obtained for the emulsions formed from the S-SEDDSs with Sylysia 320 and Aeroperl 300/30 suggested that desorption of any components of the preconcentrate was very poor

from these systems. Both these emulsions were clear and the presence of transparent system such as microemulsion or micelles was ruled out based on the particle size distribution, particularly for Sylysia 320.

In case of the emulsion formed from the S-SEDDS with Fujicalin SG, the particle size matched the original emulsion and a rough estimation of the desorbed preconcentrate was possible. Using the exponential relationship between the measured transmittance and the concentration of the preconcentrate 2A2 50: 50 (Appendix Table A.8.6), the amount of the desorbed preconcentrate was estimated to be on average 37% ± 31.6.

In the set of additional experiments (data not show in this thesis), factors such as the extended desorption time (from 15 minutes to 30 minutes), the increased amount of dispersive medium (volume increased twice) and the presence of additional surfactants (full FaSSIF-V2 used instead of blank FaSIF-V2) were employed to further examine desorption of the preconcentrate from the S-SEDDSs with Sylysia 320 and Aeroperl 300/30. None of these factors were found to improve 'recovery' of the preconcentrate or its components from these carriers and in all cases they formed emulsions were almost completely transparent.

Based on the observed emulsification behaviour the solid carriers could be classified as 1) 'poor desorption' (Sylysia 320, Aeroperl 300/30), 2) 'intermediate desorption', some components of the preconcentrate appeared to desorb to some extent (Zeofree 5161, Hubersorb 600, Neusilin US2) and 3) 'good desorption' where the preconcentrate appeared to desorb as a whole system (Fujicalin SG).

8.3.2. Desorption of Fat Red 7B dye

Desorption of SEDDS investigated by particle sizing and transmittance, relied on physical characterisation of the emulsion formed upon dilution from the S-SEDDS and the comparison of this emulsion to the emulsion that would be formed from the liquid SEDDS. It could not determine desorption of individual components of the system but evaluated emulsification of the desorbed components together by measuring physical properties the system they formed into *in situ*. Desorption of the liquid systems or their components from S-SEDDSs and S-SMEDDSs have not been studied by other researchers. These systems have been previously used to improve solubility and release of hydrophobic compounds and therefore the percentage of the dissolved drug from these compositions was used to determine good and poor desorption characteristics from the S-MEs and S-SELFs. The presence of the hydrophobic drug in the aqueous medium implies that the liquid lipid formulation system has partially desorbed as well, so the drug remains dissolved (solubilised) in the aqueous phase. Desorption of Fat Red 7B dye (FR7B), a non-ionic, water insoluble dye, was measured to further examine desorption characteristic of the solid carriers. The presence of the dissolved dye in the dispersing medium was considered as evidence that the components of the preconcentrate must have also desorbed (fully or partially) and maintained

FR7B in a solubilised form. The dye was treated in this experiment as a detectable hydrophobic marker, which was introduced into the aqueous phase via solubilisation or emulsification in the 'lipid carrier' (the components of the preconcentrate that desorbed). Therefore, the desorption of the preconcentrate or its components was examined indirectly in this experiment based on the concentration of dissolved water-insoluble marker. The percentage of dissolved FR7B was determined in the emulsions formed during the desorption test with the stained S-SEDDSs. The stained S-SEDDSs were produced as described in Chapter 2 (section 2.8.1 and 2.8.2). These were systems that adsorbed the maximum load of the preconcentrate (the PEP systems), similar to the solid (non-stained) samples used in the previous experiment. The percentage of dissolved FR7B determined in the desorbed emulsions is shown in Fig. 8.19. The dye was not detected in the emulsions formed from the S-SEDDSs with Sylysia 320 and Aeroperl 300/30, which suggested that a negligible amount of the preconcentrate or its components were released from the solid formulation. This observation was consistent with the conclusions made previously, based on the results of particle sizing and transmittance. The highest concentration of dissolved FR7B was measured in the emulsions desorbed from the S-SEDDS/Hubersorb 600, however this result was not statistically different ($p < 0.05$) to the one obtained for the emulsion/Fujicalin SG. The amount of FR7B detected in the emulsions formed after desorption of S-SEDDS/Zeofree 5161 and S-SEDDS/Neusilin US2 was similar but approximately half of the values obtained with Hubersorb 600 and Neusilin US2.

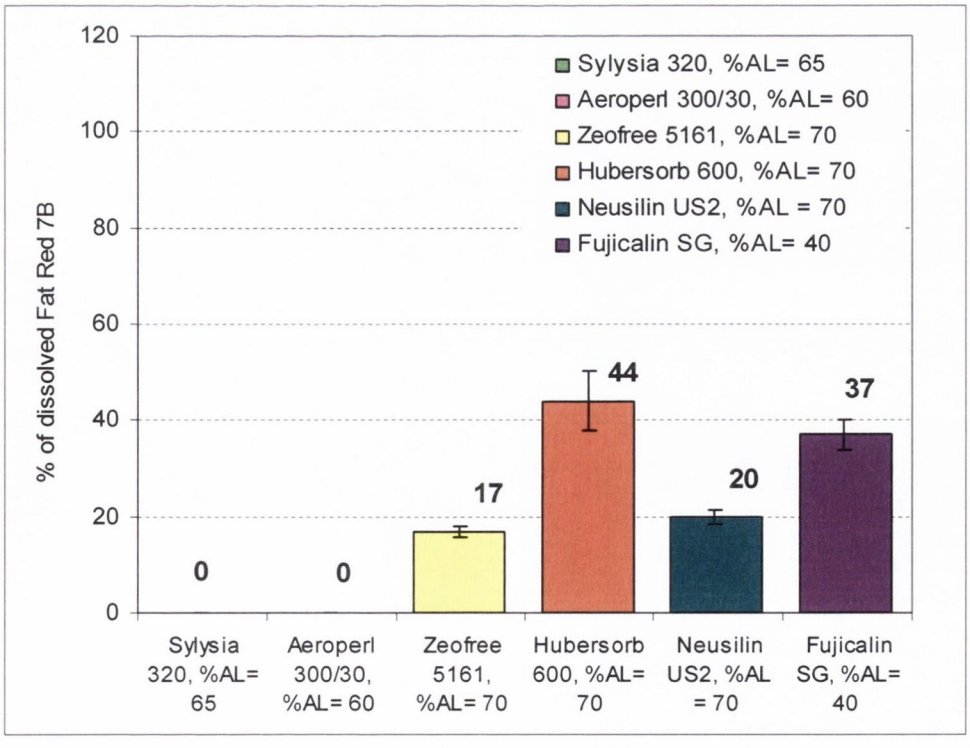

Fig. 8.19. Determination of % of dissolved Fat Red 7B in the emulsions formed in the desorption study of S-SEDDSs.

Based on the recovery of Fat Red 7B from the S-SEDDSs, the solid carriers could be again divided into the three categories: 1) 'poor desorption' – FR7B was not detected (Sylysia 320, Aeroperl 300/30), 2) 'intermediate desorption' – approximately 20% of the dissolved FR7B (Zeofree 5161, Neusilin US2), 3) 'good desorption – approximately 40% of dissolved FR7B (Hubersorb 600, Fujicalin SG).

8.3.3. SEM analysis of the desorbed S-SEDDS

SEM analysis was carried out on the solid, dried desorbed S-SEDDSs collected after the desorption test. The purpose of this analysis was to identify any differences in shape, size and appearance of the particles, which could provide additional information on the distribution of the preconcentrate onto particles. The 'desorbed' samples of Sylysia 320 (Fig. 8.20.b), Aeroperl 300/30 (Fig. 8.21.c & d), Zeofree 5161 (Fig. 8.22.c & d), Hubersorb 600 (Fig. 8.23.b) and Neusilin US2 (Fig. 8.24.c & d) did not differ from the original materials (Fig. 8.20.a, Fig. 8.21.a & b, Fig. 8.22.a & b, Fig. 8.23.a and Fig. 8.24.a & b, respectively) in terms of particle size and shape. In all these cases, the surface of particles appeared rather smoother as it was 'coated' with the preconcentrate.

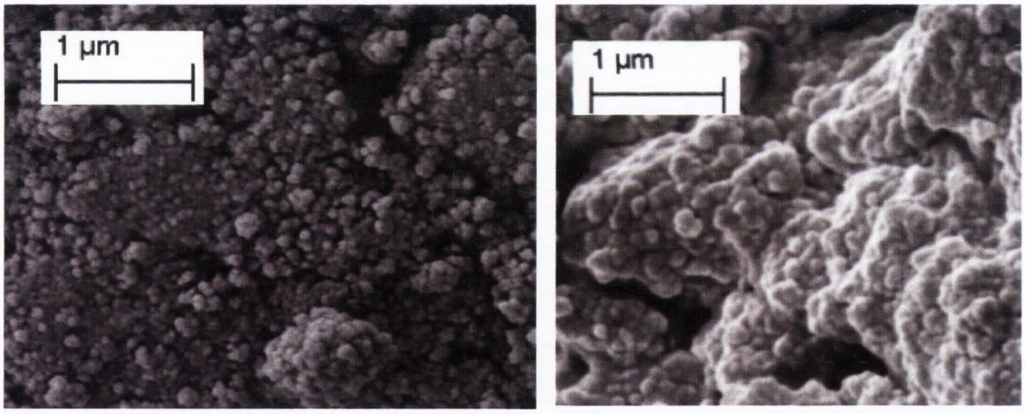

Fig. 8.20 SEM images of a) Sylysia 320 non-adsorbed, b) the desorbed S-SEDDS.

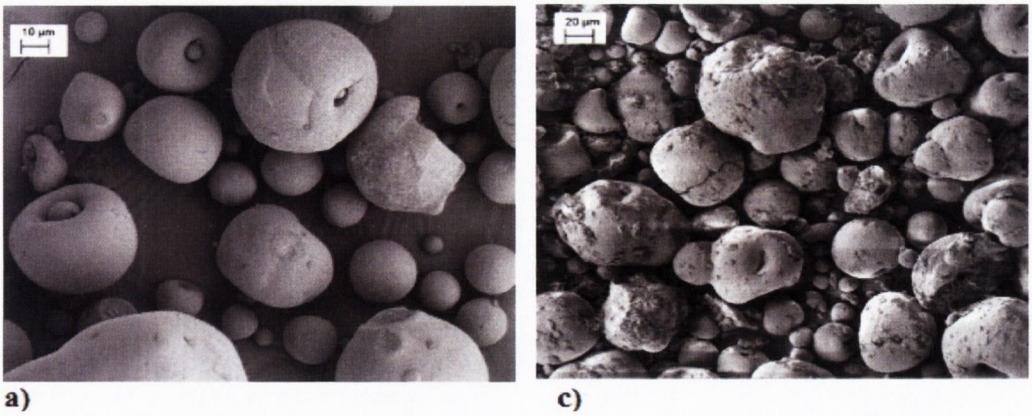

Fig. 8.21. SEM images of a) Aeroperl 300/30 non-adsorbed and c) the desorbed S-SEDDS.

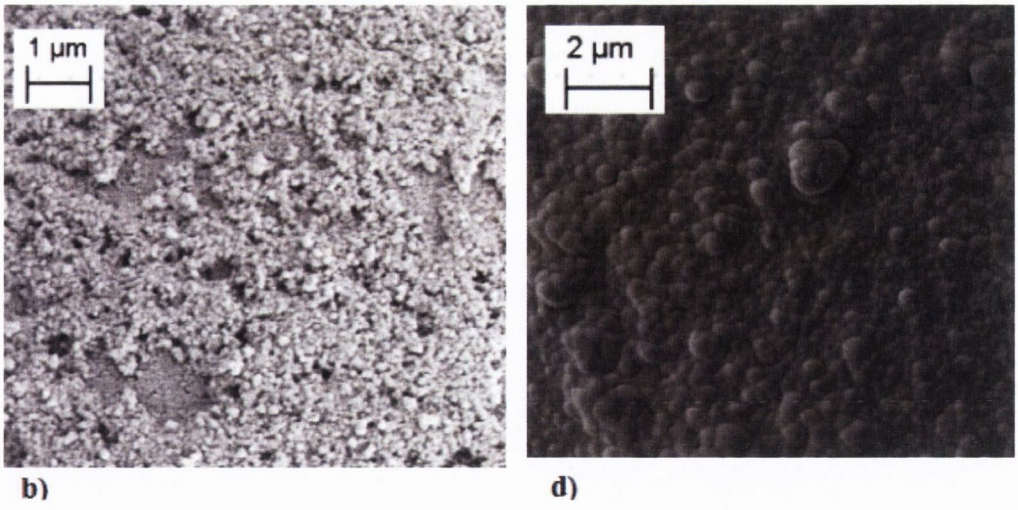

Fig. 8.21. SEM images of a, b) Aeroperl 300/30 non-adsorbed and c, d) the desorbed S-SEDDS.

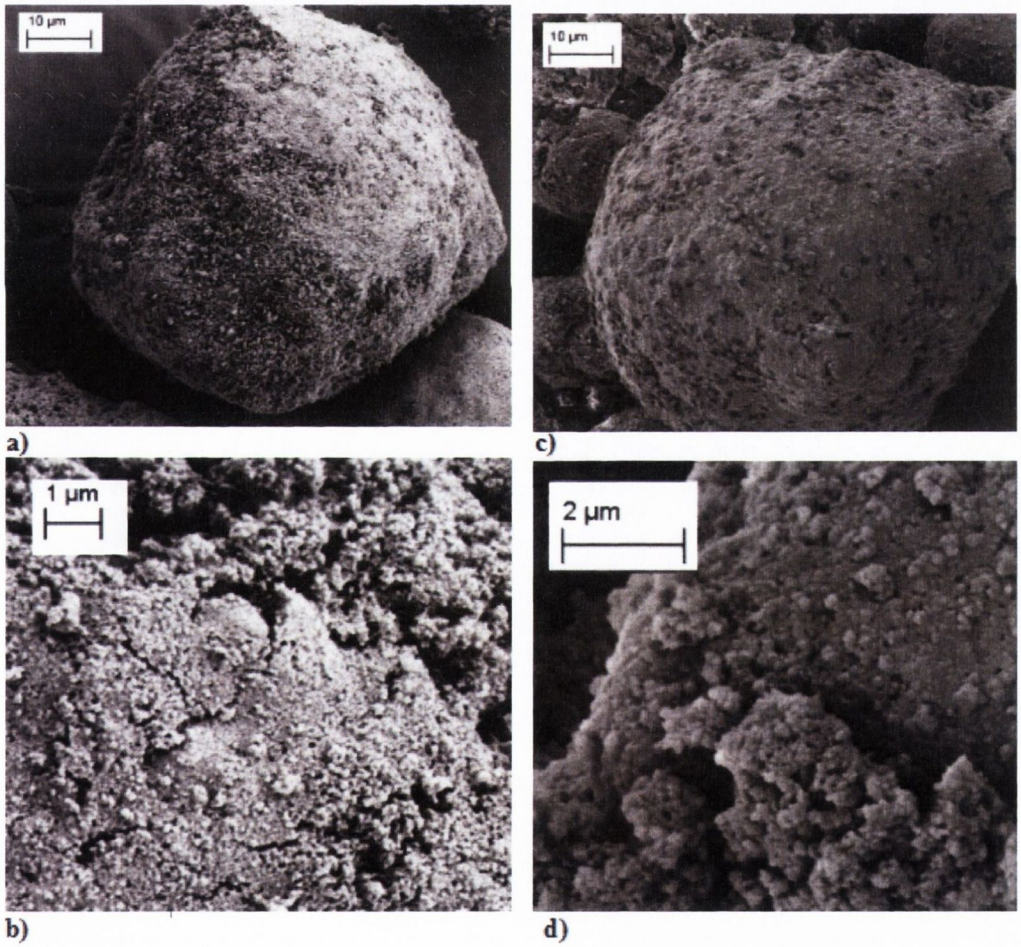

Fig. 8.22. SEM images of a, b) Zeofree 5161 non-adsorbed and c, d) the desorbed S-SEDDS.

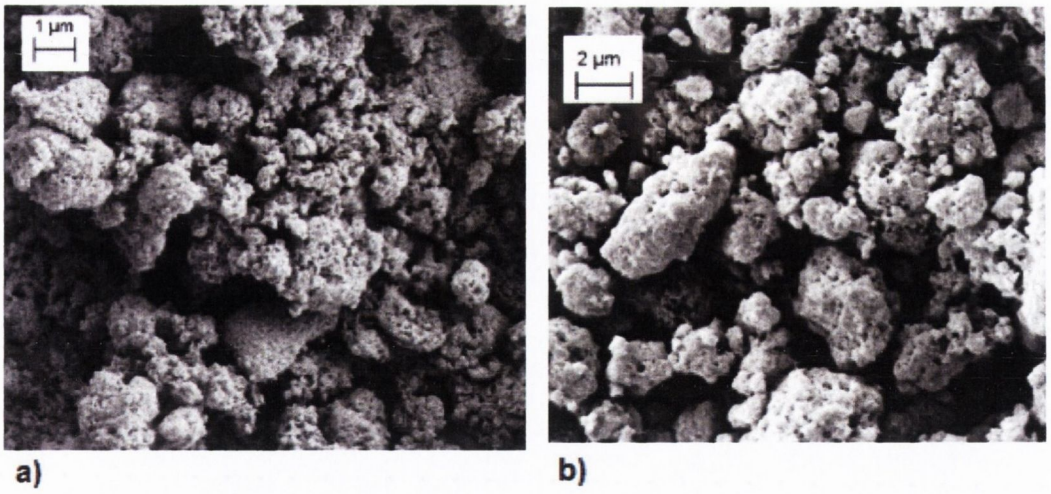

Fig. 8.23. SEM images of a) Hubersorb 600 non-adsorbed b) the desorbed S-SEDDS.

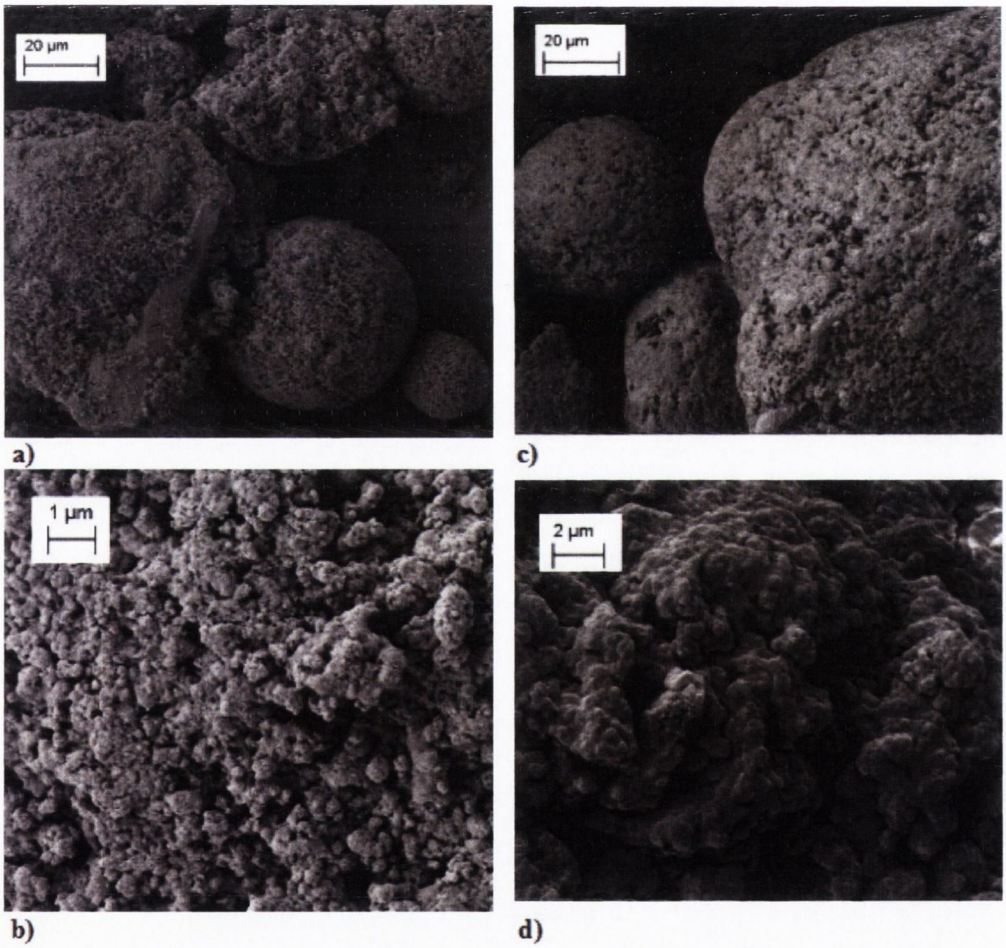

Fig. 8.24. SEM images of a, b) Neusilin US2 non-adsorbed and c, d) the desorbed S-SEDDS.

The appearance of particles in the desorbed S-SEDDS prepared with Fujicalin SG (Fig. 8.25.c & d) differed significantly from the original material (Fig. 8.25.a & b) The original, sample consisted of round, coarse granules ranging from 50-150 µm (Fig. 8.25.a), while the particles in the desorbed sample were very fine, smaller than 10 µm (Fig. 8.25.d). It appeared that the material disintegrated

into smaller particles during the dispersion test what could explain good desorption of the preconcentrate 2A2 50: 50 and Fat Red 7B dye from this S-SEDDS.

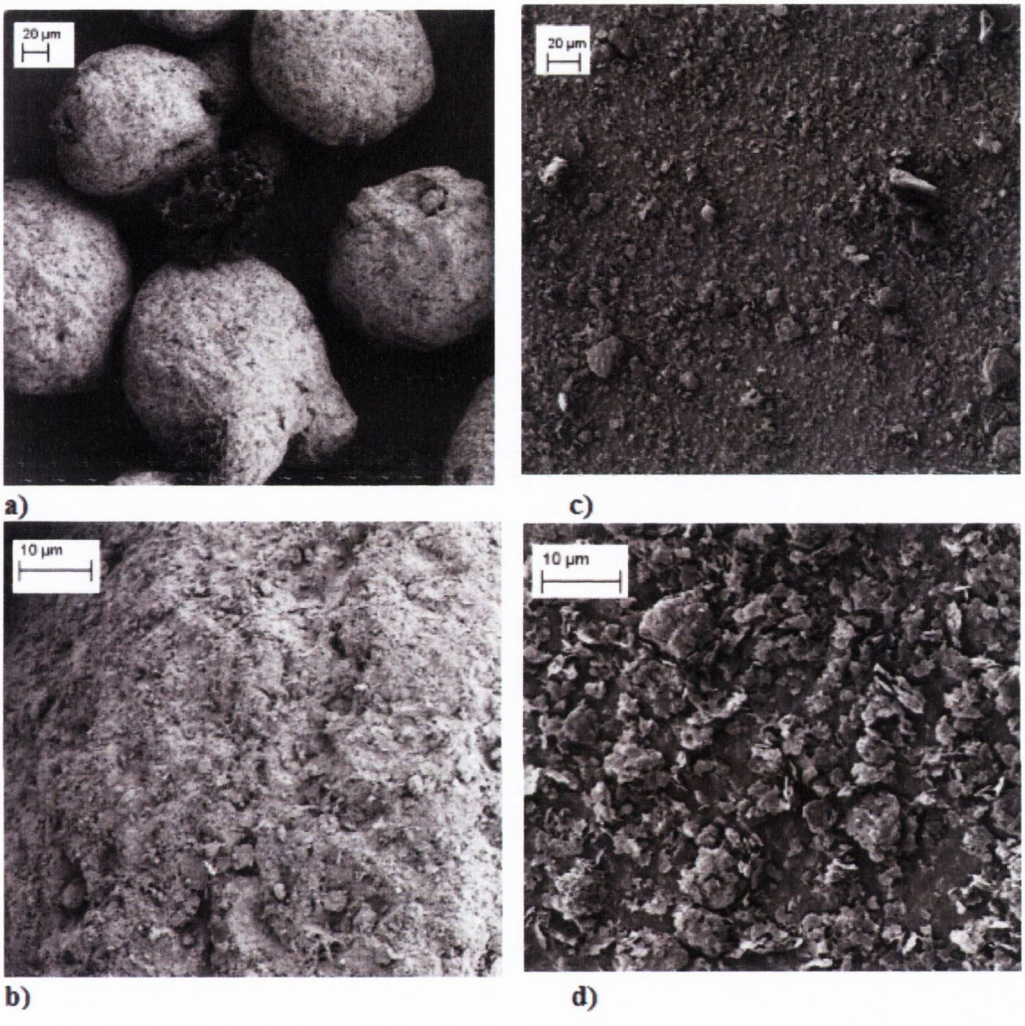

Fig. 8.25. SEM images of a, b) Fujicalin SG non-adsorbed and c, d) the desorbed S-SEDDS.

8.4. Overall Conclusions

Adsorption and desorption characteristics of the six solid carriers were investigated to select the best materials to produce S-SELFs. Very good adsorption capacity was observed for the three grades of silicon dioxide (Sylysia 320, Aeroperl 300/30, Zeofree 5161) and the other two silica materials i.e. Hubersorb 600 (calcium silicate) and Neusilin US2 (magnesium aluminum silicate). The adsorption capacity, also called the Powder End Point was determined with four different techniques that measured changes in physical properties such as flowability (BFE, SE), density (CBD) and resistance to flow (SS) as a function of gradually increasing liquid load incorporated into the samples. Each technique was capable of determining the Powder End Point in the examined samples, although the results for Sylysia 320 were the most difficult to interpret when BFE, SE and CBD measurements were employed. The Shear Stress (SS) technique was the most

sensitive and even the results for Sylysia 320 could be easily interpreted. The Final Powder End Point was chosen based on the outcomes of the four tests that assessed flow (BFE, SE) density/packing of particles (CBD) and shear properties (SS) of the S-SEDDSs (Table 8.2). The final Powder End Point for Sylysia 320 was based on the SS measurement and the appearance of the samples. The results from all four techniques were very consistent for the other five carriers and did not present ambiguities where the PEP occurred.

Table 8.2. Summary of PEP determined by different tests carried out on FT4 powder rheometer

Solid Carrier	Powder End Point (PEP) determined by				Final Powder End Point
	Basic Flowability Energy (BFE)	Specific Energy (SE)	Conditioned Bulk Density (CBD)	Shear Stress (SS)	
Sylysia 320	**50 %**	**65 %**	**60 %**	**70%**	**65%**
Aeroperl 300/30	**60 %**	**60 %**	**60 %**	**60 %**	**60 %**
Zeofree 5161	**70 %**	**70 %**	**70 %**	**70 %**	**70 %**
Hubersorb 600	**71 %**	**71 %**	**71 %**	**71 %**	**71 %**
Neusilin US2	**70 %**	**70 %**	**70 %**	**70 %**	**70 %**
Fujicalin SG	**40 %**	**40 %**	**40 %**	**40 %**	**40 %**

Based on the adsorption capacity, the best adsorbents were Hubersorb 600, Zeofree 5161 and Neusilin US2, as they could incorporate approximately 70% of Added Liquid. Their adsorption capacity was not directly correlated to the specific surface area or to the cumulative pore volume. Neusilin US2 was previously found to have almost three fold larger specific surface area (SSA_{BET}) and approximately twice larger cumulative pore volume compared to Hubersorb 600 and Zeofree 5161 (Chapter 7, section 7.4). A lack of direct correlation between the parameters that were expected to majorly influence the adsorption and the actual liquid load determined could be possibly related to the pore size. The pore size for Neusilin US2 appeared to be approximately twice smaller than that of the other materials. The diameter of pores may limit adsorption properties of a solid carrier if some pore are inaccessible or cannot be fully filled with a liquid, what might have been a case for Neusilin US2. In the case of Fujicalin SG, the gas adsorption results indicated the smallest specific surface area and cumulative pore volume among all the studied carriers, which was correlated to the findings of the adsorption experiments because this carrier could incorporate the lowest % of Added Liquid.

Desorption characteristics of the S-SEDDSs were examined in the relative dispersion test where release of the adsorbed preconcentrate was indirectly measured by particle sizing, transmittance and the percentage of dissolved dye that was water insoluble. These methods were not suitable to measure desorption of the individual components (i.e. polysorbate 80, Captex 355, etc.), neither was the dispersion test designed to give comprehensive information on how the

desorption process proceeded overtime. The dispersion (a single point) test was intended to make a relative comparison and select the carriers that had potential to release the adsorbed liquid rapidly. Sylysia 320 and Aeroperl 300/30 were found to have very poor desorption characteristics, clearly significantly worse than what was observed with the other four adsorbents. The best desorption characteristics were seen with S-SEDDSs prepared with Hubersorb 600 and Fujicalin SG. In particular, Fujicalin SG was a good desorbent which appeared to be related to disintegration of its granules in the dispersing medium creating a large surface area for the desorption process to take place. Slower desorption of the preconcentrate from the S-SEDDS prepared with Neusilin US2 was likely to be due to the porosity of the material and slow diffusion from the long pores. Agarwal et al. (2009) explained the difference between release of griseofulvin from the self-emulsified drug delivery system (SEDDS) formulated with Neusilin US2 (large particles ~80μm) and Neusilin UFL (small particles ~ 5μm) by the presence of a larger number of long and narrow intraparticular pores in Neusilin US2 compared to the other grade. The lower percentage drug released in 15 min from Neusilin US2 in comparison to Neusilin UFL was postulated as the retention and entrapment of the drug and formulation in the 'tortuous pores' (Agarwal et al., 2009).

Taking into consideration the adsorptive and desorptive characteristics of examined materials, Hubersorb 600 could be considered as the best solid carrier. However, this material was previously shown to contain impurities of lime (Chapter 7, section 7.6) which made the surface of this carrier highly alkaline and could comprise long-term stability of S-SEDDSs. In addition, the flowability of this material was also very poor (Chapter 7, section 7.5) making this carrier less suitable for directly encapsulated formulations. On the other hand, Zeofree 5161 and Neusilin US2 as silicates that typically contain free hydroxyl groups on the surface could develop chemical instability overtime between the adsorbed liquid and the carrier via formation of extra hydrogen bonds. None the materials appeared to be an ideal carrier that would show the highest adsorption capacity, rapid desorption characteristics, neutral pH of the non–reactive surface of particles and excellent flowability all at the same time. Nevertheless, Zeofree 5161, Hubersorb 600, Neusilin US2 and Fujicalin SG showed very good potential as solid carriers compared to Sylysia 320 and Aeroperl 300/30. The further selection of carrier(s) needs to be done after taking into consideration a long-term interaction between the adsorbent/adsorbate/drug and manufacturability requirements, which will be the scope of future work

Chapter 9

General Discussion

9.1. Introduction

Before carrying out the work presented in this thesis, little was known about preparations with derivatives of medium chain fatty acids, such as GIPET ® II technology (the 'Origin and Scope'). The foundation of the current work presented in the patents currently owned by Merrion Pharmaceuticals (Chapter 1, section 1.3.5) provided a limited knowledge and guidance about the formulation development of microemulsions (MEs) and self-emulsifying lipid formulations (SELFs) suitable for the incorporation of various hydrophilic compounds. The work undertaken in this thesis, focused on the development of liquid MEs and SELFs with a number of drug compounds with an emphasis on critical steps such as 1) physicochemical profiling of the model compounds to understand their solubility in aqueous and non-aqueous media and other factors that could affect their incorporation (distribution) into lipid formulations, 2) understanding the design of microemulsions and SELFs and how the type of cosurfactant, the type of oil phase and the combined HLB value of the system affects the formation of MEs/SELFs and their dilution behaviour, 3) characterisation of the model microemulsions to provide an insight into microstructure and identify the key techniques which could help to predict the drug distribution in these systems and the drug fate upon dilution, 4) incorporation of the model compounds into liquid MEs and SELFs to understand formulation limitations and constraints related to drug hydrophilicity and potential stability of capsules containing these formulations. As the last step of the current work, a new formulation approach to create a solid self-emulsifying system was initiated to overcome limitations encountered with the liquid formulations.

9.2. Physical characterisation of non-ionic microemulsions and self-emulsifying systems composed of derivatives of caprylic and capric acids.

Lipid microemulsions and SELFs composed of glycerides of medium-chain (6 to 12 carbons) fatty acids have attracted much interest as oral delivery systems for both lipophilic and hydrophilic drugs. Enhanced oral bioavailability of several drugs (ceftriaxone, cefoxitin, cyclosporine A) and peptides (SK&F 106760, GMDP) has been reported from lipid formulations comprising medium chain glycerides of caprylic and capric acids (Constantinides et al., 1995; Constantinides et al., 1994; Lyons et al., 2000, Chapter 1, section 1.3.5). Although, lipids such as Capmul MCM, Captex 335 and Captex 200P have frequently been used by other researchers in various formulations (also in combination with glycerides of long-chain fatty acids, phospholipids, lipophilic alcohols, etc.), systematic and comprehensive research to examine the impact of hydrophilicity/ hydrophobicity of the oil phase, the type of cosurfactant and its combination with the primary surfactants (such as polysorbate 80) on formation of MEs/SELFs has not been carried out before.

The oils used in the current work, Captex 355 (caprylic/capric triglyceride), Captex 200P (propylene glycol dicaprylate/dicaprate) and Capmul PG-8 (propylene glycol monocaprylate) differed in terms of hydrophilicity/hydrophobicity (Chapter 4, section 4.2.1), with Captex 355 being the most hydrophobic and Capmul PG-8 being the most hydrophilic. Capmul PG-8 was found to be miscible with the surfactants in every ratio (forming clear preconcentrates) but the microemulsion area formed upon dilution from these preconcentrates was limited and narrow (Chapter 4, sections 4.3.2 & 4.4.2). Despite its highly hydrophilic character, Capmul PG-8 did not form an extensive microemulsion region in a combination with polysorbate 80 and mono-diglycerides of caprylic/capric acids. In the work carried out by Prajapati et al. (2011), Capmul PG-8 (propylene glycol monocaprylate) effectively enlarged the microemulsion region in the pseudo-ternary systems composed of water, Cremophor EL, a mix of propylene glycol monocaprylate and propylene glycol dicaprylate. A ratio of 1: 1 between propylene glycol monocaprylate and propylene glycol dicaprylate led to the formation of an extensive microemulsion region compared to the ratio 1: 3, where the region of microemulsion was reduced and the presence of a large region of gel (liquid crystalline phase) was observed (Prajapati et al., 2011). The other two oils examined in the current work, were more hydrophobic. Captex 355 and Captex 200P were not miscible with the surfactants in every ratio. Captex 355 as the most hydrophobic oil was the least miscible with the mix of surfactants, but the preconcentrates comprising this oil showed good dilution behaviour, in particular when Capmul MCM C8 was used as a cosurfactant. The preconcentrate containing 50% of Captex 355, 32.5% of Capmul MCM C8 and 17.5% of Crillet 4 HP showed the best dilution behaviour among all examined preconcentrates (a microemulsion formed up to 30% of water at 37 °C). None of the examined preconcentrates could be considered as a SMEDDS since this system would be expected to form a very large region of the microemulsion upon dilution, up to approximately 200% of water (1: 200 is a typical dilution at which the particle size is tested to determine SEDDS/SNEDDS SMEDDS, Porter et al., 2004). Nevertheless, some preconcentrates prepared with Captex 355 and Captex 200P showed superior dilution behaviour to the preconcentrates with Capmul PG-8. Therefore as SEDDS formulations, they could potentially be used with hydrophilic, physically and enzymatically unstable drugs such as peptides, where the prolonged existence of water-in-oil microemulsion upon dilution *in vivo* could protect the drug against enzymatic degradation (Lyons et al., 2000).

In the current work, pseudoternary phase diagrams prepared with mono-diglycerides of mainly caprylic acid (Capmul MCM C8, Capmul MCM) and mono-diglycerides of mainly capric acid (Capmul MCM C10), used as a cosurfactants were prepared (Chapter 4, sections 4.3.1 & 4.4.2). In terms of chemical structure, Capmul MCM C10 (made with capric acid) could be considered as an elongated homologue of Capmul MCM C8, with one extra carbon atom in the esterified fatty acid chain. As co-emulsifying properties of these two surfactants relate to their chemical composition and structure, an evaluation of the length of the fatty acid chains affects the 'cosurfactant

performance' was made. Capmul MCM C8 was found to be a better cosurfactant than Capmul MCM C10 in both types of the systems: with the low (HLB = 6 - 9) and high (HLB = 9 - 14) combined HLB values. Capmul MCM C8 used as a cosurfactant, not only facilitated formation of larger microemulsion area upon dilution (systems with HLB = 6 - 9) but also reduced the formation of liquid crystalline regions (HLB = 9 - 14). The combined HLB values of the systems prepared with Capmul MCM C8 and Capmul MCM C10 differed by less than 1 HLB unit, since the individual HLB values of the cosurfactants were also close, approximately 5.2 and 4.1 respectively (as calculated in Chapter 4, section 4.2.2). One of the patent claims which refers to 'a surfactant or mixture of surfactants, wherein the surfactant or surfactant mixture has a hydrophilic-lipophilic balance value of from 7 to 14' (Owen et al., 1995), is quite general and the work undertaken demonstrated that a choice of cosurfactant is significant. Since Capmul MCM C10 showed poorer 'co-emulsifying' properties, a cosurfactant should be chosen carefully because, as the length of 'fatty acid chain' increased, the hydrophobic character prevailed over hydrophilic groups and the material became less useful as a cosurfactant. Capmul MCM C10 as a cosurfactant has not been studied by other researchers so far but clearly, as a cosurfactant, it has no advantage over Capmul MCM C8. When examining systems with a very high content of the cosurfactant (with a lower primary surfactant content), it was also noted that neither Capmul MCM C8 nor Capmul MCM C10 had strong enough emulsifying properties to form an extensive microemulsion area, therefore neither can perform effectively as the primary surfactant, the way polysorbate 80 acts. Another novel finding of this work relates to the ratio between the cosurfactant and the primary surfactant (polysorbate 80), in other words to the combined HLB value and its effect on formation of SELFs/microemulsions and their dilution behaviour. Among all the studied systems, the best dilution characteristics was seen in systems with the combined HLB value of 8.6, where the low HLB value surfactant (cosurfactant) was combined with the high HLB value surfactant in the ratio of 65 to 35. This narrows down the patent claim presented in the 'Origin and Scope' referring to 'a surfactant or mixture of surfactants, wherein the surfactant or surfactant mixture has a hydrophilic-lipophilic balance value of from 7 to 14'. In general, in the systems with the low combined HLB (7.9 and 8.6), the amount of the cosurfactant 'complemented' the amount of the (primary) surfactant which promoted formation of a microemulsion. When the combined HLB value was shifted towards higher values (above 9), the amount of the cosurfactant appeared insufficient to form a microemulsions in some areas of the pseudoternary phase diagrams and liquid crystalline structures were observed there.

To complement the work on selection of suitable materials for preparation of MEs/SELFs, further work evaluated the effect of additional factors on formation of MEs/SEDDSs, their physical stability and dilution behaviour. These factors included 1) the effect of temperature 2) addition of a cosolvent 3) and emulsification with a use of artificial intestinal fluids to mimic the behaviour *in vivo*. As the solubility of Crillet 4HP (polysorbate 80, a non-ionic surfactant containing

polyoxyethylene chains) increases at a lower temperature, an enlarged microemulsion area in the system with the low combined HLB value was observed at 25 °C compared to 37 °C (Chapter 4, section 4.6). In the pseudoternary phase diagrams studied by Spernath and Aserin (2006) composed of Ringers's solution, Tween 80 and the mix of glycerol monocaprylic ester and propylene glycol dicaprylic ester in the ratio 1:1, the temperature was also found to significantly affect the size of the microemulsion region in a similar manner. The reduced temperature did not affect the phase behaviour of the system with the high combined HLB value. The addition of a cosolvent to MEs/SELFs was examined, as there may be a need to incorporate another polar vehicle in a formulation for encapsulation. As the amount of water is typically restricted to a very low percentage in liquid formulations for encapsulation, other hydrophilic solvents can be added to solubilise the required dose of a hydrophilic drug in the capsule filling formulation. The addition of PEG 400 to the system with the low HLB value reduced the formation of clear SELFs and MEs (with less than 5% of water) previously formed in these systems (without the cosolvent). PEG 400 also had negligible effect on the dilution behaviour (Chapter 4, section 4.5) and therefore incorporation of this cosolvent in similar systems, could only be justified by good solubility of a drug in this vehicle. On the other hand, the addition of PEG 400 to the preconcentrates with the high combined HLB value, significantly improved formation of the microemulsion region upon dilution. It is known that partial replacement of cosurfactants and surfactants with high amounts of cosolvents such as PEG 400, could lead to a reduced solubilising capacity of these systems upon dilution (*in vivo*) where a poorly water soluble drugs may subsequently precipitate and as a consequence become less bioavailable (Pouton, 2006). On the other hand, the addition of certain amount of cosolvent(s) to the systems with the high content of surfactants promotes emulsification and reduces formation of viscous liquid crystalline structures leading to the improved dilution behaviour *in vitro*, as was demonstrated in the current work. According to Pouton (2000) at high surfactant concentrations, greater then approximately 65% depending on the materials, the progress of emulsification is compromised by viscous liquid crystalline gels, which form at the oil-water interface. These mixtures require energy to break up and in practice are not self-emulsifying systems (Pouton, 2000). Therefore, optimisation of emulsification behaviour *in vitro* aims to eliminate formation of liquid crystalline regions so emulsification and rapid release of the drug from a SELF is not compromised *in vivo*. Dilution of the model systems with the artificial intestinal fluids was carried out to examine the effect of additional surfactants on the phase behaviour. Although, pH and osmolarity are not expected to affect the dilution behaviour of non-ionic systems, the presence of additional surfactants in the artificial intestinal fluids may alter dilution behaviour. FaSSIF-V2 and FeSSIF-V2 had no significant effect on formation of the microemulsion in the system with the low HLB value, but an improved dilution behaviour was seen for the system with the high combined HLB value system (Chapter 4, section 4.7). This experiment demonstrated that water, frequently used as titrating medium, may underestimate the formation of microemulsion

in some cases and although it could be used in an initial study of dilution behaviour, it is worthy to employ intestinal media to better understand the dilution behaviour of systems where liquid crystals are detected.

Other researchers studied systems composed of the same and/or similar materials as the ones used in the current work, however the effect of various cosurfactants or the type of oil on formation of the microemulsion region was not investigated in the way presented here. Constantinides et al. (1994) constructed a pseudoternary phase diagram for a system comprising Captex 355 (the oil), Capmul MCM (a low HLB value surfactant), Tween 80 (polysorbate 80, a high HLB value surfactant) and deionised water where the pseudo-component was prepared as a fixed ratio between the oil and the low HLB value surfactant (Constantinides & Scalart, 1997). A different approach was used in the current work. Following the claims presented in patents US5444041A1, US5633226A1, US5646109A1, US5688761A1, US5707648A1 (Chapter 1, section 1.3.5), a fixed ratio between the low and the high HLB value surfactant was used. The approach undertaken, with the use of various cosurfactants and the oils provided a more comprehensive evaluation compared to the work carried out by Constantinides et al. (1994) which was limited to only one type of oil and one cosurfactant. In addition, the pseudoternary phase diagrams presented in the current work were prepared mainly at 37°C unless specified otherwise, in contrast to Constantinides et al.' work (1994) carried out at ambient temperature. The current approach examined dilution behaviour in the temperature more relevant to the human scenario, especially since non-ionic surfactants such as polysorbate 80 are sensitive to temperature. The solubilising /emulsifying character of polysorbate 80 decreases as the temperature increases. As the solubility of polysorbate 80 is reduced at 37°C, the procedure employed in the current work not only examined dilution behaviour in the 'human body temperature' but at the same time identified a number of stable, clear SELFs and microemulsions that would remain monophasic and transparent at lower temperature i.e. 25°C and 35°C. These two temperatures represent typical ICH storage conditions used to evaluate long-term and intermediate shelf life. Clear SELFs and microemulsions identified by the approach undertaken were likely to remain physically stable when stored at these conditions in a form of encapsulated dosage forms. It is also worth mentioning that a capsule filling formulation is frequently heated to 30 - 35°C during the encapsulation process to facilitate accurate dosing since its viscosity is typically reduced at higher temperatures. Therefore, the SELFs and microemulsions that did not separate at 37 °C appeared suitable for encapsulation, at least from a physical stability perspective. As mentioned earlier, the pseudoternary phase diagram published by Constantinides et al. (1994) was prepared at ambient temperature and the ambient temperature was not precisely defined. In the current work, a number of pseudoternary phase diagrams were prepared at 25°C and the temperature was carefully controlled because it has a significant impact on the phase inversion when polysorbate 80 is used. Preparing phase diagrams in ambient temperature that is not

controlled or/and accurately defined, when working with the surfactants showing phase inversion temperature (PIT) can easily lead to poorly reproducible results.

The next step of the current work focussed on characterisation of the microstructure in the model 'microemulsions' composed of derivates of caprylic/capric acid and polysorbate 80 as the primary surfactant. Identification of the microemulsion type (e.g. water-in-oil /Windsor II, bicontinuous/Windsor III, one phase/Windsor IV) helps to predict the distribution of a drug in the microemulsion and could provide an insight into probable chemical stability of the drug upon storage. Understanding how the microstructure changes upon dilution can be useful to predict the drug behaviour (e.g. possible precipitation, possible protection against enzymatic degradation). The characterisation techniques such as the SANS, DLS, cryo-TEM/ FF-TEM, conductivity, viscosity, PGSE-NMR and DSC were selected to provide comprehensive information on the structure of the selected model non-ionic colloidal samples derived from the preconcentrate 2A2 60: 40 (Chapter 5, section 5.2). This preconcentrate (together with the preconcentrate 2A2 50: 50) showed the best dilution behaviour at 25°C. The model colloidal samples represented gradual dilution of this preconcentrate with water, up to approximately 45% of the water content. The result of this comprehensive characterisation was that the model samples containing from 10% to 20% of water were identified as inverse micelles, while the samples with the water content between 20% and 45% were determined to be water-in-oil microemulsions. The PGSE-NMR and SANS were the most useful in determination of microstructure in the model colloidal samples. With regard to interpretation of the PGSE-NMR data, some differences were also seen in the sample examined compared to the 'typical PGSE-NMR criteria' for identification of the microstructure. For example, according to some researchers (Moulik & Paul, 1998, Ceglie & Lindman, 1987; Kumar & Mittal, 1999), the self-diffusion coefficients of water and the surfactant are of the same magnitude in water-in-oil microemulsions. This was not a case in the current work. The measured self-diffusion of water (10^{-10}) was significantly higher than for the surfactant (10^{-12}) in the model samples characterised in the current work. Nevertheless the examined systems were identified as water-in-oil systems based on the comparison of relative self-diffusion of water and oil (explained in detail in Chapter 5, section 5.7) and the SANS results. As the PGSE-NMR remains one of the more sophisticated techniques for studying microemulsions, it is not always available for all researchers and consequently many data presented in the scientific literature do not include these measurements. Nevertheless, as the complexity of microemulsions increases with the use of various components, there is a need to share 'non-standard' results that challenge the existing 'typical PGSE-NMR criteria' (Kumar & Mittal, 1999) and advance the understanding as to how to derive the microstructure from various self-diffusion coefficient data.

The SANS technique relies on 'unique' contrasting of the individual components in a studied system and many mathematical models are employed to translate neutron scattering patterns into various types of microstructures such as: spheres, lamellar structures, concentric cylinders, hinged

rods, etc. (King, 1999) which makes this technique very powerful and far more advanced than DLS which always assumes presence of spherical droplets. The SANS characterisation enabled determination of the type of microstructure and also provided particle size results for the samples studied. Based on the conductivity, viscosity as well as the DSC results, a transition from inverse micelles into water-in-oil microemulsions was detected when the water content reached approximately 20%. This observation combined with the particle size obtained from the SANS technique allows a characteristic particles size to be specified for water-in-oil micelles and microemulsions in systems composed of polysorbate 80 as the primary surfactant and mono-diglycerides as cosurfactants. It was mentioned in Chapter 1 (section 1.2.3) that various literature sources had reported different droplet size characteristics for microemulsions such as 15 – 150 nm (Friberg, 1990), 20- 200 nm, (Talegaonkar et al., 2008) and 10– 100 nm (Bagwe et al., 2001). In the current work, the systems containing from 10% to 20% of water, with droplets below 10 nm (Chapter 5, Table 5.6) were determined to be inverse micelles. The samples containing from 20% to 45% of water, with the particle size between 11 and 17 nm, were water-in-oil microemulsions. Although this finding applies to the systems where polysorbate 80 as a primary surfactant is used together with mono-diglycerides as cosurfactants, it contributes to the general knowledge of particle size distribution in microemulsions.

Other techniques such as conductivity, viscosity and DSC measurements that were employed to investigate the microstructure were found to be rather complementary to PGSE-NMR and SANS and not specific enough (when used alone) to give unambiguous evidence of microstructure type. In the model non-ionic colloidal samples, examined in the current work, the conductivity, viscosity and DSC measurements captured a certain change that occurred around 20% of the water content in the progressively diluted systems. However, the interpretation of this change was not obvious when the generated results were compared to the work of other researchers. The conductivity results published by other researchers for non-ionic systems are presented in Table 9.1 and Fig. 9.1. Although the shape of the conductivity curves remains similar in the published results, the existence of different types of microemulsion can be seen in the similar regions of the plots. The increase of conductivity beyond 20 % of water in Fig. 9.1 A- C, observed as a steep slope was explained by the existence of a water-in-oil microemulsion that converted into a bicontinuous phase when the conductivity began to stabilise (plateau was observed). On the other hand, in Fig. 9.1.D, the conversion of a water-in-oil microemulsion into a water-in-oil microemulsion took place in the middle of the steep slope and a bicontinuous phase was not observed in this system. Fig. 9.1.E. shows another interpretation of the conductivity data, where the bicontinuous phase was detected as the conductivity started to increase and this phase converted into an oil-in-water microemulsion in the middle of the steep slope. Phase transition between the various phases was confirmed by PGSE-NMR for the systems in Fig. 9.1 D & E (Table 9.1). Since PGSE-NMR technique appears to be the only direct way of probing the bicontinuity of microemulsions (Kumar

& Mittal, 1999), the interpretation of the results presented in Fig. 9.1.A, B and C may be found to be incorrect if further characterisation of these systems was carried out with PGSE-NMR.

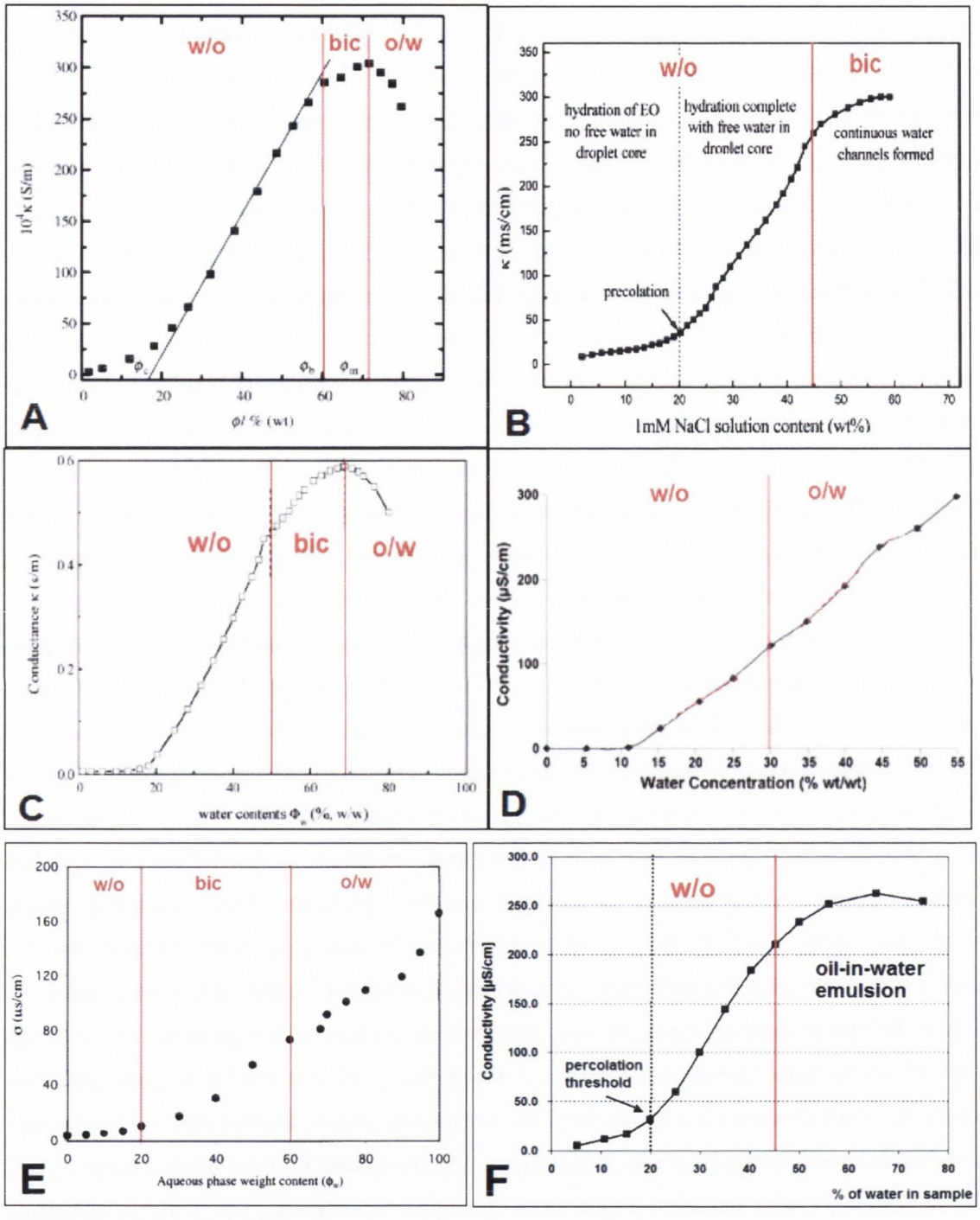

Fig. 9.1. Conductivity curves for non-ionic microemulsions published by other researchers (A-E) compared to the conductivity results collected for the non-ionic model microemulsion composed of Captex 355/Capmul MCM C8/Crillet 4 HP/purified water (F). Abbreviations: w/o = water-in-oil microstructure, bic = bicontinuous microemulsion, o/w = oil-in-water microstructure. The red line vertical lines separate different types of the microstructure defined in these systems.

Table 9.1. Determination of the microstructure of non-ionic microemulsions based on the conductivity measurements, published by other researchers.

Type of microemulsion determined	Composition of the non-aqueous phase of microemulsion	Percentage of water	Electrolyte present	Conductivity results (range)	The microstructure confirmed with other technique	Literature source
Water-in-oil	Non-ionic microemulsion composed of Span 20, Tween 80 and isopropyl myristate (IMP)	Up to 60%	Electrolyte not included, chloram-phenicol included in the oil phase of the system but not dissociated (dissolved) in the aqueous phase	0- ~ 280 x 10^4 S/m (increasing)	Not performed with more specific technique	Lv et al., 2006, **Figure 10.1. A**
Bicontinuous		60-72%		~ 280- 310 x 10^4 S/m (close to plateau)		
Oil-in-water		Above 72%		~ 310 – 260 x 10^4 S/m (decreasing)		
Water-in-oil	Non-ionic microemulsion composed of cetyl polyethylene oxide, n-butanol, heptane	Up to 45%	0.1mM NaCl solution as the aqueous phase	0- ~260 ms/cm (increasing)	water-in-oil structure suggested by UV-vis absorption of methyl orange (absorption spectrum is sensitive to medium)	Wang et al., 2008, **Figure 10.1. B**
Bicontinuous		Above 45%		~ 260 – 300 ms/cm (increasing)	Not confirmed by another technique	
Water-in-oil	Non-ionic microemulsion composed of rhamnolipid/*n*butanol/ water/n-heptane	Up to 45%	the rhamnolipid molecule existed in the ionic form in the system (as sodium salt) and therefore acted as electrolyte	0- ~ 0.5 S/m (increasing)	Not performed with more specific technique	Xie et al., 2007, **Figure 10.1. C**
Bicontinuous		45-65%		~ 0.5- 0.6 S/m (increasing)		
Oil-in-water		Above 65%		~ 0.6 –0.5S/m (decreasing)		
Water-in-oil	Non-ionic microemulsion composed of isopropyl palmitate (IPP)/water/ Brij 97/1-butanol	Up to approx 30%	the conductivity measurements were performed without deliberate incorporation of an electrolyte	0-~ 120 µS/cm (increasing)	water-in-oil structure suggested by self-diffusion NMR	Boonme et al., 2006, **Figure 10.1. D**
Oil-in-water		Above 30-35%		~120 – 300 µS/cm (increasing)	oil-in-water structure suggested by self-diffusion NMR	
Water-in-oil	Non-ionic microemulsion composed of R(+)-limonene, propylene glycol, ethanol, Tween 60	Up to 20%	a small amount of an aqueous electrolyte (a solution of 0.01 M NaCl) was added to water	0- ~ 15 µS/cm (increasing)	water-in-oil structure suggested by self-diffusion NMR	Yaghmur et al., 2003, **Figure 10.1. E**
Bicontinuous		20- 60%		~ 15- 80 µS/cm (increasing)	bicontinuous structure	
Oil-in-water		Above 60%		~ 80 – 160 µS/cm (decreasing)	oil-in-water structure suggested by self-diffusion NMR	

Conductivity of the model colloidal samples presented in the current work, was measured without the addition of any electrolyte. Although the inclusion of electrolyte in non-ionic systems would appear to be necessary to obtain measurable conductivity (Boonme et al., 2006), this was not the case in the model colloidal samples studied. The percolation threshold (a transition of inverse micelles into water-in-oil microemulsions, Fig. 9.1.F) was easily detectable at around 20% of the water content. Relatively high conductivity within the range from 5- 254 μS/cm was measured in the studied systems (electrolyte-free). High conductivity was also measured in electrolyte-free, non-ionic microemulsions studied by other researchers (Figure 9.1.A & D). Fanun (2010) investigated conductivity of an electrolyte-free microemulsion system containing mixed nonionic surfactants (sucrose laurate and ethoxylated mono-di-glyceride) and electrical conductivity shown by these systems was associated with the presence of 'conductive residues' in the components of the system.

Interpretation of viscosity results is challenging, in a similar way as the interpretation of conductivity data. Variety of oils and surfactants and their combinations produce a wide range of microemulsions where viscosity can vary significantly not only due to the type of the microstructure but mainly due to viscosity of individual components. In general the rheological behaviour of microemulsions is considered as not very revealing (Kumar & Mittal, 1999) as typically low viscosity and Newtonian flow behaviour are expected from these systems. In some systems it has been observed that around the transition from a droplet structure to a bicontinuous structure a maximum in the viscosity occurs (Kumar & Mittal, 1999). This was not a case in the studied systems, where the highest viscosity was determined for inverse micelles, while the subsequent reduction of viscosity was caused by transition into water-in-oil microemulsions (Chapter 5, section 5.6). Conductivity and viscosity are frequently used as these are simple methods that do not require expensive and technically advanced equipment. Nevertheless, the comparison of the conductivity data discussed above emphasises the need to use more specific and reliable characterisation techniques such as PGSE-NMR and SANS. Both PGSE-NMR and SANS have capability to 'access' information on the individual components of the systems while conductivity and viscosity measures only changes of the whole system. For examples, PGSE-NMR measures values of self-diffusion coefficient of water, oil and a surfactant and the relationship between these three components is used to determine the type of microstructure. The increased water content in the samples R5 - R9 (Chapter 5, section 5.11) could be correlated to the increased viscosity and the increased self-diffusion coefficient of water measured by PGSE-NMR. The viscosity analysis did not provide any additional information, while the PGSE-NMR analysis also examined diffusion behaviour of the oil and the surfactant as the content of water increased. Based on the current work, the use of PGSE-NMR and SANS would be highly recommended, especially when new systems (with new materials combined in various ratios) are explored. It is still useful to perform viscosity and conductivity measurements as complementary characterisation. Eventually,

once the systems are well characterised and certain types of microstructure are determined (with PGSE-NMR and SANS), it may be possible to 'translate' changes captured in measurements of viscosity and conductivity, and later apply these techniques to a more routine testing e.g. when minor changes (such as increased content of oil, possibly different type of oil, etc.) to the system are made and therefore minor changes in the microstructure are expected. Although, the use of advanced methods should not be avoided, it may be possible to routinely employ these inexpensive methods if the new system was fully characterised at the start of the work. This strategy was applied in the presented work. PGSE-NMR and SANS, cryo-TEM/FF-TEM, DLS together with the complementary techniques (conductivity, viscosity, DSC) were employed to thoroughly examine the model colloidal samples, which not only helped to establish the microstructure in those samples but also to explore the usefulness and applicability of each method to similar non-ionic systems composed of derivatives of caprylic and capric acids. The model colloidal samples represented the most 'dilutable preconcentrate' (2A2 60: 40), the one that could incorporate up to approximately 45% of water and therefore the diluted samples formed from it were the most likely to represent a number of different microstructures. Only inverse structures (inverse micelles and inverse microemulsions) were present, which suggested that similar compositions are likely to be inverse systems as well, which would convert into oil-in-water emulsions upon dilution.

Another technique that is widely used to characterise the particle size of microemulsions is DLS. However, this technique was found to be poorly suited for measurements of droplet size in non-diluted, concentrated samples such as the model microemulsions. The DLS results generated in the current work, despite adequate corrections being made following the work of other researchers (Cheung et al., 1987; Saint Ruth et al., 1995; Aboofazeli et al., 2000) were not in a good agreement with the SANS results. This clearly indicated that the outer phase was more complex than what was assumed. Neither SANS or PGSE-NMR was able to distinguish between Captex 355 (the oil) and Capmul MCM C8 (the cosurfactant) and therefore to determine how much of the cosurfactant was distributed in the interface and how much remained dissolved in the oil phase. As a result, the viscosity of the outer phase remained unknown. It may be possible to further investigate how the surfactant and the cosurfactant partition between the oil and the water phase in the concentrated systems, however application of DLS to concentrated samples will remain a time consuming method which may be still based on many assumptions. Although some researchers continue to apply this technique to study the microstructure of the concentrated sample, the method is widely used to study particle size of diluted microemulsions (e.g. formed by dispersing 1 g or 1 ml of microemulsion/SELF into a large volume of dissolution medium such as 200 – 1000 ml). Based on the current work, this method would not be recommended as a predictable and fast technique to study similar, concentrated microemulsions where a cosurfactant can remain partially dissolved in the oil phase.

The DSC measurements employed to probe the state of water in the colloidal samples, following the work of other researchers, provided interesting observations (Chapter 5, section 5.9). Limited studies have been published so far where thermal analysis was used to establish the microstructure of microemulsions and the detection of solidification/melting peak of water appeared to be correlated with the presence of oil-in-water or bicontinuous microemulsions (Boonme et al., 2006; Podlogar et al., 2004; Liu et al., 2009). In the work carried out here, the detection of a solidification peak was not associated with oil-in-water or bicontinuous microemulsions but indicated the formation of water-in-oil microemulsions (20% – 45% of water) while the samples 'without water peak' appeared to be solutions (5 -10% of water) and inverse micelles (10- 20% of water). The conclusions of the other researchers were supported by other characterisation techniques, which appeared to agree with their conclusions on the thermal behaviour. The results generated within the present work, demonstrated that interpretation of DSC results with regard to the microstructure should be performed carefully and considered together with other results as detection of a 'water peak' does not always indicate the presence of an oil-in-water or bicontinuous microemulsion. The DSC study, where the 'water peak' was detected in a water-in-oil microemulsion, has not been published before, therefore this work revealed a new finding in this area. The application of the DSC technique to detect 'bound', 'interfacial' and 'free/bulk' water (definitions presented Chapter 5, section 5.9) in microemulsions could also be seen as a new preformulation tool to probe the solubilising capacity of these systems to incorporate hydrophilic drugs. As a part of preformulation work, solubility of hydrophilic drug in various aqueous media is studied with the intention of dissolving the drug in one of these media and subsequently incorporate this aqueous phase (containing the drug) into a microemulsion. The DSC results generated for the samples containing 5- 20% of water, suggested that water was fully 'bound' with the surfactants and did not exist as 'bulk/free water' (a separate phase). This observation has a significant impact on the incorporation of a drug into a microemulsion. It means that the solubility of a required drug dose in the aqueous phase (before the phase is incorporated into the microemulsion) does not guarantee the solubility of this dose in the final microemulsion. Once the aqueous phase (containing the drug) is incorporated into the microemulsion, the interaction between the surfactant(s) and water may lead to precipitation of the drug (e.g. lack of sufficient solubility of the drug was observed in the aqueous microemulsions presented in Chapter 6, section 6.2). It becomes evident that interaction with the surfactant(s) alters properties of the aqueous phase and the drug may not remain soluble in the 'new vehicle' any longer. The linear plot between the water content and the normalized enthalpy (Chapter 5, Fig. 5.19) of 'water peaks' allows the percentage of 'bound water' to be determined.

Although, cryo-TEM is considered to be a very useful technique in direct imaging of microemulsions, it was not found useful in characterisation of the model colloidal samples composed of glycerides of caprylic/capric acids, likely due to insufficient contrast between the components. On the other hand, freeze fracture replicas (FF-TEM) provided interesting images of

the samples, however interpretation was still problematic without results from other techniques. The images of the samples containing 15% of water did not reveal any evident droplet –like or other structures, but the surface appeared 'rougher' compared to an image of a single solvent. When the SANS results become available, the diameter of the droplets in this sample was shown to be around 8 nm. Since the resolution of FF-TEM is limited down to 10 nm, droplets as small as 8 nm could not have been clearly displayed but the rough surface indicated multiple, overlaid small droplets. Lamellar, bilayer structures were observed in the freshly mixed sample containing 45% of water, but after 24 hours this sample resembled a bicontinuous phase to some extent. The SANS and PGSE-NMR results confirmed that this samples differed slightly from the ones with the lower content of water. With the water content exceeding 50%, an emulsion was formed. It was possible that the sample with 45% of water was a water-in-oil microemulsion where transition into a bicontinuous phase started and once 50% of water was reached the system fully converted into an oil-in-water emulsion. This explanation correlated well with the images of the observed structures. Nevertheless, based on the current work, cryo-TEM and FF-TEM would not be recommended as first choice techniques to reveal the type of the microstructure in similar microemulsions, as additional characterisation was finally required to complement the observations.

A number of significant observations were made when characterising the model colloidal samples, which not only allowed PGSE-NMR and SANS to be identified as the best tools to characterise the microstructure, but also established the techniques which provided the insight into distribution of water in microemulsions and how the interaction with surfactants could potentially limit its 'availability' as an aqueous phase.

9.3. Liquid microemulsions and self-emulsifying systems for use with BCS Class III compounds

Further work was carried out to evaluate the suitability of liquid microemulsions to incorporate protein, peptides and other organic compounds with high aqueous solubility and low permeability (BCS Class III, Amidon et al., 1995). Various aqueous phases have been used by other researchers to facilitate a high drug load in microemulsions. The amount of the aqueous phase used in these formulations varies widely from 10% (Cheng et al., 2008), 24% (Qi et al., 2011) up to 88% (Mrestani et al., 2010). Although, an improved relative oral bioavailability of the studied compounds was acquired from all aforementioned microemulsion formulations compared to the drug administered alone (dissolved in an aqueous phase), none of them appeared to contain a low amount of the aqueous phase that would ensure acceptable stability of the encapsulated final form. The aqueous versions of microemulsions for bisphosphonates were designed bearing in mind the potential stability of the final encapsulated dosage form, and therefore the content of the aqueous phase was limited to 8%. During the preformulation work sodium alendronate trihydrate was found to be the most soluble in the modified K-McIlvaine's buffer pH 7.8 (before incorporation of the

drug) and also showed high solubility in pH 2.2 (Chapter 3, Table 3.5, Fig. 3.8). When investigating solubility of this compound in non-aqueous media such as propylene glycol and the standard GIPET ®II formulation, a new solvate was identified. In propylene glycol, sodium alendronate trihydrate was found to exchange the hydrated water and form a solvate with one molecule of propylene glycol. High solubility of disodium pamidronate pentahydrate was found in the modified K-McIlvaine's buffers having initial pH of 4.4, 5.2 and 7.4 (Chapter 3, Table 3.6, Fig. 3.10) while the solubility in propylene glycol and the standard GIPET ®II formulation was very poor. The aqueous formulations developed for the bisphosphonates were equivalents of capsule fill having size/volume of 1 g/1ml of the microemulsion. This meant that the amount of the aqueous phase was limited (~80mg, 8% of 1000mg) but these formulations had a real potential to become an encapsulated physically stable dosage form if a sufficient amount of the drugs could be dissolved. The theoretical load of sodium alendronate trihydrate that should dissolve in the microemulsion prepared with the modified K-McIlvaine's buffer pH 2.2 (initial pH), should have been at a minimum 3.6 mg per 1g of formulation since the solubility of the compound in this buffer was 43.11 mg /ml (Chapter 3, section 3.2.5) and 80 mg of this buffer was incorporated into 1g of the microemulsion. The load of disodium pamidronate pentahydrate in 1g of the microemulsion prepared with the modified K-McIlvaine's buffer pH 4.4 (initial pH), should have been 6.1 mg based on the solubility of 70.47 mg/ml in this buffer (Chapter 3, section 3.2.5) and the amount of the aqueous phase (80 mg). The actual solubility of both bisphosphonates in the aqueous microemulsions was well below 1 mg/1g which was at least three times worse for alendronate and six times worse for pamidronate compared to the theoretical values predicted based on the solubility values and the content of the aqueous phases. The discrepancy between the theoretical and actual drug load was evidence for the 'bound water' that did not exist in a free form (available as a vehicle) in these microemulsions as discussed before in section 9.2. The attempt to incorporate bisphosphonates in the aqueous microemulsions was not successful due to their poor solubility in these systems. It was not possible to prepare clear microemulsion formulations with the high dose of these compounds. This work clearly highlighted that the solubility and a required drug load are the main obstacles that may prevent development of clear microemulsions with many other hydrophilic compounds. A third model compound was a novel chemical entity, a decapeptide that only recently has been administered orally in humans for the first time. As a decapeptide, it differed significantly from the bisphosphonates and the preformulation work identified a number of critical factors that affected development of encapsulated liquid microemulsions with this drug. The major problem was related to gelling. Acyline monoacetate showed an unfavourable propensity to rapidly form gels in various aqueous solutions (Chapter 3, section 3.3.5) and therefore self-emulsifying systems (SEDDSs, non-aqueous microemulsions) were developed containing approximately 5% of glycerine or propylene glycol and 19.5% of PEG 400 or PEG 300. Prolonged physical stability of dissolved acyline in propylene glycol or glycerine was a significant improvement compared to

stability in any aqueous medium. Nevertheless, the final non-aqueous formulations appeared to be physically and chemically stable at a very low temperature for a limited period of time (Chapter 6, Tables 6.2, 6.5, 6.6) while gelling was rapidly evident at higher temperature. The gelled formulations showed a significantly slower dissolution rate of acyline (Chapter 6, Tables 6.3 & 6.4 Figs. 6.1 & 6.2) compared to freshly prepared, non-gelled liquid formulations. The poor physical stability of acyline monoacetate in the liquid formulations was a significant obstacle to the development of stable commercially viable, encapsulated formulations. On the other hand, oral bioavailability of acyline was significantly improved with the liquid (non-gelled) SEDDSs.

The preclinical study presented in the current work is one of the first oral animal biostudies with acyline, as it has been previously only administered subcutaneously. All formulations were liquid, without signs of gelling at the time of administration. Acyline administered in purified water (unenhanced formulation) showed a significantly lower absorption extent in comparison to performance from two liquid SEDDS formulation (Test Item 3 and Test Item 4). The oral bioavailability of acyline from these SEDDSs was increased (on average) by 22 and 33 fold respectively and therefore considered as superior to the unenhanced formulation (statistical significance $p < 0.05$). The calculated elimination rate constant was the same for all four formulations. Acyline monoacetate administered in water showed inconsistent and variable absorption rate compared to the three SEDDSs used in the study. Although the mean values of T_{max} and $T_{1/2}$ were not statistically different between all four test items, the absorption of acyline from the unenhanced formulation was clearly impeded. All three SEDDSs showed low relative standard deviations for these parameters while variability was clearly at least twice higher for the unenhanced formulation. There could be at least two possible explanations for the more variable extent of absorption of acyline when delivered in purified water. When the unenhanced formulation was mixed with the intestinal fluids, gelling could have occurred and therefore acyline dissolved slowly (gradually) and became also slowly absorbed. If this was true, it appeared that acyline incorporated into the SEDDSs was protected from rapid gelling. Also, the absorption rate of acyline could have been slow due to its relatively large molecular weight. Again if this was the case, both rate and extent of absorption were significantly improved in the presence of SEDDSs. Table 9.2 presents a comparison of the acyline biodata and the biodata published by other researchers generated using formulations based on the same lipid materials and surfactants (used in different ratios).

Table 9.2. Comparison of the preclinical data for similar formulations based on glycerides of caprylic/capric acids published by other researchers, with the results obtained for acyline.

Compound/ Molecular weight	Animal model and administration mode	Formulation (w/w)	Biodata (Reference)
GMDP (N-acetylglucosaminyl-N-acetyl-muramyl dipeptide) / **M_W= 695** (Rajadhyaksha, & Lahey, 2004)	Fasted rats (n = 3), body weight 250-300g, items dosed via intraduodenal cannula	65% Captex 355, 22% Capmul MCM, 10% Polysorbate 80, 3% water ***1 ml of ME containing 128.3 µg of API was dosed and flushed with 0.2 ml of saline***	Fabs% (unenhanced) = 8.3% ± 4.4% Fabs% (microemulsion) = 80.1 ± 30.5% **Oral bioavailability increased by 10 fold (on average)** (Lyons et al., 2000)
SK&F 106760 (a water-soluble RGD peptide) / **M_W = 634**	Fasted rats (n = 3) average weight not disclosed, items dosed via intraduodenal cannula	65% Captex 355, 22% Capmul MCM, 10% Polysorbate 80, 3% saline ***~1 ml of ME containing ~2.5 mg of API (8.4 mg/kg) was dosed (3.3 mg/kg) and the flush volume unknown***	Fabs% (unenhanced) = 0.5% ± 0.3% Fabs% (microemulsion) = 27.4 ± 8.9% **Oral bioavailability increased by 55 fold (on average)** (Constantinides et al., 1994)
Calcein (a water-soluble marker molecule) / **M_W = 623**	Fasted rats (n= 4 - 6) average weight not disclosed, items dosed via intraduodenal cannula	65% Captex 355, 22% Capmul MCM, 10% Polysorbate 80, 3% saline ***~1 ml of ME containing ~1.9 mg of API (6.2 mg/kg) dosed (3.3 mg/kg) and the flush volume unknown***	Fabs% (unenhanced) = 2.4% ± 40.9% Fabs% (microemulsion) = 44.9 ± 9.6% **Oral bioavailability increased by 19 fold (on average)** (Constantinides et al., 1994)
Atorvastatin calcium (BCS II) / **M_W = 1155.42 (anhydrous)**	Fasted male albino rats (n= 6), body weight 150 – 200 g, items dosed orally via intubation using a 18-gauge feeding needle	38% Captex 355 34% Capmul MCM, 16% Polysorbate 80, 12% PEG 400 ***~1 ml of SEDDS containing 5 mg of API (25 mg/kg) was dosed and the flush volume unknown***	PK parameters not measured, PD response: ***Pure drug (48h)***: 1) cholesterol reduction (78.61% inhibition), 2) triglycerides reduction (63.77% inhibition), 3) LDL reduction (95.47% inhibition) ***SEDDS (48h)***: 1) cholesterol reduction (95.93% inhibition), 2) triglycerides reduction (95.47% inhibition), 3) LDL reduction (100.14 % inhibition) **Pharmacodynamic response (with SEDDS) improved by ~ 1.5 fold (on average)** (Kadu et al., 2011)

Table 9.2. Comparison of the preclinical data for similar formulations based on glycerides of caprylic/capric acids published by other researchers, with the results obtained for acyline (cont'd).

Compound/ Molecular weight	Animal model and administration mode	Formulation (w/w)	Biodata (Reference)
Valsartan (BCS III) / **M_W = 435.5**	Fasted male rabbits (n= 6) average weight 1.7 ± 0.3 kg, items dosed orally	10% Capmul MCM, 45% Polysorbate 80, 45% PEG 400 ***~0.112 ml of SMEDDS containing 5.6 mg of API was dosed and the flush volume unknown***	Frel% (SMEDDS vs suspension in capsule) = 178.70 % **Oral bioavailability increased by 1.8 fold (on average)** (Dixit et al., 2010)
Preclinical study, Chapter 6, section 6.3.1			
Acyline (free base) / **M_W = 1535.23**	Fasted beagle dogs (n=5), body weight 5.0 to 8.4 kg, items dosed via intraduodenal cannula)	5.5% Captex 355, 55% Capmul MCM C10, 15% Polysorbate 80, 5% Glycerine, 19.5% PEG 300 ***1 ml of ME containing 5 mg of API was dosed and flushed with 7 ml of purified water***	Fabs% (unenhanced) & Fabs (microemulsion) = N/A (i.v. not available) Frel% (microemulsion vs unenhanced) = 785% ± 591% **Oral bioavailability increased by 8 fold (on average)**
		5.5% Captex 355, 55% Capmul MCM, 15% Polysorbate 80, 5% Glycerine, 19.5% PEG 300 ***1 ml of ME containing 5 mg of API was dosed and flushed with 7 ml of purified water***	Fabs% (unenhanced) & Fabs (microemulsion) = N/A (i.v. not available) Frel% (microemulsion vs unenhanced) = 2610% ± 3517% **Oral bioavailability increased by 26 fold (on average)**
		45.5% Capmul PG-8, 10% Capmul MCM, 20% Polysorbate 80, 5% Glycerine, 19.5% PEG 300 ***1 ml of ME containing 5 mg of API was dosed and flushed with 7 ml of purified water***	Fabs% (unenhanced) & Fabs (microemulsion) = N/A (i.v. not available) Frel% (microemulsion vs unenhanced) = 3252% ± 3791% **Oral bioavailability increased by 33 fold (on average)**

Due to many differentiating factors including the animal model, the volume of SELFs dosed, the volume of flush, the composition of SELFs, the molecular size of the compounds, the ionic charge and chemical stability at physiological pH, etc., the direct comparison between the improved bioavailability (fold of improvement) cannot be made and therefore it is not possible to say if the SEDDSs used with acyline were more 'effective' compared to the formulations used by other

researchers. However, the dog model employed in the preclinical study with acyline can be considered as an improved 'proof of concept' model compared to the previous rat data (Constantinides et al., 1994; Lyons et al., 2000). While the rat is a reliable and versatile model suitable for initial screening and identification of the optimum prototype formulation, differences in anatomy and physiology including the lack of a gallbladder and expression levels and patterns for intestinal metabolizing enzymes make accurate quantitative bioavailability predictions in man difficult (O'Driscoll & Griffin, 2008; Cao et al., 2006). A good correlation between the bioavailability obtained in humans and rats for several hydrophilic and metabolically stable drugs (acyclovir, atenolol, nadolol, cimetidine and hydrochlorothiazide) was reported while the dogs grossly overestimated the bioavailability of nadolol and acyclovir (Li & Hu, 2011). On the other hand, Sutton (2004) reported a good correlation between small intestinal permeability in human and dog for lactulose, L-rhamose, 3-methyl-D-glucose, D-xylose. According to Cao et al. (2006), the rat model can be used to predict oral drug absorption in the small intestine of human (based on similar drug absorption profiles and similar transporter expression patterns in the small intestine), however these two species present distinct expression levels and patterns for metabolizing enzymes in the intestine and therefore there is no correlation between the oral bioavailability in human and rat. The dog is also not considered as the best model to reflect *in vivo* small intestinal metabolism as fasted state chymotrypsin activity observed in dogs is approximately 10 times higher compared to that reported in humans and therefore oral bioavailability of peptides and peptide analogues may be severely underestimated in dogs (Sinko, 1992). Other differences in GIT physiology including gastric pH and enterocyte enzymatic profile have resulted in poor correlation for bioavailability between dog and human (O'Driscoll & Griffin, 2008). On the other hand, as the GI tract, gastric transit profile and biliary secretion patterns of the dog better reflects the human situation (Porter et al., 2007), in some cases the dog model is superior over the rat model. The pig has been considered as the most suitable non-primate animal model since it very closely resembles the human in terms of eating behaviour, anatomy and physiology of the gastrointestinal tract (O'Driscoll & Griffin, 2008). The dog model employed in this work is not ideal to predict human bioavailability but certainly can be used to evaluate the relative bioavailability of tested compounds and rank the performance of various formulations, in the way it was carried out with acyline monoacetate. The preclinical results presented in this work demonstrated significantly improved oral bioavailability for the molecule at least twice larger than that reported by other researchers for other molecules (Lyons et al., 2000; Constantinides et al., 1994; Dixit et al., 2010). Obviously, the molecular size is not the only factor that affects intestinal permeability of the molecules. In fact, certain larger molecules, e.g. atorvastatin (Table 9.2) belong to BCS class II. Nevertheless the acyline results demonstrate that oral bioavailability of larger peptide molecules can be successfully improved with SEDDSs and oral administration of larger compounds should not be discounted based on their size above.

In addition, the improved bioavailability of acyline was achieved with a much smaller volume of SEDDSs compared to the previous studies. In the work published by Lyons et al. (2000), Kadu et al. (2011) and Constantinides et al. (1994), the volume of microemulsion dosed was approximately 1 ml per a rat (per body weight of 250- 300g or less). If the same ratio between volume administered and body weight was applied to calculate a human dose (~ 70kg), it would be approximately 280 ml of microemulsion or SEDDS. Clearly, this large volume was not dosed having in mind a 'scalable volume of formulation' somehow proportional to the human weight. In fact, it was clearly highlighted by Lyons et al. (2000) that their study was designed as 'proof of concept' and designed to maximise the protective and absorption enhancing properties of the formulation as well as to limit the chances of phase inversion. Taking this into consideration, these researchers admitted that additional studies would be required to determine if scaling the volumes and altering the delivery of the formulation to those more applicable to the human setting would negate the increase in bioavailability observed. The current preclinical study in dogs, is still an example of 'proof of concept' as the same volume (~1 ml = ~1 g) of the SEDDSs was administered to dogs as is intended for humans. Nevertheless, the study presents a refined 'proof of concept' where a number of critical factors that affect the oral absorption (such as a reduced volume of formulation vs weight of animals, increased volume of flush/diluting agent, etc.) were adjusted.

A number of significant novel findings were identified during preformulation, formulation and preclinical work with acyline monoacetate as this compound is also a novel chemical entity. Despite the highly desirable bio-enhancing effect achieved with the SEDDSs, physical as well as chemical stability of acyline in those formulations was found to be unacceptable from the commercial point of view. A limited shelf life and refrigerated storage were viewed as a significant threat to achieve inexpensive, safe and convenient encapsulated dosage forms. In the case of all three hydrophilic model compounds, preparation of stable, clear microemulsions appeared unfeasible. Preparation of a suspension could have been a possible solution to incorporate the required doses of bisphosphonates but it was not going to resolve the stability issue observed with acyline. As the incorporation of model drugs was unsuccessful, stability of the developed liquid microemulsions and the SEDDSs in capsules was not evaluated, although this study could have revealed another common formulation issues with SELFs such as softening and /or brittleness of the final encapsulated dosage forms. Further work focussed on development of solid forms of SELFs as alternative formulations to overcome limitations related to the high drug load and physicochemical incompatibility between the drug and microemulsion/liquid excipients.

9.4. Solid forms of self-emulsifying lipid formulations (SELFs) for use with BCS Class III compounds

Given the advantages of solid dosage forms, solid self-emulsifying lipid formulations (S-SELFs) have been extensively explored in recent years, as they frequently represent more stable

encapsulated alternatives to conventional liquid forms (Tang et al., 2008). From the perspective of dosage forms, S-MEs, S-SEDDSs, S-SMEDDSs are compressed or encapsulated solid dosage forms with self-emulsification properties. Adsorption onto solid carriers is one of the formulation strategies to produce free flowing powders and has been so far used to increase dissolution rate and subsequently absorption of lipophilic poorly water-soluble drugs (Dixit & Nagarsenker, 2010; Franceschinis et al., 2005; Tuleu et al., 2004; Sharma et al., 2005; Ito et al., 2005; Agarwal et al., 2009). Application of solid self-emulsifying lipid formulations (S-SELFs) with water-soluble compounds has not been explored by many researchers so far. Although, solubility is not an issue for BCS class III compounds and many proteins, peptides, a concomitant delivery of these drugs with the lipid formulation can improve their stability in the intestinal fluids and absorption rate/extent. A typical approach in formulating solid microemulsions and emulsifying systems observed in the literature is to select a number of materials known to be adsorbents and apply SELFs onto those materials varying the ratio of powder and liquid. Surprisingly, little effort is spent on the preformulation work to characterise and understand the physicochemical properties of the adsorbents. The work presented in Chapter 7 focused on in-depth characterisation of the preselected solid carriers. Three grades of silicon dioxide (Sylysia 320, Zeofree 5161, Aeroperl 300/30), calcium silicate (Hubersorb 600), magnesium aluminometasilicate (Neusilin US2) and dibasic calcium phosphate anhydrous (Fujicalin SG) were selected as adsorbents based on the work of other researchers and producers' recommendations. The materials differed significantly among each other in terms of particle size, porosity, specific surface area, bulk density and flowability as presented in Chapter 7. The best adsorptive characteristic preliminarily determined by the Adsorption Index (Chapter 7, section 7.10), was shown by Neusilin US2. The other materials, Zeofree 5161, Aeroperl 300/30, Sylysia 320 screened and Hubersorb 600 were slightly less effective compared to Neusilin US2, but still substantially better than Fujicalin SG. The grades of silicon dioxide were also found to differ substantially in relation to the surface of the particle, specifically with regard to free hydroxyl and siloxane groups present on the surface of particles (Chapter 7, sections 7.7 & 7.8). This was a significant observation, since hydroxyl group present on surface of silicon materials are potentially reactive. Formation of bonds stronger than van der Waals forces between an adsorbent and an adsorbed liquid, would change the adsorption process from physisorption (reversible) into chemisorption (irreversible) impeding spontaneous desorption of adsorbed liquid. Zeofree 5161 was found to be the most hydrophilic grade of silicon dioxide but its surface area was almost half of that of the other two silicon dioxide carriers which could limit the interaction with an adsorbed liquid (limited area of contact).

The adsorption process onto solid carriers resembles initial stages in the wet granulation process such as adsorption (distribution) of a binding agent onto the mass 'to be' granulated. With the addition of a granulating fluid, the powder undergoes gradual transformation into four states: pendular, funicular, capillary and dispersion states. The systematic transition of powders from one

stage to another is referred to as stepwise growing behaviour (Goldszal & Bousquet, 2001). A powder rheometer which may be used to detect endpoint for wet granulation (Freeman, 2009), was employed to determine the Powder End Point (PEP), the maximum adsorption capacity (before the powder becomes 'sticky'). The final Powder End Point was chosen reviewing the outcomes of the four tests: Basic Flowability Energy, Specific Energy, Conditioned Bulk Density and Shear Stress. These tests assessed flow, density/packing and shear properties of the solid carriers as a function of the liquid load. The significant and novel finding of the current work was that all selected adsorbents, except for Fujicalin SG, could incorporate at least the same quantity of liquid as the size of the adsorbent sample. The load of the liquid, expressed as '% of Added Liquid', was found to be between 60 -70% for all the studied adsorbents excluding Fujicalin SG. Despite significant differences in the particle size, surface area, pore volume and even pore size shown by the materials, a direct correlation was not found between the Powder End Point and any of these parameters. Fujicalin SG showed the lowest adsorptive capacity and the lowest specific surface area among all the carriers (Chapter 7, section 7.4). On the other hand, Neusilin US2, showed the same Powder End Point as Zeofree 5161 and Hubersorb 600 although its specific surface area (BET) was 2.5 fold larger than for the other two carriers. It appeared that the high adsorptive properties of the carriers were achieved by a combination of all these factors rather than by one parameter in particular.

Agarwal et al. (2009) used a powder flow analyzer, another type of powder rheometer, to determine force and torque exerted by the moving blade in the bed of particles. This method was similar to the Specific Energy test and was considered as a good tool to detect the end of adsorption. The adsorption end point established by these researchers for Neusilin US2 was 2.75: 1 (ratio between liquid: solid carrier) which is in a good agreement with the result obtained in the current study showing %AL = 70% which equals to 2.3: 1 (Chapter 8, section 8.2.2). Agarwal et al. (2009) also used another method, angle of repose, to detect the absorption end point but this method failed to delineate the different phases that the adsorbent underwent with the addition of griseofulvin-containing SEDDS. In the current work, four methods were employed to detect the adsorption end point (Powder End Point) (Chapter 8, Table 8.2). Although, the method based on Shear Stress appeared to be the most reliable as the interaction between the particles was forced by the compaction step (Chapter 1, section 1.5.2.3), each of the methods could potentially be employed to successfully determine the end of adsorption. This is an important finding as there is limited literature available on suitable techniques and tools to determine the end of adsorption. Visual techniques, which are apparently the most common, cannot precisely determine the powder end point and may also be inappropriate for cohesive materials showing continuous growing behaviour.

In the course of this thesis, desorption of the model SEDDS (preconcentrate 2A2 50: 50) was also examined to evaluate the suitability of the carriers to produce rapid release of the liquid components. The formulation concept outlined in the final part of the current work was to combine

a hydrophilic drug in a solid state (powder, non-dissolved) with a solid SELF. The physical blend, dry granulated mixture or other solid preparations containing the drug and the S-SELFs could be subsequently filled into a capsule using conventional manufacturing techniques. It is believed that a key feature of this system requires bio-enhancing components to be delivered together with the drug to the intestinal membrane where absorption can take place. While the hydrophilic drug is likely to dissolve rapidly on its own in the intestinal tract, the bio-enhancing components will need to be first desorbed from the solid carrier and form an *in situ* emulsion or a microemulsion similar to the one formed by the equivalent liquid formulation upon dilution in the same conditions. The simultaneous dissolution of the drug and emulsification of the bio-enhancing components may become especially important for peptides and proteins where entrapment of the drug in the diluted emulsion and microemulsion is expected to limit enzymatic degradation. In order to explore the concept described above, the examination of desorption characteristics (emulsifying behaviour) from the model S-SEDDS was preliminarily tested. In the solid self-emulsifying systems with the hydrophobic compounds studied by other researchers, the dissolution profile of the drug was only examined and little attention was given to desorption of the liquid system or its individual components. Desorption characteristics from the S-SEDDSs formulated with the six carriers was evaluated based on an emulsification state (using particle sizing) and comparing transparency of dilutions (Chapter 8 section 8.3). There was practically no desorption from the S-SEDDSs formulated with Sylysia 320 and Aeroperl 300/30 while Zeofree 5161, Hubersorb 600, Neusilin US2 and Fujicalin SG showed promising desorptive characteristics. A similar observation was made when desorption characteristics was evaluated with a water insoluble compound, Fat Red 7B dye used as 'desorption marker'. In the work carried out by Agarwal et al. (2009) the dissolution of griseofulvin remained incomplete (only 30 - 40% released after 60 minutes) when the solid formulations made with Neusilin US2, GL 100 (silicon dioxide, 3.6 μm), GL200 (silicon dioxide, 20 μm), ZeoPharm 5170 (silicon dioxide, 300 μm and Hubersorb 5121 (calcium silicate, 25μm) were tested. While there was no statistical difference between release of griseofulvin from Neusilin US2, GL 100 and GL200, the other two carriers (ZeoPharm 5170, Hubersorb 5121) showed the lowest dissolution rate. Based on these results, it appears that different types of silicon dioxide, could offer a better desorption profile. In the work carried out by Ito et al. (2005) with gentamicin (hydrophilic drug that belongs to BCS III), there was no evident correlation between the *in vitro* release and *in vivo* performance of the solid formulations prepared with Florite RE (microporous calcium silicate), Neusilin US2 and Sylysia 320. Still, the bioavailability of gentamicin from these solid preparations appeared to be dependent on both the type and amount of adsorbent in the formulation (Ito et al., 2005).

The adsorption and desorption processes examined in the current work with the selected six solid carriers enabled the adsorption capacity and desorption characteristics for each adsorbent to be established. The novel approach undertaken to detect the Powder End Point (the adsorption

capacity) helped to determine precisely when a material was fully adsorbed but not 'overloaded' which is a significant improvement compared to visual techniques previously used by other researchers. The work presents the parameter (PEP) that can be reproducibly measured so that a stable, repeatable adsorption process can be achieved. The desorption test employed to preliminarily examine desorption characteristics of various S-SEDDS was a modified/scaled down version of the dispersion test used to assess emulsification behaviour of liquid MEs/SELFs. This test may require further modification to establish a correlation with the *in vivo* conditions, however it was found adequate to detect differences in desorption behaviour of silicon dioxide grades and the other three materials.

This thesis provides a comprehensive study of development steps undertaken to advance knowledge about the microemulsions and self-emulsifying lipid formulations composed of derivatives of caprylic/capric acids, their characterisation, their potential to dissolve hydrophilic drugs and finally a novel formulation strategy for a solid formulation (S-SELFs) that is expected to be more flexible in relation to the drug load and drug stability. The systematic experimental approach applied throughout the current work revealed many significant and novel observations and relationships related to formation of microemulsions, characterisations of these systems and solubility/stability of the model compounds in these lipid formulations. Development of commercially viable, stable S-SELFs requires more work, but the current work provides extensive and solid foundations for the further steps.

9.5. Main findings

- Formation of a microemulsion region in the systems composed of glycerides and propylene glycol esters of caprylic and capric acids was affected by the content of the main surfactant (Crillet 4 HP), the type of the cosurfactant and the ratio between them. The systems with the low combined HLB value (7 - 8) did not form extensive liquid crystalline regions as the presence of the cosurfactant facilitated formation of a microemulsion instead.

- A very low content of the high HLB value surfactant (low combined HLB value between 6 - 7) decreased the formation of the microemulsion region upon dilution, which indicated that the cosurfactant was ineffective as the main surfactant (Crillet 4 HP).

- A limited microemulsion region was achieved when the content of the cosurfactant comprised approximately 1/3 of the mix of the surfactants (high combined HLB value between 9 - 13). Instead, an extensive liquid crystalline region was formed.

- Capmul MCM C8 (mono- and diglycerides of mainly caprylic acid) was found to be a more effective cosurfactant compared to Capmul MCM C10 (mono- and diglycerides of mainly capric acid) in the systems with the low and high combined HLB value systems (6-9 & 9-14).

- The type of oil had a significant effect on formation of preconcentrates and their dilution behaviour. Capmul PG-8 (monoester of propylene glycol and mainly caprylic acid), used as the oil, was found to be miscible with the mixes of the surfactants in all ratios, however the microemulsion area formed upon dilution was very limited. More hydrophobic oils, Captex 355 (triglycerides of caprylic and capric acids) and Captex 200P (diesters of propylene glycol and caprylic, capric acids), formed more extensive microemulsion regions but were not miscible with the surfactants in all ratios.

- The model microemulsions (derived from the preconcentrate 2A2 (60: 40) were identified as inverse micelles (containing 10 -20% of water) and water-in-oil microemulsions (containing 25- 45% of water) mainly with the aid of SANS and PGSE-NMR techniques. Other characterisation techniques such as conductivity, viscosity, DLS, DSC, cryo-TEM and FF-TEM provided complementary information regarding the microstructure but interpretation of this data without the former two techniques would have been incomplete and questionable.

- Use of differential scanning calorimetry to determine the type of the microemulsion was closely examined in the current work. The presence of a 'water peak' in the water-in-oil microemulsions was in contrast to the published results where detection of a 'water peak' by DSC indicated the presence of water in the outer phase (e.g. formation of bicontinuous and an oil-in-water microemulsion).

- Use of differential scanning calorimetry to establish the existence of the bound water was suggested as a new preformulation tool to gain better understanding of the drug distribution in the microemulsions and potentially estimate the drug load of hydrophilic compounds in such systems.

- Based on the work carried out with the model compounds, incorporation of the hydrophilic compounds into the liquid microemulsions and SELFs was found to be unfeasible for various reasons. Poor solubility of bisphosphonates (sodium alendronate trihydrate and disodium pamidronate pentahydrate) in the microemulsions prevented formation of clear systems with the sufficient drug load, while physical stability (gelling) of a model peptide (acyline) in the SEDDS led to unacceptable shelf life.

- The selected SEDDSs composed of derivatives of caprylic and capric acids, were found to significantly enhance oral bioavailability of acyline in the preclinical dog study. On average, the oral absorption of acyline incorporated in the SEDDSs: T2, T3, T4 was increased by 8, 26 and 33 fold respectively (T3 & T4 significantly better than the unenhanced formulation, $p < 0.05$). Compared to other animal studies published by other researchers with similar compositions, this study represented a refined 'proof of concept'. The bioresults demonstrated the increased oral absorption of a molecule with a molecular weight approximately twice as large as compounds previously reported.

- A high adsorption capacity between 60 - 70% was quantified for five solid carriers (Sylysia 320, Zeofree 5161, Aeroperl 300/30, Hubersorb 600, Neusilin US2) using four different, novel methods. Each method enabled the Powder End Point to be accurately determined and therefore could be employed in the future to establish the adsorption capacity of various materials.

- Desorption from the model S-SEDDSs carried out *in vitro,* demonstrated that Hubersorb 600, Neusilin US2, Fujicalin SG, Zeofree 5161 could provide a rapid desorption (release) of adsorbed liquid formulation, in contrast to the other two materials: Sylysia 320 and Aeroperl 300/30 which failed to deliver rapid release. Fujicalin SG was found to be the best desorbent.

9.6. Future work

The final work carried out in the course of this thesis presented a potential to formulate a solid self-emulsifying formulations composed of derivatives of caprylic and capric acids, where a hydrophilic compound would not be directly incorporated into the liquid systems. The proposed solid formulations could offer significant advantages over liquid formulations such as the unrestricted drug load, reduced chemical and physical instability of the drug, reduced instability in capsules, ease of manufacture, etc. Also, development of solid and 'non-interacting with a capsule shell' formulations, would allow for flexible choice of components. Currently, the choice of excipients and their content, in particular cosurfactants and surfactants, is restricted by their negative effect on capsule shell stability and therefore many potent, bio-enhancing liquid formulations never become commercially viable products. On the other hand, there is a need to establish if the proposed concept could deliver equivalent benefits to the one offered by the liquid formulations. A continuation of this work should examine:

- physical stability of acyline upon dilution and digestion of the preclinical SEDDSs, in order to understand if the relationship between the oral bioavailability of this drug and the dilution/digestion behaviour of the SEDDSs exists;
- oral bioavailability of other model compounds to validate the'bio-performance' of the preclinical SEDDSs. It may be possible to establish which SEDDS produces the highest bioavailability improvement and subsequently evaluate if the relationship between the oral bioavailability and the composition, or the overall HLB value (the dilution behaviour) or the digestion behaviour exists;
- 'bioequivalence' of S-SELFs with their liquid equivalents (is the same bioavailability improvement achieved?);
- a relationship between *in vitro* desorption characteristics of S-SELFs studied in the artificial intestinal fluids and their actual behaviour *in vivo* (e.g. if lack of desorption observed *in vitro* is not an indication of performance *in vivo*, suitability of *in vitro* tests to evaluate a long-term stability may need to be reconsidered);
- a long-term stability of the S-SELFs with the preselected carriers to understand if the desorption characteristics remain the same upon storage, also the impact of various storage conditions;
- the impact of drug incorporation, whether there is any short and long-term interaction or instability between the drug and the solid system (e.g. if the physical stability of acyline remains satisfactory when the drug in a solid form is combined with a 'solidified' liquid formulation);
- the impact of S-SELFs on capsules shell stability in comparison to their liquid equivalents.

References

ABITEC Corporation, http://www.abiteccorp.com/product-lines/capmul

Aboofazeli, R., Barlow, D.J., Lawrence, M.J., 2000. Particle size analysis of concentrated phospholipid microemulsions: II. Photon correlation spectroscopy. *AAPS Pharmsc.*, 2(2) article 19.

Afach, G., Kawanami, Y., Cheetangdee. N., Fukada, K., Izumori K., 2008. Lipase-catalyzed synthesis of D-psicose fatty acid diesters and their emulsification activities *J. Am. Oil Chem. Soc.*, 85, 755–760.

Agarwal, V., Siddiqui, A., Ali, H., Nazzal, S., 2009. Dissolution and powder flow characterization of solid self-emulsified drug delivery system (SEDDS). *Int. J. Pharm.* 366, 44-52.

Ahmad, S.I., Shinoda, K., Friberg, S.E., 1974. Microemulsions and phase equilibria: Mechanism of the formation of so-called microemulsions studied in connection with phase diagram. *J. Colloid Interface Sci.*, 47, 32–37.

Alany, R.G., Tucker, I.G., Davies, N.M., Rades, T., 2001. Characterizing colloidal structures of pseudoternary phase diagrams formed by oil/water/amphiphile systems. *Drug Dev. Ind. Pharm.*, 27(1), 31–38.

Amidon, G.L., Lennernas, H., Shah, V.P., Crison, J.R., 1995. A theoretical basis for a biopharmaceutic drug classification: The correlation of in vitro drug dissolution and in vivo bioavailability. *Pharm. Res.*, 12, 413-420.

Andrienko, D., 2006. Introduction to liquid crystals. International Max Planck Research School: Modelling of soft matter, 11-15 September 2006, Bad Marienberg, Germany.

Anklam, M.R., Prud'Homme, R.K, Warr, G.G., 1995. Shear thinning in ternary bicontinuous and water-in-oil microemulsions. *AICHE J.*, 41(3), 677–682.

Asnani, M., Vyas, K., Bhattacharya, A., Devarakonda, S., Chakraborty, S., Mukherjee, A.K., 2009. Ab initio structure determination of anhydrous sodium alendronate from laboratory powder X-Ray diffraction data. *J. Pharm. Sci.*, 98 (6), 2113 – 2121.

Astaneh, R., Nafissi-Varchehb, N., Erfana, M., 2007. Zinc–leuprolide complex: preparation, physicochemical characterization and release behaviour from in situ forming implant. *J. Pept. Sci.*, 13, 649–654.

Augustijns, A., Brewster, M., 2007. Solvent systems and their selection in pharmaceutics and biopharmaceutics. 1st edition. New York, Springer.

Aulton, M.E., 2002. Pharmaceutics: The science of dosage form design. 2nd edition. Edinburg, London, New Yourk, Oxford, Philadelphia, St Louis, Sydney, Toronto. Churchill Linvingston.

Bagwe, R.P., Kanicky, J.R., Palla, B.J., Patanjali, P.K., Shah, D.O., 2001. Improved drug delivery using microemulsions: rationale, recent progress, and new horizons. *Crit. Rev. Ther. Drug Carrier Syst.*, 18(1), 77-140.

Bahl, D., Hudak, J., Bogner, R. H., 2008. Comparison of the ability of various pharmaceutical silicates to amorphize and enhance dissolution of indomethacin upon co-grinding. *Pharm. Dev. Technol.*, 13, 255–269.

de Boer, J.H., Lippens, B.C, Linsen, B.G, Broekhoff, J.C.P., van den Heuvel, A., Osinga, Th. J., 1966. The t-curve of multimolecular N_2-adsorption. *J. Colloid. Interf. Sci.*, 21 (4), 405-414.

Bolzinger, M.A., Thevenin, Carduner C., Poelman, M.C., 1998. Bicontinuous sucrose ester microemulsion: a new vehicle for topical delivery of niflumic acid. *Int. J. Pharm.,* 176, 39–45.

Boonme, P., Krauel, K., Graf, A., Rades, T., Junyaprasert, V.B., 2006. Characterization of microemulsion structures in the pseudoternary phase diagram of isopropyl palmitate/water/Brij 97:1-butanol. *AAPS PharmSciTech.,* 7(2), article 45.

Brain, T., 2008, Chief (Scientific) Technical Officer, Centre for Ultrastructural Imaging, Guys Campus, King's College, Basement Level North, New Hunts House, London, UK, private communication.

Brunauer S., Emmett P. H., Teller E., 1938. Adsorption of gases in multimolecular layers. *J. Am. Chem. Soc.*, 60, 309-319.

Brumsen, C., Papapoulos, S.E, Lips, P., Geelhoed-Duijvestijn, P.H.L.M., Hamdy, N.A.T., Landman, J.O., Mccloskey, E.V, Netelenbos, J.C., Pauwels, E.K.J., Roos J.C, Valentijn, R.M., Zwinderman, A.H, 2002. Daily oral pamidronate in women and men with psteoporosis: a 3-year randomized placebo-controlled clinical trial with a 2-year open extension. *J. Bone Miner. Res.*, 17 (6), 1057 – 1064.

Brundrett, M.C., Kendrick, B., Peterson, C.A, 1991. Efficient lipid staining in plant material with Sudan Red 7B or fluoral yellow 088 in polyethylene glycol – glycerol. *Biotech. Histochem.,* 111-116.

Bummer, P.M., 2004. Physical chemical considerations of lipid-based oral drug delivery — solid lipid nanoparticles, *Crit. Rev. Ther. Drug Carrier Syst.,* 21, 1 – 19.

Cameron, D.R., Weber, M.E., Idziak, E.I., Neufeld, R.J., Cooper, D.J., 1991. Determination of interfacial areas in emulsions using turbidimetric and droplet size data: correction of the formula for emulsifying activity index. J. *Agric. Food Chem.,* 39, 655-659.

Carr, R.L.,1965. Evaluating flow properties of solids. *Chem. Eng.,* 72, 163-168.

Cao, X., Leyva, N., Anderson, R.S, Hancock, B.C, 2008. Use of prediction methods to estimate true density of active pharmaceutical ingredients. *Int. J. Pharm., 355,* 231–237.

Cao, Y, Sheng, J., 2010. Microstructure of microemulsion in MEEKC. *Electrophoresis* 31, 672–678.

Cao, X., Gibbs, S.T., Fang, L., Miller, H.A., Landowski, C.P., Shin, H.C., Lennernas, H., Zhong, Y., Amidon, G.L., Yu, L.X., Sun D., 2006. Why is it challenging to predict intestinal drug absorption and oral bioavailability in human using rat model. *Pharm. Res.,* 23 (8), 1657 – 1686.

Ceglie, A., Lindman, B., 1987. Microemulsion structure in four-component systems for different surfactants. *Colloids Surf.,* 28, 29-40.

Celebi, N., Turkyilmaz, A., Gonul, B., Ozogul, C., 2002. Effects of epidermal growth factor microemulsion formulation on the healing of stress-indused gastric ulcers in rats. *J. Control. Release*, 83, 197 –210.

Celis, M.T., Garcia-Rubio, L.H., 2008. Characterization of emulsions: A systematic spectroscopy study. *J. Disper. Sci. Technol.*, 29, 20–26.

Chakraborty, S., Shukla, D., Mishra, B., Singh, S., 2009. Lipid – an emerging platform for oral delivery of drugs with poor bioavailability. *Eur. J. Pharm. Biopharm.*, 73, 1–15.

Cheng, M.B., Wang, J.C., Li J.H., Liu, X.Y., Zhang, X., Chen, D.W., Zhou, S.F., Zhang, Q., 2008. Characterization of water-in-oil microemulsion for oral delivery of earthworm fibrinolytic enzyme. *J. Control. Release*, 129, 41–48.

Cheung, H. M., Qutubuddin, S., Edwards, R.V., Mann, J.A., 1987. Light scattering study of oil-in-water microemulsions: Corrections for interactions. *Langmuir,* 3 (5), 744-752.

Cheung ,W.K., Honc, F., Schoenfeld, S., Knight, R., Seaman, J., Bowen, A.T., John V., Redalieu, E., Chan, K., 1994. A single-dose bioavailability study of pamidronate disodium after oral administration as encapsulated enteric-coated pellets, enteric-coated tablets, and a solution to patients with postmenopausal osteoporosis. *Am. J. Ther.* 1(3), 221-227.

Chevalier, Y., Zemb T., 1990. The structure of micelles and microemulsions. *Rep. Prog. Phys.* 53, 279-371.

CPMP/EWP/QWP/1401/98 (Rev. 1), 2010. Guideline on the investigation of bioequivalence, EMEA. European Medicines Agency, Evaluation of Medicines for Human Use. London, 20 January 2010.
http://www.emea.europa.eu/docs/en_GB/document_library/Scientific_guideline/2010/01/WC500070039.pdf

CHMP/EWP/40326/2006, 2006. Questions & Answers on the bioavailability and bioequivalence guideline CHMP efficacy working party/ Therapeutic subgroup on pharmacokinetics (EWP-PK). EMEA. European Medicines Agency, Evaluation of Medicines for Human Use.
http://www.rsihata.com/updateguidance/emea/2006/4032606en.pdf

Choi, A., Gang, H., Chun, I., Gwak, H., 2008. The effects of fatty acids in propylene glycol on the percutaneous absorption of alendronate across the excised hairless mouse skin. *Int. J. Pharm.,* 357, 126–131

Christiansen, A., Backensfeld, T., Weitschies, W., 2010. Effects of non-ionic surfactants on in vitro triglyceride digestion and their susceptibility to digestion by pancreatic enzymes. *Eur. J. Pharm. Sci.,* 41, 376–382.

Coates, J., 2000. Interpretation of infrared spectra, a practical approach in Encyclopedia of Analytical Chemistry, R.A. Meyers (Ed.) John Wiley & Sons Ltd, Chichester.

Cole, E.T., 2007. Challenges and opportunities in the encapsulation of liquid and semisolid formulations into gelatin and non-gelatin capsules. Oral presentation, AAPS Workshop, March 2007, Washington DC, USA.

Cole, E.T, 1999. Liquid filled and sealed hard gelatin capsules. *Gattefossé Bulletin* 92.

Cole, E.T., Cade, D., Benameur, H., 2008. Challenges and opportunities in the encapsulation of liquid and semi-solid formulations into capsules for oral administration. *Adv. Drug Deliver. Rev.* 60, 747 – 756.

Constantinides, P.P., 1995. Lipid microemulsions for improving drug dissolution and oral absoprtion: physical and biopharmaceutical aspects. *Pharm. Res.,* 12 (11), 1561-1572.

Constantinides, P.P., Scalart, J.P., 1997. Formulation and physical characterization of water-in-oil microemulsions containing long- versus medium-chain glycerides. *Int. J. Pharm.,* 158, 57-68.

Constantinides, PP, Yiv, S.H., 1995. Particle size determination of phase-inverted water-in-oil microemulsions under different dilution and storage conditions. *Int. J. Pharm.,*115, 225-234.

Constantinides, P.P., Lancaster, C.M., Marcello, J., Chiossone, D.C., Orner D., Hidalgo, I., Smith, P.L., Sarkahian, A.B., Yiv S.H., Owen, A.J., 1995. Enhanced intestinal absorption of an RGD peptide from water-in- oil microemulsions of different composition and particle size. *J. Control. Release*, 34, 109-116.

Constantinides, P.P., Scalart, J.P., Lancaster, C., Marcello, J., Marks, G., Ellens H., Smith, L.P., 1994. Formulation and intestinal absorption enhancement evaluation of water in-oil microemulsions incorporating medium-chain glycerides. *Pharm. Res.,* 11 (10), 1385-1390.

Constantinides, P.P., Welzel, G., Ellens, H., Smith, P.L., Sturgis, S., Yiv, S.H., Owen, A.J., 1996. Water-in-oil microemulsions containing medium-chain fatty acids/salts: formulation and intestinal absorption enhancement evaluation. *Pharm. Res.,* 13, 210-215.

Cuine, J. F., Charman, W.N., Pouton, C.W., Edwards, G.N., Porter, C.J.H., 2007. Increasing the proportional content of surfactant (Cremophor EL) relative to lipid in self-emulsifying lipid-based formulations of danazol reduces oral bioavailability in beagle dogs. *Pharm. Res.,* 24 (4), 748-57

Daniels, R., Kerstiens, B., Tischinger-Wagner, H., Rupprecht, H., 1986. The stability of drug adsorbates on silica. *Drug Dev. Ind. Pharm.* 12, 2127–2156.

Danielsson, I., Lindman, B., 1981. The definition of a microemulsion. *Colloids Surf.*, 3, 391-392.

Davis, J.T., 1959. A quantitative kinetic theory of emulsion type, I. Physical chemistry of the emulsifying agent, gas/liquid and liquid/liquid Interface. Proceedings 2. Intern. Cong. Surface Activity, London, 1, 426-438.

Dixit, R.P., Nagarsenker, M.S., 2010. Optimized microemulsions and solid microemulsion systems of simvastatin: characterization and in vivo evaluation. *J. Pharm. Sci.,* 99 (12), 4892-4902.

Dixit, A.R., Rajput, S.J, Patel, S.G., 2010. Preparation and bioavailability assessment of SMEDDS containing valsartan. *AAPS PharmSciTech,* 11 (1), 314 – 321.

Embleton, J.K., Pouton, C.W., 1997. Structure and function of gastro-intestinal lipases. *Adv. Drug Deliv. Rev.,* 25, 15-32.

Epstein, H., Gutman, D., Cohen-Sela, E., Haber, E., Elmalak, O., Koroukhov, N., Danenberg, H.D., Golomb, G., 2008. Preparation of alendronate liposomes for enhanced stability and bioactivity: In vitro and in vivo characterization. *AAPS J.,* 10 (4), 505–515.

Ezra, A., Golomb, G., 2000. Administration routes and delivery systems of bisphosphonates for the treatment of bone resorption. *Adv. Drug Deliv. Rev.,*42, 175 –195.

Fahy, E., Subramaniam, S., Brown, H.A., Glass, C.K., Merrill Jr., A.H., Murphy, R.C., Raetz, C.R.H., Russell, D.W., Seyama, Y., Shaw, W., Shimizu, T., Spener, F., van Meer, G., Van Nieuwenhze, M.S., White, S.H., Witztum, J.L., Dennis, E.A., 2005. A comprehensive classification system for lipids. *J. Lipid Res.,* 46, 839 – 861.

Fanun, M., 2008. A study of the properties of mixed nonionic surfactants microemulsions by NMR, SAXS, viscosity and conductivity. *J. Mol. Liq.,* 142, 103–110.

Fanun, M., 2009. Properties of microemulsions with sugar surfactants and peppermint oil. *Colloid Polym. Sci.,* 287, 899–910.

Fanun, M., 2010. Microemulsions with nonionic surfactants and mint oil. *Open Colloid. Sci. J.,* 2010, 3, 9-14.

Fanun, M., Wachtel, E., Antalek, B., Aserin,A., Garti, N., 2001. A study of the microstructure of four-component sucrose ester microemulsions by SAXS and NMR. *Colloid. Surf. A*, 180, 173–186.

Fraissard, J., 1997. Physical adsorption: experiment, theory and applications. 1st edition, Kluwer Academic Publisher.

Franceschinis, E., Voinovich, D., Grassi, M., 2005. Self-emulsifying pellets prepared by wet granulation in high-shear mixer: influence of formulation variables and preliminary study on the in vitro absorption. *Int. J. Pharm.,* 291, 87-97.

Freeman, R., 2005. Measuring the flow properties of consolidated, conditioned and aerated powders – a comparative study using a powder rheometer, and a rotational shear cell, Particulate Systems Analysis, workshop, Stratford (UK) 2005.

Freeman, R., 2007. Measuring the flow properties of consolidated, conditioned and aerated powders — A comparative study using a powder rheometer and a rotational shear cell. *Powder Technol.,* 174, 25 – 33.

Freeman, R., Fu, X., 2008. Characterisation of powder bulk, dynamic flow and shear properties in relation to die filling. *Powder Metall.*, 51(3), 196-201.

Freeman, R.E., Cooke, J.R., Schneider, L.C.R., 2009. Measuring shear properties and normal stresses generated within a rotational shear cell for consolidated and non-consolidated powders. *Powder Technol.,*, 190, 65–69.

Freeman, T., 2009. Better wet granulation: development, scale-up and manufacture. Freeman Technology website, http://www.freemantech.co.uk/literature-and-downloads/articles-and-white-papers.html.

Freeman Technology Work Instructions for FT4 powder rheometer.

Friberg, S.E., 1990. Micelles, microemulsions, liquid crystals, and the structures of stratum corneum lipids. *J. Soc Cosmetic. Chem.,* 4 (1), 155-171.

Goncalves, E., Rigassi, T., 2006. Solid microemulsions prepared by adsorption of microemulsion preconcentrates onto silicas. Poster presentation, AAPS Annual Meeting and Exposition, San Antonio, USA.

Garti, N., Aserin, A., Tiunova, I., Fanun, M., 2000. A DSC study of water behavior in water-in-oil microemulsions stabilized by sucrose esters and butanol. *Colloid. Surf. A*, 170, 1–18.

Gattefossé, http://www.gattefosse.com/en/applications/?administration-route,oral

Ge, Z., Zhang, X., Gan, L., Gan, Y., 2008. Redispersible, dry emulsion of lovastatin protects against intestinal metabolism and improves bioavailability. *Acta Pharmacol. Sin.*, 29 (8), 990–997.

Geyer, R.P., Tuliani, V., 1992. US5110606A1. Non- aqueous microemulsions for drug delivery.

Gershanik, T., Benita, S., 2000. Self-dispersing lipid formulations for improving oral absorption of lipophilic drugs. *Eur. J. Pharm. Biopharm.*, 50, 179- 188.

Gi, H.J., Chen,S.N., Hwang, J.S., Tien, C., Kuo, M.T., 1992. Studies of formation and interface of oil-water microemulsion. *Chin. J. Phys.,* 30 (5), 665 – 678.

Goddeeris, C., Coacci, J., Van den Mooter, G., 2007. Correlation between digestion of the lipid phase of smedds and release of the anti-HIV drug UC 781 and the anti-mycotic drug enilconazole from smedds. *Eur. J. Pharm. Biopharm.*, 66, 173–181.

Goddeeris, C., Cuppo, F., Reynaers, H., Bouwman, W.G., Van den Mooter, G., 2006. Light scattering measurements on microemulsions: estimation of droplet sizes. *Int. J. Pharm.,* 312, 187–195.

Goldszal, A., Bousquet, J., 2001. Wet agglomeration of powders: from physics towards process optimization. *Powder Technol.* 117, 221–231.

Ghosh, P.K., Murthy, R.S.R. 2006. Microemulsions: a potential drug delivery system. *Curr. Drug Delivery*, 3(2), 167 – 180.

Gradzielski M., 2008. Recent developments in the characterisation of microemulsions. *Curr. Opin. Colloid Interface Sci.*, 13, 263–269.

Griffin, W.C., 1954. Calculation of HLB values of non-ionic surfactants. *J. Soc. Cosmet. Chem.*, 5, 249–256.

Griffin, BT, O'Driscoll CM, 2008. An examination of the effect of intestinal first pass extraction on intestinal lymphatic transport of saquinavir in the rat. *Pharm. Res.,* 25 (5): 1125-1133.

Gursoy, R.N., Benita, S., 2004. Self-emulsifying drug delivery systems (SEDDS) for improved oral delivery of lipophilic drugs. *Biomed. Pharmacother.,* 58, 173–182.

Hantzschel, D., Enders, S., Kahl, H., Quitzsch, K., 1999. Phase behaviour of quaternary systems containing carbohydrate surfactants-water-oil-cosurfactant. *Phys. Chem.,* 1, 5703-5710

Hägele, G., Szakács, Z., Ollig J., Hermens, S., Pfaff, Ch., 2000. NMR-controlled titrations: characterizing aminophosphonates and related structures. *Heteroatom Chem.*, 11 (7), 562 – 582.

Hauss D.J., 2007. Oral lipid-based formulations: enhancing the bioavailability of poorly water soluble drugs. 1st edition. New York. Informa Healthcare USA, Inc.

Healy, A.M., McDonald, B.F., Tajber, L., Corrigan, O.I., 2008. Characterisation of excipient-free nanoporous microparticles (NPMPs) of bendroflumethiazide. *Eur. J. Pharm. Biopharm.* 69, 1182-1186.

Herbst, K. L., Anawalt, B.D, Amory, J. K, Bremner, W.J, 2002. Acyline: the first study in humans of a potent, new gonadotropin-releasing hormone antagonist. *J. Clin. Endocrinol. Metab.,* 87(7), 3215–3220.

Herbst, K.L., Coviello, A.D., Page, S., Amory, J.K, Anawalt, B.D., Bremner, W.J., 2004. A single dose of the potent gonadotropin-releasing hormone antagonist acyline suppresses gonadotropins and testosterone for 2 weeks in healthy young men. *J. Clin. Endocrinol. Metab.*, 89 (12), 5959–5965.

Hild, S.A., Attardi, B.J, Reel, J.R., 2004. The ability of a gonadotropin-releasing hormone antagonist, acyline, to prevent irreversible infertility induced by the indenopyridine, CDB-4022, in adult male rats: the role of testosterone. *Biol. Reprod.*,71, 348–358.

Höhne, G., Hemminger, W. Flammersheimer, H.J., 1996. Differential scanning calorimety- an introduction for practioners. 1st edition. Berlin, New York. Springer-Verlag Heidelberg.

Ibach H., 2006. Physics of surfaces and interfaces, 1 edition, New York, Springer.

Immordino, M.L., Dosio, F., Cattel, L., 2006. Stealth liposomes: review of the basic science, rationale, and clinical applications, existing and potential. *Int. J. Nanomedicine*, 1(3) 297–315.

Israelachvili, J.N, Mitchell, D.J., Ninham, B.W., 1976. Theory of self-assembly of hydrocarbon amphiphiles into micelles and bilayers. *J. Chem. Soc. Faraday Trans II*, 72, 1525-1568.

Ito, Y., Arai, H., Uchino, K., Iwasaki, K. Shibata, N., Takada, K., 2005. Effect of adsorbents on the absorption of lansoprazole with surfactant. *Int. J. Pharm.*, 289, 69–77.

Ito, Y., Kusawake, T., Ishida, M., Tawa, R., Shibata, N., Takada, K. 2005. Oral solid gentamicin preparation using emulsifier and adsorbent. *J. Control. Release*, 105, 23–31.

Jackson, K.D.O., 1998. A guide to identifying common inorganic fillers and activators using vibrational spectroscopy. *Internet J. Vib. Spectro.*, 2.
http://www.ijvs.com/volume2/edition3/section3.html

Jannin, V., Musakhanian, J., Marchaud, D., 2008. Approaches for the development of solid and semi-solid lipid-based formulations. *Adv. Drug Delivery Rev.*, 60, 734–746.

Jantratid, E., Janssen, N., Reppas, C., Dressman, J.B., 2008. Dissolution media simulating conditions in the proximal human gastrointestinal tract: an update. *Pharm. Res.*, 25 (7), 1663 – 1676.

Jian, X., Ganzuo, L., Zhiqiang, Z., Guowei, Z., Kejian, J., 2001. A study of the microstructure of CTAB/1-butanol/octane/water system by PGSE-NMR, conductivity and cryo-TEM. *Colloid. Surf. A*, 191, 269–278.

Jiang, G., Gavini, E., Dani, B.A., Murty, S.B, Schrier, B., Thanoo, B.C, DeLuca, P.P., 2002. Identification and determination of GnRH antagonist gelling at injection site. *Int. J. Pharm.*, 233, 19–27.

Jiang, G., Miller, C., Koerber, S.C., Porter, J., Craig, A.G., Bhattacharjee, S., Kraft, P., Burris, T.P., Campen, C.A., Rivier, C.L., Rivier, J.E., 1997. Betidamino acid scan of the GnRH antagonist acyline. *J. Med. Chem.*, 40 (23), 3739-3748.

Jiang, G., Stalewski, J., Galyean, R., Dykert, J., Schteingart, C., Broqua, P., Aebi, A., Aubert, M.L., Semple, G., Robson, P., Akinsanya, K., Haigh, R., Riviere, P., Trojnar, J., Junien, J.L., Rivier, J.E.,

2001. GnRH antagonists: a new generation of long acting analogues incorporating *p*-ureido-phenylalanines at positions 5 and 6. *J. Med. Chem.*, 44 (3), 453-467.

Joshi, M, Pathak, S., Sharma, S, Patravale, V., 2008. Solid microemulsion preconcentrate (NanOsorb) of artemether for effective treatment of malaria. *Int. J. Pharm.*, 362, 172-178.

Jones, R., 2002. Successful particle analysis of dry powders. *G.I.T Laboratory Journal,* 2, 46-48.

Kadu, P.J., Kushare, S.S, Thacker, D.D, Gattani, S.G., 2011. Enhancement of oral bioavailability of atorvastatin calcium by self-emulsifying drug delivery systems (SEDDS). *Pharm. Dev. Technol.*, 16(1), 65–74.

Kang, B.K., Lee, J.S., Chon, S.K., Jeong, S.Y., Yuk, S.H., Khang, G., Lee, H.B., Cho, S.H., 2004. Development of self-microemulsifying drug delivery systems (SMEDDS) for oral bioavailability enhancement of simvastatin in beagle dogs. *Int. J. Pharm.*, 274 (1–2), 65-73.

Karamustafa, F., Celebi, N., 2008. Development of an oral microemulsion formulation of alendronate: effects of oil and cosurfactant type on phase behaviour. *J. Microencapsulation*, 25 (5): 315–323.

Karasulu, H.Y., 2008. Microemulsions as novel drug carriers: the formation, stability, applications and toxicity. *Expert Opin. Drug Deliv.*, 5(1), 119 – 135.

Kaukonen, A.M., Boyd, B.J., Porter, C. J. H., Charman, W. N., 2004. Drug solubilization behavior during in vitro digestion of simple triglyceride lipid solution formulations. *Pharm. Res.,* 21(2), 245 – 253.

Ke, W.T., Lin, S.-Y., Ho, H.-O., Sheu, M.-T., 2005. Physical characterizations of microemulsion systems using tocopheryl polyethylene glycol 1000 succinate (TPGS) as a surfactant for the oral delivery of protein drugs. *J. Control. Release,* 102, 489–507.

Keene, O.N., 1995. The Log Transformation is special. *Statistics in Medicine,* 14, 811-819.

Kerwin, B.A., 2008. Polysorbates 20 and 80 used in the formulation of protein biotherapeutics: structure and degradation pathways. *J. Pharm. Sci.*, 97 (8), 2924 – 2935.

Kim, J.M., Chang, S.M., Kong, S.M., Kim, K.S., Kim, J, Kim, W.S., 2009. Control of hydroxyl group content in silica particle synthesized by the sol-precipitation process. *Ceram. Int.* 35, 1015–1019.

King, S.M., 1999. Small Angle Neutron Scattering, Chapter 7 in Modern Techniques for Polymer Characterisation. 1st edition. Pethrick & Dawkins (editors), Chichester, UK , Wiley.

Klopman, G., Li, Ju-Yun., Wang, S., Dimayuga, M, 1994. Computer automated logP calculations based on an extended group contribution approach. *J. Chem. Inf. Comput. Sci.*, 34, 752.

Kohli, K., Chopra, S., Dhar, D., Arora, S., Khar, R.K., 2010. Self-emulsifying drug delivery systems: an approach to enhance oral bioavailability. *Drug Discov. Today*, 15 (21-22), 958 – 965.

Koleske, J. V., 1995. Oil absorption of pigments, paint and coaling testing: Gardner-Sward Handbook (Astm Manual Series), 14th edition. American Society for Testing & Materials.

Kommuru, T.R., Gurley, B., Khan, M.A, Reddy, I.K., 2001. Self-emulsifying drug delivery systems (SEDDS) of coenzyme Q10: formulation development and bioavailability assessment. *Int. J. Pharm.*, 212, 233–246.

Kowalski, J., Simple HPLC Analysis for Sudan Dyes: Monitor Sudan I, II, III, and IV in a single, isocratic analysis. Restek Corporation [electronic resource] http://www.restek.com/Technical-Resources/Technical-Library/Foods-Flavors-Fragrances/

Kuentz, M. Rothlisberger, D., 2002. Determination of the optimal amount of water in liquid-fill masses for hard gelatin capsules by means of texture analysis and experimental design. *Int. J. Pharm.*, 236, 145–152.

Kumar, A., Sharma, S., Kamble, R., 2010. Self emulsifying drug delivery system (SEDDS): future aspects. *Int. J. Pharm. Pharm. Sci.*, 2 (4), 7-13.

Kumar P., Mittal K.L, 1999. Handbook of Microemulsion Science and Technology. 1st edition. New York. Dekker,

Lagues, M., Sauterey, C., 1980. Percolation transition in water in oil microemulsions. Electrical conductivity measurements. *J. Phys. Chem.*, 84, 3503-3508.

Lawrence, M.J., Rees, G.D, 2000. Microemulsion-based media as novel drug delivery systems. *Adv. Drug Delivery Rev.*, 45, 89 –121.

Leonard, T.W., Adamczyk, B., Lee, A., O'Toole, E., 2007. Almerol™ (MER-103), poster presentation, The North American Menopause Society (NAMS) Annual Meeting, Dallas , USA.

Leonard, T.W., O'Toole, E., Brennan, F., Brayden, D.J., 2006. Promoting the oral absorption of drugs in humans using gastro-intestinal permeation enhancement technology (GIPET). *Drug Deliv. Techn.*, 6, 2.

Leonard, T.W., Lynch, J., McKenna, M.J., Brayden, D.J., 2006. Promoting absorption of drugs in humans using medium-chain fatty acid-based solid dosage forms: GIPET™. *Expert Opin. Drug Deliv.*, 3(5), 685-692.

Leung, R., Shah., D.O., 1987. Solubilization and phase equlibria of water-in-oil microemulsions: II Effects of alcohols, oils and salinity on single-chain surfactant Systems. *J. Colloid Interface Sci.*, 120 (2), 330 – 344.

Li, X., Hu, M., 2011. Oral bioavailability: basic principles, advanced concepts, and applications. 1st edition. New Jersey, Willey.

Li, P., Hynes, S.H., Haefele, T.F., Pudipeddi, M., Royce, A.E., Serajuddin, A.T.M., 2009. Development of clinical dosage forms for a poorly water-soluble drug II: formulation and characterization of a novel solid microemulsion preconcentrate system for oral delivery of a poorly water-soluble drug. *J. Pharm. Sci.*, 98 (5), 1750-1764.

Li, P., Ghosh, A., Wagner, R.F., Krill, S., Joshi Y.M., Serajuddi A.T M., 2005. Effect of combined use of nonionic surfactant on formation of oil-in-water microemulsions. *Int. J. Pharm.*, 288 (1), 27-34.

Lin, J.H., 1996. Bisphosphonates: a review of their pharmacokinetic properties. *Bone*, 18 (2), 75-85.

Lin, J.L., Chen, I.W., Deluna, F.A, 1994. On the absorption of alendronate in rats. *J. Pharm. Sci.*, 83 (12), 1741-1746.

Liu, X., Qu, S., Lu, X., Ge, X., Leng, Y., 2009. Time-of-flight secondary ion mass spectrometry study on the distribution of alendronate sodium in drug-loaded ultra-high molecular weight polyethylene. *Biomed. Mater.* 4, 65 -88.

Liu, H., Wang, Y., Lang, Y. Yao, H., Dong, Y., Li S., 2009. Bicontinuous cyclosporin A loaded water-AOT/Tween 85-isopropylmyristate microemulsion: structural characterization and dermal pharmacokinetics in vivo. *J. Pharm. Sci.,* 98 (3), 1167 – 1176.

Loper, A.E., Booth, S., Clarke, A., Olah, T.V., McLoughlin, D.A., Novak, L.B., Hettrick, L.A., Storey, D.E., 1996. Equivalence of a self-emulsifying drug delivery system (SEDDS) and soybean oil for oral delivery of a 5a-reductase inhibitor in rhesus monkeys. In: Couvreur P., Duchene D., Kalles I. (Eds.), Proc. Eur. Symp. Formulation of Poorly available Drugs for Oral Absorption. Editions de Sante, Paris, 369–372.

Lutz, R., Aserin, A., Wachtel, E.J., Shoshan, E.B., Danino, D., Garti, N., 2007. A Study of the emulsified microemulsion by SAXS, Cryo-TEM, SD-NMR, and electrical conductivity. *J. Dispersion Sci. Technol.,* 28, 1149–1157.

Lyons, K.C., Charman, W.N., Miller, R., Porter, C.J.H., 2000. Factors limiting the oral bioavailability of N-acetylglucosaminyl-N-acetylmuramyl dipeptide (GMDP) and enhancement of absorption in rats by delivery in a water-in-oil microemulsion. *Int. J. Pharm.*, 199, 17–28.

Lyogen Limited et al., 2003. WO03/053985A1. Pamidronic acid monosodium salt and preparation thereof.

Lv, F.F., Li, N., Zheng, L.Q., Tung, C.H., 2006. Studies on the stability of the chloramphenicol in the microemulsion free of alcohols. *Eur. J. Pharm. Biopharm.*, 62, 288 –294.

MacGregor, K.J., Embletona, J.K., Lacy, J.E., Perry, E.A., Solomon, L.J., Seagerb, H., Pouton, C.W., 1997. Influence of lipolysis on drug absorption from the gastro-intestinal tract. *Adv. Drug Deliver. Rev.*, 25, 33-46.

Madieh, S., Simone, M., Wilson, W., Mehra, D., Augsburger, L., 2007. Investigation of drug–porous adsorbent interactions in drug mixtures with selected porous adsorbents. *J. Pharm. Sci.*, 96 (4), 851–863.

Mahajan, R.K., Chawla, J., Bakshi, M.S., 2004. Depression in the cloud point of Tween in the presence of glycol additives and triblock polymers. *Colloid Polym. Sci.*, 282, 1165–1168.

Mahato, R.M., Narang, A.S., Thoma L., Miller, D.D., 2003. Emerging trends in oral delivery of peptide and protein drugs. *Crit. Rev. Ther. Drug,* 20 (2,3), 153–214.

Mahdi, E.S., Sakeena, M.H, Abdulkarim, M.F., Abdullah, G.Z., Sattar, M.A., Noor, A.M., 2011. Effect of surfactant and surfactant blends on pseudoternary phase diagram behavior of newly synthesized palm kernel oil esters. *Drug Des. Devel. Ther.,* 5, 311–323.

Mahmoud, E. A, Bendas, E. R, Mohamed, M.I., 2009. Preparation and evaluation of self-nanoemulsifying tablets of carvedilol, *AAPS PharmSciTech.*, 10 (1).

Mannhold, R., Kubinyi, H., Folkers, G., 2007. Molecular drug properties: measurement and prediction. 1st edition. Darmastdt, Wiley VCH.

Mehta, S.K, Bala, K, 2000. Tween-based microemulsions: a percolation view. *Fluid Phase Equilib.*, 172, 197–209.

Mehta, S.K., Kaur, G., 2011. Microemulsions: thermodynamic and dynamic properties in Thermodynamics, Mizutani Tadashi (Editor), InTech.
http://www.intechopen.com/articles/show/title/microemulsions-thermodynamic-and-dynamic-properties

Meissonnier, J. 2007. Director of Research and Development, Catalent Pharma Solutions, private communication.

Mitra, R.K., Paul, B.K., 2005. Physicochemical investigations of microemulsification of eucalyptus oil and water using mixed surfactants (AOT + Brij-35) and butanol. *J. Colloid Interface Sci.* 283, 565–577.

Motulsky H., 1995. Intuitive Biostatistics. 1st edition. New York, Oxford University Press.

Moulik, S.P., Paul, B.K, 1998. Structure, dynamics and transport properties of microemulsions. *Adv. Colloid Interface Sci.* 78, 99-195.

Mrestani, Y., Behbood, L., Härtl, A, Neubert, R.H.H., 2010. Microemulsion and mixed micelle for oral administration as new drug formulations for highly hydrophilic drugs. *Eur.J. Pharm. Biopharm.*, 74, 219–222.

MRK0345, Basic principles of particle size analysis, technical note by Rawle A. www.malvern.co.uk

MRK656, Dynamic light scattering: an introduction in 30 minutes, DLS technical note, www.malvern.co.uk

MRK809-01, Surfactant micelle characterization using dynamic light scattering, DLS technical note, www.malvern.co.uk

MRK1399, Setting new standards for laser diffraction particle size analysis, technical note by Rawle A. and Kippax P., www.malvern.co.uk.

Müllertz, A., Ogbonna, A., Ren S., Rades, T., 2010. New perspectives on lipid and surfactant based drug delivery systems for oral delivery of poorly soluble drugs. *J. Pharm. Pharmacol.*, 62: 1622–1636.

Na, G.C., Yuan, B.O., Stevens, H.J., Weekley, B.S., Rajagopalan, N., 1999. Cloud point of nonionic surfactants : modulation with pharmaceutical excipients. *Pharm. Res.*, 16 (4), 562-568.

Nanjwade, B.K., Patel, D.J., Udhani, R.A., Manvi, F.V., 2011. Functions of lipids for enhancement of oral bioavailability of poorly water-soluble drugs. *Sci. Pharm.*, 79, 705–727

Narang, A.S., Delmarre, D., Gao, D., 2007. Stable drug encapsulation in micelles and microemulsions. *Int. J. Pharm.*, 345, 9–25.

Negrea, D., Ducu, C., Moga, S., Malinovschi, V., Neamtu, J., Ristoscu C., Mihailescu, I.N., Cornelia, F., 2010. Microstructural characterization of hydroxyapatite-alendronate nanocomposites. *J. Optoelectron. Adv. M.*, 12 (5), 1194 – 1199.

Nobbmann, U., Connah, M., Fish, B., Varley, P., Gee, C., Mulot, S., Chen, J., Zhou, L., Lu, Y., Sheng, F., Yi J., Harding, S.E., 2007. Dynamic light scattering as a relative tool for assessing the molecular integrity and stability of monoclonal antibodies. *Biotechnol. Genet. Eng.*, 24, 117-128.

O'Driscoll, C.M., 2002. Lipid-based formulations for intestinal lymphatic delivery. *Eur. J. Pharm. Sci.*, 15, 405–415.

O'Driscoll, C.M., Griffin, B.T., 2008. Biopharmaceutical challenges associated with drugs with low aqueous solubility--the potential impact of lipid-based formulations. *Adv. Drug Deliver. Rev.*, 60 (6), 617-624.

Owen, A.J., Yiv, S.H., Sarkanian, B., 1995. US5444041A1, Convertible microemulsion formulations.

Owen, A.J and Yiv, S.H., 1997. US5633226A1, Convertible microemulsion formulations.

Owen, A.J and Yiv, S.H., 1997. US5646109A1, Convertible microemulsion formulations.

Owen, A.J. Yiv, S.H., Sarkanian, B., 1997. US5688761A1, Convertible microemulsion formulations.

Overbeek, J.Th.G., deBruyn, P.L., Verhoecks, F., 1985. Microemulsions in Surfactants. 1st edition, (Tadros Th.F editor), Academic Press, 111-132.

Paul, B.K., Moulik, S.P., 1997. Microemulsions: an overview. *J. Disper. Sci. Technol.,* 18 (4), 301-367.

Parida, S. K., Dash, S., Patel, S., Mishra, B.K., 2006. Adsorption of organic molecules on silica surface. *Adv. Colloid Interface Sci.,* 121, 77 – 110

Pasquali, R.C., Taurozzi, M.P, Bregni, C., 2008. Some considerations about the hydrophilic–lipophilic balance system. *Int. J. Pharm.*, 356, 44–51.

Patel, M.R., Patel, R.B, Parikh, J.R, Bhatt, K.K., Solanki, A.B, 2010. Investigating the effect of vehicle on in vitro skin permeation of ketoconazole applied in o/w microemulsions. *Acta Pharma. Sci.,* 52, 65-77.

Phillips, N., 2009. Technical Service Manager in J.M. Huber Corporation, private communication.

Planinsek, O., Kovacic, B., Vrecer, F. 2011. Carvedilol dissolution improvement by preparation of solid dispersions with porous silica. *Int. J. Pharm.*, 406, 41–48.

Podlogar, F., Gasperlin, M., Tomsi, M., Jamnik, A., Bester-Rogac, M., 2004. Structural characterisation of water–Tween 40®/Imwitor 308®–isopropyl myristate microemulsions using different experimental methods. *Int. J. Pharm.*, 276, 115–128.

Pouton, C.W., 1997. Formulation of self-emulsifying drug delivery systems. *Adv. Drug Deliver. Rev.*, 25, 47-58.

Pouton, C.W., 2000. Lipid formulations for oral administration of drugs: non-emulsifying, self-emulsifying and 'self-microemulsifying' drug delivery system. *Eur. J. Pharm. Sci.,* 11 (2), 93–98.

Pouton, C.W., 2007. Properties and uses of common formulation lipids, surfactants and cosolvents. Oral presentation, AAPS Workshop, Washington DC, USA.

Pouton, C.W., 2006. Formulation of poorly water-soluble drugs for oral administration: Physicochemical and physiological issues and the lipid formulation classification system. *Eur. J. Pharm. Sci.,* 29, 278-287.

Pouton, C.W., Porter C.J.H., 2008. Formulation of lipid-based delivery systems for oral administration: Materials, methods and strategies. *Adv. Drug Deliver. Rev.*, 60, 625 – 637

Porter, C.J.H, Kaukonen, A.M., Boyd, B.J., Edwards, G.A., Charman, W.N., 2004. Susceptibility to lipase-mediated digestion reduces the oral bioavailability of danazol after administration as a medium-chain lipid-based microemulsion formulation. *Pharm. Res.,* 21 (8), 1405 – 1412.

Porter, C.J.H., Trevaskis, N.L., Charman, W.N., 2007. Lipids and lipid-based formulations: optimizing the oral delivery of lipophilic drugs. *Nat. Rev. Drug Discov.,* 6, 231 – 248.

Porter, C.J.H., Charman, W.N., 1997. Uptake of drugs into the intestinal lymphatics after oral administration. *Adv. Drug Deliver. Rev.*, 25, 71-89.

Porter, C.J.H., Charman W.N., 2001. In vitro assessment of oral lipid based formulations. *Adv. Drug Deliver. Rev.*, 50, S127 – S147.

Powell, M.F., Fleitman, J., Sanders, L.M., Si, V.C., 1994. Peptide liquid crystals: inverse correlation of kinetic formation and thermodynamic stability in aqueous solutions. *Pharm. Res.,* 11 (9), 1352 –1354.

Powell, M.F., Sanders, L.M., Rogerson, Al., Si V., 1991. Parenteral peptide formulations: chemical and physical properties of native luteinizing hormone-releasing hormone (LHRH) and hydrophobic analogues in aqueous solution. *Pharm. Res.,* 8 (10), 1258 – 1263.

Prajapati, H.N., Patel, D.P., Patel, N.G, Dalrymple, D.M., Serajuddin, A.T.M., 2011. Effect of difference in fatty acid chain lengths of medium-chain lipids on lipid/surfactant/water phase diagrams and drug solubility. *J. Excipients and Food Chem.,* 2 (3), 73 – 88.

Prélot, B., Lantenois, S., Nedellec, Y., Lindheimer, M., Douillard, J.M., Zajac, J., 2010. The difference between the surface reactivity of amorphous silica in the gas and liquid phase due to material porosity, *Colloid. Surf. A*, 355, 67–74.

Price, W.S., 2005. Applications of pulsed gradient spin-echo NMR diffusion measurements to solution dynamics and organization. *Diffusion Fundamentals*, 2, 112.1 - 112.19.

Prince, L. M, 1977. Microemulsions Theory and Practice. 1st edition. New York. Academic Press Inc.

Qi, J., Zhuang, J., Wu, W., Lu, Y., Song, Y., Zhang, Z., Jia, J., Ping, Q., 2011. Enhanced effect and mechanism of water-in-oil microemulsion as an oral delivery system of hydroxysafflor yellow A. *Int. J. Nanomedicine,* 6, 985–991.

Q1A(R2), 2003, Stability Testing Of New Drug Substances And Products. ICH Harmonised Tripartite Guideline.
http://www.ich.org/fileadmin/Public_Web_Site/ICH_Products/Guidelines/Quality/Q1A_R2/Step4/Q1A_R2__Guideline.pdf

Qiu, Y., Chen Y., Zhang G.G.Z., Liu L., 2008. Developing solid oral dosage forms: pharmaceutical theory and practice. 1st edition. New York. Academic Press.

Rajadhyaksha, V, J. Lahey, T.P., 2004. Glycopeptides for the treatment of Als and other metabolic and autoimmune disorders. US 2007/0185012 A1.

Rivier, J.E., Jiang, G., Koerber, S.C., Porter, J., Simont, L., Craig, A.G., Hoeger, C.A., 1996. Betidamino acids: versatile and constrained scaffolds for drug discovery. *Proc. Natl. Acad. Sci.* 93, 2031-2036.

Rivier, J.E., Jiang, G., Porter, J., Hoeger, C.A, Craig, A.G, Corrigan, A., Vale, W., Rivier, C.L, 1995. Gonadotropin-releasing hormone antagonists: novel members of the azaline B family. *J. Med. Chem.,*38, 2649-2662.

Rocha, J. V., Barrera, D., Sapag, K., 2010. Improvement in the pore size distribution for ordered mesoporous materials with cylindrical and spherical pores using the Kelvin equation. *Top. Catal,* 54, 121–134.

Roldan, E.J.A., Quattrocchi, O., Zanchetta, J., Plotkin H., Araujo, G., Piccinin, E., 2002. Comparable bioavailability of two esophago-gastric protective formulations containing pamidronate. *Medicina (Buenos Aires),* 62, 317-322.

Rosen, M. J., 2004. Surfactants and Interfacial Phenomena. 3rd Edition edition. New York, Wiley.

Rouquerolt, J., Avnir, D.; Fairbridge, C. W., Everett, D. H., Haynes, J. H., Pernicone, N., Ramsay, J. D. F., Sing, K. S. W., Unger, K. K., 1994. Recommendations for the characterization of porous solids. *Pure & Appl. Chem.,* 66 (8), 1739-1758.

Rowe, R.C., Sheskey, P.J., Weller, P.J., 2003. Handbook of pharmaceutical excipients, 4th edition. APhA Publications.

Rxlist, The internet drug index, http://www.rxlist.com

Ruckenstein, E., Chi, J.C., 1975. Stability of microemulsions. *J. Chem. Soc. Faraday Trans.*, 71, 1690-1707.

Ruckenstein, E., Krishnan, R., 1979. Swollen micellar models for solubilization. *J. Colloid Interface Sci.*, 71, 321.

Ryan, P.J., Blake, G. M., Davie, M., Haddaway, M., Gibson, T., Fogelman, I., 2000. Intermittent oral disodium pamidronate in established osteoporosis: a 2 year double-masked placebo-controlled study of efficacy and safety. *Osteoporos Int.*, 11, 171–176.

Sangwichien, C., Aranovich, G.L., Donohue, M.D., 2002. Density functional theory predictions of adsorption isotherms with hysteresis loops. *Colloid. Surf. A*, 206, 313–320.

Saint Ruth, H., Attwood, D., Ktistis, G., Taylor, C.J., 1995. Phase studies and particle size analysis of oil-in-water phospholipid microemulsions. *Int. J. Pharm.,*116, 253-261.

Sarciaux, J.M., Acar, L., Sado, P.A., 1995. Using microemulsion formulations for oral drug delivery of therapeutic peptides. *Int. J. Pharm.,* 120, 127-136.

Seeballuck, F., Lawless, E., Ashford, M.B., O'Driscoll, C.M., 2004. Stimulation of triglyceride-rich lipoprotein secretion by Polysorbate 80: in vitro and in vivo correlation using Caco-2 cells and a cannulated rat intestinal lymphatic model. *Pharm. Res.* 21, 2320–2326.

Schiller, C., Frohlich, C.P., Giessmann, T., Siegmund, W., Monnikess, H., Hosten, N., 2005. Intestinal fluid volumes and transit of dosage forms as assessed by magnetic resonance imaging. *Aliment. Pharmacol. Ther.,* 22, 971–979.

Schmitz, G., Borgmann, U., Assmann, G. 1985. Analytical capillary isotachophoresis: a routine technique for the analysis of lipoproteins and lipoprotein subfractions in whole serum. *J. Chromatogr.*, 320 (1), 253-262.

Schoff, C.K., 2009. Oil absorption . *JCT. Coatings Tech.* *http://findarticles.com/p/articles/mi_hb3226/is_3_6/ai_n31566106/*

Schulman, J.H., Stoeckentuis, W., Prince, L.M. 1959. Mechanism of formation and structure of microemulsions by electron microscopy. *J. Phys. Chem.,* 63, 1677–1680.

Senatra, D., Gabrielli, G., Caminati, G., Zhod, Z., 1988. Conformational changes at the microemulsion water/oil interface and their influence on the system's dielectric temperature behavior. *IEEE Transactions on Electrical Insulation*, 23 (4), 579 – 589.

Senatra, D., 2000. Procedures for DSC analysis of percolative microemulsions. *Thermochim. Acta*, 345, 39-46.

Settle, F.A, 1997. Handbook of instrumental techniques for analytical chemistry. 1st edition. Prentice Hall.

Sha, X., Yan, G., Wu, Y., Li J., Fang, X., 2005. Effect of self-microemulsifying drug delivery systems containing Labrosol on tight junctions in Caco-2 cells. *Eur. J. Pharm. Sci.*, 24, 477 –486.

Sharma, S., Sher, P., Badve, S., Pawar, A.P., 2005. Adsorption of meloxicam on porous calcium silicate: characterization and tablet formulation. *AAPS PharmSciTech.*, 6(4), 618 – 625.

Sinko, P.J., 1992. Intestinal absorption of peptides and peptide analogues: implications of fasting pancreatic serine protease levels and pH on the extent of oral absorption in dogs and humans. *Pharm. Res.,* 9(3), 320- 325.

Shinoda, K., Friberg, S.E., 1975. Microemulsions: colloidal aspects. *Adv.Colloid Interface Sci.*, 4, 281 –300.

Sing, K. S. W., Everett, D. H., Haul, R. A. W, Moscou, L., Pierotti, R. A., Rouquerol, J., Siemieniewska, T., 1985. Reporting physisorption data for Gas/solid systems with special reference to the determination of surface area and porosity. *Pure & App. Chem.,* 57 (4), 603—619.

Siwinska-Stefanska, K., Walkowiak, J, Krysztafkiewicz, A., Jesionowski, T., 2008. Polymer adsorption on the surface of highly dispersed silica. *Appl. Surf. Sci.,* 254, 3591–3600.

Slager, J., Domb, A.J., 2004. Hetero-stereocomplexes of D-poly(lactic acid) and the LHRH analogue leuprolide. Application in controlled release. *Eur. J. Pharm. Biopharm.,* 58, 461–469.

Sneh, O., George, S.M, 1995. Thermal stability of hydroxyl groups on a well-defined silica surface. *J. Phys. Chem.,* 99, 4639-4647.

Söderman, O., Stilbs, P., Price, W.S., 2004. NMR studies of surfactants. *Concepts in Magnetic Resonance Part A*, 23A(2), 121–135.

Spernath, A., Aserin, A., 2006. Microemulsions as carriers for drugs and nutraceuticals. *Adv. Colloid Interface Sci.*, 128 – 130, 47 – 64.

Sripriya, R., Rajab, K.M., Santhosh, G., Chandrasekaran, M., Noel, M., 2007. The effect of structure of oil phase, surfactant and cosurfactant on the physicochemical and electrochemical properties of bicontinuous microemulsion. *J. Colloid Interface Sci.,* 314, 712–717.

Stegemeyer, H., 1994. Liquid crystals (Topics in physical chemistry). 1st edition. Darmstadt. Steinkopff Verlag.

Stella, V.J., 2007. Compound selection: the what, why and how of lipid-based formulations, oral presentation given at AAPS Lipids Workshop, Bethesda, USA.

Strickley, R.G., 2004. Solubilizing excipients in oral and injectable formulations. *Pharm. Res.,* 21 (2), 201 – 230.

Stubenrauch, C., 2009. Microemulsions: background, new concepts, applications, perspectives. 1st edition. West Sussex (UK). Willey.

Surjyanarayan, M., Snigdha, M.S., Naazneen, S., Vandana, P.B., Mandal, P.A.S., 2009. Design and development of saquinavir microemulsion for the oral bioavailability enhancement. *Int. J. Pharm. Tech. Res.,* 1 (4), 1442-1448.

Sutton, S.C., 2004. Companion animal physiology and dosage form performance, *Adv. Drug Deliver. Rev.*, 56, 1383 – 1398.

Swarbrick, J., 1973. Current concepts in the pharmaceutical sciences: dosage form design and bioavailability. 1st edition. Philadelphia. Lea & Febiger.

Szymula, M., 2005. The influence of ascorbic acid on the rheological properties of the microemulsion region of the SDS/pentanol/water system. *J. Cosmet. Sci.,* 56 (4): 267-77.

Tadros, T.F., 2005. Surfactants: Principles and Applications. 1st edition. Weihem, Germany. Wiley -VCH

Tajber, L., Corrigan, D.O., Corrigan, O.I., Healy, A.M., 2009. Spray drying of budesonide, formoterol fumarate and their composites-I. Physicochemical characterisation. *Int. J. Pharm.* 367, 79-85.

Tajber, L., Corrigan, O.I., Healy, A.M., 2005. Physicochemical evaluation of PVP-thiazide diuretic interactions in co-spray-dried composites - analysis of glass transition composition relationships. *Eur. J. Pharm. Sci.* 24, 553-563.

Takei, T., Kato, K., Meguro A., Chikazawa, M., 1999. Infrared spectra of geminal and novel triple hydroxyl groups on silica surface. *Colloid. Surf. A*, 150, 77–84.

Talegaonkar, S., Azeem, A., Ahmad, F.J., Khar, R.K., Pathan, S.A, Khan Z.I., 2008. Microemulsions: a novel approach to enhanced drug delivery. *Recent Pat. Drug Deliv. Formul.* 2, 238-257.

Tang, B., Cheng, G., Gu J.C., Xu, C.H., 2008. Development of solid self-emulsifying drug delivery systems: preparation techniques and dosage forms. *Drug Disc. Today,* 13 (13/14), 606 – 612.

Tang, J., Sun, J., He, Z.G., 2007. Self-emulsifying drug delivery systems: strategy for improving oral delivery of poorly soluble drugs. *Curr. Drug Ther.*, 2, 85-93.

Taupitz,T., Klein, S., 2010. Can biorelevant media be simplified by using SLS and Tween 80 to replace bile compounds? *Open Drug Deliv. J.,* 4, 30-37.

Troy, D.B., 2006. Remington: the science and practice of pharmacy, 21st edition. Philadelphia (USA). Lippincott Williams & Wilkins.

Tuleu, C., Newton, M., Rose, J., Euler, D., Saklatvala, R., Clarke, A., Booth, S., 2004. Comparative bioavailability study in dogs of a self-emulsifying formulation of progesterone presented in a pellet and liquid form compared with an aqueous suspension of progesterone. *J. Pharm. Sci.* 93, 1495–1502.

UCM070244, 2001. Statistical approaches to establishing bioequivalence. U.S. Department of Health and Human Services Food and Drug Administration Center for Drug Evaluation and Research (CDER), http://www.fda.gov/downloads/Drugs/GuidanceComplianceRegulatoryInformation/Guidances/ucm070244.pdf

Van Der Voort, P., Gillis-D'Hamers, Vrancken, K. *C,* Vansant, E.F, 1991. Effect of porosity on the distribution and reactivity of hydroxyl groups on the surface of silica gel. *J. Chem. Soc. Faraday Trans*, 87 (24), 3899-3905.

Van Hecke, G.R., Karukstis, K.K., Li H., Hendargo, H.C., Cosand, A.J., Fox M.M. 2005. Synthesis and physical properties of liquid crystals: an interdisciplinary experiment. *J. Chem. Educ.,* 82 (9), 1349 – 1354.

Van Hoogevest, P., Liu, X., Fahr, A., 2011. Drug delivery strategies for poorly water-soluble drugs: the industrial perspective. *Expert Opin. Drug Deliv.,* 8 (11), 1482 – 1500.

Vasilenko, A., Glasser, B.J., Muzzio, F.J., 2011. Shear and flow behavior of pharmaceutical blends — method comparison study. *Powder Technol.*, 208, 628–636.

Verlaan, V., van der Werf, C. H. M., Arnoldbik, W. M., Goldbach, H. D., Schropp, R. E. I., 2006. Unambiguous determination of Fourier-transform infrared spectroscopy proportionality factors: The case of silicon nitride. *Phys. Rev. B,* 73, 195333-1 – 195333-8.

Viswanadhan, V.N.; Ghose, A.K.; Revankar, G.R. & Robins, R.K. 1989. Atomic physicochemical parameters for three dimensional structure directed quantitative structure-activity relationships. 4. Additional parameters for hydrophobic and dispersive interactions and their application for an automated superposition of certain naturally occurring nucleoside antibiotics. *J. Chem. Inf. Comput. Sci.*, 29, 163-172.

Virden, A., 2010. Method development for laser-diffraction particle-size analysis. *Pharm. Technol.*, 2, 100-106.

Voigt, A., Gao, Y., Hilfert, L., Sundmacher, K., 2008. Nanodroplet cluster formation in ionic liquid microemulsions. *Chem. Phys. Chem.,* 9, 1603 – 1609.

Walsh, E.G., Fox, J.S., Leonard, T.W., 2011. Oral-absorption-enhancing drug-delivery technology. *Pharm. Technol.,* 35, s12-s14.

Wang, F., Fang, B., Zhang, Z., Zhang, S., 2008. Mechanism of electrical percolation of w/o microemulsions formed by nonionic surfactants. *J. Dispersion Sci. Technol.,* 29, 1166–1172.

Wasan, E.K., Bartlett, K., Gershkovich, P., Sivak, O., Banno, B., Wong, Z., Gagnon, J., Gates, B., Leon, C.G., Wasan, K.M., 2009. Development and characterization of oral lipid-based amphotericin B formulations with enhanced drug solubility, stability and antifungal activity in rats infected with Aspergillus fumigatus or Candida albicans. *Int. J. Pharm.* 372, 76–84.

Winsor, P.A., 1948. Hydrotropy, solubilization, and related emulsification processes. *J. Chem. Soc. Faraday Trans.*, 44, 376-382.

Whang, J., Gwak, H., 2011. Effects of amines on percutaneous absorption of alendronate. *Drug |Dev. Ind. Pharm.*, 37(5): 491–497.

White, L.D., Tripp, C.P, 2000. A Low-frequency infrared study of the reaction of methoxymethylsilanes with silica. *J. Colloid. Interf. Sci.,* 224, 417–424

Willavize, S.A., Morgenthien, E.A., 2008. Nonparametric confidence intervals for Tmax in sequence-stratified crossover studies. *Pharmaceut. Statist.*7, 9–19.

Xie, Y., Ye, R., Liu, H., 2007. Microstructure studies on biosurfactant-rhamnolipid/*n*-butanol/water/*n*-heptane microemulsion system. *Colloid. Surf. A*, 292, 189–195.

Yadav, N.N, Price, W.S., 2007. Effects of polydispersity on PGSE NMR coherence features *Diffusion Fundamentals*, 6, 2.1 - 2.12.

Yaghmur, A., Aserin, A., Antalek, B., Garti, N., 2003. Microstructure considerations of new five-component Winsor IV food-grade microemulsions studied by pulsed gradient spin-echo NMR, conductivity, and viscosity. *Langmuir,* 19, 1063-1068.

Ying, J.Y., Benziger, J.B., 1992. Structure tailoring of alkoxide silica. *J. Non-Cryst. Solids.,* 147 - 148, 222-231.

Yiv, S.H. 1998. Transparent liquid for encapsulated drug delivery. US5707648A1.

Zumbrum, M.A., 1994. Acid/base properties of fumed silica fillers used in silicone elastomers. *J Adhesion*, 46 (1,4), 181 – 196.

Appendices

Appendix to Chapter 3

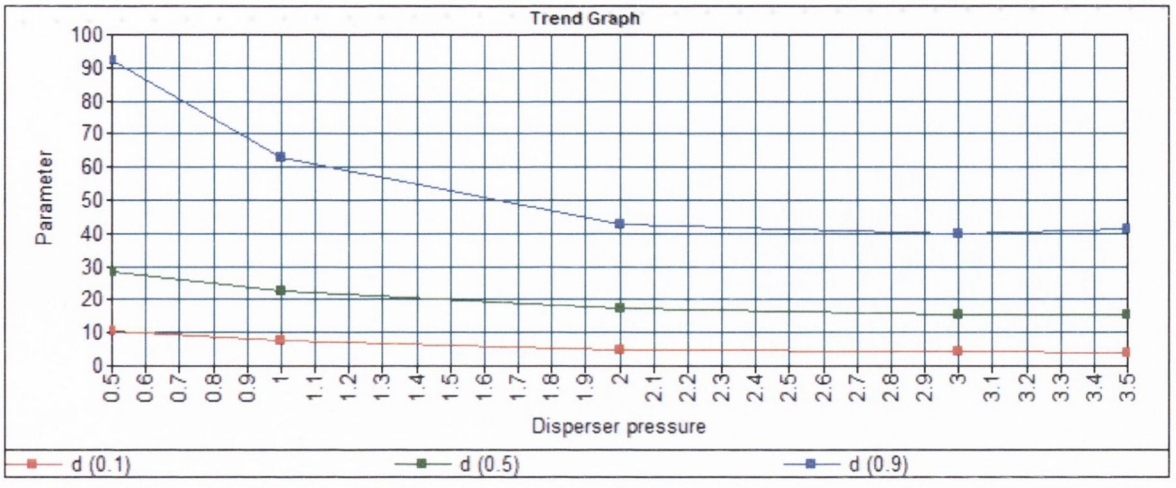

Fig. A.3.1. Pressure/particle size titration of disodium pamidronate pentahydrate (final dispersive pressure of 3 bar selected).

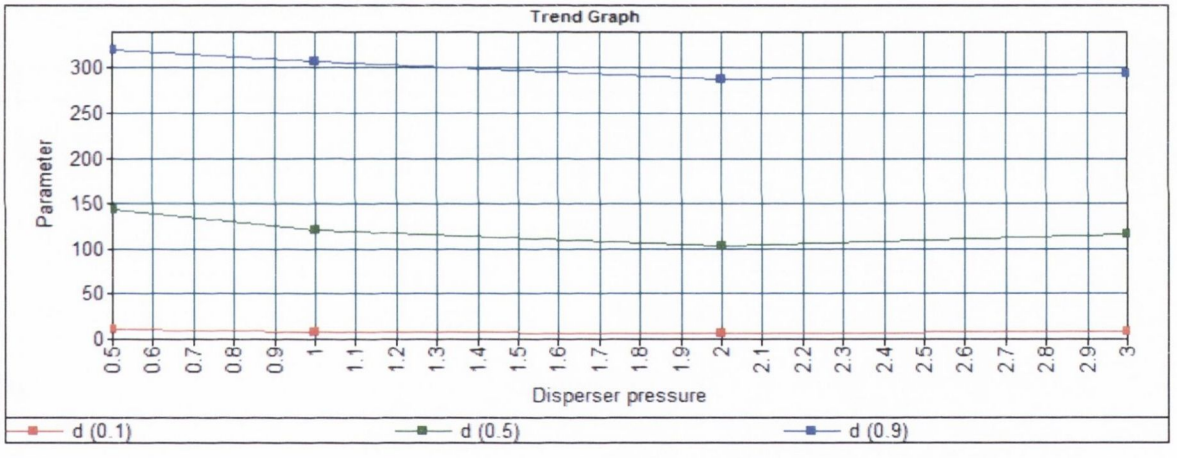

Fig. A.3.2. Pressure/particle size titration of sodium alendronate trihydrate (final dispersive pressure of 2 bar selected).

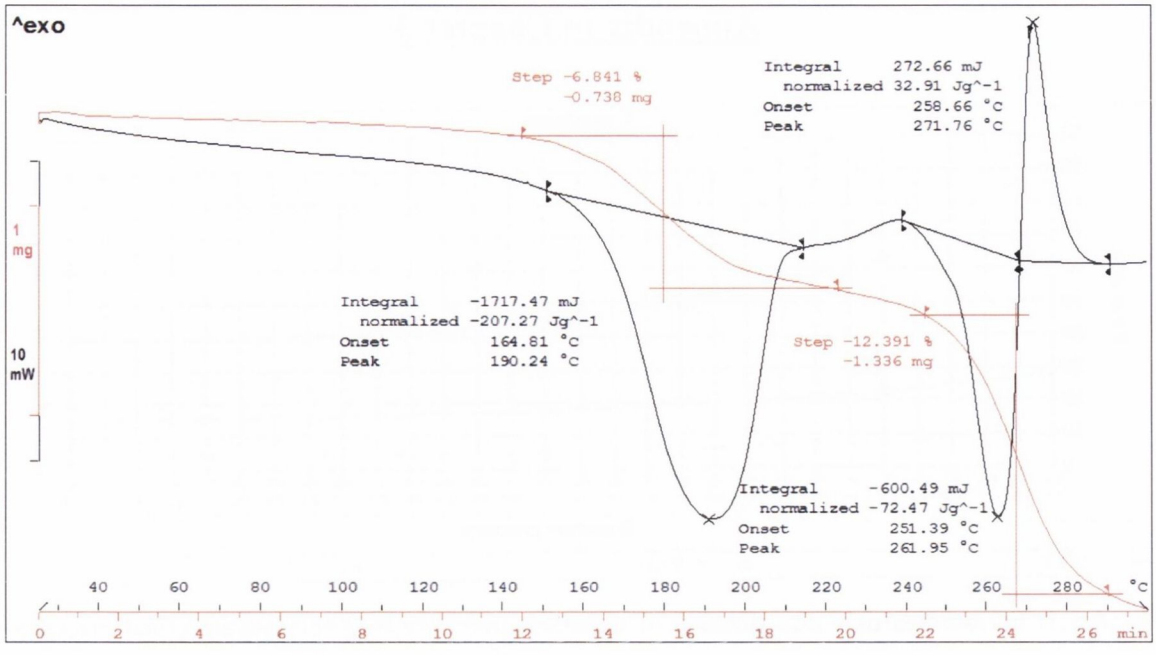

Fig. A.3.3. DSC and TGA curves of synthesized monosodium pamidronate monohydrate according to the preparation method presented in WO03/053985A1

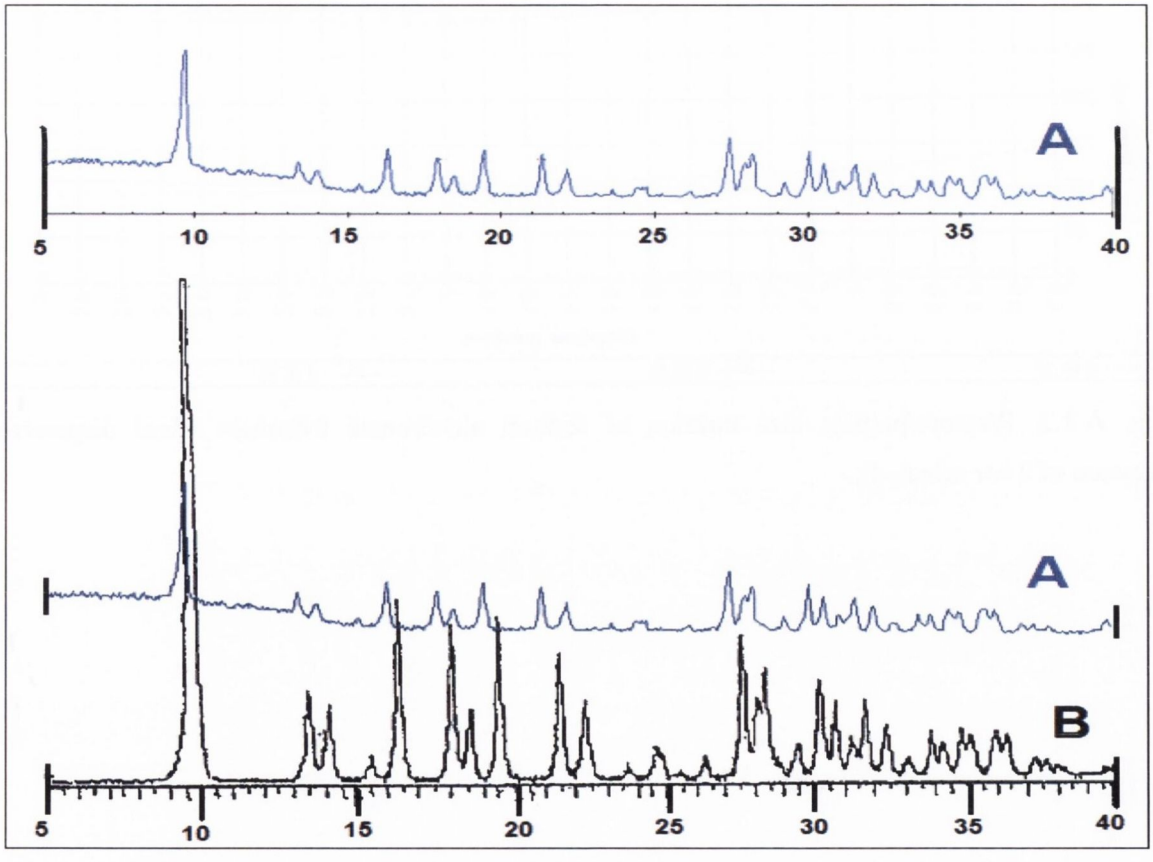

Fig. A.3.4. XRD diffractograms of the synthesized monosodium pamidronate monohydrate (A) compared with the XRD pattern of the monosodium pamidronate monohydrate presented in the patent WO03/053985A1 (B).

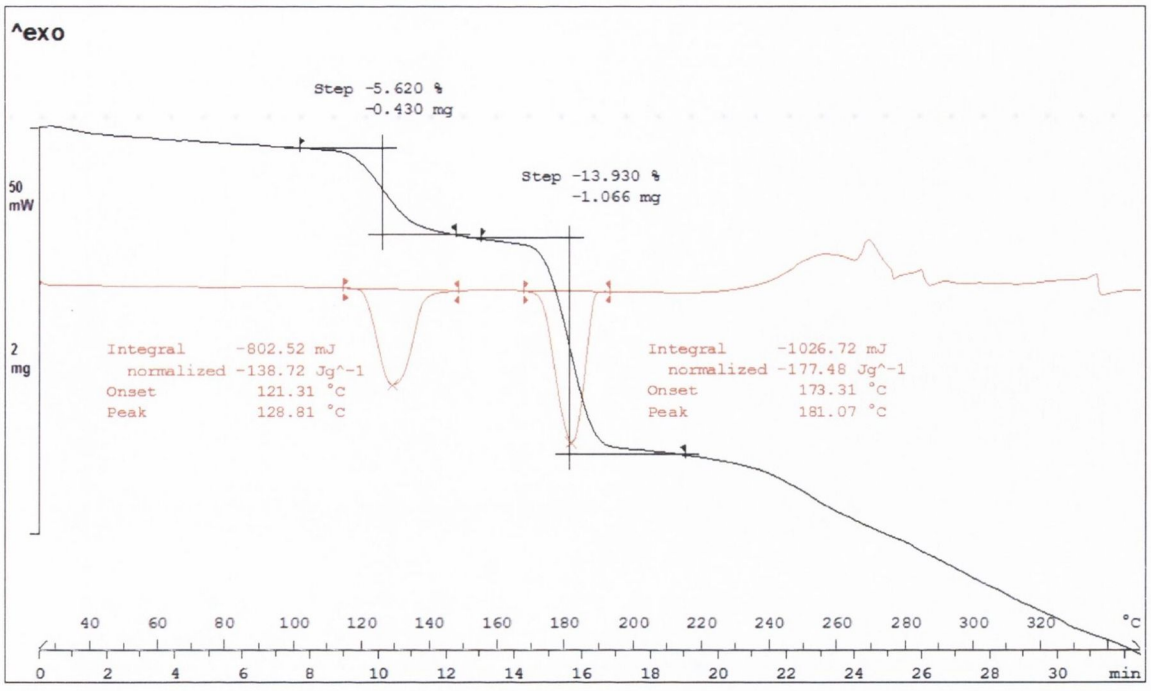

Fig. A.3.5. DSC and TGA curves overlaid for the solvate (sample 4E) of sodium alendronate recovered from propylene glycol after 322 days.

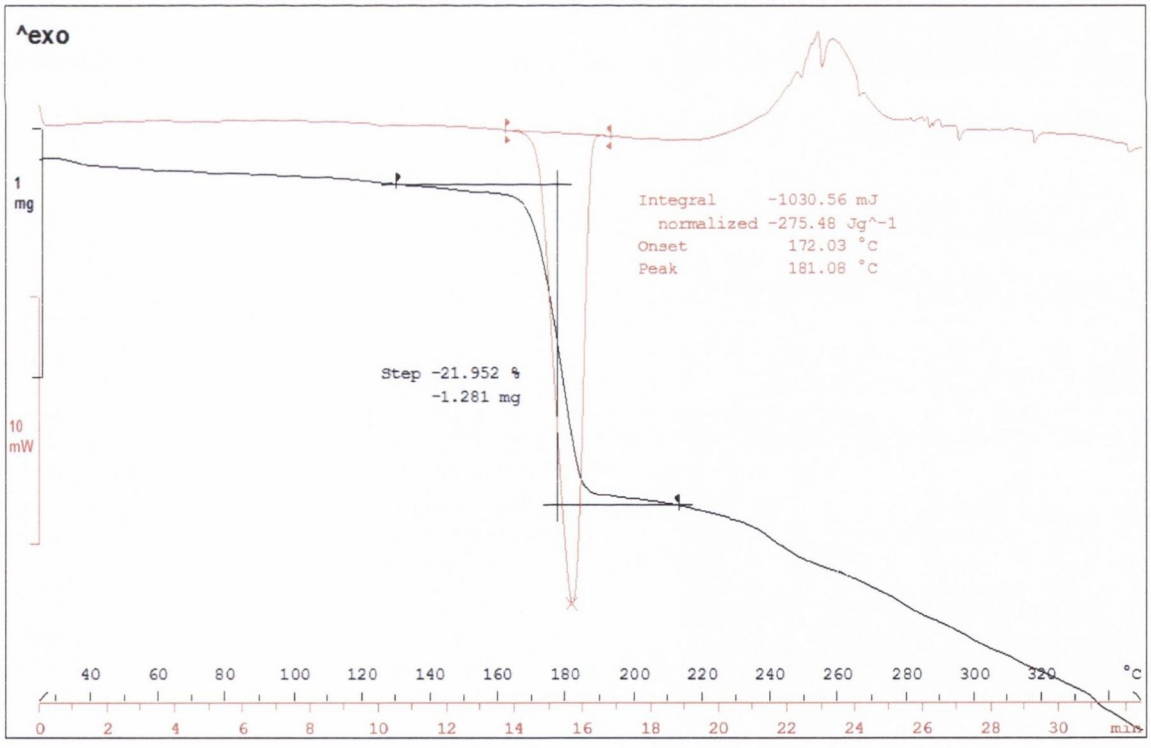

Fig. A.3.6. DSC and TGA curves overlaid for the solvate (sample 4G) of sodium alendronate recovered from propylene glycol after 382 days.

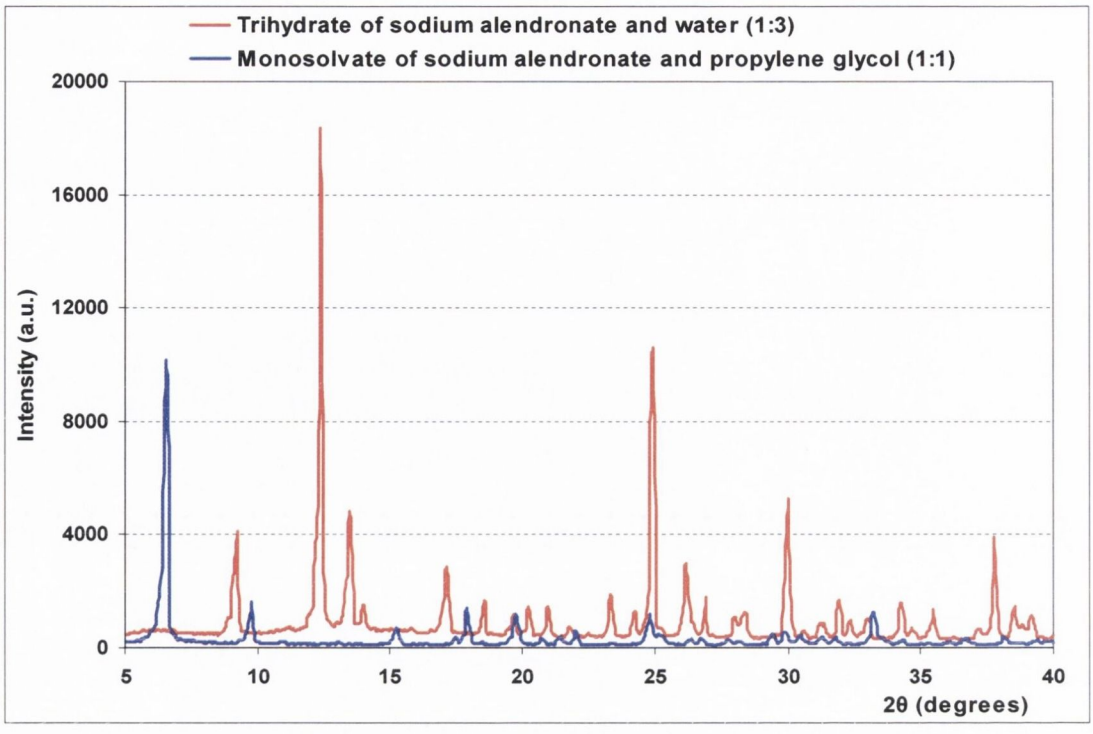

Fig. A.3.7. PXRD diffractograms overlaid for the solvate of sodium alendronate and propylene glycol versus the original material (sodium alendronate trihydrate).

Table A.3.1. Calibration curves for sodium alendronate trihydrate and disodium pamidronate pentahydrate where, *x* - corresponds to the concentration of the drug, *y* – corresponds to the peak surface area).

Sodium alendronate trihydrate			
Item	**Calibration range**	**Relationship**	**Correlation Coefficient**
Calibration curve 1	0.065 – 0.26 mg/ml	y = 30469033 x	$R^2 = 1.0000$
Calibration curve 2		y = 30397095 x	$R^2 = 0.9999$
Calibration curve 3		y = 30562605 x	$R^2 = 0.9999$
Disodium pamidronate pentahydrate			
Item	**Calibration range**	**Relationship**	**Correlation Coefficient**
Calibration curve 1	0.078 – 0.31 mg/ml	y = 18649502 x	$R^2 = 0.9985$
Calibration curve 2		y = 17714574 x	$R^2 = 0.9958$
Calibration curve 3		y = 18730477 x	$R^2 = 0.9983$

Appendix to Chapter 4

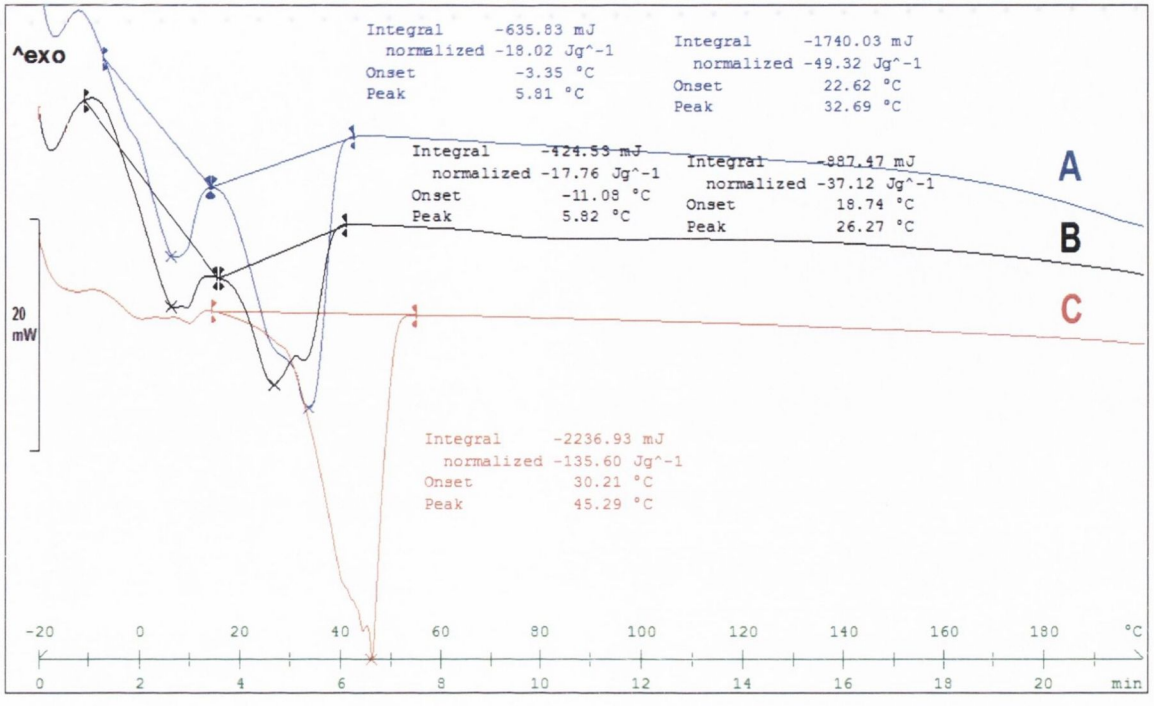

Fig. A.4.1. DSC curves of the low HLB values surfactants A) Capmul MCM, B) Capmul MCM C8, C) Capmul MCM C10

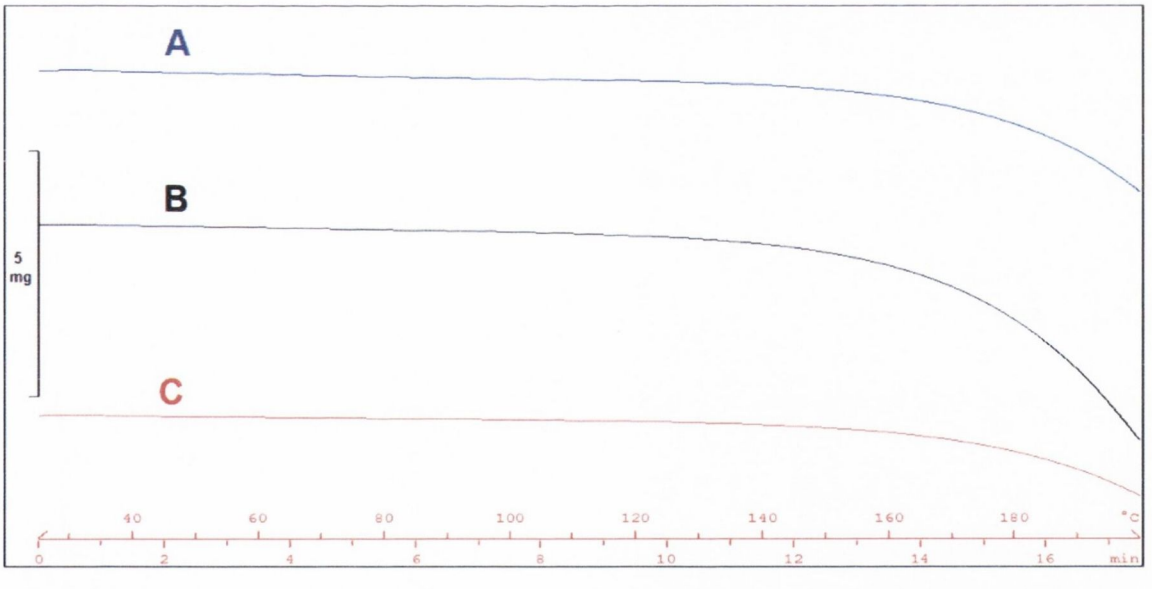

Fig. A.4.2.TGA curves of the low HLB values surfactants A) Capmul MCM, B) Capmul MCM C8, C) Capmul MCM C10

Appendix to Chapter 5

Table A.5.1.Conductivity results for samples R1 – R13.

Sample Name	1st set of samples			2nd set of samples			Average [μS/cm]	SD	RSD
	Average	SD	RSD	Average	SD	RSD			
R1	4.80	0.20	4.14	5.48	1.02	18.61	**5.14**	0.49	9.45
R2	13.41	0.30	2.23	10.35	0.10	0.95	**11.88**	2.16	18.21
R3	16.71	0.09	0.56	17.21	0.99	5.73	**16.96**	0.35	2.06
R4	29.07	0.42	1.43	34.30	0.20	0.58	**31.68**	3.70	11.68
R5	54.87	0.21	0.38	64.93	0.72	1.11	**59.90**	7.12	11.88
R6	92.30	1.11	1.21	108.37	1.40	1.30	**100.33**	11.36	11.32
R7	132.30	0.60	0.45	155.60	0.17	0.11	**143.95**	16.48	11.45
R8	177.50	0.26	0.15	189.87	0.74	0.39	**183.68**	8.74	4.76
R9	205.67	2.08	1.01	214.33	0.58	0.27	**210.00**	6.13	2.92
R10	231.00	1.00	0.43	235.00	0.00	-	**233.00**	2.83	1.21
R11	249.33	2.08	0.83	253.00	1.00	0.40	**251.17**	2.59	1.03
R12	261.33	2.52	0.96	263.67	0.58	0.22	**262.50**	1.65	0.63
R13	252.67	3.79	1.50	255.33	2.08	0.82	**254.00**	1.89	0.74

Table A.5.2.Calculated log (conductivity) and 1st derivative (conductivity) for samples R1 – R13.

volume fraction of water	***Conductivity [log]***					**Conductivity 1st derivative [d (log conductivity)/d volume fraction of water (φ w]**				
	1st set	2nd set	**Average**	SD	RSD	1st set	2nd set	**Average**	SD	RSD
0.05	0.681	0.739	**0.710**	0.041	5.8	8.023	4.958	**6.490**	2.168	33.4
0.10	1.127	1.015	**1.071**	0.080	7.4	2.117	4.886	**3.501**	1.958	55.9
0.17	1.223	1.236	**1.229**	0.009	0.7	5.024	6.263	**5.644**	0.876	15.5
0.34	1.463	1.535	**1.499**	0.051	3.4	5.461	5.486	**5.473**	0.018	0.3
0.65	1.739	1.812	**1.776**	0.052	2.9	4.558	4.488	**4.523**	0.049	1.1
1.08	1.965	2.035	**2.000**	0.049	2.5	3.134	3.149	**3.142**	0.011	0.3
1.56	2.122	2.192	**2.157**	0.050	2.3	2.457	1.664	**2.060**	0.561	27.2
1.90	2.249	2.278	**2.264**	0.021	0.9	1.297	1.067	**1.182**	0.162	13.7
2.14	2.313	2.331	**2.322**	0.013	0.5	1.048	0.831	**0.940**	0.154	16.4
2.35	2.364	2.371	**2.367**	0.005	0.2	0.562	0.543	**0.552**	0.013	2.4
2.53	2.397	2.403	**2.400**	0.004	0.2	0.212	0.187	**0.199**	0.018	9.1
2.64	2.417	2.421	**2.419**	0.003	0.1	-0.155	-0.148	**-0.151**	0.005	-3.5
2.55	2.403	2.407	**2.405**	0.003	0.1	3.205	3.211	**3.208**	0.004	0.1

Table A.5.3. Summary of DSC results for samples R1 – R13.

Sample Name	**'CAPTEX 355 peak'**			**'WATER peak'**		
	Normalized Enthalpy [Jg⁻1] of solidification					
	Average	**SD**	**RSD**	**Average**	**SD**	**RSD**
100% of Captex 355	**52.84**	2.13	4.04	N/A		
R1, 5% of water	**41.37**	1.48	3.57	Not detected		
R2, 11% of water	**39.41**	0.99	2.50	Not detected		
R3, 15% of water	**29.90**	2.56	8.55	Not detected		
R4, 20% of water	**52.20**	2.03	3.90	Not detected		
R5, 25% of water	**24.96**	3.45	13.81	**31.96**	7.60	23.77
R6, 30% of water	**27.96**	0.87	3.11	**53.58**	3.12	5.83
R7, 35% of water	**27.21**	1.01	3.73	**71.05**	1.96	2.76
R8, 40% of water	**23.41**	0.31	1.33	**89.15**	2.77	3.11
R9, 45% of water	**21.72**	0.41	1.87	**107.50**	0.64	0.59
R10, 50% of water	**20.16**	0.61	3.04	**125.95**	1.29	1.03
R11, 56% of water	**17.86**	0.40	2.24	**146.17**	2.97	2.03
R12, 65% of water	**13.22**	0.85	6.40	**168.59**	19.50	11.56
R13, 75% of water	**9.69**	0.21	2.14	**218.84**	5.83	2.67
100% of Water	N/A			**295.54**	4.56	1.54

Table A.5.3. Summary of DSC results for samples R1 – R13 (cont'd).

Sample Name	'CAPTEX 355 peak'			'WATER peak'		
	Solidification Peak [°C]					
	Average	*SD*	RSD	Average	SD	RSD
100% of Captex 355	**-44.81**	0.66	-1.48	N/A		
R1, 5% of water	**-46.37**	0.87	-1.88	Not detected		
R2, 11% of water	**-45.09**	0.58	-1.30	Not detected		
R3, 15% of water	**-45.08**	1.05	-2.33	Not detected		
R4, 20% of water	**-45.28**	0.61	-1.34	Not detected		
R5, 25% of water	**-44.23**	0.46	-1.05	**-35.28**	1.52	-4.32
R6, 30% of water	**-44.67**	0.58	-1.29	**-27.83**	1.83	-6.57
R7, 35% of water	**-43.86**	1.43	-3.25	**-20.74**	2.56	-12.35
R8, 40% of water	**-45.44**	0.08	-0.17	**-17.05**	1.63	-9.54
R9, 45% of water	**-45.39**	0.63	-1.38	**-20.62**	8.30	-40.26
R10, 50% of water	**-45.37**	0.10	-0.23	**-15.72**	1.29	-8.19
R11, 56% of water	**-44.89**	0.19	-0.43	**-12.26**	1.00	-8.19
R12, 65% of water	**-44.72**	0.17	-0.38	**-10.15**	1.32	-12.98
R13, 75% of water	**-44.23**	0.17	-0.39	**-9.29**	2.66	-28.67
100% of Water	N/A			**-13.67**	2.45	-17.91

Table A.5.4. Rheological properties of the samples R1-R13, viscosity results versus shear rate.

shear rate	R1 (1st set of samples)			R1 (2nd set of samples)			**R1 (average)**		
[s-1]	**Average**	**SD**	**RSD**	**Average**	**SD**	**RSD**	Average	SD	RSD
15.80	70.17	0.29	0.41	72.40	0.36	0.50	**71.28**	1.58	2.22
26.40	68.57	0.21	0.30	70.87	2.04	2.88	**69.72**	1.63	2.33
39.60	67.87	0.32	0.47	69.37	1.24	1.79	**68.62**	1.06	1.55
shear rate	R2 (1st set of samples)			R2 (2nd set of samples)			**R2 (average)**		
15.80	70.80	0.36	0.51	73.87	0.29	0.39	**72.33**	2.17	3.00
26.40	69.33	0.25	0.36	72.23	0.40	0.56	**70.78**	2.05	2.90
39.60	68.67	0.06	0.08	71.20	0.35	0.49	**69.93**	1.79	2.56
shear rate	R3 (1st set of samples)			R3 (2nd set of samples)			**R3 (average)**		
15.80	71.13	0.60	0.85	74.20	0.87	1.17	**72.67**	2.17	2.98
26.40	69.63	0.74	1.06	72.20	0.35	0.48	**70.92**	1.81	2.56
39.60	69.10	0.10	0.14	71.57	0.21	0.29	**70.33**	1.74	2.48
shear rate	R4 (1st set of samples)			R4 (2nd set of samples)			**R4 (average)**		
15.80	70.97	0.25	0.35	73.13	0.12	0.16	**72.05**	1.53	2.13
26.40	69.77	0.12	0.17	71.17	0.06	0.08	**70.47**	0.99	1.40
39.60	69.17	0.12	0.17	70.50	0.10	0.14	**69.83**	0.94	1.35
shear rate	R5 (1st set of samples)			R5 (2nd set of samples)			**R5 (average)**		
15.80	66.33	1.15	1.74	71.53	0.29	0.40	**68.93**	3.68	5.33
26.40	65.17	0.78	1.19	68.47	0.06	0.08	**66.82**	2.33	3.49
39.60	64.43	0.78	1.21	67.50	0.17	0.26	**65.97**	2.17	3.29
shear rate	R6 (1st set of samples)			R6 (2nd set of samples)			**R6 (average)**		
15.80	67.20	0.00	0.00	64.53	0.29	0.45	**65.87**	1.89	2.86
26.40	65.73	0.06	0.09	62.90	0.17	0.28	**64.32**	2.00	3.12
39.60	65.10	0.20	0.31	62.00	0.10	0.16	**63.55**	2.19	3.45
shear rate	R7 (1st set of samples)			R7 (2nd set of samples)			**R7 (average)**		
15.80	60.80	0.96	1.59	63.53	0.29	0.45	**62.17**	1.93	3.11
26.40	59.03	0.12	0.20	61.53	0.25	0.41	**60.28**	1.77	2.93
39.60	57.60	0.36	0.63	60.77	0.06	0.10	**59.18**	2.24	3.78
shear rate	R8 (1st set of samples)			R8 (2nd set of samples)			**R8 (average)**		
26.40	53.10	0.30	0.56	54.07	0.25	0.47	**53.58**	0.68	1.28
39.60	52.07	0.45	0.87	53.50	0.26	0.49	**52.78**	1.01	1.92
66.00	51.13	0.51	1.00	52.77	0.40	0.77	**51.95**	1.15	2.22

Table A.5.4. Rheological properties of the samples R1-R13, viscosity results versus shear rate (cont'd).

shear rate	R9 (1st set of samples)			R9 (2nd set of samples)			**R9 (average)**		
26.40	47.77	0.49	1.03	49.53	0.55	1.11	**48.65**	1.25	2.57
39.60	46.93	0.60	1.28	48.63	0.50	1.03	**47.78**	1.20	2.52
66.00	45.83	0.51	1.12	48.23	0.32	0.67	**47.03**	1.70	3.61
79.20	45.57	0.55	1.21	48.13	0.32	0.67	**46.85**	1.81	3.87
shear rate	R10 (1st set of samples)			R10 (2nd set of samples)			**R10 (average)**		
39.60	42.70	0.36	0.84	50.07	0.25	0.50	**46.38**	5.21	11.23
66.00	41.37	0.40	0.98	49.53	0.31	0.62	**45.45**	5.77	12.71
79.20	41.10	0.56	1.35	49.50	0.35	0.70	**45.30**	5.94	13.11
shear rate	R11 (1st set of samples)			R11 (2nd set of samples)			**R11 (average)**		
39.60	37.80	0.26	0.70	42.00	0.35	0.82	**39.90**	2.97	7.44
66.00	36.20	0.36	1.00	40.90	0.30	0.73	**38.55**	3.32	8.62
79.20	36.00	0.36	1.00	40.73	0.42	1.02	**38.37**	3.35	8.72
shear rate	R12 (1st set of samples)			R12 (2nd set of samples)			**R12 (average)**		
39.60	27.87	0.21	0.75	18.57	0.58	3.11	**23.22**	6.58	28.32
66.00	25.77	0.15	0.59	18.13	0.80	4.42	**21.95**	5.40	24.59
79.20	25.40	0.26	1.04	17.67	0.72	4.09	**21.53**	5.47	25.39
shear rate	R13 (1st set of samples)			R13 (2nd set of samples)			**R13 (average)**		
132.00	4.08	0.22	5.30	4.02	0.22	5.38	**4.05**	0.04	1.05

Table A.5.5. Parameters derived from the SANS measurements for samples R3-R7 & R9.

Sample ID	**Calculated volume fraction of water** (composition)	**Calculated volume fraction of water** (fitting)	**Scale factor (S_F) from FISH**	**Calculated Scale factor (S_F)**	Error/ %
R3	0.15	0.08	22	23	4.5
R4	0.20	0.12	59	62	5.1
R5	0.25	0.15	125	122	2.4
R6	0.30	0.20	236	237	0.4
R7	0.35	0.25	380	402	5.7
R9	0.45	0.37	899	939	4.4

Table A.5.6. Parameters derived from the DLS measurements for samples R3-R5 & R7 where the experimental phases were used.

Sample Name		**Viscosity [mPas]**	**Diffusion Coefficient = D_{or} [μ^2/s]**	**fraction of internal phase (water + surf) = Φ_{exp}**	**Corrected Diffusion Coefficient =D_{corr} [μ^2/s]**	**Hydrodynamic diameter = R [nm]**
R3	AVER	**52.5**	**1.59**	**0.2500**	**1.1415**	**15.9**
	SD	0.0	0.01	0.0000	0.0059	0.1
	RSD	0.0	0.51	0.0000	0.5146	0.5
R4	AVER	**41.5**	**1.67**	**0.3680**	**1.0588**	**21.0**
	SD	0.0	0.02	0.0000	0.0096	0.2
	RSD	0.0	0.90	0.0000	0.9033	0.9
R5	AVER	**36.4**	**1.88**	**0.5267**	**1.0293**	**24.2**
	SD	0.0	0.02	0.0000	0.0114	0.3
	RSD	0.0	1.11	0.0000	1.1059	1.1
R7	AVER	**32.0**	**2.25**	**0.6533**	**1.1160**	**25.0**
	SD	0.0	0.01	0.0000	0.0051	0.1
	RSD	0.0	0.46	0.0000	0.4583	0.5

Table A.5.7. Experimental distribution of the surfactants in the internal and external phase in samples R1 – R13.

Sample Name	Microemulsion composition wt%				wt% converted into mMol *			Assumed distribution in the microemulsion			
	Oil wt% (A)	Crillet 4HP wt% (B)	Capmul MCM C8 wt% (C)	Water wt% (D)	Crillet 4HP mMol (B)	Capmul MCM C8, mMol (C)	Water, Mmol (D)	**Crillet 4 HP, bound, mMol**	**Crillet 4HP non-bounded, mMol**	**Capmul MCM C8, bound, mMol**	**Capmul MCM C8, non-bounded, mMol**
R1	38	20.0	37.1	**5**	15.2	170.0	277.8	3.21	12.02	none assumed	170.0
R2	36	18.6	34.5	**11**	14.2	158.0	611.1	7.05	7.11		158.0
R3	34	17.9	33.2	**15**	13.6	152.1	833.3	9.62	4.01		152.1
R4	32	16.8	31.2	**20**	**12.8**	143.1	**1111.1**	**12.8**	none, all in the internal phase		143.1
R5	30	15.8	29.3	**25**	12.0	134.2	1388.9	12.0		54.66	79.51
R6	28	14.7	27.3	**30**	11.2	125.2	1666.7	11.2		65.60	59.63
R7	26	13.7	25.4	**35**	10.4	116.3	1944.4	10.4		76.53	39.76
R8	24	12.6	23.4	**40**	9.6	107.3	2222.2	9.6		87.46	19.88
R9	22	11.6	21.5	**45**	8.8	**98.4**	**2500.0**	8.8		**98.4**	0.00
R10	20	10.5	19.5	**50**	8.0	89.4	2777.8	8.0		89.4	none, all in the internal phase
R11	18	9.5	17.6	**56**	7.2	80.5	3111.1	7.2		80.5	
R12	14	7.4	13.7	**65**	5.6	62.6	3611.1	5.6		62.6	
R13	10	5.3	9.8	**75**	4.0	44.7	4166.7	4.0		44.7	

* Molecular weight of Polysorbate 80 = 1310 (Ke et al., 2005), molecular weight of Capmul MCM C8 (monoglyceride caprylate assumed) = 218

Table A.5.8. Experimental distribution of the surfactants in the external phase and measured physical properties of the external phase.

Sample Name	Estimation of external phase						Composition of the external phase wt%			Physical properties of external phase			
	Crillet 4HP non-bound, [mMol]	Crillet 4HP non-bound, [grams]	Oil, [grams]	Capmul MCM C8 non-bound, [mMol]	Capmul MCM C8 non-bound, [grams]	Total, [grams]	% of Crillet 4HP	% of Oil	% of Capmul MCM C8	Density, [g/cm^3]	Viscosity, [mPas]		
											Average	SD	RSD
R3	4.01	5.25	34	152.1	33.2	72.40	7.25	46.96	45.79	0.9966	52.5	0.55	1.05
R4	0	0	32	143.1	31.2	63.20	0.00	50.63	49.37	0.9952	41.5	0.15	0.37
R5	0	0	30	79.51	17.33	47.33	0.00	63.38	36.62	0.9950	36.4	1.72	4.71
R7	0	0	26	39.76	8.67	34.67	0.00	75.00	25.00	0.9949	32.0	0.36	1.13

Table A.5.9. Calculation of the fraction of internal phase (Φ), for the experimental external phases.

Distribution of the components in the internal * and external phase								Type of system
Sample Name	**% of Oil**	**% of Water**	**% of Capmul MCM C8 non-bound**	**% of Capmul MCM C8 bound**	**% of Crillet 4HP non-bound**	**% of Crillet 4HP bound**	**fraction of internal phase (core + bound surf) = Φ_{exp}**	
R3	34	15.0	33.2	0.0	5.25	12.60	0.2760	w/o
R4	32	20.0	31.2	0.0	0	16.8	0.3680	w/o
R5	30	25.0	17.3	11.9	0.0	15.8	0.5267	w/o
R7	26	35.0	8.7	16.7	0.0	13.7	0.6533	w/o

* internal phase contains the core component (e.g., water if the systems is a water-in-oil microemulsion) and the surfactants engaged in formation of the interphase surrounding droplets

Appendix to Chapter 6

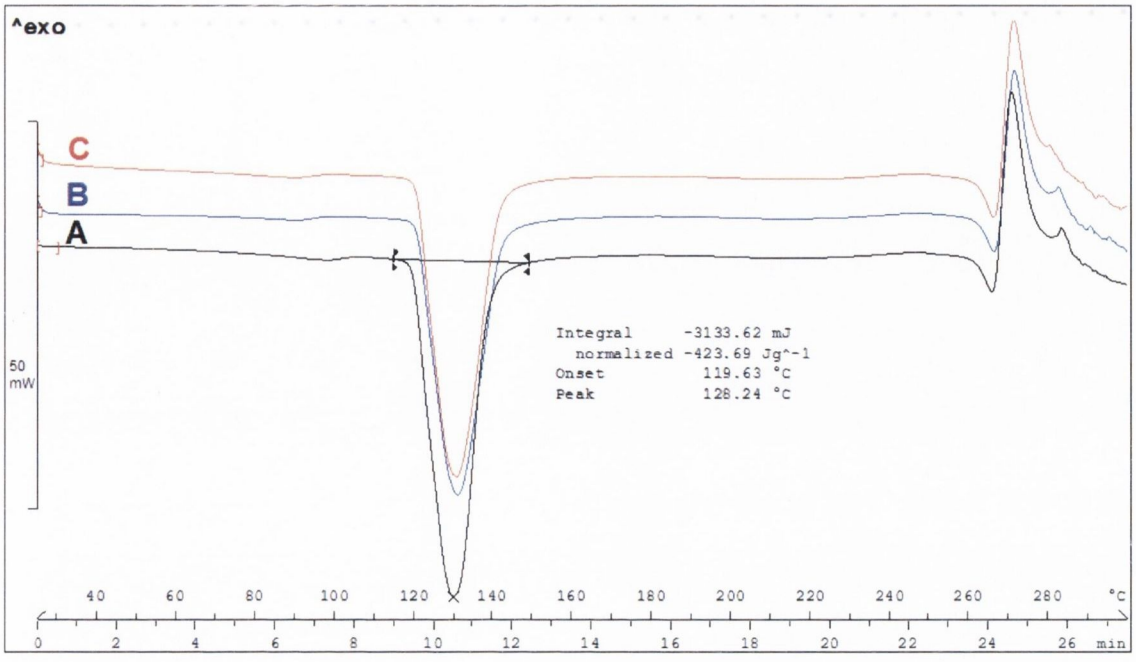

Fig. A.6.1. Comparison of DSC spectra between the original sodium alendronate trihydrate (A) and solid material recovered after incorporation study (48 hours) from 1A2_T3 formula (B) and 1B3_T4 formula (C).

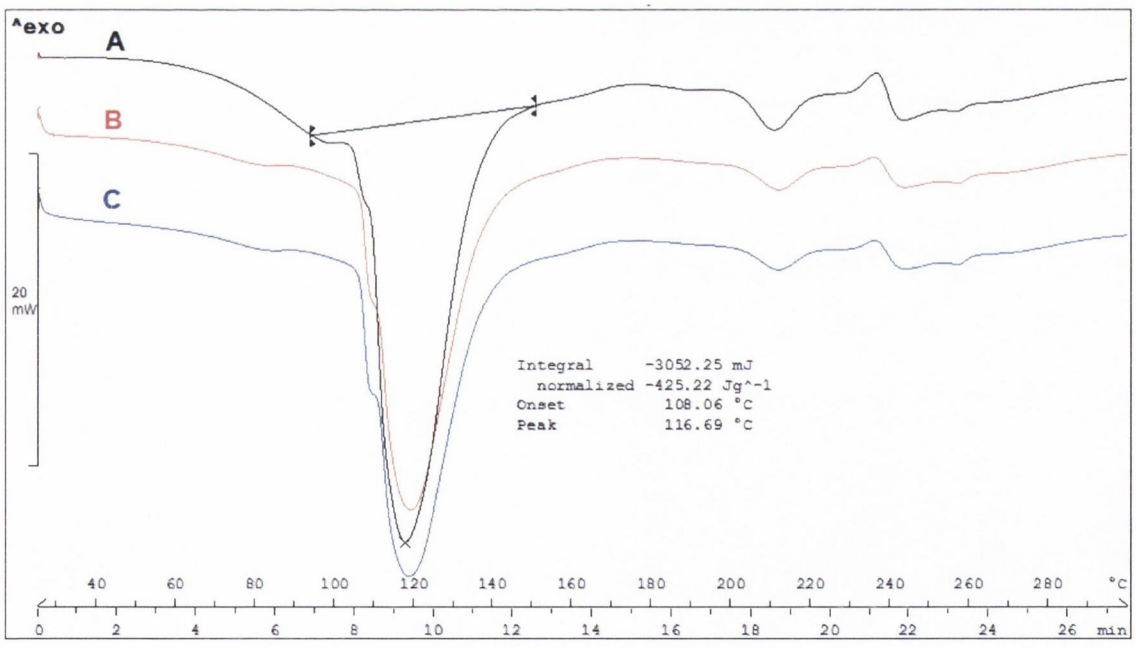

Fig. A.6.2. Comparison of DSC spectra between the original disodium pamidronate pentahydrate (A) (A) and solid material recovered after incorporation study (48 hours) from 1A2_T3 formula (B) and 1B3_T4 formula (C).

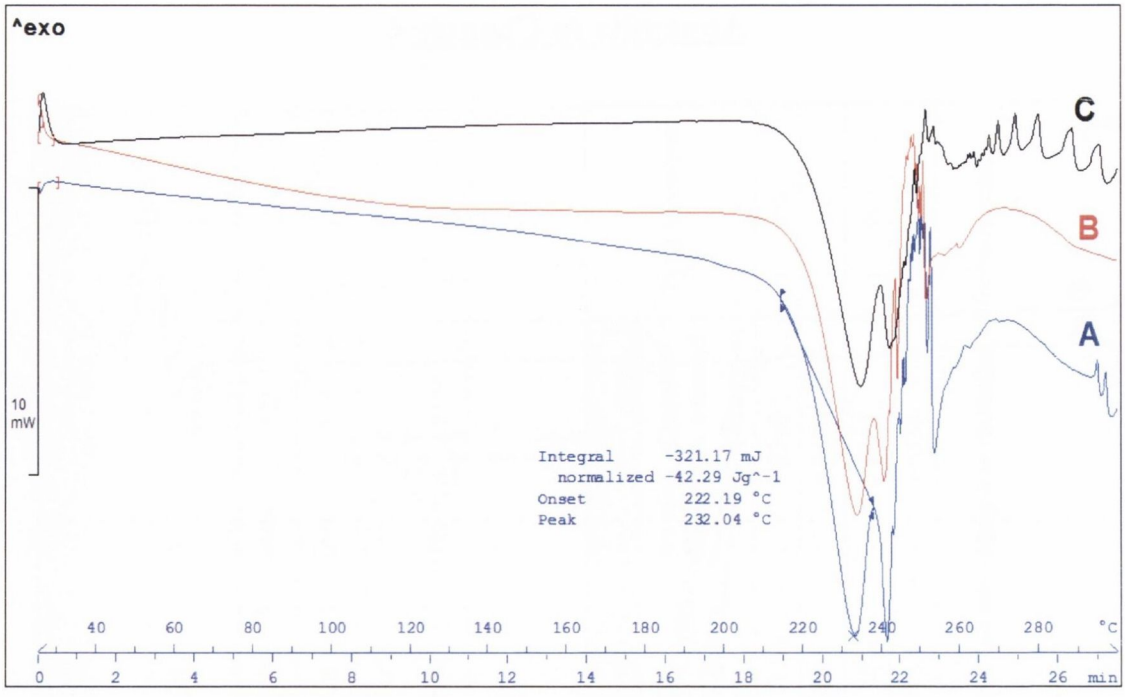

Fig. A.6.3. Comparison of DSC spectra between the original pamidronic acid (A) and the undissolved material recovered after 48 hours of solubility (exposure) in the standard non-aqueous GIPET ® II formula (B) and propylene glycol (C).

Table A.6.1.Acyline concentration (ng/ml) in serum samples after administration of the preclinical items.

Time points [h]	**Test Item 1, Unenhanced formulation - 5mg of Acyline in 5 ml of water**			**Test Item 2, 3A2_T2 (type IV) formulation - 5mg of acyline in 1g of SEDDS**			**Test Item 3, 1A2_T3 (type IV) formulation - 5mg of acyline in 1g of SEDDS**			**Test Item 4, 1B3_T4 (type IV) formulation - 5mg of acyline in 1g of SEDDS**		
	Mean	SD	RSD	**Mean**	SD	RSD	**Mean**	SD	RSD	**Mean**	SD	RSD
0	**0.00**	0.00	/	**0.00**	0.00	/	**0.00**	0.00	/	**0.00**	0.00	/
0.5	**10.24**	10.09	98.5	**89.15**	80.12	89.9	**334.26**	384.87	115.1	**417.35**	371.17	88.9
1	**9.59**	8.83	92.1	**84.81**	72.09	85	**332.37**	408.84	123	**302.96**	283.89	93.7
2	**7.46**	6.62	88.7	**44.32**	32.65	73.7	**175.79**	175.96	100.1	**222.59**	264.11	118.7
4	**5.54**	5.38	97.1	**31.53**	22.36	70.9	**42.75**	26.03	60.9	**156.26**	164.24	105.1
6	**4.91**	2.43	49.5	**26.44**	23.01	87	**69.19**	96.34	139.2	**82.41**	92.57	112.3
8	**4.72**	2.81	59.5	**16.67**	13.82	82.9	**32.88**	28.27	86	**78.98**	63.17	80
12	**2.24**	1.69	75.4	**10.36**	7.71	74.4	**23.76**	21.35	89.9	**28.92**	22.57	78
24	**1.07**	1.04	97.2	**1.97**	1.99	101	**5.29**	4.15	78.4	**6.72**	3.81	56.7
48	**0.26**	0.59	226.9	**0.22**	0.50	227.3	**0.81**	1.11	137	**0.98**	0.91	92.9

Table A.6.2. Pharmacokinetic parameters calculated from serum acyline concentration after administration of the preclinical items.

	Dog No 5048222	Dog No 5065046	Dog No 5063078	Dog No 5027110	Dog No 5008492	**AVER**	**SD**	**RSD**
Test Item 1, Unenhanced formulation - 5mg of Acyline in 5 ml of water								
AUC (0-48h) [ng/ml*h]	13.5	78.4	173.4	183.5	46.3	**99.0**	76.1	76.9
Log AUC (0-48h)	1.1303	1.8943	2.2390	2.2636	1.6656	**1.8386**	0.4679	25.4
AUC (0-inf) [ng/ml*h]	N/A	102.3	217.4	199.1	50.9	**142.4**	79.2	55.6
Cmax (0-48h) [ng/ml]	3.1	4.2	16.6	24.9	7.0	**11.2**	9.3	83.0
T1/2 (3 last time points) [h]	N/A	11.13	25.66	6.75	2.92	**11.62**	9.95	85.6
Tmax (0-48h) [h]	0.50	8.00	0.50	0.50	1.00	**2.10**	3.31	157.6
Elimination Rate Constant [ng/h]	N/A	0.06	0.03	0.10	0.24	**0.11**	0.09	81.8

Table A.6.2. Pharmacokinetic parameters calculated from serum acyline concentration after administration of the preclinical items (cont'd).

	Dog No 5048222	Dog No 5065046	Dog No 5063078	Dog No 5027110	Dog No 5008492	**AVER**	**SD**	**RSD**
Test Item 2, 3A2_T2 (type IV) formulation - 5mg of acyline in 1g of SEDDS								
AUC (0-48h) [ng/ml*h]	131.0	929.3	360.2	221.2	666.5	**461.6**	330.9	71.7
Log AUC (0-48h)	2.1173	2.9682	2.5565	2.3448	2.8238	**2.5621**	0.3459	13.5
AUC (0-inf) [ng/ml*h]	164.2	961.0	378.8	255.2	681.2	**488.1**	328.6	67.3
Cmax (0-48h) [ng/ml]	31.3	153.3	41.8	54.5	226.6	**101.5**	85.2	83.9
T1/2 (3 last time points) [h]	7.13	5.11	11.25	5.19	4.94	**6.72**	2.68	39.9
Tmax (0-48h) [h]	0.50	1.00	0.50	0.50	0.50	**0.60**	0.22	36.7
Elimination Rate Constant [ng/h]	0.10	0.14	0.06	0.13	0.14	**0.11**	0.03	27.3
Relative Bioavailability (Frel%)	970	1185	208	121	1440	**785**	591	75.3
Test Item 3, 1A2_T3 (type IV) formulation - 5mg of acyline in 1g of SEDDS								
AUC (0-48h) [ng/ml*h]	325.9	492.3	1497.2	741.1	4047.7	**1420.8**	1535.4	108.1
Log AUC (0-48h)	2.5131	2.6922	3.1753	2.8699	3.6072	**2.9715**	0.4313	14.5
AUC (0-inf) [ng/ml*h]	334.5	513.0	1523.5	770.3	4072.1	**1442.7**	1538.2	106.6
Cmax (0-48h) [ng/ml]	85.2	78.3	505.0	85.4	977.0	**346.2**	397.2	114.7
T1/2 (3 last time points) [h]	4.84	5.13	10.34	5.51	7.80	**6.72**	2.33	34.7
Tmax (0-48h) [h]	0.50	0.50	1.00	2.00	1.00	**1.00**	0.61	61.0
Elimination Rate Constant [ng/h]	0.14	0.14	0.07	0.13	0.09	**0.11**	0.03	27.3
Relative Bioavailability (Frel%)	2414	628	863	404	8742	**2610**	3517	134.8
Test Item 4, 1B3_T4 (type IV) formulation - 5mg of acyline in 1g of SEDDS								
AUC (0-48h) [ng/ml*h]	299.3	2595.7	858.5	999.3	4487.8	**1848.1**	1704.8	92.2
Log AUC (0-48h)	2.4761	3.4143	2.9337	2.9997	3.6520	**3.0952**	0.4556	14.7
AUC (0-inf) [ng/ml*h]	315.2	2611.5	885.0	1037.1	4508.8	**1871.5**	1702.5	91.0
Cmax (0-48h) [ng/ml]	56.2	566.7	298.1	293.3	988.5	**440.6**	355.6	80.7
T1/2 (3 last time points) [h]	5.57	7.34	11.06	5.16	7.49	**7.32**	2.33	31.8
Tmax (0-48h) [h]	1.00	0.50	0.50	1.00	0.50	**0.70**	0.27	38.6
Elimination Rate Constant [ng/h]	0.12	0.09	0.06	0.13	0.09	**0.10**	0.03	30.0
Relative Bioavailability (Frel%)	2217	3311	495	545	9693	**3252**	3791	116.6

Appendix to Chapter 7

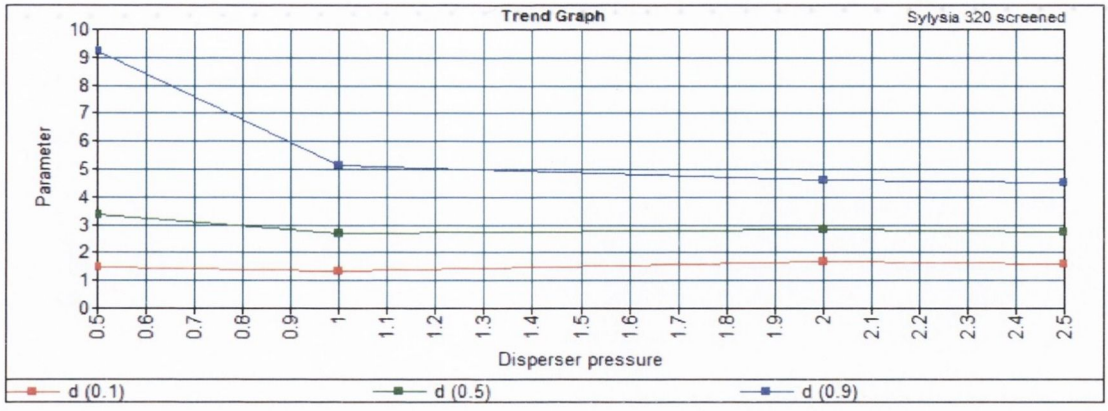

Fig. A.7.1. Pressure/particle size titration of Sylysia 320.

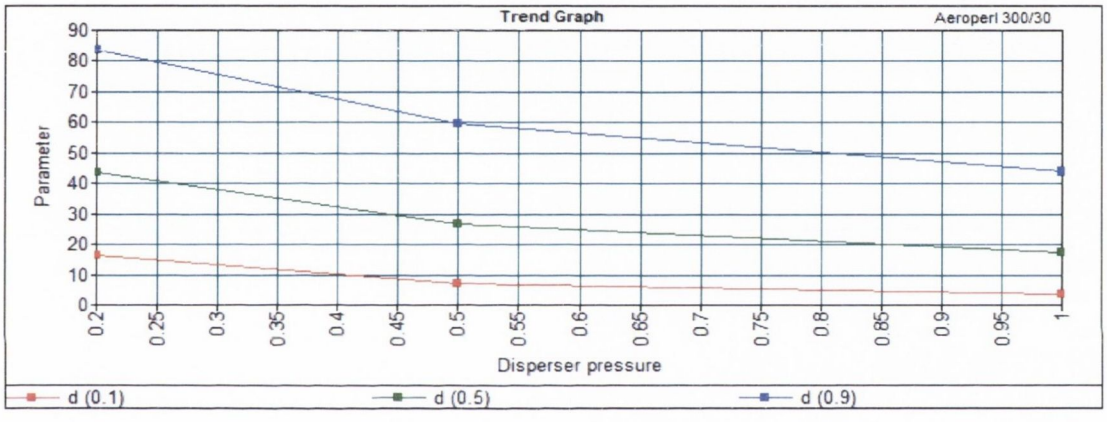

Fig. A.7.2. Pressure/particle size titration of Aeroperl 300/30

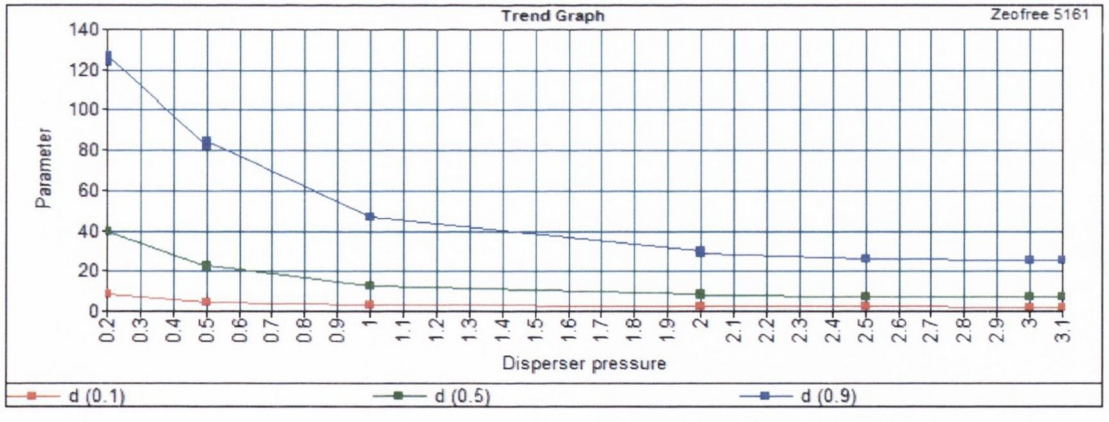

Fig. A.7.3. Pressure/particle size titration of Zeofree 5161.

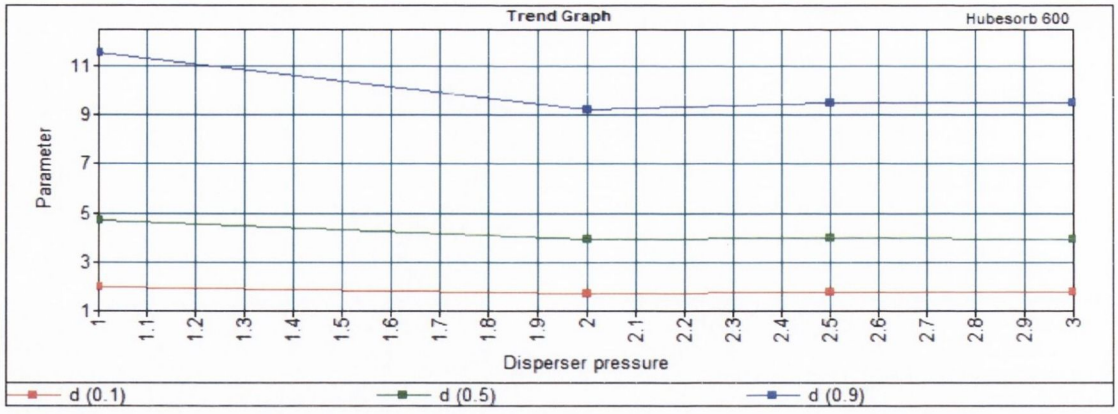

Fig. A.7.4. Pressure/particle size titration of Hubersorb 600.

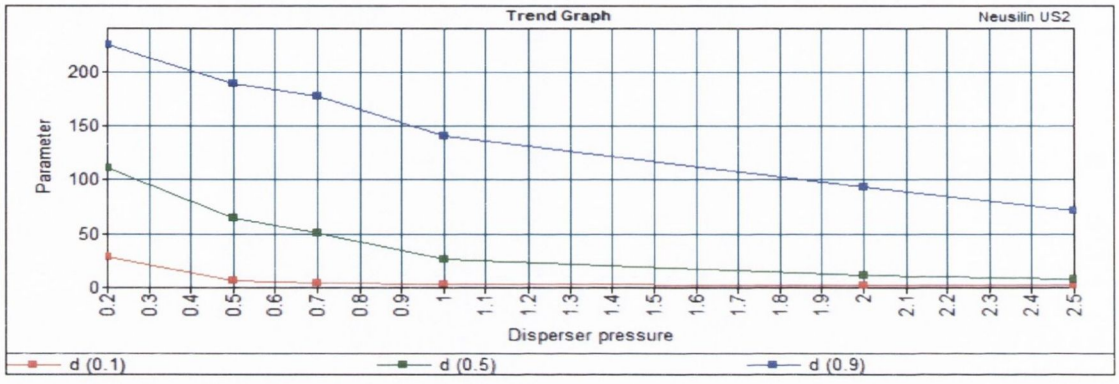

Fig. A.7.5. Pressure/particle size titration of Neusilin US2.

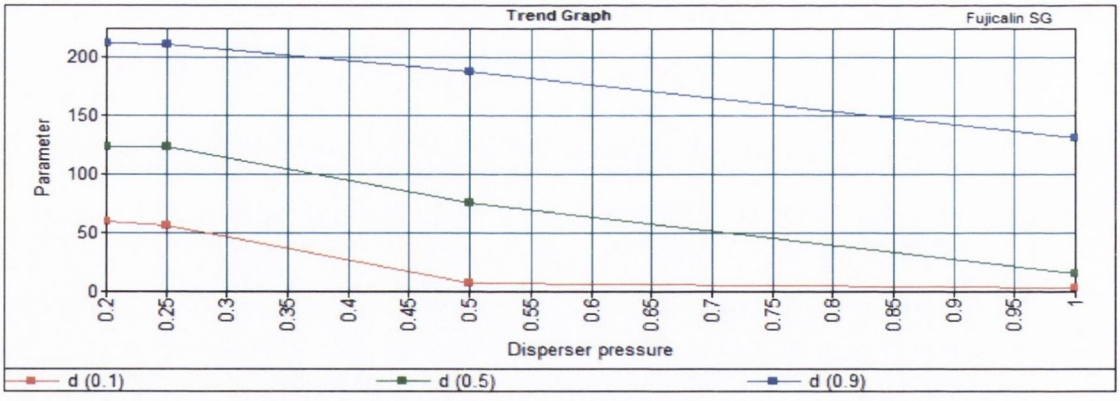

Fig. A.7.6. Pressure/particle size titration of Fujicalin SG.

Table A.7.1. True Density results.

Sample Name	True Density [g/cm3]		
	Average	SD	RSD
Sylysia 320	2.1441	0.0328	1.5
Aeroperl 300/30	2.1919	0.0045	0.2
Zeofree 5161	2.0285	0.0093	0.5
Hubersorb 600	1.8882	0.0223	1.2
Neusilin US2	2.1172	0.0078	0.4
Fujicalin SG	2.8156	0.0007	0.0

Appendix to Chapter 8

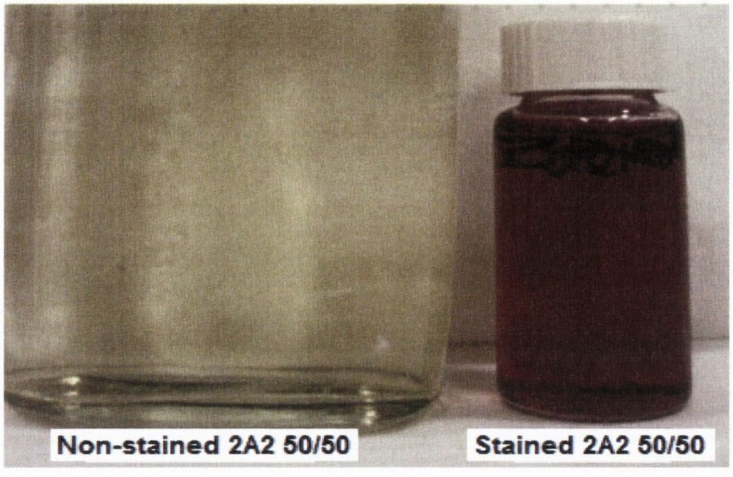

Fig. A.8.1. Non-stained and stained preconcentrate 2A2 50: 50.

Table A.8.1. Summary of BFE, SI and FRI results for raw and adsorbed solid carriers.

Sample Name / w/w%	%AL	Basic Flowability Energy (mJ) – Test 7					Stability Index			Flow Rate Index		
		Average	SD	RSD	Ratio BFE sample: BFE pure carrier	Ratio BFE sample (n): BFE sample (n-1)	Average	SD	RSD	Average	SD	RSD
Sylysia 320 : Preconcentrate/ 100:0	**0**	**11.0**	1.5	13.6	**1.0**	/	**1.08**	0.08	7.4	**1.99**	0.18	9.0
Sylysia 320 : Preconcentrate/ 60:40	**40**	**17.0**	1.7	10.0	**1.5**	**1.5**	**0.97**	0.20	20.6	**2.55**	0.06	2.4
Sylysia 320 : Preconcentrate/ 50:50	**50**	**20.9**	0.8	3.8	**1.9**	**1.2**	**1.25**	0.28	22.4	**2.82**	0.01	0.4
Sylysia 320 : Preconcentrate/ 40:60	**60**	**42.9**	5.5	12.8	**3.9**	**2.1**	**1.34**	0.02	1.5	**2.79**	0.08	2.9
Sylysia 320 : Preconcentrate/ 35:65	**65**	**51.7**	0.4	0.8	**4.7**	**1.2**	**1.10**	0.09	8.2	**1.94**	0.14	7.2
Sylysia 320 : Stained Preconcentrate/ 35:65	**65**	**58.9**	3.5	5.9	**5.4**	**1.1**	**1.01**	0.08	7.9	**1.94**	0.14	7.2
Sylysia 320 : Preconcentrate/ 30:70	**70**	**72.5**	4.1	5.7	**6.6**	**1.4**	**1.08**	0.16	14.8	**1.45**	0.21	14.5
Aeroperl 300/30: Preconcentrate/ 100:0	**0**	**14.2**	2.7	19.0	**1.0**	/	**0.84**	0.11	13.1	**1.66**	0.11	6.6
Aeroperl 300/30: Preconcentrate/ 60:40	**40**	**46.3**	5.3	11.4	**3.3**	**3.3**	**0.99**	0.03	3.0	**1.42**	0.08	5.6
Aeroperl 300/30: Preconcentrate/ 50:50	**50**	**70.1**	4.7	6.7	**4.9**	**1.5**	**0.99**	0.03	3.0	**1.32**	0.02	1.5
Aeroperl 300/30: Preconcentrate/ 40:60	**60**	**85.6**	4.2	4.9	**6.0**	**1.2**	**1.01**	0.01	1.0	**1.24**	0.01	0.8
Aeroperl 300/30: Stained Preconcentrate/ 40:60	**60**	**93.3**	0.5	0.5	**6.6**	**1.1**	**1.00**	0.03	3.0	**1.19**	0.02	1.7
Aeroperl 300/30: Preconcentrate/ 35:65	**65**	**69.2**	40.5	58.5	**4.9**	**0.8**	**0.77**	0.37	48.1	**1.26**	0.07	5.6
Aeroperl 300/30: Preconcentrate/ 30:70	**70**	**233.5**	29.0	12.4	**16.4**	**3.4**	**1.38**	0.21	15.2	**0.82**	0.07	8.5
Zeofree 5161: Preconcentrate/ 100:0	**0**	**17.1**	2.3	13.5	**1.0**	/	**1.22**	0.13	10.7	**2.66**	0.11	4.1
Zeofree 5161 : Preconcentrate/ 60:40	**40**	**42.1**	4.6	10.9	**2.5**	**2.5**	**1.05**	0.10	9.5	**2.07**	0.13	6.3
Zeofree 5161 : Preconcentrate/ 50:50	**51**	**53.9**	3.0	5.6	**3.2**	**1.3**	**1.06**	0.06	5.7	**1.91**	0.05	2.6
Zeofree 5161 : Preconcentrate/ 40:60	**60**	**75.9**	0.6	0.8	**4.4**	**1.4**	**1.04**	0.06	5.8	**1.64**	0.00	0.0
Zeofree 5161 : Preconcentrate/ 35:65	**65**	**89.5**	0.5	0.6	**5.2**	**1.2**	**1.03**	0.01	1.0	**1.54**	0.01	0.6
Zeofree 5161 : Stained Preconcentrate/ 35:65	**65**	**97.7**	0.6	0.6	**5.7**	**1.3**	**1.03**	0.01	1.0	**1.45**	0.04	2.8
Zeofree 5161 : Preconcentrate/ 30:70	**70**	**106.5**	6.4	6.0	**6.2**	**1.2**	**1.00**	0.01	1.0	**1.41**	0.05	3.5
Zeofree 5161 : Stained Preconcentrate/ 30:70	**70**	**107.0**	8.5	7.9	**6.3**	**1.2**	**1.06**	0.02	1.9	**1.36**	0.02	1.5
Zeofree 5161 : Preconcentrate/ 25:75	**76**	**431.5**	46.0	10.7	**25.2**	**4.1**	**1.30**	0.01	0.8	**1.19**	0.25	21.0

Table A.8.1. Summary of BFE, SI and FRI results for raw and adsorbed solid carriers (cont'd).

Sample Name / w/w%	%AL	Basic Flowability Energy (mJ) – Test 7					Stability Index			Flow Rate Index		
		Average	SD	RSD	Ratio BFE sample: BFE pure carrier	Ratio BFE sample (n): BFE sample (n-1)	Average	SD	RSD	Average	SD	RSD
Hubersorb 600: Preconcentrate/ 100:0	**0**	**9.6**	2.4	25.0	**1.0**	/	**0.86**	0.00	0.0	**2.08**	0.03	1.4
Hubersorb 600 : Preconcentrate/ 40:60	**61**	**33.3**	1.6	4.8	**3.5**	**3.5**	**1.11**	0.01	0.9	**1.79**	0.09	5.0
Hubersorb 600 : Stained Preconcentrate/ 40:60	**60**	**31.9**	0.1	0.3	**3.3**	**3.3**	**0.90**	0.20	22.2	**1.99**	0.14	7.0
Hubersorb 600 : Preconcentrate/ 30:70	**71**	**98.1**	0.0	0.0	**10.2**	**2.9**	**1.17**	0.01	0.9	**1.11**	0.17	15.3
Hubersorb 600 : Stained Preconcentrate/ 30:70	**70**	**97.3**	25.0	25.7	**10.1**	**2.9**	**1.05**	0.02	1.9	**1.25**	0.17	13.6
Hubersorb 600 : Preconcentrate/ 25:75	**75**	**837.9**	1179.6	140.8	**87.3**	**8.5**	**0.77**	1.07	139.0	**0.23**	0.31	134.8
Neusilin US2: Preconcentrate/ 100:0	**0**	**24.1**	**0.1**	0.4	**1.0**	/	**0.95**	0.03	3.2	**1.32**	0.02	1.5
Neusilin US2 : Preconcentrate/ 40:60	**60**	**89.9**	**0.7**	0.8	**3.7**	**3.7**	**1.02**	0.00	0.0	**1.15**	0.03	2.6
Neusilin US2 : Stained Preconcentrate/ 40:60	**60**	**89.1**	5.7	6.4	**3.7**	**3.7**	**1.02**	0.03	2.9	**1.13**	0.01	0.9
Neusilin US2 : Preconcentrate/ 30:70	**70**	**117.5**	0.7	0.6	**4.9**	**1.3**	**1.06**	0.01	0.9	**1.18**	0.00	0.0
Neusilin US2 : Stained Preconcentrate/ 30:70	**70**	**114.0**	2.8	2.5	**4.7**	**1.3**	**1.07**	0.03	2.8	**1.20**	0.01	0.8
Neusilin US2 : Preconcentrate/ 25:75	**75**	**107.1**	29.6	27.6	**4.4**	**0.9**	**0.95**	0.35	36.8	**0.89**	0.05	5.6
Fujicalin SG: Preconcentrate/ 100:0	**0**	**106.0**	1.4	1.3	**1.0**	/	**1.02**	0.03	2.9	**1.14**	0.03	2.6
Fujicalin SG: Preconcentrate/ 70:30	**30**	**199.0**	9.9	5.0	**1.9**	**1.9**	**0.97**	0.04	4.1	**1.15**	0.01	0.9
Fujicalin SG: Stained Preconcentrate/ 70:30	**31**	**194.0**	9.9	5.1	**1.8**	**1.8**	**1.02**	0.01	1.0	**1.12**	0.00	0.0
Fujicalin SG: Preconcentrate/ 60:40	**40**	**220.5**	4.9	2.2	**2.1**	**1.1**	**1.02**	0.02	2.0	**1.10**	0.01	0.9
Fujicalin SG: Stained Preconcentrate/ 60:40	**40**	**220.0**	0.0	0.0	**2.1**	**1.1**	**1.07**	0.02	1.9	**1.09**	0.02	1.8
Fujicalin SG: Preconcentrate/ 55:45	**45**	**147.0**	21.2	14.4	**1.4**	**0.7**	**1.24**	0.02	1.6	**0.89**	0.00	0.0

Table A.8.2 Summary of SE results for raw and adsorbed solid carriers

Sample Name / w/w%	%AL	Specific Energy (mJ/g)			Ratio SE sample: SE pure carrier	Ratio SE sample(n): SE sample(n-1)
		Average	SD	RSD		
Sylysia 320 : Preconcentrate/ 100:0	**0**	**5.58**	0.17	3.0	1.0	/
Sylysia 320 : Preconcentrate/ 60:40	**40**	**5.83**	0.06	1.0	1.0	1.0
Sylysia 320 : Preconcentrate/ 50:50	**50**	**5.93**	0.16	2.7	1.1	1.0
Sylysia 320 : Preconcentrate/ 40:60	**60**	**7.41**	0.45	6.1	1.3	1.2
Sylysia 320 : Preconcentrate/ 35:65	**65**	**6.30**	0.11	1.7	1.1	0.9
Sylysia 320 : Stained Preconcentrate/ 35:65	**65**	**6.11**	0.81	13.3	1.1	0.8
Sylysia 320 : Preconcentrate/ 30:70	**70**	**5.42**	0.07	1.3	1.0	0.9
Aeroperl 300/30: Preconcentrate/ 100:0	**0**	**2.14**	0.09	4.2	1.0	/
Aeroperl 300/30: Preconcentrate/ 60:40	**40**	**2.49**	0.02	0.8	1.2	1.2
Aeroperl 300/30: Preconcentrate/ 50:50	**50**	**2.73**	0.14	5.1	1.3	1.1
Aeroperl 300/30: Preconcentrate/ 40:60	**60**	**2.62**	0.18	6.9	1.2	1.0
Aeroperl 300/30: Stained Preconcentrate/ 40:60	**60**	**2.84**	0.12	4.2	1.3	1.0
Aeroperl 300/30: Preconcentrate/ 35:65	**65**	**4.11**	1.62	39.4	1.9	1.6
Aeroperl 300/30: Preconcentrate/ 30:70	**70**	**10.76**	1.19	11.1	5.0	2.6
Zeofree 5161: Preconcentrate/ 100:0	**0**	**4.69**	0.25	5.3	1.0	/
Zeofree 5161 : Preconcentrate/ 60:40	**40**	**5.05**	0.14	2.8	1.1	1.1
Zeofree 5161 : Preconcentrate/ 50:50	**51**	**4.88**	0.01	0.2	1.0	1.0
Zeofree 5161 : Preconcentrate/ 40:60	**60**	**4.60**	0.23	5	1.0	0.9
Zeofree 5161 : Preconcentrate/ 35:65	**65**	**4.67**	0.06	1.3	1.0	1.0
Zeofree 5161 : Stained Preconcentrate/ 35:65	**65**	**4.71**	0.13	2.8	1.0	1.0
Zeofree 5161 : Preconcentrate/ 30:70	**70**	**4.80**	0.11	2.3	1.0	1.0
Zeofree 5161 : Stained Preconcentrate/ 30:70	**70**	**4.81**	0.03	0.6	1.0	1.0
Zeofree 5161 : Preconcentrate/ 25:75	**76**	**11.9**	/	/	2.5	2.5
Hubersorb 600: Preconcentrate/ 100:0	**0**	**5.11**	0.64	12.5	1.0	/
Hubersorb 600 : Preconcentrate/ 40:60	**61**	**5.84**	0.28	4.8	1.1	1.1
Hubersorb 600 : Stained Preconcentrate/ 40:60	**60**	**5.58**	0.13	2.3	1.1	1.1
Hubersorb 600 : Preconcentrate/ 30:70	**71**	**8.41**	0.14	1.7	1.6	1.4
Hubersorb 600: Stained Preconcentrate/ 30:70	**70**	**8.03**	2.05	25.5	1.6	1.4
Hubersorb 600 : Preconcentrate/ 25:75	**75**	**14.78**	15.59	105.5	2.9	1.8
Neusilin US2: Preconcentrate/ 100:0	**0**	**2.39**	0.16	6.7	**1.0**	/
Neusilin US2 : Preconcentrate/ 40:60	**60**	**3.54**	0.01	0.3	**1.5**	**1.5**
Neusilin US2 : Stained Preconcentrate/ 40:60	**60**	**3.72**	0.35	9.4	**1.6**	**1.6**
Neusilin US2 : Preconcentrate/ 30:70	**70**	**4.06**	0.12	3.0	**1.7**	**1.1**
Neusilin US2 : Stained Preconcentrate/ 30:70	**70**	**4.04**	0.07	1.7	**1.7**	**1.1**
Neusilin US2 : Preconcentrate/ 25:75	**75**	**6.64**	2.24	33.7	**2.8**	**1.6**
Fujicalin SG: Preconcentrate/ 100:0	**0**	**3.52**	0.11	3.1	**1.0**	/
Fujicalin SG: Preconcentrate/ 70:30	**30**	**4.38**	0.23	5.3	**1.2**	**1.2**
Fujicalin SG: Stained Preconcentrate/ 70:30	**31**	**4.34**	0.16	3.7	**1.2**	**1.2**
Fujicalin SG: Preconcentrate/ 60:40	**40**	**4.34**	0.15	3.5	**1.2**	**1.0**
Fujicalin SG: Stained Preconcentrate/ 60:40	**40**	**4.46**	0.13	2.9	**1.3**	**1.0**
Fujicalin SG: Preconcentrate/ 55:45	**45**	**5.99**	0.16	2.7	**1.7**	**1.4**

Table A.8.3 Summary of CBD results for raw and adsorbed solid carriers.

Sample Name/ w/w%	%AL	Conditioned Bulk Density (g/ml)		
		Average	SD	RSD
Sylysia 320 : Preconcentrate/ 100:0	0	0.067	0.005	7.5
Sylysia 320 : Preconcentrate/ 60:40	40	0.142	0.004	2.8
Sylysia 320 : Preconcentrate/ 50:50	50	0.181	0.005	2.8
Sylysia 320 : Preconcentrate/ 40:60	60	0.239	0.008	3.3
Sylysia 320 : Preconcentrate/ 35:65	65	0.238	0.007	2.9
Sylysia 320 : Stained Preconcentrate/ 35:65	65	0.254	0.030	11.8
Sylysia 320 : Preconcentrate/ 30:70	70	0.320	0.012	3.8
Aeroperl 300/30: Preconcentrate/ 100:0	0	0.244	0.001	0.4
Aeroperl 300/30: Preconcentrate/ 60:40	40	0.419	0.003	0.7
Aeroperl 300/30: Preconcentrate/ 50:50	50	0.528	0.010	1.9
Aeroperl 300/30: Preconcentrate/ 40:60	60	0.700	0.114	16.3
Aeroperl 300/30: Stained Preconcentrate/ 40:60	60	0.684	0.044	6.4
Aeroperl 300/30: Preconcentrate/ 35:65	65	0.402	0.057	14.2
Aeroperl 300/30: Preconcentrate/ 30:70	70	0.354	0.014	4.0
Zeofree 5161: Preconcentrate/ 100:0	0	0.161	0.001	0.6
Zeofree 5161 : Preconcentrate/ 60:40	40	0.259	0.004	1.5
Zeofree 5161 : Preconcentrate/ 50:50	51	0.321	0.002	0.6
Zeofree 5161 : Preconcentrate/ 40:60	60	0.405	0.015	3.7
Zeofree 5161 : Preconcentrate/ 35:65	65	0.446	0.002	0.4
Zeofree 5161 : Stained Preconcentrate/ 35:65	65	0.456	0.000	0.0
Zeofree 5161 : Preconcentrate/ 30:70	70	0.460	0.009	2.0
Zeofree 5161 : Stained Preconcentrate/ 30:70	70	0.460	0.006	1.3
Zeofree 5161 : Preconcentrate/ 25:75	76	0.415	0.040	9.6
Hubersorb 600: Preconcentrate/ 100:0	0	0.093	0.004	4.3
Hubersorb 600 : Preconcentrate/ 30:60	61	0.201	0.019	9.5
Hubersorb 600 : Stained Preconcentrate/ 30:60	60	0.232	0.001	0.4
Hubersorb 600 : Preconcentrate/ 30:70	71	0.262	0.005	1.9
Hubersorb 600 : Stained Preconcentrate/ 30:70	70	0.255	0.032	12.5
Hubersorb 600 : Preconcentrate/ 25:75	75	0.414	0.037	8.9
Neusilin US2: Preconcentrate/ 100:0	0	0.182	0.001	0.5
Neusilin US2 : Preconcentrate/ 30:60	60	0.423	0.001	0.2
Neusilin US2 : Stained Preconcentrate/ 30:60	60	0.422	0.001	0.2
Neusilin US2 : Preconcentrate/ 30:70	70	0.527	0.003	0.6
Neusilin US2 : Stained Preconcentrate/ 30:70	70	0.522	0.009	1.7
Neusilin US2 : Preconcentrate/ 25:75	75	0.329	0.023	7.0
Fujicalin SG: Preconcentrate/ 100:0	0	0.476	0.004	0.8
Fujicalin SG: Preconcentrate/ 70:30	30	0.651	0.003	0.5
Fujicalin SG: Stained Preconcentrate/ 70:30	31	0.661	0.008	1.2
Fujicalin SG: Preconcentrate/ 60:40	40	0.733	0.009	1.2
Fujicalin SG: Stained Preconcentrate/ 60:40	40	0.732	0.011	1.5
Fujicalin SG: Preconcentrate/ 55:45	45	0.507	0.035	6.9

Table A.8.4 Summary of Shear Stress measurements for raw and adsorbed solid carriers.

Sample Name / w/w%	Actual Normal Stress (kPa)			Actual Pro-Rated Shear Stress (kPa)		
	Average	SD	RSD	Average	SD	RSD
Sylysia 320 : Preconcentrate / 100:0, %AL= 0%	**7.71**	0.25	3.20	**6.72**	1.01	15.00
	7.00	0.34	4.90	**5.97**	0.57	9.50
	5.32	0.02	0.40	**4.84**	1.23	25.40
	4.23	0.17	4.00	**4.00**	1.31	32.80
	3.27	0.01	0.30	**3.26**	1.21	37.10
Sylysia 320 : Preconcentrate / 60:40, %AL= 40%	**7.93**	0.05	0.60	**6.36**	0.16	2.50
	6.71	0.45	6.70	**5.60**	0.39	7.00
	5.43	0.15	2.80	**4.55**	0.31	6.80
	4.52	0.15	3.30	**3.88**	0.06	1.50
	3.23	0.05	1.50	**2.88**	0.01	0.30
Sylysia 320 : Preconcentrate / 50:50, %AL= 50%	**8.02**	0.00	0.00	**6.43**	0.14	2.20
	6.62	0.51	7.70	**5.57**	0.25	4.50
	5.47	0.16	2.90	**4.79**	0.13	2.70
	4.54	0.12	2.60	**4.01**	0.06	1.50
	3.53	0.09	2.50	**3.24**	0.08	2.50
Sylysia 320 : Preconcentrate / 40:60, %AL= 60%	**8.27**	0.26	3.10	**6.91**	0.25	3.60
	6.88	0.42	6.10	**6.05**	0.36	6.00
	5.64	0.23	4.10	**5.26**	0.22	4.20
	4.62	0.30	6.50	**4.48**	0.18	4.00
	3.75	0.04	1.10	**3.84**	0.08	2.10
Sylysia 320 : Preconcentrate / 35:65, %AL= 65%	**8.39**	0.02	0.20	**6.94**	0.02	0.30
	6.53	0.21	3.20	**6.03**	0.09	1.50
	5.57	0.04	0.70	**5.36**	0.08	1.50
	4.56	0.01	0.20	**4.63**	0.04	0.90
	3.44	0.02	0.60	**3.71**	0.10	2.70
Stained Sylysia 320 : Preconcentrate / 35:65, %AL= 65%	**8.16**	0.03	0.40	**6.99**	0.09	1.30
	7.16	0.06	0.80	**6.43**	0.11	1.70
	5.61	0.15	2.70	**5.42**	0.04	0.70
	4.52	0.04	0.90	**4.62**	0.10	2.20
	3.54	0.01	0.30	**3.77**	0.18	4.80
Sylysia 320 : Preconcentrate / 30:70, %AL= 70%	**8.41**	0.01	0.10	**6.97**	0.11	1.60
	6.55	0.01	0.20	**5.99**	0.13	2.20
	5.57	0.03	0.50	**5.40**	0.07	1.30
	4.41	0.05	1.10	**4.54**	0.12	2.60
	3.35	0.09	2.70	**3.79**	0.09	2.40
Sylysia 320 : Preconcentrate / 25:75, %AL= 75%	**8.62**	0.27	3.10	**8.65**	0.08	0.90
	8.07	0.07	0.90	**8.44**	0.24	2.80
	5.41	0.00	0.00	**7.10**	0.23	3.20
	4.38	0.02	0.50	**6.37**	0.16	2.50
	3.35	0.01	0.30	**5.38**	0.32	5.90
Aeroperl 300/30: Preconcentrate / 100:0, %AL= 0%	**7.60**	0.12	1.60	**3.25**	0.39	12.00
	6.29	0.26	4.10	**2.58**	0.02	0.80
	5.00	0.21	4.20	**2.00**	0.09	4.50
	3.94	0.04	1.00	**1.63**	0.18	11.00
	3.01	0.16	5.30	**1.64**	0.67	40.90
Aeroperl 300/30: Preconcentrate / 60:40, %AL= 40%	**7.93**	0.12	1.50	**3.35**	0.13	3.90
	6.63	0.01	0.20	**2.74**	0.00	0.00
	5.14	0.03	0.60	**2.09**	0.05	2.40
	4.17	0.00	0.00	**1.61**	0.01	0.60
	3.13	0.01	0.30	**1.23**	0.02	1.60
Aeroperl 300/30: Preconcentrate / 50:50, %AL= 50%	**7.81**	0.14	1.80	**3.26**	0.09	2.80
	6.71	0.03	0.40	**2.83**	0.01	0.40
	5.12	0.11	2.10	**2.06**	0.08	3.90
	4.20	0.06	1.40	**1.65**	0.03	1.80
	3.16	0.08	2.50	**1.23**	0.04	3.30

Table A.8.4. Summary of Shear Stress measurements for raw and adsorbed solid carriers (cont'd).

Sample Name / w/w%	Actual Normal Stress (kPa)			Actual Pro-Rated Shear Stress (kPa)		
	Average	SD	RSD	Average	SD	RSD
Aeroperl 300/30: Preconcentrate / 40:60, %AL= 60%	**7.91**	0.16	2.00	**3.37**	0.15	4.50
	6.88	0.14	2.00	**2.94**	0.11	3.70
	5.25	0.05	1.00	**2.15**	0.04	1.90
	4.20	0.04	1.00	**1.75**	0.06	3.40
	3.19	0.02	0.60	**1.33**	0.09	6.80
Stained Aeroperl 300/30: Preconcentrate / 40:60, %AL= 60%	**7.91**	0.14	1.80	**3.69**	0.62	16.80
	6.69	0.01	0.10	**3.08**	0.49	15.90
	5.20	0.07	1.30	**2.26**	0.40	17.70
	4.51	0.37	8.20	**2.09**	0.78	37.30
	3.43	0.52	15.20	**1.69**	0.78	46.20
Aeroperl 300/30: Preconcentrate / 35:65, %AL= 65%	**7.98**	0.07	0.90	**5.03**	0.16	3.20
	6.78	0.50	7.40	**4.49**	0.42	9.40
	5.59	0.12	2.10	**3.92**	0.04	1.00
	4.57	0.07	1.50	**3.37**	0.17	5.00
	3.54	0.01	0.30	**2.85**	0.11	3.90
Aeroperl 300/30: Preconcentrate / 30:70, %AL= 70%	**8.22**	0.00	0.00	**7.32**	0.04	0.50
	7.33	0.01	0.10	**6.82**	0.02	0.30
	5.71	0.02	0.40	**5.89**	0.01	0.20
	4.71	0.06	1.30	**5.22**	0.08	1.50
	3.69	0.03	0.80	**4.49**	0.01	0.20
Zeofree 5161: Preconcentrate / 100:0, %AL= 0%	**8.27**	0.03	0.40	**5.04**	0.17	3.40
	7.32	0.14	1.90	**4.35**	0.04	0.90
	5.25	0.02	0.40	**3.14**	0.17	5.40
	4.22	0.01	0.20	**2.59**	0.18	6.90
	3.19	0.01	0.30	**2.06**	0.11	5.30
Zeofree 5161 : Preconcentrate / 60:40, %AL= 40%	**8.30**	0.04	0.50	**4.99**	0.08	1.60
	7.29	0.05	0.70	**4.30**	0.04	0.90
	5.29	0.05	0.90	**3.13**	0.07	2.20
	4.22	0.02	0.50	**2.59**	0.07	2.70
	3.21	0.03	0.90	**2.05**	0.04	2.00
Zeofree 5161 : Preconcentrate / 50:50, %AL= 51%	**8.31**	0.03	0.40	**4.91**	0.00	0.00
	7.30	0.03	0.40	**4.24**	0.04	0.90
	5.25	0.04	0.80	**3.11**	0.02	0.60
	4.26	0.00	0.00	**2.61**	0.02	0.80
	3.22	0.02	0.60	**2.08**	0.01	0.50
Zeofree 5161 : Preconcentrate / 40:60, %AL= 60%	**8.37**	0.01	0.10	**5.17**	0.23	4.40
	7.30	0.02	0.30	**4.39**	0.21	4.80
	5.44	0.23	4.20	**3.36**	0.01	0.30
	4.24	0.02	0.50	**2.77**	0.11	4.00
	3.22	0.07	2.20	**2.25**	0.18	8.00
Zeofree 5161 : Preconcentrate / 35:65, %AL= 65%	**8.26**	0.08	1.00	**5.20**	0.39	7.50
	6.72	0.64	9.50	**4.30**	0.13	3.00
	5.32	0.02	0.40	**3.48**	0.38	10.90
	4.29	0.04	0.90	**3.02**	0.47	15.60
	3.22	0.05	1.60	**2.40**	0.37	15.40
Stained Zeofree 5161 : Preconcentrate / 35:65, %AL= 65%	**8.34**	0.01	0.10	**5.13**	0.04	0.80
	7.30	0.04	0.50	**4.43**	0.08	1.80
	5.30	0.00	0.00	**3.35**	0.09	2.70
	4.25	0.01	0.20	**2.82**	0.08	2.80
	3.21	0.01	0.30	**2.20**	0.04	1.80
Zeofree 5161 : Preconcentrate / 30:70, %AL= 70%	**8.34**	0.11	1.30	**5.36**	0.12	2.20
	6.43	0.05	0.80	**4.34**	0.01	0.20
	5.32	0.02	0.40	**3.68**	0.01	0.30
	4.32	0.03	0.70	**3.15**	0.04	1.30
	3.28	0.01	0.30	**2.47**	0.01	0.40

Table A.8.4. Summary of Shear Stress measurements for raw and adsorbed solid carriers (cont'd).

Sample Name / w/w%	Actual Normal Stress (kPa)			Actual Pro-Rated Shear Stress (kPa)		
	Average	SD	RSD	Average	SD	RSD
Stained Zeofree 5161 : Preconcentrate / 30:70, %AL= 70%	**8.34**	0.01	0.10	**5.38**	0.11	2.00
	7.17	0.00	0.00	**4.59**	0.06	1.30
	5.32	0.06	1.10	**3.75**	0.11	2.90
	4.28	0.01	0.20	**3.15**	0.08	2.50
	3.26	0.00	0.00	**2.58**	0.04	1.60
Zeofree 5161 : Preconcentrate / 25:75, %AL= 75%	**8.21**	0.11	1.30	**8.77**	0.30	3.40
	7.74	0.06	0.80	**8.48**	0.62	7.30
	5.35	0.06	1.10	**7.08**	0.58	8.20
	4.33	0.02	0.50	**6.40**	0.68	10.60
	3.31	0.01	0.30	**5.71**	0.82	14.40
Hubersorb 600: Preconcentrate / 100:0, %AL= 0%	**8.28**	0.04	0.50	**5.15**	0.11	2.10
	7.09	0.21	3.00	**4.46**	0.42	9.40
	5.00	0.09	1.80	**3.55**	0.08	2.30
	4.19	0.06	1.40	**3.04**	0.08	2.60
	3.13	0.06	1.90	**2.42**	0.07	2.90
Hubersorb 600 : Preconcentrate / 30:60, %AL= 61%	**8.25**	0.05	0.60	**6.50**	0.18	2.80
	6.90	0.11	1.60	**5.83**	0.06	1.00
	5.07	0.14	2.80	**4.76**	0.28	5.90
	4.02	0.06	1.50	**4.00**	0.18	4.50
	3.29	0.45	13.70	**3.32**	0.28	8.40
Stained Hubersorb 600 : Preconcentrate / 30:60, %AL= 60%	**8.29**	0.03	0.40	**6.31**	0.19	3.00
	7.25	0.14	1.90	**5.88**	0.18	3.10
	5.04	0.36	7.10	**4.55**	0.25	5.50
	4.11	0.04	1.00	**3.92**	0.16	4.10
	3.10	0.09	2.90	**3.03**	0.06	2.00
Hubersorb 600 : Preconcentrate / 30:70, %AL= 71%	**8.47**	0.09	1.10	**8.62**	0.29	3.40
	7.13	0.77	10.80	**8.02**	0.64	8.00
	5.61	0.06	1.10	**7.14**	0.35	4.90
	4.59	0.11	2.40	**6.38**	0.25	3.90
	3.56	0.18	5.10	**5.65**	0.19	3.40
Stained Hubersorb 600 : Preconcentrate / 30:70, %AL= 70%	**8.36**	0.01	0.10	**8.30**	0.08	1.00
	7.37	0.10	1.40	**7.81**	0.01	0.10
	5.66	0.01	0.20	**6.64**	0.00	0.00
	4.80	0.09	1.90	**6.09**	0.04	0.70
	3.72	0.01	0.30	**5.10**	0.06	1.20
Hubersorb 600 : Preconcentrate/ 25:75, %AL= 75%	**6.99**	0.19	2.70	**10.40**	1.56	15.00
	7.25	0.45	6.20	**9.77**	1.04	10.60
	5.38	0.35	6.50	**8.93**	1.29	14.40
	4.47	0.04	0.90	**8.63**	0.59	6.80
	3.96	0.83	21.00	**7.74**	1.51	19.50
Neusilin US2: Preconcentrate / 100:0, %AL= 0%	**8.49**	0.08	0.90	**4.17**	0.05	1.20
	7.06	0.03	0.40	**3.21**	0.16	5.00
	5.07	0.05	1.00	**2.12**	0.04	1.90
	4.32	0.06	1.40	**1.72**	0.03	1.70
	3.38	0.04	1.20	**1.31**	0.04	3.10
Neusilin US2 : Preconcentrate / 30:60, %AL= 60%	**8.50**	0.01	0.10	**4.48**	0.06	1.30
	7.34	0.08	1.10	**3.77**	0.06	1.60
	5.38	0.02	0.40	**2.56**	0.09	3.50
	4.36	0.16	3.70	**2.06**	0.00	0.00
	3.38	0.16	4.70	**1.64**	0.04	2.40
Stained Neusilin US2 : Preconcentrate / 30:60, %AL= 60%	**8.48**	0.01	0.10	**4.49**	0.10	2.20
	7.39	0.04	0.50	**3.87**	0.04	1.00
	5.31	0.03	0.60	**2.57**	0.03	1.20
	4.56	0.08	1.80	**2.19**	0.01	0.50
	3.59	0.00	0.00	**1.74**	0.03	1.70

Table A.8.4. Summary of Shear Stress measurements for raw and adsorbed solid carriers (cont'd).

Sample Name / w/w%	Actual Normal Stress (kPa)			Actual Pro-Rated Shear Stress (kPa)		
	Average	SD	RSD	Average	SD	RSD
Neusilin US2 : Preconcentrate / 30:70, %AL= 70%	**8.42**	0.01	0.10	**4.77**	0.06	1.30
	7.48	0.01	0.10	**4.15**	0.13	3.10
	5.35	0.02	0.40	**2.93**	0.16	5.50
	4.40	0.16	3.60	**2.45**	0.16	6.50
	3.43	0.18	5.20	**2.02**	0.10	5.00
Stained Neusilin US2 : Preconcentrate / 30:70, %AL= 70%	**8.35**	0.06	0.70	**4.73**	0.01	0.20
	7.44	0.05	0.70	**4.11**	0.02	0.50
	5.46	0.06	1.10	**3.02**	0.01	0.30
	4.58	0.04	0.90	**2.51**	0.01	0.40
	3.64	0.02	0.50	**2.09**	0.05	2.40
Neusilin US2 : Preconcentrate / 25:75, %AL= 75%	**8.48**	0.08	0.90	**6.24**	0.12	1.90
	7.80	0.01	0.10	**5.76**	0.07	1.20
	5.52	0.05	0.90	**4.64**	0.11	2.40
	4.54	0.03	0.70	**4.02**	0.07	1.70
	3.64	0.01	0.30	**3.48**	0.10	2.90
Fujicalin SG: Preconcentrate / 100:0, %AL= 0%	**8.94**	0.06	0.70	**4.57**	0.08	1.80
	7.50	0.11	1.50	**3.94**	0.12	3.00
	5.12	0.01	0.20	**2.42**	0.06	2.50
	4.14	0.04	1.00	**1.96**	0.11	5.60
	3.24	0.23	7.10	**1.49**	0.04	2.70
Fujicalin SG: Preconcentrate / 70:30, %AL= 30%	**8.62**	0.02	0.20	**4.49**	0.40	8.90
	7.47	0.03	0.40	**4.07**	0.44	10.80
	5.38	0.08	1.50	**2.77**	0.20	7.20
	4.56	0.04	0.90	**2.43**	0.09	3.70
	3.63	0.00	0.00	**1.95**	0.10	5.10
Stained Fujicalin SG: Preconcentrate / 70:30, %AL= 31%	**8.49**	0.05	0.60	**4.57**	0.05	1.10
	7.45	0.02	0.30	**3.98**	0.23	5.80
	5.39	0.06	1.10	**2.73**	0.13	4.80
	4.52	0.09	2.00	**2.34**	0.16	6.80
	3.56	0.04	1.10	**1.95**	0.14	7.20
Fujicalin SG: Preconcentrate / 60:40, %AL= 40%	**8.51**	0.14	1.60	**4.64**	0.02	0.40
	7.51	0.05	0.70	**4.16**	0.03	0.70
	5.39	0.01	0.20	**2.97**	0.06	2.00
	4.61	0.06	1.30	**2.58**	0.00	0.00
	3.72	0.04	1.10	**2.14**	0.06	2.80
Stained Fujicalin SG: Preconcentrate / 60:40, %AL= 40%	**8.44**	0.04	0.50	**4.75**	0.08	1.70
	7.57	0.02	0.30	**4.30**	0.10	2.30
	5.35	0.01	0.20	**3.12**	0.01	0.30
	4.49	0.09	2.00	**2.66**	0.08	3.00
	3.55	0.01	0.30	**2.16**	0.07	3.20
Fujicalin SG: Preconcentrate / 55:45, %AL= 45%	**8.26**	0.05	0.60	**5.58**	0.08	1.40
	7.58	0.03	0.40	**5.23**	0.03	0.60
	5.57	0.13	2.30	**4.24**	0.03	0.70
	4.73	0.06	1.30	**3.81**	0.02	0.50
	3.74	0.01	0.30	**3.24**	0.06	1.90

Table A.8.5. Particle size calibration curves for diluted preconcentrate 2A2 50:50 in blank FaSSIF-V2.

Calibration Curve 1 of Preconcentrate 2A2 50: 50 in blank FaSSIF-V2								
Sample Name	Concentration of Preconcentrate [mg/ml]	% of the Initial sample	Particle Size [nm]			Polydispersity Index		
			Average	SD	RSD%	Average	SD	RSD%
A	3.7850	100.00	**104**	1.2	1.2	**0.233**	0.014	6.0
A1	2.7036	71.43	**101**	1.6	1.6	**0.207**	0.009	4.3
A2	2.1028	55.56	**107**	1.2	1.1	**0.242**	0.004	1.7
B	1.8925	50.00	**106**	1.6	1.5	**0.239**	0.004	1.7
B1	1.2617	33.33	**104**	1.9	1.8	**0.236**	0.008	3.4
B2	1.1132	29.41	**103**	1.9	1.8	**0.219**	0.008	3.7
C	0.9463	25.00	**104**	2.1	2.0	**0.228**	0.008	3.5
D	0.7570	20.00	**102**	1.9	1.9	**0.208**	0.010	4.8
E	0.5407	14.29	**103**	1.5	1.5	**0.211**	0.011	5.2
F	0.3785	10.00	**104**	1.8	1.7	**0.212**	0.005	2.4
G	0.1992	5.26	**100**	1.3	1.3	**0.182**	0.013	7.1
Calibration Curve 2 of Preconcentrate 2A2 50: 50 in blank FaSSIF-V2								
Sample Name	Concentration of Preconcentrate [mg/ml]	% of Initial sample	Particle Size [nm]			Polydispersity Index		
			Average	SD	RSD %	Average	SD	RSD%
A	3.7750	100.00	**124**	1.4	1.1	**0.229**	0.010	4.4
A1	2.6964	71.43	**123**	0.6	0.5	**0.236**	0.011	4.7
A2	2.0972	55.56	**121**	0.9	0.7	**0.225**	0.013	5.8
B	1.8875	50.00	**114**	0.8	0.7	**0.188**	0.009	4.8
B1	1.2583	33.33	**119**	1.0	0.8	**0.229**	0.005	2.2
B2	1.1103	29.41	**123**	1.2	1.0	**0.223**	0.008	3.6
C	0.9438	25.00	**119**	1.2	1.0	**0.222**	0.016	7.2
D	0.7550	20.00	**119**	0.8	0.7	**0.219**	0.004	1.8
E	0.5393	14.29	**116**	0.7	0.6	**0.205**	0.007	3.4
F	0.3775	10.00	**117**	1.1	0.9	**0.204**	0.015	7.4
G	0.1798	4.76	**117**	1.5	1.3	**0.201**	0.012	6.0

Table A.8.6. Calibration curves for preconcentrate 2A2 50:50 where, x - corresponds to the concentration of the preconcentrate, y – corresponds to the measured transmittance.

Preconcentrate 2A2 50: 50 in blank FaSSIF-V2			
Item	**Calibration range**	**Relationship**	**Correlation Coefficient**
Calibration curve 1	0.2 – 3.8 mg/ml	$y = 99.8807\ e^{-0.5959\ x}$	$R^2 = 0.9991$
Calibration curve 2		$y = 99.7836e^{-0.6003\ x}$	$R^2 = 1.0000$
Calibration curve 3		$y = 101.1888\ e^{-0.6220\ x}$	$R^2 = 0.9978$

Table A.8.7. Particle size and polydispersity index data obtained after desorption of S-SEEDS prepared with the solid carriers.

Sample Name	Particle Size [nm]			Polydispersity Index		
	Average	SD	RSD	Average	SD	RSD
BL Sylysia 320, AL%= 65 - 38A (r=6)	386	5.3	1.4	0.165	0.035	21.2
BL Sylysia 320, AL%= 65 - 38B (r=6)	546	5.6	1.0	0.176	0.023	13.1
BL Sylysia 320, AL%= 65 - 38C (r=6)	412	8.1	2.0	0.249	0.012	4.8
BL Sylysia 320, AL%=65 (n=3)	**448**	85.9	19.2	**0.197**	0.046	23.4
BL Aeroperl 300/30, AL%= 60 - 31A (r=6)	164	1.2	0.7	0.105	0.028	26.7
BL Aeroperl 300/30, AL%= 60 - 31B (r=6)	180	4.8	2.7	0.264	0.022	8.3
BL Aeroperl 300/30, AL%= 60 - 31C (r=10)	144	4.9	3.4	0.228	0.035	15.4
BL Aeroperl 300/30, AL% = 60 (n=3)	**163**	18.0	11.0	**0.199**	0.083	41.7
BL Zeofree 5161, AL%= 70 - 37A (r=6)	144	1.5	1.0	0.234	0.009	3.8
BL Zeofree 5161, AL%= 70 - 37B (r=6)	167	2.4	1.4	0.363	0.041	11.3
BL Zeofree 5161, AL%= 70 - 37C (r=6)	162	2.3	1.4	0.376	0.039	10.4
BL Zeofree 5161, AL%=70 (n=3)	**158**	12.1	7.7	**0.324**	0.079	24.4
BL Hubersorb 600, AL%=71 - 45A (r=6)	156	0.7	0.4	0.246	0.007	2.8
BL Hubersorb 600, AL%=71 - 45B (r=6)	194	1.9	1.0	0.405	0.021	5.2
BL Hubersorb 600, AL%=71 - 45C (r=6)	188	1.5	0.8	0.395	0.016	4.1
BL Hubersorb 600, AL%=71 - 56A (r=6)	171	2.2	1.3	0.322	0.032	9.9
BL Hubersorb 600, AL%=71 - 56B (r=12)	214	35.9	16.8	0.422	0.052	12.3
BL Hubersorb 600, AL%=71 - 56C (r=6)	157	3.0	1.9	0.325	0.036	11.1
BL Hubersorb 600, AL%=71 (n=6)	**180**	22.8	12.7	**0.353**	0.067	19.0
BL Neusilin US2, AL%=70 - 42A (r=6)	122	0.9	0.7	0.264	0.004	1.5
BL Neusilin US2, AL%=70 - 42B (r=12)	144	1.9	1.3	0.304	0.025	8.2
BL Neusilin US2, AL%=70 - 42C (r=6)	145	1.7	1.2	0.296	0.025	8.4
BL Neusilin US2, AL%=70 - 57A (r=18)	242	3.6	1.5	0.503	0.010	2.0
BL Neusilin US2, AL%=70 - 57C (r=12)	280	27.6	9.9	0.511	0.038	7.4
BL Neusilin US2, AL%=70 (n=5)	**187**	69.8	37.3	**0.376**	0.121	32.2
BL Fujicalin SG, AL%=40 - 40A (r=6)	92	0.5	0.5	0.233	0.010	4.3
BL Fujicalin SG, AL%=40 - 40B (r=6)	109	0.6	0.6	0.234	0.009	3.8
BL Fujicalin SG, AL%=40 - 40C (r=6)	121	1.0	0.8	0.203	0.007	3.4
BL Fujicalin SG, AL%=40 - 59A (r=6)	146	0.6	0.4	0.248	0.007	2.8
BL Fujicalin SG, AL%=40 - 59B (r=6)	121	0.5	0.4	0.205	0.004	2.0
BL Fujicalin SG, AL%=40 - 59C (r=6)	117	1.0	0.9	0.245	0.007	2.9
BL Fujicalin SG, AL%=40 (n=6)	**118**	17.7	15.0	**0.228**	0.020	8.8

Table A.8.8. Transmittance data obtained after desorption of S-SEDDSs prepared with the solid carriers.

Sample Name	Transmittance [%]		
	Average	SD	RSD
BL Sylysia 320, AL%=65 - 38A (r=3)	53.47	0.03	0.1
BL Sylysia 320, AL%=65 - 38B (r=3)	99.80	0.09	0.1
BL Sylysia 320, AL%=65 - 38C (r=3)	99.76	0.16	0.2
BL Sylysia 320, AL%=65 (n=3)	**84.34**	26.74	31.7
BL Aeroperl 300/30, AL%=60 - 31A (r=3)	91.88	0.26	0.3
BL Aeroperl 300/30, AL%=60 - 31B (r=3)	82.82	0.21	0.3
BL Aeroperl 300/30, AL%= 60 - 31C (r=3)	91.74	0.24	0.3
BL Aeroperl 300/30, AL%=60 (n=3)	**88.81**	5.19	5.8
BL Zeofree 5161, AL%=70 - 37A (r=3)	53.15	0.01	0.0
BL Zeofree 5161, AL%=70 - 37B (r=3)	28.45	0.06	0.2
BL Zeofree 5161, AL%=70 - 37C (r=3)	34.55	0.03	0.1
BL Zeofree 5161, AL%=70 (n=3)	**38.72**	12.87	33.2
BL Hubersorb 600, AL%=70 - 45B (r=3)	0.79	0.00	0.0
BL Hubersorb 600, AL%=70 - 45C (r=3)	0.96	0.01	1.0
BL Hubersorb 600, AL%=70 - 56A (r=3)	11.95	0.06	0.5
BL Hubersorb 600, AL%=70 - 56B (r=3)	0.64	0.01	1.6
BL Hubersorb 600, AL%=70 - 56C (r=3)	4.98	0.03	0.6
BL Hubersorb 600, AL%=70 (n=6)	**4.60**	4.72	102.6
BL Neusilin US2, AL%=70 - 42A (r=3)	43.73	0.18	0.4
BL Neusilin US2, AL%=70 - 42B (r=3)	6.48	0.03	0.5
BL Neusilin US2, AL%=70 - 42C (r=3)	2.91	0.00	0.0
BL Neusilin US2, AL%=70 - 57A (r=3)	0.75	0.01	1.3
BL Neusilin US2, AL%=70 - 57B (r=3)	0.63	0.01	1.6
BL Neusilin US2, AL%=70 - 57C (r=3)	0.73	0.00	0.0
BL Neusilin US2, AL%=70 (n=6)	**9.21**	17.06	185.2
BL Fujicalin SG, AL%=40 - 40A (r=3)	76.01	0.51	0.7
BL Fujicalin SG, AL%=40 - 40B (r=3)	58.46	0.03	0.1
BL Fujicalin SG, AL%=40 - 40C (r=3)	48.67	0.16	0.3
BL Fujicalin SG, AL%=40 - 59A (r=3)	10.24	0.02	0.2
BL Fujicalin SG, AL%=40 - 59B (r=3)	52.48	0.22	0.4
BL Fujicalin SG, AL%=40 - 59C (r=3)	57.87	0.02	0.0
BL Fujicalin SG, AL%=40 (n=6)	**50.62**	21.89	43.2

Table A.8.9. Calibration curves for Fat Red 7B where, x - corresponds to the concentration of Fat Red 7B , y – corresponds to the peak surface area.

Preconcentrate 2A2 50: 50 in blank FaSSIF-V2			
Item	**Calibration range**	**Relationship**	**Correlation Coefficient**
Calibration curve 1	0.5 – 7 µg/ml	y = 211046 x	$R^2 = 0.9997$
Calibration curve 2		y = 210710 x	$R^2 = 0.9995$

Table A.8.10. Standard solutions of Fat Red 7B spiked with Preconcentrate 2A2 50/50.

Excipients screening - samples spiked with Preconcentrate 2A2 50/50							
Sample Name	Concentration of FR7B [mg/ml]	Concentration of Preconcentrate 50/50 [mg/ml]	Diluent	Appearance	Peak Surface Area		
					Average (2 injections)	**SD**	**RSD%**
SPM1	7.147	11.700	methanol	clear solution	1541543	4378.41	0.3
SPM2	7.147	12.000	methanol	clear solution	1574465	3428.05	0.2
1A	7.147	-	methanol	clear solution	1505538	5787.67	0.4
Spiked Samples vs non spiked (Average/SD/RSD based on SPM1, SPM2, 1A)					**1540515**	34475	2.2
SPM3	1.021	10.860	methanol	clear solution	223103	409.41	0.2
SPM4	1.021	10.280	methanol	clear solution	228695	466.69	0.2
1D	1.021	-	methanol	clear solution	215569	4154.25	1.9
Spiked Samples vs non spiked (Average/SD/RSD based on SPM3, SPM4, 1D)					**222456**	6587	3.0

Table A.8.11. Solutions and emulsions with Fat Red 7B and Preconcentrate 2A2 50/50.

Sample Name	Stock X of FR7B in methanol [ml]	Concentration of Preconcentrate 2A2 50/50 [mg/ml]	Diluent	Final volume [ml]	Appearance	Peak Surface Area		
						Average (2 injections)	**SD**	**RSD%**
CX1 (1st sub-sample)	1.4	10.200	blank FaSSIF-V2	10	cloudy red/pink emulsion, non-separating easily	1096557	32397.51	3.0
CX1 (2nd sub-sample)						1184152	29876.68	2.5
CX1 (3rd sub-sample)						1185852	10782.88	0.9
CX1 (4th sub-sample)						1139278	1798.17	0.2
CX1 (5th sub-sample)						1145681	1866.05	0.2
CX1 Average/SD/RSD based on 5 sub-samples						**1150304**	36882	3.2
CX2	1.4	-	blank FaSSIF-V2	10	purple solution with precipitate	not tested		
CX3	1.4	-	methanol	10	clear red solution	1162192	4391.84	0.4
CX4	1.4	11.690	methanol	10	clear red solution	1175137	0.0	0.0
Average/SD/RSD based on CX1, CX3, CX4						**1162544**	12420	1.1

Table A.8.12. Recovery of Fat Red 7B in the filtrates after desorption from the final stained S-SEDDSs prepared with the solid carriers.

Sample Name	Peak Surface Area			**Fat Red 7B Concentration [µg/ml]**			Adsorbed Preconcentrate [mg]	Fat Red 7B [µg] – measured in 20 ml of media	(% of Recovery from the original sample of FR7B)	
	Average	**SD**	**RSD**	**Average**	**SD**	**RSD**				
Sylysia 320, AL%= 65 - 69A	**Peak not detected**	/	/	/	/	/	**73.0**	**146.0**	**0**	
Sylysia 320, AL%= 65 - 69B	**Peak not detected**	/	/	/	/	/	**71.7**	**143.4**	**0**	
Sylysia 320, AL%= 65 - 69C	**Peak not detected**	/	/	/	/	/	**71.4**	**142.8**	**0**	
BL ST Sylysia 320, AL%= 65 (n=3)									**Average = 0 %**	
									SD = 0	**RSD= /**
Aeroperl 300/30, AL%= 60 -70A	**Peak not detected**	/	/	/	/	/	**71.9**	**143.8**	**0**	
Aeroperl 300/30, AL%= 60 - 70B	**Peak not detected**	/	/	/	/	/	**72.4**	**144.8**	**0**	
Aeroperl 300/30, AL%= 60 - 70C	**Peak not detected**	/	/	/	/	/	**74.7**	**149.4**	**0**	
BL ST Aeroperl 300/30, AL%=60 (n=3)									**Average = 0 %**	
									SD = 0	**RSD= /**
Zeofree 5161, AL%=70 - 67A – sample 1	1894.34	0.7	1.29	0.11	0.1	1894.34	**74.3**	**148.6**	**18.0**	
Zeofree 5161, AL%=70 - 67A – sample 2	2847.52	1.0	1.32	0.11	0.1	2847.52				
Zeofree 5161, AL%=70 - 67A (average)				**1.304**	**0.03**	**2.1**				
Zeofree 5161, AL%=70 - 67B – sample 1	244000.0	246.78	0.1	1.16	0.11	0.1	**71.5**	**143.0**	**16.0**	
Zeofree 5161, AL%=70 - 67B – sample 2	250318.0	876.81	0.4	1.19	0.11	0.1				
Zeofree 5161, AL%=70 - 67B (average)				**1.172**	**0.02**	**1.8**				
Zeofree 5161, AL%=70 - 67C – sample 1	248280.0	3585.74	1.4	1.18	0.11	0.1	**74.3**	**148.6**	**16.0**	
Zeofree 5161, AL%=70 - 67C – sample 2	260646.0	1175.92	0.5	1.24	0.11	0.1				
Zeofree 5161, AL%=70 - 67C (average)				**1.207**	**0.04**	**3.5**				
BL ST Zeofree 5161, AL%=70 (n=3)									**Average = 17 %**	
									SD = 1.15	**RSD= 6.8**
Hubersorb 600, AL%=70 - 65A –sample 1	679832.0	374.8	0.1	3.22	0.11	0.1	**72.3**	**144.6**	**46.0**	
Hubersorb 600, AL%=70 - 65A –sample 2	726101.0	2718.8	0.4	3.44	0.11	0.1				
Hubersorb 600, AL%= 70 - 65A (average)				**3.334**	**0.15**	**4.6**				
Hubersorb 600, AL%=70 - 65B –sample 1	563033.0	429.2	0.1	2.67	0.11	0.1	**74.1**	**148.2**	**37.0**	
Hubersorb 600, AL%=70 - 65B –sample 2	578807.0	5076.3	0.9	2.75	0.11	0.1				
Hubersorb 600, AL%= 70 - 65B (average)				**2.708**	**0.05**	**2.0**				
Hubersorb 600, AL%=70 - 65C –sample 1	706565.0	3170.0	0.4	3.35	0.11	0.1	**70.4**	**140.8**	**49.0**	
Hubersorb 600, AL%=70 - 65C –sample 2	740584.0	2008.2	0.3	3.51	0.11	0.1				
Hubersorb 600, AL%= 70 - 65C (average)				**3.432**	**0.11**	**3.3**				
BL ST Hubersorb 600, AL%=70 (n=3)									**Average = 44 %**	
									SD = 6.24	**RSD=14.2**

Table A.8.12. Recovery of Fat Red 7B in the filtrates after desorption from the final stained S-SEDDSs prepared with the solid carriers (cont'd).

Sample Name	Peak Surface Area			Fat Red 7B Concentration [µg/ml]			Adsorbed Preconcentrate [mg]	Fat Red 7B [µg] – measured in 20 ml of media	(% of Recovery from the original sample of FR7B)	
	Average	SD	RSD	Average	SD	RSD				
Neusilin US2, AL%=70 - 61A – sample 1	292047.0	1437.55	0.5	1.39	0.11	0.1	**73.6**	**147.2**	**20.0**	
Neusilin US2, AL%=70 - 61A – sample 2	324224.0	5951.01	1.8	1.54	0.11	0.1				
Neusilin US2, AL%= 70 - 61A (average)				**1.461**	**0.11**	**7.4**				
Neusilin US2, AL%=70 - 61B – sample 1	323621.0	0.00	0.0	1.54	0.11	0.1	**71.6**	**143.2**	**22.0**	
Neusilin US2, AL%=70 - 61B – sample 2	330563.0	586.90	0.2	1.57	0.11	0.1				
Neusilin US2, AL%= 70 - 61B (average)				**1.552**	**0.02**	**1.5**				
Neusilin US2, AL%=70 - 61C – sample 1	271041.0	2190.62	0.8	1.29	0.11	0.1	**71.8**	**143.6**	**19.0**	
Neusilin US2, AL%=70 - 61C – sample 2	292597.0	1774.13	0.6	1.39	0.11	0.1				
Neusilin US2, AL%= 70 - 61C (average)				**1.337**	**0.07**	**5.4**				
BL ST Neusilin US2, AL%= 70 (n=3)									**Average = 20 %**	
									SD = 1.53	**RSD= 7.7**
Fujicalin SG, AL%=40 - 63A – sample 1	536779.0	95.46	0.0	2.55	0.11	0.1	**73.1**	**146.2**	**35.0**	
Fujicalin SG, AL%=40 - 63A – sample 2	538796.0	2867.32	0.5	2.56	0.11	0.1				
Fujicalin SG, AL%= 40 - 63A (average)				**2.550**	**0.01**	**0.3**				
Fujicalin SG, AL%=40 - 63B – sample 1	540609.0	1193.60	0.2	2.56	0.11	0.1	**72.4**	**144.8**	**36.0**	
Fujicalin SG, AL%=40 - 63B – sample 2	544889.0	4504.27	0.8	2.58	0.11	0.1				
Fujicalin SG, AL%= 40 - 63A (average)				**2.574**	**0.01**	**0.5**				
Fujicalin SG, AL%=40 - 63C – sample 1	632003.0	1881.61	0.3	3.00	0.11	0.1	**74.1**	**148.2**	**41.0**	
Fujicalin SG, AL%=40 - 63C – sample 2	654267.0	2964.90	0.5	3.10	0.11	0.1				
Fujicalin SG, AL%= 40 - 63A (average)				**3.050**	**0.07**	**2.5**				
BL ST Fujicalin SG, AL%= 40 (n=3)									**Average = 37 %**	
									SD = 3.21	**RSD= 8.7**